Final Research Report

REVISED

PREDICTION OF REINFORCEMENT LOADS IN REINFORCED SOIL WALLS

by

Tony M. Allen, P.E.
Washington State Department of Transportation
E&EP Materials Laboratory Geotechnical Division
Olympia, Washington

and

Richard J. Bathurst, Ph.D., P.Eng.
Professor of Civil Engineering
Royal Military College of Canada
Kingston, Ontario, Canada

Prepared for

Washington State Department of Transportation
and in cooperation with
US Department of Transportation
Federal Highway Administration

December 2003

TECHNICAL REPORT STANDARD TITLE PAGE

1. REPORT NO.	2. GOVERNMENT ACCESSION NO.	3. RECIPIENT'S CATALOG NO.
WA-RD 522.2		

4. TITLE AND SUBTITLE	5. REPORT DATE
Prediction of Reinforcement Loads in Reinforced Soil Walls	December 2003
	6. PERFORMING ORGANIZATION CODE
7. AUTHOR(S)	8. PERFORMING ORGANIZATION REPORT NO.
Tony M. Allen, Richard J. Bathurst	
9. PERFORMING ORGANIZATION NAME AND ADDRESS	10. WORK UNIT NO.
Washington State Transportation Center (TRAC) University of Washington, Box 354802 University District Building; 1107 NE 45th Street, Suite 535 Seattle, Washington 98105-4631	11. CONTRACT OR GRANT NO.
12. SPONSORING AGENCY NAME AND ADDRESS	13. TYPE OF REPORT AND PERIOD COVERED
Research Office Washington State Department of Transportation Transportation Building, MS 47370 Olympia, Washington 98504-7370 Keith Anderson, Project Manager, 360-709-5405	Research report
	14. SPONSORING AGENCY CODE

15. SUPPLEMENTARY NOTES

This study was conducted in cooperation with the U.S. Department of Transportation, Federal Highway Administration.

16. ABSTRACT

Proper estimation of soil reinforcement loads and strains is key to accurate design of the internal stability of geosynthetic and steel reinforced soil structures. Current design methodologies use limit equilibrium concepts to estimate reinforcement loads for internal stability design, with empirical modifications to match the prediction to observed reinforcement loads at working stresses. This approach has worked reasonably well for steel reinforced walls but appears to seriously overestimate loads for geosynthetic walls.

A large database of full-scale geosynthetic walls (16 fully instrumented, full-scale geosynthetic walls and 14 walls with limited measurements) and 24 fully instrumented, full-scale steel reinforced wall sections was utilized to develop a new design methodology based on working stress principles, termed the K-Stiffness Method. This new methodology considers the stiffness of the various wall components and their influence on reinforcement loads. Results of simple statistical analyses to evaluate the ratio of predicted to measured peak reinforcement loads in geosynthetic walls were telling: the AASHTO Simplified Method results in an average ratio of measured to predicted loads of 0.45 with a coefficient of variation (COV) of 91 percent, whereas the proposed method results in an average of 0.99 and a COV of 36 percent. The proposed method remains accurate up until the point at which the soil begins to fail (approximately 3 to 5 percent strain). For steel reinforced MSE walls the improvement was more modest: AASHTO's Simplified Method results in an average ratio of predicted to measured loads of 1.12 with a (COV) of 45 percent, whereas the new K-Stiffness Method results in an average of 0.95 and a COV of 32 percent. The objective of the method is to design the wall reinforcement so that the soil within the wall backfill will not reach a state of failure consistent with the notion of working stress conditions. This soil failure limit state is not considered in the design methods currently available, yet, given the research results presented herein, is likely to be a controlling limit state for geosynthetic structures.

The fruit of this research is a more accurate method for estimating reinforcement loads, thereby reducing reinforcement needs and improving the economy of reinforced soil walls. The scope of this research was limited to reinforced soil walls that utilize granular (non-cohesive, relatively low silt content) backfill.

17. KEY WORDS	18. DISTRIBUTION STATEMENT
Reinforcement, walls, loads, strains, creep, design	No restrictions. This document is available to the public through the National Technical Information Service, Springfield, VA 22616

19. SECURITY CLASSIF. (of this report)	20. SECURITY CLASSIF. (of this page)	21. NO. OF PAGES	22. PRICE
None	None		

TABLE OF CONTENTS

FIGURES

TABLES

EXECUTIVE SUMMARY

This report represents an update to Report WA-RD 522.1. Continued technical review of this work by the research team, as well as by the geotechnical engineering profession at large, and the availability of new data have resulted in some changes in the interpretation of the data and some modifications to the recommendations. This additional technical evaluation has also provided the opportunity to improve the analysis of the data and the resulting design model. While the basic structure and content of the report as presented herein remains unchanged relative to Report WA-RD 522.1, the data and analysis results provided in the original report have been updated, with the text modified as necessary.

This report is the culmination of over ten years of research on the estimation of reinforcement loads and strains in reinforced soil walls. This effort began as a Federal Highway Administration (FHWA) Experimental Features Project (the I-90 Rainier Avenue Geotextile Wall in Seattle), progressed into a multi-phase research project on geosynthetic walls at the University of Washington, continued with the development of a database of both geosynthetic and steel reinforced soil walls in support of proposed revisions to the AASHTO Standard Specifications for Highway Bridges, and is continuing at present as a multi-agency pooled fund research project at the Royal Military College of Canada. This pooled fund project involves construction and analysis of full-scale, reinforced soil test walls subjected to surcharge loading in excess of working stress levels. The focus of all this effort is to develop a new design methodology based on working stress principles that provides more accurate estimates of reinforcement loads and strains. This is especially important for geosynthetic walls, as engineers have long recognized that current geosynthetic wall designs are excessively conservative, given observed performance to date. It is also important to consider the behavior of steel reinforced walls, to ensure that any new design method will encompass the full range of soil reinforcement properties and not be limited to geosynthetic reinforced soil wall structures. Such a new method could also help to remove the somewhat arbitrary distinctions made between various reinforcement types, as is currently done to attempt to match the empirical data. A seamless design approach with consistent limit states and levels of safety for all reinforcement materials is desirable.

Proper estimation of soil reinforcement loads and strains is key to the accurate design of internal stability for reinforced soil structures. Accurate estimation of reinforcement loads and strains will result in more accurate estimation of reinforcement strength and spacing requirements, facing connection strength, facing design, and reinforcement length required to resist pullout.

Because current design specifications, such as the AASHTO Load and Resistance Factor Design (LRFD) Bridge Design Specifications and the Eurocode, now utilize a limit states approach, an objective of any new methodology must be to make it fully adaptable to limit states design. To this end, adequate statistical information that demonstrates the accuracy of the design, both for loads and resistances, is an important objective. Such data can be used to develop accurate load and resistance factors so that a consistent and known overall level of safety can be quantified. Currently, the true level of safety in these systems is not very well known, as empirical or theoretical assumptions have been combined with poorly defined material properties, resulting in "hidden" safety factors. Furthermore, the true limit states for reinforced soil wall systems need to be better defined to accurately understand the true performance limits of these structures.

Research Approach

The scope of this study was limited to reinforced soil walls that utilize granular (non-cohesive, relatively low silt content) backfill. The scope of this study was also limited to static conditions (i.e., no seismic loading). Extension of the methodology developed herein to non-select fills and seismic load environments can only be carried out once the behavior of reinforced soil walls is well defined for the simplest soil and loading conditions.

To develop an improved design approach, a database of numerous case histories of both geosynthetic and steel reinforced walls was assembled (28 fully instrumented, full-scale, field wall case histories comprising 37 different wall sections and surcharge conditions, plus five fully instrumented, full-scale, laboratory test walls, plus an additional six field wall case histories comprising 14 different wall sections that were not fully instrumented). For each wall, this database included the wall geometry, reinforcement properties and spacing, measured soil properties (strength and unit weight), any available long-term performance data, and for the fully

instrumented walls the measured reinforcement strains or loads. The range of material properties and wall geometries encompassed by this database included the following:

- For the geosynthetic wall case histories, reinforcement products included geotextiles and geogrids, different polymers (polypropylene (PP), high density polyethylene (HDPE) and polyester (PET)), strip and continuous reinforcements, and a range of tensile strengths from 12 to 200 kN/m and reinforcement stiffness values from 45 to 7,400 kN/m. Reinforcement vertical spacing varied from 0.3 to 1.6 m. Wall facing batter angles varied from 0^o (vertical) to 27^o, although most of the walls had facing batter angles of 8^o or less. Wall heights vary from 3.0 m to 12.6 m, with surcharge heights of up to 5.3 m of soil. Facing types included geosynthetic wrapped-face, welded wire, pre-cast concrete panels, and modular concrete blocks. Plane strain peak soil friction angles, estimated from measured triaxial or direct shear test data, varied from 42^o to 57^o. Some of these walls have been in service for up to 25 years, although long-term strain measurements were available only for walls up to 11 years old.
- For steel reinforced soil wall case histories, reinforcement products included steel strip, bar mat, and welded wire reinforcement, and reinforcement stiffness values of from 18,000 kN/m to 166,000 kN/m. Most of the steel walls utilized pre-cast concrete panel facings, although one wall had a welded wire facing. The facing for all of the steel reinforced soil walls was near vertical. Walls with and without significant soil surcharges, narrow base and wide base-width walls, walls with trapezoidal cross-sections, and very tall walls of up to 18 m high were included in the database. Reinforcement coverage ratios varied from 0.053 to 1.0, while vertical spacing of the reinforcement varied from 0.3 to 0.75 m. The wall backfill materials had a range of peak plane strain soil shear strengths (35^o to 56^o).

The new design methodology proposed herein, called the K-Stiffness Method, was developed empirically through analysis of these full-scale wall case histories within a working stress framework. In most cases, reinforcement loads in these case histories had to be estimated through measured reinforcement strains converted to load with reinforcement stiffness values. Therefore, the correct stiffness as a function of both time and temperature was estimated, at least for geosynthetic walls, to accurately determine the reinforcement loads. For steel reinforced walls, the conversion of strain to load was relatively straightforward.

The soil reinforcement in geosynthetic walls is loaded at a very slow rate during construction in contrast to the loading rate in typical index tensile test methods. Typically, wall construction takes 500 to 1,500 hours to be completed. To account for this slow loading rate, the analysis of the long-term load-strain properties of geosynthetics determined that the geosynthetic reinforcement stiffness could be accurately estimated by using isochronous creep data. Stress relaxation tests, very slow constant rate of strain, or constant rate of stress tests may be more appropriate for quantifying the long-term stiffness of geosynthetic reinforcement than constant load tests. However, from a practical point of view, for most geosynthetics little difference was found in the reinforcement stiffness at the times of interest, regardless of the type of test used. The accuracy of the method used to estimate the correct time-dependent geosynthetic stiffness was verified by comparing the loads predicted from measured strains to load cell readings, typically at the reinforcement-facing connection but in one case within the backfill. The accuracy of the reinforcement loads was also verified by comparing the measured post-construction creep strains and rates to laboratory in-isolation creep data obtained at the reinforcement load level estimated from measured strain data. In most cases, the laboratory creep strains and rates were found to be the same as or greater than (i.e., more conservative for design than) the creep strains and rates measured in the full-scale walls. An important implication of this result is that reinforcement loads estimated from strain readings with the reinforcement stiffness at the end of construction are reasonably accurate.

Once the correct load levels in the reinforcement layers had been established, the reinforcement loads obtained from the full-scale wall case histories were compared to values predicted by the current methodologies found in design guidelines and design codes, including the Coherent Gravity Method and the Simplified Method (AASHTO, 2002), and by the proposed methodology. Conventionally, these predicted reinforcement loads are compared to the "measured" values in the form of a ratio (predicted/measured) to statistically quantify the relative accuracy of various prediction methods. All of the existing design methodologies were found to provide very poor predictions of reinforcement load for geosynthetic walls and only marginally acceptable predictions for steel reinforced structures. The average and coefficient of variation (COV) of the ratio of predicted to measured peak reinforcement load (T_{max}) calculated by the Simplified Method were 4.2 and 120 percent, respectively, for geosynthetic walls, and 0.9 and 50.6 percent, respectively, for steel reinforced soil walls, given all of the full-scale field walls in

the database. These statistics were based on the use of the plane strain friction angle of the soil to calculate reinforcement loads. Note that the Simplified Method was developed to yield an average of just over 1.0 for steel reinforced walls when more conventional triaxial or direct shear strength test results are used (the average when using the triaxial or direct shear friction angle was found to be 1.04, and the COV was 50.7 percent). Current AASHTO design specifications (AASHTO 2002) specifically exclude polymer strap walls and heavily battered walls. If these walls are eliminated from the database, and if a triaxial/direct shear soil friction angle is used, the average and COV of the Simplified Method predictions for geosynthetic walls are 7.6 and 82 percent, respectively. The most recent AASHTO design specifications (AASHTO 2003) recommend that the triaxial/direct shear soil friction angle be limited to 40^{o}, even if the measured value is greater. If this is considered, the average and COV of the Simplified Method predictions for steel walls are 1.12 and 45.3 percent, respectively. The K-Stiffness Method, however, was found to produce average and COV values for this ratio of 1.14 and 38.4 percent, respectively, for geosynthetic walls, and 1.16 and 32.9 percent, respectively, for steel reinforced soil walls. This was a marked improvement, regardless of which soil friction angle was chosen for use with the Simplified Method.

Sources of variability in the measured strains used to estimate loads in reinforcements and in the stiffness used to convert strains to load were also investigated. Although the variability in the measurements can be considerable, with variations of $\pm$10 to 40 percent possible in the measurement of strain and $\pm$5 to 50 percent in the measurement of stiffness (combined uncertainty in the actual reinforcement loads of approximately 14 to 60 percent, assuming that variability in parameter values are uncorrelated), redundancy in the measurements, careful data interpretation, and a large quantity of data can be used to reduce the effect of this variability. While it can be argued that some sources of uncertainty are correlated, the treatment of the variability of primary parameters as uncorrelated values follows conventional practice in bridge design and simplifies the investigation of parameter variability on predicted design loads. The authors believe that the best overall practical indicator of uncertainty in the new method is the comparison of the predicted loads to the best estimates of the actual loads in the reinforcement.

K-Stiffness Method

This new methodology considers, directly or indirectly, the stiffness of all wall components relative to the soil stiffness to estimate the distribution and magnitude of T_{max}. As such, it uses working stress principles to estimate the load and strain in the reinforcement. However, the method is empirical in nature, since it was calibrated to accurately predict the reinforcement loads in nine full-scale field geosynthetic wall cases (13 different wall sections and surcharge conditions with 56 individual data points) and 19 full-scale field steel reinforced soil wall cases (24 different wall sections and surcharge conditions with 102 individual data points). An additional five full-scale test wall cases were also analyzed to assess the effect of variables that could not be easily assessed with only the field case studies. This new methodology was determined to provide a reasonably accurate prediction up to the point at which the soil begins to fail, making it possible to use the load predictions from this method for both a serviceability and strength limit state prediction.

The K-Stiffness Method considers the following variables:

- for wall geometry, H (the total height of the wall), S (the average surcharge height above the wall), S_v (tributary area, equivalent to the average vertical spacing of the reinforcement near each layer location when analyses are carried out per unit length of wall), and Φ_{fb} (a factor to account for the effect of wall face batter)
- for reinforcement properties, S_{local} (the local reinforcement stiffness, equal to J/S_v where J is the reinforcement stiffness), and S_{global} (the global wall stiffness, equal to $J_{ave}/(H/n)$ where J_{avg} is the average stiffness for all reinforcement layers and n is the number of layers)
- for facing stiffness, Φ_{fs} (facing stiffness factor, which considers the structural stiffness of the facing column)
- for soil properties, γ (the backfill soil unit weight), and K_0 (the at-rest earth pressure coefficient based on the peak plane strain soil friction angle).

The K-Stiffness Method was developed by first considering the conventional equation for earth pressure behind walls, assuming nothing about the distribution of that pressure, as follows:

$$\sigma_h = \frac{1}{2} K \gamma (H + S) \tag{1.1}$$

"K", a lateral earth pressure coefficient, was set equal to K_0. For steel reinforced systems, a lower bound cap for $K_0 = 0.3$ (this corresponds to an approximate plane strain soil friction angle of 44^o) was required to provide the best correlation between K_0 and T_{max}. The use of K_0 in this proposed method is not to imply that at rest conditions exist within the reinforced backfill. K_0 is simply used as an index parameter to approximately characterize the soil behavior, as is discussed in more detail in the report. The distribution of maximum tensile forces in the wall reinforcement layers was determined empirically from the case history data and through limited analytical modeling. A trapezoidal distribution was found to work well for the geosynthetic walls, but a distribution that was more triangular in shape worked best for steel reinforced soil walls. A factor (D_{tmax}) was introduced to characterize these distributions. Therefore, applying D_{tmax} to Equation 1.1 resulted in a distributed earth pressure of the proper shape. Applying the vertical spacing of the reinforcement, S_v, which in effect would become a tributary area if reinforcement loads were being evaluated on the basis of unit of wall width, converted Equation 1 to represent the force carried by the reinforcement layer, as shown below:

$$T_{max} = \frac{1}{2} K\gamma(H+S)S_v D_{tmax}\Phi \tag{1.2}$$

All that was left to do at this point was to empirically adjust this equation using the function Φ to accurately fit the equation to the empirical reinforcement load data. This function, Φ, was found to be affected by the global wall stiffness, the facing stiffness, the facing batter, and the local stiffness of the reinforcement. Using simple regression techniques to fit the equation to the empirical data, the final expanded form of the equation to predict the maximum load, T_{max}, in each reinforcement layer was determined as follows:

$$T_{\max} = 0.5S_v K_0\gamma\ (H+S)D_{t\max}\left(\frac{S_{local}}{S_{global}}\right)^a\left(\frac{K_{abh}}{K_{avh}}\right)^{0.25} 0.5\left(\frac{1.5H^4}{ELb^3\left(h_{eff}/H\right)}p_a\right)^{0.14} 0.25\left(\frac{S_{global}}{p_a}\right)^{0.25} \tag{1.3}$$

where "a" is a coefficient (currently set equal to 1 for geosynthetic walls and 0 for steel reinforced walls); K_{abh} is the horizontal component of active earth pressure coefficient accounting for wall face batter; K_{avh} is the horizontal component of active earth pressure coefficient, assuming the wall is vertical; d is a constant coefficient (currently set equal to 0.25), p_a is the atmospheric air pressure (a constant equal to 101 kPa); and all other variables are as

defined previously. $(S_{local}/S_{global})^a$ is a factor that accounts for the effects of local stiffness, and $(K_{abh}/K_{avh})^d$ is the batter factor Φ_{fb}. The facing stiffness factor, Φ_{fs}, is calculated, treating the facing column as a cantilevered beam, as follows:

$$\Phi_{fs} = \eta (F_f)^{\kappa} \tag{1.4}$$

where, F_f is the facing stiffness parameter, which is a function of the facing column geometry and stiffness, and η and κ are empirically determined coefficients equal to 0.5 and 0.14, respectively. This equation is applicable to both geosynthetic and steel reinforced soil walls. This equation can be used to estimate both reinforcement loads and strains, since strain can be estimated by simply dividing T_{max} by the reinforcement stiffness.

To properly apply this equation to design, it must be used with conceptually correct limit states. The research found that this equation predicts the reinforcement loads accurately for geosynthetic reinforced structures up until the soil begins to fail, at which point the reinforcement load begins to increase. When the soil begins to fail, its modulus begins to decrease rapidly, causing the reinforcement to carry more load to maintain equilibrium in the wall system. In the past, failure has been defined in terms of reinforcement rupture, as it has been assumed that all wall components reached a state of failure at the same time (i.e., limit equilibrium). For geosynthetic reinforced structures, the soil will fail first, and then eventually, if destabilizing loads are great enough, the reinforcement will fail. Although steel reinforcements reach yield well before the soil begins to fail, rupture of the steel will most likely occur after the soil has reached a failure state. Therefore, one limit state that must be considered for reinforced soil walls is failure of the wall backfill. Reinforcement failure is a second limit state that must be considered. In most cases, at least for granular soils, if the reinforcement strains can be kept below approximately 3 to 3.5 percent strain, soil failure will be avoided. The K-Stiffness Method can be used to design the reinforcement to limit the strain so that soil failure is avoided. Furthermore, the reinforcement load predicted by this method can be used to estimate the ultimate tensile strength required to prevent reinforcement rupture. This method can also be used to estimate reinforcement requirements to meet serviceability criteria, although more research is required to link the estimated reinforcement strains to short-term and long-term wall face deformations.

Additional Research

Additional research will be needed to refine the magnitude of parameters needed to calculate T_{max} by this method and possibly to develop more accurate expressions for the factors that appear in the fundamental equation introduced as Equation 1.3. The available data at the time of this study suggest that best estimates of parameter values are based on a reasonable fit to the empirical data, so that the method can be used with confidence. Additional research is recommended in the following areas:

- improved quantification of how facing stiffness and wall toe restraint affect reinforcement loads, especially for steel reinforced walls and very tall walls
- better quantification of the load distribution factor, D_{tmax}, especially for very soft or very stiff foundation conditions and for intermediate values of global wall stiffness (i.e., is the distribution a function of global wall stiffness?), as well as how local reinforcement stiffness affects the distribution of reinforcement load
- better quantification of the effect of reinforcement coverage ratio on reinforcement loads
- better quantification of the effect of wall face batter on reinforcement loads, especially for steel reinforced systems
- better quantification of the relationship between reinforcement strain and the shear strain needed to reach the soil peak strength
- improved methods of characterizing the soil to deal with working stress conditions (i.e., is the effect of the soil strength and stiffness characteristics on reinforcement load also related to the global reinforcement stiffness?)
- improved methodology for predicting global deformation of reinforced soil walls
- quantification of wall face connection loads, considering all mechanisms of load development at the connection
- quantification of load and resistance factors for designing limit states through the assessment of the variability in key parameters
- additional analytical modeling, properly calibrated to match the existing case history data, to provide some theoretical verification of the trends observed herein, and to extrapolate the available case history data to a broader range of wall geometries and conditions.

1.0 THE PROBLEM

Accurate prediction of loads, strains, and their distribution for backfill reinforcement in reinforced soil walls is necessary to produce cost effective, internally stable wall designs. The predicted reinforcement loads affect the strength and spacing required for the reinforcement as well as the reinforcement length required to resist pullout. Predicted strains affect the assessment of reinforced soil wall serviceability.

The methods identified in the most recent design codes and design guidelines in North America for estimating reinforcement loads in reinforced soil walls (e.g., the Simplified Method in AASHTO 2002) are semi-empirical in nature. They use limit equilibrium concepts to develop the design model but working stress observations to adjust the model to fit what has been observed in full-scale structures. These approaches have worked reasonably well for typical steel reinforced soil walls, but they appear to be overly conservative for predicting loads in geosynthetic reinforced structures and their performance (Bell et al. 1983, Rowe and Ho 1993; Allen, et al. 2001). Furthermore, these methods cannot be used to accurately estimate reinforcement strains and deformations. Given that problems with current design methodologies have tended to result in excessively conservative designs, especially for geosynthetic walls, design method improvements should result in cost savings for these types of structures.

The reasons for the lack of reinforcement load and strain prediction accuracy appear to be two-fold:

- Limit equilibrium concepts do not accurately reflect mechanisms of load and strain development in a mass composed of elements that are vastly different in their load-strain properties and that are seldom at incipient collapse under operating conditions in the field. Modifications to limit equilibrium-based methods to improve the prediction of reinforcement loads by using measured reinforcement load and strain data are fundamentally impossible.
- The properties of the reinforcement, especially the geosynthetic reinforcement, have not been correctly characterized to provide an accurate estimate of the reinforcement loads and strains under typical operating conditions in the field.

In general, loads in soil reinforcement layers in walls must be estimated from strain measurements and converted to load by using the stiffness of the reinforcement material. There are two requirements for estimating reinforcement load:

1. accurate determination of the strain in the reinforcement, accounting for sources of strain measurement error due to gauge location and calibration, and redundancy in the measurements
2. accurate determination of the stiffness of the reinforcement, accounting for the time dependence of the stiffness, the effect of soil confinement, the effect of installation damage, and other sources of stiffness measurement error. The selection of an appropriate stiffness value is mainly an issue for geosynthetic reinforcement, as the stiffness of steel reinforcement is constant with time and temperature and is relatively straightforward to determine.

Selection of the correct stiffness value to calculate actual reinforcement loads in full-scale reinforced soil walls will provide an accurate basis for developing any improved methodology for designing the internal stability of reinforced soil walls. The interpretation of empirical reinforcement load data using the appropriate stiffness values also enables analytical models to be properly calibrated. Finally, empirical data also provide a baseline against which any new design methods can be compared and their accuracy quantified.

The accuracy of any new design methodology can be assessed by its ability to predict reinforcement loads, as well as its ability to predict performance of the wall over the service life of the structure. Ultimately, the goal is to produce a wall design with the least cost, but with acceptable and predictable long-term performance.

The following approach has been taken to systematically evaluate the current methodologies for designing the internal stability of reinforced soil walls so that improvements can be made:

1. Develop a comprehensive database of wall case histories that will allow reinforcement loads, long-term performance, or both to be assessed. Chapter 2.0 presents the basic database for geosynthetic walls. The report by Allen et al. (2001) contains the corresponding database for steel reinforced soil walls. Additional key measurements and properties (e.g., short- and long-term strain gauge measurements, stiffness properties, estimated reinforcement loads, etc.) for both types of walls are provided in subsequent chapters.

2. Evaluate how heavily reinforced walls have been built in the past and for which long-term performance data are available. Then compare that level of reinforcement to what would be required by current design methodologies, considering both short-term and long-term stability and performance relative to the demand the reinforcement must resist. From this comparison, begin to assess the sources of conservatism in the design of reinforced soil walls. This comparison is also provided in Chapter 2.0.
3. Evaluate measured reinforcement strains and how they were obtained to assess their accuracy and reliability so that further analysis and interpretation of the data can be conducted with confidence. This is accomplished for geosynthetic walls in Chapter 3.0. Allen et al. (2001) address this issue for steel reinforced walls.
4. Evaluate the time, temperature, and strain dependency of the stiffness for geosynthetics, considering all potential load-strain-time regimes for geosynthetic reinforcement confined in the wall backfill. Develop a model to predict the stiffness near the end-of-wall construction and beyond. Next, assess the accuracy of the long-term stiffness prediction model through comparison with direct reinforcement load cell measurements recorded in laboratory and full-scale structures. This evaluation is described in Chapter 4.0 and applied in Chapter 5.0.
5. Verify the accuracy of reinforcement loads estimated from strain measurements based on long-term creep measurements by using the relationship between load level and creep rate. If the load levels are accurate, the creep rate observed should be reasonably close to the laboratory creep rate at that same load level, given the effect of load application rate and soil confinement. This is described in Chapter 6.0.
6. Geosynthetic walls have been viewed by the civil engineering profession, in general, as a new technology whose performance has not been established. Yet geosynthetic walls have been in use for almost 25 years. Is enough case history data available and has the science of geosynthetic material degradation prediction advanced enough to demonstrate the long-term performance of geosynthetic walls? The long-term creep data obtained from full-scale geosynthetic walls mentioned previously will also be used to answer this question, so that any new design approach developed can be tied directly to the long-term performance expected. This is also described in Chapter 6.0.

7. Compare the "measured" reinforcement loads to the loads predicted by the current design methodologies for both geosynthetic and steel reinforced walls to assess any patterns that develop in prediction error, sources of conservatism, and appropriateness of the design model used. This will form the baseline of comparison from which to evaluate design model improvements. The primary emphasis of these analyses will be on full-scale field walls. Full-scale laboratory test walls will also be considered for controlled evaluation of specific variables, provided the test wall boundary conditions are well enough understood to know how to extrapolate the test wall behavior regarding those controlled variables to field wall conditions. This is described in Chapter 5.0 for geosynthetic walls and in the report by Allen et al. (2001) for steel reinforced walls.
8. Develop a new design approach for estimating reinforcement loads in reinforced soil walls. Compare predicted to measured loads and strains for the full-scale field wall case histories and evaluate all variables observed to influence reinforcement loads and strains. The approach used will be empirical in nature but will consider, from a theoretical standpoint, what should influence the development of reinforcement loads and strains at working stresses. The approach should also consider reinforced soil walls as a whole, providing as much as possible a "seamless" design approach across all reinforcement types. This new methodology is developed for geosynthetic walls in Chapter 7.0 and extended to steel reinforced walls in Chapter 8.0.
9. Finally, implement the new reinforcement load prediction methodology for designing the internal stability of reinforced soil walls. Use a limit states approach that will be suitable for load and resistance factor design (LRFD) and use key examples to illustrate how the new method compares to current practice. This will be done in a companion report to be published in the future.

Because of the complexity of the analysis required, the scope of the development of this new methodology is limited to granular backfill materials. Silt and clay backfills add complexity to the prediction of reinforcement load and long-term wall performance. Therefore, the application of the proposed design methodology to silt and clay backfills is reserved for a future study.

2.0 GLOBAL LEVEL OF SAFETY AND PERFORMANCE OF GEOSYNTHETIC WALLS: A HISTORICAL PERSPECTIVE

2.1 Introduction

The first geosynthetic reinforced soil walls were built in France in 1970 and 1971 (Leflaive 1988, Leclercq et al. 1990, Puig et al. 1977). Geosynthetic reinforced walls have been in use in the United States since 1974. Bell and Steward (1977) described some of these early applications, which were primarily geotextile wrapped-face walls that supported logging roads in the northwestern United States. Since these early examples, the use of geosynthetic walls has increased steadily, both in the private and public sectors (Yako and Christopher 1987, Elias et al. 2001). The history of geosynthetic wall design in North America has been summarized by Allen and Holtz (1991) and Berg et al. (1998).

Procedures for designing the internal stability of geosynthetic walls, which define the required strength, spacing, and length of the reinforcement, have become more conservative over the past 20 years, primarily because of the increase in knowledge regarding the durability of geosynthetics (Berg et al. 1998). Attention to the resistance element of internal stability equations has produced more accurate (though likely conservative) estimates of reduction factors for installation damage, creep (at least in air), and durability (at least in the laboratory). This knowledge has generally caused an increase in the magnitude of strength reduction factors that are used to calculate the long-term strength of geosynthetics (Allen and Elias 1996). However, design methods for estimating reinforcement loads have changed little in the past 20 years, resulting in generally more conservative design over time (Berg et al. 1998).

A careful reexamination of the global "level of safety" of older, carefully documented geosynthetic reinforced soil walls and their observed performance over many years offers the possibility to quantify the expected global level of safety and performance of geosynthetic reinforced soil walls constructed today. The performance of older geosynthetic structures will provide a conservative indication of the performance that should be expected for geosynthetic structures built today.

The first objective of this chapter is to provide a database of selected, well-documented geosynthetic reinforced soil walls constructed as long as 25 years ago. The walls selected in this

study were constructed with granular backfill materials to simplify interpretation and analyses. Only case histories that have a post-construction wall performance evaluation were selected.

The second objective of this chapter is to quantify the global level of safety for the one or more wall sections or loading conditions corresponding to each wall case history, and to compare these values to visual observation of wall behavior. Global level of safety is quantified in terms of a resistance-demand ratio, RD, which is the ratio of the sum of reinforcement strengths to the total horizontal load in the soil reinforcement layers. This global level of safety or "resistance to demand ratio" concept provides a common basis of comparison between wall structures and design methods (Allen 1997, Berg et al. 1998). The calculation of global level of safety values is explained in detail in Section 2.3.

The resistance-demand ratio for existing geosynthetic retaining walls is calculated and compared to the resistance-demand ratio that would be required by current design practice and the AASHTO (2002) design code in the USA. This comparison, together with observed post-construction wall performance, allows the identification of potential sources of current design conservatism, and the proposal of directions for improving current geosynthetic reinforced wall design methodologies.

2.2 Summary of Geosynthetic Wall Case Histories

2.2.1 Early French Experience

The first geosynthetic wall in the world was built near Poitiers, France, in 1970 using woven polyester straps. Leflaive (1988) and Leclercq et al. (1990) reported on the long-term durability observed for the polyester reinforcement and provided some details about this wall. The polyester straps were of a type similar to safety belts and were anchored directly to the concrete facing units. The total wall height was approximately 4.5 meters, with six levels of straps installed at a vertical spacing that varied from 0.6 m to 1.1 m. The particle size distribution and soil type were not reported, but in a published photograph (Leclercq et al. 1990) the soil appeared to be gravelly. The pH of the soil was reported to be 8.5, and near the back of the facing panels, the pH was as high as 13 to 14. Samples of the straps taken nine years after the wall had been constructed indicated that the straps had lost significant strength near the connections to the concrete panels. Consequently, an earth berm was placed in front of the wall

to prevent the possibility of collapse should the strength loss continue. Samples were taken and tested again 17 years after the wall had been built. Significant losses on the order of 45 to 50 percent relative to the original strength of the straps had occurred near the wall face, but no significant strength loss was observed in the straps in the backfill away from the face (Leclercq et al. 1990). Observers concluded that at least a portion of this strength loss was due to hydrolysis caused by a high pH level at the wall face, with the remainder of the strength loss due to mechanical damage.

The second geosynthetic wall built, in 1971, was also located in France, at Rouen, on the A15 motorway. Details of this wall are provided by Delmas, et al. (1987), Gourc and Matichard (1992) and Leclercq et al. (1990). The wall was vertically faced and 4 m in height with a geotextile face. This temporary wall was considered experimental and was backfilled with earth in front of the wall after nine months of service. A nonwoven, needlepunched, polyester geotextile with an ultimate tensile strength of 10 kN/m was placed at a vertical spacing of 0.5 m. The fill material was a fine grained mixture of chalk, clay, and flint, with a soil pH of 9 to 10. The wall was placed over a compressible layer of peat and settled more than 1 meter, making interpretation of the wall strains, estimated to be in the order of 1.5 to 2 percent, very difficult (Gourc and Matichard 1992). After the wall had been in place for 15 years, samples of the geotextile were exhumed and tested. Samples revealed a loss in strength of 20 to 30 percent (Gourc and Matichard 1992, Leclercq et al. 1990). Since no chemical changes in the geotextile had occurred, all of the strength loss was attributed to mechanical damage that had occurred during construction.

2.2.2 Detailed Case Histories

Case histories used in the current and subsequent chapters are summarized in Table 2.1 and figures 2.1 through 2.20. The table provides information on material types, material properties, wall geometry, and surcharge details. Additional project details and performance observations are provided in the following sections. A total of 20 different projects, with data from 35 analysis cases (i.e., combinations of wall geometry and loading condition), are presented in the database. The writers were directly involved in many of the project case studies described below. For other walls the writers contacted the original investigators to confirm project details and to collect unpublished information. The earliest geosynthetic walls described in Section 2.1 were not well

documented in terms of material properties and are not used in calculations that appear later in the report.

For the case histories described in the following sections, almost all were built with high quality backfill material (i.e., clean sand or gravel), and with the exception of two wall sites, all the walls were placed on firm foundation soils. It must therefore be recognized that the conclusions drawn later in the report are only applicable to these conditions. Beyond this, the wall case histories described include 17 wrapped-face, four welded wire, one modular concrete block, six full-height propped panel, and four incremental panel-faced wall analysis cases, and they encompass a wide range of geosynthetic reinforcement types, strengths, and spacing. A wide range of soil surcharge conditions was also encompassed by these case histories.

Table 2.1. Summary of wall height and material properties for geosynthetic wall case histories.

Case Study	Project	Height and Surcharge	Soil Description	Soil Gradation d_{max} d_{50} <75μm (mm/mm/%)	Soil Unit Weight γ (kN/m^3)	Design ϕ_{des} (^{o})	Triaxial or Direct Shear ϕ_{trx} or ϕ_{ds} (^{o})	Estimated Plane Strain ϕ_{ps} (^{o})	Project Section or Panel Number	Depth Zone	Geosynthetic Product Name/ Mass/unit area	Product Type/ Polymer	Index Strength T_{ult} (kN/m)
GW1	Snailback Wall, 1974	2.9 m plus 0.9 m soil surcharge	uniform subrounded fine to medium sand.	4.76 1.2 2	21.2[1]	34^o	38^o[8]	43^o	NA	All	Fibretex 420 (420 g/m^2)	NW-NP-GT/PP	19.0
GW2	Olympic National Forest Wall, 1975	5.6 m	crushed rock	75 35 -	18.1[2]	40^o	NA	50^o[3]	A	1 & 2	Bidim C-28 (200 g/m^2)	NW-NP-GT/PET	14.4
										3 & 4	Bidim C-38 (420 g/m^2)	NW-NP-GT/PET	24.7
									B	1 & 2	Fibretex 420 (420 g/m^2)	NW-NP-GT/PP	15.8
										3 & 4	Fibretex 600 (600 g/m^2)	NW-NP-GT/PP	22.1
GW3	CDOT Glenwood Canyon Walls, 1982	4.8 m	pit run, well-graded, clean sandy gravel (rounded)	100 19 -	22.3[1]	35^o	42^o[7]	46^o	1 & 9	1 & 2	Typar 3601	HB-NW-GT/PP	12.6[5]
										3	Trevira 1155	NW-NP-GT/PET	28.9[5]
									2 & 10	1 & 2	Trevira 1127	NW-NP-GT/PET	16.6[5]
										3	Trevira 1155	NW-NP-GT/PET	28.9[5]
									3	1 & 2	Supac (200 g/m^2)	NW-NP-GT/PP	24.3[5]
										3	Trevira 1155	NW-NP-GT/PET	28.9[5]
									4	1 & 2	Fibretex 400	NW-NP-GT/PP	9.9[5]
										3	Trevira 1155	NW-NP-GT/PET	28.9[5]

Table 2.1, Continued.

Case Study	Project	Height and Surcharge	Soil Description	Soil Gradation d_{max} d_{50} <75μm (mm/mm/%)	Soil Unit Weight γ (kN/m^3)	Design ϕ_{des} (^{o})	Triaxial or Direct Shear ϕ_{trx} or ϕ_{ds} (^{o})	Estimated Plane Strain ϕ_{ps} (^{o})	Project Section or Panel Number	Depth Zone	Geosynthetic Product Name/ Mass/unit area	Product Type/ Polymer	Index Strength T_{ult} (kN/m)
GW3	CDOT Glenwood Canyon Walls, 1982	4.8 m plus 2 m soil surcharge	pit run, well-graded, clean sandy gravel (rounded)	100 19 -	22.3[1]	35^o	42^o[7]	46^o	5	1	Typar 3401	HB-NW-GT/PP	7.7[5]
										2	Typar 3601	HB-NW-GT/PP	12.6[5]
										3	Trevira 1155	NW-NP-GT/PET	28.9[5]
									6	1	Trevira 1115	NW-NP-GT/PET	6.8[5]
										2	Trevira 1127	NW-NP-GT/PET	16.6[5]
										3	Trevira 1155	NW-NP-GT/PET	28.9[5]
		4.8 m							7	1 & 2	Supac (135 g/m^2)	NW-NP-GT/PP	12.1[5]
										3	Trevira 1155	NW-NP-GT/PET	28.9[5]
									8	1	Fibretex 200	NW-NP-GT/PP	5.8[5]
										2	Fibretex 400	NW-NP-GT/PP	9.9[5]
										3	Trevira 1155	NW-NP-GT/PET	28.9[5]
GW4	Devils Punch Bowl Wrapped-Face Wall, 1982	8.8 m	crushed basalt	50 4 to 5 10	22.0[3]	40^o	NA	50^o[3]	NA	All	Tensar SR-2	E-GG/ HDPE	73.0[4]
GW5	Tanque Verde Wall, 1984	4.9 m	clean well graded gravelly sand	75[3] 0.7[3] 3[3]	19.6[1]	34^o	53 ^{o}[6] [10]	53 ^{o}[10]	Wall 26-32	All	Tensar SR-2	E-GG/ HDPE	73.0[4]

Table 2.1, Continued**.**

Case Study	Project	Height and Surcharge	Soil Description	Soil Gradation d_{max} d_{50} <75μm (mm/mm/%)	Soil Unit Weight γ (kN/m^3)	Design ϕ_{des} (^{o})	Triaxial or Direct Shear ϕ_{trx} or ϕ_{ds} (^{o})	Estimated Plane Strain ϕ_{ps} (^{o})	Project Section or Panel Number	Depth Zone	Geosynthetic Product Name/ Mass/unit area	Product Type/ Polymer	Index Strength T_{ult} (kN/m)
GW6	Lithonia Georgia Wall, 1985	6.1 m	well graded sandy gravel	NA	21.2[3]	40^o	43^o[3]	48^o	NA	All	Tensar SR-2	E-GG/ HDPE	79.0[5] (x 0.60 for partial coverage)
GW7	Oslo, Norway Wall, 1987	4.8 m plus 3 m soil surcharge (64^o facing batter from horizontal)	uniformly graded fine to medium sand	16 0.25 3	17.0[1]	33^o	41^o[8]	46^o	J	All	Tensar SR-55 (primary)	E-GG/ HDPE	47.0[5]
											Tensar SS1 (secondary)	E-GG/ PP	19.6[5]
									N	All	Tensar SR-55 (primary)	E-GG/ HDPE	47.0[5]
											Tensar SS1 (secondary)	E-GG/ PP	19.6[5]
GW8	Algonquin HDPE Wall, 1988	6.1 m plus 2.1 m soil surcharge	well graded clean gravelly sand	50 4 0	20.4[1]	40^o	40^o[7]	43^o	FHWA Wall 2	All	Tensar SR-2	E-GG/ HDPE	67.8[5]
GW9	Algonquin PET Wall, 1988								FHWA Wall 9	All	Miragrid 5T	W-GG/ PET	39.2[5]
GW10	Algonquin Geotextile Wall, 1988	5.9 m but supported by 2.1 m of water at base of wall							FHWA Wall 6	All	Quline 160	W-GG/ PET	19.3[5]
		5.9 m after water removed								All	Quline 160	W-GG/ PET	1 9.3[5]

Table 2.1, Continued**.**

Case Study	Project	Height and Surcharge	Soil Description	Soil Gradation d_{max} d_{50} <75μm (mm/mm/%)	Soil Unit Weight γ (kN/m^3)	Design ϕ_{des} (^{o})	Triaxial or Direct Shear ϕ_{trx} or ϕ_{ds} (^{o})	Estimated Plane Strain ϕ_{ps} (^{o})	Project Section or Panel Number	Depth Zone	Geosynthetic Product Name/ Mass/unit area	Product Type/ Polymer	Index Strength T_{ult} (kN/m)
GW11	RMCC Geogrid Wrapped-Face Wall, 1986	2.85 m plus 0.6 m soil surcharge	clean uniform-size washed sand with some gravel	8 1.2 0	17.6[1]	40^o	46^o to 53$^{0(8)}$	55$^{o(11)}$	NA	All	Tensar SS2	E-GG/PP	16.0[5]
GW12	RMCC Timber Propped Panel Wall, 1987	3 m plus effective surcharge of 42 kPa			18.0[1]					All	Tensar SR2	E-GG/ HDPE	67.0[5]
GW13	RMCC Timber Incremental Panel Wall, 1987	3 m plus effective surcharge of 42 kPa	clean uniform-size washed sand with some gravel	8 1.2 0	18.0[1]	40^o	46^o to 53$^{0(8)}$	55$^{o(11)}$	NA	All	Tensar SR-2	E-GG/ HDPE	67.0[5]
GW14	RMCC Full-Height Aluminum Propped Panel Wall, 1989	3 m								All	Tensar SS1	E-GG/PP	12.0[5]
		3 m plus effective surcharge of 70 kPa									Tensar SS1	E-GG/PP	12.0[5]
GW15	RMCC Incremental Aluminum Panel Wall, 1989	3 m								All	Tensar SS1	E-GG/PP	12.0[5]
		3 m plus effective surcharge of 60 kPa									Tensar SS1	E-GG/PP	12.0[5]

Table 2.1, Continued**.**

Case Study	Project	Height and Surcharge	Soil Description	Soil Gradation d_{max} d_{50} <75μm (mm/mm/%)	Soil Unit Weight γ (kN/m^3)	Design ϕ_{des} (^{o})	Triaxial or Direct Shear ϕ_{trx} or ϕ_{ds} (^{o})	Estimated Plane Strain ϕ_{ps} (^{o})	Project Section or Panel Number	Depth Zone	Geosynthetic Product Name/ Mass/unit area	Product Type/ Polymer	Index Strength T_{ult} (kN/m)
GW16	WSDOT Rainier Ave. Wall, 1989	12.6 m plus 5.3 m soil surcharge	well graded gravelly sand	60 2 -	21.1[1]	36^o	45^{o}[7] [9]	54^o	NA	1 2 3 4	Exxon GTF200 Exxon GTF375 Exxon GTF500 Exxon GTF1225T	W-GT/PP W-GT/PP W-GT/PP W-GT/ PET	31.0[5] 62.0[5] 92.0[5] 186[5]
GW17	London, Ontario Propped Panel Wall, 1989	7.1 m	silty sand and gravel	27 4.75 10	20.4	36^o	NA	45^{o}[3]	Panel 39	All	Tensar UX1600	E-GG/ HDPE	118[4]
GW18	Fredericton, New Brunswick Propped Panel Wall, 1990	6.1 m	pit run coarse sand and gravel	76 - 12	20.4[3]	40^o	NA	45^{o}[3]	NA		Tensar SR2 (except 2nd layer from top is SR1)	E-GG/ HDPE	73.0[4] 55.0[4] for SR-1 (x 0.77 for partial coverage)
GW19	PET Strip St. Remy Test Wall, 1993	6.4 m	uniform size fine to medium (Fountaine-bleu) sand	1.5 0.15 to 0.2 4	16.4	37^o	39^{o}[7] [10]	42 ^{o}	NA	All	Paraweb 2S	PET	200

Table 2.1, Continued**.**

Case Study	Project	Height and Surcharge	Soil Description	Soil Gradation d_{max} d_{50} <75μm (mm/mm/%)	Soil Unit Weight γ (kN/m^3)	Design ϕ_{des} (^{o})	Triaxial or Direct Shear ϕ_{trx} or ϕ_{ds} (^{o})	Estimated Plane Strain ϕ_{ps} (^{o})	Project Section or Panel Number	Depth Zone	Geosynthetic Product Name/ Mass/unit area	Product Type/ Polymer	Index Strength T_{ult} (kN/m)
GW20	Vicenza, Italy Wall, 1998	4 m	clayey, sandy gravel	50 10 10	21.1[2]	40^o	49^o[7] [10]	57^o	1	All	Tenax TT 201 SAMP	E-GG/ HDPE	58.0[5]
		4 m plus 3.5 m soil surcharge									Tenax TT 201 SAMP	E-GG/ HDPE	58.0[5]
		4 m							2		Tenax LBO 220 SAMP	E-GG/PP	23.7[5]
		4 m plus 3.5 m soil surcharge									Tenax LBO 220 SAMP	E-GGPP	23.7[5]

Notes: (1) Measured in-situ during compaction of backfill
(2) Estimated from laboratory compaction tests
(3) Estimated based on data for similar soil
(4) From manufacturer product testing not specific to project wall
(5) From project-specific testing of geosynthetic materials
(6) Multiaxial cubic triaxial test results
(7) Triaxial compression test
(8) Direct shear test
(9) Plane strain test
(10) (c-ϕ) soil peak strength envelopes corrected to equivalent peak secant friction angle using $\tan\phi_{secant} = c/\gamma H + \tan\phi$ where c = soil cohesion
(11) peak direct shear friction angle corrected to peak plane strain shear angle using method by Bolton (1986)

NW-NP-GT = nonwoven needlepunched geotextile
HB-NW-GT = heat bonded nonwoven geotextile
E-GG = extruded geogrid
W-GG = woven geogrid
W-GT = woven geotextile
PP = polypropylene
PET = polyester
NA = not available.

2.2.2.1 Snailback Geotextile Shotcrete Wrapped-Face Wall, 1974 (Case GW1, Figure 2.1)

The Snailback Wall, built by the US Forest Service in 1974 near Cave Junction, Oregon, in the Siskyou National Forest, was the first geosynthetic wall built in North America and the third geosynthetic wall built in the world. Details regarding the Snailback Wall and its performance after 25 years were reported by Greenway et al. (1999), and their paper is the primary source of information on this structure. Direct shear tests were conducted on the backfill to determine its shear strength (Bell 1998). The wall reinforcement was placed to develop tensile load in the cross-machine direction. The ultimate wide-width tensile strength of the reinforcement layers was estimated from the results of the Oregon State University (OSU) ring test, grab tensile tests, and correlation with wide width tensile tests. Because of the unusually long overlap of the geotextile behind the wrapped face (1.5 m), the facing overlaps were considered to contribute to the internal stability of the reinforced zone. Post-construction evaluation of the geotextile strength and durability has not been carried out. However, the non-aggressive nature of the backfill soil and wall environment is believed to have kept installation damage and long-term strength losses to a minimum.

Recent observations of the long-term performance of the wall after 25 years of service reported by Greenway et al. (1999) indicate that the wall has performed well. Although no deformation measurements are available, they concluded that little if any deformation has occurred since the shotcrete facing was installed. They reported no evidence of facing distortion or significant cracking. Forest Service records reveal that no maintenance has been performed on the wall since its construction.

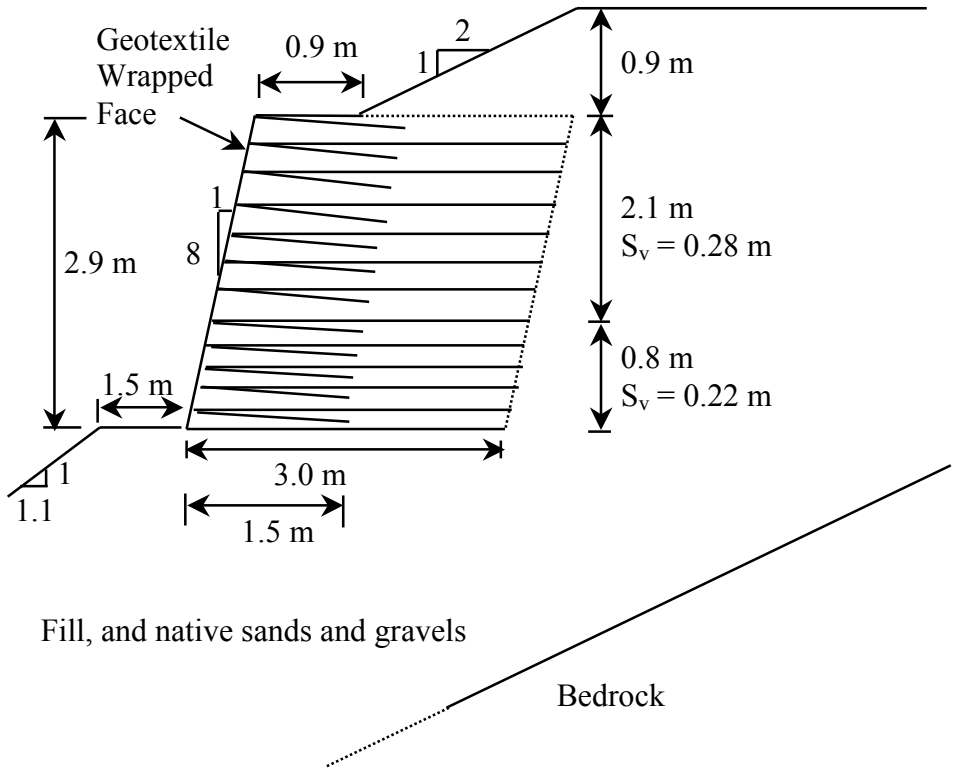

Figure 2.1. Cross-section for Snailback Wall.

2.2.2.2 Olympic National Forest Geotextile Wrapped-Face Wall, 1975 (Case GW2, Figure 2.2)

The Olympic National Forest wall located near Shelton, Washington, built in 1975, was the second geosynthetic reinforced soil wall built in the USA (Steward et al. 1977). The wall backfill is a crushed rock. The wall was built using two different reinforcement designs (Sections A and B). The ultimate wide-width tensile strength of the reinforcement layers was estimated from the results of OSU ring tests, grab tensile tests, and correlation with wide-width test results (Powell and Mohney 1994).

Lateral movements of 25 to 50 mm were measured with magnet extensometers attached to horizontal inclinometers. These deformations occurred during the first 1.5 years of service and within 1 meter of the front of the wall (Steward et al. 1977). This movement is attributed, in part, to downhill creep of the foundation that was seated on a relatively steep slope. In 1993, 18 years after construction, the wall was surveyed by the US Forest Service (Powell and Mohney 1994). They observed that wall movements had ceased. Nevertheless, the geotextile at the wrapped face had degraded significantly under exposure to ultraviolet radiation because of the

poor performance of the spray-coated asphalt emulsion that was originally applied to the facing. A facing repair with shotcrete is planned. Samples of the geotextile reinforcement were exhumed to measure strength degradation and to identify the cause of any degradation. The geosynthetic revealed obvious signs of installation damage (holes and punctures), and a strength loss based on tensile test results on the order of 50 percent for the polyester geotextile and 40 percent for the polypropylene geotextile. Powell and Mohney concluded that most of this strength loss could be attributed to installation damage.

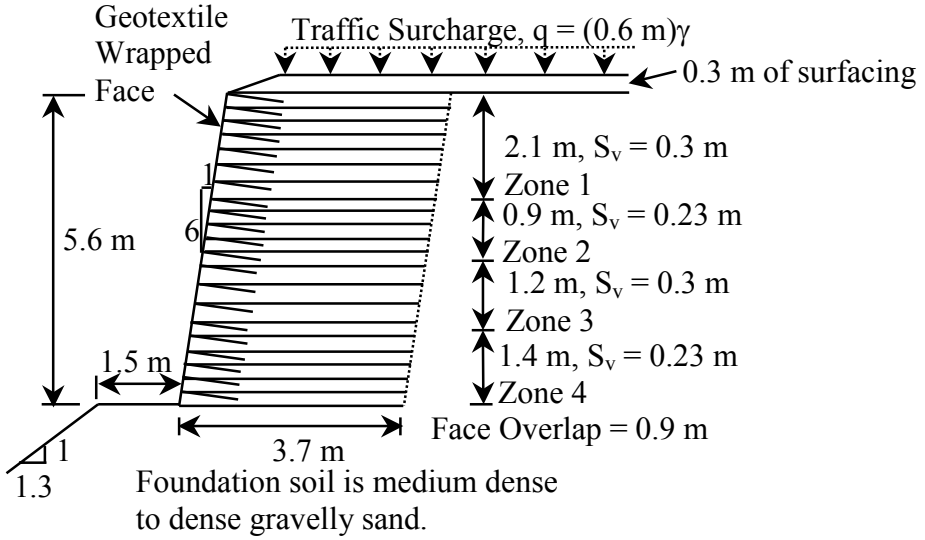

Figure 2.2. Cross-section for Olympic National Forest wall.

2.2.2.3 Glenwood Canyon Geotextile Shotcrete Faced Walls, 1982 (Case GW3, Figure 2.3)

A full-scale test wall was constructed by the Colorado Department of Transportation (CDOT) in 1982 (Bell et al. 1983). This wall consisted of ten different test sections and used a large number of different nonwoven geotextile products. Sections 2 and 9, at the opposite ends of the wall, used identical designs. Two of the wall sections (sections 5 and 6) were surcharged with soil after wall construction had been completed in an attempt to fail the wall. Soil shear strength was determined from the results of large diameter (100-mm) triaxial compression tests (Bell 1998). Wide-width tests using a precursor to ASTM D4595 were conducted by the first writer in 1982 to determine the ultimate strength of the geotextile products. A low mass per unit area geotextile was used as a separator at the top of all reinforced wall sections, but these layers are not considered to have contributed to wall internal stability.

Lateral movements of 50 to 75 mm or less were measured. Most of this movement occurred during construction (Bell et al. 1983). The greatest lateral movements occurred at the top of the wall, but this may be due to the 150 to 450 mm of vertical foundation settlement recorded at the site. All of the walls appeared to be stable with respect to lateral movements within 6 months after construction, including the surcharged sections. Post-construction strains in the geotextile were too small in magnitude to be measurable.

Portions of the wall were excavated in 1986 to obtain samples of the geotextile reinforcement. Tensile test results indicated strength losses on the order of 15 to 38 percent, which appeared to be primarily due to installation damage (Allen and Bathurst 1994, Bell and Barrett 1995). The wall sections were buried in 1993. At that time visual observations by the first writer revealed no signs of distress.

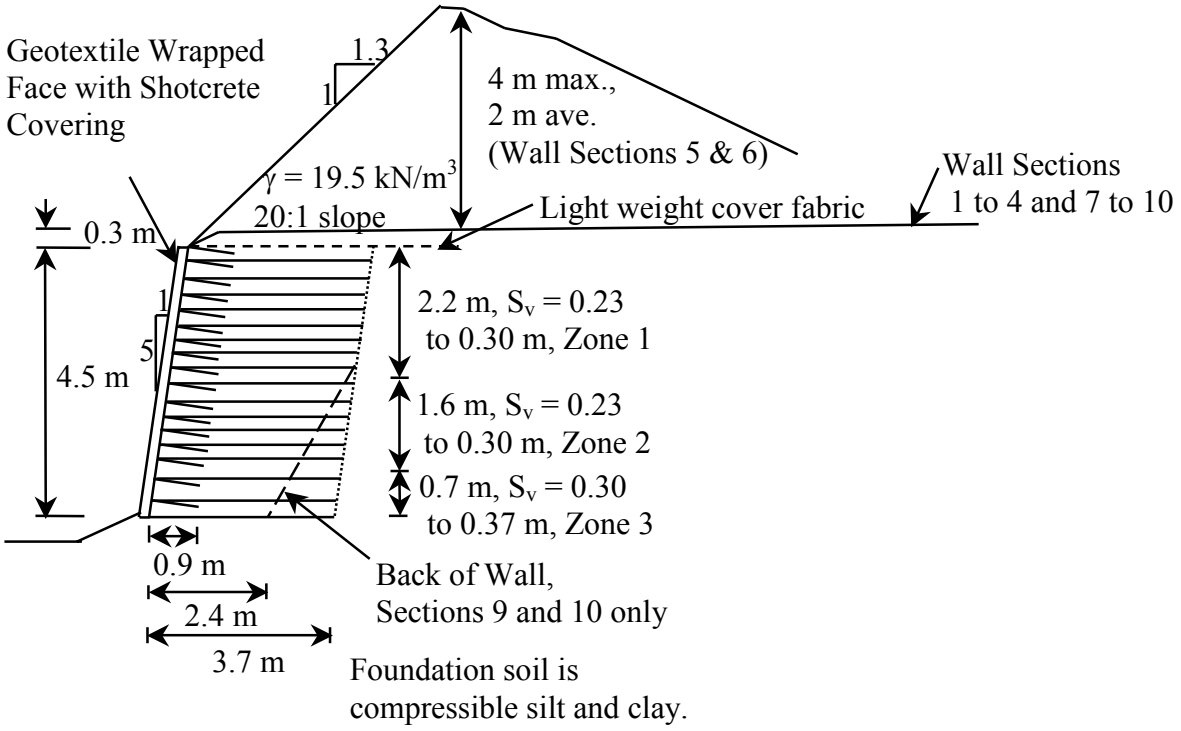

Figure 2.3. Cross-section for Colorado Department of Transportation Glenwood Canyon shotcrete faced walls.

2.2.2.4 Devils Punch Bowl Wrapped-Face Geogrid Wall, 1982 (Case GW4, Figure 2.4)

The first permanent geogrid wall constructed in the U.S. was built in 1982 to support a roadway access to Devils Punch Bowl State Park on the central Oregon coast, USA (Bell et al. 1985). Personal observations by the first writer in 1993 indicated that little wall movement had

occurred since construction and that the geogrid reinforcement still appeared shiny and new, with no apparent degradation.

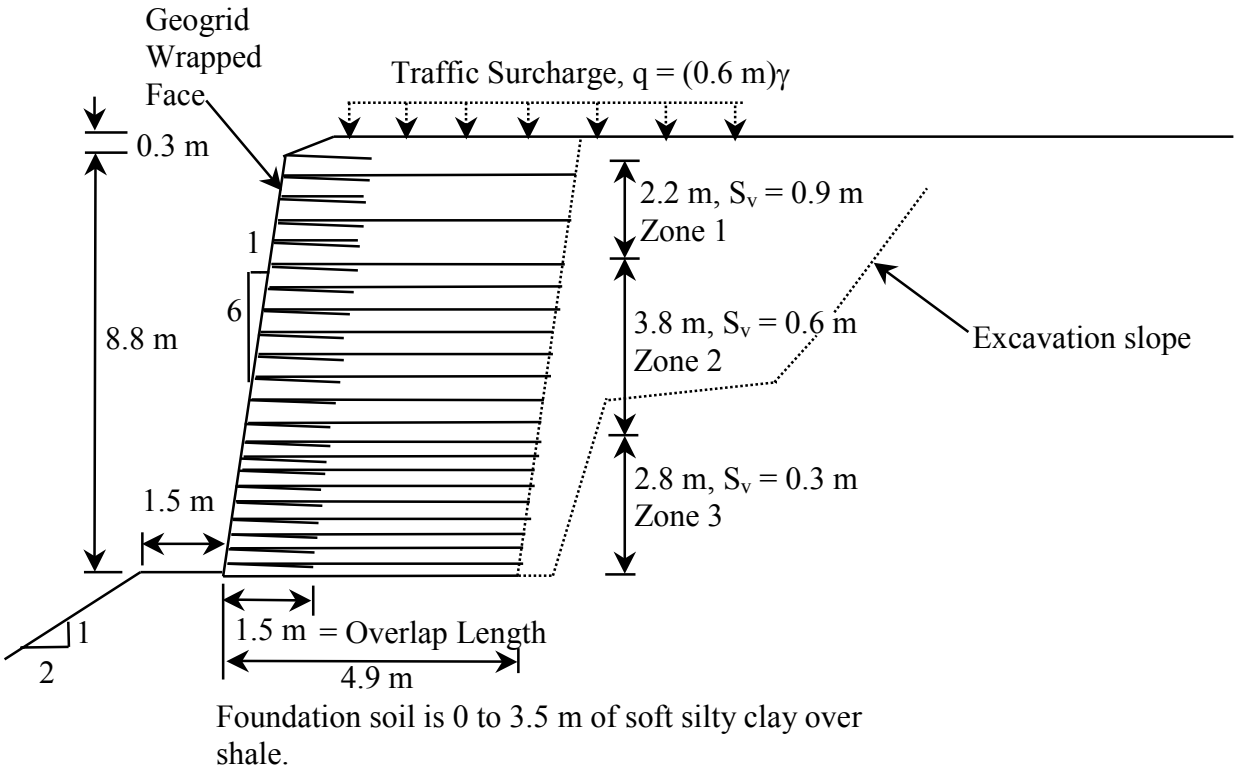

Figure 2.4. Cross-section for Devils Punch Bowl wrapped-face HDPE geogrid wall.

2.2.2.5 Tanque Verde Geogrid Concrete Panel Wall, 1984 (Case GW5, Figure 2.5)

Forty-six geogrid reinforced retaining wall sections (1600 lineal meters of wall) were constructed to provide grade separations for the Tanque Verde-Wrightstown-Pantano Roads intersection in Tucson, Arizona (Bright et al. 1994). Full-height, precast concrete panels were used for the facing. The panels were externally braced (propped) until two-thirds of the backfill behind the panels were in place.

Multiaxial cubic triaxial tests were carried out on specimens of the granular backfill soil screened to a No. 4 sieve (Desert Engineering 1989). Interpretation of these data by the writers gave a peak friction angle of 53°. This value was not adjusted to give an equivalent peak plane strain angle (see Section 2.3.3), as the cubic triaxial test was considered to adequately approximate plane strain conditions.

The southwest USA location of these structures made the temperature within the wall backfill unusually high. The measured temperatures were as high as 38^{o} C, with an average of 25

to 30° C. The maximum strains at the end of construction were about 0.3 percent and were located at the connections between the panel facing and the reinforcement layers (Desert Engineering 1987). After 8 years, the maximum geogrid strains increased to approximately 0.5%. Maximum deformation of the face at the top of the wall was approximately 65 mm (Berg et al. 1986). Exhumation of geogrid reinforcement samples in 1992 indicated that no significant change in tensile strength had occurred relative to the initial strength as a result of installation and eight years of in-service loading (Bright et al. 1994).

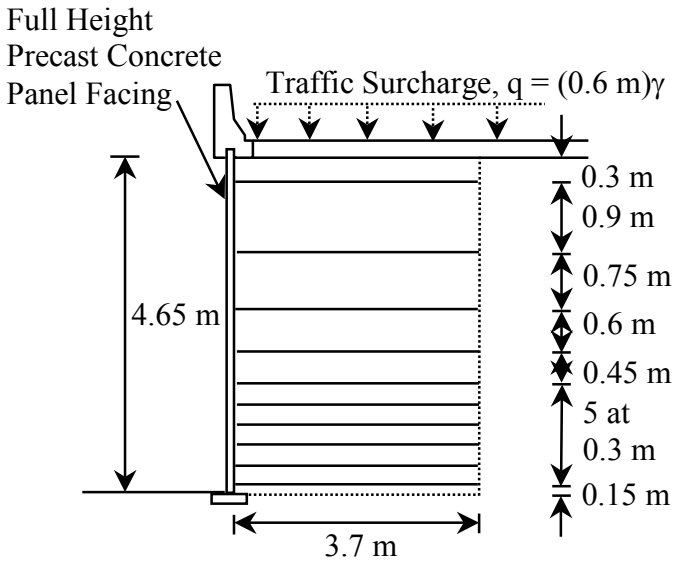

Figure 2.5. Cross-section for Tanque Verde HDPE geogrid concrete panel wall.

2.2.2.6 Lithonia Geogrid Concrete Panel Wall, 1985 (Case GW6, Figure 2.6)

An incremental concrete panel demonstration wall was constructed near Lithonia, Georgia, USA, in 1985 (Berg et al. 1986). The concrete facing panels were not directly attached to the soil reinforcement layers. Geogrid tabs, 1.3 m long, were cast directly into concrete facing units and overlapped with the primary reinforcement layers. The overlap lengths were separated vertically by a 75-mm thickness of soil. At the bottom of the wall, three additional layers of reinforcement were installed that were not connected to the facing units.

The structure is now in service as a materials handling platform, with trucks dumping quarry stone over the top of the wall into bins located at the front of the structure. Maximum lateral movement of the wall face during construction and during the first year of service was on the

order of 100 to 150 mm. Wall performance has been acceptable, with no signs of deterioration or unacceptable deformation.

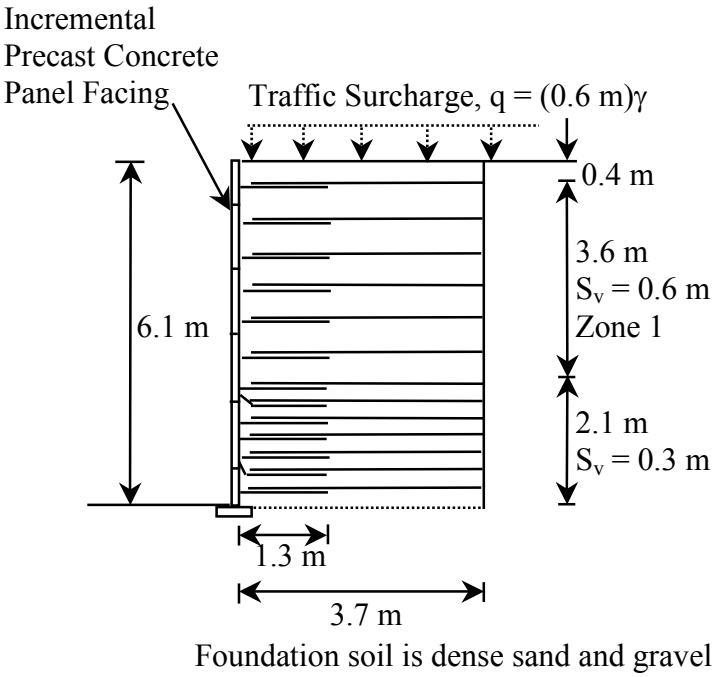

Figure 2.6. Cross-section for Lithonia, Georgia, demonstration HDPE geogrid concrete panel wall.

2.2.2.7 Oslo, Norway, Geogrid Walls, 1987 (Case GW7, figures 2.7 and 2.8)

A full-scale, welded, wire-faced test wall was constructed in Oslo, Norway, in 1987 (Fannin and Hermann 1990). This wall was designed in two sections with different reinforcement spacing and lengths. The wall face is inclined at an angle of about 63^o from the horizontal. In practice, this structure could be classified as a slope. However, because of the high quality data for this structure and because earth force calculations described later in this paper were carried out by using Coulomb theory (i.e., the wall facing angle is included explicitly in the calculation of earth forces), this case study is included. Note that the primary reinforcement layers simply abut against the back of the welded wire facing form, and did not wrap back into the backfill as is typical of wrapped-face wall systems. Material properties for the wall, including direct shear testing for the wall backfill, were reported by Fannin (1988). The wall has been monitored continuously for 12 years for deformations and load. Total maximum strains in the reinforcement are less than 1 percent and occurred largely during construction. Strains in the reinforcement have stabilized (Fannin and Hermann 1991; Fannin 1994, 2001).

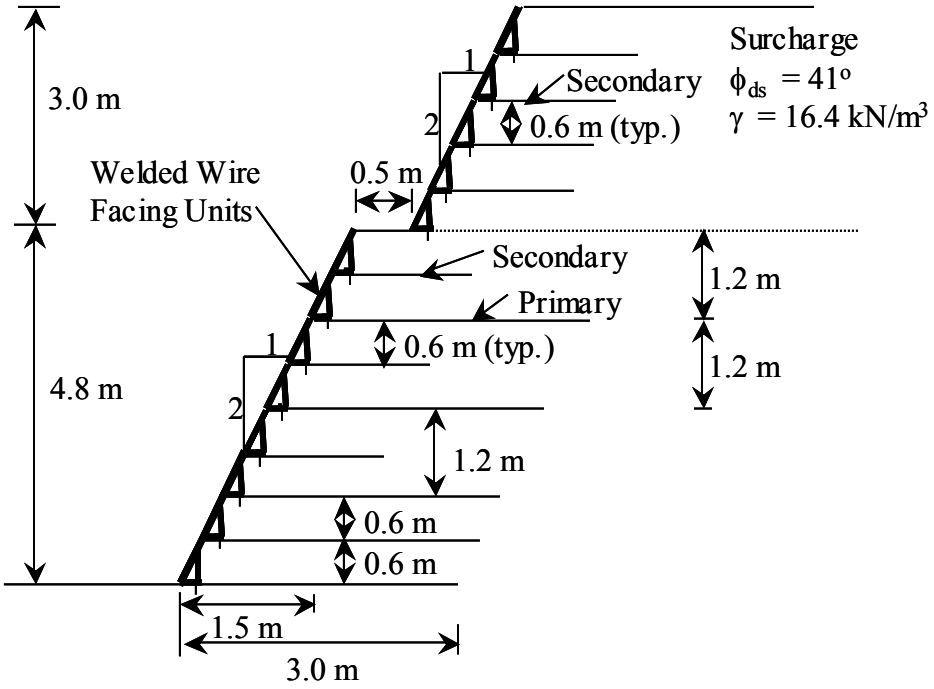

Figure 2.7. Cross-section for Oslo, Norway, (HDPE geogrid) walls, Section J.

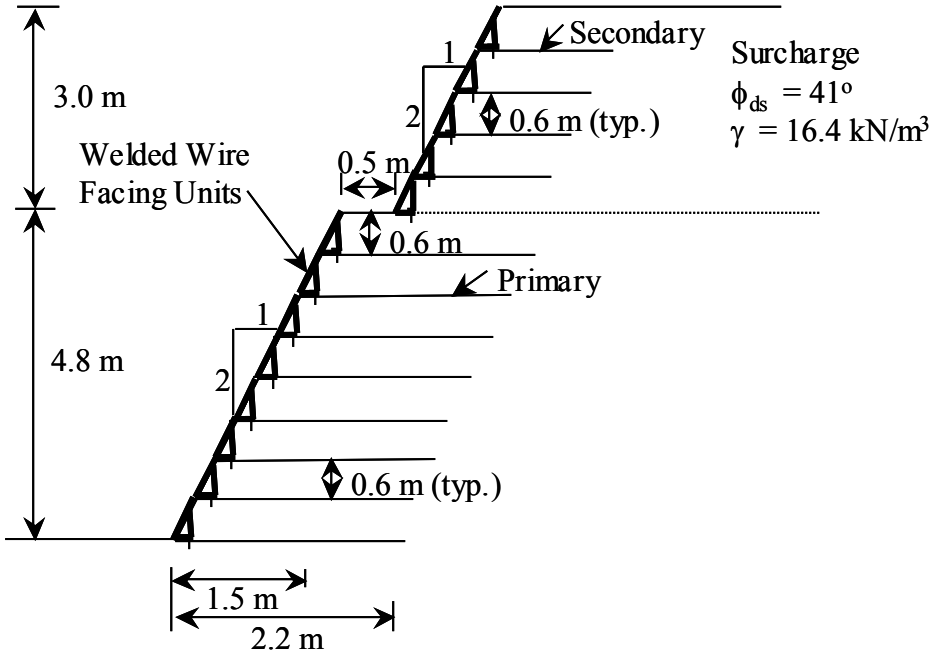

Figure 2.8. Cross-section for Oslo, Norway, (HDPE geogrid) wall, Section N.

2.2.2.8 Algonquin, HDPE Geogrid Concrete Panel Wall, 1988 (Case GW8, Figure 2.9)

A series of full-scale test walls were constructed in a gravel pit in Algonquin, Illinois, USA, as part of a Federal Highway Administration (FHWA) study to investigate the behavior of mechanically stabilized earth (MSE) walls (Christopher 1993). Seven wall sections, 6.1 m high by 10 m long, were constructed with different reinforcement products but the same precast concrete facing panels. The section constructed with high density polyethylene (HDPE) geogrid reinforcement is reported here.

Measured maximum lateral movement of this wall was 35 mm, most of which occurred during construction. The wall was monitored for two years after construction. At that time the measured total strains were less than 1 percent, and lateral movements appeared to have stopped (Christopher 1998).

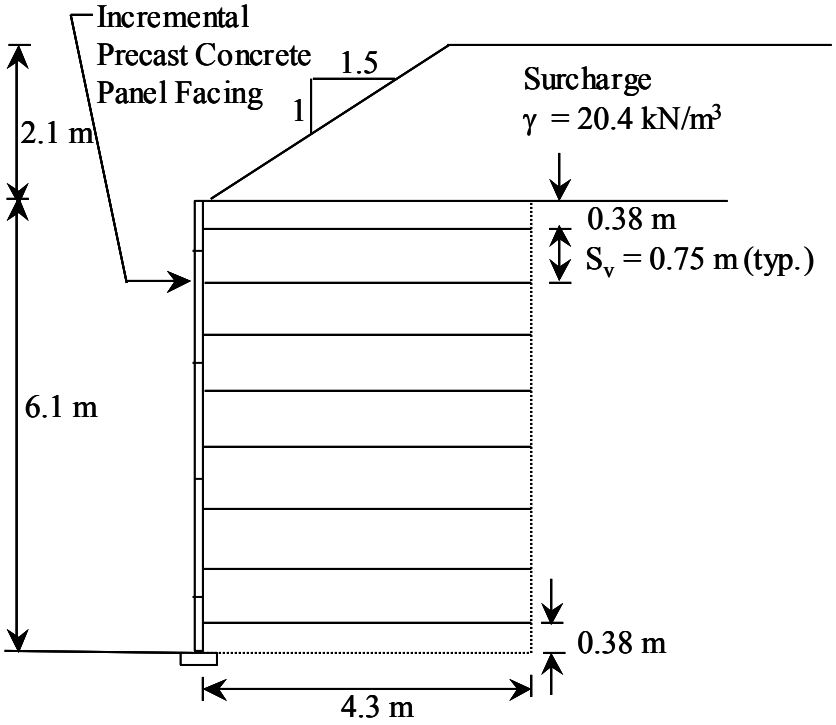

Figure 2.9. Cross-section for Algonquin HDPE geogrid concrete panel wall.

2.2.2.9 Algonquin, Polyester (PET) Geogrid Modular Block Faced Wall, 1988 (Case GW9, Figure 2.10)

This wall was constructed at the Algonquin, Illinois, site described in the previous case study and was part of the same FHWA research program (Bathurst et al. 1993b). The geometry

of this wall was similar to other Algonquin walls, except that the wall was 15 m long and was constructed with a battered facing column of dry cast concrete modular blocks (segmental retaining wall).

The measured maximum lateral movement for this wall was about 150 mm, the majority of which occurred during construction. Measured maximum total strains were approximately 1.2 percent, and strains and deformations appeared to have stabilized one year after construction.

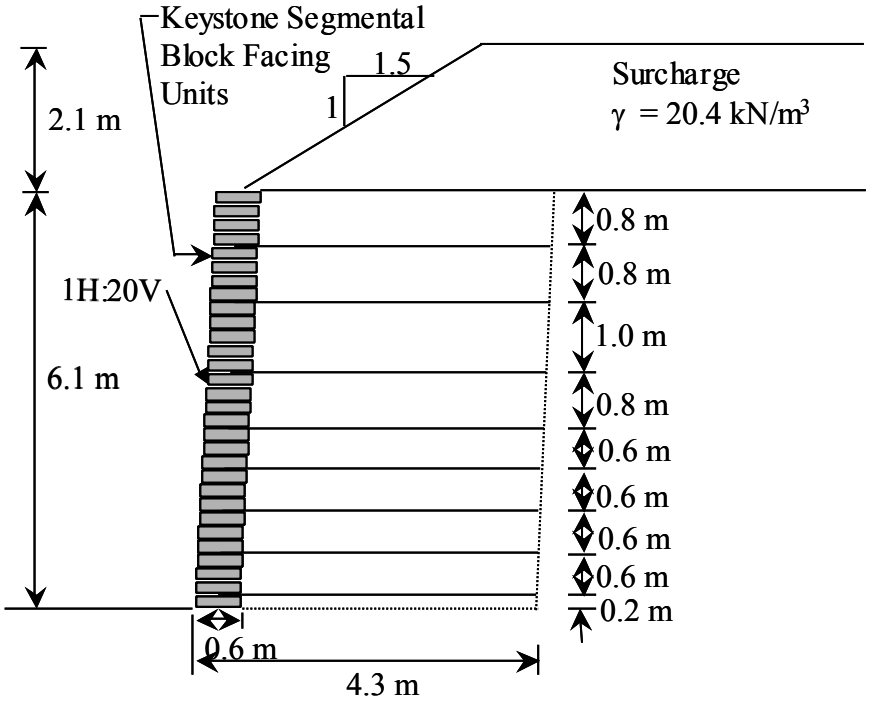

Figure 2.10. Cross-section for Algonquin PET geogrid modular block faced wall.

2.2.2.10 Algonquin, Geotextile Wrapped-Face Wall, 1988 (Case GW10, Figure 2.11)

This wall was constructed at the Algonquin, Illinois, site described in the two previous case studies and was part of the same FHWA research program (Christopher 1993). A geotextile wrapped-face construction was used. In-soil confined tensile tests were also conducted on reinforcement layers in the wall backfill.

The wall was purposely under-designed to produce an internal stability failure. The wall was supported laterally over the bottom half of the structure during construction and for about four months thereafter by using a pond of water contained within a geomembrane. Total lateral wall deformations of approximately 150 mm were measured, as were maximum reinforcement strains

of 2 to 3 percent at end-of-construction. The large strains were not unexpected since the wall was purposely under-designed using a very extensible, nonwoven geotextile. The surface of the backfill soil did not exhibit tension cracks at this point, indicating that the geotextile remained in a confined state and that the soil had not reached a state of failure. Following release of the external support, the wall face deflected an additional 450 mm at the crest, and reinforcement strains exceeded the capacity of the strain gauges mounted directly on the geotextile (strains were likely well in excess of 3 percent, as indicated by the last reliable measurement of reinforcement strain). The soil exhibited signs of failure (i.e., tension cracks in the backfill surface behind the wall face). The wall continued to strain with time, resulting in additional soil cracks. However, the rate of strain increase decreased with time, and reinforcement rupture did not occur over the five years of post-construction observation (Christopher 1998).

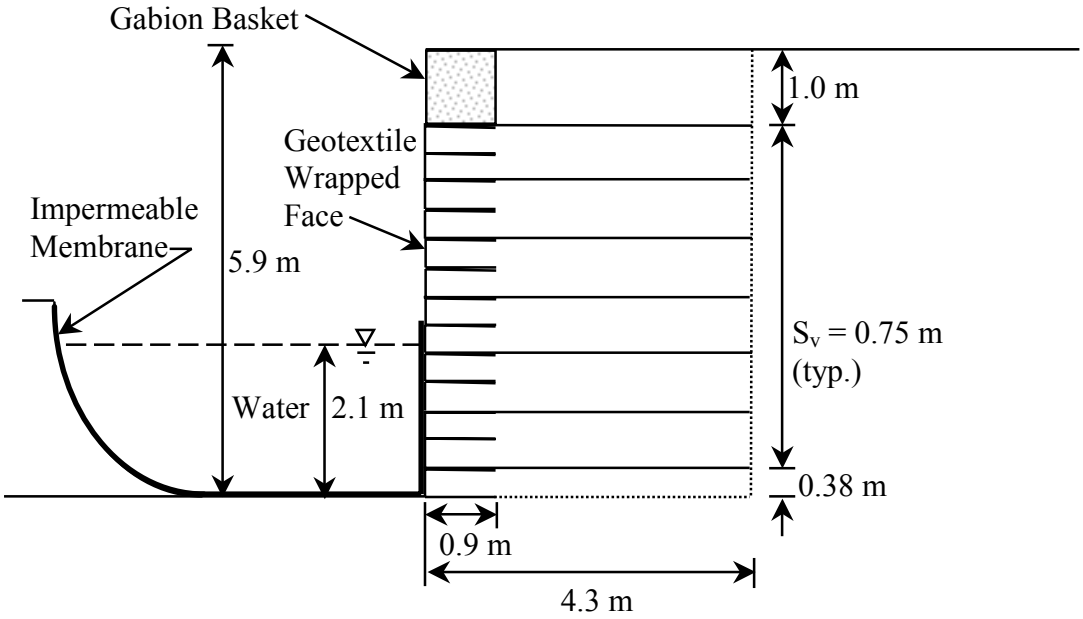

Figure 2.11. Cross-section for Algonquin geotextile wrapped-face wall.

2.2.2.11 RMCC Geogrid Wrapped-Face Wall, 1986 (Case GW11, Figure 2.12)

A full-scale, geogrid, wrapped-face test wall was constructed and monitored at the Royal Military College of Canada (RMCC) in Kingston, Ontario (Bathurst et al. 1988). The test wall was approximately 2.9 m high, 2.4 m wide, and retained a soil volume extending approximately 6 m behind the facing. Potential boundary effects of the full-scale test wall facility were

quantified by carrying out a full-scale experiment in which the external support to an unreinforced full-height facing panel was slowly released to generate an active earth failure in the soil. In addition, direct shear testing of the side wall friction-reducing interfaces (multiple layers of lubricated polyethylene sheeting) were carried out (Bathurst 1993). Fully mobilized side wall friction angles were calculated to be 10 to 15^{o}.

The wall was purposely under-designed by using a weak biaxial geogrid oriented with the weakest direction in the direction of tensile loading and by using large vertical spacings. Strains measured during construction were as large as 2.6 percent, with additional creep strains after 600 hours of surcharging of up to 1.5 percent. Maximum facing deformations were 20 mm or less at the geogrid layer locations, with additional long-term deformations of 10 mm or less. Most wall deformations were confined to the front 0.6 m of the wall and were due to local failure of the soil in the slumped, wrapped-face portions. However, the geogrid reinforcement showed no signs of failure, and strain rates were observed to decrease with time. The geogrid reinforcement was excavated and tested for residual tensile strength. No signs of installation damage were observed, which was as expected since the soil was placed very carefully. No tensile strength loss was observed from index tensile wide-width strip tests on exhumed specimens of geogrid, indicating that the long-term creep strains had not affected the residual tensile strength of the geogrid reinforcement (Bathurst et al. 1988).

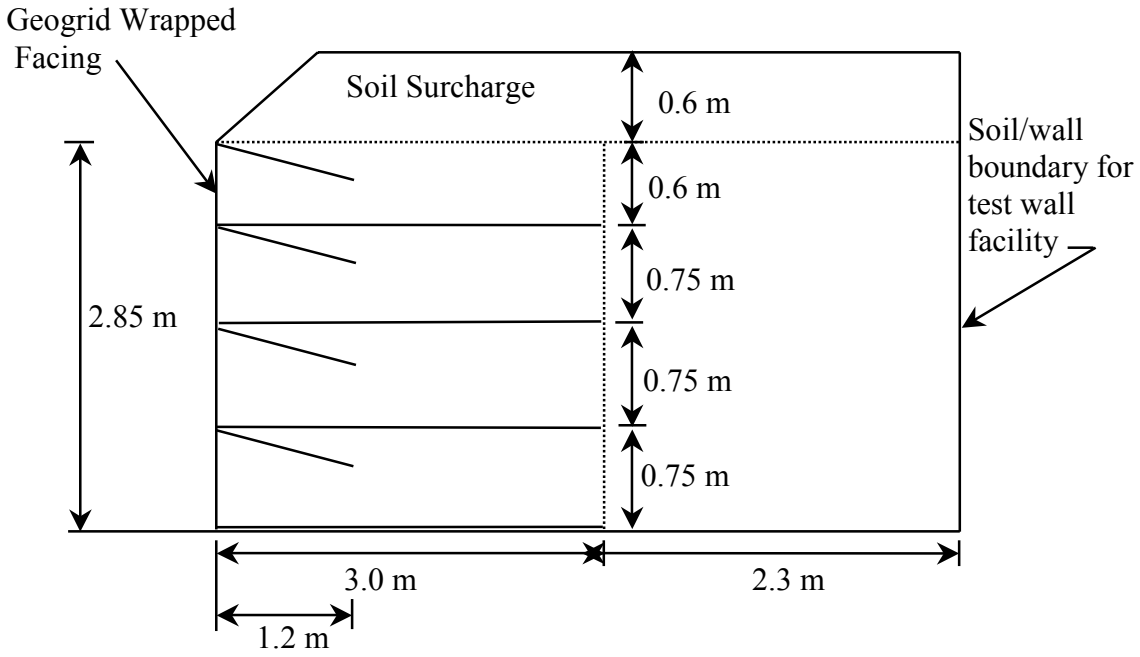

Foundation for wall is concrete floor.

Figure 2.12. Cross-section for RMCC polypropylene (PP) geogrid wrapped-face wall.

2.2.2.12 RMCC Full-Height Propped Timber Panel Geogrid Test Wall (Case GW12,) and Incremental Timber Panel (Case GW13) Geogrid Test Wall, 1987 (Figure 2.13)

Full-scale, instrumented, full-height, propped panel and incremental panel test walls were constructed and surcharged at RMCC (Bathurst et al. 1987). The test walls were 3 m high and 2.4 m wide, and they were constructed with timber and plywood bulkhead facings. See Case GW11 for additional details regarding backfill testing.

The full-height panel wall was braced externally for the duration of backfill placement. For the incremental panel wall, each row of panels was temporarily braced during backfilling behind the row, and the bracing was removed once the next row of facing panels was in place and backfilled.

The soil backfill in each test was uniform surcharge loaded in stages by using a system of airbags that covered the entire 6-m length of the RMCC Retaining Wall Test Facility. Friction reducing membranes were introduced between the airbags and soil surface. (The influence of side wall friction in the RMCC Retaining Wall Test Facility was discussed in the previous section (Case GW11).) A three-dimensional wedge analysis estimated that boundary effects in

these tests contributed approximately 14 percent to wall capacity at collapse under surcharge loading (Bathurst and Benjamin 1990, Bathurst 1993).

Maximum lateral movement for the incremental panel wall was 18 mm, and reinforcement strains were 0.3 percent or less at the end of construction. For the companion full-height, propped panel wall, the maximum lateral movement during wall construction and before external prop removal was about 1 mm, and the maximum geogrid strain about 0.03 percent. The wall was stage surcharge loaded up to a maximum 50 kPa pressure (an effective surcharge pressure of 42 kPa after correction for boundary effects, according to Bathurst (1993)). At the end of the surcharging, the maximum outward face deformation and strain were approximately 40 mm and 0.9 percent, respectively, for the incremental panel wall, and approximately 12 mm and 0.88 percent, respectively, for the full-height propped panel wall. No strength reduction of the geogrid due to installation or time effects was apparent after wide-width tensile testing and constant load creep testing of exhumed reinforcement specimens (Bush and Swan 1987).

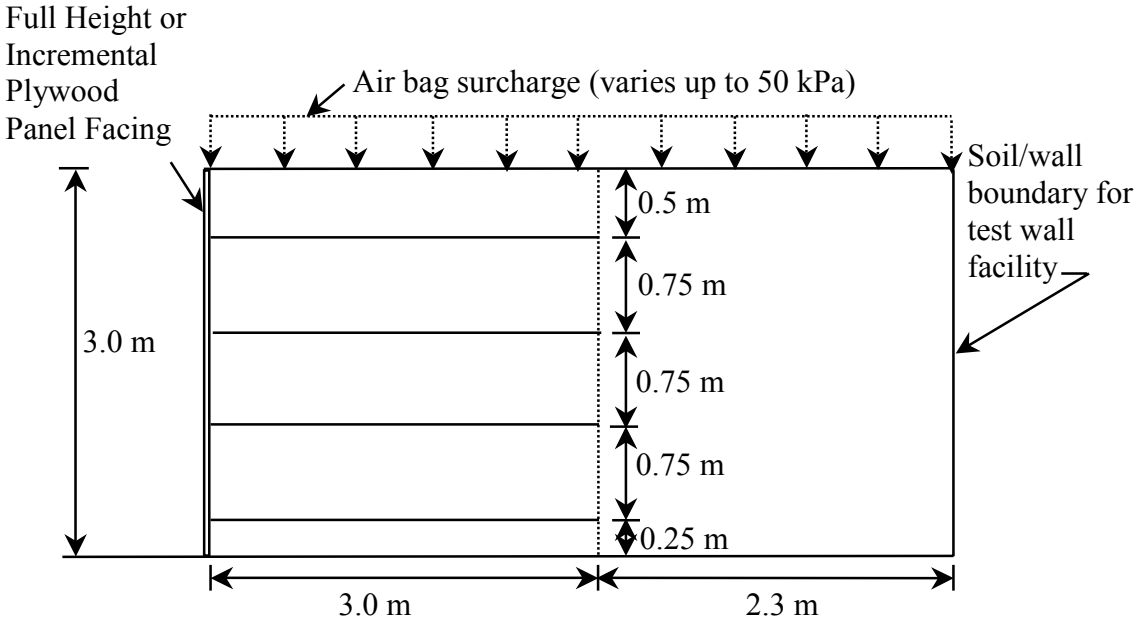

Figure 2.13. Cross-section for RMCC incremental and full-height plywood propped panel HDPE geogrid walls.

2.2.2.13 RMCC Full-Height Propped Aluminum Panel Geogrid Test Wall, 1989 (Case GW14, Figure 2.14)

A full-scale, instrumented, full-height propped panel wall was constructed and surcharged to failure at RMCC (Bathurst and Benjamin 1990). This wall differed from the previous case study (GW12) in the use of a stiffer aluminum panel for the facing, a pinned connection at the wall toe to measure toe forces (in Cases GW12 and GW13 the wall toe was only restrained by base friction), more instrumentation, and a weaker, more extensible geogrid reinforcement. In addition, the surcharge capacity of the RMCC Retaining Wall Facility was increased. Otherwise, the wall geometry and backfill soil were the same as in case GW12.

Measured maximum lateral movement of this wall was about 10 mm, and reinforcement strains were 1 percent or less at the end of construction, immediately after external prop release (Bathurst and Benjamin 1990). The wall was stage surcharge loaded, with each surcharge load increment maintained for a minimum of 100 hours to measure reinforcement creep, to a maximum load of 80 kPa created by airbags located at the top of the soil surface. The equivalent surcharge for an infinitely wide wall structure was estimated through back-analysis to be about 70 kPa because of the contribution of sidewall boundary effects (Bathurst 1993). Approximately 250 hours after this last surcharge load had been applied, the soil in the reinforced zone exhibited signs of failure. Approximately 350 hours into the final load increment, the upper geogrid layer ruptured, and the wall was purposely unloaded to examine internal failure modes. At reinforcement failure, the maximum lateral deflection of the propped panel face was approximately 100 mm, and maximum reinforcement strains were approximately 10 to 12 percent at the facing connection and 7 to 8 percent near the soil failure surface.

2.2.2.14 RMCC Incremental Aluminum Panel Geogrid Test Wall, 1989 (Case GW15, Figure 2.14)

This test wall was similar to the full-height, propped panel RMCC test wall presented in the previous case study, except that the aluminum facing panels were incremental rather than full-height (Bathurst et al. 1993a). The construction technique was the same as that described for case GW13.

Measured maximum lateral movement for this wall was 13 mm, and reinforcement strains were 1 percent or less at the end of construction but before surcharging. The wall was stage

surcharge loaded to a maximum pressure of 70 kPa, with each surcharge load increment held for a minimum of 100 hours to measure reinforcement creep. Three-dimensional stability calculations suggested that approximately 10 kPa of the 70-kPa surcharge were carried by side wall friction (Bathurst 1993). Approximately 100 hours after the last surcharge load had been applied, the soil exhibited signs of failure, and approximately 380 hours later the upper geogrid layers ruptured and the wall failed catastrophically. At incipient collapse, the maximum lateral deflection was approximately 100 mm, and maximum reinforcement strains were approximately 10 percent.

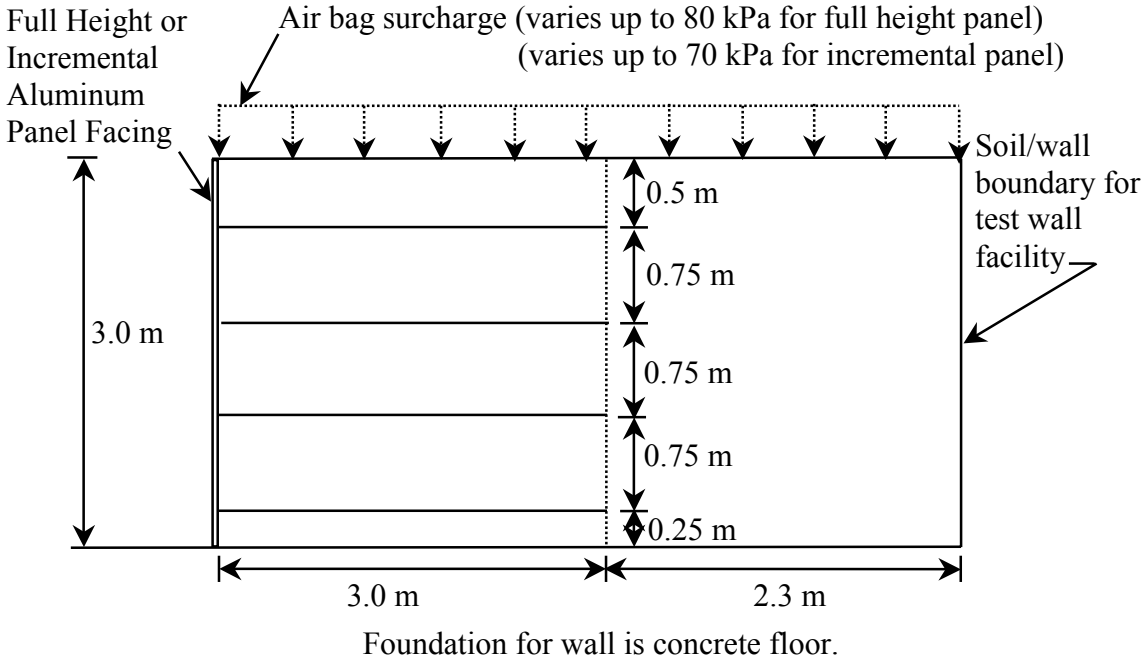

Figure 2.14. Cross-section for RMCC incremental and full-height propped panel geogrid test walls.

2.2.2.15 WSDOT Rainier Avenue Wrapped-Face Geotextile Wall, 1989 (Case GW16, Figure 2.15)

Six geotextile walls were built to support a preload fill for the reconstruction of a major freeway interchange at Rainier Avenue in Seattle, Washington, USA (Allen et al. 1992). Although the walls were intended to be temporary, they were in place long enough (about 1 year) to assess long-term behavior. At the time of construction, the instrumented wall section at

this interchange was the largest geotextile wall in the world. Soil shear strength was determined by using large-diameter (100-mm) triaxial tests and plane strain shear strength testing.

The measured maximum lateral movement of the instrumented section was 140 mm during construction, with an additional 30 mm of movement after construction. The wall was monitored for approximately one year after construction. Measured maximum total strains were approximately 1.5 percent, and wall movement appeared to be stable after one year. Installation damage to the geotextile reinforcement was evaluated immediately after construction. Strength losses of approximately 10 to 30 percent due to installation damage were measured.

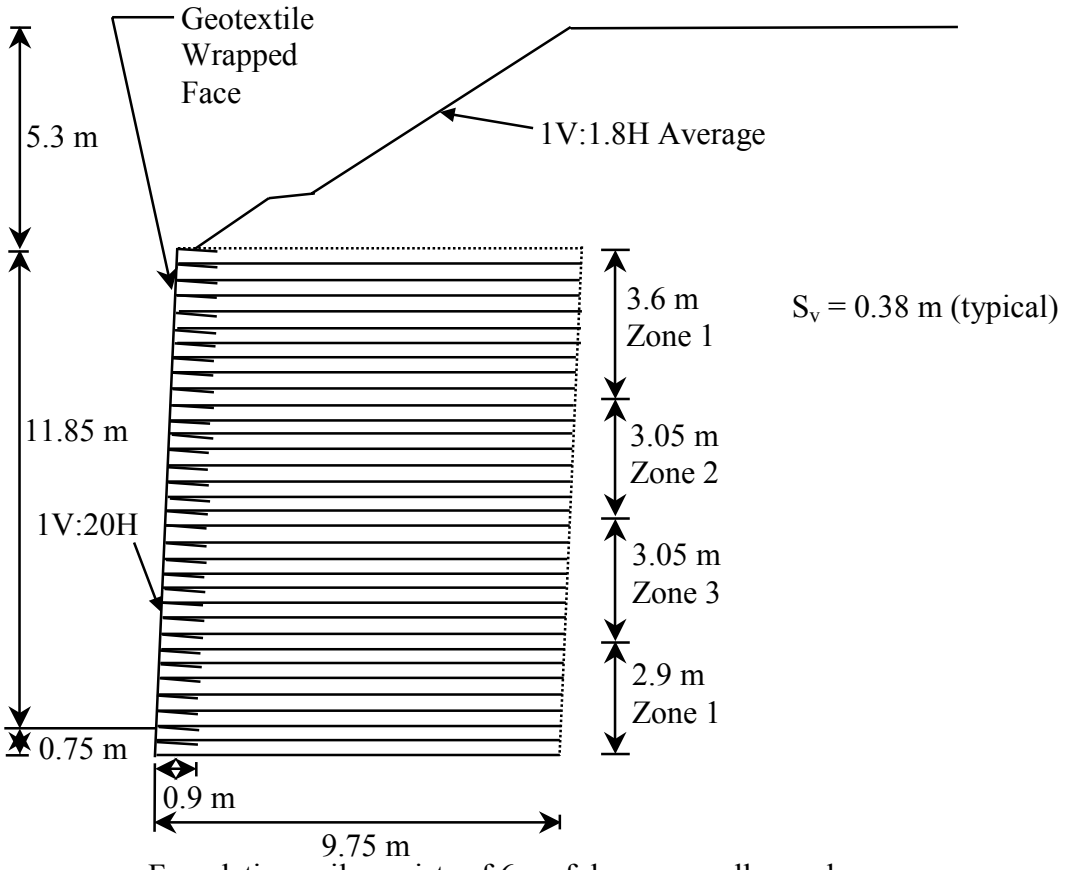

Figure 2.15. Cross-section for WSDOT Rainier Avenue wrapped face geotextile wall.

2.2.2.16 London, Ontario, Propped Panel Geogrid Wall, 1989 (Case GW17, Figure 2.16)

A geogrid reinforced, full-height, propped, precast concrete panel wall was constructed as part of the Highbury Avenue reconstruction and widening in London, Ontario, Canada (Bathurst 1992). Because of the coarse nature of the backfill, laboratory shear strength tests were not carried out, but the shear strength was estimated on the basis of experience with similar soil.

Maximum wall deformations of 44 mm and geogrid strains of 3 to 3.5 percent, most of which occurred within 6 months after prop removal, were measured in the tallest (7.1-m-high) instrumented panel. The largest strains occurred near the wall face, which can be explained by downward soil movement behind the relatively stiff facing panel. No signs of distress have been observed in the wall since it was constructed.

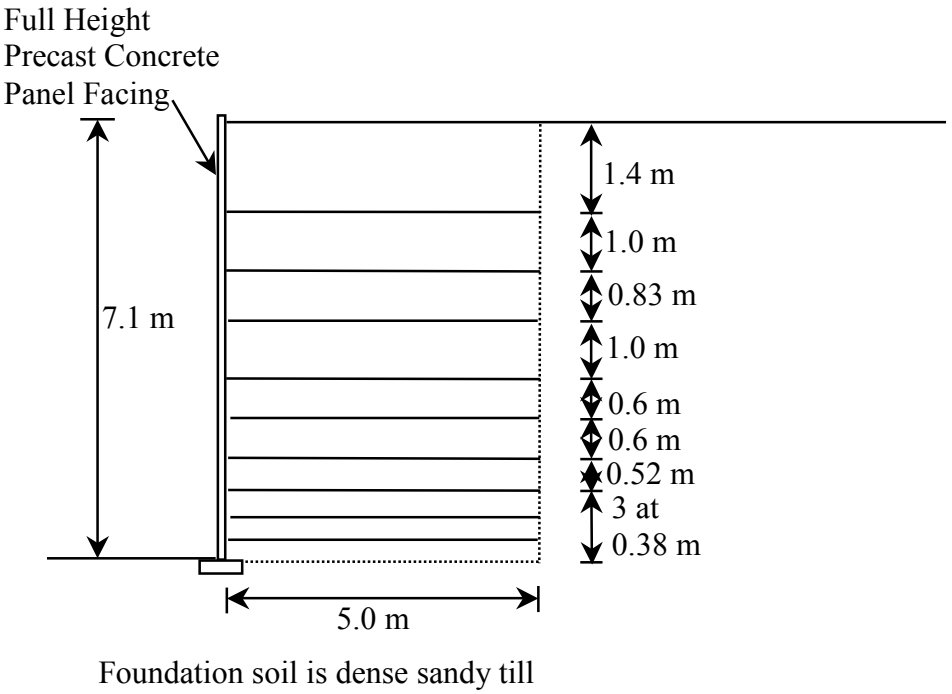

Figure 2.16. Cross-section for London, Ontario, propped panel (HDPE geogrid) wall.

2.2.2.17 Fredericton, New Brunswick, Propped Panel Geogrid Wall, 1990 (Case GW18, Figure 2.17)

A geogrid reinforced, full-height, propped, precast concrete panel wall was constructed in Fredericton, New Brunswick, Canada (Knight and Valsangkar 1993). Maximum wall deformations of 28 mm and geogrid strains of up to 2.1 percent, most of which occurred within 6

months after prop removal, were reported. No signs of distress have been observed in the wall since it was constructed.

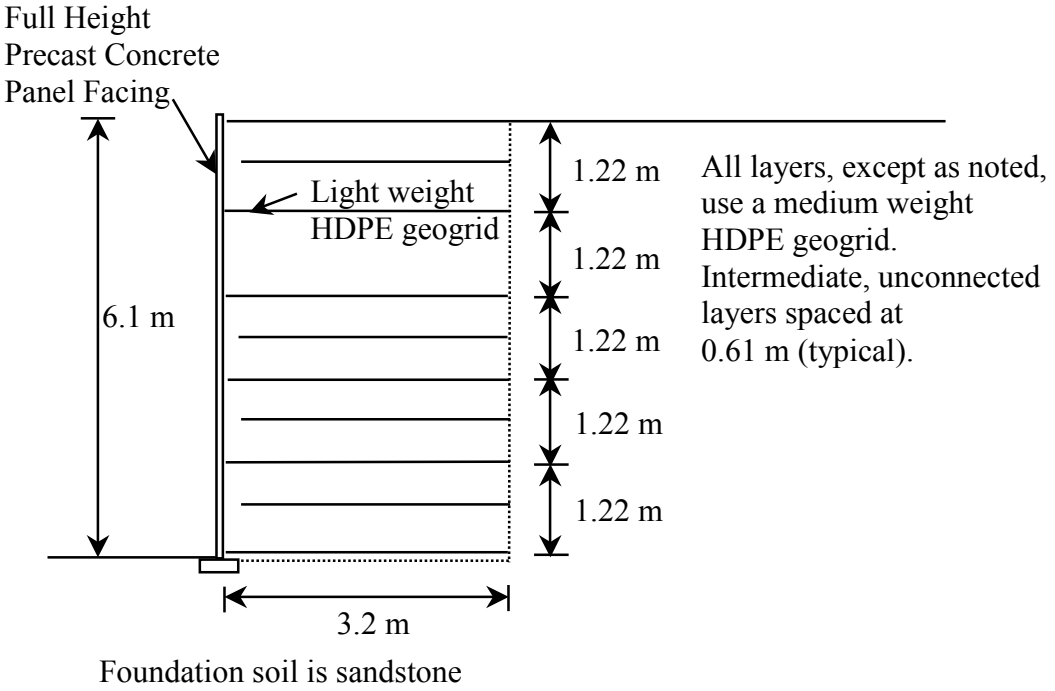

Figure 2.17. Cross-section for Fredericton, New Brunswick, propped panel (HDPE geogrid) wall.

2.2.2.18 Remy, France, Polyester Strap Concrete Panel Wall, 1993 (Case GW19, Figure 2.18)

A polyester strap, reinforced, incremental concrete panel wall 6.4 m high was constructed at the Centre Experimental du Batiment at St. Remy in 1993 (Schlosser et al. 1993). Total wall deformations were generally less than 50 mm, most of which occurred during construction.

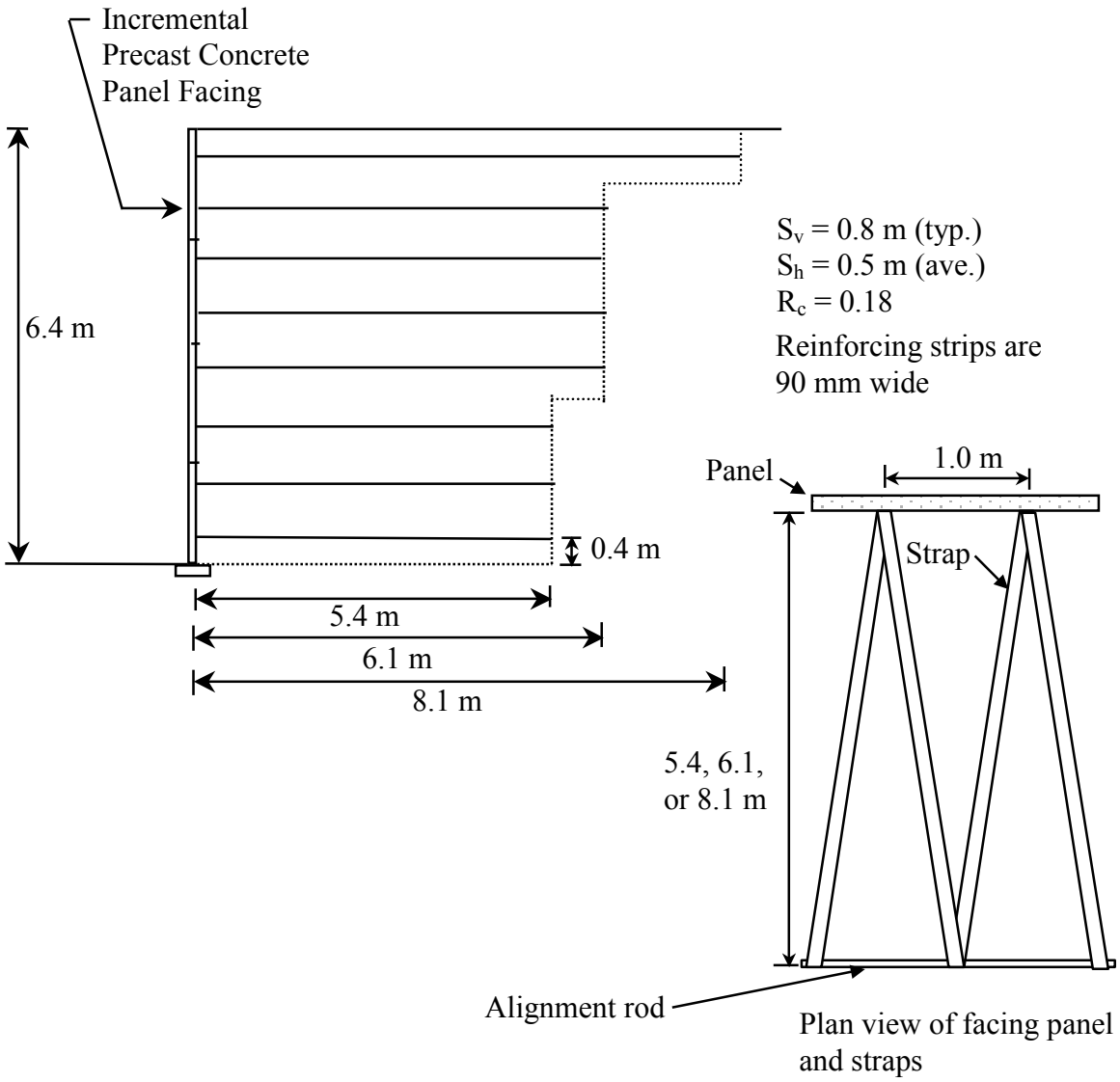

Figure 2.18. Cross-section for Freyssisol-Websol St. Remy test wall.

2.2.2.19 Vicenza, Italy, Geogrid Welded Wire-Faced Wall, 1998 (Case GW20, figures 2.19 and 2.20)

A 4-m-high welded wire-faced geogrid wall near Vicenza, Italy, was constructed and surcharged in an attempt to produce an internal failure (Carruba et al. 1999). Large diameter (100 mm) triaxial tests were conducted to determine the shear strength of the soil. The wall consisted of two sections 5.0 m wide. One section was constructed with a uniaxial HDPE geogrid, and the other section with a biaxial PP geogrid. The foundation below the wall was rigid.

The wall was surcharged in three stages to a maximum surcharge height of 3.5 m. At the maximum surcharge, maximum strains in the reinforcement ranged up to 1.6 percent for the HDPE geogrid section and up to 4.2 percent for the PP geogrid section. Before surcharging, the maximum reinforcement strains were generally less than 0.5 percent. There was some indication that the HDPE section exhibited signs of pullout under the highest surcharge height (Montanelli 2000). However, 2,000 hours of creep data indicated that creep strains and strain rates were decreasing with time after the final surcharge was placed.

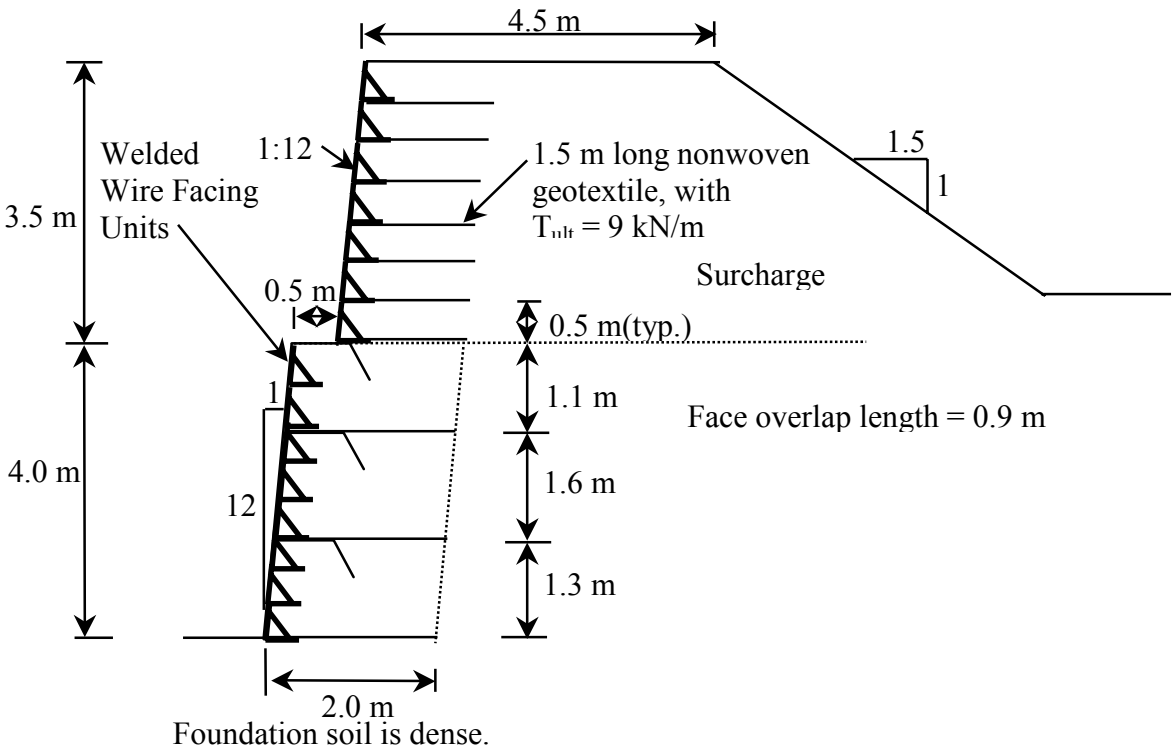

Figure 2.19. Cross-section for Vicenza, Italy, HDPE geogrid welded wire-faced wall.

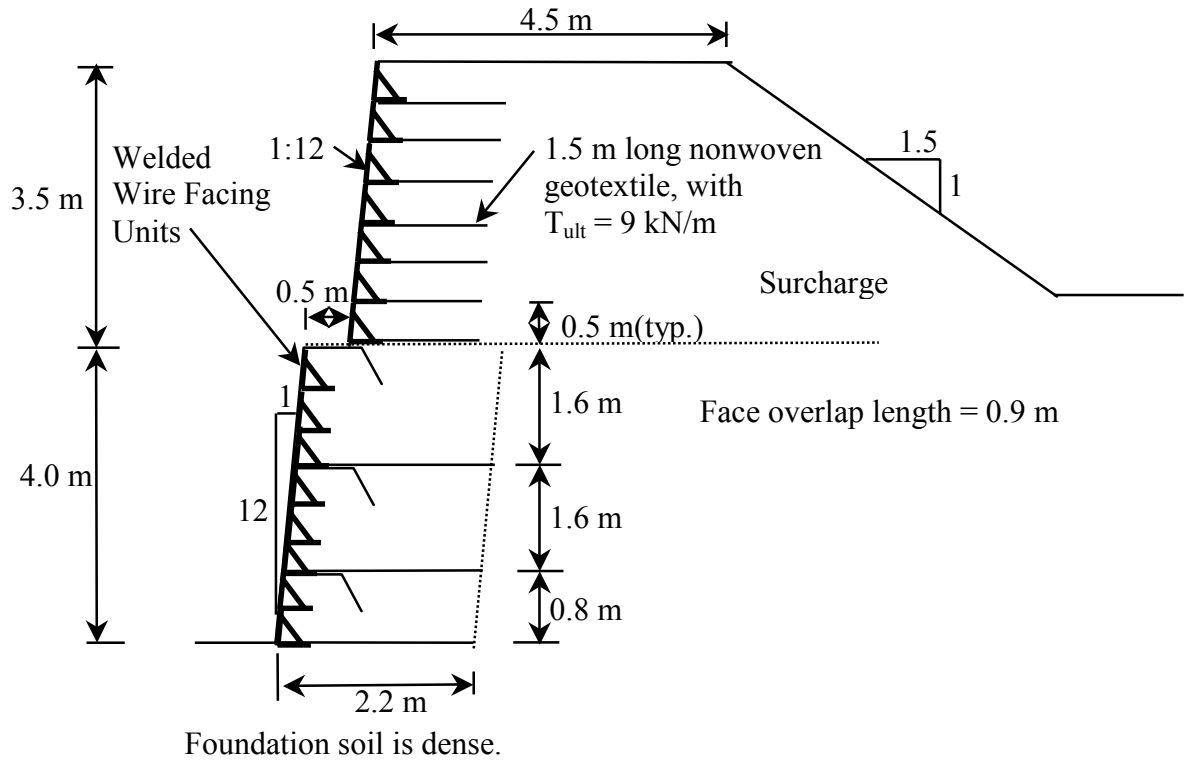

Figure 2.20. Cross-section for Vicenza, Italy, PP geogrid welded wire-faced wall.

2.3 Determination of Resistance-Demand Ratio

2.3.1 General

In this chapter the global level of safety is represented by the resistance-demand (RD) ratio of a reinforced soil wall, as described by expressions that have the following general form:

$$RD = \frac{R}{D} = \frac{\sum_{i=1}^{n} T_i}{D_{actual}} \qquad (2.1)$$

Conceptually, R (resistance) = the total tensile capacity of the reinforcement layers in the structure and, D (demand) = the total horizontal earth force to be carried by the reinforcement layers. The resistance term is calculated as the sum of the tensile reinforcement capacities (T_i) of

n layers of reinforcement in the wall. The interpretation and computational details of the resistance term vary for different resistance-demand ratio expressions introduced below.

The denominator used to calculate the RD ratio, D_{actual}, is based on the measured shear strength of the soil. This is calculated from plane strain peak friction angles estimated from triaxial or direct shear data (see Section 2.3.3) or directly measured in a plane strain test apparatus. D_{actual} is used in all RD ratio calculations that follow in order to provide a common basis of comparison.

Figure 2.21 illustrates resistance-demand concepts. The RD ratios shown in the figure are global parameters and therefore do not represent the RD ratio for individual layers within the structure. The quantities R_{index} and $R_{ultdesign}$ represent short-term resistance values, and R_{actual} and R_{design} represent long-term resistance values (i.e., at the end of the wall design life). D_{actual} is as defined previously, and D_{design} represents the magnitude of demand (total tensile load) on the reinforcement layers based on the design value of soil shear strength. Irrespective of how the demand term is calculated, the magnitude of this value is assumed to be constant over the design life of the structure. D_{design} is used only to estimate R_{design} in the RD calculations that follow. In practice, project-specific backfill shear strength tests are seldom conducted for wall design purposes, and if they are conducted for design, triaxial or direct shear strength tests are almost always used rather than plane strain testing. Hence, design values of soil shear strength are used to estimate D_{design} and R_{design} to determine the RD ratio that would be required if the wall were designed in accordance with the current design practice.

The short-term (index or ultimate) strength of the soil reinforcement (T_{ult}) is based on wide-width strip tensile test results and is the simplest and most consistent way to calculate the resistance term in Equation 2.1 (i.e., $R = R_{index} = \Sigma T_{ult}$). The *index* resistance-demand ratio RD_{index} (Equation 2.5) is illustrated in Figure 2.21a. At the very least this quantity provides a relative measure of how heavily reinforced a wall is.

Figure 2.21a represents the *idealized* case when the *actual* total available resistance at the end of design life is known (R_{actual}). This value can be calculated by carrying out wide-width strip tensile tests on exhumed samples of reinforcement materials at the design life of the structure. Alternatively, if the magnitude of index strength reduction due to installation damage, durability, and creep is known with certainty, then the predicted value of R_{actual} can be calculated as in Equation 2.11. The dashed line in the figure symbolizes that resistance values before the

end of design life are assumed to decrease with time, but the actual degradation rate is unknown. Regardless, the time history of reinforcement strength loss does not enter into the calculations reported in this chapter.

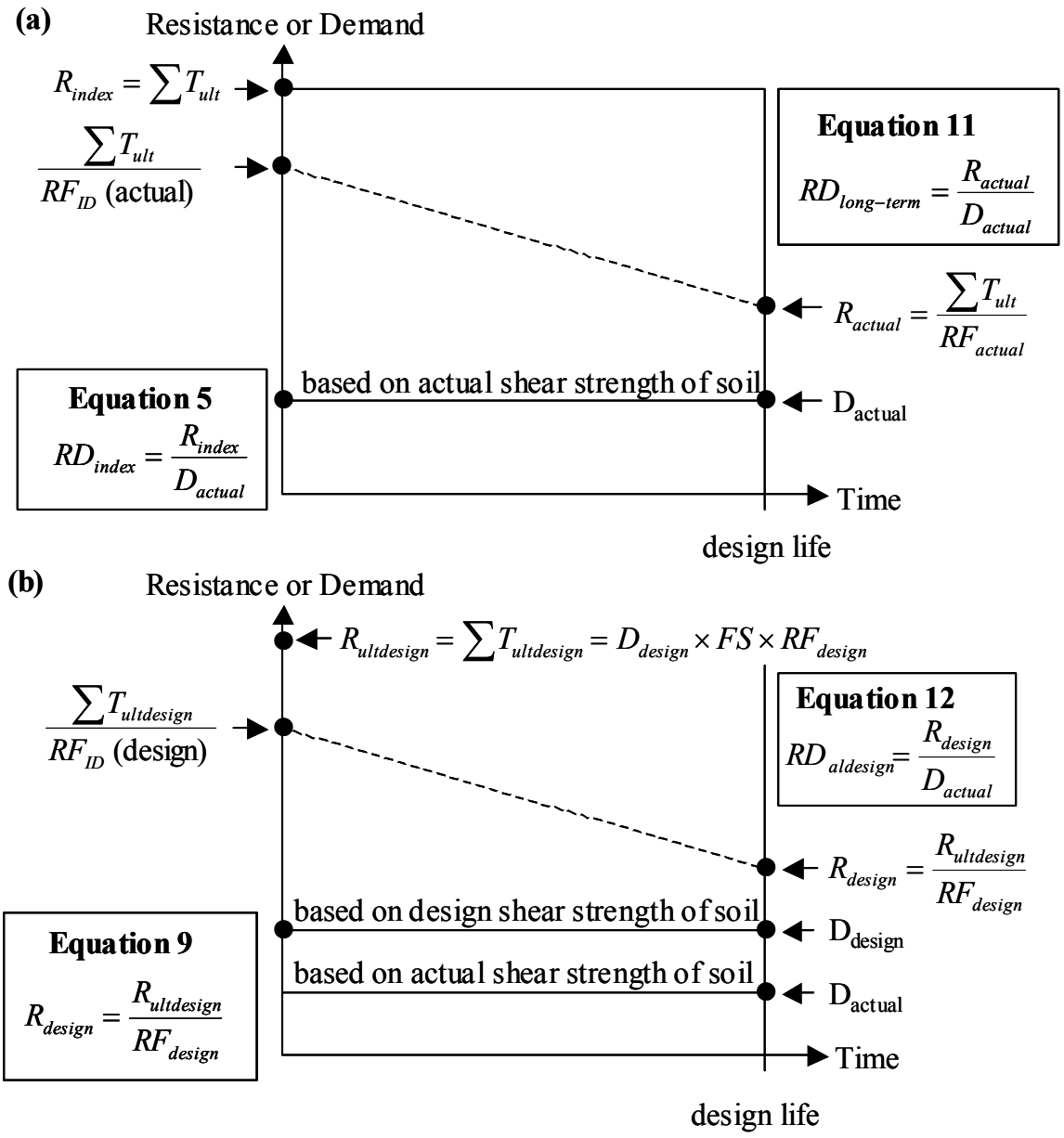

Figure 2.21. Resistance-demand concepts: (a) actual; (b) design.

"Actual" strength reduction factors (RF_{actual}) were estimated on the basis of current knowledge of geosynthetic durability (Elias et al. 2001, Elias 2001, WSDOT 1998) and site conditions for the selected case histories. For some of the case histories, reduction factors were calculated from laboratory tests of exhumed reinforcement specimens (Section 2.3.3).

Figure 2.21b illustrates the calculation of resistance-demand ratios on the basis of current design practice in North America. The demand term D_{design} is typically calculated by using shear strength values for the soil that are less than actual values, hence $D_{design} > D_{actual}$ in the figure. According to conventional AASHTO practice, the sum of the ultimate wide-width strip tensile strengths of the reinforcement layers ($\Sigma T_{ultdesign}$) must be at least equal to the product of the design demand load (D_{design}), a design global factor of safety (FS) to account for overall uncertainty, and a design reduction factor (RF_{design}) to account for the combined effect of installation damage, durability, and creep. Design values for the short-term and long-term resistance-demand ratios are calculated according to equations 2.9 and 2.12, respectively.

RF_{design} was calculated for each of the case histories. Current AASHTO requirements to estimate long-term geosynthetic strength reduction factors were used, and the calculations were based on what would have been known at the time of the wall case history regarding the aggressiveness of the backfill and the long-term geosynthetic properties. If little was known about the durability of the product used in the case history, the default reduction factor RF = 7.0 was used to calculate R_{design}.

RD ratio values should not be interpreted as a quantitative measure of the factor of safety against wall collapse because these values do not capture specific failure modes associated with geosynthetic reinforced soil walls (see also Section 2.3.2 regarding the potential accuracy of the method used to calculate demand). Rather, the global RD ratios introduced here are a convenient way to make a relative comparison of the best estimate of the RD ratio for the actual walls, based on measured soil and reinforcement properties, to the RD ratio needed to satisfy current AASHTO practice, based on typical design properties. Through this comparison, the degree of conservatism in the current design practice relative to the "actual" RD ratios for this database of wall case histories can be assessed.

For brevity in the following text, the term "global level of safety" or "level of safety" is understood to mean "resistance-demand ratio" as defined above. Both short-term and long-term RD ratios are calculated for each case study in Table 2.2 to provide insight into the global level of safety of geosynthetic walls built to date.

2.3.2 Calculation of Demand

The calculation method used to determine the value of demand (D) in Equation 2.1 is essentially the Simplified Method, which is specified in design practice for geosynthetic walls by AASHTO in the USA (AASHTO 1999, Elias et al. 2001). However, in the sections that follow, demand (D) is expressed as a total active force applied to the wall reinforcement rather than a force per reinforcement layer. For geosynthetic walls, the Simplified Method is essentially the same as the tieback wedge method that has been used to design geosynthetic walls for the past 20 years in North America (Allen and Holtz 1991). The total active earth force in the following sections was calculated by using the horizontal component of Coulomb earth force, since Coulomb theory explicitly includes the influence of wall batter. Interface friction, δ, between the wall facing and soil was assumed to be 0.0, and all soil volumes above the wall crest were treated as an equivalent uniform surcharge. The zero interface friction assumption is consistent with U.S. design codes and practice. However, it is recognized that this assumption is likely conservative.

The Simplified Method is a limit equilibrium approach and contains two key assumptions for calculating reinforcement load:

1. The magnitude of tensile load in each reinforcement layer is proportional to the soil overburden stress. Hence, reinforcement load will increase linearly with increasing depth of soil below the crest of the wall.
2. Tensile load in the reinforcement is a direct indicator of the state of stress in the soil, since the reinforcement layer is assumed to carry the full-lateral active earth pressure in the soil near the layer (i.e., the contributory area approach).

Both the design demand, used only to calculate the amount of reinforcement required per the current AASHTO specifications (AASHTO 1999), and the "actual" demand were calculated with this method, but with different shear strength parameters as discussed previously. It should not be assumed that the actual demand accurately represents the stress levels that would be measured in geosynthetic reinforcement in actual walls. The two assumptions used by the Simplified Method listed above may not necessarily be correct (Rowe and Ho 1993, Zornberg et al. 1998a). The actual demand is simply the best estimate of demand possible when using the Simplified Method.

Table 2.2. Summary of global resistance to demand and performance based on calculated reinforcement loads for geosynthetic walls.

Case Study	Height and Sur-charge	Sec-tion	Wall Perfor-mance to Date	K_{ah} Using Design ϕ	K_{ah} Using Plane Strain ϕ	Index RD Ratio for Actual Wall (Eq. 2.5)	Ultimate RD Ratio if Designed per AASHTO 2002 – Typical Practice (Eq. 2.9)	Ultimate RD Ratio if Designed per AASHTO 2002 – Perfect Match to Demand (Eq. 2.9)	Estimated Long-Term RD Ratio for Actual Wall (Eq. 2.11)	Long-Term RD Ratio if Designed per AASHTO 2002 – Typical Practice (Eq. 2.12)	Long-Term RD Ratio if Designed per AASHTO 2002 – Perfect Match to Demand (Eq. 2.12)
GW1	2.9 m plus 0.9 m soil surcharge	NA	Good	0.24	0.15	29	28	14	3.7	3.9	2.15
GW2	5.6 m	A	Good	0.17	0.085	13	23	19	2.2	3.2	2.7
	5.6 m	B	Good	0.17	0.085	12	23	19	1.1	3.2	2.7
GW3	4.8 m	1 & 9	Good	0.20	0.10	10	30	22	1.8	4.3	3.2
	4.8 m	2 & 10	Good	0.20	0.10	12	30	22	2.6	4.3	3.2
	4.8 m	3	Good	0.20	0.10	17	30	22	2.5	4.3	3.2
	4.8 m	4	Good	0.20	0.10	8.7	30	22	1.4	4.3	3.2
	4.8 m plus 2 m soil surcharge	5	Good	0.20	0.10	5.0	26	22	0.90	3.7	3.1
	4.8 m plus 2 m soil surcharge	6	Good	0.20	0.10	5.4	26	22	1.2	3.7	3.1
	4.8 m	7	Good	0.20	0.10	9.9	30	22	1.6	4.3	3.2
	4.8 m	8	Good	0.20	0.10	7.4	30	22	1.3	4.3	3.2
GW4	8.8 m	NA	Good	0.17	0.085	17	16	15	4.2	4.1	3.7
GW5	4.9 m	NA	Good	0.28	0.11	25	17	14	6.1	4.5	3.7
GW6	6.1 m	NA	Good	0.22	0.15	8.9	12	9.0	2.2	3.1	2.1
GW7	4.8 m plus 3 m soil surcharge	J	Good	0.14	0.04	21	30	25	4.8	7.1	6.0
		N	Good	0.14	0.04	26	30	25	6.4	7.1	6.0
GW8	6.1 m plus 2.1 m soil surcharge	2	Good	0.22	0.19	5.3	12	6.5	1.3	2.9	1.6

Table 2.2. Continued.

Case Study	Height and Sur-charge	Sec-tion	Wall Perfor-mance to Date	K_{ah} Using Design ϕ	K_{ah} Using Plane Strain ϕ	Index RD Ratio for Actual Wall (Eq. 2.5)	Ultimate RD Ratio if Designed per AASHTO 2002 – Typical Practice (Eq. 2.9)	Ultimate RD Ratio if Designed per AASHTO 2002 – Perfect Match to Demand (Eq. 2.9)	Estimated Long-Term RD Ratio for Actual Wall (Eq. 2.11)	Long-Term RD Ratio if Designed per AASHTO 2002 – Typical Practice (Eq. 2.12)	Long-Term RD Ratio if Designed per AASHTO 2002 – Perfect Match to Demand (Eq. 2.12)
GW9	6.1 m plus 2.1 m soil surcharge	9	Good	0.20	0.17	6.6	5.2	1.1	2.1	1.7	6.6
GW10	5.9 m but supported by 2.1 m of water at base of wall	6	Fair to good	0.22	0.19	30	18	0.62	4.4	2.5	30
	5.9 m after water removed	6	Poor. Failed by excessive deformation	0.22	0.19	20	12	0.41	2.9	1.7	20
GW11	2.85 m plus 0.6 m soil surcharge	NA	Good, except for sagging at face	0.22	0.10	37	20	1.5	6.4	3.4	37
GW12	3 m plus effective surcharge of 42 kPa	NA	Good	0.22	0.10	17	12	3.8	4.4	3.1	17
GW 13	3 m plus effective surcharge of 42 kPa	NA	Good	0.22	0.10	17	12	3.8	4.4	3.1	17

Table 2.2. Continued.

Case Study	Height and Sur-charge	Sec-tion	Wall Perfor-mance to Date	K_{ah} Using Design ϕ	K_{ah} Using Plane Strain ϕ	Index RD Ratio for Actual Wall (Eq. 2.5)	Ultimate RD Ratio if Designed per AASHTO 2002 – Typical Practice (Eq. 2.9)	Ultimate RD Ratio if Designed per AASHTO 2002 – Perfect Match to Demand (Eq. 2.9)	Estimated Long-Term RD Ratio for Actual Wall (Eq. 2.11)	Long-Term RD Ratio if Designed per AASHTO 20029 – Typical Practice (Eq. 2.12)	Long-Term RD Ratio if Designed per AASHTO 2002 – Perfect Match to Demand (Eq. 2.12)
GW14	3 m	NA	Good	0.22	0.10	6.0	34	18	1.2	6.0	3.1
	3 m plus effective surcharge of 70 kPa		Failed by excessive deformation and rupture	0.22	0.10	1.7	23	18	0.32	4.0	3.1
GW15	3 m	NA	Good	0.22	0.10	6.0	34	18	1.2	6.0	3.1
	3 m plus effective surcharge of 60 kPa		Poor. Failed by excessive deformation and rupture	0.22	0.10	1.9	24	18	0.36	4.1	3.1
GW16	12.6 m plus 5.3 m soil surcharge	NA	Good	0.24	0.09	14	32	28	3.4	4.6	4.0
GW17	7.1 m	NA	Good	0.26	0.17	12	11	8.7	3.2	2.9	2.2
GW18	6.1 m	NA	Good	0.22	0.17	7.6	12	8.7	1.9	3.0	2.1
GW19	6.4 m	NA	Good	0.25	0.23	24	9.3	4.7	9.1	3.5	1.8
GW20 (HDPE)	4 m	1	Good	0.19	0.066	16	26	23	3.7	6.6	5.9
	4 m plus a 3.5 m soil surcharge		Good	0.19	0.066	7.6	47	28	1.7	10	5.9
GW20 (PP)	4 m	2	Good	0.19	0.066	8.5	37	33	1.3	6.4	5.8
	4 m plus a 3.5 m soil surcharge		Fair	0.19	0.066	3.7	56	34	0.53	8.8	5.6

2.3.3 Material Properties Used to Calculate Resistance-Demand Ratio

The reinforcement and soil properties used to calculate the resistance-demand (RD) ratio are based on measured properties rather than on design properties (sections 2.3.4 and 2.3.6). The exceptions are calculations performed to determine the resistance required for each case history wall with the current AASHTO design specifications (AASHTO 2002) (Sections 2.3.5 and 2.3.7).

Reinforcement strengths from wide-width strip tensile test results (ASTM D4595) on project-specific materials were used in many of the case histories to calculate the index and estimated long-term RD ratios (sections 2.3.4 and 2.3.6). In some cases, minimum average roll values (MARV) for wide-width tensile strength were used if lot-specific test data were not available. For the two oldest case studies (GW1 and GW2), lot-specific tensile test results were correlated to equivalent wide-width test results to estimate tensile strengths for analysis.

To calculate the long-term RD ratio (Section 2.3.6), reduction factors for installation damage, creep, and chemical durability were typically estimated on the basis of site-specific conditions. Unless specific information was available to the contrary, the soil condition at each case history site was assumed to be non-aggressive according to the AASHTO (2002) definition for geosynthetic walls. Installation damage reduction factors were based on the results of wide-width tensile testing of exhumed reinforcement samples. If these data were not available, the installation damage reduction factor for the geosynthetic was estimated on the basis of product-specific installation damage test results, backfill gradation, and other site characteristics. Product-specific stress rupture or creep data were used to estimate reinforcement creep reduction factors if available. For most of the geotextiles in the current study, product-specific creep data were not available. Hence, creep reduction factors were estimated on the basis of the polymer used in the geosynthetic and corresponding values reported in the literature (Jewell and Greenwood 1988, Elias et al. 2001, Allen 1991, Allen and Bathurst 1996). In general, a creep reduction factor of 4.5 was used for polypropylene geosynthetics and 1.8 for polyester geosynthetics, if product-specific data were not available. Durability reduction factors were estimated on the basis of the characteristics of the polymer used in the geosynthetic, the backfill environment, and typical long-term durability test results reported in the literature (Elias 2001, Elias et al. 1997, Salman et. al. 1997, 1998). Durability reduction factors for non-aggressive

environments varied from 1.3 to 1.5 for polypropylene geosynthetics, 1.15 to 1.6 for polyester geosynthetics, and 1.1 for high density polyethylene geosynthetics. None of the case histories had soil environments that would be considered chemically aggressive.

Soil shear strength values from triaxial compression or direct shear test results were generally available. Plane strain or equivalent shear strength results were available only for case studies GW11 through GW16. In two cases (GW5 and GW19), peak strengths from triaxial compression testing were converted by the writers from reported (c - ϕ) values to peak secant friction angle values that corresponded to a vertical pressure of γH, where γ is the bulk unit weight of the reinforced soil and H is the height of the wall.

Plane strain conditions were assumed to be applicable to all the walls in the current study. Furthermore, recent work indicates that the peak plane strain friction angle controls the internal capacity of geosynthetic structures, rather than the plane strain constant volume or critical state soil friction angle (Rowe and Ho 1993, Bathurst 1993, Zornberg et al. 1998a,b).

Peak plane strain peak friction angle values, ϕ_{ps} , for compacted granular fills are larger than values inferred from triaxial compression and direct shear results. To form a common basis of comparison, peak triaxial friction angles, ϕ_{tx} , were corrected to peak plane strain friction angles by using the following equation by Lade and Lee (1976):

$$\phi_{ps} = 1.5\phi_{tx} - 17 \text{ (in degrees)} \qquad (2.2)$$

On the basis of data interpretation presented by Bolton (1986) and Jewell and Wroth (1987), for dense sands, peak plane strain friction angles, ϕ_{ps} , were calculated from peak direct shear friction angles, ϕ_{ds} , by using the following relationship:

$$\phi_{ps} = \tan^{-1} (1.2 \tan \phi_{ds}) \qquad (2.3)$$

2.3.4 Index Resistance-Demand Ratio

Equation (2.1) can be used to calculate an *index* resistance-demand (RD) ratio. Term R is calculated as the sum of the ultimate tensile capacities of the reinforcement layers, given a standard laboratory (index) tensile strength value (T_{ult}) (e.g., ASTM 4595). The demand term D

is equal to the *horizontal* component of earth force $P_{ah}(\phi_{ps})$ calculated by using classical earth pressure theory. Hence:

$$P_{ah}(\phi_{ps}) = 0.5\, K_{ah}\, \gamma\, H^2 + K_{ah}\, q\, H \qquad (2.4)$$

where $K_{ah} = K_a(\phi_{ps}, \delta, \omega) \times \cos(\delta - \omega)$; ϕ_{ps} = the peak plane strain friction angle of the soil; ω = wall batter; δ = interface shear angle between wall facing and backfill soil (assumed to be zero on the basis of current practice as defined in AASHTO, 2002); H = total wall height measured from the toe of the wall to the soil surface immediately behind the wall facing; γ = the bulk unit weight of the soil and; q is the magnitude of any uniformly distributed surcharge load at the soil surface. For broken back surcharges, an equivalent uniform surcharge was calculated by using the total weight of the surcharge over the reinforced soil zone divided by the width of the reinforced soil zone. The index RD ratio is as follows:

$$RD_{index} = \frac{R_{index}}{D_{actual}} = \frac{\sum_{i=1}^{n} T_{ult}^{i}}{P_{ah}(\varphi_{ps})} \qquad (2.5)$$

Example 2.1. Calculate index resistance-demand ratio for Case Study GW9 with surcharge in place (Figure 2.10).

Soil properties: $\gamma = 20.4$ kN/m^3; $\phi = \phi_{ps} = 43°$

Number of reinforcement layers: 8

Reinforcement index tensile strength: $T_{ult} = 39.2$ kN/m (ASTM 4595)

Wall height and batter and interface friction: $H = 6.10$ m; $\omega = 3°$; $\delta = 0$

Average soil surcharge load: $q = \gamma \times D_q = 20.4$ kN/m^3 $\times$ 1.30 m $= 26.5$ kN/m^2

Coefficient of horizontal active earth pressure: $K_{ah} = K_a\,(\phi, \delta, \omega) \cos(\delta - \omega) = 0.171$

The total demand is equal to the horizontal component of earth force (Equation 2.4):

$$P_{ah} = 0.5 K_{ah} \gamma H^2 + K_{ah} q H = 0.5 \times 0.171 \times 20.4 \frac{\text{kN}}{\text{m}^3} (6.10)^2 \text{m}^2 + 0.171 \times 26.5 \frac{\text{kN}}{\text{m}^2} \times 6.10 \text{m} = 92.8 \frac{\text{kN}}{\text{m}}$$

From Equation 2.5:

$$RD_{index} = \frac{\sum_{i=1}^{n} T_{ult}^{i}}{P_{ah}(\varphi_{ps})} = \frac{8 \times 39.2 \ \frac{kN}{m}}{92.8 \ \frac{kN}{m}} = \frac{314}{92.8} = 3.38$$

END OF EXAMPLE 2.1

2.3.5 Ultimate Resistance-Demand Ratio Using AASHTO Design Method

In current design practice (AASHTO 2002) the maximum allowable design load T_{max}^{i} for a reinforcement layer is calculated as follows:

$$T_{max}^{i} \leq \frac{T_{al}^{i}}{FS} = \frac{T_{ult}^{i}}{FS \times RF_{design}} = \frac{T_{ult}^{i}}{FS \times RF_{ID} \times RF_{CR} \times RF_{D}} \tag{2.6}$$

According to AASHTO terminology, the quantity T_{al} = long-term reinforcement strength, and FS is a factor of safety to account for overall uncertainty. The reduction factors used to account for other forms of degradation are RF_{ID} = installation damage, RF_{CR} = creep rupture and, RF_{D} = chemical and biological degradation. For brevity, the product of these terms for design using the AASHTO method can be expressed as $RF_{design} = RF_{ID} \times RF_{CR} \times RF_{D}$.

The maximum load to be carried by a reinforcement layer using the Simplified Method is:

$$T_{max}^{i} = S_i K_{ah}(\gamma z_i + q) \tag{2.7}$$

The load in reinforcement layer i is calculated on the basis of the integrated lateral pressure acting over a contributory unit face area, S_i. The quantity K_{ah} is calculated by using the *design* friction angle for the soil ($\phi = \phi_{des}$), as reported in Table 2.1. Equating expressions 6 and 7 leads to the following:

$$T_{ultdesign}^{i} = FS \times RF_{design} \times T_{max}^{i} \tag{2.8}$$

An *ultimate* design resistance-demand ratio can now be expressed as follows:

$$RD_{ultdesign} = \frac{R_{iultdesign}}{D_{actual}} = \frac{\sum_{i=1}^{n} T^{i}_{ultdesign}}{P_{ah}(\varphi_{ps})} \tag{2.9}$$

The numerator in the above expression is the sum of the reinforcement layer index strengths required to just satisfy the current AASHTO design method for calculating the maximum allowable design load T^{i}_{max}. The demand term in the denominator (total horizontal earth force acting on the wall) is calculated as before, using $\phi = \phi_{ps}$ to provide a common basis of comparison. The least conservative estimate of $RD_{ultdesign}$ can be obtained by matching the reinforcement strength required to the demand at each reinforcement layer level, termed "perfect match-to-demand" in Table 2.2. However, typical design practice is to determine the reinforcement strength required by using the calculated demand at the bottom of a constant reinforcement strength or vertical spacing zone within the wall cross-section, and using the strength calculated in this manner for the entire constant strength or vertical spacing zone. This is termed "typical practice" in Table 2.2. In all cases, this typical practice calculation will result in a higher $RD_{ultdesign}$ than will the perfect match-to-demand calculation.

Example 2.2. Calculate the ultimate design resistance-demand ratio using the AASHTO design method for Case Study GW9 with surcharge in place (Figure 2.10), for the perfect match-to-demand case. Additional parameter values from those in Example 2.1 are as follows:

Design friction angle: $\phi = \phi_{des} = 40°$

Coefficient of horizontal active earth pressure: $K_{ah} = K_a(\phi_{design}, \delta, \omega) \times \cos(\delta - \omega) = 0.199$

Product-specific reduction factors: $RF_{CR} = 1.85$, $RF_{ID} = 1.30$, $RD_D = 1.30$

Reinforcement spacing: $S_8 = 1.2$ m; $S_7 = 0.9$ m; $S_6 = 0.9$ m; $S_5 = 0.7$ m; $S_4 = 0.6$ m; $S_3 = 0.6$ m; $S_2 = 0.6$ m; $S_1 = 0.4$ m

Depth of reinforcement layers: $z_8 = 0.8$ m; $z_7 = 1.6$ m; $z_6 = 2.6$ m; $z_5 = 3.4$ m; $z_4 = 4.0$ m; $z_3 = 4.6$ m; $z_2 = 5.2$ m; $z_1 = 5.8$ m

Example calculations for layers 4 and 1 using Equation 2.7:

$$T_{max}^{4} = S_4 \times K_{ah} \times \left(\gamma z_4 + q\right) = 0.6\ \text{m} \times 0.199 \times \left(20.4\ \frac{\text{kN}}{\text{m}^3} \times 4.0\ \text{m} + 26.5\ \frac{\text{kN}}{\text{m}^2} \right) = 12.9\ \frac{\text{kN}}{\text{m}}$$

$$T_{max}^{1} = S_1 \times K_{ah} \times \left(\gamma z_1 + q\right) = 0.4\ \text{m} \times 0.199 \times \left(20.4\ \frac{\text{kN}}{\text{m}^3} \times 5.8\ \text{m} + 26.5\ \frac{\text{kN}}{\text{m}^2} \right) = 11.5\ \frac{\text{kN}}{\text{m}}$$

The product of reduction factors is the following:

$RF_{design} = RF_{ID} \times RF_{CR} \times RF_{D} = 1.85 \times 1.30 \times 1.30 = 3.13$

Example calculations for the ultimate design strength for layers 4 and 1 using Equation 2.8 are:

$$T_{ultdesign}^{4} = FS \times RF_{design} \times T_4 = \left(1.5 \times 3.13\right) \times 12.9\ \frac{\text{kN}}{\text{m}} = 60.6 \frac{\text{kN}}{\text{m}}$$

$$T_{ultdesign}^{1} = FS \times RF_{design} \times T_8 = \left(1.5 \times 3.13\right) \times 11.5\ \frac{\text{kN}}{\text{m}} = 54.0 \frac{\text{kN}}{\text{m}}$$

The *ultimate* design resistance-demand ratio is calculated using Equation 2.9:

$$RD_{ultdesign} = \frac{\sum_{i=1}^{8} T_{ultdesign}^{i}}{P_{ah}(\varphi_{ps})} = \frac{\left(54.0 + 74.3 + 67.5 + 60.6 + 62.9 + 66.9 + 49.7 + 48.0\right)\frac{\text{kN}}{\text{m}}}{92.8\ \frac{\text{kN}}{\text{m}}} = \frac{484}{92.8} = 5.21$$

END OF EXAMPLE 2.2

2.3.6 Estimated Long-Term Resistance-Demand Ratio

The actual reinforcement strength available at the end of design life (long-term) is difficult to estimate given the current state of knowledge. However, the current AASHTO approach that uses "best estimate" values for degradation mechanisms, or actual measured losses from exhumation and testing of the reinforcement, if reported, can be used to calculate available long-term reinforcement strength for comparison purposes. The available reinforcement capacity T_i is:

$$T_{al}^{i} = \frac{T_{ult}^{i}}{RF_{actual}} = \frac{T_{ult}^{i}}{RF_{ID} \times RF_{CR} \times RF_{D}} \tag{2.10}$$

where RF_{actual} is calculated by using "best estimate" values for reduction factors RF_{ID}, RF_{CR}, and RF_{D}. The *estimated* long-term resistance-demand ratio can now be calculated as follows:

$$RD_{long\text{-}term} = \frac{R_{actual}}{D_{actual}} = \frac{\sum_{i=1}^{n} \frac{T_{ult}^{i}}{RF_{actual}}}{P_a(\phi_{ps})} \tag{2.11}$$

Example 2.3. Calculate the estimated long-term resistance-demand ratio for Case Study GW9 with surcharge in place (Figure 2.10).

"Best estimate" reduction factors: $RF_{CR} = 1.85$, $RF_{ID} = 1.30$, $RD_{D} = 1.30$

The product of estimated reduction factors is:

$RF_{actual} = RF_{ID} \times RF_{CR} \times RF_{D} = 1.85 \times 1.30 \times 1.30 = 3.13$

The estimated long-term resistance-demand ratio is calculated using Equation (11):

$$RD_{long\text{-}term} = \frac{\sum_{i=1}^{8} \frac{T_{ult}^{i}}{RF_{actual}}}{P_a(\varphi_{ps})} = \frac{8 \times \left(\frac{39.2}{3.13}\right)\frac{kN}{m}}{92.8\frac{kN}{m}} = \frac{100}{92.8} = 1.08$$

END OF EXAMPLE 2.3

2.3.7 Allowable Long-Term Resistance-Demand Ratio Using AASHTO Method

The resistance-demand ratio for all case histories in the current study can be calculated by using long-term reinforcement strength values ($T_{aldesign}^{i}$). The *allowable* long-term design resistance-demand ratio using the AASHTO method can expressed as follows:

$$RD_{aldesign} = \frac{R_{design}}{D_{actual}} = \frac{\sum_{i=1}^{n} T_{aldesign}^{i}}{P_a(\phi_{ps})} = \frac{\sum_{i=1}^{n} \frac{T_{ultdesign}^{i}}{RF_{design}}}{P_a(\phi_{ps})} \tag{2.12}$$

where $T^{i}_{ultdesign}$ is calculated with Equation 2.8, and RF_{design} is calculated with AASHTO-recommended values for reduction factors RF_{ID}, RF_{CR}, and RF_{D}, given what would have been known about the wall backfill and long-term properties of the reinforcement product at the time the wall was designed. As described in Section 2.3.5, $RD_{aldesign}$ can be obtained by matching the reinforcement strength required to the demand at each reinforcement layer level (termed "perfect match to demand" in Table 2.2), or it can be calculated in accordance with typical practice using constant zones of strength and spacing (termed "typical practice" in Table 2.2).

Example 2.4. Calculate the allowable long-term resistance-demand ratio using the AASHTO method for Case Study GW9 with surcharge in place (Figure 2.10), for the perfect match-to-demand case.

From Example 2:

$RF_{design} = RF_{ID} \times RF_{CR} \times RF_{D} = 1.85 \times 1.30 \times 1.30 = 3.13$

The *allowable* design resistance-demand ratio is calculated using Equation 2.12:

$$RD_{aldesign} = \frac{\sum_{i=1}^{8} T^{i}_{aldesign}}{P_a(\varphi_{ps})} = \frac{\sum_{i=1}^{8} \frac{T^{i}_{ultdesign}}{RF_{design}}}{P_a(\varphi_{ps})} = \frac{\frac{(54.0+74.3+67.5+60.6+62.9+66.9+49.7+48.0)\frac{kN}{m}}{3.13}}{92.8\frac{kN}{m}} = \frac{156}{92.8} = 1.67$$

END OF EXAMPLE 2.4

2.4 Summary of Global Level of Safety and Performance for Case Histories

The calculated resistance to demand ratios, or level of safety, both short (equations 2.5 and 2.9) and long term (equations 2.11 and 2.12), for all case histories are summarized in Table 2.2. The table also compares the calculated level of safety for the case history to the level of safety that would be required by current AASHTO design specifications (AASHTO 2002). The long-term level of safety has been estimated at the end of a 75-year design life, which is a typical design life used for these types of walls.

Table 2.2 also records the observed long-term performance of each wall as "good" or "poor." The following definition for "good" long-term performance was used (see Chapter 6.0):

- Total reinforcement strains are small (typically less than 3 percent).
- Creep strains and strain rates decrease as time increases (i.e., only primary creep observed).
- The wall backfill soil does not exhibit signs of failure (cracking, slumping, etc.).
- Post-construction deformations, which are typically greatest at the wall top, are less than 30 mm within the first 10,000 hours.

Evidence of "poor" long-term performance included the following:

- The total reinforcement strains are relatively large (typically 5 percent or more).
- The creep strain rates are relatively constant or increase as a function of time.
- The wall backfill exhibits signs of failure (cracking, slumping, etc.)
- A reinforcement rupture occurs either at the connection or in the backfill (typically, the top reinforcement layer will fail first).
- Post-construction wall face deformations are greater than 35 mm in the first 10,000 hours after the end of wall construction, and increase at a constant or increasing rate.

In some cases, wall performance was described as fair, indicating a borderline case.

The average index RD ratios, based on measured properties, both short-term and long-term, and for walls that exhibited either good or poor performance, are compared in Table 2.3 to the RD ratios that would be required if the walls were designed in accordance with current AASHTO specifications. Additionally, figures 2.22 and 2.23 illustrate how the RD ratios are distributed statistically for the actual versus the AASHTO design RD ratio. Figure 2.24 illustrates the level of conservatism that current AASHTO design requirements would require relative to the actual RD ratio inherent in the wall case histories that exhibited good long-term performance. These figures and Table 2.3 clearly illustrate the difference in resistance-demand ratio between what has been built successfully in the past versus what is now required by current AASHTO specifications.

Table 2.3. Average global resistance to demand for all geosynthetic wall case histories.

Wall Performance	Number of Walls, Test Sections, or Load Cases	Average Resistance to Demand Ratio (RD)			Ratio: AASHTO to Actual RD	Conservatism due to Soil Strength Selection: Design K_{ah} / Plane Strain K_{ah}	Conservatism Due to Imperfect Match to Demand	Ratio of AASHTO RD, with Conservatism Due to Soil Strength Selection and Imperfect Demand matching Removed, to Actual RD
		Actual Wall	Designed per AASHTO (2002), Typical Practice, with Typical Soil Design Parameters	Designed per AASHTO (2002), Perfect Match to Demand, with Typical Soil Design Parameters				
good performance, short-term (index or ultimate)	30	12	25	18	2.8	2.1	1.4	0.9
fair or poor performance, short-term (index or ultimate)	5	2.5	31	20	12	1.9	1.5	4.5
good performance, long-term (estimated or allowable)	30	2.7	4.6	3.4	2.4	2.1	1.4	0.8
fair or poor performance, long-term (estimated or allowable)	5	0.45	4.8	3.2	9.9	1.9	1.5	3.8

*This "conservatism" is relative to the theoretical demand based on Coulomb theory, but with zero soil-wall interface friction, using measured soil strength parameters from which plane strain parameters were estimated. If the load calculation theory itself is conservative (i.e., measured reinforcement loads are below the theoretical reinforcement loads calculated), then additional conservatism will be present that is not shown in this table.

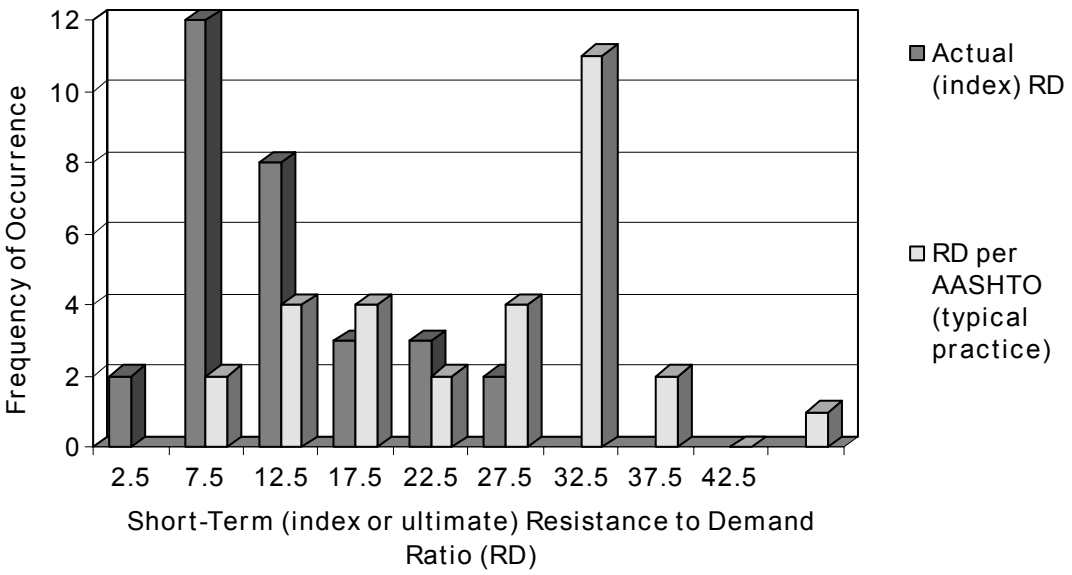

Figure 2.22. Comparison between the index (short-term) resistance-demand ratio for the actual walls and the ultimate resistance-demand ratio required by current AASHTO design specifications for geosynthetic wall case histories with good performance.

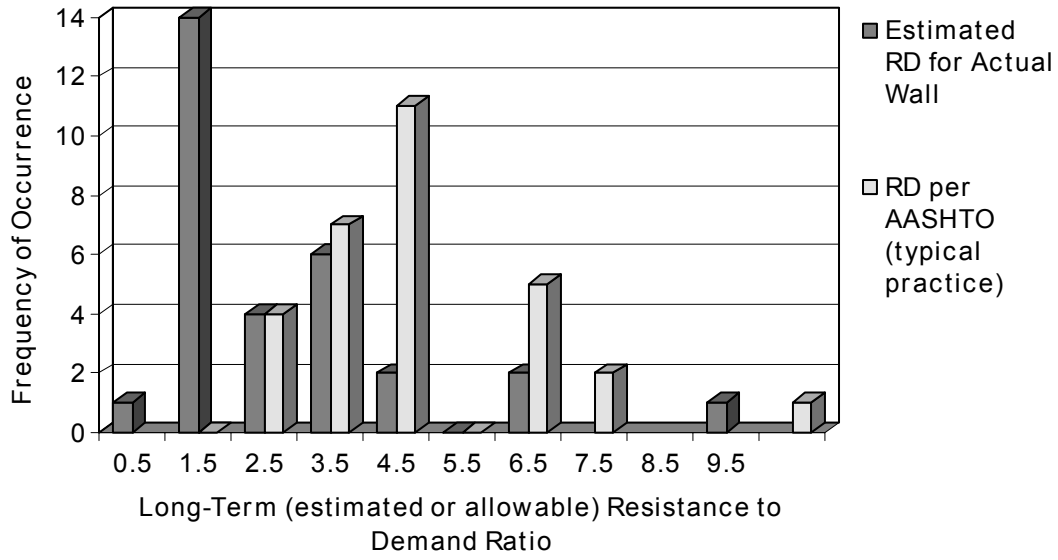

Figure 2.23. Comparison between the estimated long-term resistance-demand ratio for the actual walls and the allowable long-term resistance-demand ratio required by current AASHTO design specifications for geosynthetic wall case histories with good performance.

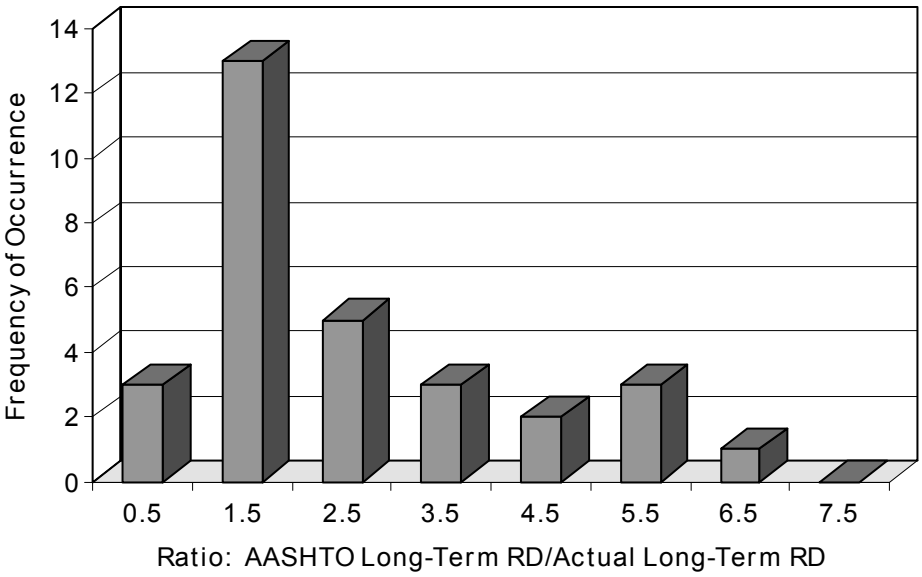

Figure 2.24. Degree of conservatism in long-term resistance-demand ratio when following current practice (AASHTO 2002) for case histories with good long-term performance.

2.5 Discussion of Wall Case History Performance and Level of Safety

The case histories summarized in tables 2.1 and 2.2 cover a variety of heights, surcharge conditions, foundation conditions, facing types and batter, reinforcement types and stiffness, and reinforcement spacings. The performance of these walls is considered to be representative of geosynthetic reinforced soil walls that are constructed with granular backfills.

Table 2.3 indicates that, for short-term strength, case study walls contain approximately one third of the reinforcement that would typically be required if the walls were designed in accordance with the current AASHTO specifications using typical soil design properties. For long-term level of safety, actual walls that exhibited good performance contain less than one half of the reinforcement that would typically be required if the walls were designed in accordance with the current AASHTO specifications. In some cases, only one-eighth of the reinforcement required by current AASHTO specifications was used.

As for the case study walls that exhibited poor performance, these walls contained only one tenth to one twelfth of the reinforcement that would typically be required if the walls were designed in accordance with the current AASHTO specifications for both short-term and long-term reinforcement strength. Given these observations, it appears that the reinforcement actually required to provide adequate internal strength for good long-term performance is somewhere

between one half and approximately one tenth of what current design practice, in particular the AASHTO specifications, would require. Clearly, there must be some significant sources of conservatism in current design practice. Possible sources of conservatism in internal stability design are discussed below.

In current design practice for walls with granular backfill, a design soil friction angle of 34 to 40 degrees is typically used, even for well-graded granular backfills with angular particles. It is generally not feasible to perform laboratory soil shear strength tests on project-specific backfill soils in advance of design, since the backfill source is typically not known at this stage. In those rare cases where measured backfill soil shear strength properties are available for design, the data are from direct shear box tests or triaxial tests, and peak friction angles are not converted to larger plane strain values.

The case histories reviewed here suggest that the use of a conservative soil shear strength value resulted in overestimation of reinforcement loads by a factor of 1.2 to 3.5, with an average value of about 2.0 (Table 2.3). Not considered here is potentially greater soil shear strength due to apparent soil cohesion (in general, 10 kPa or less) that could increase this overestimation factor even more. However, most designers are reluctant to rely on apparent cohesion over the long term.

Another source of conservatism, based on Table 2.3, is an imperfect match between the reinforcement strength available and the demand at each reinforcement level. An imperfect match may occur in design if the reinforcement strength used in calculations is determined at the base of a group (or zone) of reinforcement layers of the same strength, or of a group of layers with the same vertical spacing, and this strength is applied over the entire zone. As indicated in Table 2.3, this causes reinforcement loads, on average, to be overestimated by a factor of 1.4 to 1.5 for the case histories evaluated.

Combining both the soil shear strength and imperfect matching as sources of conservatism and applying them to reduce R_{design} for calculating $RD_{ultdesign}$ and $RD_{aldesign}$ (Table 2.3) indicates that the wall case histories, on average, have about the right amount of reinforcement relative to the theoretical minimum amount AASHTO would require for walls that performed well, and approximately one-fourth of the reinforcement for walls that performed fairly to poorly. Furthermore, for the walls that performed well, 13 of the wall case histories had less reinforcement than the theoretical minimum amount AASHTO would require (as low as one half

of the reinforcement required by AASHTO), as indicated in Figure 2.25, which summarizes the distribution of values for each case history used to develop the averages presented in the far right column of Table 2.3. This suggests that even after removing sources of conservatism such as soil strength parameter selection and imperfect matching of the reinforcement to the AASHTO demand, additional conservatism is still hidden in the current design methodology for walls that are known to perform well. It is likely that the magnitude of this hidden conservatism is somewhere between a factor of 1.5 and 4, with the larger value corresponding to walls with marginal to poor performance.

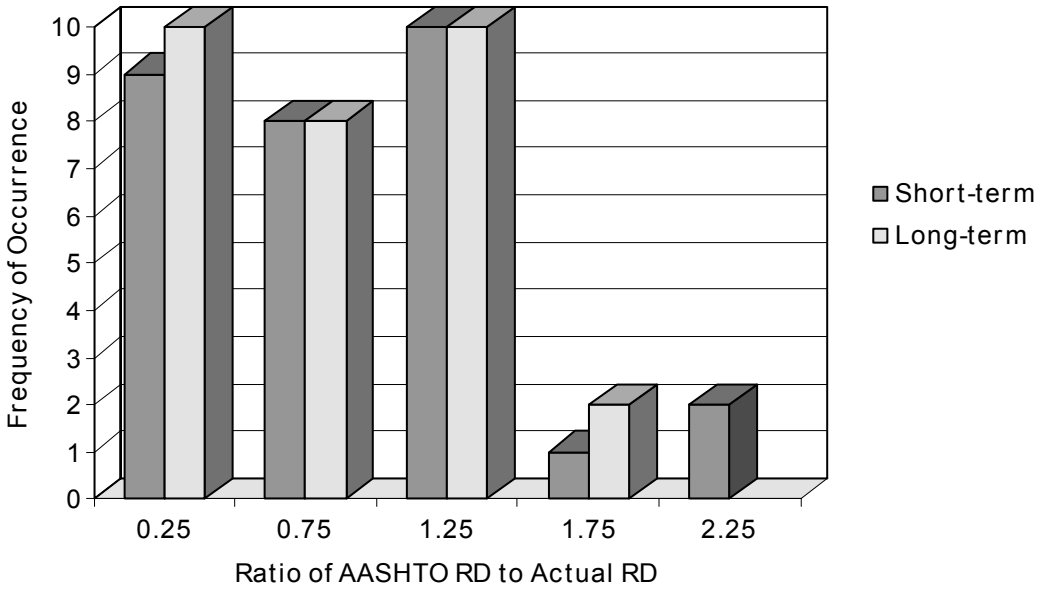

Figure 2.25. Ratio of the theoretical minimum AASHTO RD to the actual RD for walls with good long-term performance (conservatism due to soil strength selection and imperfect demand matching removed).

Even when measured soil properties are considered, loads interpreted from measured reinforcement strains in geosynthetic reinforced wall systems have consistently been observed to be significantly lower than the calculated load. Later chapters and other previous publications (e.g., Rowe and Ho 1993) provide detailed evidence of this observation.

Current methods of characterizing long-term geosynthetic reinforcement strength (e.g., Elias et al. 2001, Elias 2001, AASHTO 1999, WSDOT 1998) may also contribute to design conservatism. The paper by Allen and Elias (1996) contains a discussion of how current and

proposed durability laboratory test protocols are likely to produce a conservative estimate of geosynthetic polymer life. Chapter 6.0 discusses evidence that as long-term creep occurs, the remaining reinforcement tensile strength does not decrease until just before creep rupture is reached. Hence, the tensile strength of the reinforcement does not, in reality, decrease monotonically with the logarithm of elapsed time due to creep, as is often assumed in design. Hence, creep becomes a non-issue, especially if conservative soil strength parameters are used, causing reinforcement resistance and the overall level of safety to be underestimated.

2.6 Summary and Conclusions

A summary of 20 geosynthetic wall case histories with a total of 35 analysis conditions has been presented. These case histories cover a variety of wall heights, surcharge conditions, foundation conditions, facing types and batter, reinforcement types and stiffness, and reinforcement spacings. All of the walls that were designed as production walls, including structures in place for 25 years, performed well with low strains and minimum deflections, both in the short term and long term. Some of the walls that were built for research rather than production were purposely under-designed so that failure could occur, providing an indication of the design limits of these types of wall systems. Some of these under-designed walls (e.g., Bell et al. 1983) could not be taken to failure even though they were intended to fail, indicating that the internal stability of geosynthetic walls has been greater than one could expect based on what is currently known.

Each of the walls was characterized globally with respect to internal level of safety, or resistance-demand (RD) ratio. The geosynthetic walls in these case histories that performed well appear to be significantly under-designed relative to the design that would result from using current North American design codes and practices. Even when sources of conservatism are considered, such as soil parameter selection and imperfect matching of the reinforcement strengths to the demand (Simplified Method), the Simplified Method still appears to require approximately 1.5 to 4 times as much geosynthetic reinforcement as would to be needed to achieve acceptable performance based on the actual long-term performance of many walls.

This analysis indicates that there would be significant benefit in reevaluating the current approach used to design geosynthetic walls for internal reinforcement rupture. Furthermore, designers who use the Simplified Method should consider the “hidden” conservatism that results

from current design practices applied to geosynthetic walls. For example, a more aggressive approach to the selection of soil design parameters and matching of the reinforcement strength to demand should be considered.

3.0 SHORT-TERM STRAIN AND DEFORMATION BEHAVIOR OF GEOSYNTHETIC WALLS AT WORKING STRESS CONDITIONS

3.1 Introduction

The previous chapter summarized a number of geosynthetic wall case histories and evaluated the internal stability of those case histories from a global perspective. That global analysis revealed substantial design conservatism exists in how design parameters are selected, how the design procedures are applied, and in the design procedure itself. It is possible that the conservatism in the design procedure alone could produce 1.5 to 4 times the amount of reinforcement needed to obtain good, long-term performance.

To better understand the generally good performance of geosynthetic reinforced walls (in some cases after 25 years in service) and to quantify this performance in a way that can be used to develop improved design procedures, it is valuable to review available data on the loads and strains that have been recorded in carefully instrumented and monitored structures. Measured strains and loads can then be used to guide the development of improved design methods that will result in less conservative designs while ensuring satisfactory long-term performance.

To determine actual geosynthetic reinforcement loads, the strain in the reinforcement must be measured and strain readings correctly interpreted. This chapter reviews the strain measurement techniques that were used, how measurements were interpreted, accuracy of reinforcement strain measurements, and some advantages and disadvantages of different reinforcement strain instrumentation techniques. In addition, the relationship between measured wall facing deflections and reinforcement strains is examined.

The strain data reported in this study are used in a later chapter to estimate loads in reinforcement layers and finally to support a new geosynthetic wall design methodology.

3.2 Geosynthetic Wall Case Histories

Only the case histories reported in Chapter 2.0 that have good quality reinforcement and strain data, as well as wall deformation measurements, are considered. The key characteristics of each of these case histories are summarized in Table 3.1. Additional details of each wall can be found in Chapter 2.0. Table 3.2 summarizes the instruments used to measure the strains in the

walls. The case histories in the tables span the past 18 years and include a range of wall heights (3 to 12.6 m), surcharge conditions, reinforcement types, and arrangement. Most of the walls used geogrid reinforcement products, although some employed woven geotextiles and one a nonwoven geotextile.

Table 3.1. Summary of geometry for selected case histories.

Wall Case No.	Case History	Date Built	Wall Height (m)	Surcharge Conditions
GW5	Tanque Verde Tensar Concrete Panel Wall	1984	4.9	None
GW7	Oslo, Norway (Tensar) Walls (Sections J and N)	1987	4.8	3 m steeply sloping soil surcharge
GW8	Algonquin Tensar Concrete Panel Wall	1988	6.1	2.1 m sloping surcharge
GW9	Algonquin Miragrid Modular Block-Faced Wall	1988	6.1	2.1 m sloping surcharge
GW10	Algonquin Geotextile Wrapped-Face Wall	1988	6.1	None
GW11	RMCC Geogrid Wrapped-Face Full-Scale Test Wall	1986	2.85	0.7 m soil surcharge
GW12	RMCC Full Height Propped Plywood Panel Full-Scale Test Wall	1987	3	Full test wall top coverage with air bag loading system, up to effective pressure of 42 kPa
GW13	RMCC Incremental Plywood Panel Full-Scale Test Wall	1987	3	Full test wall top coverage with air bag loading system, up to effective pressure of 42 kPa
GW14	RMCC Full Height Propped Panel Full-Scale (Tensar) Test Wall	1989	3	Full test wall top coverage with air bag loading system, up to effective pressure of 70 kPa
GW15	RMCC Incremental Panel Full-Scale (Tensar) Test Wall	1989	3	Full test wall top coverage with air bag loading system, up to effective pressure of 60 kPa
GW16	WSDOT Rainier Avenue WrappedFace Geotextile Wall	1989	12.6	5.3 m sloping surcharge
GW17	London, Ontario Propped Panel (Tensar) Wall	1989	7.1	None
GW18	Fredericton, New Brunswick Propped Panel (Tensar) Wall	1990	6.1	None
GW20	Vicenza, Italy Welded Wire-Faced Geosynthetic Walls (HDPE test section)	1998	4	3.5 m steeply sloping soil surcharge
GW20	Vicenza, Italy Welded Wire-Faced Geosynthetic Walls (PP test section)	1998	4	3.5 m steeply sloping soil surcharge

Table 3.2. Summary of instrumentation details for measuring strain for each case history.

Wall Case No.	Strain Measurement Method	Gauge Type	Number of Measurement Points	Number of Gauges Per Point	Method used to Attach Gauges to Geosynthetic	Gauge Length (mm)	Gauge Calibration Method	Strain Gauge Calibration Factor	Reference for Details
GW5	Strain gauges (local reinforcement strain)	Bonded Resistance Strain Gauges: Micro Measurements Type CAE-06-25OUT-350	50 points distributed among two wall sections	2 (top and bottom)	AE-10 adhesive beneath entire gauge. Gauge was attached to the rib	6.3	In-isolation wide width test on specimens with gauge attached	1.0	Desert Earth 1987
GW7	Inductance coils (global strain)	Bison inductance coils, 54 mm in diameter and 7 mm thick	23 points Section J, 37 points Section N	2 (one at each end of the rib)	Bolted through small hole drilled through rib nodes	Length of rib between nodes (156 mm)	Laboratory calibration using physical measurements of distance in comparison to readings	1.0	Fannin 1998
GW8	Strain gauges (local strain)	Hottinger-Baldwin gauge 6/120 LY61	28 points	2 (top and bottom)	Micro Measurements M Bond 200 adhesive; attached to rib	60 mm	In-isolation wide width test on specimens with gauge attached	1.0	Christopher 1993
GW9	Strain gauges (local reinforcement strain)	Kyowa Dengyo high elongation foil gauge type KFE-5-C1	42 points	2 (top and bottom)	Tokyo Sokki Kenyujo Type CN cynoacrylate adhesive	5 mm	In-isolation wide width test on specimens with gauge attached	1.4	Bathurst et al. 1993
	Extensometers (global reinforcement strain)	Gloetzl extensometers	13 points	1	Not reported, but likely similar to method used for GW15 extensometers	Varies	N/A	1.0	Bathurst et al. 1993

Table 3.2. Continued.

Wall Case No.	Strain Measurement Method	Gauge Type	Number of Measurement Points	Number of Gauges Per Point	Method used to Attach Gauges to Geosynthetic	Gauge Length (mm)	Gauge Calibration Method	Strain Gauge Calibration Factor	Reference for Details
GW10	Strain gauges (local strain)	Hottinger-Baldwin gauge 10/120 LD20	28 points	2 (top and bottom)	Micro Measurements AE15 adhesive; attached only at ends of gauge	10 mm	In-isolation wide width test and in-soil tests on specimens with gauge attached	Approx. 1.5	Christopher 1993
GW11	Strain gauges (local strain)	Bonded resistance gauges: Showa Measuring Instruments Type Y11-FA-5-120	14 points	3 gauges on different ribs but at nominally identical distances from wall face	RTC epoxy beneath entire gauge	5 mm	In-isolation wide width test on specimens with gauge attached	1.33	Benjamin 1989, Lescoutre 1986, Bathurst et al. 1988
GW12 and GW13	Strain gauges (local strain)	Bonded resistance gauges: Showa Measuring Instruments Type Y11-FA-5-120	20 points	3 gauges on different ribs but at nominally identical distances from wall face	RTC epoxy beneath entire gauge	5 mm	In-isolation wide width test on specimens with gauge attached	1.05	Benjamin 1989

Table 3.2. Continued.

Wall Case No.	Strain Measurement Method	Gauge Type	Number of Measurement Points	Number of Gauges Per Point	Method used to Attach Gauges to Geosynthetic	Gauge Length (mm)	Gauge Calibration Method	Strain Gauge Calibration Factor	Reference for Details
GW14 and GW15	Strain gauges (local strain)	Bonded resistance gauges: Showa Measuring Instruments Type Y11-FA-5-120	24 points	3 gauges on different ribs but at nominally identical distances from wall face	RTC epoxy beneath entire gauge	5 mm	In-isolation wide width test on specimens with gauge attached	1.05	Benjamin 1989
	Extensometers (global strain)	Wire extensometers	16 points	1	Bolted to grid node with very small set screw	varies	N/A	1.0	Benjamin 1989
GW16	Strain gauges (local reinforcement strain)	Bonded resistance gauges: BLH, Inc., SR-4 type PA3 gauges for the PET geosynthetic, Tokyo Lokki Kenkyojo Ltd. YL-20 Gauges for the PP geosynthetics	45 installed (69% survived throughout wall life)	2 (top and bottom)	High elongation, low creep adhesive beneath entire gauge	50 mm for PA3 gauge, 31 mm for YL-20 gauge	In-isolation wide width test on specimens with gauge attached, tested at a strain rate of 1% and 10% per minute	1.4 for PET geosynthetics, 2.0 for PP geosynthetics	Allen et al. 1992, Boyle and Holtz 1998
	Extensometers (global reinforcement strain)	Glotzl Instrument Co. mechanical extensometer, with a fiberglass rod	14 (11 survived wall construction)	1	Wire placed through geosynthetic layer and glue at anchor head	varies	N/A	N/A	Allen et al. 1992

Table 3.2. Continued.

Wall Case No.	Strain Measurement Method	Gauge Type	Number of Measurement Points	Number of Gauges Per Point	Method used to Attach Gauges to Geosynthetic	Gauge Length (mm)	Gauge Calibration Method	Strain Gauge Calibration Factor	Reference for Details
GW17	Strain gauges (local reinforcement strain)	High elongation bonded resistance gauges: Kyowa Electronic Instruments Type KFE	20 points	1	RTC epoxy beneath entire gauge, mounted to rib	5 mm	In-isolation wide width test on specimens with gauge attached, tested at a strain rate of 2% per minute	1.25	Bathurst 1992
GW18	Strain gauges (local reinforcement strain)	Bonded Resistance Strain Gauges: Micro Measurements Type AE-13-125BT-120	12 (50% of the gauges survived construction)	2 (top and bottom)	Not reported	Not reported	Correction to gross strain was estimated based on similar work by Bathurst, 1992	1.25	Knight and Valsangkar 1993
GW20	Strain gauges (local reinforcement strain)	Bonded Resistance Strain Gauges: Tokyo Sokki KenkyujoType TFLA-5	63 points (62 gauges survived construction)	1	Gauge mounted to rib, near junction with cross rib, using cynoacrylate adhesive	5 mm	In-isolation wide width test on specimens with gauge attached, tested at various strain rates	1.05 for HDPE geogrid, 1.1 for PP geogrid	Carrubba et al. 1999

Although other wall case histories in the literature reported reinforcement strain readings, they are not listed in the tables. These case histories were deficient with respect to soil shear strength and/or reinforcement load-strain properties. Other walls used nonwoven geotextiles and lack site- and product-specific in-soil stiffness data. Walls with unusual or complicated boundary conditions were also omitted from this study.

Most of the case histories used redundant instrumentation schemes either in terms of multiple gauges at a given point and/or an independent measurement technique to verify measured strains (e.g., strain gauges and extensometers). In many of the cases, the strain gauge response was compared to global strains in the reinforcement by using in-isolation tensile tests. The comparison was used to quantify under-registration of average strain in the reinforcement as a result of gauge attachment method, gauge-reinforcement interaction, or variation of geosynthetic properties with location (e.g., integral drawn polyolefin geogrids). Where these data were available, correction factors (if required) could be applied to strain gauge readings to estimate global strains in the reinforcement. Global strain values are required to estimate loads in polymeric reinforcement materials from in-isolation isochronous tensile load-strain data.

Finally, many of the case histories reported wall face deformation measurements. These deformations were used to check the reasonableness of the reinforcement strain measurements.

3.3 Interpretation of Strain Measurements

Interpretation of strain or displacement readings from devices attached to geosynthetic reinforcement layers depends on the type of device (Perkins and Lapeyre 1997). The most common types of devices are strain gauges bonded directly to the surface of the geosynthetic reinforcement material and extensometers. Displacements recorded by pairs of extensometers are used to calculate global strains assumed to be constant over the distance between the monitoring points.

3.3.1 Strain Gauges

Small, high elongation strain gauges glued to the reinforcement material must be calibrated against the “true” global strain in the reinforcement. In this chapter “local strain” or “gauge strain” values refer to strains recorded by a strain gauge at the point of attachment. “Global strain” refers to strain averaged over a length that is much larger than the strain gauge or the

repeating structure of a geotextile or, in the case of a geogrid, one or more aperture lengths. Strain gauges bonded to woven geogrids or geotextiles typically generate a local "hard spot," causing under-registration of global tensile strains. Strain gauges bonded to integral drawn polypropylene (PP) and high density polyethylene (HDPE) geogrids will record the local strain at the attachment point, which may vary from point to point on the reinforcement material because of product geometry (cross-sectional area) and polymer modulus (a result of the drawing process during manufacture). The calibration factor for a particular combination of gauge, bonding technique, reinforcement type, and location of gauge is typically established from constant rate of strain, in-isolation, wide-width strip tensile testing (ASTM D 4595). Strain gauges may be mounted on one or both sides of the geosynthetic specimen during in-isolation tensile testing. Examples of in-isolation strain gauge calibration tests on four different products are illustrated in figures 3.1 to 3.4.

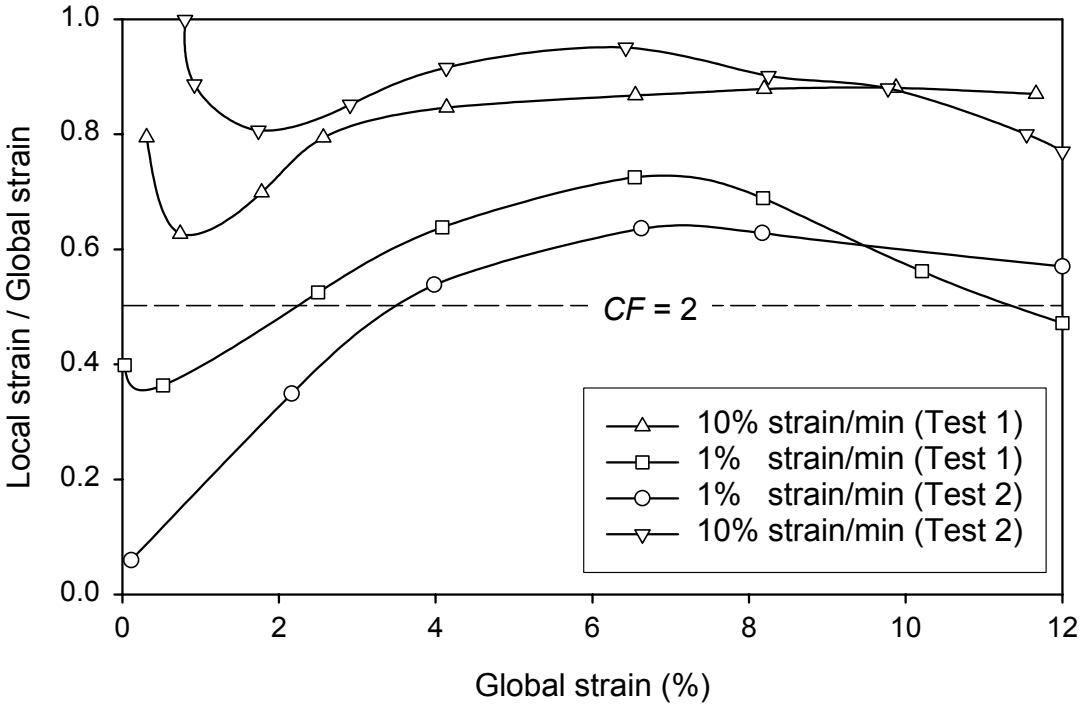

Figure 3.1. Ratio of local strain from strain gauges to global strain versus global strain for polypropylene woven slit film geotextile (adapted from Boyle and Holtz 1998). Note: *CF* = calibration factor.

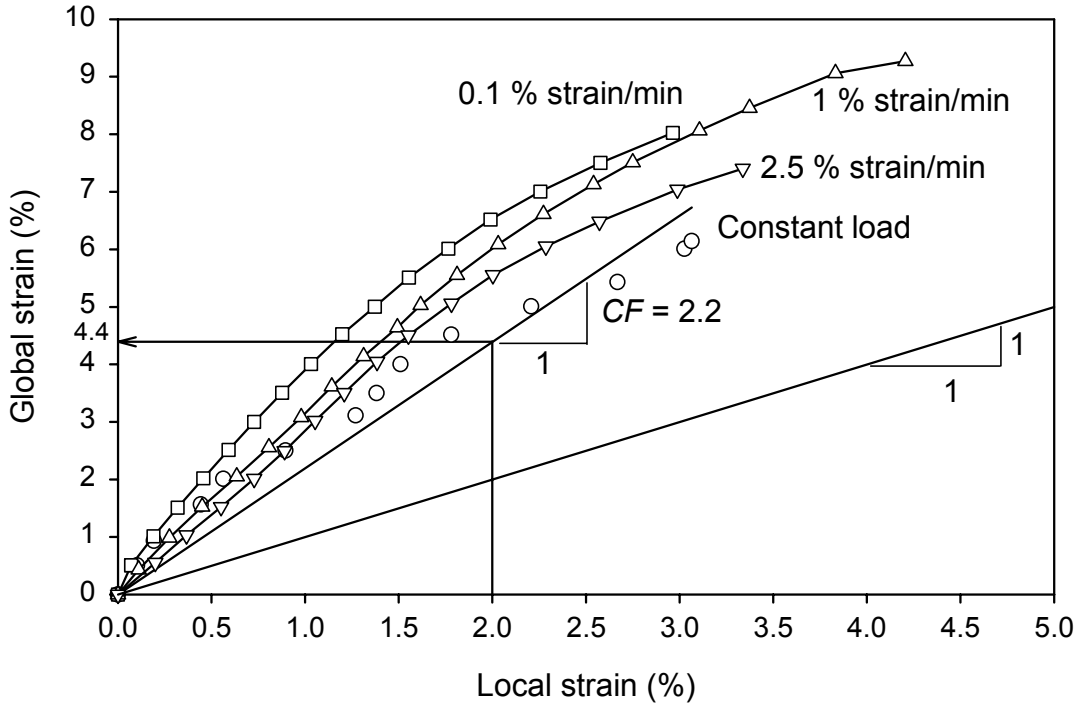

Figure 3.2. Example of in-isolation strain gauge response versus global strain for woven polyester (PET) geogrid (adapted from Saunders 2001). Note: *CF* = calibration factor.

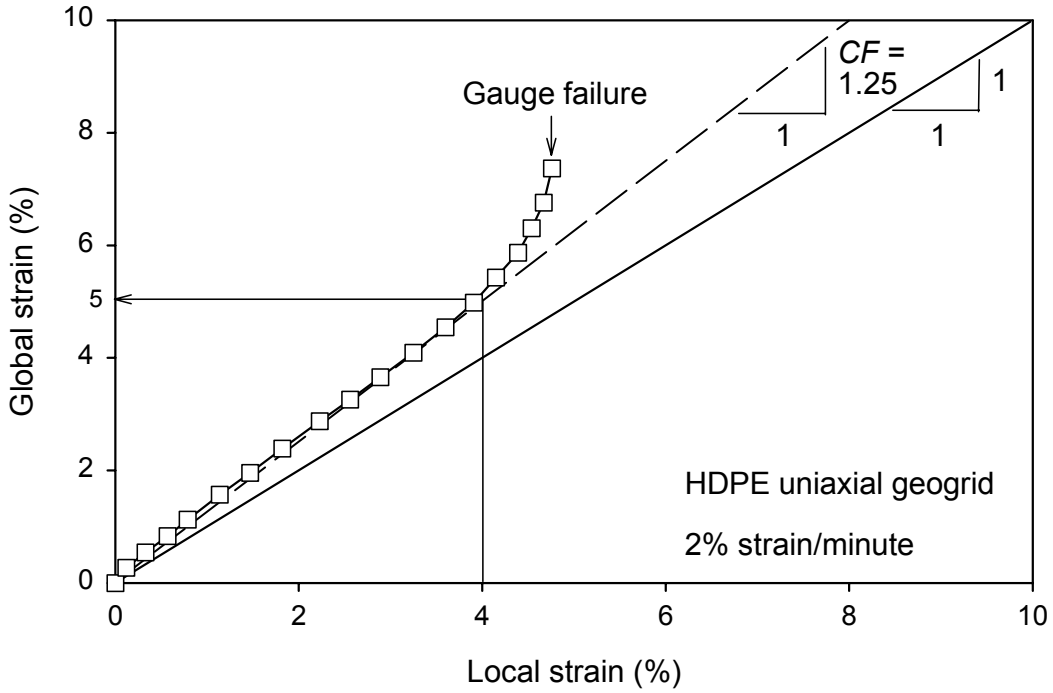

Figure 3.3. Example in-isolation global strain versus strain gauge response for HDPE geogrid (adapted from Bathurst 1992). Note: *CF* = calibration factor for local strain ≤ 4%.

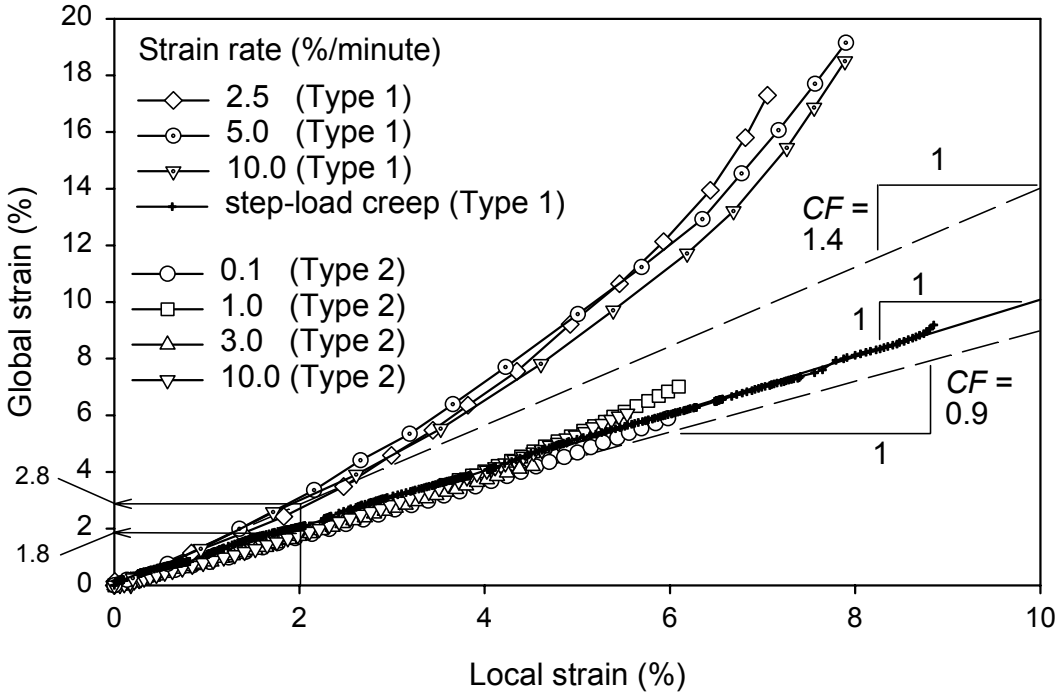

Figure 3.4. Example in-isolation global strain versus strain gauge response for PP biaxial geogrids. Notes: *CF* = calibration factor at 2% local strain. Type 1 - T_{ult} = 13 kN/m, $J_{2\%}$ = 250 kN/m. Type 2 (adapted from Bathurst et al. 2003) - T_{ult} = 19 kN/m, $J_{2\%}$ = 375 kN/m using ASTM 4595 method of test.

Figure 3.1 reports data for a polypropylene woven slit film geotextile that was used in the Rainer Avenue wall (GW16). Strain gauges 30 mm long were centered over an instrumented 75 mm length of specimen (Boyle and Holtz 1998). The data show the ratio of strain gauge reading to global strain reading as a function of global strain. A ratio of 1.0 represents perfect correspondence between strain gauge readings and global strain. The data show that the magnitude of under-registration varied widely with rate of loading and magnitude of global strain, and that the registration (calibration) factor (CF) varied between nominally identical tests. The differences between calibration curves for the multiple tests in Figure 3.1 are likely due to a combination of variations in the specimen stiffness, as well as the properties and thickness of the glue and waterproof coating used. A single-value calibration factor from these data over a range of 4 percent strain is about 2. In other words, the strain gauge values must be doubled to represent "true" global strains. Clearly, interpretation of strain gauge readings can be problematic for woven geotextiles, and any strain gauge readings should be corroborated by extensometer or inductance coil readings in the field, or at least multiple strain gauges at

nominally identical locations to provide adequate redundancy. For the Rainier Avenue wall, a calibration factor CF = 1.4 to 2.0 was used to convert measured strain gauge strains to true global strains after in-isolation strain data had been reviewed and measured strain gauge readings in-situ had been compared with corresponding extensometer readings.

Figure 3.2 shows similar data for a knitted polyester (PET) geogrid with an index strength of T_{ult} = 16 kN/m (Saunders 2001). The response curves for constant rate of strain tensile loading fall within a relatively narrow band. The significant under-registration of global strains is considered to be the result of the impregnation of the longitudinal polyester fiber bundles by gauge epoxy glue, which creates a locally stiff region in the longitudinal member (a "hard spot"). Also shown on the figure are data from a constant load (creep) test. The calibration factor for the constant rate of loading test is about CF = 2.2 and is a lower bound on the constant rate of strain calibration curves. It can be argued that the actual loading history of a reinforcement layer during construction falls between the two idealized loading conditions performed in the laboratory. Case study GW9 describes a wall with a woven PET geogrid as the reinforcement. The calibration factor from a single constant rate of tension test gave CF = 1.4. The difference in magnitude of calibration factor between the two products may be attributed to differences in geogrid manufacture, strength, strain gauge type, and gauge adhesive.

In Figure 3.3 the strain registration response of a typical calibration tensile test on an extruded, drawn uniaxial HDPE geogrid is presented (Bathurst 1993). The gauges in this case study (GW17) were mounted directly on longitudinal members at the mid-point between cross-members. These data show a reasonably constant calibration factor of CF = 1.25 up to a global strain of 4 percent. The non-linearity in the response thereafter may be related to debonding of the gauge from the geogrid surface.

Figure 3.4 shows strain calibration data for two different extruded, drawn PP geogrids. Type 1 is very similar to the material used in the RMC test walls (GW14 and GW15). Type 2 material is from the same family of products as Type 1 but with a higher stiffness and strength. The gauges were mounted at the mid-point between transverse members. For both sets of in-isolation constant-rate-of-strain data, the strain gauge readings were independent of rate of strain testing. However, the magnitude of calibration factor increased with magnitude of global strain. A stepped constant load test was also carried out on the Type 1 material, which gave a one-to-one correspondence between global and local strain values (CF = 1). In this test the load history was

applied in increments that were held constant for about 100 hours to simulate the loading history in typical full-scale test walls at the RMC as a result of stepped-uniform surcharge loading (Bathurst et al. 2000). Benjamin (1989) reported that constant-rate-of-strain tests with the PP geogrid product used in the RMC walls (GW14 and GW15) also produced a calibration factor close to unity (i.e. CF =1.05) (Table 3.2). The data in Figure 3.4 illustrate that for the same manufacturer product type, significant differences in calibration factor are possible even when the same strain gauge type and attachment technique are used.

On the basis of a review of available in-isolation tensile strain gauge calibration test data the following observations can be made:

1. The magnitude of strain gauge under-registration (and hence magnitude of calibration factor CF) at a local strain of 2% is greatest for woven geotextiles or knitted geogrids and least for extruded, drawn HDPE geogrids.
2. Variability in strain gauge response is greatest for woven geotextiles.
3. Non-linearity in CF values with magnitude of global strain is greatest for woven geotextiles and geogrids and least for uniaxial HDPE geogrids.
4. In all cases reviewed the magnitude of the calibration factor was 1.0 or better (i.e., CF ≥ 1).
5. In-isolation constant load calibration tests for the two cases reviewed in this study produced lower CF values than the results for the same materials tested under constant rate of strain conditions.

The experience of the writers with strain gauge installation techniques and the interpretation of strain readings from actual field monitoring has led to several important observations. Flexure of reinforcement longitudinal members in the direction of loading may cause additional strain at the gauge location or may attenuate strains, depending on the direction of flexure. For example, local bending may occur as the longitudinal members of stiff, extruded geogrids are compressed flat under soil lifts. In addition, local contact with gravel or cobble particles can cause a local increase or attenuation of strain gauge readings. Flexure of the reinforcement at the connections with hard facings may tend to reduce strain readings because of convex-down reinforcement geometry or may increase strain readings near the wrapped face for flexible geosynthetic-faced walls because of convex-up geometry. A strategy to avoid flexure-induced strain readings is to attach bonded gauges in pairs on opposite sides of the reinforcement and to arrange the two

gauges in a bridge completion that gives a pure tension strain (Gnanendran and Selvadurai 2001). The majority of the case studies included in this investigation in which strains were measured with strain gauges utilized pairs of gauges to account for bending. Other case histories reported herein did use single gauges, but additional gauges were placed in the wall at nominally identical locations for redundancy.

Finally, it is also possible that strain gauges can malfunction because of electronic problems resulting from exposure to moisture, damage during the reinforcement installation and backfilling process, or debonding of the gauge from the reinforcement because of glue failure. Allen et al. (1992) provided a detailed assessment of these issues as they were applied to Wall GW16. Judgment is often required to identify strain gauge readings that may misrepresent global strains in the reinforcement for the reasons noted above.

3.3.2 In-situ Global Strains from Extensometer Readings

A correction factor is not needed if extensometers are mounted to the geosynthetic. Nevertheless, strains inferred from extensometers may overestimate geosynthetic yarn or rib strains because of initial surface wrinkles or warps in the geosynthetic that occur during placement or may under-estimate strains because of initial slackness in the extensometer cables.

3.3.3 Other Devices

In one case study (GW7), inductance coil pairs attached to and in the same plane as the geogrid reinforcement were used to infer strains. Average global strains based on sets of three devices located at the same nominal distance from the wall face were as great as 0.9 percent at the end of surcharging (Fannin and Hermann 1990) and were reported to have a resolution of ±0.1 percent (Fannin 1988). These devices are calibrated in-isolation and do not require a correction factor. However, the signal from inductance coil pairs is sensitive to the magnitude of out-of-plane movements that may be generated under the conditions described earlier regarding sources of flexure-induced strain gauge readings.

3.3.4 Redundancy of Reinforcement Measurements

In several case studies, multiple strain gauges were placed at nominally identical locations from the wall facing. This approach allows readings to be averaged across the width of the wall

and also provides redundancy in the event of failure of an individual gauge in a set of two or more gauges. Data showing variation in strain gauge response for nominally identical gauges are not reported for the case studies considered herein. However, data from recent full-scale polypropylene and polyester geogrid reinforced soil walls reported by Bathurst et al. (2000,2001) do give a quantitative indication of the variation in strain gauge response that may be expected *in-situ* under carefully controlled laboratory conditions corresponding to the RMCC test walls in the current study.

Figure 3.5 shows that the uncorrected response of a pair of strain gauges mounted on a PP geogrid may vary by about ±15 percent of the mean reading of 2 percent strain at a prediction level of 95 percent. Here the prediction limits on the figure represent the range of gauge strain values that would be expected for any single point value on the X-axis with a 95 percent probability of occurrence if a new set of readings were taken.

Coefficients of variation (*COV*) values can also be calculated for different ranges of average strain in Figure 3.5. *COV* values are calculated here as the standard deviation of the ratio of Y/X divided by the mean of Y/X values where Y and X denote vertical and horizontal axis values for each data point. The mean of Y/X values is simply one in this data set. For average strain values greater than 0.01 percent, *COV* = 29 percent, but it reduces to *COV* = 13 percent for average strain values greater 0.02 percent. A similar analysis of data reported by Saunders (2001) for the same strain gauges mounted on a knitted PET geogrid reinforcement layers (Bathurst et al. 2001) produced *COV* = 23 percent and 14 percent for average strain readings greater than 0.02% and 0.1 percent, respectively. The higher threshold strain level needed to obtain similar levels of reliability for similar strength PET and PP products (0.02 percent and 0.1 percent, respectively) is consistent with the observation that the structure of drawn polyolefin geogrids is much simpler than that of a multi-filament knitted polyester product.

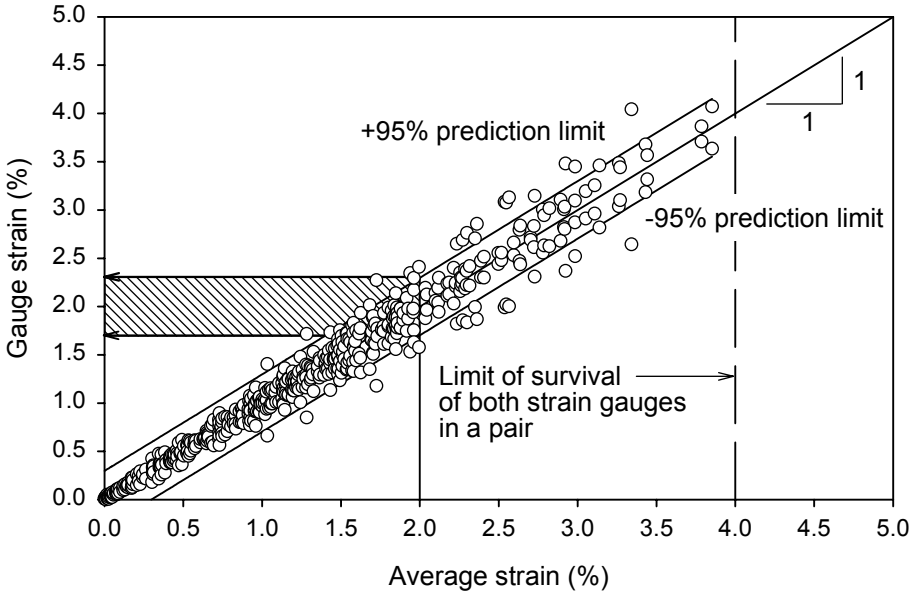

Figure 3.5. Variation in strain gauge response versus average of strain gauge pair mounted at nominally identical positions on a PP geogrid (adapted from Burgess 1999).

One strategy for providing a check on strain gauge readings is to use strain gauges and extensometers. An example of the variation between uncorrected strain gauge readings and in-situ strains using pairs of extensometer points bracketing each strain gauge location is shown in Figure 3.6 from one of the full-scale walls described above (Burgess 1999). The data show that in this carefully controlled experiment there is a linear correspondence between gauge strain readings and extensometer strains measured in-situ. The strain gauge readings vary by ±0.6 percent strain of the extensometer values over the entire range of extensometer data at a 95 percent prediction level. In general, the correspondence is better for extensometer strains ≥ 2 percent strain after possible local bending of the geogrid and slackness in the extensometer cables have been taken out. Assuming that strain gauge readings are accurate, it is possible to estimate the reliability of the extensometer readings. For example, the *COV* value calculated from the data set in Figure 3.6 is 9 percent for extensometer strains ≥ 2 percent. The accuracy of extensometers was marginal at lower strain levels (i.e. *COV* = 56 percent for 0.2 to 1 percent strain, *COV* = 38 percent for 0.5 to 1 percent, and *COV* = 23 percent for 1 to 2 percent strain). Note that *COV* values calculated here are independent of the constant *CF* value multiplier required to correct the strain gauge readings.

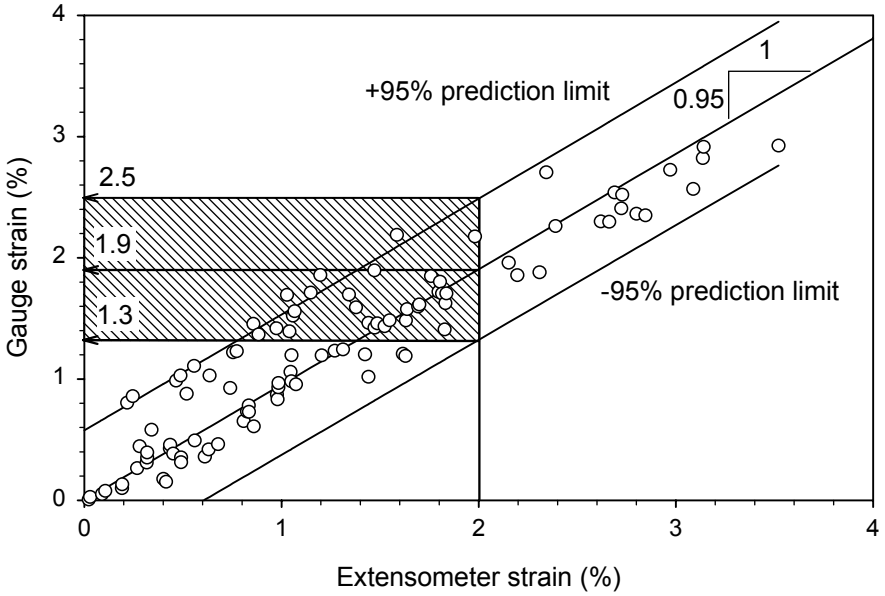

Figure 3.6. Average response of uncorrected strain gauge pair strain readings versus strain calculated from extensometer measurements at the same nominal distances from the wall face on layers of PP geogrid (adapted from Burgess 1999).

Corrected peak strain gauge readings in the current case studies can also be compared to peak in-situ extensometer strain measurements (if available). Figure 3.7 shows generally good agreement between the two types of strain measurement, although there are a few points in which the strain gauge values appear to be too high, which may be due to the reasons noted above. In this data set, the strain gauge readings vary by ±0.4 percent strain from extensometer values over the range of extensometer data at a 95 percent prediction level. The *COV* value calculated from the data set in Figure 3.7 is 29 percent for extensometer readings in the range 0.2 to 1 percent strain.

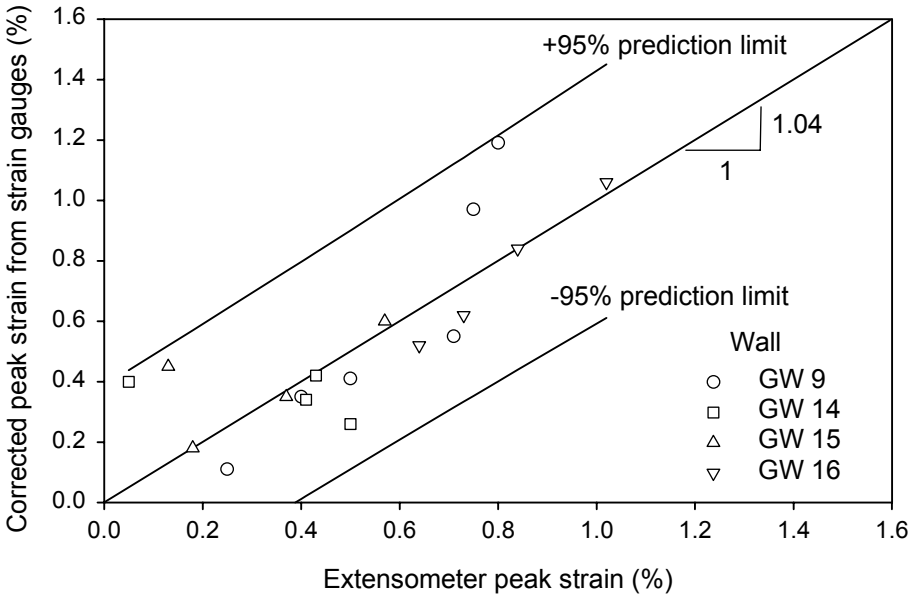

Figure 3.7. Comparison of in-situ corrected peak strain gauge values with peak strains calculated from extensometer pairs at nominal identical distances behind wall face. Note: Readings taken at the end of construction under working load conditions.

On the basis of the *COV* values for the data in figures 3.5 through 3.7, it can be concluded that corrected strain gauge readings are sufficiently accurate (i.e., *COV* < 15 percent) for strains of greater than 0.02 percent for integrally drawn polyolefin geogrids, 0.1 percent strain for woven PET geogrids, and extensometer strains for strains of greater than 2 percent.

In case history (GW7), inductance coil readings were used to calculate reinforcement strains. On the basis of the data reported by Fannin (1988), the calculated variabilities in strain measurements for average strains in excess of 0.1 percent and 0.2 percent were *COV* = 40 percent and 32 percent, respectively.

Estimated minimum resolution strains and the reliability of different instrument types using the data available are summarized in Table 3.3.

Table 3.3. Summary of estimated resolution and reliability of instrument readings.

Reinforcement type	Instrument type	Resolution strain (%)	Reliability		
			Strain range (%)	*COV* (%)	Data source
PP geogrid	Strain gauge	±0.01	> 0.01 > 0.02	29 13	Figure 5
PET geogrid	Strain gauge	±0.02	> 0.02 > 0.1	23 14	Saunders (2001)
PP geogrid	Extensometer	0.2	0.2 – 1 0.5 – 1 1 – 2 > 2	56 38 23 9	Figure 6
PET/PP geogrids and woven PP/PET geotextiles	Extensometer	- *	0.2 – 1	29	Figure 7
HDPE geogrid	Inductance coil	±0.1	> 0.1 > 0.2	40 32	Fannin (1988)

Note: * A minimum resolution value is not attempted here because data are for different reinforcement-extensometer combinations.

3.3.5 Distribution of Strains at the End of Construction

For all walls the peak (maximum) strain readings were determined from inspection of strain readings along the length of the reinforcement layer, with the exception of strains in the immediate vicinity of the facings (i.e., near the connections) or at locations where the facing slumped for wrapped-face walls. Hence, the possibility of reinforcement curvature effects on the magnitude of strain gauge readings was minimized.

Examples of strain distributions are shown in figures 3.8 to 3.10. Figure 3.8 is from case study GW16 – the Rainier Avenue wrapped-face geotextile wall. The strain gauge readings in the figure are uncorrected and are generally lower than those reported from interpretation of extensometer readings, which is consistent with the results of the in-isolation testing of woven geotextiles discussed in Section 3.3.1. However, the focus here is on the distribution of strains, which in this case study were generally coincident with a potential log-spiral internal failure surface through the reinforced soil zone. Note that for the second instrumented layer in case study GW16, the maximum strain locations indicated by extensometers and strain gauges were different. However, the strain gauge readings that caused this difference were identified as questionable, which is explained in detail by Allen et al. (1992). In the summary data to follow, peak strains for this particular wall have been taken from the internal locations roughly

coincident with the hatched area in the figure. This wall provides an example of the need for correct interpretation of strain data, based on redundant strain measurement systems, analysis of gauge behavior, and overall development of strain patterns within the wall.

Figure 3.9 shows strain distributions recorded under a uniform 50 kPa surcharge (working stress level) for nominally identical walls constructed with a propped panel face and an incremental panel face (Case studies GW14 and GW15, respectively). The data illustrate the influence of facing type on the distribution of strains in the reinforcement. For the propped panel wall the strains were largest at the connections as a result of downward movement of the soil behind the connections as the wall facing rotates outward. The incremental panel wall was constructed with panels that had some vertical compressibility, and as a result, peak strains no longer occurred at the connections in the top two layers.

Figure 3.10 shows strain distributions from uncorrected strain gauge readings for a modular block-faced wall (Case study GW9) taken immediately after surcharge loading. The data show distinct peaks. One peak is at the facing and the other peaks are within the soil mass. There was no systematic change in the magnitude of strains with the exception of the facing, where connection strains decreased, perhaps as a result of reinforcement stress relaxation with time and possible redistribution of load between reinforcement layers.

In the chapters to follow, a distinction is made between strains generated in the reinforcement layers because of lateral earth pressures and those generated as a result of local facing effects (e.g., down-drag forces as the reinforced fill moves down with respect to the facing). Peak strain readings that occurred immediately at the facing were generally disregarded in favor of peak strain readings within the soil reinforced zone in order to correlate peak strain levels in the reinforcement to reinforced soil properties.

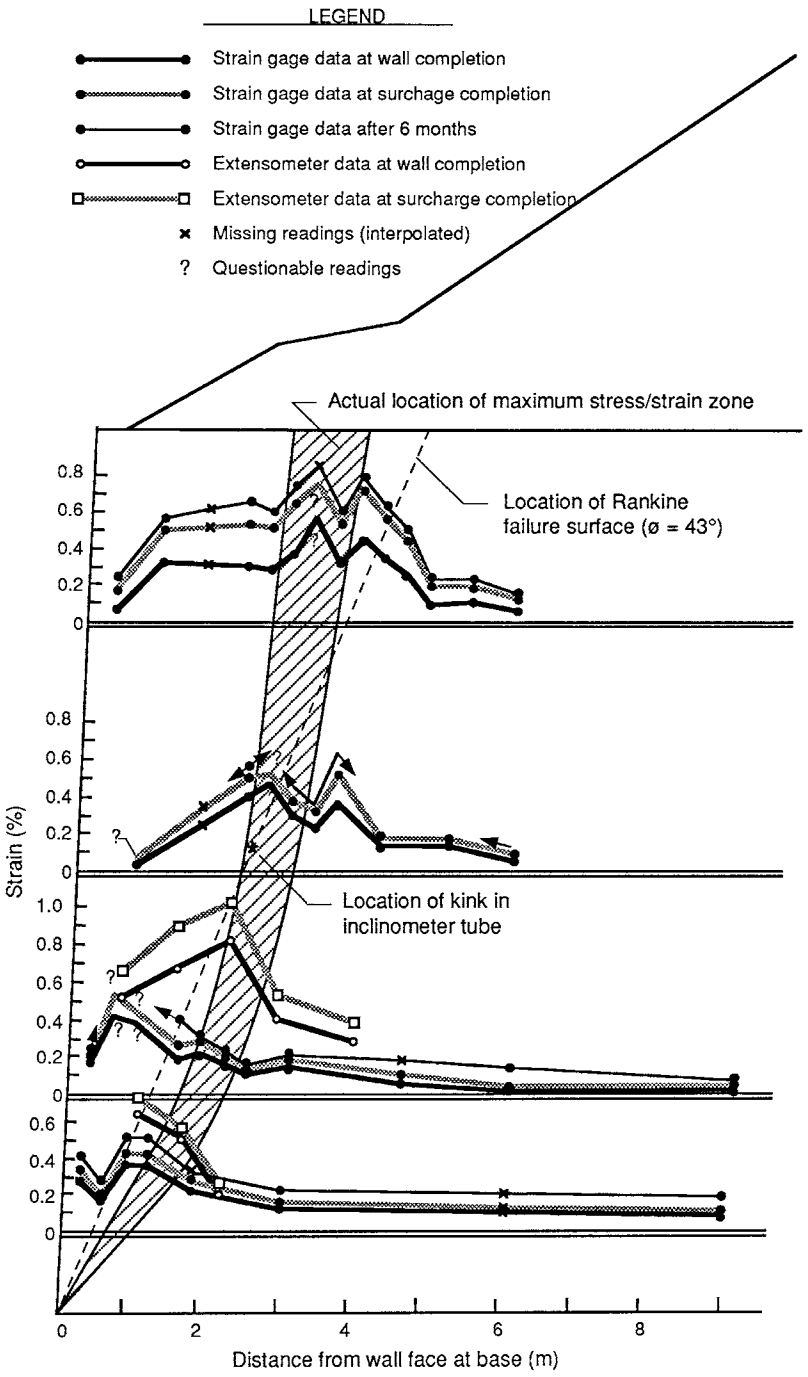

Figure 3.8. Strain distributions (strain gauge readings as plotted are uncorrected) recorded for Rainier Avenue Wall (Allen et al. 1992).

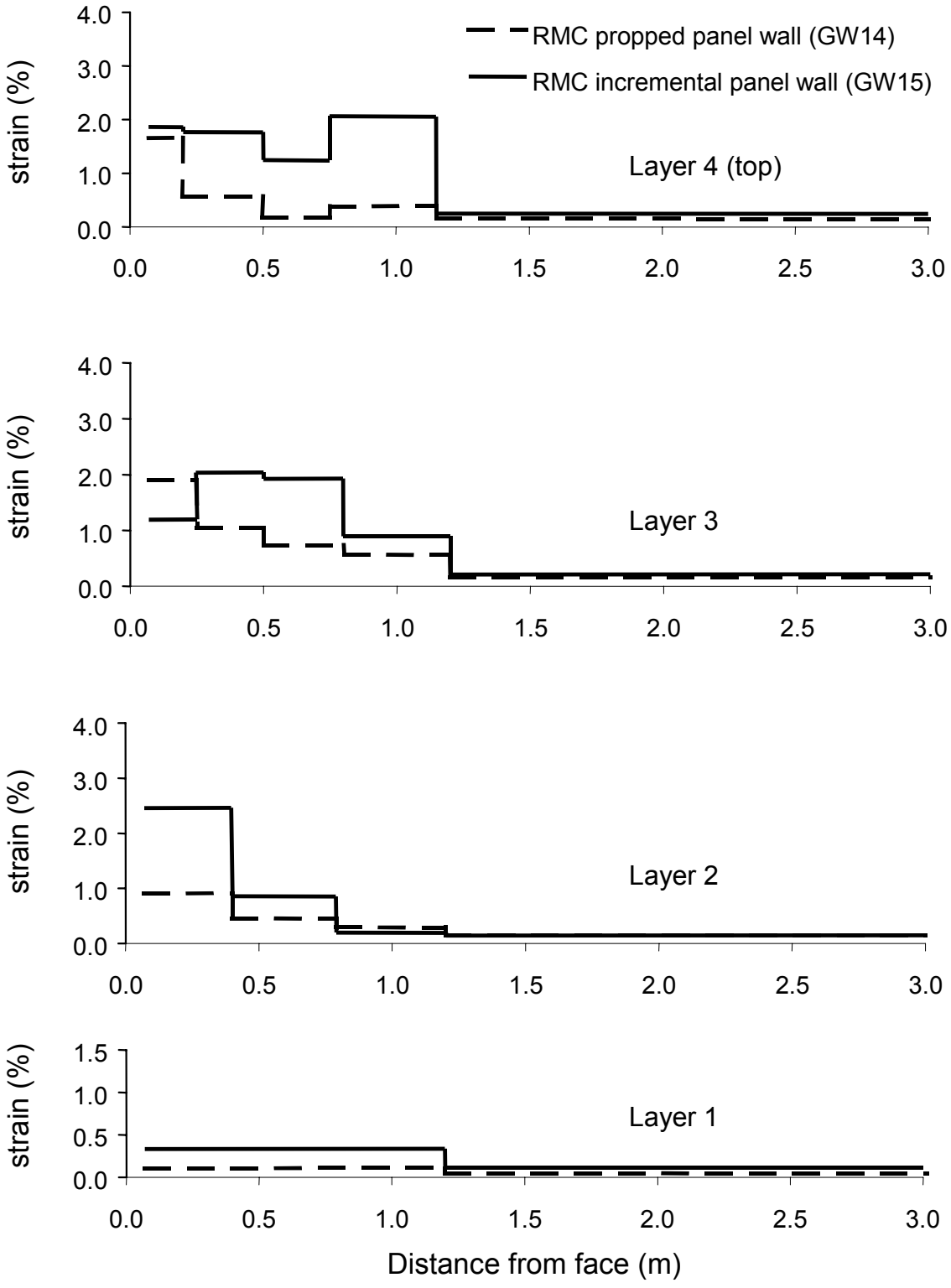

Figure 3.9. Summary of reinforcement strains at 50 kPa surcharge load for the RMCC propped panel and incremental panel walls (after Benjamin 1989).

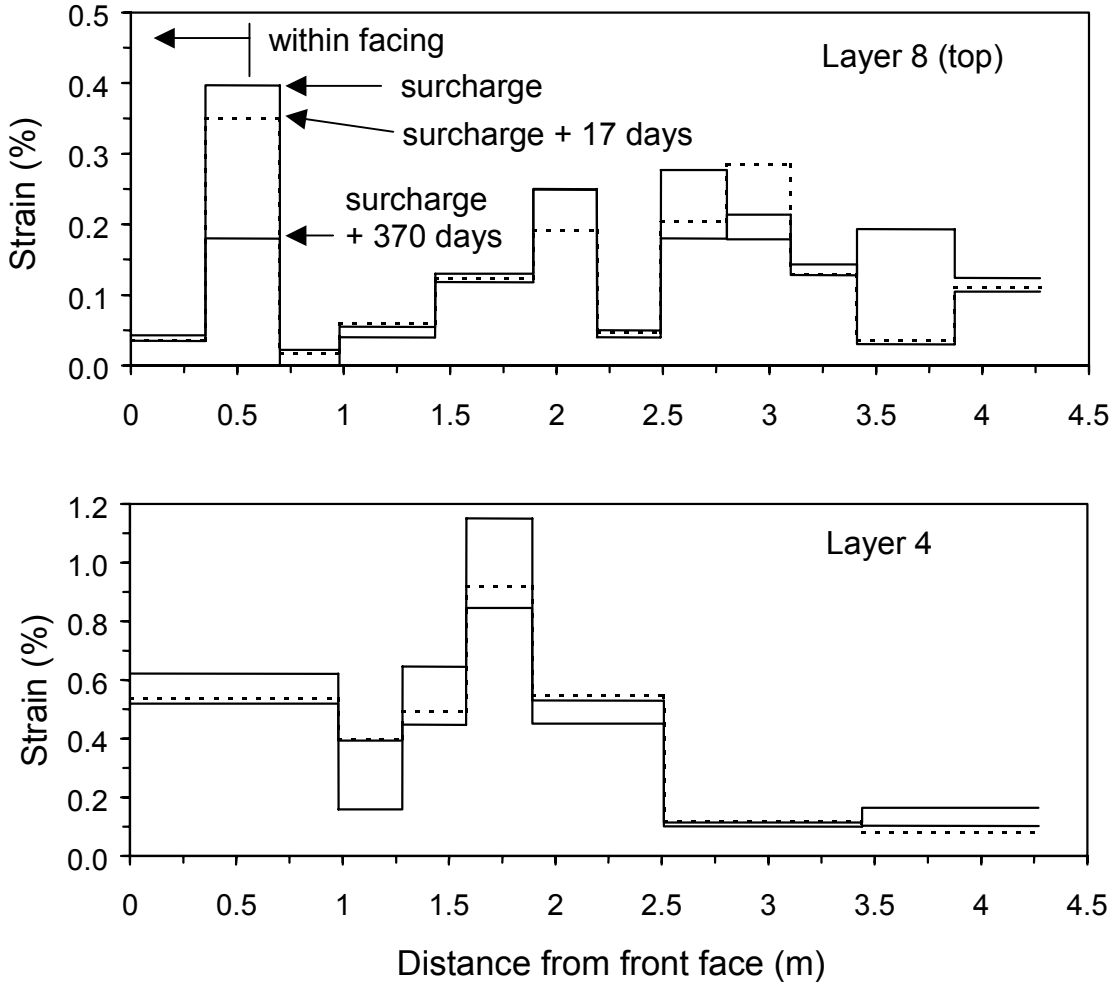

Figure 3.10. Summary of reinforcement strains for modular block-faced wall after end of construction with 2.1-m sloped surcharge (Case study GW9, uncorrected strains) (after Bathurst et al. 1993b).

3.3.6 Summary of Short-Term Peak Strains from Case Studies

Tables 3.4 through 3.18 summarize global strains from extensometers, inductance coils, and corrected local strain measurements (if applicable) for the case studies identified earlier. The readings correspond to end of construction (which in some case studies included a surcharge). These tables provide case-specific comparisons, where such comparisons could be made, between different methods of strain estimation or measurement, illustrating the use of redundant measurement systems. The data presented in these tables can also be used, in conjunction with an appropriate reinforcement stiffness, to estimate wall reinforcement loads, given both the

magnitude and accuracy of the measurements, to assess the accuracy of current or proposed internal wall stability design methods (see Chapter 5).

Table 3.4. Measured peak strains in the geosynthetic reinforcement for the Tanque Verde wall (GW5).

Event	Depth Below Wall Top (m)	Measured Strain from Strain Gauges (%)	Strain Gauge Calibration Factor from Lab Testing	Calibrated Strain from Strain Gauges (%)
End of wall construction	1.14	0.18	1.0	0.18
	3.28	0.33	1.0	0.33
	4.2	0.25	1.0	0.25

Table 3.5. Measured peak strains in the geosynthetic reinforcement for the Oslo Wall, Section J (GW7).

Event	Depth Below Wall Top (m)	Global Strain from Inductance Coils (%)
End of wall construction	1.2	0.37
	2.4	0.42
	3.6	0.26
	4.2	0.28
	4.8	0.08
Completion of Surcharge	1.2	0.52
	2.4	0.70
	3.6	0.28
	4.2	0.79
	4.8	0.10

Table 3.6. Measured peak strains in the geosynthetic reinforcement for the Oslo Wall, Section N (GW7).

Event	Depth Below Wall Top (m)	Global Strain from Inductance Coils (%)
End of wall construction	0.6	0.66
	1.2	0.56
	1.8	0.37
	2.4	0.52
	3.0	0.63
	3.6	0.43
	4.2	0.43
	4.8	0.30
Completion of Surcharge	0.6	0.92
	1.2	0.82
	1.8	0.78
	2.4	0.79
	3.0	0.80
	3.6	0.79
	4.2	0.70
	4.8	0.31

Table 3.7. Measured peak strains in the geosynthetic reinforcement for the Algonquin HDPE geogrid wall (GW8).

Event	Depth Below Wall Top (m)	Measured Strain from Strain Gauges (%)	Strain Gauge Calibration Factor from Lab Testing	Calibrated Strain from Strain Gauges (%)
End of wall construction	1.2	0.35	1.0	0.35
	2.5	0.71	1.0	0.71
	4.2	0.76	1.0	0.76
	5.0	0.74	1.0	0.74
	5.7	0.18	1.0	0.18

Table 3.8. Measured peak strains in the geosynthetic reinforcement for the Algonquin PET geogrid wall (GW9).

Event	Depth Below Wall Top (m)	Measured Strain from Strain Gauges (%)	Strain Gauge Calibration Factor from Lab Testing	Calibrated Strain from Strain Gauges (%)	Global Strain from Extensometers (%)
End of wall construction	0.8	0.08	1.4	0.11	0.25
	2.6	0.29	1.4	0.41	
	4.0	0.29	1.4	0.41	0.50
	5.2	0.39	1.4	0.55	0.71
	5.8	0.11	1.4	0.15	
Completion of Surcharge	0.8	0.25	1.4	0.35	0.40
	2.6	0.65	1.4	1.91	
	4.0	0.85	1.4	1.19	0.80
	5.2	0.69	1.4	0.97	0.75
	5.8	0.19	1.4	0.27	

Table 3.9. Measured peak strains in the geosynthetic reinforcement for the Algonquin geotextile wall (GW10).

Event	Depth Below Wall Top (m)	Measured Strain from Strain Gauges (%)	Strain Gauge Calibration Factor from Lab Testing	Calibrated Strain from Strain Gauges (%)
End of wall construction, before water at wall face released	1.0	1.4	1.5	2.1
	2.6	1.2	1.5	1.8
	4.2	1.25	1.5	1.9
	4.9	0.95	1.5	1.4
	5.65	0.75	1.5	1.1
End of wall construction, after water at wall face released	1.0	2.0+	1.5	3.0+
	2.6	2.0+	1.5	3.0+
	4.2	1.35	1.5	2.0
	4.9	1.05	1.5	1.6
	5.65	0.75	1.5	1.1

Table 3.10. Measured peak strains in the geosynthetic reinforcement for the RMCC geogrid, wrapped–face, full-scale test wall (GW11).

Event	Depth Below Wall Top (m)	Measured Strain from Strain Gauges (%)	Strain Gauge Calibration Factor from Lab Testing	Calibrated Strain from Strain Gauges (%)
End of wall construction	0.6	1.48	1.33	1.97
	1.35	2.00	1.33	2.66
	2.1	0.94	1.33	1.25
	2.85	0.15	1.33	0.20

Table 3.11. Measured peak strains in the geosynthetic reinforcement for the RMCC full height, plywood panel, full-scale test wall (GW12).

Event	Depth Below Wall Top (m)	Measured Strain from Strain Gauges (%)	Strain Gauge Calibration Factor from Lab Testing	Calibrated Strain from Strain Gauges (%)
End of wall construction (no surcharge)	0.5	0.038	1.05	0.04
	1.25	0.019	1.05	0.02
	2	0.018	1.05	0.02
	2.75	0.008	1.05	0.01
With 50 kPa surcharge	0.5	0.66	1.05	0.50
	1.25	0.47	1.05	0.49
	2	0.31	1.05	0.33
	2.75	0.21	1.05	0.22

Table 3.12. Measured peak strains in the geosynthetic reinforcement for the RMCC incremental plywood panel, full-scale test wall (GW13).

Event	Depth Below Wall Top (m)	Measured Strain from Strain Gauges (%)	Strain Gauge Calibration Factor from Lab Testing	Calibrated Strain from Strain Gauges (%)
End of wall construction (no surcharge)	0.5	0.03	1.05	0.03
	1.25	0.26	1.05	0.27
	2	0.30	1.05	0.32
	2.75	0.32	1.05	0.34
With 50 kPa surcharge	0.5	0.76	1.05	0.8
	1.25	0.76	1.05	0.79
	2	0.57	1.05	0.6
	2.75	0.48	1.05	0.53

Table 3.13. Measured peak strains in the geosynthetic reinforcement for the RMCC full height, propped aluminum panel, full-scale test wall (GW14).

Event	Depth Below Wall Top (m)	Measured Strain from Strain Gauges Located at Extensometer Peak Strain (%)	Strain Gauge Calibration Factor from Lab Testing	Calibrated Strain from Strain Gauges Located at Extensometer Peak Strain (%)	Global Strain from Extensometers (%)
End of wall construction (no surcharge)	0.5	0.38	1.05	0.40	0.05
	1.25	0.32	1.05	0.34	0.41
	2	0.25	1.05	0.26	0.50
	2.75	0.40	1.05	0.42	0.43
With effective 70 kPa surcharge	0.5				2.93
	1.25				3.47
	2				2.00
	2.75				1.45

Table 3.14. Measured peak strains in the geosynthetic reinforcement for the RMCC incremental, aluminum panel, full-scale test wall (GW15).

Event	Depth Below Wall Top (m)	Measured Strain from Strain Gauges Located at Extensometer Peak Strain (%)	Strain Gauge Calibration Factor from Lab Testing	Calibrated Strain from Strain Gauges Located at Extensometer Peak Strain (%)	Global Strain from Extensometers (%)
End of wall construction (no surcharge)	0.5	0.17	1.05	0.18	0.18
	1.25	0.57	1.05	0.60	0.57
	2	0.33	1.05	0.35	0.37
	2.75	0.42	1.05	0.45	0.13
With effective 60 kPa surcharge	0.5				4.0
	1.25				4.15
	2				1.20
	2.75				0.42

Table 3.15. Measured peak strains in the geosynthetic reinforcement for the Rainier Avenue wall (GW16).

Event	Depth Below Wall Top (m)	Measured Strain from Strain Gauges (%)	Strain Gauge Calibration Factor from Lab Testing	Calibrated Strain from Strain Gauges (%)	Global Strain from Extensometers (%)
End of wall construction	3.1	0.57	2.0	1.14	
	6.5	0.46	2.0	0.92	
	9.6	0.42	2.0	0.84	0.84
	11.5	0.37	1.4	0.52	0.64
Completion of Surcharge	3.1	0.75	2.0	1.50	
	6.5	0.53	2.0	1.06	
	9.6	0.53	2.0	1.06	1.02
	11.5	0.44	1.4	0.62	0.73

Table 3.16. Measured peak strains in the geosynthetic reinforcement for the London, Ontario, propped panel, HDPE geogrid wall (GW17).

Event	Depth Below Wall Top (m)	+Measured Strain from Strain Gauges (%)	Strain Gauge Calibration Factor from Lab Testing	Calibrated Strain from Strain Gauges (%)	*Global Strain from Inclinometers (%)
End of wall construction	2.4	2.42	1.25	3.02	0.7
	4.23	1.58	1.25	1.97	0.5
	5.4	1.30	1.25	1.62	0.35
	6.33	0.70	1.25	0.87	0.3

*Obtained from differential movement between two inclinometers, one at face and one 1.5 m behind face. Because the strain in the wall was restricted by the prop restraint during wall construction, all movement recorded by the inclinometers should reflect movement that occurred in the reinforcement. Note that this is an average strain, yet it is known from the nature of propped panel walls that the highest strains will occur at the face, dropping rapidly with distance from the face. The available strain gauge data, though erratic, appear to indicate this type of strain pattern. It is estimated that the peak strains within this 1.5-m zone could be on the order of 50 to 70 percent higher than the average strain.

+Obtained at a point in time when the equilibrium condition was judged to occur after prop release. Because the soil behind the wall was frozen during the initial months of wall life after prop release, equilibrium was not reached until the following summer after construction. Note that the gauges were highly erratic, and some judgment was required to establish peak strains from the strain gauges.

Table 3.17. Measured peak strains in the geosynthetic reinforcement for the Fredericton, New Brunswick, full height, propped panel, HDPE geogrid wall (GW18).

Event	Depth Below Wall Top (m)	Measured Strain from Strain Gauges (%)	Strain Gauge Calibration Factor from Lab Testing	Calibrated Strain from Strain Gauges (%)
End of wall construction	2.44	0.33	1.25	0.43
	4.88	0.38	1.25	0.50

Table 3.18. Measured peak strains in the geosynthetic reinforcement for the Vicenza, Italy, welded wire-faced geosynthetic wall (GW20).

Wall Section	Event	Depth Below Wall Top (m)	Measured Strain from Strain Gauges (%)	Strain Gauge Calibration Factor from Lab Testing	Calibrated Strain from Strain Gauges (%)
1 (HDPE geogrid)	With soil surcharge	1.1	0.87	1.05	0.91
		2.7	1.42	1.05	1.49
2 (PP geogrid)	With soil surcharge	1.6	2.85	1.1	3.13
		3.2	1.84	1.1	2.02

3.4 Comparison of Wall Deformations with Strain Measurements

A strategy for checking the interpretation of reinforcement strains is to integrate reinforcement strains over the length of the reinforcement and to compare the result with wall deformations recorded at each reinforcement elevation during construction. Allen et al. (1992) attempted to make such a comparison for the Rainier Avenue Geotextile Wall (Wall GW16). An updated comparison is presented in Figure 3.11 with calibrated strain gauge data that were not available in 1992. Integration was accomplished by using the average values of the measured strain over the length segments, and the product of the average strain and the segment length was summed to estimate the total extension of the reinforcement layer. This approach assumes that there is no deformation at the free end of the reinforcement layer and that all of the reinforcement strain results in horizontal movement of the facing. The cumulative deformation from integration of the strains is compared to the lateral deflection measured at the wall face at the same elevation as the reinforcement layer and with respect to the time the reinforcement layer was installed. Hence, the curves in the figure are not wall deformation profiles but rather curves representing deflections measured (or estimated) from the time of installation of the reinforcement layer.

Figure 3.11 shows that there are significant differences between predicted wall deflections based on integrated strain measurements and surveyed deflections. Some of the discrepancy may be attributed to the accuracy of the wall face survey deflection measurements, which are typically on the order of $\pm$ 10 mm. However, in this particular case, lateral movements behind the wall were found to be small, 5 mm or less, and lateral movements below the wall were 10 mm or less (Allen et al. 1992). In addition, for wrapped-face walls, localized strains and

deflections due to face bulging between reinforcement layers can be significant. Allen et al. (1992) found that soil strains within the face wrap were as high as 7 percent based on Bison (inductance) coil measurements. These localized facing deformations could significantly affect the facing deflections measured by using the survey method, and they are likely the reason for the discrepancies between the curves in this case.

Similar data for the RMCC geogrid, wrapped-face wall (GW11) are presented in Figure 3.12**.** In this case the wall face deflections estimated from the integrated strain gauge data were greater than the measured lateral facing deflections. A large vertical spacing (0.75 m) was used between reinforcement layers in this wall, which resulted in vertical sagging of the wrapped face when each layer facing form was removed (Bathurst et al. 1988). This resulted in additional reinforcement strain that was not reflected in the lateral facing deformation (i.e., reinforcement strains were generated as a result of local vertical deformations, particularly at the top of the wall).

Figure 3.13 shows a comparison of measured lateral wall facing deflections versus estimated deflections from integrated strains for case study GW8, which was constructed with concrete panels (incremental panel construction). In this case, the facing deflection profiles are similar in shape, and the magnitude of calculated strains are within the accuracy of the facing survey method used to calculate the facing deflection values.

Taken together, the results of this comparison suggest that integration of reinforcement strains to estimate peak wall deflections during construction is difficult, particularly for wrapped-face walls.

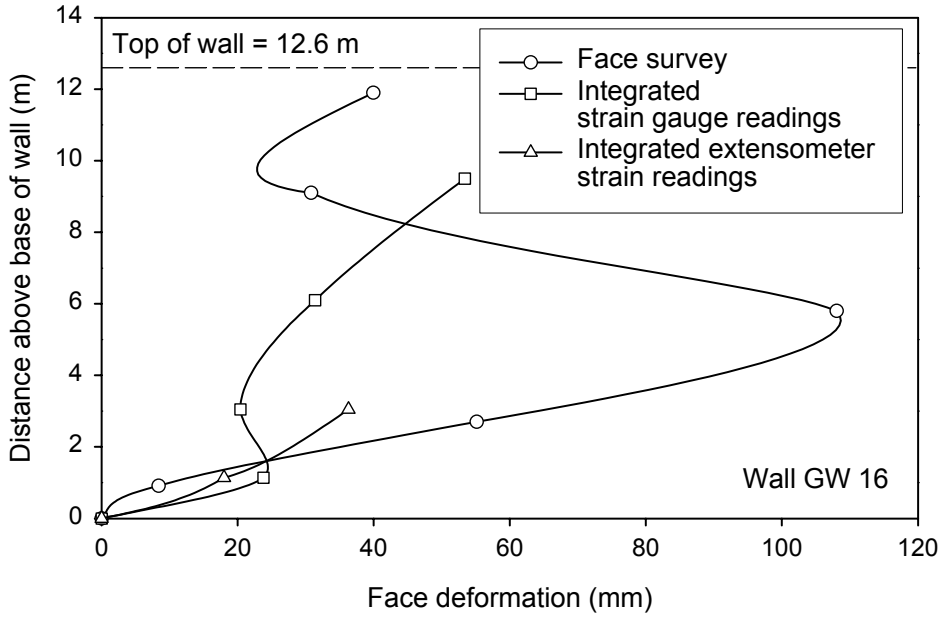

Figure 3.11. Comparison of measured wall facing deflections with estimated values from integration of reinforcement strains (Case study GW16 – wrapped face).

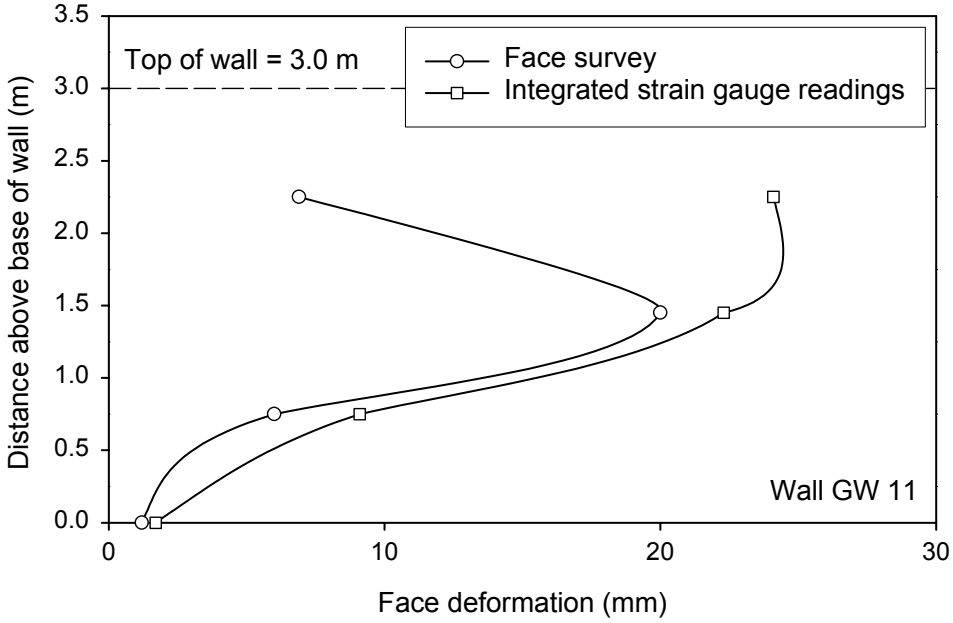

Figure 3.12. Comparison of measured wall facing deflections with estimated values from integration of reinforcement strains (Case study GW11 – wrapped face).

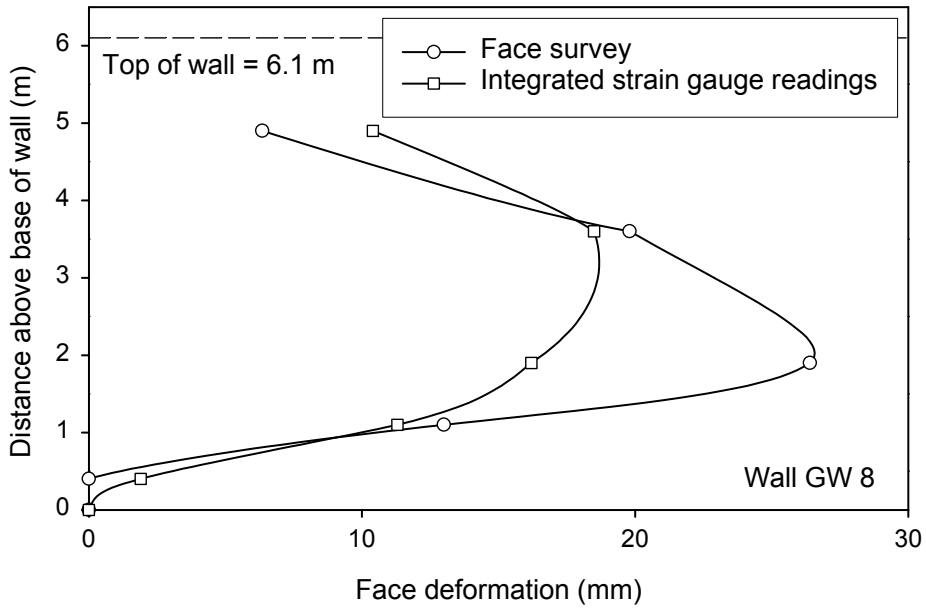

Figure 3.13. Comparison of measured wall facing deflections with estimated values from integration of reinforcement strains (Case study GW8 – incremental concrete panel face).

Finally, it is useful to normalize the surveyed lateral facing deflection curves for the three walls investigated in this section to provide empirical guidance on the magnitude of end-of-construction deflection that may be anticipated in the field. They were normalized in the following manner:

- The location of each lateral deformation measurement was normalized by the wall height (a geometrical normalization).
- The lateral deformation was normalized by the wall height plus average surcharge height to approximate the difference in total loading applied in each wall case.

This is done in Figure 3.14, and the data show that peak lateral movements recorded between the time a reinforcement layer was installed and the end of construction ranged from 0.4 to 0.7 percent of the height of the structures. As may be expected, the wall with a hard facing (GW8) and a stiffer reinforcement deformed less than the two wrapped-face walls. In all cases the largest relative deformations occurred at heights above the base of the wall corresponding to 30 to 50 percent of the height of the facing.

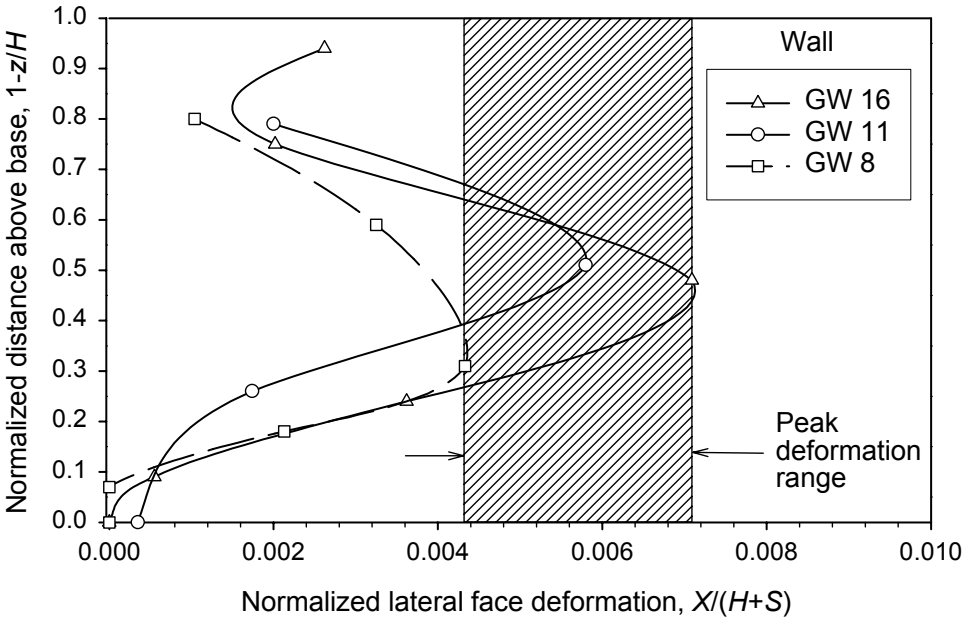

Figure 3.14. Normalized lateral facing deflections from wall facing survey measurements taken with respect to initial reading (Case study GW8 – incremental concrete panel face; Case study GW11 and GW16 – wrapped face).

3.5 Summary and Conclusions

This chapter focuses on the interpretation of strain readings from instruments used in well-documented case studies of geosynthetic reinforced soil walls. The major conclusions from this review regarding the determination of reinforcement strains are as follows:

- Strain gauge readings in the field must be corrected to true global strains by using in-isolation tensile tests of instrumented reinforcement products. Under-registration of global strains was shown to vary from a factor of 1 to as high as 2.2 at strain levels of 2 percent or less.
- The ratio of global strain to strain gauge measurements (calibration factor) was shown to vary from 0.9 to 2.2 at strain levels of 2 percent or less on the basis of constant-rate-of-strain testing.
- On the basis of limited data, the calibration factor for strain gauges tested with constant load (creep) testing was lower than that for tests that use constant-rate-of- strain loading.
- In general, under-registration of global strains by strain gauges increases with global strain level.

- Local strain readings at nominally identical locations on a reinforcement layer can be expected to vary. On the basis of data available for an instrumented, drawn PP geogrid, the coefficient of variation (*COV*) for strain gauge readings was calculated to be 13 percent for strains ≥ 0.02 percent. Similar data for a knitted polyester geogrid produced a *COV* = 14 percent for strains ≥ 0.1 percent. Possible explanations for the variation in readings include non-uniform load distribution across reinforcement layers and reinforcement type, the gauge type and technique used to attach the strain gauges to the reinforcement (e.g., glue and waterproof coating thickness and properties), and possible local bending of the reinforcement.
- On the basis of data for instrumented PP geogrids, strain gauges have proved accurate for estimating reinforcement strains at low strain levels (0.02 to 2 percent). Extensometers are more reliable for reinforcement strains ≥ 2 percent. For a knitted polyester geogrid, strain gauges gave reliable readings for strains of greater than 0.1 percent.
- Analysis of inductance coil readings showed that these instruments produced the least reliable readings of the three measurement techniques investigated (e.g., *COV* = 32 percent for strains in the range of 0.2 to 0.9 percent).
- Bonded strain gauges in the field typically produced a non-linear response or failed at strains greater than 3 percent, hence extensometers provide the only practical means of estimating reinforcement strains at large strain levels.
- On the basis of the data available, the coefficient of variation (*COV*) for extensometer readings was shown to be in the range of 29 to 56 percent for strains from 0.2 to 1 percent, but they improved to a value of 9 percent if the devices were restricted to strains of ≥ 2 percent.
- Strategies for improving confidence with interpretation of strain readings from field monitoring are to use both strain gauges and extensometers, include multiple strain gauges at nominally identical locations in the wall, and use strain gauge pairs mounted top and bottom at each reinforcement monitoring point.

In general, wall face deformations are difficult to predict using integrated reinforcement strain readings. Integrated strain gauge readings do not account for movements of the soil mass

due to deformations behind and below the wall, localized sagging of the face (wrapped-face walls), or soil down-drag behind stiff wall facings.

The review of physical data from a database of well instrumented wall structures has allowed the writers to comment on the reliability of the strain data, both qualitatively and quantitatively. One possible use of these data is to estimate the mean and spread of reinforcement loads and compare estimated values to predicted values by using current and proposed design methods for the internal stability of geosynthetic reinforced soil walls (see Chapter 5).

4.0 CONVERSION OF GEOSYNTHETIC WALL STRAINS TO LOAD BY USING IN-SOIL REINFORCEMENT MODULUS

4.1 Introduction

Knowledge of both soil reinforcement strains and loads is required to fully understand the internal stability behavior of reinforced soil walls so that design procedures can be improved. Measurements indicative of the internal behavior of full-scale walls typically consist of reinforcement strains and overall deformations, since it is difficult to directly measure reinforcement loads. Chapter 3.0 summarizes the strain measurements obtained in several geosynthetic wall case histories to provide a baseline for analysis.

For steel reinforced MSE walls, the conversion of reinforcement strain to load is relatively straightforward, since the modulus of the steel reinforcement is affected by neither soil confinement nor time. For geosynthetic reinforcement, on the other hand, the reinforcement stiffness can be affected by soil confinement, time under load, strain level, and temperature. The determination of the correct stiffness value for a geosynthetic is potentially complicated because of the factors noted above and also because of potential differences in the time dependent behavior of the reinforcement and the soil.

Approaches used in the past to estimate reinforcement loads from strain measurements have varied. For example, Christopher (1993) used the stiffness determined from short-term index tensile tests (ASTM D 4595) and short-term confined load-strain tests to convert measured strains to load. Others have used isochronous creep load-strain data to estimate loads from reinforcement strain measurements (Bathurst et al. 1987, Desert Earth Engineering 1989, Bathurst 1990, Fannin and Hermann 1991). Boyle et al. (1996) suggested that results of constant-rate-of-strain (CRS) tests conducted at strain rates comparable to the strain rate that would be encountered during wall construction (or extrapolated to actual wall strain rates) be used to estimate reinforcement loads in geosynthetic reinforced structures. Nevertheless, the validity of these different approaches has not been systematically investigated nor the results compared against measured reinforcement loads.

The focus of this chapter is the development of a methodology that can be used to convert measured strains reported for full-scale, geosynthetic reinforced structures to load. Ideally, the

methodology must take into consideration the visco-elastic-plastic behavior of the geosynthetic, the effect of soil confinement, how the geosynthetic is loaded in full-scale structures, and other factors that may affect reinforcement stiffness values. In-isolation and in-soil test data are summarized for a variety of products to demonstrate the influence of soil confinement and loading type on soil-geosynthetic interaction. This chapter attempts to quantify the uncertainty in the assessment of reinforcement stiffness values. Finally, example calculations are presented, and the estimated reinforcement load values are compared against directly measured values for the few case studies from which data are available. Estimates of the error in predicted loads are quantified on the basis of the combined effect of uncertainty in the estimated stiffness values and measured reinforcement strains.

The scope of this chapter is limited to geogrids and woven geotextiles in granular backfill soils.

4.2 The Development of Reinforcement Load and Strain in Geosynthetic Walls—Concepts

The time-dependent properties of the geosynthetic reinforcement, soil, and their interactions must be known to accurately predict the mechanical response of a geosynthetic under load in a wall. Geosynthetics are visco-elastic-plastic materials, which means that the molecules of the constituent polymer will undergo time dependent rearrangement when subjected to an external load or distortion, regardless of the loading mechanism and load level. While typically ignored, granular soils also exhibit viscous creep effects under conditions of constant stress or load (Kuhn and Mitchell 1993). If the soil is, for practical purposes, perfectly bonded to the geosynthetic (i.e., no relative slippage), the soil and the geosynthetic must deform together. Therefore, if the geosynthetic strains under constant load due to creep, the soil must take on more load or must creep under constant load to maintain strain compatibility with the geosynthetic. The time-dependent equilibrium between these two very different materials will likely cause the geosynthetic reinforcement to exhibit behavior between that of pure creep and pure stress relaxation, if the soil creep rate is less than the geosynthetic creep rate. Kuhn and Mitchell have show that creep of sands, even at typical working stress levels, can be significant. Therefore, whether or not stress relaxation or creep occurs will depend on the load-strain-time properties of the geosynthetic relative to that of the soil backfill.

The stiffness of the geosynthetic will be affected by the magnitude, sequence, and rate of loading. In most geosynthetic reinforced soil walls, the peak strain has been 2 percent or less at the end of construction (Bathurst et al. 2002). In a typical index tensile strength test carried out at a strain rate of 10 percent/minute (ASTM D 4595), the test specimen takes 12 seconds to reach a strain of 2 percent. Figure 4.1 gives example construction histories (wall height versus time) for geosynthetic reinforced soil walls from a number of sources. The construction times range from 8 to 70 days (200 to 1700 hours). Assuming that a maximum reinforcement strain of 2 percent was achieved at the end of construction, then the rate of loading of the reinforcement is four to five orders of magnitude less than the conventional tensile test (ASTM D 4595). Furthermore, the loading sequence in geosynthetic reinforced soil walls is not continuous, but rather a series of step-wise load increases. In many cases, the steps are small enough that for practical purposes, the loading rate is continuous.

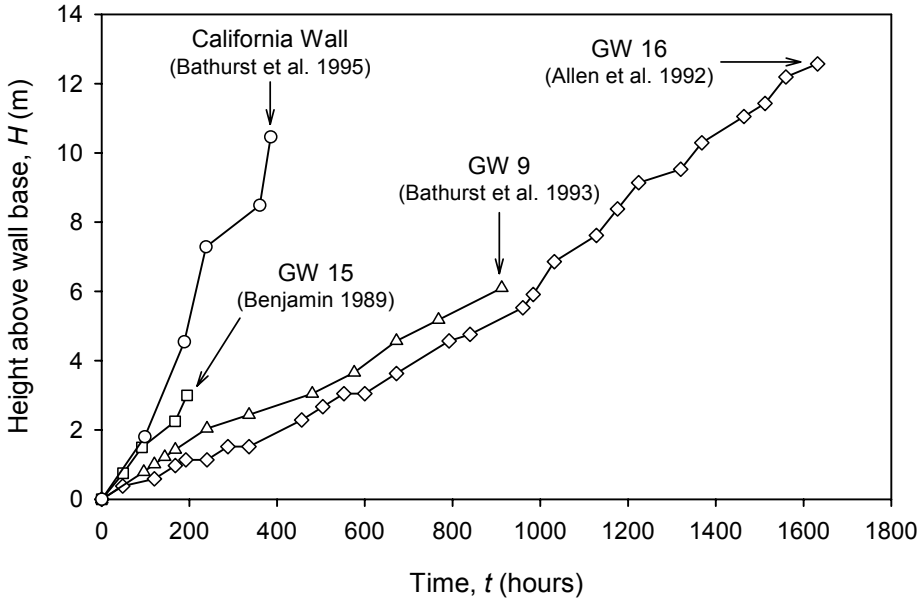

Figure 4.1. Wall construction rates observed for some geosynthetic reinforced soil walls adapted from Bathurst et al. 1995, Bathurst et al. 1993b, Benjamin 1989, and Allen et al. 1992).

4.3 Determination of Geosynthetic Stiffness from Laboratory Tests

Laboratory in-isolation tests include standard wide-width strip tensile tests in which a constant rate of strain is applied to the specimen (ASTM D 4595 or D 6637), creep tests in which a constant load is applied to the specimen (ASTM D 5262), and stress relaxation tests that maintain a constant strain on the specimen (ASTM E 328). For creep and stress relaxation tests, a series of specimens is tested by using different load levels or different initial strain levels to produce a family of curves. For CRS wide-width tensile tests, specimens are loaded at different strain rates to produce a family of curves.

In-soil characterization of geosynthetic reinforcement load-strain-time behavior has been accomplished in the laboratory by using devices in which the load is applied to the geosynthetic through the surrounding soil, and devices in which the load is applied directly to the geosynthetic. Examples are illustrated conceptually in Figure 4.2. Elias et al. (1998) provide detailed descriptions and evaluations of devices that have been used to quantify in-soil behavior of geosynthetic reinforcement. Ideally, if the soil creep rate is less than the geosynthetic creep rate, the load should be applied through the soil to simulate the effect of the soil to restrict geosynthetic creep (Figure 4.2a).

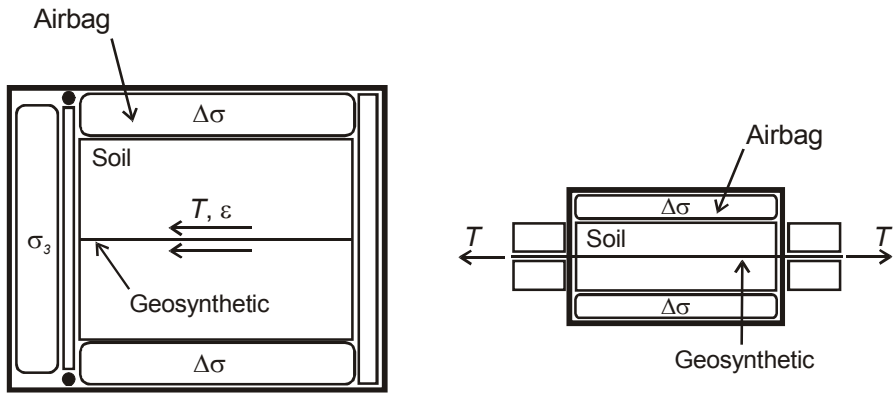

a. Device in which soil loads geosynthetic b. Device in which geosynthetic is loaded directly

Figure 4.2. Laboratory tensile load/creep devices to test geosynthetic reinforcement confined in-soil.

The stiffness of a geosynthetic at a given time or loading rate, strain level, and temperature is essentially the slope of a load-strain curve from a tensile test, or the slope of an isochronous load-strain curve from either a creep test or stress relaxation test. A secant slope is used to

define the reinforcement stiffness in this report. The stiffness obtained from a family of creep curves is denoted as the "creep stiffness" (J_c), and similarly, the "relaxation stiffness" (J_r) is obtained from a family of stress relaxation curves. The creep stiffness, J_c (typically kN/m), is expressed as follows:

$$J_c = \frac{T_i}{\varepsilon_i} \qquad \text{(Eq. 4.1)}$$

where T_i is the load per meter width and ε_i is the strain at any time. The same equation can be used for the relaxation stiffness, although the creep stiffness is not necessarily equal to the relaxation stiffness. Figure 4.3 illustrates how the stiffness of a geosynthetic reinforcement product can be determined from constant rate of strain tensile tests, constant load (creep) tests, and stress relaxation tests.

4.4 Factors That Affect Geosynthetic Stiffness

The following variables are considered to influence the magnitude of geosynthetic reinforcement stiffness *in-situ* at the end of construction (Bush 1990, Rimoldi and Montanelli 1993, Allen and Bathurst 1994, Boyle et al. 1996, Yuan et al. 1998):

1. loading sequence
2. rate of loading and time after application of load
3. soil confinement
4. strain level
5. temperature
6. installation damage.

4.4.1 Loading Sequence, Loading Rate, and Soil Confinement

Geosynthetic reinforcement *in-situ* may experience creep, stress relaxation, or step-wise increases in load, as discussed in Section 4.2. Idealization of these loading histories can be simulated by different laboratory tests that are conducted with the reinforcement in-isolation or confined in soil (Section 4.3). Data from studies, where comparisons between creep, stress relaxation and/or CRS test results can be made for the same geosynthetic product, are evaluated

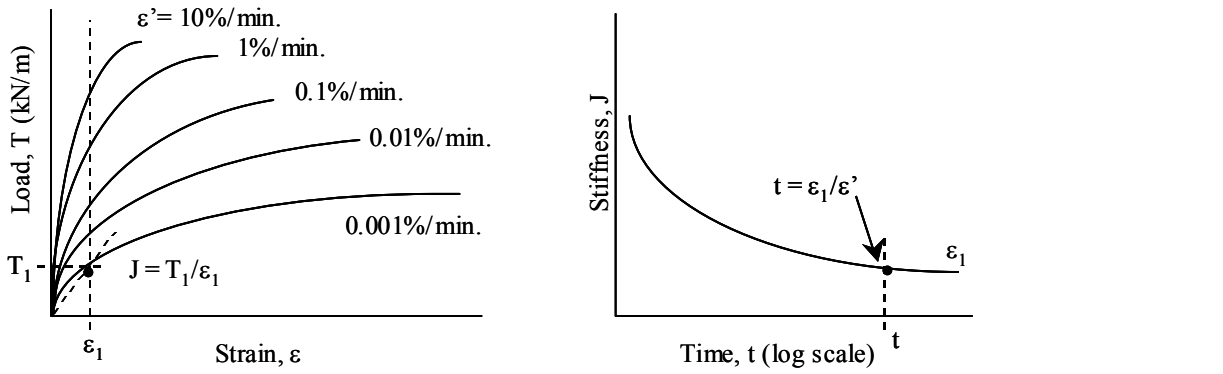

a. Constant rate of strain tensile test

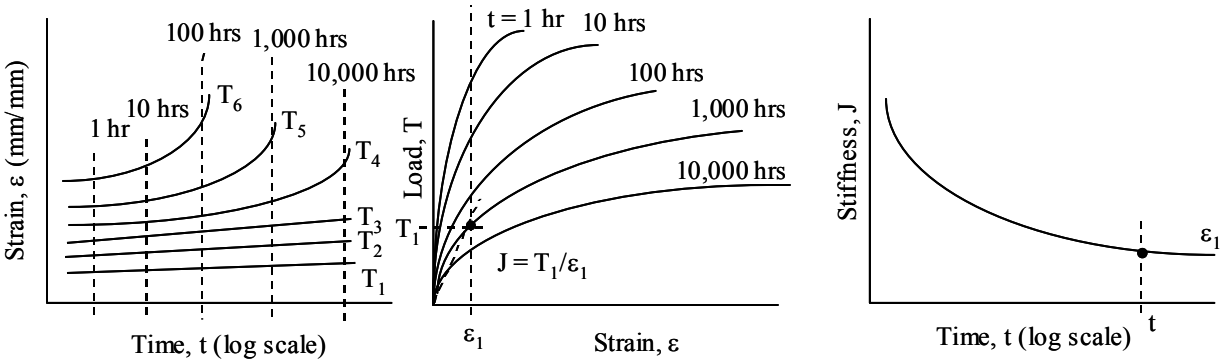

b. Constant load (creep) test

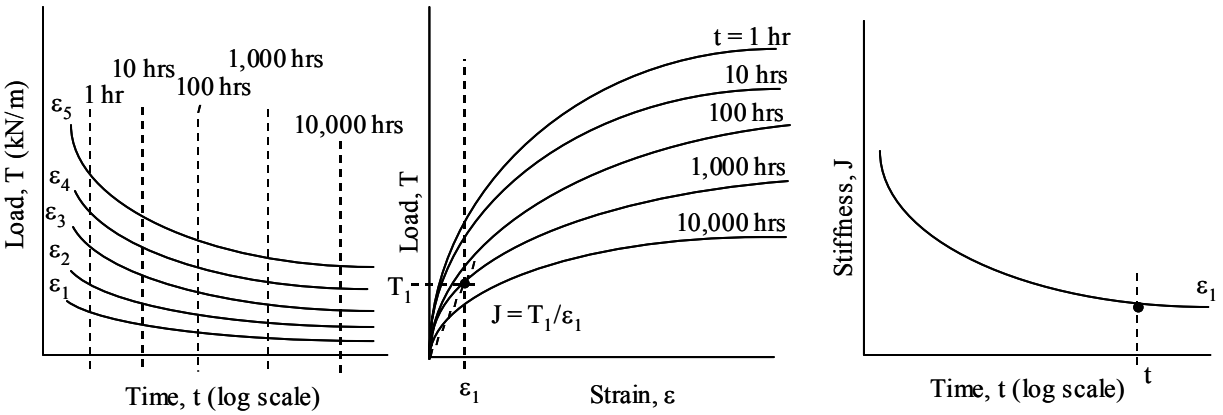

c. Constant strain (stress relaxation) test

Figure 4.3. Determination of stiffness from various types of laboratory tests.

in the following sections to assess the effects of test type (i.e., loading sequence and soil confinement) on short- and long-term stiffness values. The geosynthetic materials are summarized in Table 4.1. Specimens denoted as EGG-3 and EGG-4 are the same polypropylene (PP) material taken from the same roll, but were tested by researchers with different equipment (Burgess 1999 and Kaliakin et al. 2000, respectively).

Table 4.1. Geosynthetic materials used in previous and current studies.

Designation	Product Name	Type	Polymer	Index Tensile Strength, T_{ult} (kN/m)	Reference
WGT-1	Exxon GTF375	Woven geotextile	PP	62.0	Boyle 1995
EGG-1	Tensar SS1	Extruded biaxial geogrid	PP	12.0	Yeo 1985, and Benjamin 1989
EGG-2	Tensar SR-2	Extruded uniaxial geogrid	HDPE	70.5	Yeo 1985
EGG-3	Tensar BX1100	Extruded biaxial geogrid	PP	13.0	Burgess 1999
EGG-4	Tensar BX1100	Extruded biaxial geogrid	PP	13.0	Kaliakin et al. 2000
EGG-5	Tensar UX1000 SB	Extruded uniaxial geogrid	HDPE	38.0	Kaliakin et al. 2000
EGG-6	Tensar UX1500 SB	Extruded uniaxial geogrid	HDPE	72.0	Kaliakin et al. 2000
WGG-1	Fortrac 35/20-20	Woven biaxial geogrid with PVC coating	PET	36.0	Kaliakin et al. 2000
WGG-2	Miragrid 5T	Woven biaxial geogrid with acrylic coating	PET	41.0	Kaliakin et al. 2000
WGG-3	Stratagrid 100	Woven biaxial geogrid with PVC coating	PET	15.8	Saunders 2001

4.4.1.1 In-Isolation Data from Previous Studies

Kaliakin et al. (2000) reported creep and stress relaxation test results for several geogrids (Table 4.1). Creep and relaxation stiffness values calculated from these data are shown in

figures 4.4, 4.5 and 4.6. Creep and CRS test data from Yeo (1985) and Benjamin (1989) were used to calculate stiffness values for other materials, as shown in figures 4.7 and 4.8. All stiffness values are expressed as a function of time using the approaches illustrated in Figure 4.3. The following general trends can be observed for stiffness values calculated at 2 percent strain:

1. Stiffness values decrease at a decreasing rate with a logarithm of time for all the materials tested, regardless of the method of test.
2. The stiffness of polyester (PET) products is least affected by time in comparison to polypropylene (PP) and high density polyethylene (HDPE) geosynthetics, at least for strains of up to 2 percent.
3. The relaxation stiffness value is typically less than the creep stiffness value for all three polymer types (see figures 4.4, 4.5 and 4.6).
4. The stiffness values obtained from the different test methods tend to converge at longer times for PP geosynthetics (see Figure 4.6). However, there was no consistent trend regarding convergence or non-convergence for the PET and HDPE geosynthetic materials tested.
5. The stiffness values obtained from the CRS tests as a function of time for HDPE and PP geosynthetics are roughly the same or slightly lower than the stiffness values obtained from creep testing, especially at longer times (see figures 4.7 and 4.8).
6. The stiffness curves based on creep testing are significantly flatter at elapsed times in excess of 100 hours, which is less than the time required to construct the walls identified in Figure 4.1.

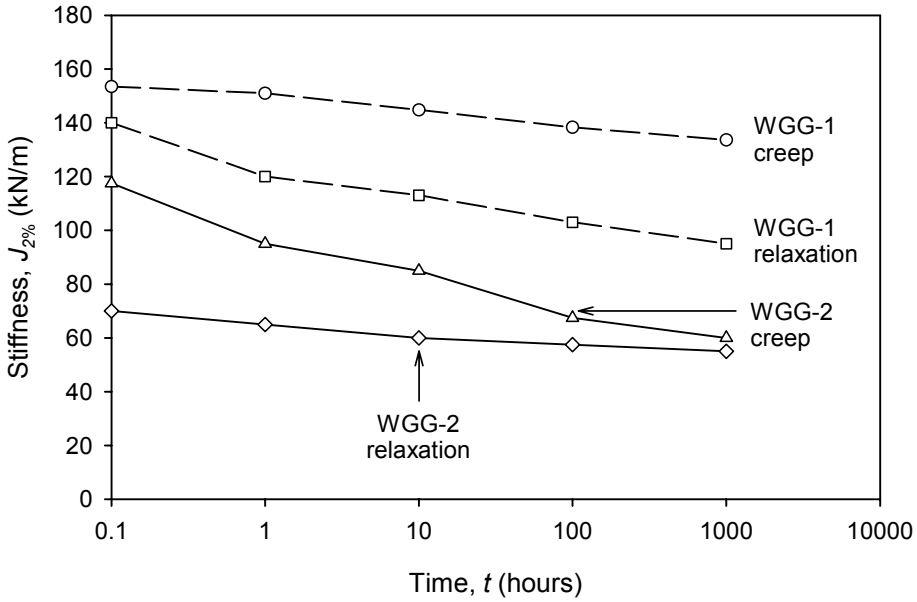

Figure 4.4. In-isolation relaxation and creep stiffness values at 2 percent strain for woven PET geogrids (WGG-1 and WGG-2) using data reported by Kaliakin et al. (2000).

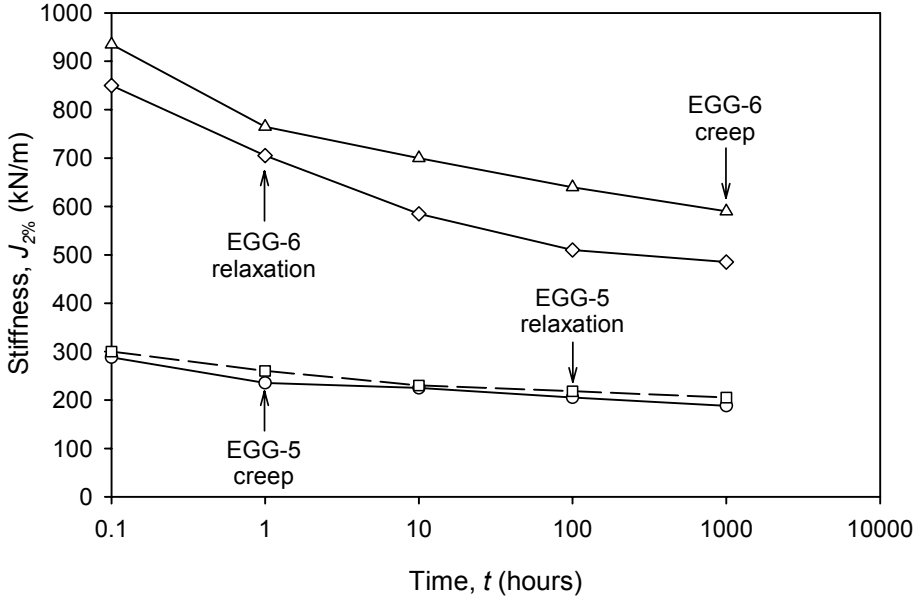

Figure 4.5. In-isolation relaxation and creep stiffness values at 2 percent strain for uniaxial HDPE geogrids EGG-5 and EGG-6 using data reported by Kaliakin et al. (2000).

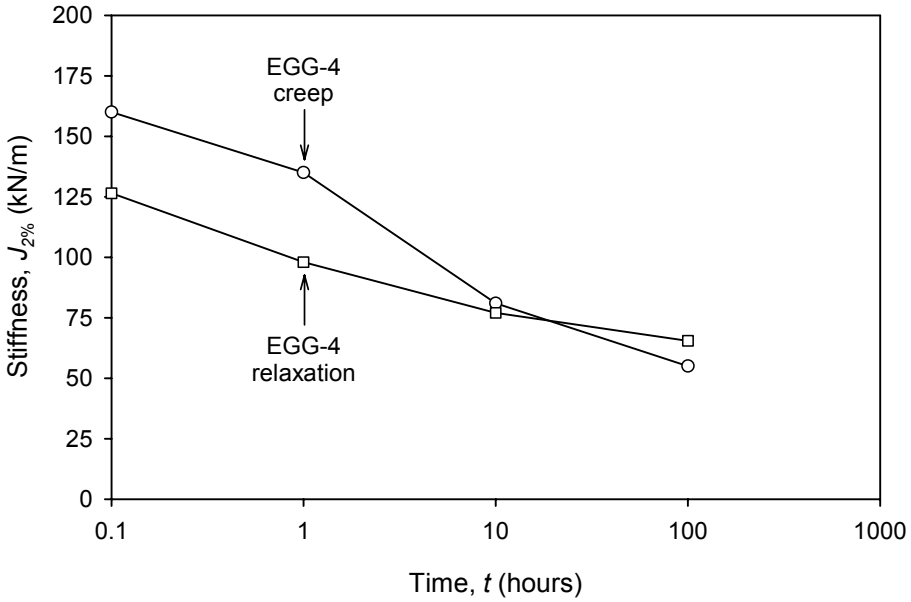

Figure 4.6. In-isolation relaxation and creep stiffness values at 2 percent strain for biaxial PP geogrid EGG-4 using data reported by Kaliakin et al. (2000).

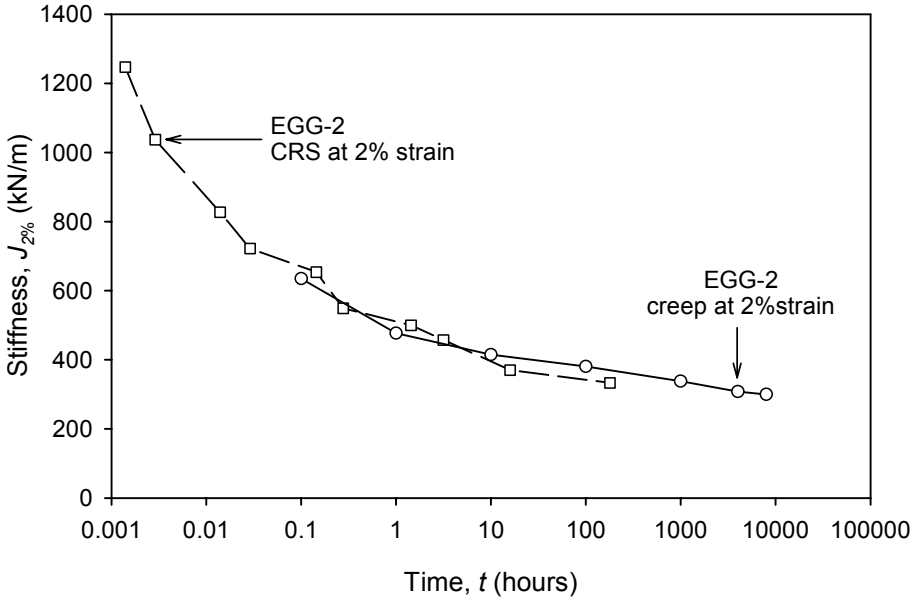

Figure 4.7. In-isolation constant rate of strain (CRS) and creep stiffness values at 2 percent strain for uniaxial HDPE geogrid EGG-2 using data reported by Yeo (1985) and Benjamin (1989).

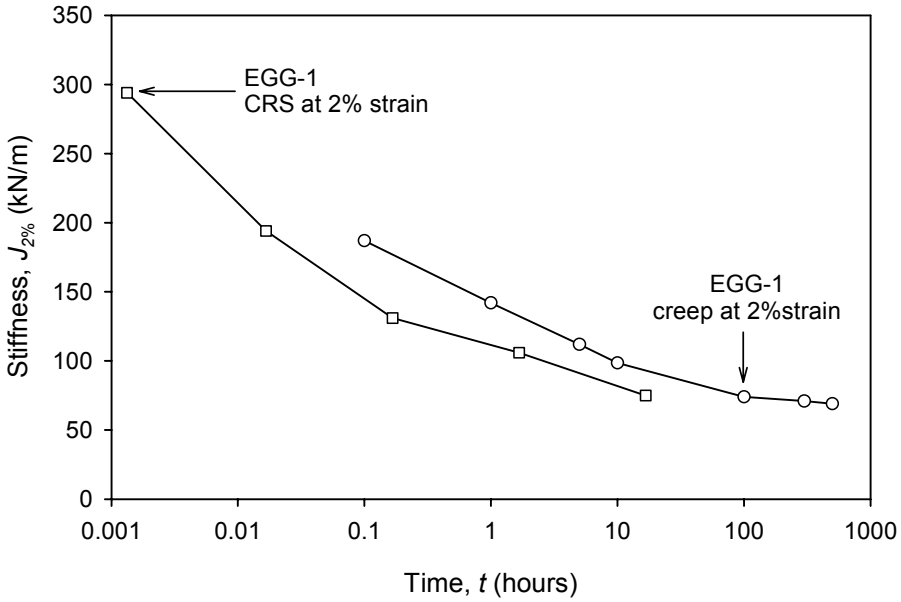

Figure 4.8. In-isolation CRS and creep stiffness values at 2 percent strain for biaxial PP geogrid EGG-1 loaded in weak direction using data reported by Yeo (1985) and Benjamin (1989).

Figures 4.9 through 4.11 were developed from data presented by Kaliakin et al. (2000). The figures show that for the three types of geogrids, the stiffness values appear to converge at low strain levels. The relaxation stiffness values were calculated directly from the data, but the creep stiffness data presented in figures 4.4 through 4.11 were extrapolated down to 2 percent strain from data reported at a 4 to 5 percent strain or higher. Hence, it is difficult to conclude whether the creep curve for a particular data set falls above or below the relaxation curve at low strain values. Nevertheless, the trend in the data suggests that both curves are close at low strain levels.

Creep and stress relaxation test data were presented by Thornton (2001) to characterize the time dependent behavior of EGG-3 at low load levels from specimens of material from the same roll of geogrid used by Kaliakin et al. (2000) and Burgess (1999). Using the data from the in-isolation tests corresponding to strain levels of less than 1 percent and for times of less than 10 minutes, Thornton (2001) concluded that the creep stiffness and the relaxation stiffness were approximately equal, with the creep stiffness exhibiting a tendency to be slightly greater than the relaxation stiffness. However, using the Stepped Isothermal Method (SIM) of Time Temperature Superposition and vertically shifting the stress relaxation master curve, Thornton concluded that in the long term, the relaxation stiffness would be greater than the creep stiffness.

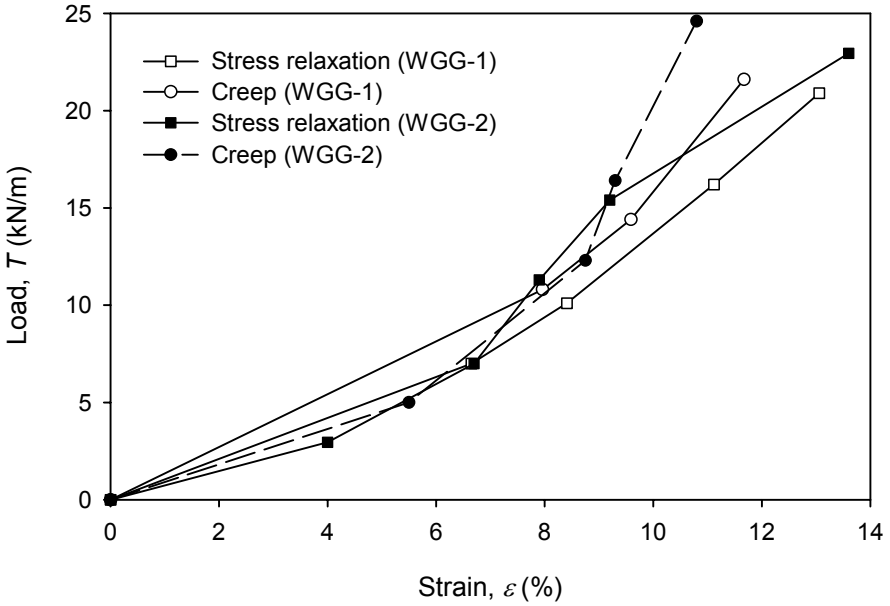

Figure 4.9. In-isolation 1000-hour isochronous curves for woven PET geogrids WGG-1 and WGG-2 from stress relaxation and creep testing using data reported by Kaliakin et al. (2000).

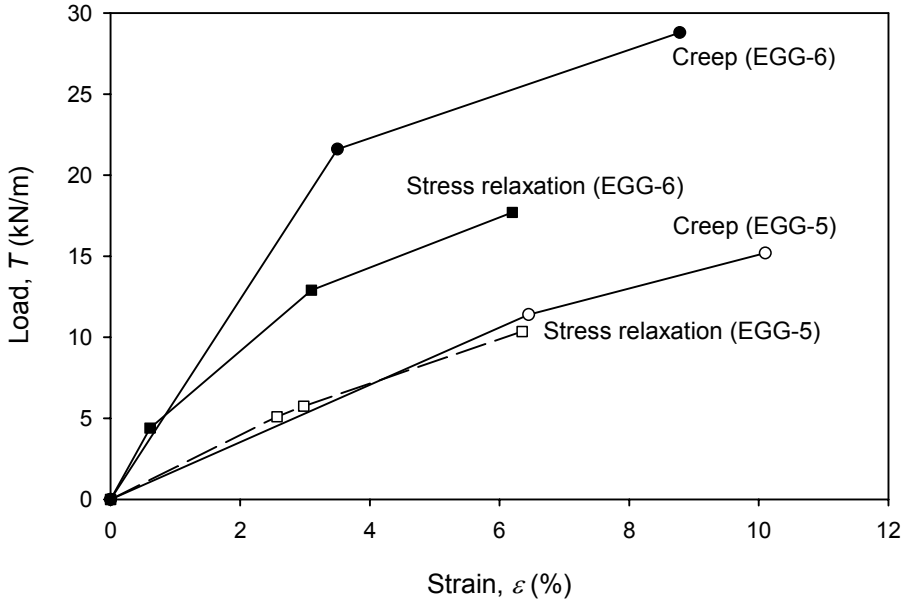

Figure 4.10. In-isolation 1000-hour isochronous curves for uniaxial HDPE geogrids EGG-5 and EGG-6 from stress relaxation and creep testing using data reported by Kaliakin et al. (2000).

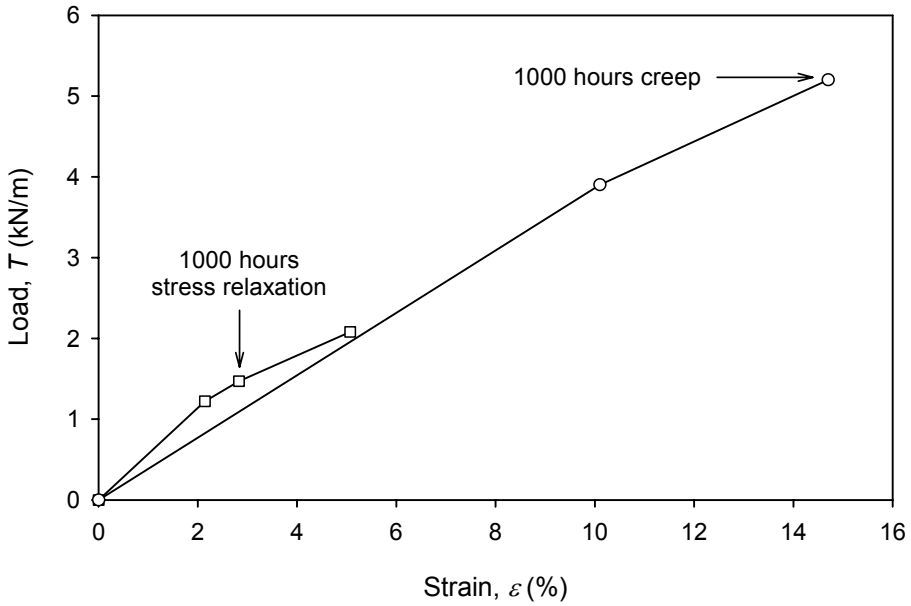

Figure 4.11. In-isolation 1000-hour isochronous curves for biaxial PP geogrid EGG-4 from stress relaxation and creep testing using data reported by Kaliakin et al. (2000).

4.4.1.2 In-Isolation Data from the Current Study

Creep, stress relaxation, and CRS tests were not conducted on the same sample of material in the studies reported previously. Hence, a direct comparison of results from all these different types of tests cannot be made. Furthermore, as noted earlier, low strain data from in-isolation tests at the times of interest were not available, requiring extrapolation to lower strain values.

In order to compare the influence of test type on material response, additional tests were carried out on specimens of EGG-3 and a knitted, high tenacity PET geogrid (WGG-3) (figures 4.12 and 4.13). The tests were specifically focused on low strain behavior. These geosynthetics are very weak (T_{ult} = 13 and 16 kN/m for the PP and PET geogrids, respectively) and were specifically chosen to generate large strains in instrumented full-scale, reinforced soil retaining wall structures (Bathurst et al. 2000).

In-isolation creep and CRS testing of EGG-3 were conducted on 200-mm-wide specimens, and single rib specimens were used for the stress relaxation tests. All in-isolation tests for the PET material were conducted with single rib specimens to avoid the problem of non-uniform loading of the multiple-strand knitted PET geogrid specimens (Saunders 2001).

Creep testing was conducted in accordance with ASTM D 5262. The gauge length of the test specimens was approximately 500 mm, and creep strains were measured with displacement-type

potentiometers clamped to the specimens (Burgess 1999, Saunders 2001). The test specimens from each geosynthetic product were taken from the same roll and loaded for 1000 hours or to creep rupture of the specimen, whichever occurred first.

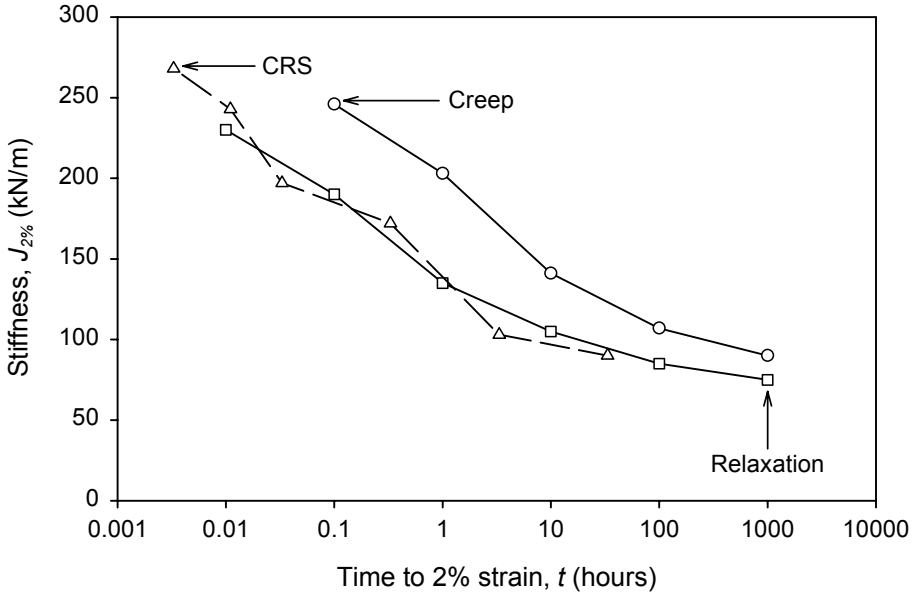

Figure 4.12. Comparison of in-isolation constant rate of strain (CRS) stiffness, isochronous $J_{2\%}$ creep stiffness, and $J_{2\%}$ stress relaxation stiffness for biaxial PP geogrid EGG-3.

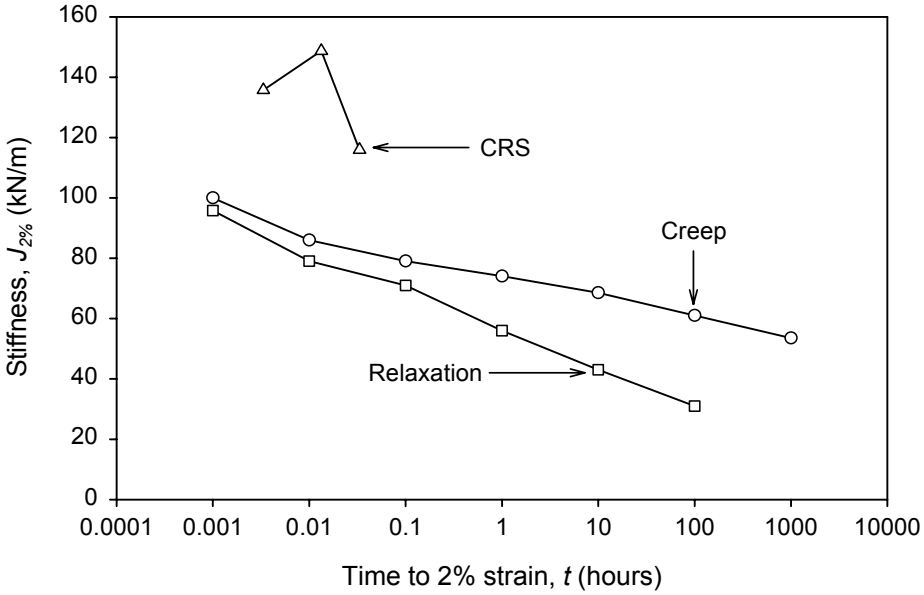

Figure 4.13. Comparison of in-isolation constant rate of strain (CRS) stiffness, isochronous $J_{2\%}$ creep stiffness, and $J_{2\%}$ stress relaxation stiffness for woven PET geogrid WGG-3.

Relaxation testing was in general accordance with recommendations in ASTM E 328. The ends of the single rib specimens were cast in a cylindrical mold of molten Ostalloy (Saunders 2001) and gripped by the spring-loaded jaws of a standard laboratory tensometer machine. A specimen length of approximately 320 mm was used, and a series of tests was conducted at different initial strain values. The initial strain was applied rapidly (a strain rate of 110 percent/minute), and each test was monitored for a minimum of 100 hours.

CRS testing to determine the index strength of both materials was conducted in accordance with ASTM D 4595. Additional CRS tests were also conducted at strain rates of 1, 0.1, 0.01 and 0.001 percent/minute for EGG-3, and at 3 and 1 percent/minute for WGG-3. The specimens had an overall length of 300 mm and a gauge length of 100 mm. Displacement-type potentiometers were attached to the specimens to measure the strain during testing. All tests described here were carried out at a temperature of $20^{o} \pm 2^{o}$ C.

The data in Figure 4.12 for the PP material show that all three curves appear to converge with increasing time and that at low strain levels (i.e., 2 percent) the stiffness values follow the relative trends expressed as:

$$\text{Creep Stiffness} > \text{CRS Stiffness} \geq \text{Relaxation Stiffness}$$

The relative trends for the PET geogrid curves in Figure 4.13 are less clear, and convergence was not observed for this data set. In particular, the CRS tests were not carried out at very slow strain rates to confirm that the CRS curve is tending toward values observed for the creep and relaxation curves at greater elapsed times. Nevertheless, the creep stiffness values are greater than the relaxation stiffness values, as noted for the PET data in the previous section.

4.4.2 In-Soil Data

Yuan et al. (1998) performed in-soil tests of the type shown conceptually in Figure 4.2b, at a constant strain rate of 10 percent/minute. The soil used was a beach sand. The results of these tests on one nonwoven PP geotextile (PP-10), two woven PP geotextiles (PP-11 and PP-12), one extruded HDPE geogrids (PE-13), and one woven PET geogrids (PET-14), are provided in Figure 4.14. The test results show that soil confinement has only a minor effect, if any, on the

stiffness values of woven geotextiles and geogrids (an increase of 5 to 30 percent over the in-isolation value) but a large effect on the stiffness values of nonwoven geotextiles (an increase of up to 500 percent depending on the confining pressure and soil type). A similar study performed by Wilson-Fahmy et al. (1993) showed that soil confinement had a negligible effect on woven geotextiles, but a large effect on nonwoven geotextiles. Taken together, the two studies suggest that load-strain response from in-isolation tests can be used to estimate the short-term stiffness of woven geotextiles under soil confinement but not of nonwoven geotextiles.

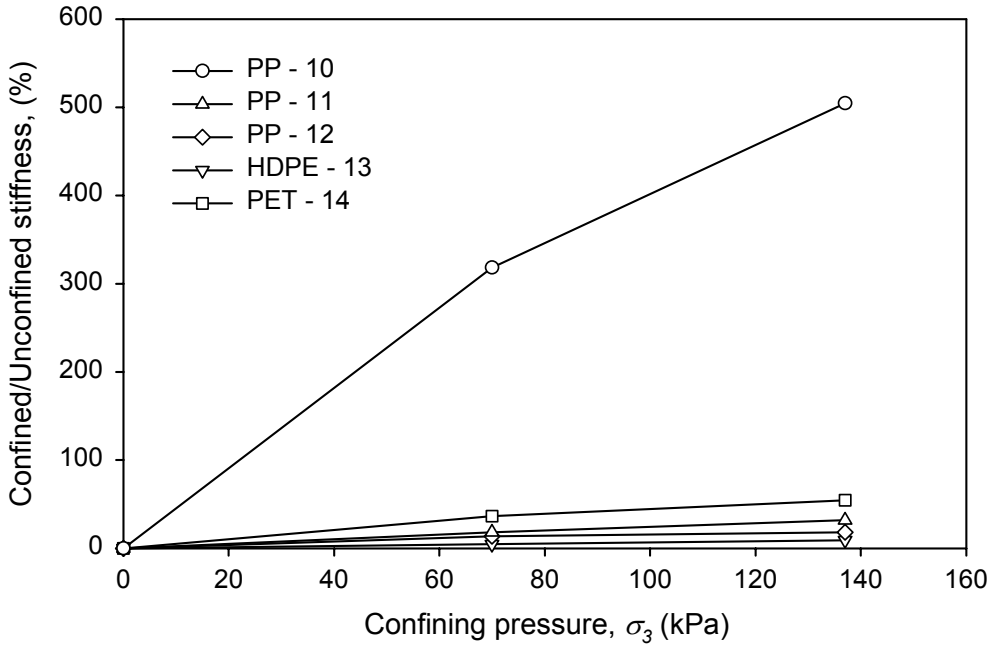

Figure 4.14. Soil confinement effect on the secant stiffness modulus at 5 percent strain for selected geosynthetic materials confined in beach sand (after Yuan et al. 1998).

Boyle (1995) and Boyle et al. (1996) reported the results of in-soil load-strain tests using a unit cell device (see Figure 4.2a), by which the geosynthetic response to a constant deviator stress applied to the soil could be monitored through direct measurement of both load and strain in the reinforcement. Boyle concluded that although some non-uniformity in the strain distribution did exist in some tests, indicating some deviation from true unit cell conditions, the error caused by this deviation was small.

Measurements of short-term in-soil geosynthetic stiffness from the unit cell device are summarized in Figure 4.15. This figure also shows the stiffness obtained from in-isolation tests on the same geosynthetics. Note that the in-soil unit cell test is conducted as a constant rate of soil loading test, rather than as a constant rate of strain test, to better simulate how a soil/geosynthetic composite is loaded in real structures. If there is a confinement effect, because the normal confining stress on the geosynthetic is not held constant, the effect of confining stress can only be determined approximately. This issue is only significant for nonwoven geotextiles, as the effect of confining stress on woven geotextiles is minimal. Because the test is controlled by the soil loading rate, the in-soil strain rates reported in Figure 4.15 are average rates determined over the duration of the test.

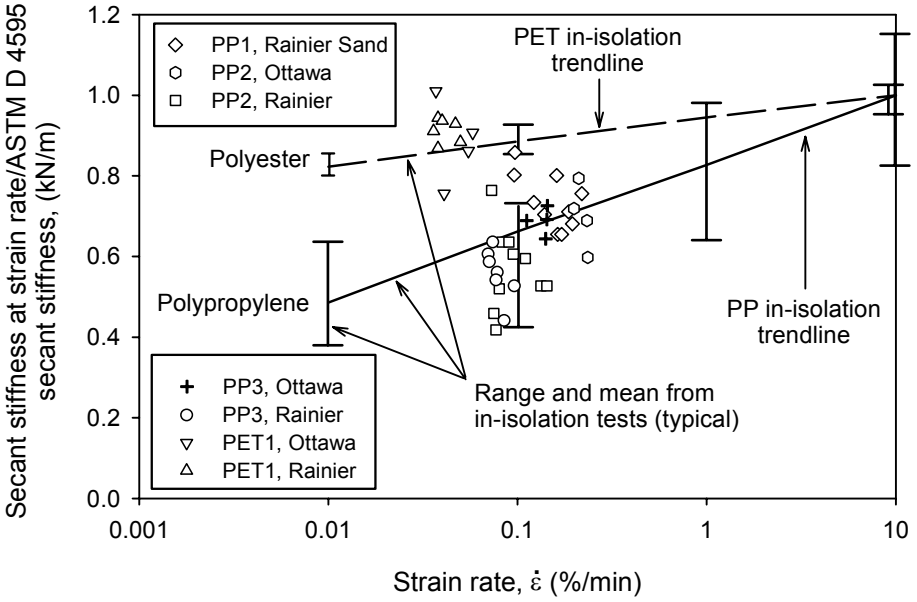

Figure 4.15. Five percent secant stiffness versus strain rate from in-soil and in-isolation CRS tests on woven PP and PET geotextiles (adapted from Boyle et al. 1996).

The first observation that can be made from Figure 4.15 is that the log-linear curve describing the trend in data for the ratio of in-isolation stiffness to index stiffness versus strain rate passes through the data sets for the in-soil PET and PP results. It may be argued that the in-soil stiffness values measured for the PET geotextile are, on average, slightly above the in-isolation trend line for the PET geotextile data points. This observation is consistent with the data provided in Figure 4.14, which showed a slight improvement in stiffness of PET geotextiles because of soil confinement. The second observation is that the in-soil stiffness values for the

geosynthetic products tested at an average rate of 0.1 percent strain/minute were less than the in-isolation modulus at 10 percent strain rate/minute. It is reasonable to assume that the log-linear trend for the in-isolation tests is preserved and, therefore, that the in-soil stiffness of geosynthetics can be expected to also decrease with a decreasing logarithm of strain rate.

Boyle (1995) and Boyle and Holtz (1996) also evaluated the creep behavior of the PP woven geotextiles confined in soil with the unit cell device described previously. Figure 4.16 provides the test results for a woven PP geotextile (WGT-1 in Table 4.1) confined in a gravelly sand tested in the device under constant deviator stress, σ_1. The test was conducted at a confining pressure of σ_3 = 20 kPa. This figure shows that both creep and stress relaxation occurred in the unit cell simulation of geosynthetic reinforcement confined in soil under wall or reinforced slope conditions (i.e., measured strain continued to increase, albeit only marginally, while the load in the reinforcement as measured by load cells located at each end of the specimen decreased with time).

Helwany and Shih (1998) performed similar experiments with a heatbonded nonwoven geotextile confined in sand with σ_1 = 70 kPa and σ_3 = 3.5 kPa. They alsoreported that both stress relaxation and creep occurred when the soil applied the load to the geosynthetic through a deviator stress. However, as shown in Figure 4.17, the stress relaxation did not occur immediately but was delayed approximately 20 hours after the initial application of the vertical deviator stress. A plausible explanation for the unusual shape of the stress relaxation curve obtained from the test was that it took time, possibly because of soil creep, for the load to transfer along the geosynthetic back to the end of the geosynthetic where the load was measured. This delayed load transfer could have caused the load as measured by the load cell to increase during the first 20 hours of loading. In any case, once full load transfer occurred, stress relaxation did occur, as it did in the tests by Boyle (1995). Together, the in-soil test results reviewed here confirm that stress relaxation is a potential time-dependent mechanism in geosynthetic reinforced structures, at least at working stress conditions. However, the magnitude and variation of stress relaxation with time may be expected to be influenced by the boundary conditions in the unit cell devices and how reinforcement loads and strains are measured.

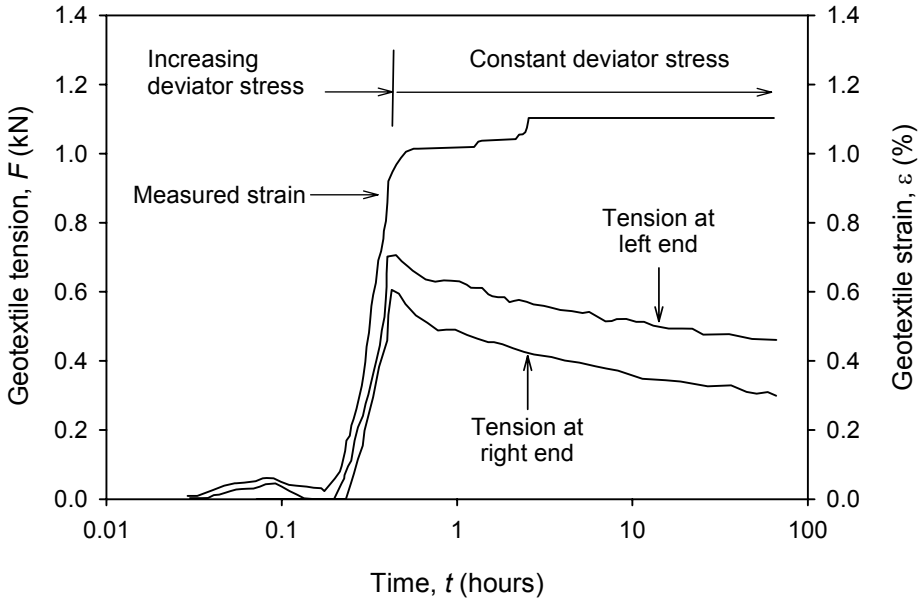

Figure 4.16. Confined creep and stress relaxation response of woven PP geotextile WGT-1 in Rainier Avenue gravelly sand at 20 kPa confining pressure (adapted from Boyle and Holtz 1996).

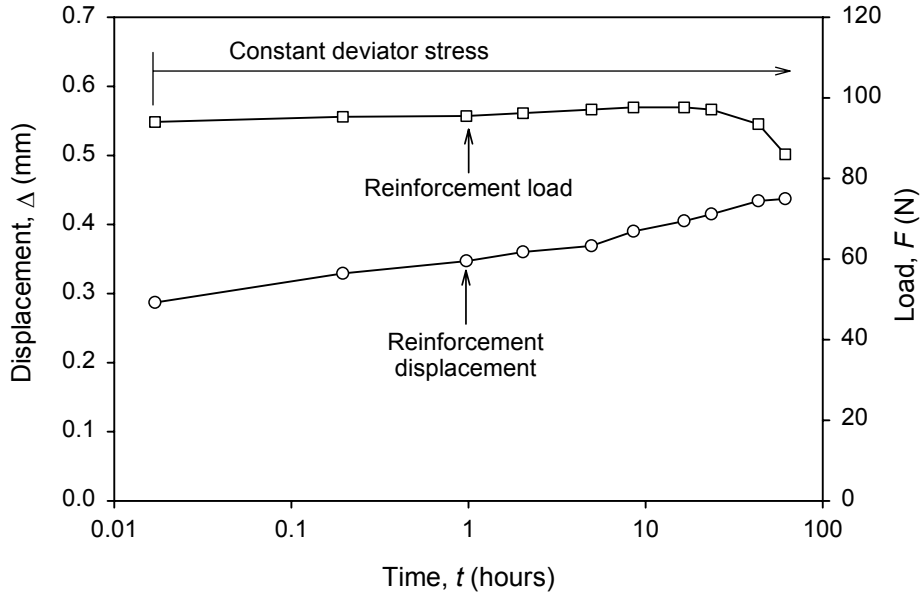

Figure 4.17. Confined creep of a PP heatbonded nonwoven geotextile at a confining stress of 3.5 kPa (adapted from Helwany and Shih, 1998).

Figure 4.18 provides a comparison of the stiffness values obtained from the in-isolation and in-soil CRS and creep tests conducted by Boyle (1995) and Boyle et al. (1996) on a woven PP geotextile. The stiffness values reported in this figure were determined at 1 percent strain rather than at the 2 percent strain used for the data presented elsewhere in this chapter. The creep test

data at higher strain values were insufficient to develop isochronous curves at all times of interest. The in-soil "creep" response was strongly affected by stress relaxation/load transfer, as demonstrated in Figure 4.16. Hence, the difference between the in-isolation and in-soil "creep" responses at short durations was likely the result of the difference between the stiffness obtained in stress relaxation versus creep tests, as observed in Sections 4.1.1.1 and 4.1.1.2. In general, there appears to be a convergence of stiffness value curves from in-soil and in-isolation test methods in Figure 4.18 at longer times.

Chapter 6.0 compares the in-isolation and in-soil data in figures 4.16 and 4.18 to the long-term measurements obtained for geosynthetic reinforcement layers in full-scale walls. The conclusion, based on the measured creep rates from the reinforcement in Wall GW16, is that the unit cell device may have led to more stress relaxation than occurred in the actual wall.

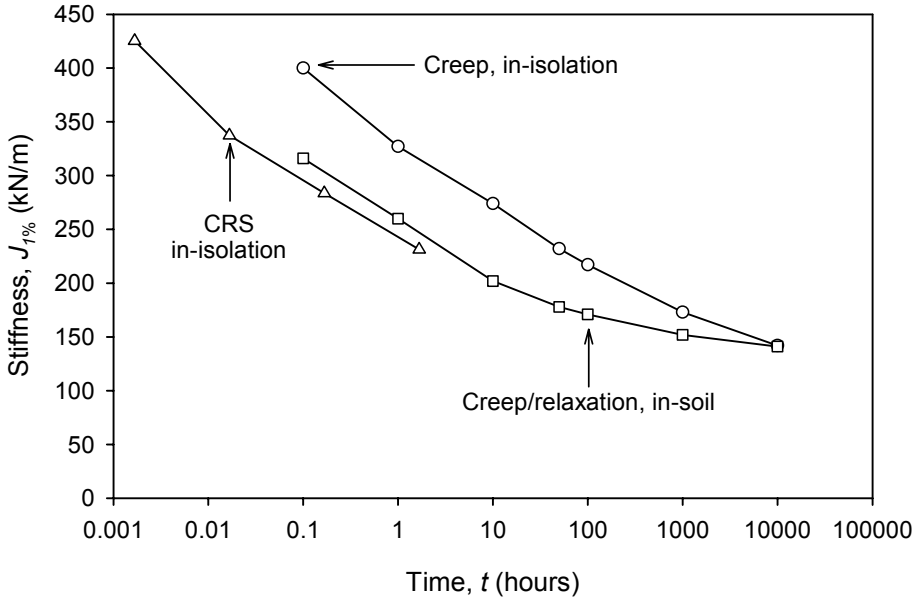

Figure 4.18. Comparison of CRS and isochronous creep $J_{1\%}$ values from in-isolation and in-soil tests on woven PP geotextile WGT-1 (based on data from Boyle 1995).

4.4.3 Strain Level

The load-strain relationship for most geosynthetics is non-linear, especially at relatively high strain levels. Therefore, the magnitude of strain in a geosynthetic reinforcement is important when the reinforcement stiffness is estimated. At very low strains (e.g., 2 percent or lower) non-linearity is typically small, and for practical purposes the isochronous creep stiffness is constant. Laboratory assessment of reinforcement stiffness at strains of 1 percent or less is difficult, depending on how slack in the specimen is handled and the gripping technique used,

and will likely have a greater uncertainty (see Section 4.6). Hence, it is recommended that the 2 percent secant stiffness be used to characterize the stiffness at low strains. PET geosynthetics may be an exception, as they characteristically have sigmoidal (i.e., S-shaped) load-strain curves at low strains because of their crystalline structure. Isochronous creep curves also tend to exhibit this sigmoidal shape. If the sigmoidal shape of the PET geosynthetic load-strain curve is significant at strains of 2 percent or less (i.e., near the maximum stiffness range), a lower strain stiffness should be used at very low strains. If strains are expected to exceed 3 to 4 percent, the reinforcement stiffness should be determined at higher strain levels.

4.4.4 Temperature

Temperature will affect the stiffness value of geosynthetics, with increasing temperature resulting in lower stiffness, especially for polyolefin materials (e.g., Bush 1990). Time-temperature superposition techniques are used to estimate the stiffness at any specific temperature (e.g., WSDOT 1998). The stiffness value used to estimate load from strain measurements should be determined at the temperature in the wall. Current U.S. design practice considers the effective wall temperature to be the temperature that is the mean of the average yearly air temperature and the normal daily air temperature for the hottest month at the site (AASHTO 2002). The data presented in this report were obtained at a temperature of 20^{o}C unless otherwise noted.

4.4.5 Installation Damage Effects on Geosynthetic Stiffness

Allen and Bathurst (1994) investigated the effect of installation damage on the stiffness of different types of geosynthetic reinforcement. They determined that for woven geotextiles, the decrease in stiffness is minor for levels of damage that result in less than 40 percent peak tensile strength loss. For geogrids, the stiffness loss is insignificant until very high levels of damage are achieved.

Allen and Bathurst (1996) also investigated and summarized the combined effect of installation damage and creep on the strain response to load of various geosynthetics. They determined that the creep strain response is the same before and after installation damage, which indicates that the creep stiffness will also be the same before and after damage. However, if the installation damage is great enough to cause a significant stiffness reduction based on short-term

tensile tests, the creep strain response before damage may be different than the creep strain response after damage. From these previous analyses, it can be concluded that, in general, installation damage does not need to be considered when the stiffness of geosynthetics is assessed to convert measured strains to load, unless the damage level is exceptionally severe.

4.5 Analysis of Laboratory Geosynthetic Stiffness Trends

Geosynthetic stiffness trends, as a function of time, have been presented for CRS, creep, and stress relaxation laboratory tests, both in-isolation and in-soil. The next step is to assess which type(s) of test best represents the true stiffness of the geosynthetic, both experientially and theoretically, as well as to assess the amount of error that can be incurred if a simpler test is used to determine the stiffness.

4.5.1 Effect of Test Type on Geosynthetic Stiffnesss Determination (Experimental Analysis)

Figures 4.15 and 4.18 show that stiffness values measured for most times of interest were approximately the same in-soil or in-isolation for the geosynthetics tested. Elias et al. (1998) concluded that if the fibers/yarns/ribs cannot reorient or straighten significantly under tensile load in-isolation, which is the case with most woven geotextiles and all geogrids, soil confinement will have little effect on the in-situ stiffness. The average of a 10 to 15 percent stiffness increase for woven geotextiles and a 5 percent or less increase for geogrids observed when under confinement, based on short-term tensile tests (see Figure 4.14), is likely statistically insignificant, given the other sources of variability in the stiffness determination. Therefore, in-isolation stiffness determinations are probably accurate enough to convert strains to loads for most woven geotextiles and all geogrids, without consideration for time effects.

In-isolation stiffness values also appear to be adequate even when time effects are considered. Although the soil may tend to restrict creep deformation, soil confinement does not change the visco-elastic or visco-plastic properties of the geosynthetic material. Therefore, if the geosynthetic cannot creep, then it will stress relax instead, as illustrated in figures 4.16 and 4.17. Either way, the stiffness is reduced because of time effects (e.g., Figure 4.18).

On the basis of the available test data, the stiffness values determined with CRS tests for HDPE and PP geogrids were lower than the stiffness values determined with creep tests at a

given time, As shown in Table 4.2, the average ratio of the CRS stiffness (J_{crs}) to the creep stiffness (J_c) at times of 100 hours or more, except for WGG-3, was 0.84 to 0.92. Convergence of stiffness values obtained from the two types of tests typically occurs at longer times. This observation of convergence is supported by Figure 4.19, which shows that at longer times, the strain response tends to be the same whether the load was applied rapidly or slowly for the HDPE geogrids tested, which is also consistent with the findings of Yeo (1985). This supports the conclusion of Thornton et al. (1997), based on visco-elastic theory, that the creep or relaxation rate becomes independent of the loading ramp rate at times of greater than 3 to 10 times the loading ramp time. That is, the stress history is partially or fully erased as strain- or time-dependent molecular rearrangement continues to occur.

Table 4.2. Ratio of stiffness values at a given time and strain from different test methods.

Material Designation	Polymer	At 2% Strain, at 100 hrs		At 2% Strain, at 1000 hrs	
		J_{crs}/J_c	J_r/J_c	J_{crs}/J_c	J_r/J_c
WGT-1	PP	0.78*	0.8*[+]	0.99*	1.0*[+]
EGG-1	PP	0.83		0.85*	
EGG-2	HDPE	0.92		0.95*	
EGG-3	PP	0.84		1.0	
EGG-4	PP		1.2		1.3
EGG-5	HDPE		1.1		1.1
EGG-6	HDPE		0.80		0.82
WGG-1	PET		0.75		0.71
WGG-2	PET		0.85		0.92
Average		0.84	0.92	0.95	0.98
COV (%)		6.9	20	7.2	21
WGT-1	PP	0.78*	0.8*[+]	0.99*	1.0*[+]

J_c = reinforcement stiffness from constant load (creep) tests (creep stiffness); J_{crs} = reinforcement stiffness from constant-rate-of-strain (CRS) tests (CRS stiffness); J_r = reinforcement stiffness from constant strain (stress relaxation) tests (relaxation stiffness); *COV* = coefficient of variation = (standard deviation of ratio of stiffness values/mean of ratio of stiffness values) x 100%;

*Estimated based on visual extrapolation with time.

[+] In-soil "creep" data for this product were assumed to be representative of stress relaxation and were therefore used to compute J_r.

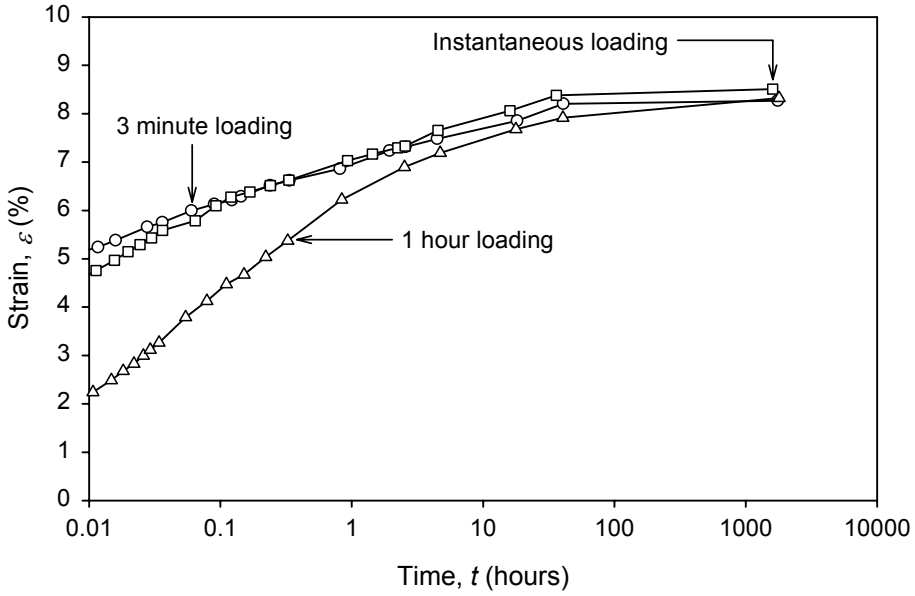

Figure 4.19. Effect of load application rate on in-isolation creep response of HDPE geogrid (adapted from Rimoldi and Montanelli 1993).

Stiffness values determined from the CRS test for the PET geogrid in Figure 4.13 (WGG-3) were about 30 percent greater than the creep stiffness at short times, which is quantitatively different from the curves for creep and CRS tests using polyolefin geogrid products. This difference is a manifestation of the complex molecular structure of PET and possibly the macro-structure of the woven or knitted PET geogrids investigated in this study. There are also some differences in the stiffness values from relaxation and creep tests, as shown in Table 4.2. Excluding WGG-3, the ratio of the relaxation stiffness to the creep stiffness varied from 0.7 to 1.3, with an average of about 0.92 at 100 hours to 0.98 at 1,000 hours.

4.5.2 Effect of Test Type on Geosynthetic Stiffness Determination (Theoretical Analysis)

Figure 4.20 illustrates the theoretical relationship between the creep stiffness and the stress relaxation stiffness for a geosynthetic material. At the start of both tests and shortly thereafter, the constituent polymers possess high and approximately equal creep and relaxation stiffness because of the elastic properties of the material. At very long times during the tests, the viscous behavior of the polymers dominates the mechanical response to the applied load or deformation, resulting in the material exhibiting low and approximately equal creep and relaxation stiffness values. At this stage, the material response is in equilibrium with the applied load or deformation. Between the two extreme times, the creep stiffness differs from the relaxation

stiffness, and Williams (1980) showed that the difference is approximately 10 percent, with the creep stiffness greater than the relaxation stiffness. The time required for the geosynthetic material to exhibit the full range of stiffness values illustrated in the figure depends on the mobility of the molecular chains of the constituent polymers. At 20°C, the molecules in polyolefin-based materials (PP and HDPE) are mobile in a rubbery state, which is in contrast to the glassy state of PET molecules. Hence, PET geosynthetics may require longer testing periods to attain the equilibrium condition during creep and relaxation tests than PP and HDPE geosynthetics.

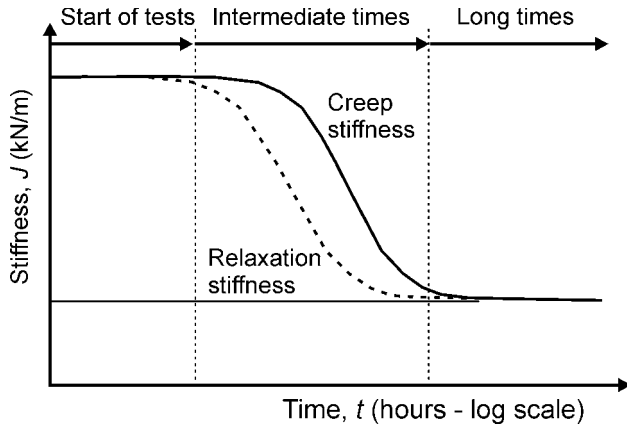

Figure 4.20. Creep and relaxation stiffness as a function of time (adapted from Williams 1980).

In general, the experimental data summarized in this report support the theoretical trends noted above. For practical purposes, the creep and relaxation stiffness determined for HDPE geosynthetics WGG-5 and WGG-6 may be considered equal, at least at low strain levels (figures 4.5, 4.9 and 4.10). The PET geogrids tend to have larger differences between the creep and relaxation stiffness values, and were not converging consistently at the end of the observation times (Figures 4.4, 4.6 and 4.13). It may be argued, on the basis of the molecular structure of PET and this theoretical model, that the observation times in the experiments were within the first half of the intermediate times (Figure 4.20), when there appears to be a trend toward diverging stiffness values.

The other stiffness values of interest are those determined from the CRS test. The load-strain relationship for geosynthetics is shown schematically in Figure 4.3a. At very high strain rates, the initial segments of the curves are linear, reflecting the relatively stiff response of the material at the start of the tests. However, the stiffness of the initial response decreases with decreasing

strain rates, revealing the strain rate dependence of the CRS stiffness values. At later times during the tests, the non-linearity of the relationship is due to the bending of the curves toward the horizontal strain axis. This trend in the curves is attributed to the increased length of time available for the constituent polymer molecules to become aligned in the direction of loading and for the load to accommodate the strain (McCrum et al. 1988). Stress relaxation occurs as the molecular chains slide past each other, resulting in a decrease in the load per unit strain. PP and HDPE geosynthetics exhibit this type of response at 20^{o}C, and the stiffness determined from a CRS test for these materials will be approximately equal to the stiffness determined from a stress relaxation test, as shown in Figure 4.12.

In contrast, the characteristic sigmoidal shape of PET at 20^{o}C is attributed to a maximum stiffness, not at the start of the test but in the range of 0.5-1 percent strain (Voskamp and van Vliet 2001). The stiffness then decreases to a minimum value, followed by an increase in stiffness with increasing strain up to rupture of the specimen. However, Davis and Talbot (1985) and Boyce et al. (2000) showed that at elevated temperatures, PET fibers exhibit a load-strain relationship at low strains similar to that illustrated in Figure 4.3a. Materials that exhibit such load-strain response (PP and HDPE) tend to demonstrate some convergence in the stiffness values at long times. Hence, it is likely that because of longer-term relaxation processes the CRS stiffness will also tend to converge with the creep and relaxation stiffness values of the polyester geogrid WGG-3 shown in Figure 4.13.

Mechanical models consisting of combinations of springs and dashpots have been used to simulate the visco-elastic behavior of geosynthetics. The Standard Linear Solid (Three Element) Model (Sawicki 1999) is the simplest model for predicting the generic stiffness responses shown in Figure 4.20. However, the Standard Linear Solid Model has limited capabilities for simulating the history of the stiffness values from very short to very long periods of time. More complex models such as the Multiple Kelvin Model (Soong and Koerner 1998, Zhang and Moore 1997) and the Multiple Maxwell Model (Soong and Lord 1998) are therefore used for the theoretical analyses of the effect of complex loading histories on the geosynthetic stiffness beyond the observation times of the experiments.

4.5.3 Effect of Test Type on Geosynthetic Stiffness Determination (Analysis Summary)

The differences in the stiffness values obtained from a variety of test types at the times of interest (100 to 1,000 hours or more) are relatively small. For woven geotextiles and geogrids, soil confinement appears to have little effect on the stiffness (less than a 5 to 15 percent increase). Therefore, in-isolation testing should be sufficient for these materials. The available data show that the in-isolation creep test from which stiffness values are easily calculated tend to give the highest estimates of the long-term stiffness values. Thus the results of this test are conservative for the estimation of reinforcement loads in design. Furthermore, analysis of full-scale walls (see Chapter 6.0) suggests that at the end of wall construction, the reinforcement tends to exhibit primarily creep, while at long times after construction, the reinforcement tends toward pure relaxation once the soil ceases to deform. Therefore, it can be concluded that the in-isolation creep test can be used to conservatively estimate the reinforcement stiffness at longer times (e.g., 500 to 1,000 hours or more) for woven geotextiles and geogrids for the purpose of calculating reinforcement loads in field-scale walls.

4.6 Accuracy of the Geosynthetic Stiffness Determination

Material variability and uncertainty in test interpretation can become a significant issue for the determination of stiffness values at very low strains. Statistical analyses performed on data obtained by Gallagher (1995) for undamaged specimens of geotextiles are summarized in figures 4.21 and 4.22. These plots show that there is a general trend of increasing magnitude of coefficient of variation (*COV*) for stiffness values with decreasing magnitude of strain. However, there is not a consistent trend for *COV* values with magnitude of strain rate.

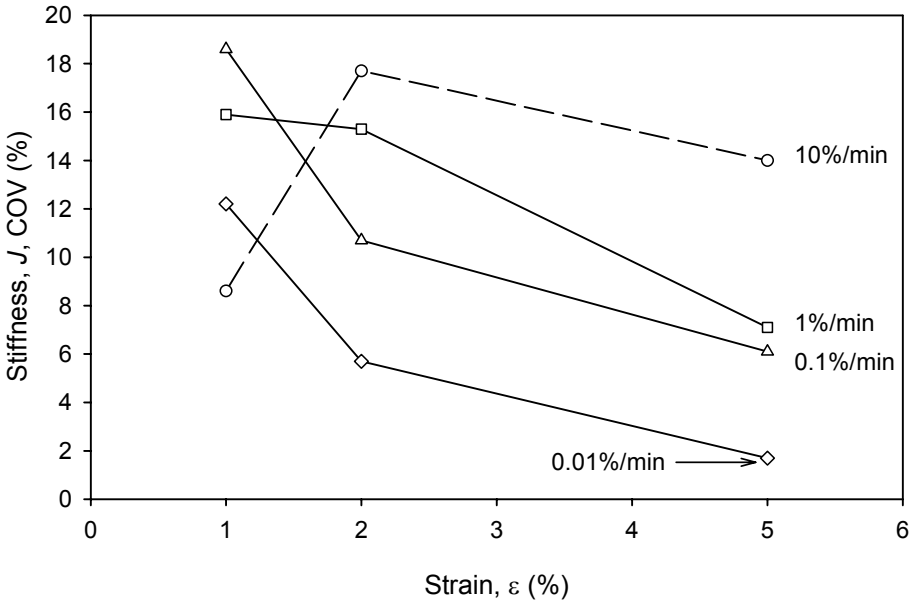

Figure 4.21. Coefficient of variation (COV) for stiffness values at various strains for a woven PP geotextile tested at various strain rates using data reported by Gallagher (1995**)**.

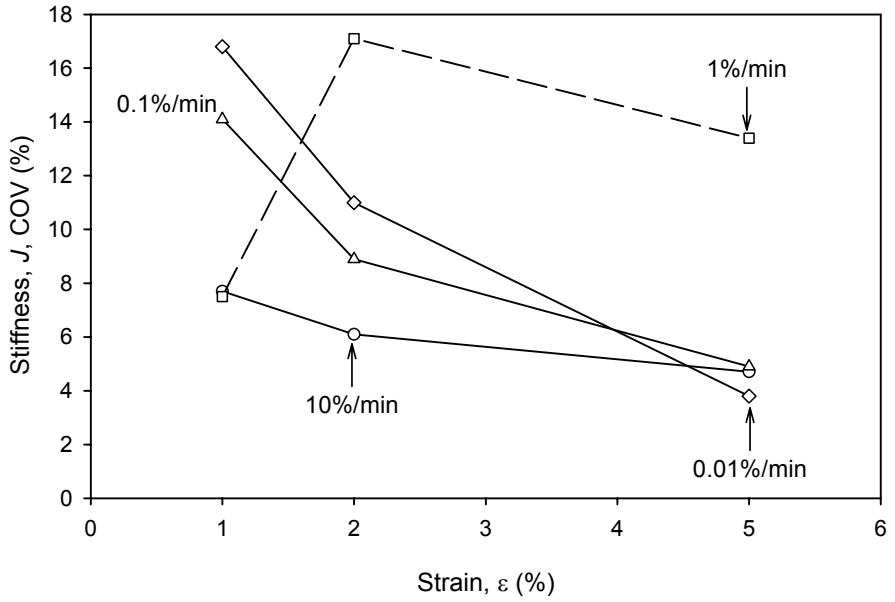

Figure 4.22. Coefficient of variation (COV) for stiffness values at various strains for a woven PET geotextile tested at various strain rates using data reported by Gallagher (1995).

Table 4.3 provides data presented by Allen and Bathurst (1994), who quantified variability in stiffness values caused by installation damage. This table also shows the magnitude of *COV* values for different geosynthetics. Geosynthetic stiffness variability, including the effect of damage and strain levels, can be summarized as follows:

- At 5 percent strain, the short-term CRS stiffness value had a *COV* of 3 to 10 percent. Calculating the stiffness at lower strains, say 1 to 2 percent strain, increases the *COV* value, on average, by a factor of approximately 1.7 relative to the *COV* measured at 5 percent strain, given the data for woven geotextiles presented in figures 4.21 and 4.22. For geogrids, based on tensile test data available to the writers (Allen and Bathurst 1994), the *COV* value for geogrids appears to increase, on average, by a factor of 1.5 relative to the stiffness values at 5 percent strain. Furthermore, installation damage increases the *COV* value by a factor of 1.2 for geogrids (on average) and by 1.5 for woven geotextiles.
- The COV did not appear to consistently be affected by time effects. Therefore, the short-term stiffness COV is assumed to be approximately the same as the long-term COV value.

These data lead to the conclusion that the COV of the stiffness at 2 percent strain, given the effects of significant installation damage and time, can be expected to vary from 5 percent to 18 percent for geogrids to approximately 26 percent for woven geotextiles. If installation damage is light (say, strength losses of less than 20 percent), the COV values will likely be less.

Table 4.3. Coefficient of variation of reinforcement modulus at 5 percent strain for various geosynthetics in both virgin and damaged conditions.

Product Type	Condition	COV (%) of CRS Stiffness value at 5% strain	% Increase in COV Due to Damage
Geotextile	*Virgin*	10.3	
	Damaged	15.2	47.6
HDPE Geogrid	Virgin	2.6	
	Damaged	3.1	19.2
PET Geogrid	Virgin	6.4	
	Damaged	7.1	10.9
PP Geogrid	Virgin	8.2	
	Damaged	10.3	25.6

Note: All tests carried out at 10% strain/minute.

4.7 Approach to Determine the Reinforcement Stiffness Value to Convert Geosynthetic Strain to Load

On the basis of arguments presented in the previous sections, a practical approach for calculating the in-soil reinforcement stiffness is to use the stiffness from in-isolation creep tests, at least for geogrids and woven geotextiles. If in-isolation creep data are used, the stiffness of the geosynthetic can be estimated as follows:

1. Determine the total length of time necessary to complete construction of the wall at a given section (i.e., the time after which no additional loading will occur – see Figure 4.1 as an example).
2. Using the procedures illustrated in Figure 4.3, develop an in-isolation creep stiffness versus time curve at constant strain levels of interest, and select the creep stiffness on the basis of the elapsed time to the end of wall construction. For the example walls in Figure 4.1, this time is 500 to 1,500 hours. Select the stiffness at the anticipated maximum working strains for the wall, as the stiffness is likely to be strain level dependent. For design purposes, a 2 percent secant stiffness at 1,000 hours is likely reasonable. If strains of 3 to 4 percent or more are anticipated, determine the stiffness at the higher strain level. If strains of significantly less than 2 percent are anticipated, and a geosynthetic material is being used that is known to have a highly non-linear load-strain curve over the strain range of interest (e.g., some PET geosynthetics), then a stiffness value determined at a lower strain should be considered. This recognizes the difficulties of accurately measuring the stiffness at such low strains.
3. If the effective site temperature is anticipated to be significantly different from 20^{o}C, the creep stiffness value may need to be temperature shifted, requiring creep data at higher or lower temperatures to establish the appropriate shift factors. See Bush (1990) for an example of temperature shifting.

Correct the stiffness obtained in Step 3 for soil confinement effects if the reinforcement is not a geogrid or slit film woven geotextile. For multi-filament woven geotextiles, the in-isolation stiffness may need to be increased by a factor of 1.1 to 1.2 and for nonwoven geotextiles by a factor of 2 to 5. In-soil load-strain tests are recommended for nonwoven geotextiles.

Estimates of the ratio of the creep stiffness value at typical working conditions (i.e., strains at say, 2 percent and loading times of 1000 hours) to the stiffness value from a conventional CRS test (e.g., ASTM D 4595) are summarized in Table 4.4. The data show that for polyolefin products the CRS stiffness from tests run at 10 percent strain/minute is approximately 3 to 4 times that of the creep stiffness value. These data imply that using the index stiffness value in reinforcement load calculations for polyolefin products can be expected to overestimate the reinforcement loads by a similar factor, thus leading to excessively conservative design. The corresponding error for PET products is less, resulting in an over-estimation of reinforcement loads in the range of about 20 to 30 percent. This table is also useful for estimating long-term creep stiffness values for back-analysis of instrumented walls when creep data for the reinforcement materials are not available.

Table 4.4. Ratio of typical working stress stiffness (at 1,000 hours) to the stiffness obtained in a CRS test at 10 percent/minute, per ASTM D4595.

Geosynthetic Polymer	$J_{1000\ hrs}/J_{D4595}$
PP	0.25 to 0.35
HDPE	0.25 to 0.35
PET	0.75 to 0.85

4.8 Conversion of Strains to Loads and Estimate of Error

Equation 4.1 can be rewritten as:

$$T_i = J_c \times \varepsilon_i \tag{4.2}$$

to estimate the reinforcement load from the reinforcement stiffness value and measured strain. Associated with each load value is uncertainty in the predicted value that varies with the magnitude of the estimate of error of the stiffness and strain measurements. The reliability of stiffness values has been summarized in Section 4.6 and quantified using a coefficient of variation (*COV*) value. The resolution and reliability of stain measurements using different combinations of instrument and reinforcement types are examined in Chapter 3.0. Uncertainty in strain measurements (COV_ε) and stiffness values (COV_J) are uncorrelated (i.e. independent). Therefore, total uncertainty in estimated reinforcement loads can be quantified by a coefficient of variation (COV_T) value calculated as follows (Ang and Tang 1975):

$$COV_T = \sqrt{COV_\varepsilon^2 + COV_J^2} \quad (4.3)$$

In the following section, the error on the estimated reinforcement load from strain measurements is expressed as ± one standard deviation using COV_T values.

4.9 Full-Scale Geosynthetic Wall Case Histories with Measured Loads and Measured Strains

One full-scale field case history (a welded wire-faced, steep reinforced slope), and only a few full-scale laboratory geosynthetic reinforced soil walls have produced direct measurements of both the reinforcement load and strain.

4.9.1 Wall GW7

Wall GW7 is technically a steep reinforced slope with a facing batter of 2V:1H and was built with two different reinforcement sections (see Chapter 2.0**)**. Fannin and Hermann (1991) reported isochronous creep curves that are considered to be representative of the geogrid used in the wall (the source of the data was from the product manufacturer but was not lot-specific). The average temperature in the wall was approximately 8°C, and the average temperature for the warmest month was approximately 12°C (Fannin 2001). Data from Fannin (1988, 2001**)** indicated that the temperature in the wall during its construction typically varied from 10 to 12°C, although peaks as high as 20°C did occur. A temperature of 10°C was used to estimate the stiffness of the reinforcement on the basis of the procedures outlined in Section 4.4.4. Fannin and Hermann (1991) also characterized the wall temperature as 10°C.

The procedure illustrated in Figure 4.3b was used to estimate the creep stiffness at the end of wall construction (960 hours) and at the end of surcharge construction (2,600 hours). Using the isochronous creep curves obtained for the product used in the wall at 10°C, and a strain level of 2 percent to characterize the low strain stiffness of the geogrid, a creep stiffness versus time curve out to 1,000 hours at 10°C was created. A similar curve was created for 20°C. Using the approach provided by Bush (1990), the 20°C curve was used to extrapolate the 10°C curve to 2,600 hours. From the extrapolated 10°C creep stiffness curve at 2 percent strain, a reinforcement stiffness of 362 kN/m at 960 hours (end of construction) and 353 kN/m at 2,600 hours (surcharge in place) was obtained. Figure 4.23 illustrates the creep stiffness curves, the

extrapolation using time-temperature superposition, and how these stiffness values were determined. As indicated in Table 4.3, for an HDPE geogrid, a typical value for the *COV* of the stiffness at 5 percent strain is approximately 3.1 percent. At low strains (2 percent or less), the *COV* will increase, on average, by a factor of 1.5 for geogrids (Section 4.6), resulting in *COV* = 4.7 percent. Lot-specific tensile strength data were not available for this particular case history. Therefore, a value of COV_J = 6 percent was assumed to capture uncertainty in the estimated stiffness values for the HDPE geogrid. Strain readings were determined by using the average of readings from sets of three Bison inductance coils located at nominal identical locations in the cross-plane strain direction of the two sections. Values for uncertainty in calculated strains from inductance coil readings were taken as COV_ε = 40 and 32 percent for strains less of than and greater than 0.1 percent, respectively (Table 4.3; see Chapter 3.0). The combined uncertainty using Equation 4.3 is therefore 40 percent for strains of greater than 0.1 percent. Note that in this example case study, the uncertainty in estimated load values is due largely to uncertainty in the measured strains.

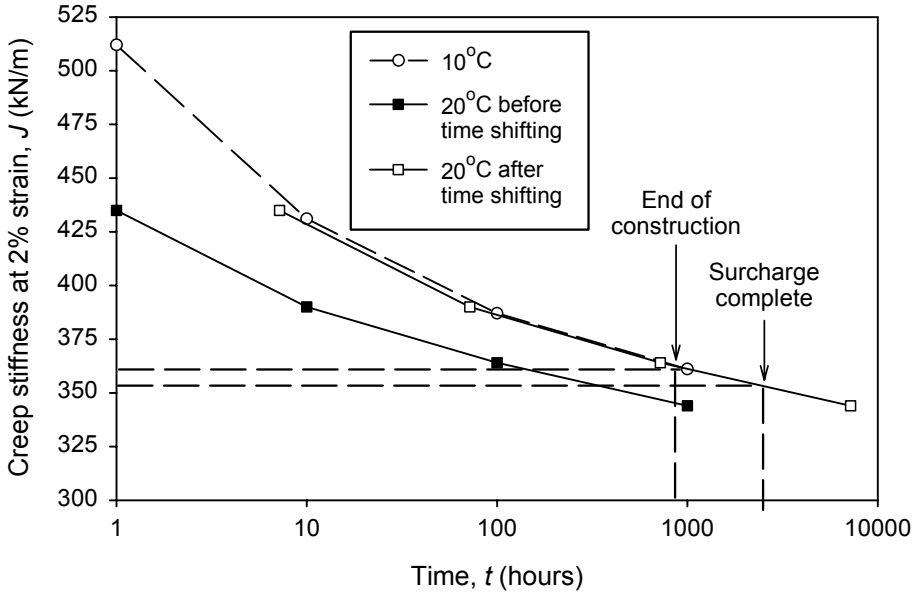

Figure 4.23. Creep stiffness data to convert measured strains to load for Wall GW7, Sections J and N.

Figure 4.24, developed from data provided by Fannin and Hermann (1990), shows loads measured by load cells placed directly in the reinforcement layers and loads estimated from the

inductance coils. Data to estimate uncertainty in load cell readings are not available; hence error bars on load cell readings do not appear in the figure.

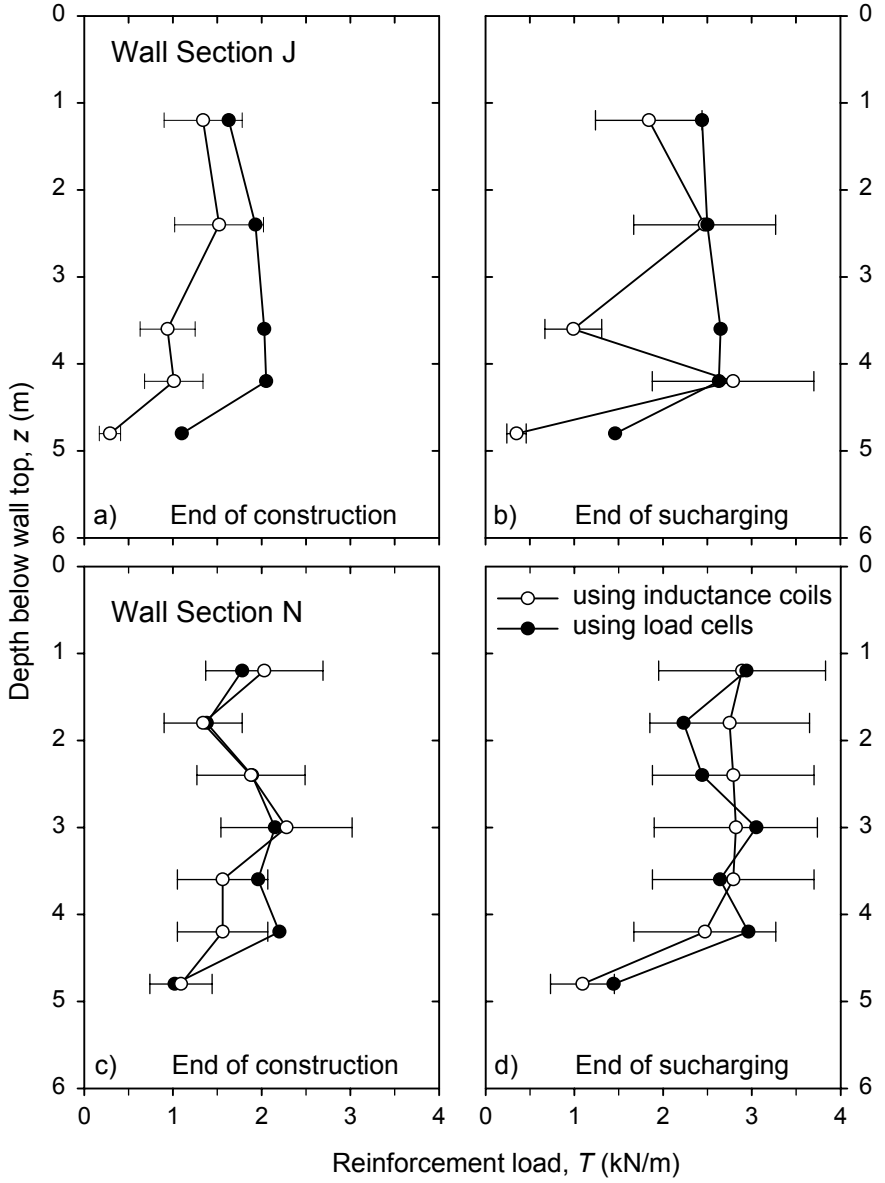

Figure 4.24. Measured reinforcement loads, and loads predicted from inductance coil readings for Wall GW7. Note: Error bars represent ±1 standard deviation on estimates of reinforcement load using inductance coils.

The loads estimated from inductance coils were less than the values measured by the load cells for Section J (with one exception), and about the same for Section N. The largest difference was at the end of construction for Section J (estimated loads from inductance coils were 26 to 82

percent of measured load values). This discrepancy may be related to the ability of the load cells to attract additional load as a result of soil-load cell interaction and their inability to creep or stress relax. Consequently, as soil creep occurs, the load cells may tend to gain load while the geosynthetic reinforcement stiffness continues to soften. Nevertheless, it is interesting to note that for each plot the range of measured values from load cells was reasonably consistent with the range of loads estimated from inductance coil readings and best estimates of reinforcement stiffness.

4.9.2 Propped Panel Wall GW14

A propped panel-faced geogrid wall was built to full scale in the laboratory to a maximum height of 3.0 m (Benjamin 1989; see Chapter 2.0). Reinforcement forces were measured directly by load cells at the connection with the facing and estimated from strains measured by strain gauges and extensometers attached to the reinforcement just beyond the load cells. The distance between the load cells and the strain gauges on the reinforcement was 0.07 m or less. Isochronous creep data, obtained at 20^{o}C to correspond with the ambient temperature of the laboratory, was used to determine the stiffness on the basis of construction time, duration of surcharging and the strain level in the reinforcement. Strains in the wall varied from 0.5 to 1.5 percent at the end of construction to almost 8 percent maximum for the maximum surcharge load applied to the wall top. The wall was constructed in 184 hours, and the final 80-kPa surcharge load was placed at 1,026 hours from the start of wall construction. The stiffness values obtained from the creep data varied, depending on the strain level and the time, from 84 to 90 kN/m at end-of-construction and from 43 to 78 kN/m once the 80-kPa surcharge was placed. Figure 4.25, developed from data reported by Benjamin (1989), provides a comparison of loads measured by load cells at the facing connection and loads estimated from the nearest location of strain gauges and extensometer points. Extensometer readings were used for strains in excess of 2 percent. On the basis of Table 4.3, a typical value for the *COV* of the stiffness for PP geogrid at 5 percent strain is approximately 10 percent (installation damage was negligible in this case history). At low strains (2 percent or less), the *COV* will increase, on average, by a factor of 1.5 for geogrids (Section 4.6), resulting in a *COV* value of approximately 15 percent. No additional uncertainty in the stiffness value was required because lot-specific tensile strength data were available for this particular case history. Therefore, a value of COV_J = 15 percent was assumed to capture

uncertainty in the estimated stiffness values for the PP geogrid in this case study at the end of construction and COV_J = 10 percent at the highest surcharge level, consistent with larger measured strain levels. Values for uncertainty in magnitude of strains were taken as COV_ε = 13 percent for strain gauge readings and COV_ε = 9 percent for extensometer readings (Table 4.3; see Chapter 3.0). The combined uncertainty in the loads using Equation 4.3 ranged from 16 to 20 percent, depending on the strain level and instrument type. In this particular example the contribution to estimate of error in the calculated reinforcement load is similar for both the stiffness value and strain measurements.

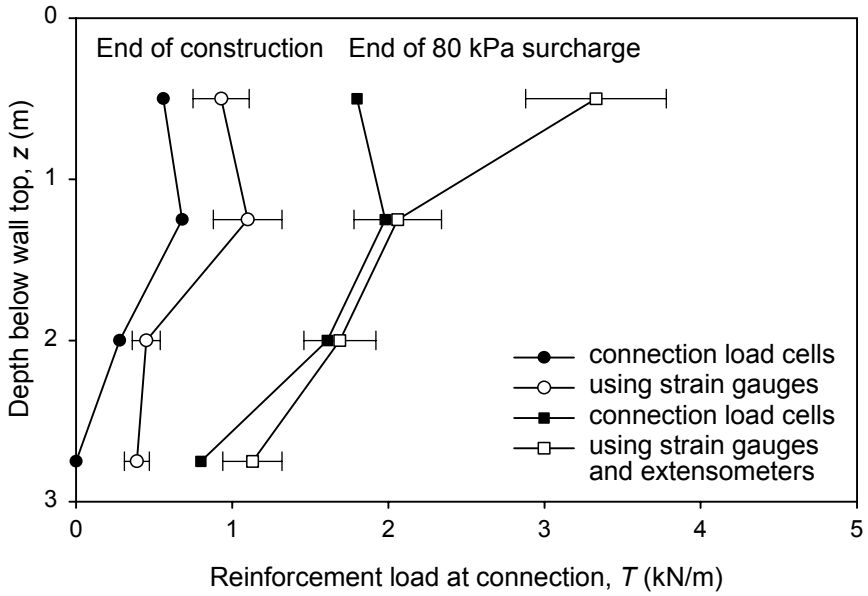

Figure 4.25. Measured reinforcement connection loads and connection loads predicted from strain gauge and extensometer measurements, for Wall GW14. Note: Error bars represent ± 1standard deviation on estimates of reinforcement load using strain gauge and extensometer readings.

The load levels from the load cells at the connection are slightly lower than those estimated from the strain gauge readings. The high value of the load estimated with the strain gauge in the top reinforcement layer relative to the load measured by the load cell is thought to be due to vertical settlement of the soil directly behind the facing, which can lead to the generation of additional downdrag strains. The strain gauges are able to record additional strains because of changes in the reinforcement out-of-plane geometry, whereas the load cells were configured to record only the in-plane horizontal load in the reinforcement. Notwithstanding the complications

noted above, the measured loads and loads estimated from interpretation of reinforcement strains are considered to be in reasonable agreement.

4.9.3 RMCC Segmental Block-Faced Walls

A series of segmental block-faced geogrid reinforced soil walls built to full scale in the laboratory to a maximum height of 3.6 m were reported by Bathurst et al. (2000). Figure 4.26 shows a cross section of Wall 1 as an example of the typical configuration and instrumentation of these test walls and is the wall used here to compare connection loads estimated from reinforcement strains and stiffness values, and loads measured by facing connection load cells. Reinforcement forces were measured directly by load cells at the connection with the facing and estimated from strains measured with strain gauges and extensometers attached directly to the reinforcement near the load cells. The distance between the load cells and the strain gauges on the reinforcement was 0.13 m or less.

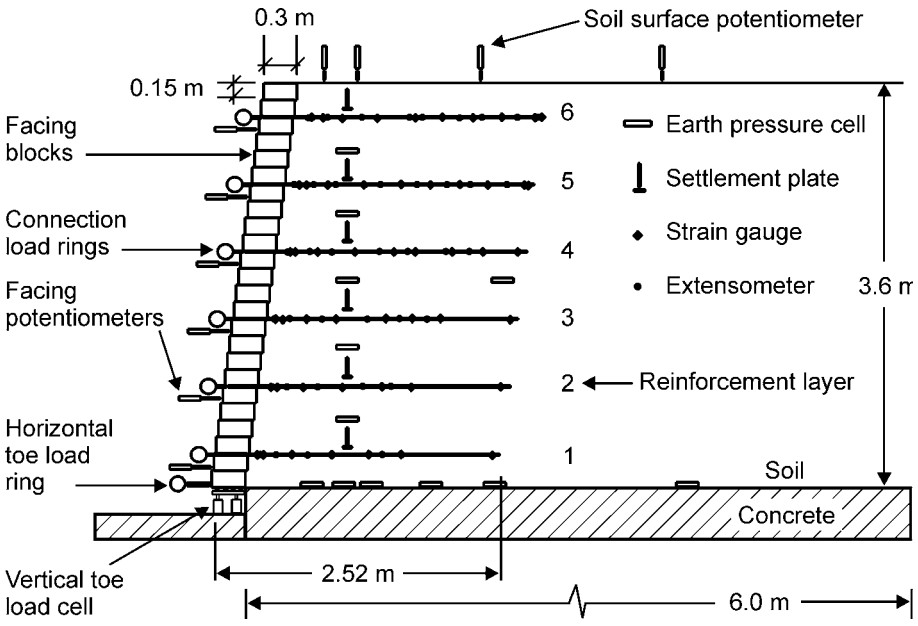

Figure 4.26. Typical cross-section for RMC Walls 1 and 2 (after Bathurst et al. 2000).

Using the approach described in Section 4.7, isochronous creep data were used to estimate the stiffness on the basis of the duration of construction time, surcharging, and measured strains as the criteria for establishing the correct reinforcement stiffness. The data used were from lot-specific 1,000-hour 20°C creep testing reported by Burgess (1999). Strains in these walls varied from 0.06 to 0.7 percent close to the connections at the end of construction to about 2 percent during the 50-kPa uniform surcharge load applied to the soil backfill. The wall was constructed in 2,020 hours and maintained at an ambient temperature of approximately 20° C. The final surcharge load was placed at approximately 3,500 hours relative to the start of wall construction. The stiffness values obtained from the creep data varied, on the basis of strain level and elapsed time, from 110 to 122 kN/m at end-of-construction and from 39 to 95 kN/m at the highest surcharge load. Values of COV_J = 15 percent and COV_ε = 13 percent were used in this case study for the reasons described in the previous example and contributed approximately equally to the uncertainty in the estimate of reinforcement load from strain readings.

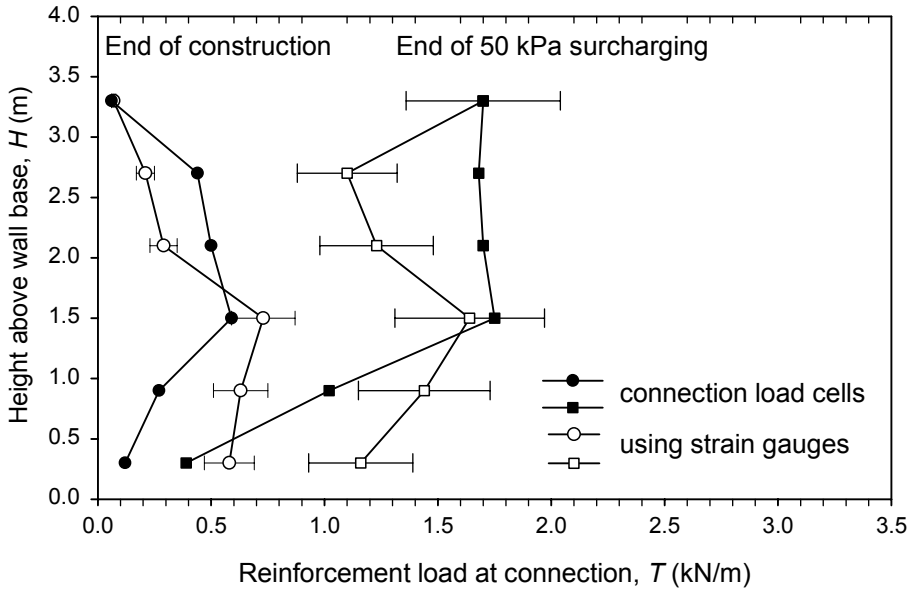

Figure 4.27. Measured reinforcement connection loads and connection loads predicted from strain gauge measurements, for RMC Wall 1 from data reported by Burgess (1999). Note: Error bars represent ± 1 standard deviation on estimates of reinforcement load using strain gauge readings.

Figure 4.27 was developed from data provided by Burgess (1999) and shows a comparison of loads measured by connection load cells and loads estimated from the nearest location of strain

gauge pairs. As shown in the figure, the range in magnitude of load estimated from strain gauge readings overlaps the range in loads measured by the load cells with the exception of the two lowest layers at 50-kPa surcharge. Possible sources of local differences in measured and inferred loads from strain readings have been noted in the previous section.

4.10 Summary and Conclusions

The primary means of assessing the load level in geosynthetic reinforcement in full-scale reinforced soil structures is to convert reinforcement strains to load using the reinforcement stiffness. Because the geosynthetic stiffness is a function of time, and to some extent loading history, the reinforcement stiffness must be determined with consideration to the time over which the load is applied. Past practice regarding the determination of the correct reinforcement stiffness value to convert strains to load has been varied, ranging from direct use of a short-term index tensile test stiffness (e.g., ASTM D 4595) to in-isolation isochronous creep data. The most common method has been the in-isolation isochronous creep approach. The report demonstrates that the loading rate in a typical index the test (ASTM D 4595) is approximately 5 orders of magnitude larger than the loading rate of the reinforcement in several example full-scale walls. This difference in loading rate leads to a large difference in the estimated stiffness value for the reinforcement at end-of-construction and beyond. For example, the simple use of stiffness values taken at 2 percent strain during an index CRS test run at 10 percent strain/minute (ASTM D 4595) can lead to an over-estimation of reinforcement loads for polyolefin products by a factor of 3 to 4 and, hence, lead to excessively conservative design. The corresponding error for PET products is less, resulting in an over-estimation of reinforcement loads in the range of about 20 to 30 percent.

Both stress relaxation and creep may occur in geosynthetic reinforcement embedded in soil in full-scale structures. This report has provided a detailed evaluation of the various approaches for measuring or estimating the long-term stiffness of geosynthetic reinforcement, using in-isolation and confined in-soil creep, relaxation, and constant-rate-of-strain laboratory test results reported in the literature, as well as data developed specifically for the current study. It was found that although there are minor differences in the results among the various test types, they were not large enough to be significant, given the natural variation in the material properties.

Uncertainty in the estimate of reinforcement stiffness due to material variability can be significant, and installation damage can cause this variability to increase, with the coefficient of variation (*COV*), after installation damage, ranging from 5 to 18 percent for geogrids and up to approximately 26 percent for woven geotextiles. The magnitude of uncertainty in stiffness values due to material variability is larger than the differences in the stiffness values due to test methodology (i.e., in-isolation versus in-soil, creep versus stress relaxation or CRS tests). Furthermore, the primary approach recommended here, in-isolation creep testing, tends to provide a conservative estimate for the purpose of estimating reinforcement load. It is also shown that the contribution of the error in the estimate of reinforcement strain measurements is typically equal to or greater than the error associated with the variability in estimate of reinforcement stiffness based on in-isolation creep data.

In summary, the use of in-isolation creep stiffness data, determined for the time required to reach the end of wall construction, the reinforcement temperature, and the strain in the reinforcement, is considered to be sufficiently accurate for estimating reinforcement loads from strain measurements, at least for geogrids and most woven geotextiles.

The approach provided in this chapter has been used to estimate reinforcement loads from measured reinforcement strain data in carefully instrumented wall case histories. A comparison of load values with directly measured values shows that that reinforcement loads estimated from measured reinforcement strain data and reinforcement stiffness values are reasonably accurate and give values that are generally within the range of values for multiple layers of reinforcement reported for the instrumented wall case studies.

5.0 SOIL REINFORCEMENT LOADS IN GEOSYNTHETIC REINFORCED SOIL WALLS AT WORKING STRESS CONDITIONS

5.1 Introduction

Knowing the load in geosynthetic reinforcements in full-scale reinforced soil walls is an important step toward improving the procedures for designing the internal stability of these structures. The internal design of reinforced soil walls uses the reinforcement load to assess the reinforcement strength and spacing required, as well as the length of the reinforcement for pullout design. The study of such empirical reinforcement load data enables analytical models to be properly calibrated, and the empirical data also provide a baseline upon which any new design methods can be compared to assess their accuracy.

In general, loads in MSE wall soil reinforcements must be estimated from strain measurements and converted to load through the stiffness of the reinforcement material. Two requirements to estimate reinforcement load are as follows:

1. determination of the strain in the reinforcement that accounts for sources of strain measurement error through proper gauge location, calibration, and redundancy in the measurements
2. determination of the stiffness of the reinforcement, accounting for the dependence of reinforcement stiffness on time, strain level, temperature, the effects of soil confinement, installation damage, and variability in the measurement of stiffness from laboratory tests.

The first issue is addressed in Chapter 3.0, where a summary of measured strains in actual geosynthetic walls and an assessment of the accuracy and reliability of the strain measurements are provided. The second issue is addressed in Chapter 4.0, where a detailed assessment of the time dependence of the stiffness of geosynthetics and an assessment of the accuracy and reliability of the stiffness values are provided.

The purpose of this chapter is to use the data and principles developed in the previous chapters to determine the peak loads estimated from measured strains in the reinforcement layers in several well documented geosynthetic wall case histories. Once the correct reinforcement loads have been determined and summarized, general trends in the data are compared to predictions from current design practice. All of the case histories involved relatively clean

granular backfills (i.e., less than 15 percent silt content and little, if any, plasticity), and were placed on relatively competent foundation soils (see Chapter 2.0). Therefore, the scope of this chapter is limited to geosynthetic walls with relatively clean, non-cohesive sand or gravel backfill, placed on competent foundation soils.

5.2 Geosynthetic Stiffness Assessment for Geosynthetic Wall Case Histories

Chapter 4.0 provides a protocol that can be used to determine the best geosynthetic stiffness for converting measured strain from strain gauges or extensometers to estimated reinforcement loads. The stiffness of geosynthetics is typically time dependent, tending to decrease with the amount of time over which the load is applied, as well as strain level and temperature dependent. While this behavior is well known, these factors have not always been considered by those who have attempted to convert measured geosynthetic strains to load. Wall reinforcements are loaded at a much slower rate than is applied in conventional tensile strength index tests, causing the stiffness values from these tests to be too high for accurate conversion of wall reinforcement strains to load. To properly assess the correct stiffness, the visco-elastic-plastic processes that are dominant for polymeric geosynthetic reinforcement products in walls must be identified. In consideration of overall wall behavior (see Chapter 6.0), laboratory simulations of geosynthetic in-soil creep behavior, and data presented in Chapter 4.0, the processes that result in time-dependent changes in reinforcement stiffness can include both creep and stress relaxation of the surrounding granular soils before soil failure. For example, the soil may restrict the time-dependent deformation of the geosynthetic, forcing it to exhibit some stress relaxation. In some cases, the loading of the reinforcement may be simulated by a constant-rate-of-loading or constant-rate-of-strain (CRS) test, since the load and strain levels within a wall during construction typically increase with the height of the wall. Test results reported in Chapter 4.0 show that the stiffness value determined from creep tests is not necessarily the same as the stiffness value obtained from stress relaxation tests or constant-rate-of-strain tests. Fortunately, the differences are not large, especially at the times of interest for assessing the stiffness of geosynthetic reinforcement at the end of wall construction. It was concluded in Chapter 4.0 that the use of in-isolation creep data to assess the time, strain, and temperature-dependent stiffness of geosynthetic reinforcements in walls is sufficiently accurate for the purpose of converting strains to loads in reinforced walls, even after other sources of variability in the geosynthetic

material properties have been considered, such as the effect of soil confinement, variability in the reinforcement properties, and uncertainty in strain measurements. Chapter 4.0 also compares the reinforcement loads determined through this approach to loads measured in the reinforcement directly using load cells for those case histories in which these data were available, and concludes that the range of predicted reinforcement loads is in reasonable agreement with directly measured values.

Key properties and parameters for each of the case histories for which reinforcement loads are determined and analyzed in this chapter are summarized in Table 5.1. Details for each of these case histories, including wall and reinforcement geometry, reinforcement type, soil properties, and construction history, are provided in Chapter 2.0. Using the strain measurements from Chapter 3.0 and the stiffness assessment approach provided in Chapter 4.0, the reinforcement loads for each of the wall case histories can be determined.

Table 5.2 provides a summary of measured peak strains, reinforcement stiffness values, estimated reinforcement loads in the reinforcement layers and the estimated accuracy of these values expressed in terms of the coefficient of variation (*COV*). The coefficient of variation values for strain measurements (COV_ε) in Table 5.2 have been estimated from data presented in Chapter 3.0 corresponding to the case studies in Table 5.1 and more recent full-scale wall trials at the Royal Military College of Canada (Bathurst et al. 2000). The method of calculating reinforcement loads and the corresponding accuracy of computed values are discussed in Section 5.3. For each case history, the determination of the recommended stiffness is provided in the sections that follow. In-isolation creep data are first used to determine the creep stiffness by using the procedure described in Chapter 4.0 at the time corresponding to the end of construction and at the desired strain level, though typically a strain level of 2 percent was used. This value is then adjusted for the average temperature within the wall and any soil confinement and installation damage effects. Note that in most cases, soil confinement effects are minor (nonwoven geotextiles are the exception). In addition, the reliability and accuracy of the stiffness determination is discussed. Because the complexity of the factors that affect the accuracy of the stiffness value, a strict statistical determination of the variability in stiffness values is not possible. However, the combined potential variation in the stiffness due to factors such as material variability, installation damage effects, lack of lot-specific test data, and time effects can be roughly estimated.

Table 5.1. Summary of properties and parameters used to calculate geosynthetic stiffness for each case history.

Wall Case History	Time for Wall Construction (hours)	Wall Temperature (^oC)	Geosynthetic	$J_{2\%}$, kN/m (10%/min. Strain rate, 20^o C)	$J_{2\%}$, kN/m (at the End of Construction - EOC)	Global Wall Stiffness at End of Construction (kN/m^2) (Equation 5)
Tanque Verde HDPE geogrid wall (GW5)	350	27	Tensar SR-2	980	340	720
Oslo, Norway Wall, Sections J and N (GW7)	960 to top of wall, 2600 to surcharge completion	10	Tensar SR-55	670 at 20^o C, 750 at 10^o C	360 at EOC, 350 at surcharge completion (100 at surcharge completion for secondary reinforcement)	430 for Section J, 590 for Section N at surcharge completion
Algonquin Tensar geogrid wall (GW8)	920	17	Tensar SR-2	2040	500	660
Algonquin Miragrid wall (GW9)	920		Miragrid 5T	500	200	260
Algonquin Geotextile wall (GW10)	8000 for wall construction, then 10 hours to remove water supporting bottom part of wall		Quline 160	180 confined in soil	Approximately 180	210
RMC geogrid wrapped-face wall (GW11)	65	20	Tensar SS2, weak direction	430	110	150
RMC full-height plywood panel-faced wall (GW12)	100 hours after prop release, 880 hours to final surcharge		Tensar SR-2	980	550 at EOC, 500 at surcharge completion	730 at EOC, 660 at surcharge completion
RMC incremental plywood panel-faced wall (GW13)	220, 3080 hours to final surcharge		Tensar SR-2	980	530 at EOC, 460 at surcharge completion	710 at EOC, 610 at surcharge completion
RMC full-height (GW14) aluminium panel- and incremental panel- (GW15) faced wall	EOC at 200 hours for incremental panel wall, 100 hours for propped panel wall		Tensar SS1, weak direction	250	Varies from 43 to 95, depending on strain and time after loading	Varies from 81 to 121, depending on strain and time after loading

Table 5.1. Continued.

Rainier Ave. wall (GW16)	1630 to EOC, 1920 to surcharge completion	14	GTF 200 from 0 to 3.1 m below wall top	220	100 to 120	1000 to 1100
			GTF 375 from 3.2 to 6.5 m	370	190	
			GTF 500 from 6.6 to 9.6 m	670	340 to 350	
			GTF 1225T from 9.7 to 12.5 m	1,300	1,000	
Fredericton, New Brunswick wall (GW18)	100 hours after prop release	10	Tensar SR-2	Unknown	500	740
St Remy PET strip test wall (GW19)	1800 hours	20 (assumed)	Paraweb 2S Strip	9,600	7,400	9,200
Vicenza, Italy HDPE wall (GW20)	150 to EOC, 5500 to end of surcharge	20 (assumed)	Tenax TT201 SAMP	900	300	220
Vicenza, Italy PP wall (GW20)			Tenax LBO 220 SAMP	500	90 to 100	75

Table 5.2. Summary of measured peak strains and estimated loads, including uncertainty, for geosynthetic reinforcement layers in walls.

Wall	Depth below Wall Top, z (m)	Measured Peak Strain (%)	Estimated Strain COV_ε (%)	Reinforcement Stiffness (kN/m)	Estimated Stiffness COV_J (%)	Reinforcement Load (kN/m)	Calculated COV_T for Reinforcement Load (%)
Tanque Verde HDPE geogrid wall (GW5)	1.14	0.18	13	340	6	0.59	14
	3.28	0.33	13	340	6	1.09	14
	4.2	0.25	13	340	6	0.84	14
Oslo, Norway geogrid steep slope, Section J (GW7) (with soil surcharge)	1.2	0.52	32	350	6	1.84	33
	2.4	0.70	32	350	6	2.47	33
	3.6	0.28	32	350	6	0.99	33
	4.2	0.79	32	350	6	2.79	33
	4.8	0.10	40	350	6	0.35	40
Oslo, Norway geogrid steep slope, Section N (GW7) (with soil surcharge)	0.6	0.92	32	350	6	3.25	33
	1.2	0.82	32	350	6	2.89	33
	1.8	0.78	32	350	6	2.75	33
	2.4	0.79	32	350	6	2.79	33
	3	0.80	32	350	6	2.82	33
	3.6	0.79	32	350	6	2.79	33
	4.2	0.70	32	350	6	2.47	33
	4.8	0.31	32	350	6	1.09	33
Algonquin HDPE geogrid wall (GW8)	1.2	0.35	13	500	30	1.75	33
	2.5	0.71	13	500	30	3.55	33
	4.2	0.76	13	500	30	3.80	33
	5	0.74	13	500	30	3.70	33
	5.7	0.18	13	500	30	0.90	33
Algonquin PET geogrid wall, no surcharge (GW9)	0.8	*0.18	29	200	11	0.36	31
	2.6	*0.41	29	200	11	0.82	31
	4	*0.46	29	200	11	0.92	31
	5.2	*0.63	29	200	11	1.26	31
	5.8	*0.17	29	200	11	0.34	31
Algonquin PET geogrid wall, with surcharge (GW9)	0.8	*0.38	29	200	11	0.76	31
	2.6	*0..87	29	200	11	1.74	31
	4	*1.0	29	200	11	2.00	31
	5.2	*0.86	29	200	11	1.72	31
	5.8	*0.22	29	200	11	0.44	31

Table 5.2. Continued

Algonquin geotextile wall (GW10)	1.0	3.00[+]	29[++]	180	50	[+]5.25	58
	2.6	3.00[+]	29[++]	180	50	[+]5.25	58
	4.2	2.00	29[++]	180	50	3.50	58
	4.9	1.60	29[++]	180	50	2.80	58
	5.65	1.10	29[++]	180	50	1.93	58
RMC geogrid wrapped-face wall (GW11)	0.6	1.97	13	110	17	2.17	21
	1.35	2.66	13	105	17	2.79	21
	2.1	1.25	13	110	17	1.38	21
	2.85	0.20	13	110	17	0.22	21
RMC full-height plywood panel-faced wall (GW12) (no surcharge)	0.5	0.04	13	550	4.5	0.22	14
	1.25	0.02	13	550	4.5	0.11	14
	2.0	0.02	13	550	4.5	0.10	14
	2.75	0.01	29	550	4.5	0.04	29
RMC full-height plywood panel-faced wall (GW12) (50 kPa surcharge)	0.5	0.50	13	500	4.5	2.48	14
	1.25	0.49	13	500	4.5	2.43	14
	2.0	0.33	13	500	4.5	1.63	14
	2.75	0.22	13	500	4.5	1.09	14
RMC incremental plywood panel-faced wall (GW13) (no surcharge)	0.5	0.03	13	530	4.5	0.19	14
	1.25	0.27	13	530	4.5	1.43	14
	2.0	0.32	13	530	4.5	1.70	14
	2.75	0.34	13	530	4.5	1.80	14
RMC incremental plywood panel-faced wall (GW13) (50 kPa surcharge)	0.5	0.80	13	460	4.5	3.68	14
	1.25	0.79	13	460	4.5	3.63	14
	2.0	0.60	13	460	4.5	2.76	14
	2.75	0.53	13	460	4.5	2.44	14
RMC full-height aluminium panel (GW14) (no surcharge)	0.5	0.40	13	95	15	0.38	20
	1.25	0.34	13	90	15	0.31	20
	2.0	0.26	13	90	15	0.23	20
	2.75	0.42	13	90	15	0.38	20
RMC full-height aluminium panel (GW14) (70 kPa surcharge)	0.5	2.93	9	53	15	1.56	17
	1.25	3.47	9	48	15	1.67	17
	2.0	2.00	23	67	15	1.34	27
	2.75	1.45	23	74	15	1.07	27
RMC Incremental aluminium panel-faced wall (GW15) (no surcharge)	0.5	0.18	13	93	15	0.17	20
	1.25	0.60	13	89	15	0.53	20
	2.0	0.35	13	87	15	0.30	20
	2.75	0.45	13	90	15	0.41	20

Table 5.2. Continued

RMC Incremental aluminium panel-faced wall (GW15) (60 kPa surcharge)	0.5	4.00	9	43	15	1.72	17
	1.25	4.15	9	45	15	1.87	17
	2.0	1.20	13	80	15	0.96	20
	2.75	0.42	13	90	15	0.38	20
Rainier Ave. wall (GW16) (no surcharge)	3.1	1.14	29	120	25	1.32	38
	6.5	0.92	29	190	25	1.75	38
	9.6	0.84	29	350	25	2.92	38
	11.5	0.52	29	1,000	25	5.19	38
Rainier Ave. wall (GW16) (with soil surcharge)	3.1	1.50	29	100	25	1.50	38
	6.5	1.06	29	190	25	1.96	38
	9.6	1.06	29	340	25	3.59	38
	11.5	0.62	29	1,000	25	6.19	38
Fredericton, New Brunswick wall (GW18)	2.44	0.43	13	500	30	2.15	33
	4.88	0.50	13	500	30	2.50	33
St Remy PET Strip Test Wall (GW19)	0.4	0.03 [a]	20 [b]	7,400	25	1.93	32
	1.2	0.06 [a]	20 [b]	7,400	25	4.80	32
	2	0.10 [a]	17 [b]	7,400	25	7.10	30
	2.8	0.12 [a]	17 [b]	7,400	25	9.20	30
	3.6	0.13 [a]	17 [b]	7,400	25	9.40	30
	4.4	0.16 [a]	15 [b]	7,400	25	11.6	29
	5.2	0.17 [a]	15 [b]	7,400	25	12.9	29
	6	0.09 [a]	17 [b]	7,400	25	6.54	30
Vicenza, Italy HDPE Wall (GW20)	1.1	0.91	13	300	6	2.70	14
	2.7	1.49	13	300	6	4.43	14
Vicenza, Italy PP Wall (GW20)	1.6	3.13	13	90	20	2.75	24
	3.2	2.02	13	100	20	2.06	24

***** Based on extensometer and calibrated strain gauge readings.

+ Gauges failed at this strain. Therefore, it is possible that the true strains are greater for this loading condition.

[++] No COV_ε data for strain gauges available; extensometer COV_ε values used.

[a] Only loads were reported. Strains were estimated from the reported loads using the reinforcement stiffness value.

[b] Estimated from multiple strain readings at nominally identical locations as reported by Schlosser et al. (1993).

Coefficient of variation (COV_T) calculated as follows (Ang and Tang 1975): $COV_T = \sqrt{COV_\varepsilon^2 + COV_J^2}$ where COV = coefficient of variation = (standard deviation of values/mean of values) x 100%. See Walters et al. (2002).

5.2.1 Tanque Verde HDPE Geogrid Wall (GW5)

The long-term stiffness for the high density polyethylene (HDPE) product used in this wall was determined by using 8,000 hours of in-isolation creep data and 180 hours of in-isolation CRS data, both at 20°C, reported by Yeo (1985). These are the same data used to characterize the geogrid properties for this wall by Desert Earth Engineering (1989) when the wall was constructed. Both types of data produced the same stiffness value at 2 percent strain at 350 hours—the time it took to construct the wall (see Chapter 4.0). To estimate the creep stiffness at the site temperature of 27°C reported by Desert Earth Engineering, a time-temperature superposition shift factor was estimated by using the approach described by Bush (1990). On the basis of data obtained by Yeo at lower temperatures, a shift factor of approximately one log cycle of time per 10°C appears to be appropriate. Bush obtained slightly larger shift factors (1.3 log cycles of time per 10°C) but for a later generation of the product used in the wall. However, he did find that the shift factor above and below 20°C was approximately constant. A shift factor of one log cycle of time per 10°C was used. To shift the 20°C creep data to 27°C, the time was multiplied by a factor of 0.2 (i.e., the 1,000-hour isochrone at 20°C becomes a 200-hour isochrone at 27°C). Once the new isochronous creep curves were established, a creep stiffness curve at 2 percent strain was established. Because the facing panels were externally braced (propped) until two-thirds of the backfill behind the panels was in place, reinforcement loading was not expected to begin until the props were released, resulting in an approximate "wall construction time" of 350 hours. The stiffness value used to convert measured strains to load was estimated from this curve at 350 hours. Installation damage was not great enough to cause significant reductions in stiffness (Allen and Bathurst 1994; see Chapter 2.0). Therefore, no additional adjustment to the stiffness value was made.

On the basis of 17 sets of wide-width tensile tests on installation-damaged, high density polyethylene (HDPE) geogrid specimens that are not project-specific, the coefficient of variation (COV_J) for stiffness values is estimated to be approximately 3 percent at a stain level of 5 percent and to increase by a factor of 1.5 on average at a strain of about 2 percent (see Chapter 4.0). resulting in COV_J = 4.5 percent. This assumes that the variability in the creep stiffness data is approximately the same as the variability in the tensile test data, which the writers believe, on the basis of experience, to be a reasonable assumption and is also consistent with how geosynthetic

material variability is handled in North American design practice (AASHTO 2002, Elias et al. 2001). There is some additional uncertainty because of lack of lot-specific data for the tensile strength and creep. Therefore, the total variance in the stiffness values may be higher than 4.5 percent. A value of 6 percent is used for this case study.

5.2.2 Oslo, Norway, Geogrid Steep Slope (GW7)

Geogrid 1,000-hour creep data supplied by the manufacturer (not lot-specific) was used in this investigation (Fannin and Hermann 1991). Details of the primary reinforcement stiffness estimation for this particular case history, considering the strain level, time, and temperature, are provided in Chapter 4.0. Secondary reinforcement, a biaxial PP geogrid, was used in the upper half of one of the GW7 wall sections. Creep data for this particular product in the machine direction were not available. However, creep data for the next stronger product, oriented in the weak direction (machine direction), were available (Yeo 1985). Because the ultimate tensile strength was approximately the same for both products in the directions indicated (20 kN/m), and because both products were produced by the same manufacturer and were part of the same product line, it was assumed that the creep stiffness obtained from these data was approximately the same as that from the specific product used in the wall as secondary reinforcement. No strain measurements were taken for the secondary reinforcement in this case study. However, the secondary reinforcement affects only the calculation of predicted reinforcement loads in the primary reinforcement layers and the global stiffness of the structure.

The uncertainty in the modulus would be similar to the uncertainty for the Tanque Verde wall as discussed above (COV_J estimated to be 6%).

5.2.3 Algonquin HDPE Geogrid Wall (GW8)

The long-term stiffness value for the product used in this wall was determined using 8,000 hours of in-isolation creep data obtained at 10 and 20^{o}C and 180 hours of in-isolation CRS data reported by Yeo (1985) and described in Section 4.2.1. These creep data were obtained for the same product specified for the wall, although the creep data were likely 5 to 7 years older than the material actually used and for a material produced in the United Kingdom rather than in the U.S.A. Using the time-temperature superposition approach described by Bush (1990), a creep stiffness curve at 2 percent strain was created at an effective site temperature of 17^{o}C to represent

the low strain stiffness of the reinforcement. The site temperature was based on regional climate data. Using a wall construction time of 920 hours, a creep stiffness of 350 kN/m was obtained. The stiffness at 2 percent strain for the reinforcement used by Yeo and tested at 10 percent strain/minute was 980 kN/m, and the ultimate tensile strength of the material was approximately 71 kN/m. However, even though the reinforcement used in the wall had the same product name as the one investigated by Yeo, a wide-width stiffness of 2,040 kN/m at 2 percent strain was obtained from lot-specific specimens (Christopher 1993). The tensile strength of the geogrid reported by Christopher was 67.7 kN/m. This apparent difference in the stiffness of the product used in the creep testing versus the lot-specific data may be the result of the difference in the source as well as product upgrades that may have occurred since the Yeo data were obtained (Berg 2002). If the creep stiffness value used to characterize the reinforcement used for this wall is increased by a factor of 2040/980 = 2.1, to account for the difference between the apparent stiffness of the material used for the creep testing and the stiffness measured for the lot of material used for the wall, the reinforcement creep stiffness is 730 kN/m. Analysis of recent creep test data reported by Kaliakin et al. (2000) on a later generation of the same product (produced in the U.S.A) indicates that a creep stiffness value of 600 kN/m, corresponding to 920 hours and 17^{o}C, is reasonable. The tensile strength of the product tested by Kaliakin et al. was 72 kN/m. The later generation product should be stiffer than the older generation product used in the wall (Berg 2002). Given this observation, a creep stiffness value of 730 kN/m appears to be too high. It was concluded that 500 kN/m, a slightly lower stiffness value than for the product tested by Kaliakin et al., is a reasonable estimate for the reinforcement used in this wall.

The uncertainty in the stiffness value should be similar to the uncertainty for the Tanque Verde wall (up to 6 percent). However, the large difference in the lot-specific stiffness and the stiffness value obtained for the material used by Yeo and Kaliakin et al. add uncertainty that is difficult to quantify. On the basis of the difference between the stiffness values reported for this product, COV_J = 30 percent was assigned to the reinforcement stiffness value for this wall.

5.2.4 Algonquin PET Geogrid Modular Block Wall (GW9)

The long-term stiffness for the polyester (PET) geogrid used in this wall was determined from Bathurst et al. (1993b), using 2,000 hours of in-isolation creep data obtained at 20^{o}C from the same lot of material used in wall, interpolated log-linearly to 920 hours. Although the

effective site temperature was 17°C (see Section 5.2.3), this minor difference in temperature relative to 20°C should not affect the stiffness value obtained, since temperature sensitivity of PET is not as great as that for HDPE or PP geosynthetics. Using these creep data, a strain level of 2 percent, and a wall construction time of 920 hours, the end-of–construction creep stiffness was estimated to be 200 kN/m.

On the basis of 40 sets of wide-width tensile tests on non-project-specific, installation-damaged acrylic coated PET geogrid specimens, the coefficient of variation (COV_J) is estimated to be 7 percent at a strain level of 5 percent and to increase by a factor of 1.5 on average at a strain of about 2 percent, resulting in a COV_J value of 11 percent. Because the creep stiffness was determined from lot-specific tests, no additional uncertainty was considered.

5.2.5 Algonquin PET Geotextile Wrapped-Face Wall (GW10)

Only in-isolation, wide-width (ASTM D4595) data and confined wide-width data from zero span (Christopher, et al. 1986) and pullout testing on lot specific material were available. The stiffness values at 5 percent strain were approximately 35 kN/m unconfined and 180 kN/m under a soil confining pressure equal to the pressure at the mid-height of the wall (Christopher 1993, 1998). Because the material was a polyester, time dependent stiffness reductions would be minimal (approximately 15 percent or less), and because of the approximate nature of the stiffness values, no additional reduction was applied. It was assumed that the stiffness was approximately linear in the range of 1 to 5 percent strain. The temperature correction for the stiffness to reflect a temperature of 17° C was not significant. The reduction in stiffness due to installation damage was minor up to peak tensile strength losses of 40 percent, which was the amount of loss estimated to occur at this site (Allen and Bathurst 1994; see also Chapter 2.0). Therefore, no additional reduction in stiffness was applied to account for installation damage effects.

On the basis of 13 sets of wide-width tensile tests on installation damaged, PET nonwoven geotextile specimens that were not project specific, the coefficient of variation (COV_J) was estimated to be approximately 26 percent (see Chapter 4.0). Because the number of specimens tested was very limited and only short-term, significant additional uncertainty is likely. Because of this, the uncertainty could be twice as high as the COV_J resulting from material variability after installation damage (i.e., on the order of 50 percent).

5.2.6 RMCC Geogrid Wrapped-Face Wall (GW11)

Creep data out to 3,000 hours obtained at 20°C from Yeo (1985) on the same product used in the wall were used to estimate the stiffness of the wall reinforcement. Wide-width index tensile test data for the product used in the wall, but at a strain rate of 2 percent/minute, and confirmation lot-specific, wide-width index tensile testing at a strain rate of 2 percent/minute gave a stiffness of 360 kN/m from tests reported by Yeo and 350 kN/m for tests carried out on the lot used in the wall (Bathurst et al. 1988). Because the index stiffness values for the Yeo data and the lot-specific test data were approximately the same, the accuracy of the Yeo data for estimating the end-of-construction stiffness for this wall was considered adequate. Bathurst et al. reported that it took 65 hours to construct the wall. Because the wall was constructed in an in-door laboratory environment, the temperature during loading was assumed to be 20°C. Strains measured in the wall at the end of construction were generally less than 2 percent, with the exception of one layer, in which a 2.7 percent strain was measured. Using the Yeo creep data and a strain level of 2 percent, the creep stiffness was estimated at 65 hours to be 110 kN/m. For the layer that exhibited a larger strain (2.7 percent), an additional creep stiffness curve was created at the higher strain, resulting in a creep stiffness value of 105 kN/m.

On the basis of 22 sets of wide-width tensile tests on installation-damaged, polypropylene (PP) geogrid specimens that were not project-specific, the coefficient of variation (COV_J) is estimated to be 10 percent at 5 percent strain and to increase by a factor of 1.5 on average at a strain of about 2 percent, resulting in a COV_J value of approximately 15 percent. Because the wide-width stiffness was determined from creep data in which the index tensile test stiffness was about the same as the lot-specific index tensile test stiffness, additional uncertainty was not considered. Hence, the total uncertainty is estimated to be 17 percent.

5.2.7 RMCC Full Height Plywood Panel-Faced Wall (GW12)

Roll-specific samples were used to obtain the short- and long-term properties of the HDPE geogrid used in the wall (Bathurst et al. 1987). The measured strains in the wall were generally less than 1 percent and were generated after prop release. The rate at which load was applied to the reinforcement depended on how rapidly load could transfer between the soil and geosynthetic reinforcement as the wall face panel deflected outward. Given the granular nature of the soil and the relatively low strains observed, it was assumed that the load was fully applied to the

reinforcement approximately 100 hours after prop release and that any remaining time-dependent deformation was due to reinforcement creep. With the 1,000-hour creep data for the product used in this wall, the in-isolation creep stiffness curve was created, by using a 2 percent strain level to characterize the low strain behavior of the geogrid. From this curve, the stiffness at 100 hours and 2 percent strain was estimated to be 550 kN/m. Once the final surcharge was in place (880 hours), the stiffness dropped to 495 kN/m.

On the basis of 17 sets of wide-width tensile tests on installation-damaged, HDPE geogrid specimens that were not project-specific, the coefficient of variation (COV_J) for the stiffness at 2 percent strain is estimated to be 4.5 percent as discussed for the Tanque Verde Wall. Because roll-specific tensile and creep test data were used for this wall, this *COV* value adequately reflects the uncertainty in the stiffness value for this wall.

5.2.8 RMCC Incremental Plywood Panel-Faced Wall (GW13)

The assessment of the reinforcement stiffness for this wall is the same as that described for the full-height, plywood, panel-faced test wall (Section 5.2.7), since the same product was used. However, the time to end-of-construction was 220 hours and to final surcharge placement 3,100 hours, resulting in stiffness values of 530 and 460 kN/m, respectively.

5.2.9 RMCC Full Height and Incremental Aluminum Panel-Faced Wall (GW14 and GW15)

Lot-specific PP geogrid 1,000-hour creep data obtained at 20^{o}C from Benjamin (1989) were available for these walls. Because the walls were built in a laboratory environment, the temperature at the wall was at room temperature, or approximately 20^{o}C. The time to end-of-construction was estimated to be 100 hours after prop release for Wall GW14 (full-height, propped panel wall) and 200 hours for Wall GW15 (incremental panel wall). Both walls were incrementally surcharged, over an additional 2,500 hours to reach the heaviest surcharge condition. The isochronous creep curves were used to estimate the creep stiffness at various times from the beginning of wall construction. Creep stiffness curves were developed at different strain levels, which varied from less than 1 percent strain at the end of wall construction to over 4 percent strain at the highest surcharge load. It was assumed that the step surcharge loading history had little effect on the reinforcement stiffness value and that the elapsed time

between the end of a surcharge load increment and the beginning of wall construction could be used to calculate the stiffness values.

On the basis of 22 sets of wide-width tensile tests on installation-damaged, PP geogrid specimens that are not project specific, the coefficient of variation (COV_J) for the stiffness at 2 percent strain is estimated to be 15 percent, as discussed for the RMC geogrid wrapped-face wall (GW11). Because lot-specific tensile and creep test data were used for this wall, and only minor time extrapolation was needed to estimate some of the stiffness values, the *COV* value calculated above was used to quantify the uncertainty in the stiffness values for this wall.

5.2.10 Rainier Avenue Geotextile Wrapped-Face Wall (GW16)

Approximately 70 hours of in-soil creep/relaxation data, 70 hours of in-isolation creep data, and 2 hours of in-isolation CRS data from the same roll of one of the PP woven geotextiles used in the wall were available. All of these data were obtained at approximately 20°C. These data were log-linearly extrapolated to 1,630 hours and 1,920 hours to estimate the stiffness at the end of construction and at surcharge completion, respectively. The focus of the creep testing for the materials used in this wall was the low strain behavior. Hence, data at higher strains matching values recorded in the wall (i.e., greater than 1 percent strain) were not available. Because the measured strains in the wall were approximately 1 percent or less, end-of-construction stiffness values were calculated at a strain of 1 percent. A creep stiffness versus time curve was developed from the in-isolation creep data to estimate the end-of-construction creep stiffness for this wall. The effective site temperature was determined to be approximately 14°C. The laboratory creep data were shifted in time to 14°C using typical shift factors observed for PP and HDPE geosynthetics (Yeo 1985). On the basis of the approach by Bush (1990) and using a shift factor of one log cycle of time per 10°C temperature, the 20°C laboratory data were shifted in time by a factor of 4 to obtain the curve at 14°C. This resulted in a stiffness value of 190 kN/m at the end of construction and at surcharge completion. Creep data were only available for one of the PP woven stitch-bonded geotextiles used in the wall. The other two PP geotextiles differed from this product with respect to the number of stitch-bonded layers. The stiffness values for the other PP geotextiles were estimated by using the low strain wide-width test (ASTM D 4595) stiffness values for each geotextile to normalize the end-of-construction and surcharge completion stiffness values.

For the woven PET geotextile used in the wall, only 2 hours of in-isolation CRS data were available (Boyle et al. 1996, Boyle and Holtz 1996; see also Chapter 4.0). Use of these data as well as general knowledge of PET creep behavior led the writers to use 75 percent of the 2 percent strain stiffness value ($J_{2\%}$) from a standard wide-width test. Wide-width tests were carried out with material taken from the wall. The PET geotextile stiffness value was assumed to be unaffected by temperature, and therefore, no further adjustment was required.

On the basis of wide-width tensile tests on installation-damaged, PP geotextile specimens taken from the wall, the coefficient of variation (COV_J) was approximately 18 percent. Because long-term stiffness data were obtained for roll-specific specimens tested under in-soil conditions, no additional uncertainty resulted from the test method and source of the material. However, a large extrapolation was required, resulting in a potential additional 7 percent uncertainty based on the WSDOT (1998) creep extrapolation protocol. Therefore, the final COV_J value was taken as 25 percent.

5.2.11 Fredericton Propped Panel Geogrid Wall (GW18)

The long-term stiffness for the product used in this wall was based on 1000 hours of in-isolation creep data obtained at 10°C reported by Yeo (1985). These creep data were obtained on the same product specified for the wall, although those creep data were likely about 7 years older than the material used in the wall. Lot-specific tensile strength or creep data were not reported for this wall. A creep stiffness versus time curve was developed from the creep data at a 2 percent strain level and an elapsed time of 100 hours (see discussion in Section 2.7). Site-specific temperature readings were approximately 10°C; hence, no temperature shifting of the creep data was necessary. The creep stiffness at 100 hours was determined to be approximately 440 kN/m. Because the likelihood of product upgrades between the generation of the creep data and the time of wall construction, the stiffness value of 500 kN/m reported in Section 2.3 at 920 hours and 17°C was increased by a factor of 440/350 = 1.26 to account for the lower temperature and shorter "construction" time. This resulted in a stiffness value of 630 kN/m. The coverage ratio for this wall (i.e., the width of the reinforcement divided by the center-to-center horizontal spacing of the reinforcement) was 0.77 (Knight and Valsangkar 1993). Reducing the stiffness value by this ratio to obtain an average stiffness per unit of reinforcement width yields

approximately 500 kN/m. Installation damage was not great enough to cause significant reductions in stiffness (Allen and Bathurst 1994; see also Chapter 2.0).

The uncertainty in the stiffness value of the HDPE geogrid used in this wall is likely similar to that for the Algonquin HDPE geogrid wall (approximately 30 percent).

5.2.12 St. Remy PET Strap Wall (GW19)

Isochronous creep data for the reinforcement reported by Schlosser et al. (1993) were used. "Instantaneous" tensile test results indicated a stiffness of 9,600 kN/m (i.e. the stiffness used by Schlosser et al. to convert measured strain from strain gauges to load). Schlosser et al. also provided isochronous creep data for the product used in the wall. However, both the rapid tensile test and creep data were not lot-specific to this wall. The test temperature used was not reported but was assumed to be approximately 20^{o}C. The effective site temperature was also not reported for this wall, but fortunately PET is not as sensitive to temperature effects as other polymers used for geosynthetic reinforcement. Therefore, temperature was not considered to have a significant effect on the accuracy of estimates of reinforcement load for this wall. For an 1,800-hour wall construction time and a strain level of 1 percent, (strains in the wall were well below 1 percent), the creep stiffness value was estimated to be 7,400 kN/m, or about 75 percent of the short-term stiffness of the material used by Schlosser et al. to convert strains to load. Because the reported loads were determined from the measured strains using the instantaneous, short-term stiffness, they were reduced by a factor of 0.75 to reflect the lower stiffness determined from the isochronous creep data.

The variability in the stiffness value for this wall could not be estimated from product-specific data. However, the reported isochronous creep data appears to be stronger and stiffer than the actual material used in the wall, if the “instantaneous” curve shown with the isochronous data is the load-extension curve for the specific material used in the creep tests. If this is the case, the creep stiffness used to interpret the strain readings for this wall could be as low as 50 percent of the stiffness used by Schlosser et al.. In general, for PET geogrid reinforced walls, uncertainty in the stiffness value of 10 to 15 percent can be anticipated (see Section 5.2.4). Because of the lack of lot-specific creep data for the reinforcement used for this wall, a larger COV_J value, estimated to be 25 percent, was selected for this wall.

5.2.13 Vicenza, Italy, HDPE Wall (GW20)

Lot-specific tensile test data showed that the product used in the wall had an ultimate tensile strength of approximately 58 kN/m (Alberto 1998). Product-specific, but not lot-specific, creep data out to 1,000 hours at both 20 and 40°C were available for this material (Cazzuffi and Sacchetti 1999). The data yielded a stiffness value of 330 kN/m after a wall construction time of 150 hours, and 270 kN/m at an end of surcharge construction time of 5,500 hours, although the product tested for creep was weaker (T_{ult} = 52.7 kN/m) than the lot-specific test results indicated. Adjusting the creep stiffness to account for the higher strength of the lot of materials used in the wall produced a creep stiffness value of approximately 300 kN/m. Site-specific temperature data were not available. Therefore, no temperature adjustment to the creep stiffness at 20°C was made.

The uncertainty in the stiffness value for the HDPE geogrid used in this wall was similar to that for the Tanque Verde Wall (COV_J = 6 percent).

5.2.14 Vicenza, Italy, PP Wall (GW20)

On the basis of lot-specific data, the wide-width 2 percent stiffness value obtained at a strain rate of 10 percent/minute was approximately 500 kN/m, and the ultimate tensile strength was 23.7 kN/m, for the PP geogrid used in this wall (Alberto 1998). No creep data were available for this product. On the basis of data from drawn PP geogrids (see Chapter 4.0), the long-term stiffness at the end of wall construction should be approximately 25 to 35 percent of the wide-width stiffness value, or approximately 150 to 170 kN/m. Creep data were available for a similar strength PP biaxial geogrid made by another manufacturer (the same creep data, obtained at 20°C, to characterize the creep stiffness for wall GW11 in Section 5.2.6). For this wall, the time required for wall construction was 150 hours, and 5,500 hours to wall surcharge completion. The site temperature was not reported but assumed to be 20°C. Measured strains varied from 2 to 3 percent. Calculating the creep stiffness from these creep data was the same as for Wall GW11, but at a surcharge completion time of 5,500 hours and at strains of 2 and 3 percent, the creep stiffness values were estimated to be 86 kN/m at 2 percent strain and 74 kN/m at 3 percent strain. Adjusting these values for the slightly higher ultimate tensile strength of the geogrid used in the wall yielded a stiffness value of 100 kN/m and 90 kN/m for 2 and 3 percent strain levels,

respectively. No additional adjustment of these values for temperature was made because site-specific temperatures were not known.

On the basis of 22 sets of wide-width tensile tests on installation-damaged PP geogrid specimens from a similar strength product, the coefficient of variation (COV_J) for the mean stiffness value at 2 percent strain is estimated to be 15 percent (Section 5.2.7). Although lot-specific tensile test data were available, some uncertainty exists because neither product- nor lot-specific creep data were available. Consequently, the total uncertainty is assumed to be higher, an estimated 20 percent.

5.3 Estimated Reinforcement Loads for Geosynthetic Wall Case Histories

Reinforcement load, T, at a given time is calculated according to the following equation:

$$T = J_c \times \varepsilon \tag{5.1}$$

where J_c and ε are best estimates of the creep stiffness value and strain measurement in the reinforcement, respectively, at the location and time of interest.

Uncertainty in the calculation of reinforcement loads is the result of uncertainty in both the magnitude of strain measurements and the estimate of stiffness values. An attempt was made in the previous section to estimate uncertainty in the reinforcement stiffness values for each wall case history.

Uncertainty in strain measurements has been estimated in Chapter 3.0. The accuracy of the strain readings is dependent on the reinforcement type, the instrumentation used to measure strain, attachment technique, how the calibration factor to equate local strain readings to global strains is carried out, in-situ bending, and non-uniform strain distribution along the width of a reinforcement layer, among other factors.

Chapter 4.0 shows how coefficients of variation for uncorrelated stiffness and strain measurements (COV_J and COV_ε, respectively) are used to estimate the coefficient of variation of the resulting estimate of reinforcement load (COV_T). The same procedure is used here.

The measured strains, uncertainty in strain values, estimated stiffness values, uncertainty in the stiffness values, estimated reinforcement load, and the total uncertainty in the load for each wall case history are summarized in Table 5.2. The strains shown in Table 5.2 represent the

highest measured strain in each layer as reported in Chapter 3.0. In some cases, strains were obtained from more than one strain measurement method (i.e., strain gauges and extensometers). In general, strain gauge readings were used for small reinforcement strains. In some cases, however, as noted in the table and shown in Chapter 3.0, there were significant differences between the extensometer and strain gauge readings. In such cases, a strain level was selected that best reflected readings from both sources. In almost all of those cases, the differences were well within the variances mentioned above. Data to calculate uncertainty in strain gauge and extensometer readings for instrumented HDPE geogrids were not available at the time of writing. However, it is reasonable to assume that COV_ε values reported for PP geogrids in Chapter 3.0 are representative of instrumented HDPE geogrids, since the instrumentation techniques were similar, and both classes of integral drawn products used in the case studies examined here were manufactured by the same process. Data on uncertainty with respect to strain measurements were not available for wall case studies GW10 and GW16. For these case studies COV_ε = 29 percent was used to match the value reported in Chapter 3.0 for extensometers.

5.4 Analysis of Reinforcement Loads

Once reinforcement loads and their uncertainty have been defined, general trends in the loads can be evaluated. Understanding trends in reinforcement load can be helpful in assessing the accuracy of current methods for designing the internal stability of geosynthetic walls and in providing direction to improve upon current approaches.

5.4.1 Current Design Methods for Estimating Reinforcement Loads

Two primary methods can be found in recent North American design specifications to estimate loads in geosynthetic reinforced soil walls: a) the Tieback Wedge/Simplified Method (AASHTO 1996, 2002, Elias et al. 2001) and b) the FHWA Structure Stiffness Method (Christopher et al. 1990). Note that both of these methods are semi-empirical in nature. Both methods produce similar load predictions, with the exception of the Structure Stiffness Method for geogrid reinforced walls. Both use limit equilibrium concepts to develop the design model but use working stress observations to adjust the models to fit what has been observed in full-scale structures. Small-scale models taken to failure have also been used to evaluate these design models at true limit equilibrium conditions (e.g., Adib 1988). These methods are applicable only

to walls with relatively high quality granular backfill (i.e., a maximum of 15 percent silt and no clay) and seated on competent foundation soils.

5.4.1.1 Tieback Wedge/Simplified Method

This method was developed by Bell et al. (1975) and the U.S. Forest Service (Steward et al. 1977) for geosynthetic reinforced soil walls as an adaptation of the earliest work by Lee et al. (1973) for steel strip reinforced soil wall design (Allen et al. 2001). In the Tieback Wedge/Simplified Method (AASHTO 1996, 2002), the wall is assumed for internal design to be flexible with enough deformation to generate an active state of stress. Hence, the lateral earth pressure coefficient K_a is used to convert vertical stress to lateral stress. K_a is determined in this method by assuming a horizontal backslope and no wall-soil interface friction in all cases. The reinforcement is assumed to resist lateral stresses occurring within the wall, with each reinforcement layer designed to resist the lateral stress over a tributary area. The Rankine failure wedge is held in horizontal equilibrium by the reinforcement layers that act as tiebacks. Polymer strap walls have been more recently excluded from this method (AASHTO 2002, Elias et al. 2001) together with any wall that has a face inclination of less than 70^o from the horizontal.

The maximum tensile load in a reinforcement layer, T_{max} (in units of force per running unit length of wall) is calculated as follows:

$$T_{max} = S_v K_a \left(\gamma \left[z + S \right] + q\right) \tag{5.2}$$

where S_v is the tributary area (assumed equivalent to the vertical spacing of the reinforcement when analyses are carried out per unit length of wall), K_a is the active lateral earth pressure coefficient, γ is the soil unit weight, z is the depth to the reinforcement level relative to the wall top at the wall face, S is the average soil surcharge depth above the wall top, and q is the vertical stress due to traffic surcharge.

5.4.1.2 FHWA Structure Stiffness Method

The Structure Stiffness Method was developed as the result of a major FHWA research project in which a number of full-scale MSE walls were constructed and monitored (Christopher et al. 1990, Christopher 1993). Model walls were also constructed and numerical modelling carried out (Adib 1988). This method is similar to the Tieback Wedge Method, but the active

earth pressure coefficient, $\underline{K_a}$, is increased by a factor that is a function of depth below the wall crest, reinforcement type, and global wall stiffness. The multiplier to K_a used for steel reinforced walls was developed from direct calibration with empirical data, by using measured triaxial or direct shear strength parameters for the backfill. For geosynthetic walls, although empirical data were evaluated, the multiplier to K_a was set to a minimum value of 1.0 for geotextiles, and as high as 1.5 near the wall crest for geogrid reinforced walls. The design methodology is summarized in equations 5.3, 5.4, and 5.5. The maximum load in the reinforcement is expressed as follows:

$$T_{max} = S_v K_r \left(\gamma \left[z + S\right] + q\right) \tag{5.3}$$

where

$$K_r = K_a \left(\Omega_1 \left(1 + 0.4 \frac{S_r}{47880} \right) \left(1 - \frac{z}{6} \right) + \Omega_2 \frac{z}{6} \right) \qquad \text{if } z \le 6\,\text{m} \tag{5.4a}$$

$$K_r = K_a \Omega_2 \qquad \text{if } z > 6\,\text{m} \tag{5.4b}$$

and

$$S_r = \frac{J}{(H/n)} \tag{5.5}$$

Here, K_r = lateral earth pressure coefficient, S_r = global reinforcement stiffness for the wall (i.e., the average reinforcement stiffness over the wall face area), Ω_1 = dimensionless coefficient equal to 1.0 for strip and sheet reinforcements or equal to 1.5 for geogrids and welded wire mats, Ω_2 = dimensionless coefficient equal to 1.0 if $S_r \le 47{,}880$ kPa or $\Omega_2 = \Omega_1$ if $S_r > 47{,}880$ kPa, J = average reinforcement stiffness for the wall (in units of force per running unit length of wall), and H/n = average vertical spacing of the reinforcement, where n = total number of reinforcement layers.

5.4.2 Comparison of "Measured" Reinforcement Loads to Loads Estimated from Current Procedures

A total of 16 geosynthetic wall cases (the same wall with and without a surcharge is considered to be one case) were analyzed (see tables 5.1 and 5.2), and the results were compared

to predictions made with current design methodologies. Eleven walls were full-scale field structures, and five were instrumented, full-scale walls built in an in-door laboratory environment. The cases included a variety of wall geometries and facing types, surcharge conditions, and a range of granular backfills. Wall reinforcement included geotextiles and geogrids, a variety of polymers—including PP, HDPE, and PET—strip and continuous reinforcements, a wide range of index tensile strengths from 12 to 200 kN/m (see Chapter 2.0), and reinforcement stiffness values from 43 to 7,400 kN/m. Reinforcement vertical spacings varied from 0.3 to 1.6 m. Wall facing batter angles varied from 0^o (vertical) to 27^o, although most of the walls had facing batter angles of 8^o or less. Wall heights varied from 3.0 m to 12.6 m, with surcharge heights of up to 5.3 m of soil. Facing types included geosynthetic wrapped-face, welded wire, pre-cast concrete panels, and modular concrete blocks. Measured peak soil shear strengths from triaxial or direct shear tests varied from 39^o to 49^o (42° to 57° plane strain). Although in general it is not possible to make direct comparisons to isolate the effect of a specific variable, most of the conditions that are likely to be encountered in practice were included in these case histories.

Figure 5.1 provides an overall view of how well the Tieback Wedge/Simplified Method predicts reinforcement loads in geosynthetic walls built in the field. The error bars in the figure show the potential variance (± one standard deviation) in the "best estimate of measured" reinforcement loads, given the estimate of variance in strain and reinforcement stiffness measurement reported in Section 5.3. Note that triaxial or direct shear peak soil friction angles and unit weights estimated from measured data were used to calculate loads by using the methods described in Section 5.4.1. Plane strain conditions likely prevail in these types of reinforced structures (Rowe and Ho 1993, Zornberg et al. 1998b) but it is recognized that in practice triaxial or direct shear backfill friction angles would be used with this design method (AASHTO 2002). No safety factors were applied to calculate the predicted loads. Figure 5.2 shows results for full-scale walls built in the laboratory.

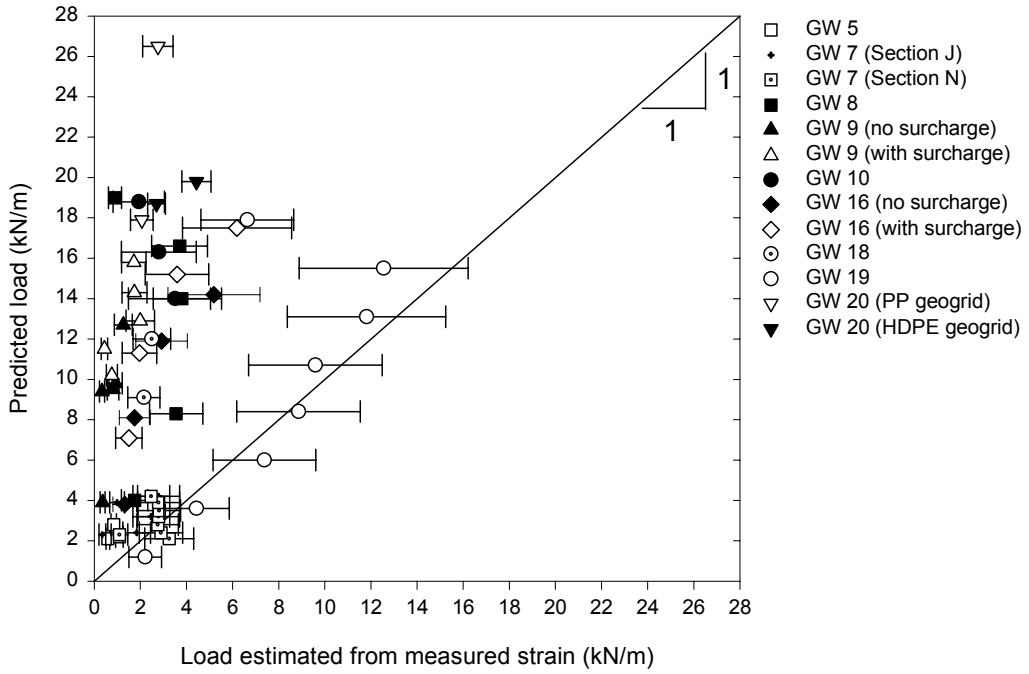

Figure 5.1. Predicted versus reinforcement load estimated from strain measurements for full-scale field geosynthetic walls, using the AASHTO Tieback Wedge/Simplified Method and triaxial or direct shear peak shear strength values. Note: Error bars represent best estimate of measured load ± 1 standard deviation.

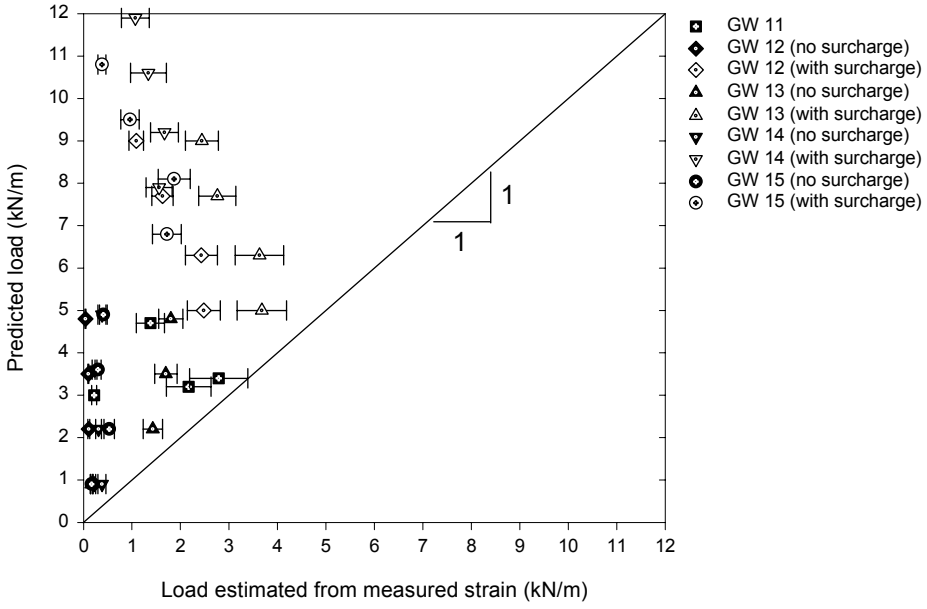

Figure 5.2. Predicted versus reinforcement load estimated from strain measurements for full-scale laboratory RMC geosynthetic walls, using the AASHTO Tieback Wedge/Simplified Method and triaxial or direct shear peak strain shear strength values. Note: Error bars represent best estimate of measured load ± 1 standard deviation.

Table 5.3 provides a summary of how well the Tieback Wedge/Simplified Method and the FHWA Structure Stiffness Method predict the measured loads by using the coefficient of variation of the ratio of the predicted reinforcement loads to loads estimated from strain measurements. Because loads in the reinforcement layers for geosynthetic walls have never been adjusted by calibration against full-scale wall data (i.e., a minimum multiplier applied to K_a of 1.0 is assumed), the issue of which measure of soil strength is used here is not critical to be consistent with the derivation of the Tieback Wedge/Simplified and Structure Stiffness Methods. Therefore, statistics for load predictions using the plane strain friction angle estimated from these measured friction angles (if the measured plane strain friction angle was not available) are provided in addition to predictions based on triaxial/direct shear data. As can be observed in the table, use of the plane strain soil friction angle for predicting the load, which should produce the least conservative estimate of load, does not fully account for the conservatism observed in the load predictions for either method (i.e., compare magnitude of ratio values for similar data sets with different friction angle values). The effect of assuming no wall-soil interface friction, which is the case for the Tieback Wedge/Simplified Method, and accounting for full wall-soil interface friction (the Tieback Wedge/Simplified Method modified to use the horizontal component of the Coulomb active earth pressure coefficient) can also be observed in Table 5.3, which shows that even accounting for full interface friction, the two methods are conservative for design.

The loads predicted with these methods are conservative relative to the loads estimated from strain measurements, even given the potential variance in those loads, with the exception of a few specific walls. For example, the reinforcement loads in walls GW7 and GW19 were predicted more accurately (i.e., with minimal conservatism) than the other walls with the Tieback Wedge/Simplified Method (see also figures 5.3a, 5.3b, and 5.3h in Section 5.4.3). Interestingly, the Tieback Wedge/Simplified Method specifically excludes walls classified as reinforced slopes because of the face inclination and walls constructed with polymer strips (Elias et al. 2001, AASHTO 2002). If these two walls are excluded from the calculation of the mean and *COV* of the predicted/measured ratio values discussed above, a better estimate of conservatism in the prediction using the Tieback Wedge/Simplified Method can be observed, as on average, the method over-predicts the loads by a factor of approximately 4 to 5. The *COV* improves significantly in this case but is nevertheless high.

Table 5.3. Summary of the ratio of predicted to best estimate of measured reinforcement load for geosynthetic walls.

Prediction Method	**Data Subset**	**Number of Data Points**	**Average Value of Ratio: Predicted/Measured Reinforcement Load**		**COV of Ratio (%)**	
			Triaxial or direct shear (ϕ)	Plane strain friction angle (ϕ)	Triaxial or direct shear (ϕ)	Plane strain friction angle (ϕ)
AASHTO Simplified/Tieback Wedge	All full-scale field walls	56	5.4	4.2	110	120
	All full-scale field walls, not including GW7 and GW19	35	7.6	6.1	82	90
	All RMC full-scale laboratory walls with full toe restraint and/or stiff facing	12	20	15	150	150
	RMC full-scale laboratory walls with low wall facing stiffness/toe restraint	16	3.6	2.7	89	89
	RMC laboratory walls with toe restraint, near failure	8	9.5	7.2	86	86
FHWA Structure Stiffness	All full-scale field walls	56	6.2	4.8	100	110
	All full-scale field walls, not including GW7 and GW19	35	8.7	7.0	77	85
	All RMC full-scale laboratory walls with full toe restraint and/or stiff facing	12	26	20	140	140
	RMC full-scale laboratory walls with low wall facing stiffness/toe restraint	16	4.8	3.6	84	84
	RMC laboratory walls with toe restraint, near failure	8	12.6	9.5	80	80
Simplified/Tieback Wedge, but using Coulomb K_a and fully mobilized wall-soil interface friction angle (modified AASHTO)	All full-scale field walls	56	4.1	3.2	110	120
	All full-scale field walls, not including GW7 and GW19	35	5.7	4.6	83	91
	All RMC full-scale laboratory walls with full toe restraint and/or stiff facing	12	14	11	150	150
	RMC full-scale laboratory walls with low wall facing stiffness/toe restraint	16	2.6	1.9	89	89
	RMC laboratory walls with toe restraint, near failure	8	6.8	5.1	86	86

Data for Wall G10 were not included in Table 5.3. Wall GW10 loads were under-predicted near the top of the wall, where loads are expected to be lower, and significantly over-predicted near the bottom of the wall, where loads are expected to be higher. Wall GW10 is the only wall reported here that was reinforced with a nonwoven geotextile and was so lightly reinforced in terms of reinforcement stiffness and vertical spacing that strains were high enough to allow the soil at the top of the wall to develop cracking and large facing deformations, both indicators of incipient soil failure (Christopher 1993). Note that the strains in the upper two layers of this wall (see Table 5.2) were likely greater than what was reported, as the gauges failed before an equilibrium strain was obtained, indicating that the strains could have been considerably higher. Therefore, the loads estimated from the last strain reading in these two layers were not included in any of the statistics in Table 5.3.

Overall, there is a tremendous amount of scatter in the predicted loads. A comparison plot for the FHWA Structure Stiffness Method results versus measured results is not presented here for brevity, but the visual impression of the data is the same as in **f**igures 5.1 and 5.2. However, Table 5.3 shows that the FHWA Structure Stiffness Method is more conservative (for design) than the Tieback Wedge/Simplified Method and therefore offers no significant advantage, at least for geosynthetic walls.

Note that Table 5.3 indicates that the measured reinforcement loads from full-scale laboratory walls deviate even more from predicted loads than do the results for full-scale field walls. The boundary conditions in the test walls, in particular the combination of facing stiffness and degree of toe restraint, appear to have much to do with the poorer match to the Tieback Wedge/Simplified Method predictions. One of the boundary conditions, side wall friction, was crudely taken into account by reducing the effective surcharge height by approximately 15 percent in this analysis (Bathurst 1993). The influence of the restrained toe in these laboratory tests is more pronounced for short walls (3 m high) than for the hard-faced walls in the field case histories (typically 4 m high or greater). Although detailed analytical modelling can be used to address these boundary issues and extend the test wall data to typical field walls, such modelling is beyond the scope of this report. The full-scale laboratory test wall data are presented here to demonstrate the general effect of certain variables on the behavior of geosynthetic walls (e.g., wall toe restraint, facing type) that cannot be easily isolated in the full-scale field wall data.

The uniform surcharge loading of these laboratory test walls was carried out to generate catastrophic failure of the soil-geosynthetic system (i.e., achieve limit equilibrium conditions). For walls GW14 and GW15 under surcharge loading, the reinforcement strains were high enough (on the order of 4 percent or more) to cause soil failure, given observations reported by Bathurst et al. (1993a) and Bathurst and Benjamin (1990).

5.4.3 Load Distribution with Depth

Figure 5.3 (a through h) shows distributions of the reinforcement load estimated from measured strains and predicted values as a function of depth below the wall top for several selected case histories. The predicted values have been plotted by using triaxial or direct shear peak friction angles and peak friction angle values corrected to plane strain values unless noted otherwise. These figures support the observation made previously that the current design methods may significantly over-estimate the reinforcement loads in geosynthetic walls, particularly over the bottom half of the wall. Note that each figure contains a curve representing the AASHTO Tieback Wedge/Simplified method, a curve representing use of the FHWA Structure Stiffness Method, and a curve representing the use of the Coulomb method to calculate K_a, assuming the wall interface friction angle is equal to the soil backfill friction angle, using only the horizontal component of the Coulomb earth pressure (modified AASHTO). Full interface friction was assumed for the Coulomb method because continuous or nearly continuous reinforcement layers attached to a facing will restrict downward movement of the backfill soil against the face, effectively resulting in a fully mobilized interface friction angle at the back of the wall face equal to the backfill soil friction angle. The exception is wall GW19 because the reinforcement was placed in discrete strips and likely generated much less shear transfer to the back of the facing than that calculated by assuming fully mobilized facing panel-soil interface friction. For this wall, an interface friction angle of two-thirds of the soil backfill friction angle was used to calculate the Coulomb K_a value, which is a typical concrete-soil interface friction angle.

Figure 5.4 shows the distribution of reinforcement loads, T_{max}, estimated from measured strains in the full-scale field walls, normalized to the maximum reinforcement load within the wall, T_{mxmx}. These normalized loads are plotted against the relative depth below the elevation of the average soil surcharge height to take into account the effect of the surcharge on load levels

near the top of the wall. The load distribution is not triangular, as is currently assumed for design, but rather is trapezoidal in shape. An approximate trend line is superimposed on the data in the figure to help emphasize the shape of the load distribution in the figure. The wall case histories represented in this paper do not include walls with very soft foundation conditions or multi-tiered walls. Therefore, the trend shown may not apply to these conditions.

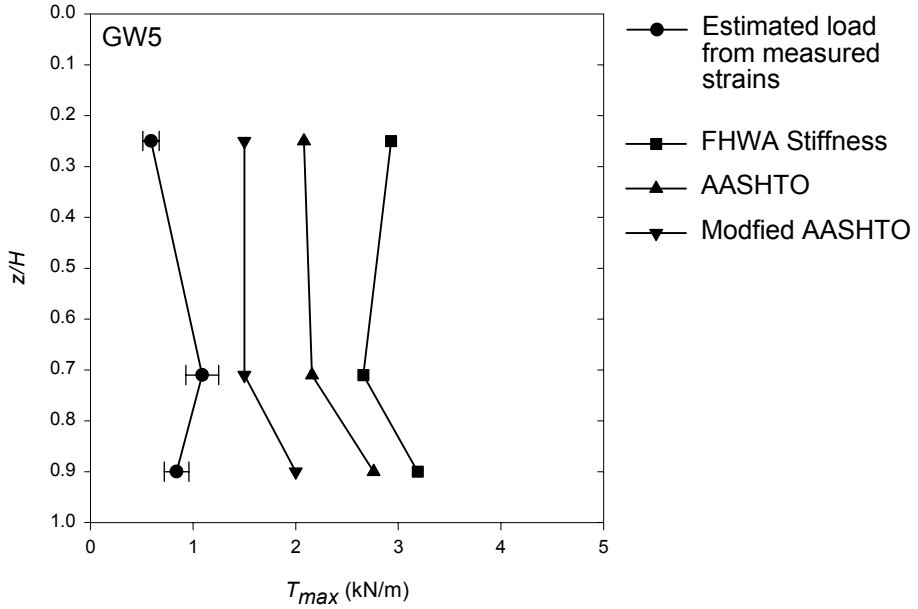

a) Wall GW5 (using measured cubic triaxial ϕ value

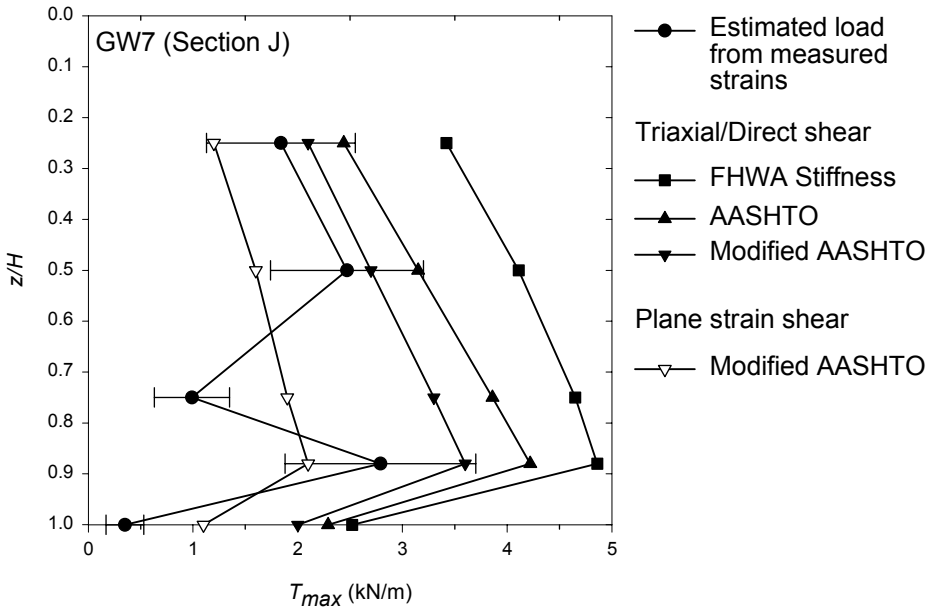

b) Wall GW7, Section J (with surcharge)

Figure 5.3. Predicted peak reinforcement peak loads, and peak loads estimated from measured strains. Note: Error bars represent best estimate of measured load $\pm$ 1 standard deviation.

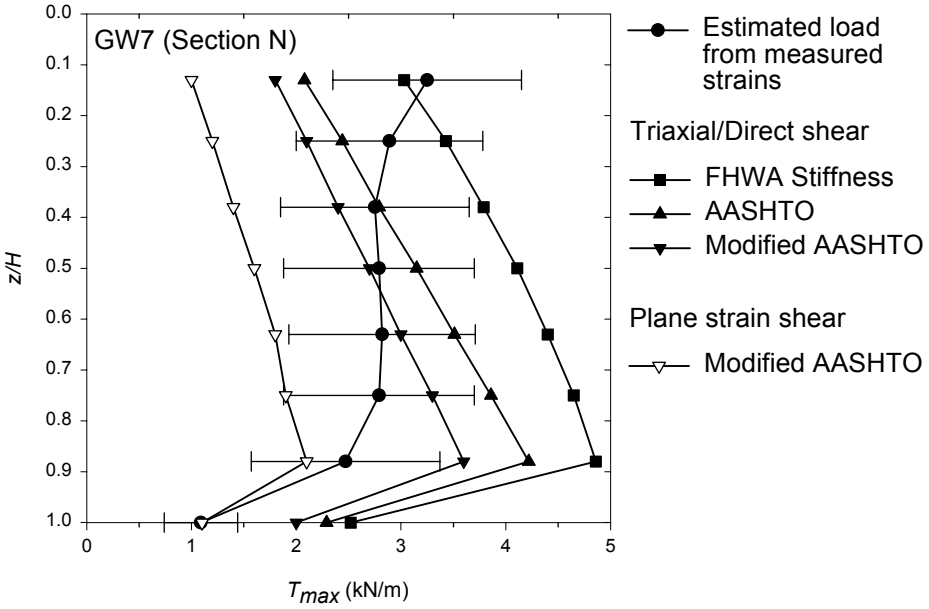

c) Wall GW7, Section N (with surcharge)

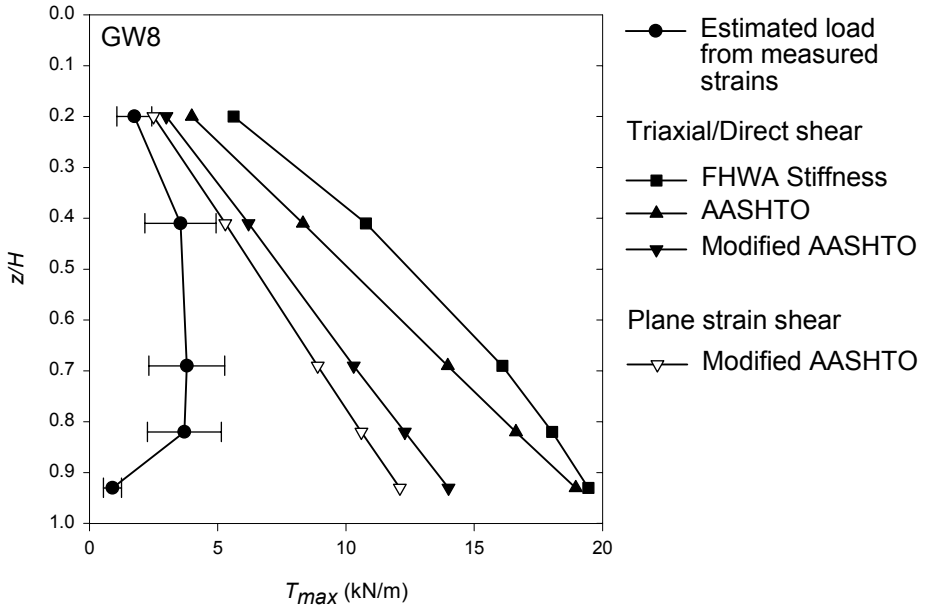

d) Wall GW8

Figure 5.3. Predicted peak reinforcement peak loads, and peak loads estimated from measured strains. Note: Error bars represent best estimate of measured load ± 1 standard deviation.

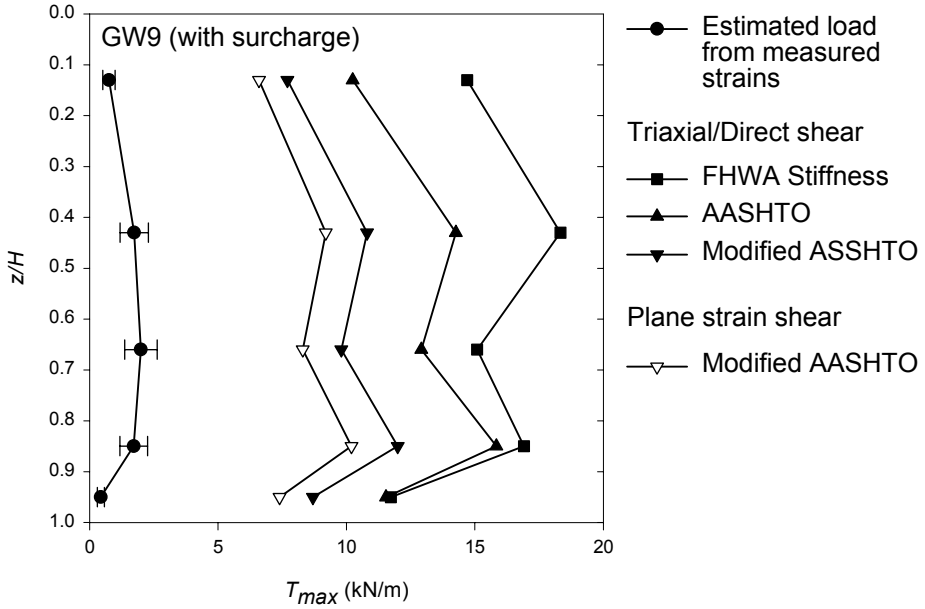

e) GW9 (with surcharge)

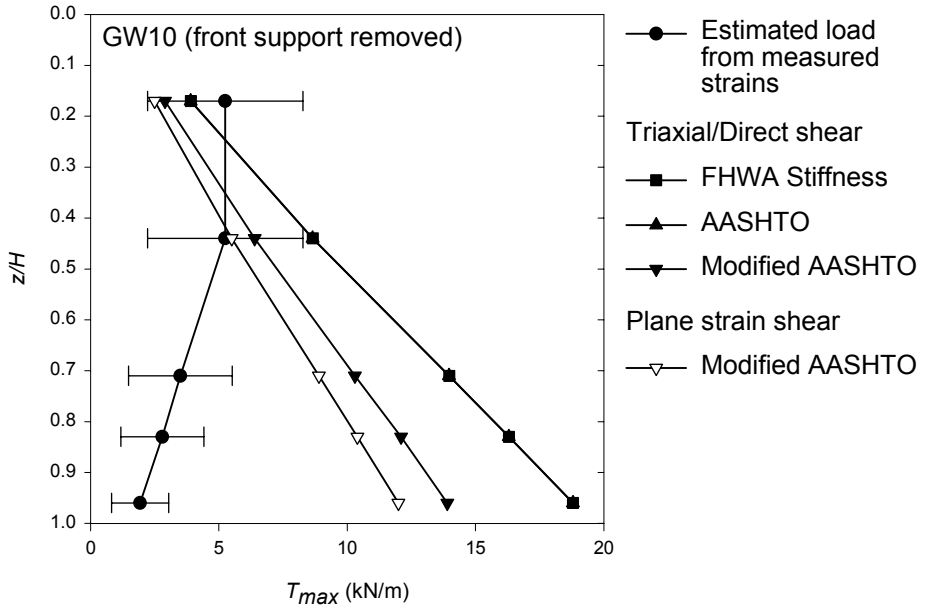

f) Wall GW10 (after wall face support removed)

Figure 5.3. Predicted peak reinforcement peak loads, and peak loads estimated from measured strains. Note: Error bars represent best estimate of measured load ± 1 standard deviation.

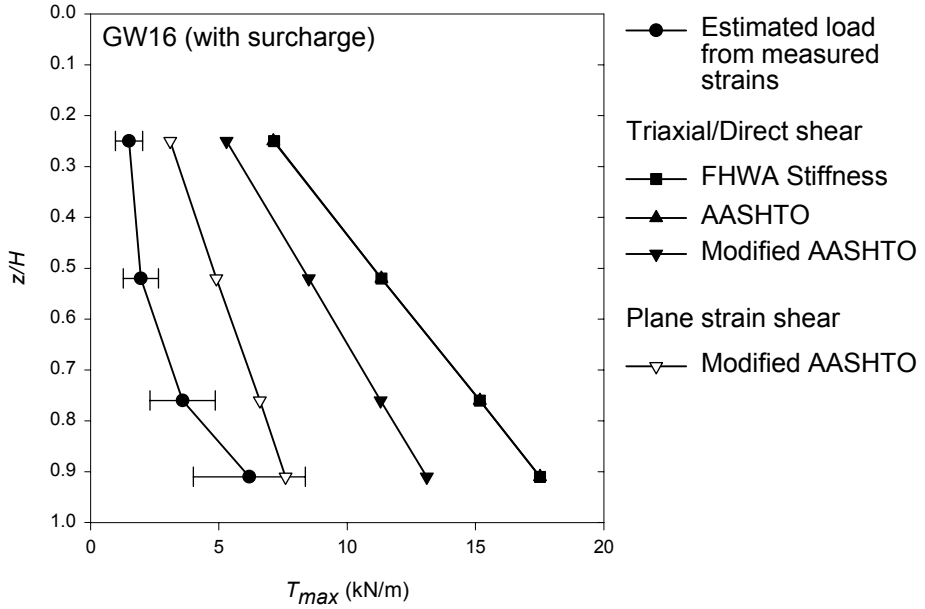

g) Wall GW16 (with surcharge)

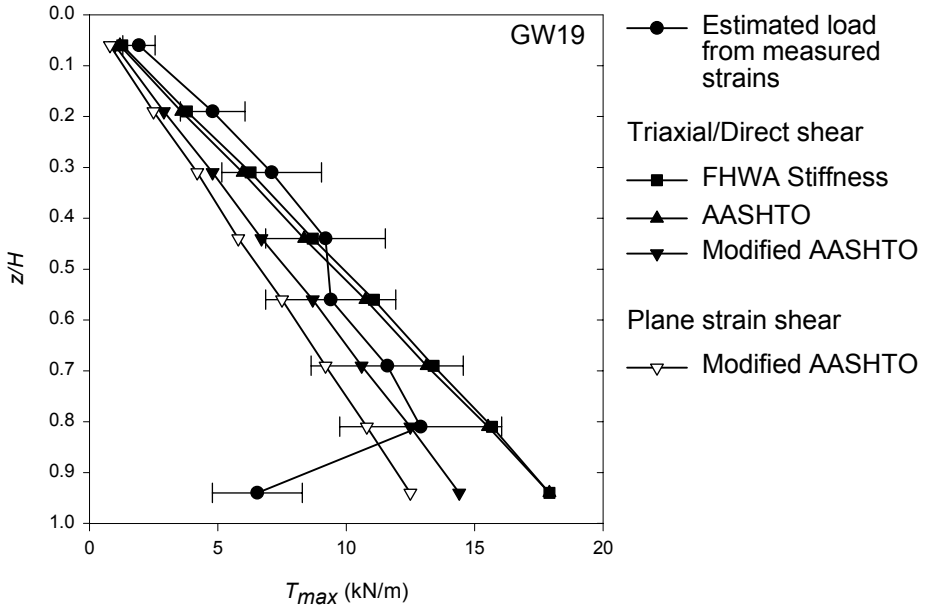

h) Wall GW19

Figure 5.3. Predicted peak reinforcement peak loads, and peak loads estimated from measured strains. Note: Error bars represent best estimate of measured load ± 1 standard deviation.

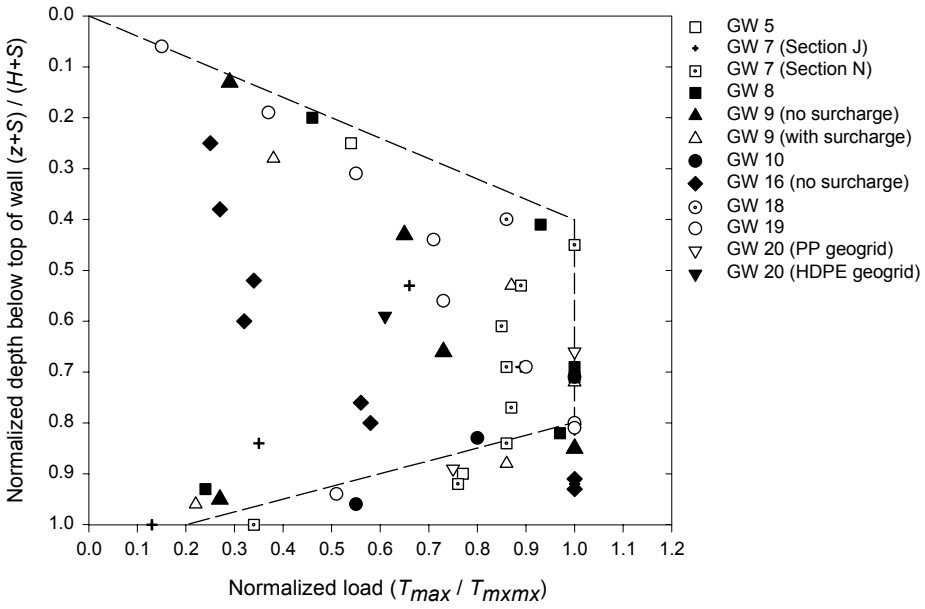

Figure 5.4. Normalized load estimated from strain measurements as a function of normalized depth below wall top.

5.5 Discussion

The empirical evidence reviewed herein suggests that conservative predictions of reinforcement loads can be expected even when fully mobilized peak plane strain soil shear strength parameters are used in reinforcement load calculations. Using the constant volume shear strength for the soil can be expected to lead to even more conservative designs. For most geosynthetic walls built to date, the reinforcement strains have been at or below the strains required to mobilize peak soil shear strength. Furthermore, it is undesirable to allow the soil to strain beyond peak shear strength over the majority of the failure surface, since the load carrying capacity of the soil at post peak strength may be very much less, and this would lead to over-stressing of the reinforcement. This condition was observed for the RMCC test walls (GW14 and GW15) subjected to high surcharge loads (Bathurst 1993), as well as the Algonquin wrapped-face geotextile wall (GW10) (see Chapter 2.0). Fortunately, even after the soil reaches failure, the geosynthetic reinforcement can be expected to continue to strain with time (see Chapter 2.0 regarding wall GW10). This points to the built-in safety of geosynthetic systems because of their inherent flexibility and large rupture strains. Other test wall studies appear to confirm that the peak soil shear strength is a key parameter that is closely related to observed wall loads and predictions of failure (Zornberg et al. 1998).

Note that relative to the peak plane strain soil shear strength derived from backfill-specific soil shear strength tests, design soil friction angles typically used for geosynthetic wall design result in a built-in additional factor of safety that is on average approximately 2.0. This is simply because of the choice of soil strength parameters alone (see Chapter 2.0). Therefore, the selection of soil strength parameters is a major source of design conservatism for geosynthetic walls.

A key assumption in current design methodologies is that internally the wall is at a state of limit equilibrium. That is, the strength of the soil and the reinforcement is fully mobilized everywhere, and all components of the wall system are at a state of incipient collapse. However, most of the measurements that have been used to estimate actual reinforcement loads have been taken at working stress conditions. The mechanisms of load development and distribution in geosynthetic soil reinforcement under conditions of limit equilibrium may not be the same as those at working stress conditions. Related to this question is the validity of the assumption that the load in the reinforcement, distributed over the reinforcement tributary area, is representative of the soil state of stress. Rowe and Ho (1993) suggested that the reinforcement loads do not represent the soil state of stress for two primary reasons:

1. The force in the reinforcement depends solely on the strain and the stiffness of the reinforcement.
2. Equating the soil stress (K_a or K_o) to the reinforcement load distributed over the tributary area implicitly assumes that principle stress directions remain vertical and horizontal, which further implies that there is no shear stress at the soil/reinforcement interface. Yet shear stress is known to occur at the soil/reinforcement interface, and principle stress directions do rotate in a reinforced soil mass by up to 20^o to 40^o (Murray and Farrar 1990).

The empirical data provided in Figure 5.1 support the argument that the soil state of stress is not represented by the lateral stress calculated from the reinforcement force distributed over the tributary area, as the lateral earth pressure determined from the reinforcement loads estimated from measured strains is significantly less than the active state or at-rest earth pressure. Although it does appear, given Table 5.3 and Figure 5.3, that use of the Coulomb active earth pressure coefficient (reduced to consider only the horizontal component and accounting for full wall interface friction) does help to bring the predicted load closer to the measured load, it does

not completely remove the difference, and other factors must contribute to the reduced load measured in the reinforcement. Note that the Coulomb analysis results presented herein do account for the rotation of principle stresses by assuming full interface friction and taking only the horizontal component of the active force. Therefore, the rotation of principle stresses does not fully account for the conservatism illustrated in the table and figures.

The first point made above provides part of the key to assessing what governs the development and distribution of reinforcement loads in geosynthetic walls. Data reported by Bathurst and co-workers for the RMC walls (e.g., Bathurst and Benjamin 1990, Bathurst et al. 1993b) show that the stiffness of the facing system and degree of wall toe restraint relative to the stiffness of the reinforcement significantly affect how much load is carried by the reinforcement. Rowe and Ho (1993) came to a similar conclusion. Since stresses are not fully mobilized in each of the load carrying components of a wall at working stress conditions, the distribution of loads will be governed by the relative stiffness of each component. Furthermore, the component that has the greatest stiffness will tend to carry the largest portion of the load. The data provided herein, especially in Figure 5.2 and Table 5.3, demonstrate that all wall components are involved in carrying the load: the soil reinforcement, the soil, the wall facing, the wall toe, and the wall foundation soil. Note that current limit equilibrium methods used in the AASHTO Tieback Wedge/Simplified Method and the FHWA Structure Stiffness Method do not consider the effect of the wall facing and toe resistance, as well as the wall foundation soil, on wall load capacity. Bathurst (1993) also came to this conclusion as a result of back analysis of two of the full-scale RMC test walls reported herein, and comparison with measured reinforcement loads and wall toe loads. The distribution of maximum reinforcement loads versus depth below the wall top (Figure 5.3) shows that the foundation soil below the wall may also carry a portion of the lateral load, as the reinforcement load tends to decrease substantially near the bottom of the wall.

Because the stiffness of the wall components greatly affects the magnitude and distribution of load in the reinforcement, the Structure Stiffness Method should have some advantages. However, the equation for this method was developed so that the load in the reinforcement distributed over the tributary area of the reinforcement would never be less than K_a, regardless of how low the stiffness value gets (see Section 5.4.1). This, in effect, maintains the assumption that the force in the reinforcement directly reflects the state of stress in the soil for geosynthetic reinforced systems. The empirical adjustments made to develop this method were based on

reinforcement loads derived from measured strains converted to load using a short-term geosynthetic stiffness rather than a longer term stiffness value, causing the loads in the empirical database used at that time to be too high. Therefore, at least for geosynthetic reinforcement, the Structure Stiffness Method does not provide an advantage regarding the issue of stiffness for geosynthetic reinforced walls because of the assumptions noted and database used to develop it.

Of the methods currently available for estimating reinforcement loads in geosynthetic walls, all characterize the soil response by using the active earth pressure coefficient. However, at working stress conditions, the amount of load carried by the reinforcement depends on the stiffness of the reinforcement relative to the soil stiffness, as well as the stiffness of the other wall components, if the soil shear strength is not fully mobilized. The stiffer the reinforcement relative to the soil modulus, the more load the reinforcement will attract. However, accurately estimating the soil modulus is not a simple task, and currently the soil modulus value is restricted to numerical modelling exercises of wall performance (for example, finite element or finite difference modelling of reinforced soil walls (Rowe and Ho 1996, Hatami et al. 2001, Bathurst and Hatami 1998, 2001). It is for this reason that a semi-empirical approach, using a more readily measurable soil parameter such as the peak soil friction angle, will continue to be used. The writers believe that a fundamental property of reinforced soil walls is the soil stiffness, as demonstrated by the results of numerical modelling (e.g., Bathurst and Hatami 1998, Rowe and Ho 1993). However, more work is required to establish explicit relationships between soil stiffness and conventional soil properties such as peak soil strength and lateral earth pressure coefficient.

Figure 5.3c and the related data in Table 5.3 indicate that the AASHTO Tieback Wedge/Simplified Method and the FHWA Structure Stiffness Method, for walls with large facing batters, are less conservative than for walls with little or no face batter. That is, these methods do not predict loads in a consistent manner across a wide range of facing batter. This appears to provide additional evidence that the assumption the reinforcement load directly reflects the soil state of stress is not correct; instead, the relative stiffness between the various wall components governs how the load is distributed. approach is inaccurate for predicting reinforcement loads at working stress conditions.

For the walls that were surcharged to fail the soil (a true ultimate limit equilibrium condition), the measured reinforcement loads were slightly to well below the predicted loads

using current design methods (see figures 5.2 and 5.3f, and Table 5.3). For the full-scale test walls with aluminium panel facings, the combination of toe restraint and facing stiffness may account for the majority of this difference. Base restraint due to good foundation soil conditions may also partially contribute to the difference. However, it should also be recognized that the current design methodology assumes no wall friction when active earth pressure coefficients are calculated, resulting in a Rankine earth pressure. When the current limit equilibrium approaches for design are considered in relation to the data presented in Table 5.3 and Figure 5.3f, comparing the Rankine earth pressure with the Coulomb earth pressure, the assumption that there is no wall interface friction appears to be too conservative even when ultimate limit equilibrium conditions are approached.

Figure 5.4 indicates that the distribution of load to each reinforcement layer is different than what is derived or assumed from limit equilibrium concepts (i.e., the distribution is trapezoidal rather than triangular). The inaccurate load distribution is a significant contributor to the poor correlation between the measured loads and the predicted loads in geosynthetic walls. The distribution observed in Figure 5.4 is similar to that proposed for other soil reinforced wall systems using empirical and numerical modelling results. For example, Broms (1978) proposed a uniform distribution for geosynthetic walls. Collin (1986) proposed a trapezoidal distribution for geogrid walls based on finite element model results. Trapezoidal distributions have been in use for many years for anchored walls and braced excavations (Terzaghi and Peck 1967, Sabatini et al. 1999). Zornberg et al. (1998a) indicated that a rectangular or trapezoidal distribution is more accurate than a triangular distribution for geosynthetic walls for one or both of the following reasons:

- Force redistribution between reinforcement layers, especially as the wall approaches failure.
- In the case of heavily battered walls, the vertical overburden stress may be reduced because of the facing batter, thereby causing the reinforcement force to not increase monotonically with depth below the wall top, as is often assumed.

Rowe and Ho (1993) also indicated that the stiffness of the reinforcement may contribute to the relatively uniform distribution observed for geosynthetic walls at working stress conditions. They found, on the basis of numerical analysis and field observations, as well as a review of the numerical and centrifuge modelling by Adib (1988) and Jaber (1989), that the load distribution

becomes more uniform as the reinforcement stiffness decreases. Bathurst et al. (1987) and Bathurst (1993) also showed that the wall foundation may influence this distribution, causing reinforcement loads to decrease near the wall base if firm foundation conditions exist. These results and conclusions give support to the distribution presented in Figure 5.4.

5.6 Summary and Conclusions

The principles of estimating the geosynthetic reinforcement stiffness as a function of time, as described in Chapter 4.0, was applied to 16 full-scale geosynthetic wall case histories to calculate a best-estimate of the load levels in geosynthetic reinforcement in walls. Uncertainties in the measurement values were estimated in the calculation of the loads estimated from measured strains in comparison to loads predicted with current design methodologies. On the basis of this evaluation, it was determined that the differences between measured and predicted values were significant, both in terms of consistency of the prediction and the tendency of the current design methods to substantially over-estimate reinforcement loads, warranting re-evaluation of the current methods used to predict reinforcement loads in walls.

On the basis of the evaluation of the geosynthetic wall reinforcement loads derived from strain measurements, the following conclusions are made:

1. Reinforcement loads derived from strain measurements at working stress conditions are in general much lower than would be predicted by current design methods that are based on limit equilibrium approaches and use Rankine earth pressure theory, even when the best estimates of the peak plane strain shear strength of the backfill soil are used in the calculations. Variability in the strain measurements and the stiffness used to convert strains to loads does not account for this difference.
2. The current limit equilibrium design methods provide a very poor correlation to the reinforcement loads estimated from measured strains. Possible reasons for the poor correlation include the following:
    - The mechanism of load distribution within the wall is different at working stress conditions than at limit equilibrium (i.e., incipient collapse of the wall). It appears that the differences in the stiffness of the various wall components dictate how load is

distributed to the reinforcement layers. Therefore, the measured reinforcement loads do not necessarily represent the soil state of stress.

- The combination of the wall face and the wall toe restraint carries a significant portion of the internal load for geosynthetic walls, thereby reducing the load the reinforcement must carry. The stiffer the wall face/wall toe restraint, the less load the reinforcement must carry.
- The foundation soil may also provide some restraint to strain development within the reinforced wall mass, acting as a boundary condition not considered in current design methodologies.
- Because of the factors mentioned above, the distribution of forces to each of the reinforcement layers is not triangular, as is currently assumed, but is instead trapezoidal.

3. Neither Rankine nor Coulomb earth pressure coefficients properly account for the effect of wall face batter on geosynthetic wall reinforcement loads. This results in under-prediction of load for heavily battered walls. This may be further evidence that the wall reinforcement loads do not directly correlate with the soil state of stress.
4. If current limit equilibrium-based design methodologies are used, it appears that assuming the wall interface friction to be zero is conservative. Assuming full interface friction, except where noted above, will produce safe estimates of reinforcement load. Using peak plane strain friction angles in calculations generally improves the prediction of reinforcement loads.

The low reinforcement strains and loads measured to date in geosynthetic walls point to the desirability of using peak soil shear strengths rather than constant volume shear strengths for design purposes. Doing so will help keep design conservatism more reasonable and will be consistent with the philosophy of preventing failure of a major component of the reinforced soil system, the soil. However, at working stress conditions, the modulus of the soil may be a more important parameter than soil shear strength for estimating reinforcement loads. Because it is difficult to estimate the soil modulus and to implement this parameter into close-formed design analyses, the use of a soil shear strength parameter is still desirable. Furthermore, because the geosynthetic reinforcement can reach much higher strains than can the soil without failure, as was observed for the RMCC test walls GW14 and GW15 and the Algonquin geotextile wall

GW10, the current focus of design, which is to prevent failure of the reinforcement, may need to be changed. The focus instead should be to prevent reinforcement strains from becoming high enough at any time during the design life of the structure to allow failure of the soil, defined as allowing the soil to strain beyond peak shear strength over the majority of the developing wall failure surface. Once enough of the soil along the developing failure surface in the wall has reached or gone beyond its peak strength such that the wall behavior can no longer be characterized as "working stress" (e.g., slumping of the wall begins or cracking of the backfill soil is observed at the wall top), even if the wall reinforcement is not near rupture, for all practical purposes the wall has failed.

6.0 OBSERVED LONG-TERM PERFORMANCE OF GEOSYNTHETIC WALLS, AND IMPLICATIONS FOR DESIGN

6.1 Introduction

Considerable focus has been given in recent years to establishing the long-term performance of geosynthetic reinforcement as a material, addressing such issues as installation damage, creep, and durability. However, only limited effort has been expended to establish the long-term performance of geosynthetic walls as a whole. Geosynthetic walls have been viewed by the civil engineering profession, in general, as a new technology whose acceptable long-term performance is yet to be established. Nevertheless, geosynthetic walls have been in use for over 25 years. Chapter 5.0 demonstrates, through back-analysis of available wall case histories, that geosynthetic reinforcement load levels appear to be significantly lower than values estimated with the current North American design methods (e.g., AASHTO 2002). That chapter also identifies several sources for this conservatism. The results from that chapter have led the writers to investigate whether measured long-term deformation and strain measurements are consistent with the hypothesis that actual load levels are significantly lower than values determined from design, and whether geosynthetic reinforced soil walls, other than those specifically identified as having poor performance, can be expected to be stable over their target design life.

The objectives of this chapter are as follows:

1. Identify and analyze the long-term behavior observed in well-documented, full-scale wall case studies and determine their long-term stability.
2. Provide at least an approximate verification of the load levels identified in a number of full-scale wall case histories reported in chapters 2.0 and 5.0. Accomplish this by comparing the measured creep data from these walls to laboratory in-isolation creep data for the same geosynthetic material.
3. Establish some quantitative guidelines to distinguish between walls that can be expected to exhibit good long-term performance and those that can be expected to exhibit marginal or poor performance.

Only case histories where granular soil was used as backfill are considered in this investigation (see Chapter 2.0).

6.2 Long-Term Performance Factors and Design

Current North American geosynthetic reinforcement design procedures recognize the potential for loss of reinforcement strength as a result of installation damage, creep, and durability. The available (allowable) reinforcement design strength is expressed as follows:

$$T_a = \frac{T_{ult}}{RF \times FS} = \frac{T_{ult}}{RF_{ID} \times RF_{CR} \times RF_D \times FS} \tag{6.1}$$

Here, T_{ult} is the ultimate wide-width strip tensile strength of the geosynthetic. RF is a combined factor to account for geosynthetic strength loss during the wall design life and is equal to RF_{ID} x RF_{CR} x RF_D, where RF_{ID} is a reduction factor that accounts for strength loss due to installation damage, RF_{CR} is a reduction factor for strength loss due to creep, and RF_D is a reduction factor for strength loss due to chemical and biological degradation.

The reduction factors RF_{ID} (installation damage—a short-term strength loss), RF_{CR} (creep—a long-term strength loss), and RF_D (chemical and biological degradation—a long-term strength loss) are not uncertainty factors but are reduction factors used to calculate the long-term strength remaining in the geosynthetic reinforcement after a given period of time. These reduction factors are analogous to the reduction in steel area used to account for corrosion losses in steel reinforcement products. Material strength variation is taken into account during the selection of T_{ult} and is based on standardized quality control and quality assurance procedures used by geosynthetics manufacturers. The Minimum Average Roll Value (MARV), which is defined as the strength that is two standard deviations below the mean tensile strength, is used for design rather than the mean tensile strength.

In past years, in particular before 1990, protocols for determining these reduction factors, to some extent creep and especially chemical durability factors, were either nonexistent or practically unusable. The long-term geosynthetic strength data that were available at that time were either inconsistent or extremely conservative because of the use of laboratory procedures that did not simulate in-situ conditions. This resulted in unrealistically conservative assessments of potential strength degradation. Because of this, geosynthetic walls at that time were considered too unreliable to use for long-term permanent applications. Simply too much was unknown, and not enough long-term performance history was available for geosynthetic walls.

A detailed description of durability issues is provided by Allen (1991) and Allen and Elias (1996).

At present, protocols for determining the long-term strength and behavior of geosynthetic reinforcement are much better developed. Examples of these protocols are now included in design codes through the AASHTO Bridge Specifications (AASHTO 2002), FHWA manuals (Elias et al. 2001, Elias 2000), and in one state department of transportation test method (WSDOT 1998).

6.3 Overview of Case Histories

Only case histories with enough deformation and strain data to determine long-term creep rates are considered herein. However, comparison of the long-term performance of these selected case histories to the overall long-term performance of all the case histories provided in Chapter 2.0 can be used to extrapolate the lessons learned to geosynthetic walls in general. Key characteristics of each of these case histories are summarized in tables 6.1 and 6.2. The type of long-term data available for each case history is summarized in Table 6.3. Instrumentation details can be found in Chapter 3.0 for each case history. Table 6.2 provides best estimates of the actual long-term resistance to demand ratio for the case histories that had long-term deformation and strain data available, as well as the global resistance to demand ratio that would be obtained if the current AASHTO specifications were used for design (a total of 10 case histories and 12 wall sections). In Chapter 2.0, this comparison was made for all of the case histories in which some indication of long-term performance was available (35 wall sections). Table 6.4 compares the average long-term resistance to demand ratio for the 12 wall sections that had detailed long-term deformation data to the average long-term *RD* value for all of the case histories. These case histories have been grouped by their observed long-term performance in accordance with the criteria provided later in this chapter. As shown in the table, the average global resistance to demand ratio for the 12 selected wall sections with good long-term performance data is similar to the average resistance to demand ratio for the entire database of walls. Furthermore, as shown in tables 6.1 and 6.2, the range of wall heights, surcharge conditions, and reinforcement types and polymers used span the range of what is typical today for geosynthetic walls. Therefore, the long-term deformation data reported herein for these 12 selected wall sections can be considered representative of the larger database of geosynthetic

Table 6.1. Summary of geometry, observation period, and data source for selected case histories.

Case History	Date Built	Wall Height (m)	Surcharge Conditions	Time for Wall Construction (hrs)	Wall Temper-ature (^oC)	Years of Monitoring Available	Source of Data Used for Analysis
Tanque Verde GeogridConcrete Panel Wall, GW5	1984	4.9	None	350	27^o C	11 years	Desert Earth Engineering (1989); McMahhon and Mann Consulting Engineers (1996)
Oslo, Norway Geogrid Walls (Sections J and N), GW7	1987	4.8	3 m steeply sloping soil surcharge	960 to top of wall, 2,600 to surcharge completion	10^o C	11 years	Fannin (1988); Fannin and Hermann (1991); Fannin (2000)
Algonquin Geogrid Concrete Panel Wall, GW8	1988	6.1	2.1 m sloping surcharge	920	17^o C	1 year	Christopher (1993, 1998)
Algonquin Geogrid Modular Block-Faced Wall, GW9	1988	6.1	2.1 m sloping surcharge	920	17^o C	1 year	Bathurst et al. (1993)
RMC Geogrid Wrapped-Face Full-scale Test Wall, GW11	1986	3	0.7 m soil surcharge	65	20^o C	1 month	Bathurst, et al. (1988)
RMC Full Height Propped Panel Full-scale (Geogrid) Test Wall, GW14	1989	3	Full test wall top coverage with air bag loading system, up to 80 kPa	100 after prop release, 1,000 to end of surcharging	20^o C	2 months	Benjamin (1989)
RMC Incremental Panel Full-scale (Geogrid) Test Wall, GW15	1989	3	Full test wall top coverage with air bag loading system, up to 70 kPa	200, 2,500 to end of surcharing	20^o C	2 months	Benjamin (1989)
WSDOT Rainier Avenue Wrapped-Face Geotextile Wall, GW16	1989	12.6	5.3 m sloping surcharge	1650	14^o C	1 year	Allen, et al. (1992)
Fredericton, New Brunswick Propped Panel Geogrid Wall, GW18	1990	6.1	None	100 after prop release	10^o C	1.2 years	Knight and Valsangkar (1993)
Vicenza, Italy Welded Wire-Faced Geosynthetic Walls (HDPE and PP test sections with final surcharge), GW20	1998	4	3.5 m steeply sloping soil surcharge	5,500 to surcharge completion	20^o C, assumed	1 year	Carrubba, et al. (1999); Alberto, (1998)

walls, especially given the similarities in observed long-term performance between this subset and the entire database. Note that most of these case histories were designed less conservatively than would be required by the current AASHTO design specifications (AASHTO 2002), in some cases much less conservatively.

Table 6.2. Summary of materials and design for selected case histories.

Case History	Geosynthetic Type	Geosynthetic Polymer	Long-Term Global Resistance to Demand Ratio (RD) for Actual Wall, (Chapter 2.0)	Long-Term Global Resistance to Demand Ratio if Designed per AASHTO (2002) and Typical Practice, (Chapter 2.0)
GW5	Extruded uniaxial geogrid	HDPE	6.1	4.5
GW7	Extruded uniaxial geogrid	HDPE	Section J - 4.8 Section N - 6.4	7.1 for both sections
GW8	Extruded uniaxial geogrid	HDPE	1.3	2.9
GW9	Woven geogrid	PET	1.1	2.1
GW11	Extruded biaxial geogrid	PP	1.5	6.4
GW14	Extruded biaxial geogrid	PP	1.2 end of construction, 0.32 with full surcharge	6.0 end of construction, 4.0 with full surcharge
GW15	Extruded biaxial geogrid	PP	1.2 end of construction, 0.36 with full surcharge	6.0 end of construction, 4.1 with full surcharge
GW16	Woven geotextile	PP for upper 75% of wall, PET for lower 25% of wall	3.4	4.6
GW18	Extruded uniaxial geogrid	HDPE	1.9	3.0
GW20	Extruded uniaxial geogrid	HDPE	1.7	10
GW20	Biaxial geogrid	PP	0.53	8.8

Table 6.3. Summary of the type of measurements that are available for each case history.

Case History	Strain	Deformation	Load
GW5	Resistance strain gauges, Bison coils for soil and geogrid strain	--	Lateral and vertical earth pressure cells
GW7	Bison coils attached to geogrid	--	Load cells attached to geogrid; vertical earth pressure
GW8	Resistance Strain Gauges, Bison coils near geogrid	Inclinometers, survey measurement of facing panels	Lateral earth pressure behind face
GW9	Resistance strain gauges, extensometers on geogrid	Inclinometers	Lateral and vertical earth pressure cells
GW11	Resistance strain gauges, extensometers on geogrid	Survey measurement of facing	Vertical earth pressure cells
GW14	Resistance strain gauges, extensometers on geogrid	Survey measurement of facing	Load cells at geogrid connection to facing; vertical earth pressure; load cells at wall toe
GW15	Resistance strain gauges, extensometers on geogrid	Survey measurement of facing	Load cells at geogrid connection to facing; vertical earth pressure; load cells at wall toe
GW16	Resistance strain gauges, extensometers; Bison coils for soil strain	Inclinometers, face survey measurements	Lateral and vertical earth pressure cells
GW18	Strain gauges	Survey measurement of facing	Lateral earth pressure cells
GW20	Strain gauges	Wall base lateral deformation only	Vertical earth pressure; load cells attached to geogrid

Table 6.4. Average global resistance to demand ratio for all wall case histories (a total of 35) vs. the 12 case histories with detailed long-term creep/deformation data.

	Average Resistance to Demand Ratio (RD)	
Wall Type/Performance	**Actual Wall**	**Designed per AASHTO (1999) with Typical Design Practice and Soil Design Parameters**
Geosynthetic walls with good performance; all case histories	2.7	4.6
Geosynthetic walls with poor performance; all case histories	0.45	4.8
Geosynthetic walls with good performance; case histories with detailed long-term creep data	2.8	5.5
Geosynthetic walls with poor performance; case histories with detailed long-term creep data	0.40	5.6

6.4 Geosynthetic Load-Strain-Time Behavior Overview – Use of Laboratory Data to Evaluate Field Performance

6.4.1 Introduction

Recent work by Elias (2001), in which 24 geosynthetics from 12 retrieval sites were evaluated, confirmed that little, if any, chemical degradation has occurred in geosynthetics in reinforcement applications in full-scale structures up to 25 years old. The researchers concluded that observed strength losses could be largely or wholly attributed to installation damage for polypropylene (PP) and high density polyethylene (HDPE) geosynthetics, as well as for high tenacity-high viscosity polyester (PET) products. Some measurable strength losses of 0.25 to 0.5 percent per year due to chemical degradation were observed for low tenacity-low molecular weight PET geotextiles, which is consistent with the laboratory studies reported by Elias et al. (1998a). Note that all of the case histories with PET reinforcement products used high tenacity-high viscosity PET geosynthetics, although some of the additional case histories reported by Allen et al. (2002) did utilize lower viscosity PET geotextiles. For the PP and HDPE products, some antioxidant consumption appeared to have occurred during the 20- to 25-year observation period but not enough to allow degradation of the polymer to occur. This is consistent with the laboratory studies reported by Salman et al. (1998).

In general, it can be concluded that the largest contributors to strength loss and reduced wall performance (i.e., excessive deformation) for the geosynthetic reinforcement products in use today are installation damage and possibly creep. Installation damage has limited impact on the initial working stress performance of geosynthetic walls, since for most geosynthetics used as reinforcement (i.e., woven geotextiles and geogrids), the load-strain-time behavior of the geosynthetic is not significantly affected by installation damage at typical or even relatively high working strains for the levels of installation damage observed in full-scale walls (Allen and Bathurst 1994). Allen and Bathurst (1996) also provided strong evidence that installation damage will have little, if any, effect on creep strains and rates for the typical levels of installation damage in full-scale structures. As a result of the observations summarized above, an accurate assessment of long-term performance can be obtained through measurement and extrapolation of the creep deformations and strains recorded in the wall case histories.

Creep is simply the visco-elastoplastic response of the geosynthetic to sustained load. Creep results in time-dependent deformation that may continue to occur as long as the reinforcement is loaded. At low to intermediate load levels, depending on the polymer type, the creep rate will continue to decrease with time and may eventually stabilize, at least within the accuracy of the measurements. At higher load levels, creep will continue until rupture occurs.

In general, up to three stages of creep are observed in polymeric materials. These include primary, secondary or steady-state, and tertiary creep. Primary creep strains are characteristically linear when plotted against a logarithmic time scale and increase at a decreasing rate on an arithmetic time scale. Secondary creep strains are typically linear when plotted against an arithmetic time scale. Tertiary creep is the rupture phase of creep and is characterized by a rapidly increasing creep rate with time. Geosynthetic structure tends to dominate primary creep (at least for nonwoven geotextiles, but much less so for woven geotextiles and not at all for geogrids), and the polymer characteristics tend to dominate secondary and tertiary creep mechanisms (Allen 1991). Polyolefins (HDPE and PP) tend to exhibit all three stages of creep, whereas PET tends to exhibit only primary and tertiary creep.

6.4.2 Long-Term Wall Stability Evaluation

To meet the objectives of this chapter it is necessary to a) define what is meant by good long-term behavior, b) determine whether the existing wall case histories are exhibiting good long-term behavior, and c) determine whether the walls will be stable throughout their design lifetime. This can be accomplished by establishing whether the wall reinforcements are exhibiting only primary creep, or better yet, determining whether logarithmic strain rates are decreasing and thus approaching complete stabilization within the observation period. Establishing whether the measured creep strains are well below what would be observed for the material from laboratory in-isolation data near the creep limit can also help in this determination.

6.4.3 Verification of Reinforcement Loads

Another objective of this chapter is to at least approximately verify the load levels identified in the available wall case histories. This will be accomplished by comparing the measured creep data from these walls to laboratory in-isolation creep data for the same geosynthetic material at actual load levels in the wall. In Chapter 5.0**,** measured strains at the

end of wall construction, and an estimated geosynthetic stiffness value that correctly accounts for the loading rate that occurred during wall construction, were used to determine a best-estimate of the reinforcement load level in each of the case histories reported herein. A summary of the load levels estimated for each wall case history in Chapter 5.0 is provided in Table 6.5.

The creep strains and rates observed for polymers typically used in geosynthetics are strongly influenced by the load level applied (e.g., Wilding and Ward 1981, Allen 1983, Yeo 1985, and Koutsourais 1995). PP and HDPE materials are in general more sensitive to load level than PET materials, except near the rupture limit, where PET creep is very sensitive to load level. Because of this sensitivity, it should be possible to provide an approximate verification of the load levels determined in Chapter 5.0. The creep rates and strains determined from laboratory in-isolation tests, at least for geogrids and woven geotextiles, can be compared to the creep rates and strains observed for the reinforcement in the full-scale walls.

Table 6.5. Reinforcement load levels estimated from strain measurements for selected case histories.

Wall Case	Depth Below Wall Top, z (m)	Load Level (% of T_{ult})	Wall Case	Depth Below Wall Top, z (m)	Load Level (% of T_{ult})
GW5	1.14	1	GW11	0.6	14
	3.28	2		1.35	18
	4.2	1		2.1	9
GW7 (Section J)	1.2	4		2.85	1
	2.4	5	GW14, with 80 kPa surcharge, at connection	0.5	26
	3.6	2		1.25	16
	4.2	6		2	15
	4.8	1		2.75	9
GW7 (Section N)	0.6	7	GW15, with 70 kPa surcharge, at connection	0.5	16
	1.2	6		1.25	23
	1.8	6		2	20
	2.4	6		2.75	13
	3.0	6	GW16, with surcharge	3.1	5
	3.6	6		6.5	3
	4.2	5		9.6	4
	4.8	2		11.5	3
GW8	1.2	3	GW18	2.44	3
	2.5	5		4.88	3
	4.2	6	GW20 (HDPE Section)	1.1	5
	5.0	6		2.7	8
	5.7	1	GW20 (PP Section)	1.6	12
GW9 (with surcharge)	0.8	2		3.2	9
	2.6	4			
	4.0	5			
	5.2	4			
	5.8	1			

If the strain level is held constant and the stress level in the reinforcement is allowed to decrease with time, stress relaxation occurs. The stress relaxation process has similarities to creep, in that molecules within the polymer must slip past one another in response to load. Both stress relaxation and creep can occur in the reinforcement, depending on the creep rate of the soil relative to the creep rate of the geosynthetic.

The writers reviewed typical sand creep data from triaxial compression tests presented by Kuhn and Mitchell (1993) that show that the creep of sands can be significant. After triaxial strain rates were adjusted to account for plane strain boundary conditions (i.e., plane strain values are about 2 to 2.5 times less than comparable triaxial test values according to Lee (2000)), it became apparent that sand strain rates can be of the same order of magnitude, or slightly less than, tensile creep rates observed in-situ for geosynthetic reinforcement materials under working stress conditions.

An implication of this comparison is that the soil, provided it has not reached its peak shear stress, can restrict the creep deformation of the geosynthetic, but only if the creep rate of the backfill soil is less than the creep rate of the geosynthetic reinforcement. If the soil controls the creep rate of the composite system, the molecules within the geosynthetic polymer can still slip past one another because of the load applied to the polymer, resulting in stress relaxation. Note that if stress relaxation does occur and composite creep strain levels are restricted by the soil, measured creep rates for reinforcement in granular backfill soil can be expected to be lower than values measured during in-isolation laboratory creep tests.

For geosynthetics that have significant macro-structure complexity (e.g., nonwoven geotextiles), reduced time-dependent macrostructure rearrangements should be expected in soil relative to creep behavior of the same geosynthetics tested under in-isolation laboratory conditions (Elias et al. 1998b). However, reduced macro-structure creep will not be a significant factor for most geogrids and woven geotextiles.

Temperature can also affect the creep rates observed, particularly for polyolefins. Temperature needs to be considered when comparing creep data from laboratory testing and creep measurements in full-scale field structures.

6.5 Long-Term Creep and Deformation Observations

Long-term measurements of creep strains, creep strain rates, and lateral wall deformations are provided later in this chapter. The sources for all of the long-term creep strain and deformation data used to produce these figures are identified in Table 6.1. Note that strains reported from strain gauges have been corrected with strain gauge calibration data (see Chapter 3.0). In all cases, the creep strains presented are from locations with the largest strains in a given layer, which were typically located near the boundary between the active and resistant zones, and in some cases near the connection with the face. Therefore, the measured creep strains are representative of the maximum load levels in the reinforcement layers.

There is a significant difference between the way the geosynthetic is loaded in the laboratory and the way it is loaded in full-scale walls. Laboratory creep specimens are brought up to the creep load rapidly (on the order of seconds), whereas in the field the loading of the geosynthetic up to its final load is very slow (on the order of 1,000 hours). This large difference in loading rate does have a significant influence on the short-term creep rates observed in the wall versus what is observed in the laboratory. The difference is illustrated in Figure 6.1 for an HDPE geogrid, taken from work by Rimoldi and Montanelli (1993). However, in the long term the strains in the specimen are not influenced by the initial loading condition. Yeo (1985) also observed a similar effect caused by loading rate. In the current investigation, time zero was adjusted to the beginning of wall construction to provide a meaningful evaluation of creep strain rates from both in-isolation and in-wall data (Figure 6.2).

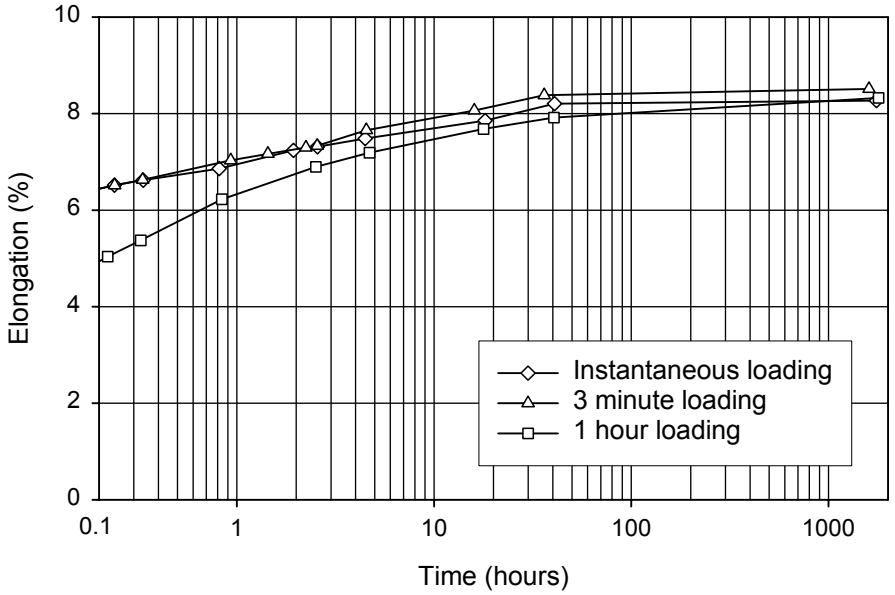

Figure 6.1. Effect of loading rate on measured creep strains for an HDPE geogrid (after Rimoldi and Montanelli 1993).

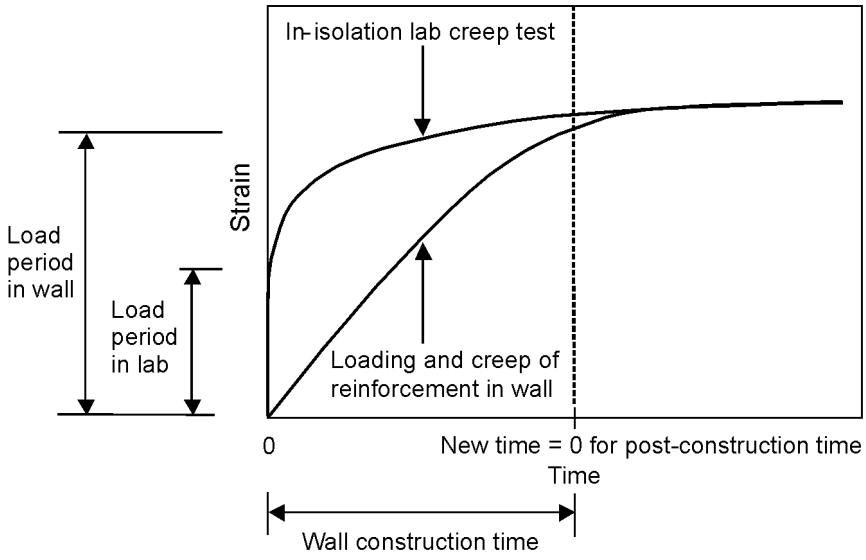

Figure 6.2. Conceptual illustration for comparing the creep measured in walls to in-isolation laboratory creep data.

Two types of creep strain rate plots are provided: Sherby-Dorn plots and log-strain rate versus log-time plots. A Sherby-Dorn plot is a well known plotting technique used in polymer science (McGown et al. 1984, WSDOT 1998). Each curve represents a specific geosynthetic

layer in a wall or a specific geosynthetic specimen tested at a specific load level. Creep strain rates observed under constant load are plotted against the total strain in the specimen or layer measured at the time the creep strain rate was calculated. The creep strain rate is simply the slope of the creep strain curve at a given point in time. Curves that are linear or concave downward indicate that only primary creep is occurring, and that stabilization (no rupture) is likely (e.g., Figure 6.7b, curves in lower left corner of plot). Curves that are concave upward indicate that secondary or tertiary creep is occurring, and that rupture is likely (e.g., Figure 6.11b, curve in upper right corner). The closer the curves are to the bottom left corner of the plot, the better the creep performance of the material. The closer the curves are to the upper right corner, the more likely creep rupture will occur.

For the log-strain rate versus log-time plots, curves that are linearly decreasing with time or concave downward indicate that only primary creep is occurring and that stabilization will eventually occur. Curves that are horizontal or concave upward indicate that secondary or tertiary creep is occurring, potentially resulting in rupture at some future time (see Figure 6.11c for examples of both).

Note that some interpretation of the creep curves through curve fitting is required to determine strain rates, since local jumps in the measured creep strain curves can cause wide variations in calculated creep strain rates. The jumps in the curves are typically the result of the short increments of time used in the calculations and the small magnitude of changes in strain readings that may be at the limit of the resolution of the measuring devices. Hence, the slope of the measured creep curves must be calculated over fairly long increments of time to be meaningful. Such an approach was taken to determine the creep rates for this study.

Estimating the in-isolation creep curves at the load levels in the wall reinforcement required interpolation between the load levels used to generate the isochronous curves, or extrapolation to load levels below the lowest load levels tested. Because the load levels were quite low in most of the case histories, log-linear time extrapolation beyond the available data was usually feasible, even while the desired accuracy was maintained. In some cases, more sophisticated extrapolation techniques were needed (Yeo 1985, WSDOT 1998). The extrapolation of the creep data was likely not a significant source of error in these comparisons. Curve fitting was applied to some data to provide both smooth and consistent isochronous curve sets. Curve fitting can reduce the variability in the results, but it can also introduce error. These errors can contribute to the

differences determined between the creep rates observed in the wall and the in-isolation creep rates estimated from the laboratory data. The error should not be greater than the coefficient of variation in the creep data itself, which the writers have found is typically about the same as the coefficient of variation in the wide-width strength (e.g., ASTM D4595) for the geosynthetic. Therefore, the error will not be great enough to mask the trends in the data observed.

As necessary, the in-isolation creep curves and strain rates produced as described above were temperature shifted to account for the difference between the test temperature and the temperature in the wall. Details regarding the temperature shifting for these wall cases are provided in chapters 4.0 and 5.0.

6.5.1 Comparison of Strain and Deformation Data

Figures 6.3 and 6.4 provide a comparison of strains and deformations measured as a function of time for walls GW9 and GW16. Note that for these walls creep strains were generally less than 0.4 percent, and at some locations less than 0.1 percent strain. Creep deformations at the wall face were also small, on the order of 20 mm or less. Similar comparisons can be made for Walls GW11 and GW18. What can be observed from these comparisons are similar trends of decreasing creep strain rate and deformation rate for most of the measurements. One strain gauge installed in Wall GW9 appeared to be the exception to this trend, and conflicts with the extensometer readings obtained at the same location.

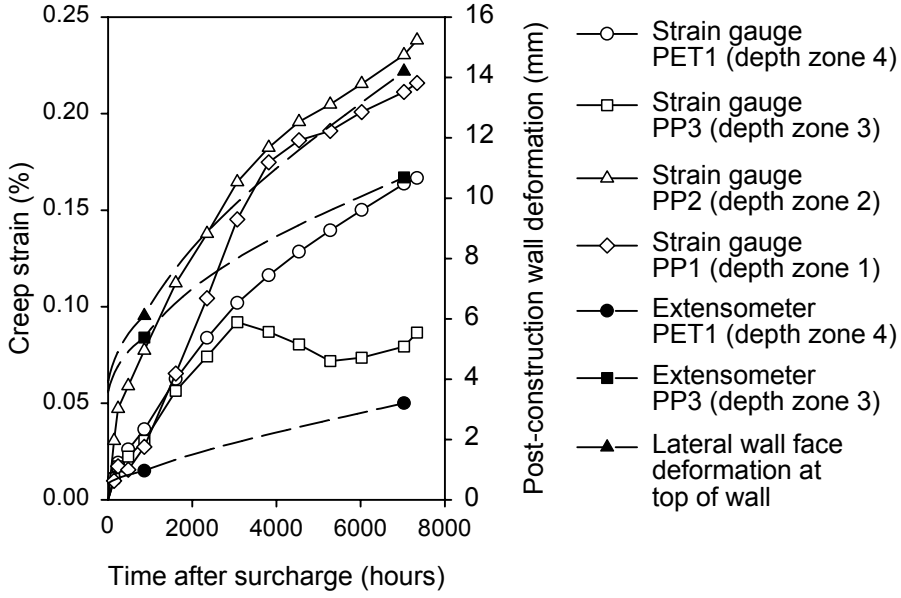

Figure 6.3. Measured creep strains and deformations for Wall GW16.

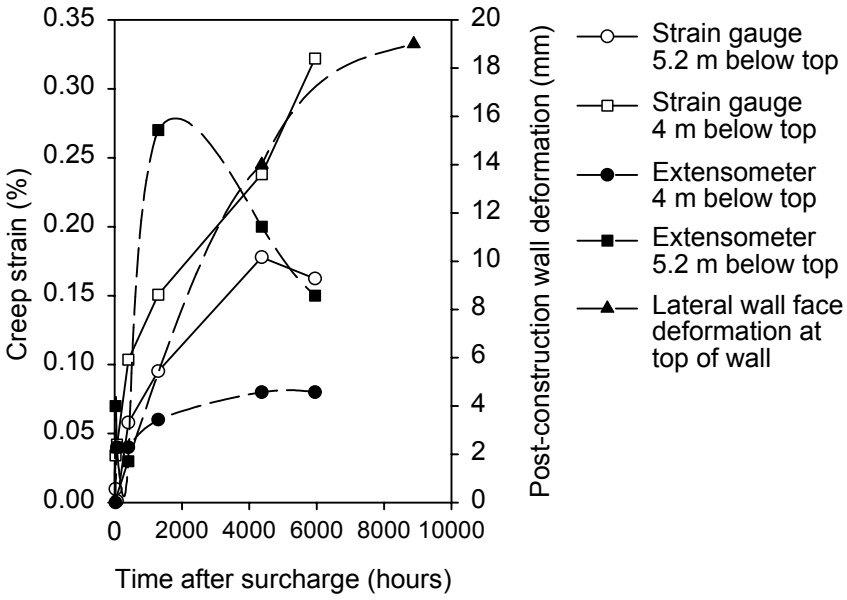

Figure 6.4. Measured creep strains and deformations for Wall GW9.

6.5.2 Creep Strain and Strain Rate Data

For each case history, plots of total strain as a function of time from the beginning of wall construction or laboratory creep test loading, as well as creep strain rates, are provided and compared to in-isolation creep strains and rates. The in-isolation laboratory creep strains correspond to load levels in the wall reinforcement estimated from in-situ strain measurements at the end of wall construction (see Chapter 5.0 and Table 6.5). The in-isolation creep curves for load levels estimated from the Simplified Method (AASHTO 2002) using measured peak plane strain soil shear strength values and soil unit weights are also plotted in the figures. The calculation of load level with the Simplified Method is explained in Chapter 5.0.

In all cases, except for the highest surcharge loading for the full-scale test walls GW14 and GW15, the creep strains can be seen to be increasing at a decreasing rate with time, indicating that only primary creep was occurring. The last strain readings for GW5 (Figure 6.5) and GW7 (Figure 6.6) indicate that strain was actually decreasing.

Note that creep data from Wall GW9 (Figure 6.4) are not included in these creep rate figures. In-isolation laboratory creep curves could not be accurately estimated from the available isochronous creep curves because of the lack of very low strain data (the load levels were estimated to be very low for this wall) and the tendency for PET isochronous creep curves to be nonlinear in the low strain range. Furthermore, at the load level range of interest, the creep strain

rates for PET are not very sensitive to load level. Therefore, a meaningful comparison between the in-isolation and in-wall creep rates could not be made. However, the creep strain rates observed in the wall indicated that only primary creep was occurring, which implies that load levels in that wall were significantly below the creep limit of the material.

6.5.2.1 Wall GW5 (Figure 6.5)

This wall was a propped panel wall. Little, if any, strain occurred in the wall until after the props had been released, which was approximately when the wall backfilling was two-thirds complete (Desert Earth Engineering 1989). For the purposes of establishing the load level in the reinforcement layers, that all of the load was assumed to be transferred to the reinforcement 100 hours after the wall construction was complete. Thereafter, any additional strain was considered to be creep. This wall is unique in that creep data were available for an exceptionally long time after construction (10 years). Furthermore, the wall site temperature was unusually high (on average, 27^{o} C), and the reinforcement polymer used was HDPE, a polymer that would be expected to exhibit significant creep, especially at such a high site temperature.

These data show that the measured creep strains and rates remained low over the observation period and were an order of magnitude lower over the long term than the creep strain rates estimated from the in-isolation laboratory tests. Furthermore, the creep strains appeared to be coming to a halt, indicating stabilization of the reinforcement creep. The creep strain level in the wall increased more rapidly at first than occurred in the in-isolation creep data. The creep strains and strain rates at the load level predicted by the Simplified Method (AASHTO 2002) were significantly higher than what was observed in the wall, but not high enough to result in eventual instability.

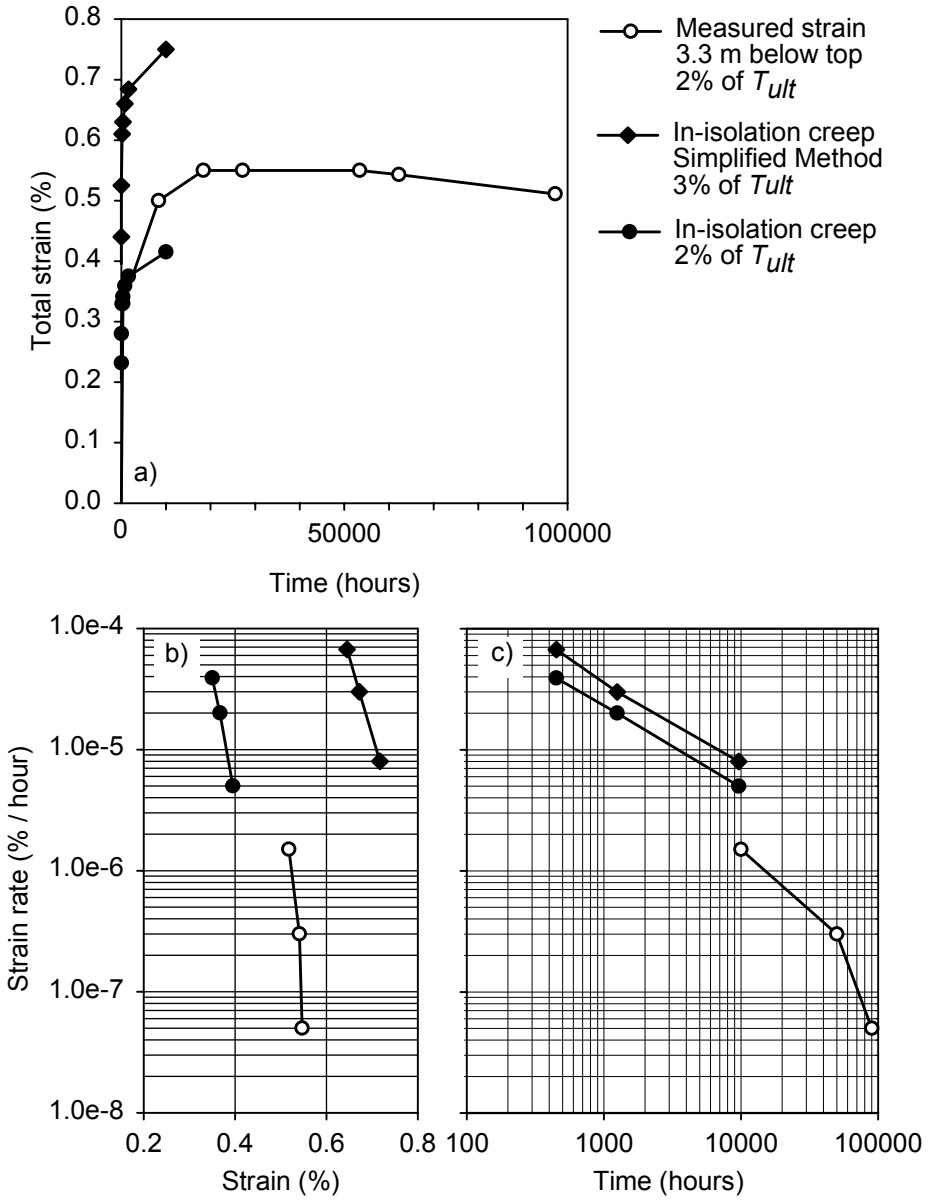

Figure 6.5. Tanque Verde HDPE geogrid wall (GW5): a) total strain versus time, b) Sherby-Dorn plots, c) strain rate versus time.

6.5.2.2 Wall GW7 (Figure 6.6)

Exceptionally long-term post-construction creep strain measurements were also available for this wall (up to 10 years of data). An HDPE reinforcement was also used in this wall, but the average site temperature was much lower than was the case for Wall GW5 (i.e., 10^{o} C). The strain readings after 50,000 hours began to decrease significantly with time (Fannin 2000). The reason for this decrease could not be specifically determined. Only the first 50,000 hours of creep data are shown.

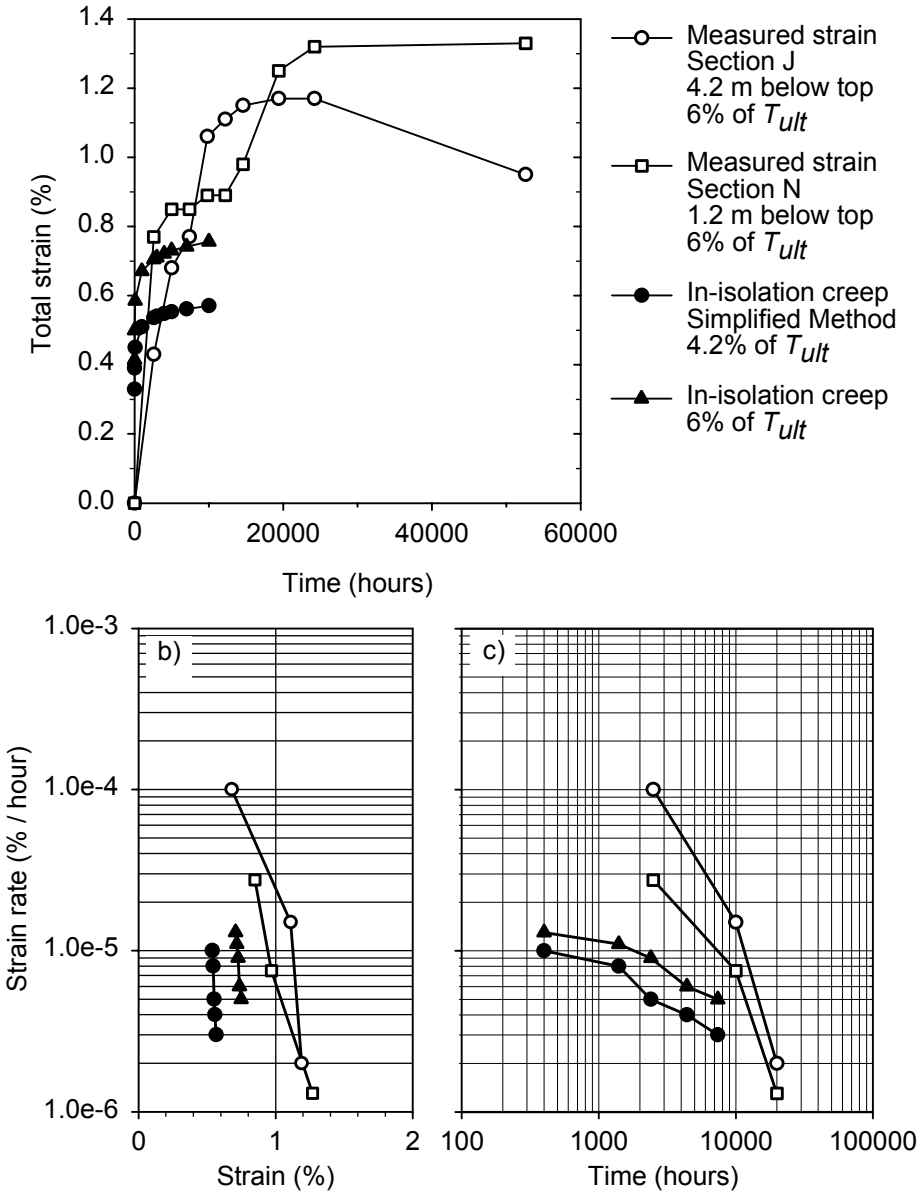

Figure 6.6. Oslo, Norway, HDPE geogrid wall (GW7): a) total strain versus time, b) Sherby-Dorn plots, c) strain rate versus time.

Figure 6.6a shows an interesting jump in the creep strain curves for both wall sections at approximately 7,000 to 10,000 hours after wall construction. Fannin (2000) postulated that soil creep near the sloping wall face could have contributed to an increase in load, which was also recorded with load cells embedded in the reinforcement layers. Nevertheless the jump in load at the times noted was not as large as the jump in recorded strain measurements. In spite of the potential load increase, the observed strain rates in the wall, though initially higher than those

estimated from the in-isolation creep test data, eventually decreased to lower creep strain rates than observed for the in-isolation data.

6.5.2.3 Wall GW16 (Figure 6.7)

The wall was constructed with three PP geotextiles and one PET woven geotextile. The three PP geotextiles were all from the same product line, as defined in WSDOT Test Method 925 (WSDOT 1998), and were constructed of one to three layers of the same slit film woven geotextile stitch-bonded together to form products of different strengths. Creep data are provided for the upper two geotextile products (PP1 and PP2 – see Chapter 2.0). However, in-isolation creep data were only available for PP2, the stronger of the two products. In-isolation creep data for PP2 were extrapolated to the PP1 product by normalizing the applied load by the ultimate strength of the product, creating a load level as a percentage of the ultimate tensile strength. This normalizing approach, but with the short-term stiffness of each product obtained via ASTM D4595, was also adopted to estimate the load in the reinforcement on the basis of the measured strain at the end of construction for each of the products, since only long-term stiffness data were available for product PP2.

Figure 6.7 indicates that the total strains observed in the wall and the corresponding in-isolation total strains matched reasonably well for the PP2 product, but that the in-isolation creep strains were slightly overestimated for PP1. However, the in-isolation creep strain rates for both reinforcement layers were greater than the measured creep rates in the wall, indicating that overall, the in-isolation creep data estimated at the actual load levels in the wall were conservative. The creep strain rates at the load level predicted by the Simplified Method were an order of magnitude higher than the measured creep rates. Furthermore, on the basis of the Sherby-Dorn plot (Figure 6.7b), it appears that the reinforcement would be predicted to be unstable at that load level (based on the curvature of the creep strain rate versus strain curve).

Note that the confined in-soil laboratory creep rates were considerably lower than the measured creep rates, even though in Figure 6.7a the total strains for the confined creep test data match the wall strains fairly well. It appears that significant stress relaxation occurred in the confined test (see Chapter 4.0), and this may have contributed to the lower creep strain rates observed.

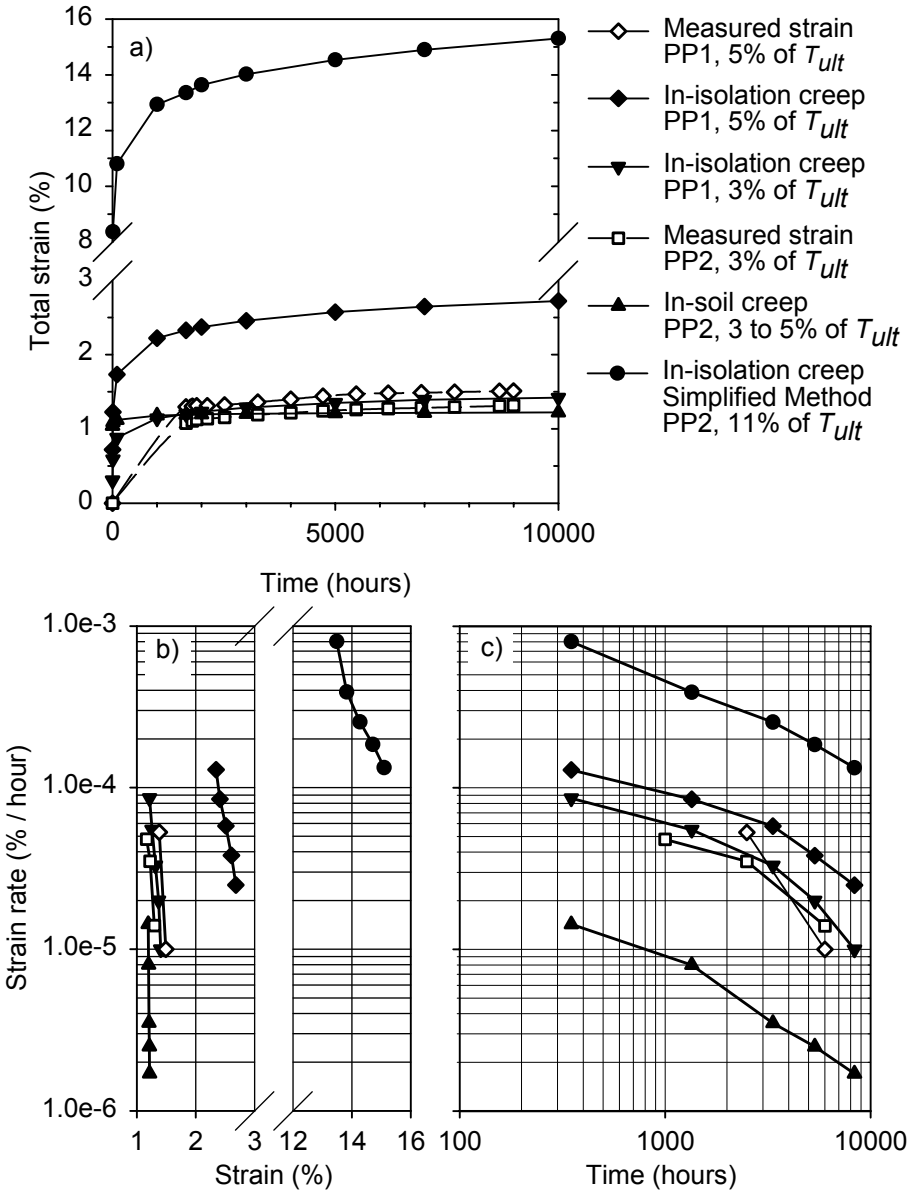

Figure 6.7. Rainier Ave. Wall (GW16) (PP geotextiles): a) strain versus time, b) Sherby-Dorn plots, c) strain rate versus time.

6.5.2.4 Wall GW18 (Figure 6.8)

This wall was a propped panel wall. Little, if any, strain occurred in the wall until after the end of wall construction, once the props had been released. For the purposes of establishing the load level in the reinforcements, all load was assumed to be transferred to the reinforcement 100 hours after prop release. Thereafter, any additional strain was considered to be creep.

Although the creep strain levels in the wall matched well with the laboratory in-isolation data initially, the strain levels in the wall increased more rapidly than the in-isolation data for the first 300 to 2,000 hours. In the long term, the measured creep strain rates in the wall were less than the in-isolation creep rates.

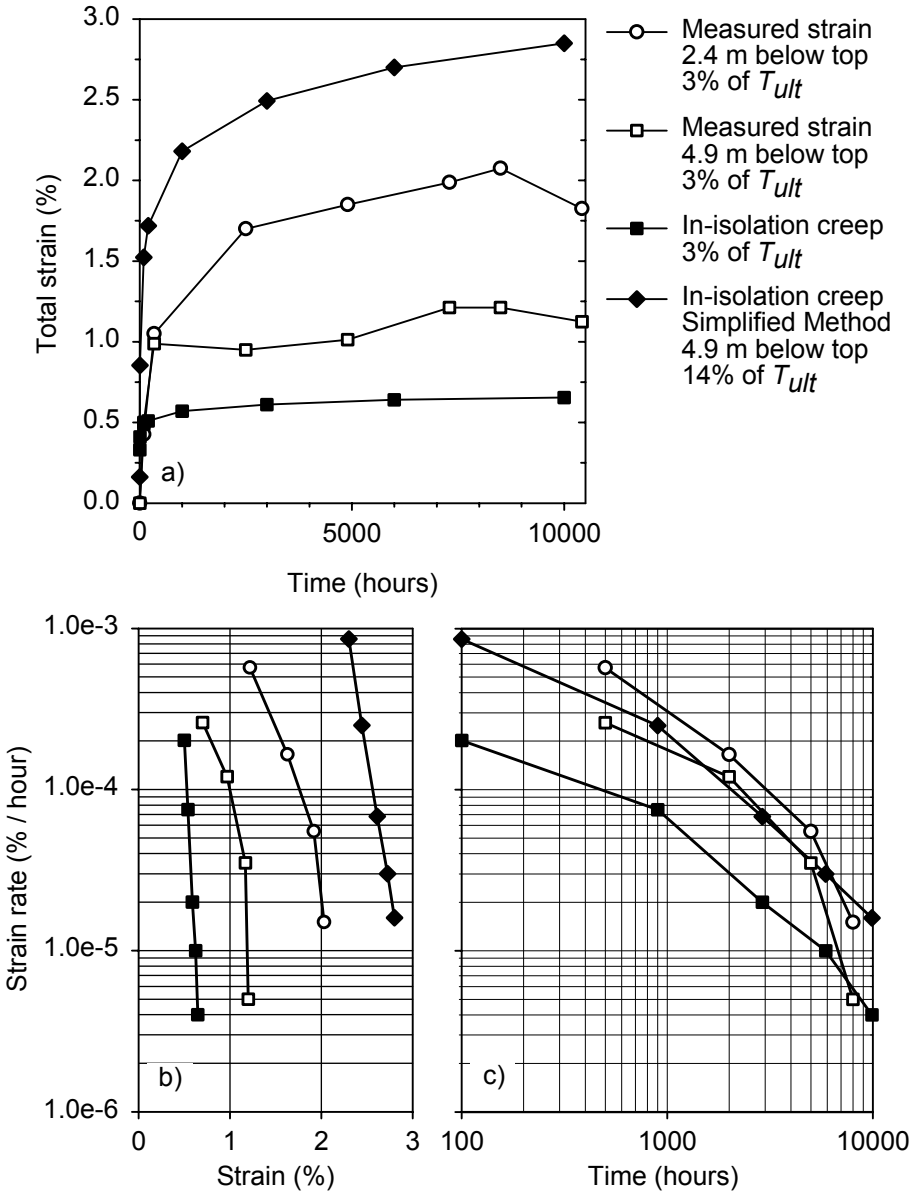

Figure 6.8. Fredericton HDPE geogrid wall (GW18): a) strain versus time, b) Sherby-Dorn plots, c) strain rate versus time.

6.5.2.5 Wall GW20 (figures 6.9 and 6.10)

This wall had widely spaced weak reinforcement, together with a flexible welded wire facing. The wall was designed to fail under the heavy surcharge load applied to the backfill.

Figures 6.9 and 6.10 show that the creep strains were accurately predicted by the in-isolation creep data during initial load application. However, the creep strain rates measured in both wall sections were greater than the in-isolation creep strain rates at the same load level, at least for the short-term. In the long term, with the exception of the upper layer in the PP section, the creep rates measured in the wall eventually dropped to approximately the same magnitude as the in-isolation creep rates. For the upper layer of the PP section, the measured creep rate in the wall was consistently higher than the in-isolation rate. In the case of the PP section, the reinforcement strains were unusually high—more than 3 percent at the end of surcharge placement and greater than 4.5 percent after 1,000 hours. The maximum creep strain was high enough to allow the soil to begin exhibiting what appears to be post-peak behavior. In the case of the HDPE section, the strains were much smaller than in the PP section. However, Currubba et al. (1999) concluded that the upper reinforcement layer in the HDPE section was beginning to pull out. This could have allowed transfer of load to the next reinforcement layer below, increasing the load level and total creep strain measured in that middle layer. This may explain the higher creep rate in that layer. However, in all the layers, except the upper layer of the PP section, the creep rates measured in the wall continued to decrease with time, and in the case of the HDPE, were even approaching stabilization, indicating that the reinforcement layers were not in danger of rupturing at some future time. Figures 6.9a and 6.10a also show that the creep strains at the load level predicted by the Simplified Method were significantly higher than the measured creep strains. For the PP wall section, the in-isolation creep strain rates predicted from the Simplified Method are not shown because the reinforcement would fail rapidly at such a high load level and could not be plotted using the time scale in the figure.

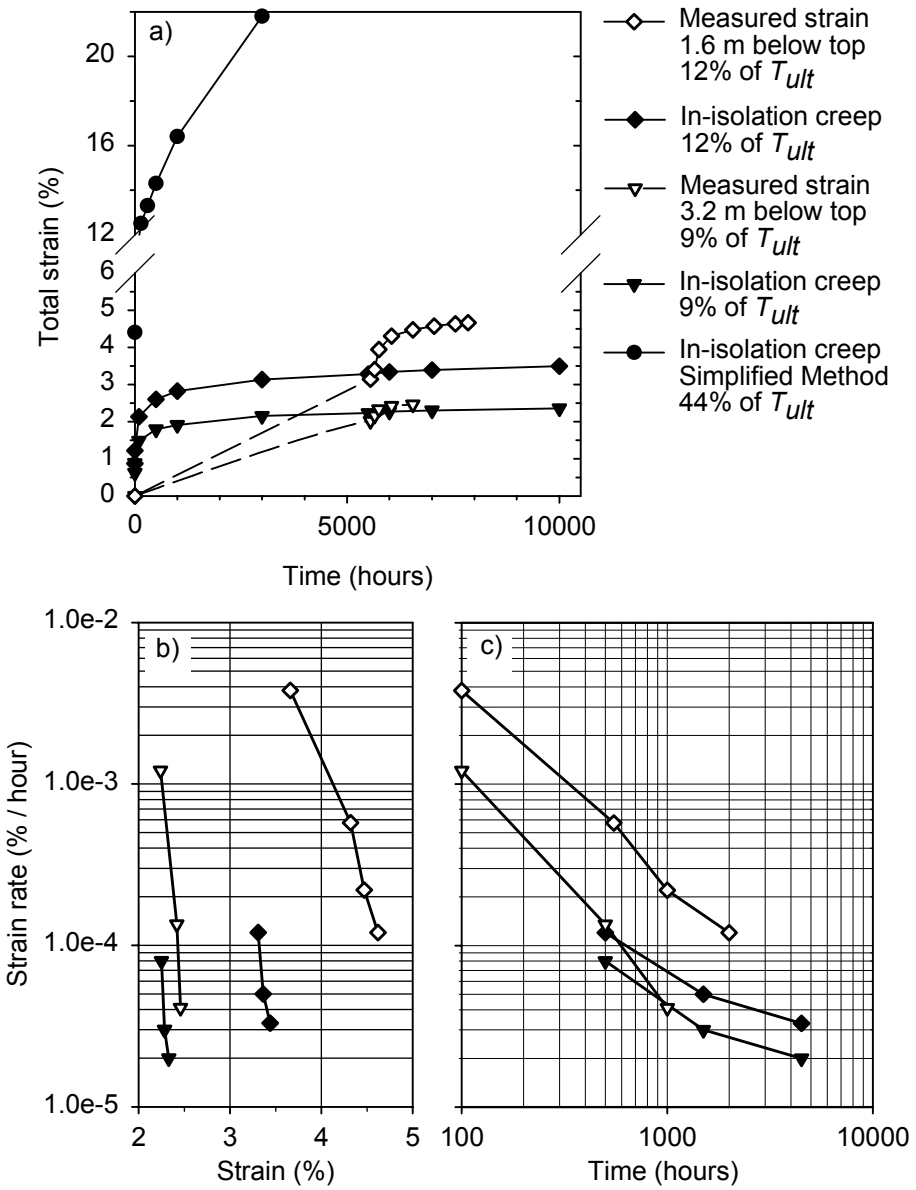

Figure 6.9. Wall GW20 (PP section): a) strain versus time, b) Sherby-Dorn plots, c) strain rate versus time.

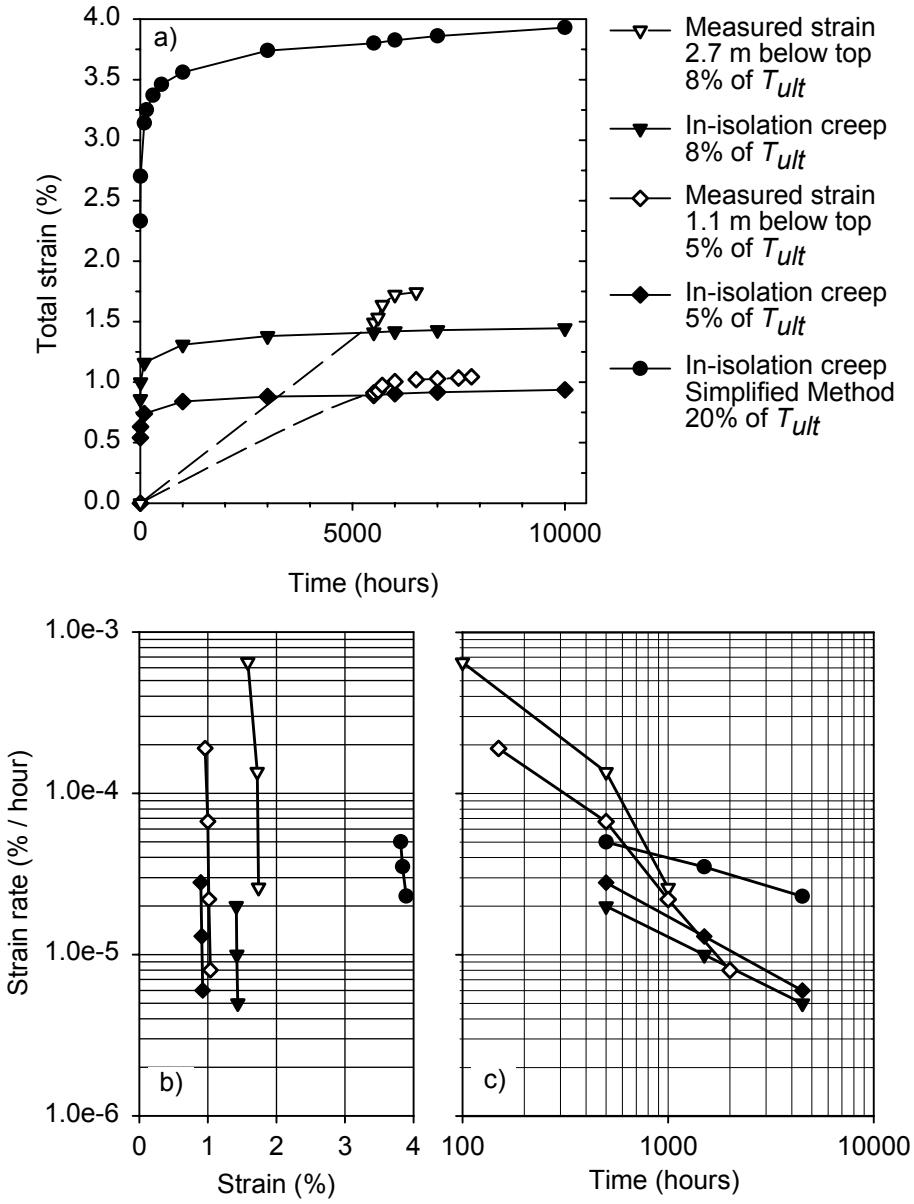

Figure 6.10. Wall GW20 (HDPE section): a) strain versus time, b) Sherby-Dorn plots, c) strain rate versus time.

6.5.2.6 Wall GW14 (Figure 6.11)

This wall was a full-scale propped panel wall built in a laboratory environment and surcharged with increasing load until failure was obtained (see Chapter 2.0). Little, if any, strain occurred in the wall until after the end of wall construction, once the props had been released. For the purposes of establishing the load level in the reinforcements, all load was assumed to be transferred to the reinforcement 100 hours after prop release. Thereafter, any additional strain was considered to be creep.

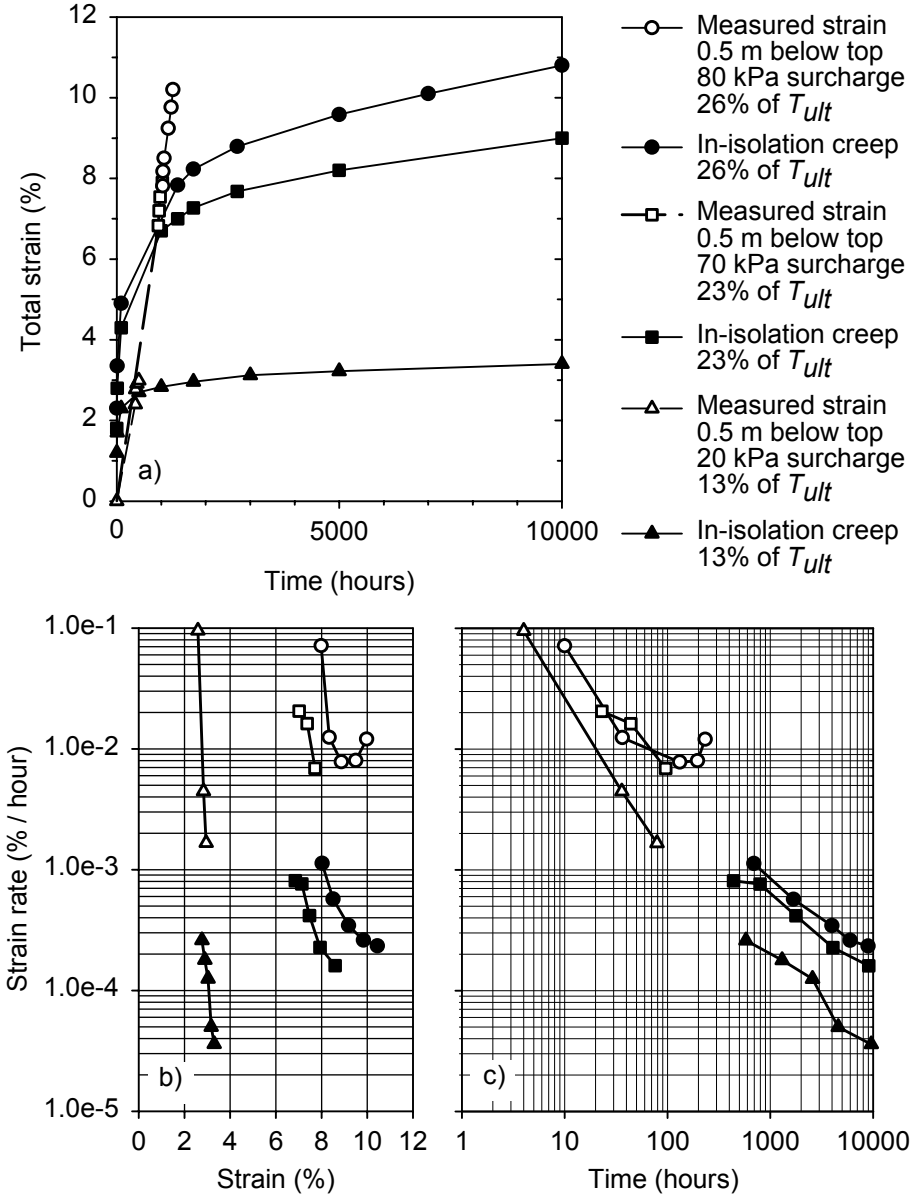

Figure 6.11. Wall GW14: a) strain versus time, b) Sherby-Dorn plots, c) strain rate versus time.

Figure 6.11a shows that the creep strains from both the wall and the in-isolation creep data matched fairly well initially but diverged significantly with time at the highest surcharge loads. Figures 6.11b and 6.11c show that the measured creep rates in the wall at the highest surcharge loads were much higher than indicated from the in-isolation data, and the shape of the curves suggest that they were approaching failure. Even the in-isolation data at the highest loads appears to predict that creep rates should increase, resulting in eventual creep rupture. Since the strains were high (7 to 8 percent or more), it is likely that the soil in the wall was exhibiting significant post-peak behavior, causing more load to be shed to the reinforcement and increasing

the creep observed. This wall did collapse at the highest surcharge load within a few hundred hours of the last surcharge application.

6.5.2.7 Wall GW15 (Figure 6.12)

This wall was a full-scale incremental panel wall built in a laboratory environment and surcharged to failure (see Chapter 2.0). The interpretation of the data in Figure 6.12 is the same as that described for the companion wall in the previous section.

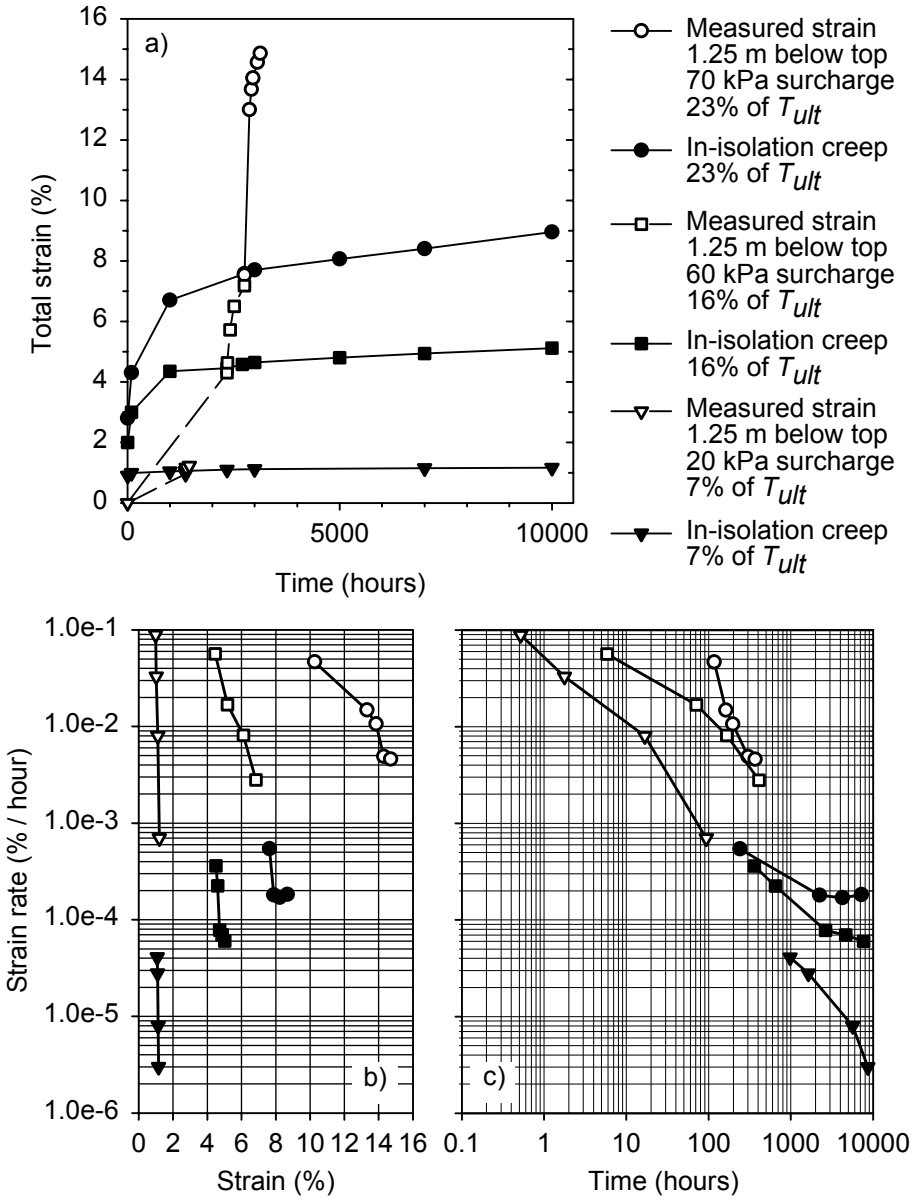

Figure 6.12. Wall GW15: a) strain versus time, b) Sherby-Dorn plots, c) strain rate versus time.

6.6 Analysis and Discussion

6.6.1 Long-Term Wall Performance

6.6.1.1 Creep at Working Stress Conditions

The creep data for all the walls (figures 6.5 through 6.12), except GW14 and GW15 at the higher surcharge levels and possibly the PP section for GW20, strongly indicate that only primary creep occurred in the reinforcement and that for some of the walls creep had virtually stopped within the observation period available. The creep behavior was consistent with the low load levels determined in Chapter 5.0 and were well below the load levels required to cause rupture within the design life of these walls. Given that these results already include any installation damage effects, and that chemical degradation has been shown to be minimal for all of the case histories observed to date, it can be concluded, with the exception of the walls noted, that the full-scale geosynthetic walls were stable and not expected to become unstable over their design life.

Furthermore, Greenwood et al. (2001), Orsat et al. (1998), Greenwood (1997), and Bernardi and Paulson (1997) provided evidence that demonstrates that as long-term creep occurs, the remaining reinforcement tensile strength does not decrease until the tertiary creep phase (i.e., the creep rupture phase) had been reached, which is in contrast to the monotonic decrease in strength with time assumed in design. This means that the factor of safety against reinforcement rupture is significantly higher than current design protocols would indicate for working stress conditions.

6.6.1.2 Creep Beyond Working Stress Conditions

Analysis of the creep strains and rates observed for walls GW20, GW14, and GW15 at the highest surcharge loads is instructive to understand what happens as a wall approaches failure. At lower surcharge levels in these walls and in the other field walls, the in-isolation laboratory creep strains and rates were similar to those observed in-situ, and maximum reinforcement strains in the walls were generally low (i.e., less than 3 percent). However, at the highest surcharge levels, reinforcement and soil strains were generally high, and the in-isolation creep rates under-estimated the creep rates observed in these walls, both in magnitude and, if rupture occurred, the time for onset of tertiary creep. As more strain occurs, the soil in a larger portion of the developing backfill shear surface becomes weaker and less stiff and approaches a residual

strength value. The overall behavior of the wall system is affected by the softer, weaker condition of the soil, beginning near the top of the wall and eventually propagating downward (e.g., walls GW20, GW14, GW15 and Wall GW10 – see chapters 2.0 and 5.0). Soil weakening and softening, in turn, requires that the soil reinforcement carry additional load, resulting in greater reinforcement creep strain and creep strain rates. In essence, the soil approaches a strength limit state, defined here as backfill soil failure. Eventually, the soil begins to exhibit cracks at the wall top, and the upper soil layers may lose confinement and possibly pull out if too short, or rupture if the reinforcement is too weak. If this occurs load transfer to lower layers can occur, increasing the strains and creep rates observed in the lower layers as time progresses. It should be emphasized, however, that reinforcement rupture is not a given in this situation (see Chapters 2.0 and 5.0).

This hypothesis explains the reinforcement strain response observed for walls GW14 and GW15 at the higher surcharge levels and both sections of Wall GW20. For Wall GW15 at 70 kPa surcharge, a jump in strain occurred at approximately 90 hours after surcharge loading because of the rupture of the reinforcement layer above the layer for which data are shown (see figures 6.12a and 6.12b), resulting in additional load transfer to the next lower layer (Benjamin 1989). This increase in load may be the cause of the greater under-prediction of strain and strain rate based on the in-isolation creep data for Wall GW14 (Figure 6.11). Wall GW14 failed catastrophically because of a wall face connection failure in the highest reinforcement layer (Bathurst and Benjamin 1990). For the HDPE section of Wall GW20 (Figure 6.10), pull-out of the upper layer appeared to result in a time dependent load increase in the next lower layer. For the PP section of this wall (Figure 6.9), the wall appeared to be initially stable. However, because the reinforcement was creep susceptible, the reinforcement allowed enough strain to build up in the soil to allow the soil shear surface to fully develop and begin exhibiting post-peak behavior. Once the soil began to weaken as creep strain continued, the reinforcement had to take on more load, accelerating the problem. This demonstrates the importance of considering the potential of the soil to develop long-term strains that are high enough to cause the wall system to exhibit post-peak behavior. Therefore, Wall GW20 should be considered marginal with respect to the soil failure limit state as defined above.

6.6.1.3 Creep Deformations at the Wall Face

Wall face post-construction lateral deformations as a function of normalized depth below the wall top are summarized in Figure 6.13. The data points in Figure 6.13b were calculated by extrapolating measured wall deformations on a log-linear plot out to 75 years. Three observations can be made from the data:

1. The post-construction face deformations increase linearly with increasing height above the wall base for four out of the five walls shown, with the maximum deformation near the wall top.
2. The post-construction face deformations do not appear to be a function of total wall height, nor do they appear to be a function of wall facing type based on the available database of case studies.
3. Comparison of the magnitude of deformations in figures 6.13a and 6.13b shows that for practical purposes most of the wall deformations occurred within 10,000 hours of wall construction.

It appears that the linear increase in wall face deformation with height above the wall base for most of the structures was the result of the wall facing rotating outward from the wall toe. The soil at the wall base was largely confined by the rigid foundation (in these case studies) as the restrained toe had little, if any, ability to creep outward as a function of time. As height above the wall base increased, the reinforcement layers were less constrained by the toe of the wall, allowing more long-term deformation to occur.

The walls included in Figure 6.13 had total heights that ranged from 3 to 12.6 m, yet the normalized deformation curves fall within a narrow band. Furthermore, these walls encompassed a variety of facing types, including a geosynthetic wrapped face, a precast concrete panel face, a full-height propped panel facing, and a modular block facing. The one exception to the linear trend in wall deformations is the data for Wall GW9, which was a modular block-faced wall. The data for all of the walls summarized in this figure were obtained from either optical facing survey or extensometers/potentiometers, whereas the data for Wall GW9 were obtained from an inclinometer attached to the face. Allen et al. (1992) discussed the difference between deformation measurements obtained from optical survey/potentiometers and inclinometers and noted that inclinometers represent total deformation relative to beginning of wall construction,

whereas optical facing survey measurements represent movement relative to time of installation of the survey device. Nevertheless, taken together the data for all five case studies fall within a reasonably narrow band.

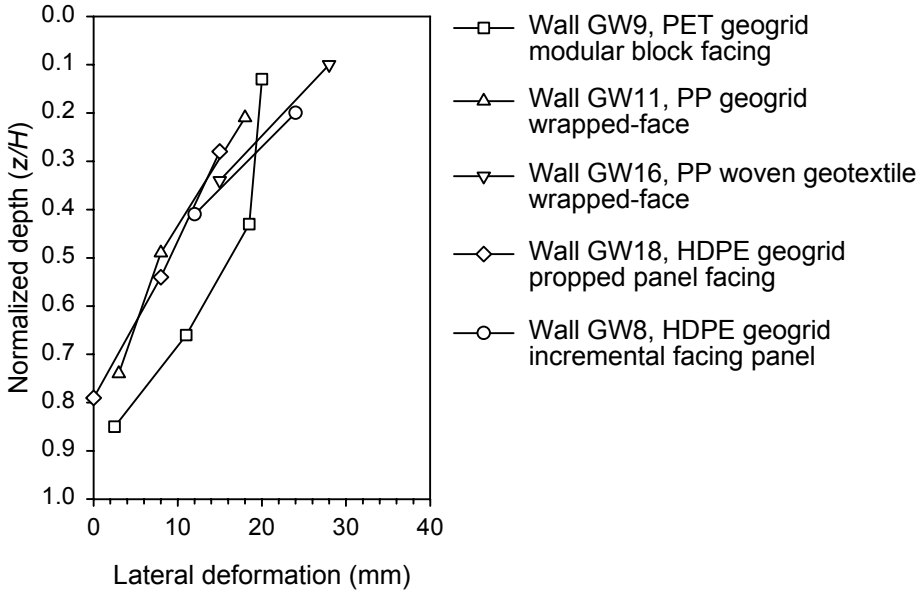

a) from end of wall construction to 10,000 hours after wall construction

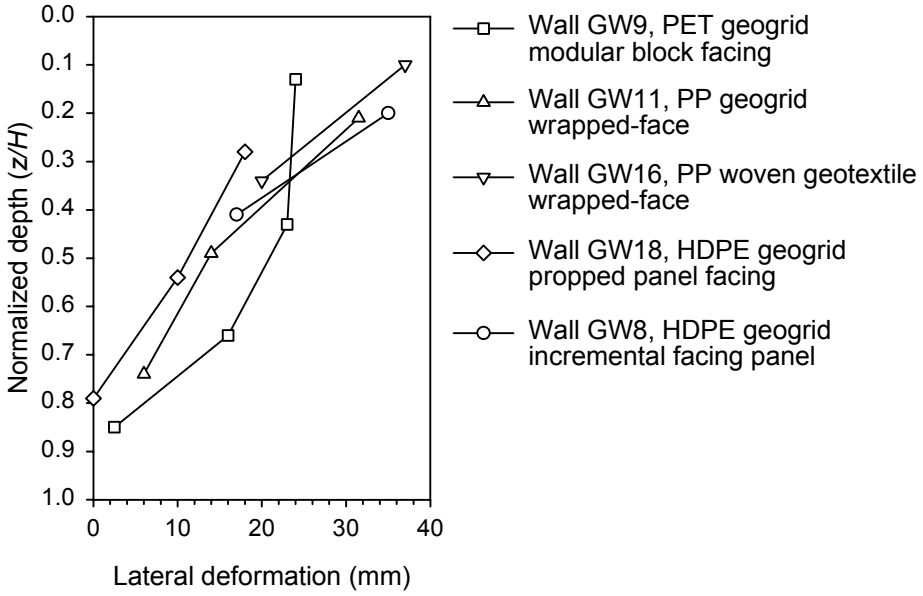

b) from end of wall construction to 75 years after wall construction (estimated)

Figure 6.13. Lateral post-construction long-term wall face deflection versus normalized depth of reinforcement z/H.

6.6.2 Comparison of Measured to In-Isolation Creep Behavior, and Implications Regarding the Actual Load Level in the Reinforcement

6.6.2.1 Comparison of Creep Strains

The creep strain and creep strain rate data presented in this chapter appear to provide at least an approximate verification of the load levels determined in Chapter 5.0 with isochronous creep stiffness data, taking into consideration the time required to construct the wall and to achieve a constant load in the reinforcement. In several cases (see data for walls GW5, GW11, GW16, the top layer for the HDPE section of GW20, the middle layer for the PP section of Wall GW20, and the lowest surcharge load level for walls GW14 and GW15), the creep strain rates determined from in-isolation data at the load levels summarized in Table 6.5 were approximately the same as or greater than corresponding values in the field (Table 6.6), indicating that these load levels are reasonably accurate or slightly conservative. However, in some cases, the initial creep rates after wall construction were significantly higher than the in-isolation rates, or the total strains were higher than the corresponding in-isolation values. For those cases in which the in-isolation creep strains and rates were less than field values, it appears, given the observed creep behavior, that the long-term load levels may have been greater than those estimated at the end of wall construction. The specific walls and the reasons for this increased load after end of wall construction appear to be as follows:

1. As discussed in Section 6.6.1.2, the wall backfill reached a failure state, causing the soil to become more plastic. Therefore, the stiffness of the soil decreased significantly, resulting in more load being shed to the reinforcement. If reinforcement failure occurred in the upper layer(s), the load originally carried by that reinforcement was shed to the adjacent lower layer, causing the load in the lower layer to increase.
2. For propped panel walls, the measured strain response to prop release is the result of load being transferred to the reinforcement from the props in addition to creep. It may take longer than 100 hours (the time assumed for end of construction in this study) for the load in the reinforcement to reach equilibrium with the soil in this type of wall. Based on Wall GW18 (Figure 6.8), it appears to take approximately 300 to 1,000 hours or more for the wall reinforcement loads to reach equilibrium after prop release, such that load increase comes to a stop and pure creep begins.

3. Figures 6.1 and 6.2 indicate that some additional time beyond the end of construction is required for the soil and reinforcement to reach equilibrium, given all of the time dependent processes involved and depending on how rapidly the load is applied. However, this source of increased load after end of wall construction is likely to be small.
4. Other sources of load may occur after the end of wall construction, such as snow load, water buildup in the backfill, or surface soil creep. Wall GW7 may be a case in point, given the significant jump in strain that occurred after the end of wall construction (Figure 6.6a). This behavior appeared similar to the strain jump that occurred for wall GW18 (a propped panel wall).

Vertical earth pressures measured at the base of the foundation zone in walls GW14 and GW15 remained constant or even decreased slightly after load application at all levels, an indicator that, overall, loads did not increase as a function of time. The same is true of full-scale field walls in which vertical earth pressures have been measured (see Table 6.3): no time dependent increases have been observed.

If soil creep toward the wall face is a mechanism that increases reinforcement loads with time, as has been postulated for Wall GW7, the reinforcement (at least PP and HDPE geosynthetics) would, in general, need to be less susceptible to creep than the soil. However, as discussed previously, the reinforcement typically has similar or greater ability to creep than granular backfill soils. Because of this, any creep that occurs in the soil after end of construction will be offset by the decrease in reinforcement stiffness that occurs during that time. Furthermore, if soil creep is contributing to a time dependent increase in reinforcement load, steel reinforcement loads should theoretically increase as a function of time, as the steel has much less ability to creep than does the soil. The writers have found that time dependent increases in steel reinforcement loads have generally not been observed for granular backfills.

Table 6.6. Comparison of in-isolation and measured creep strains and rates for full-scale walls.

Wall	Reinforcement Type	Depth below Wall Top (m)	Time Increment after End of Construction (hours)	Average Ratio of In-Isolation to Measured Creep Rate
GW5	HDPE geogrid	1.14 and 3.28	0 to 50,000 50,000 to 100,000	3.3 23
GW7	HDPE geogrid	1.2 and 4.2	0 to 10,000 10,000 to 100,000	0.4 1.5
GW11	PP Geogrid	0.6 0.6, in slump zone 1.35 2.1	0 to 300 300 to 500 0 to 300 300 to 500 0 to 300 300 to 500 All	1.2 3.7 0.7 2.5 2.0 7.2 1.9
GW14	PP Geogrid	0.5 m, 20 kPa surcharge 0.5 m, 80 kPa surcharge	All 0 to 100 100 to 200	0.8 0.6 0.15
GW15	PP Geogrid	1.25 m, 20 kPa surcharge 1.25 m, 70 kPa surcharge	All All	0.8 0.12
GW16	PP Woven Geotextile	3.1 6.5	0 to 3,000 3,000 to 7,000 All	1.3 3.2 1.1
GW18	HDPE geogrid	2.44	0 to 2,000 7,000 to 10,000	0.4 1.0
GW20	HDPE geogrid	1.1 2.7	0 to 500 500 to 1,500 0 to 500 500 to 1,500	0.4 1.4 0.15 1.0
GW20	PP Geogrid	1.6 3.2	All 0 to 500 500 to 1,500	0.25 0.6 1.0

It is this additional long-term load—possibly due to surficial soil creep in the case of Wall GW7, to time dependent load transfer from the props to the reinforcement in the case of Wall GW18, or to post-peak soil shear strength behavior or rupture of the upper layer of soil reinforcement in the case of walls GW14, GW15, and GW20—that may explain why the measured strain rates are greater than the in-isolation laboratory test strain rates in these wall cases and, thus, are the exceptions to the trends reported here. Because the strain at the end of wall construction was used to estimate the load, these other time dependent load increases were not considered in the calculation of loads summarized in Table 6.5. In spite of these long-term

load increases, it appears that the under-estimation of load in the case of walls GW7 and GW18 is typically 10 to 20 percent or less. In the case of walls GW14 and GW15, and possibly Wall GW20. the load increase is not really relevant, since it would generally be undesirable to design a wall that promoted soil failure, as the wall in that case would likely not meet serviceability requirements.

Note that for several of the walls, the long-term creep rate, though initially higher than predicted from the in-isolation creep data, eventually decreased to the point that the measured wall creep rates were lower than the in-isolation creep rates, forming a "knee" in the creep strain rate versus time curve. This was specifically observed in walls GW5, GW7, GW18, and the HDPE section of Wall GW20. This knee could be the result of one of the following scenarios:

1. The load level decreased in the long term because of load transfer between layers or gain of strength in the soil.
2. The ability of the soil to creep decreased with time (i.e., primary creep), forcing the geosynthetic to stress relax.
3. The initial high creep rate was a combination of creep strain and load increase, and once the load increase stopped, the creep strain rate dropped back to the true pure creep rate that more accurately reflected the final load level being applied to the reinforcement.

Scenarios 2 and 3 are more likely, or possibly a combination of 2 and 3. If scenario 2 was the cause, then the creep rate measured in the wall would have continued to decrease at a significantly more rapid rate with time than the in-isolation creep rates. If scenario 3 was the cause, the measured creep rate would have decreased at a more rapid rate than the in-isolation data at first, but then level out to decrease at approximately the same rate of decrease as the in-isolation data at longer times. Walls GW5 and GW7 appear to have followed the former trend (scenario 2), while GW20 appears to have followed the latter trend (scenario 3). It is uncertain whether Wall GW18 followed the former or latter trend (more creep data would be needed to fully evaluate the trend for this wall).

6.6.2.2 Stress Relaxation versus Creep

In Chapter 4.0, the plane strain in-soil creep tests conducted by Boyle (1995) were analyzed. The geosynthetic creep rate in these tests was controlled by the soil creep rate, as evidenced by the stress relaxation that occurred in the geosynthetic. The in-soil creep rates obtained by Boyle were an order of magnitude less than the in-isolation creep rates for the same geosynthetic at the same load level (see Figure 6.7). Yet the measured creep rates in the wall (GW16) were much closer to the in-isolation creep rate than the creep rate measured from the in-soil creep tests. The strain magnitudes measured in the wall were also very close to those measured for the in-isolation and the in-soil tests, indicating that the load level determined for the GW16 wall reinforcement is reasonably accurate (see Figure 6.7b and 6.7c). These observations indicate that little, if any, stress relaxation was occurring during the one-year observation period after the end of wall construction. The in-soil tests by Boyle appear, on the basis of these observations, to have under-estimated the geosynthetic and soil creep relative to what was observed in the wall, and over-estimated the amount of stress relaxation that likely occurred. Side wall friction in the test device may have contributed to this difference in creep rates. Because of the dense and angular geometry of the sand used in the tests conducted by Boyle, it would be expected that this sand would tend to be at the lower end of creep susceptibility relative to the full range of granular materials that could be used as wall backfill. Therefore, if a looser, weaker sand had been used in the tests conducted by Boyle, it is possible that less stress relaxation, if any, would have been observed. Therefore, at least in the short term after wall construction, significant stress relaxation must not be occurring in the reinforcement for Wall GW16. However, in the long term, stress relaxation would become more likely, once the soil creep rate had decreased to the point that the soil significantly restricted the ability of the geosynthetic to creep, as discussed previously.

The main point here is that at the end of construction, and for a time beyond the end of construction, the geosynthetic appears to be primarily exhibiting creep. Therefore, the correct stiffness for converting strain to load can be determined directly from the isochronous creep stiffness of the material. For geogrids and most woven geotextiles (which is the case for all of the case histories evaluated herein), the in-isolation creep data appear to be adequate for this

purpose. For geosynthetics with greater macro-structure influence on load-strain-time response, confined creep data are required.

6.6.3 Criteria for Good and Poor Wall Performance

The long-term deformation and strain data presented here can be used to establish criteria that indicate whether a wall will perform well throughout its design life. Since the observations from these case histories can be considered representative of the larger database reported in Chapter 2.0, the criteria presented below are considered by the writers to be generally true for a wide range of geosynthetic reinforced walls constructed with granular backfill soils up to a wall height of approximately 13 m.

A geosynthetic wall can be considered to exhibit good performance and adequate long-term stability if all of the following are true:

1. Total reinforcement strains are small (typically less than 3 percent).
2. Creep strains and strain rates are decreasing with time (i.e., only primary creep is observed).
3. The wall backfill soil does not show signs of failure (cracking, slumping, etc.).
4. Post-construction deformations, which are typically greatest at the wall top, are less than 25 to 30 mm within the first 10,000 hours for walls 13 m or shorter.

A geosynthetic wall can be considered to be performing poorly or be potentially unstable during the wall design life if any one of the following is true:

1. The total reinforcement strains are relatively large (typically 5 percent or more).
2. The creep strain rates are relatively constant or increasing with time.
3. The wall backfill shows signs of failure (cracking, slumping, etc.).
4. A reinforcement rupture occurs either at the connection or in the backfill (typically reinforcement layers near the top of the wall will fail first).
5. Post-construction wall face deformations are greater than 35 mm in the first 10,000 hours after the end of wall construction, and are increasing at a constant or increasing rate (for walls 13 m or shorter).

Implicit in these recommendations is the assumption that lifetime boundary loads and ground conditions for the structures do not change from those operating at the end of construction.

6.7 Summary and Conclusions

Long-term creep data from ten full-scale geosynthetic wall case histories (twelve wall sections) have been presented and analyzed. These case histories span a wide range of geometries, geosynthetics, and granular soil properties, and they include observations at both working stress conditions and near failure. With extrapolation of the data, including due consideration for potential chemical degradation (which was minimal in all cases) and installation damage, wall strain levels and trends were identified that are characteristic of walls that will be stable for typical design lifetimes of 75 to 100 years or more. The difference between good and poor wall performance appears to be linked to whether reinforcement strain levels are large enough to allow the soil shear surface in the backfill to develop to the point that the wall system can exhibit post-peak soil behavior. That is, if the reinforcement strains are low enough to prevent the soil from reaching failure, reinforcement creep will be minimal and the wall will remain stable. Specific criteria have been provided to identify the potential for the wall to exhibit good or poor long-term performance.

The creep strains measured in the full-scale walls were compared to the creep that would be expected on the basis of laboratory creep tests conducted in-isolation (unconfined), and in one case on the basis of laboratory in-soil creep tests. The creep measured in the walls should be comparable to the laboratory creep rates if the load levels determined from the measured strains in the wall, converted to load through a creep stiffness, have been determined correctly, if the laboratory creep curves are accurate, and if pure creep is occurring, rather than a combination of stress relaxation and creep. Though there were some notable exceptions, in the majority of cases, the laboratory in-isolation creep rates were the same as or greater than the measured geosynthetic reinforcement creep rates in full-scale walls, providing an approximate corroboration of the reinforcement load levels for these walls determined in Chapter 5.0. This also indicates that in-isolation laboratory creep data, in general, produce a conservative estimation of creep in walls.

Whether significant stress relaxation occurred in the reinforcement near the end of construction for each of the wall case histories could not be determined with certainty from the available case study data. It appears that the effect of any stress relaxation that is occurring at the end of wall construction is sufficiently small that that creep rates measured in the walls and during laboratory in-isolation tests are approximately equivalent, at least within the first 200 to

10,000 hours after the end of construction. However, at longer times, the creep rate measured in the wall reinforcement layers dropped off more quickly with time than did the laboratory in-isolation creep rates. This indicates that the ability of the soil to creep decreased more rapidly than the ability of the geosynthetic to creep, forcing the geosynthetic to exhibit a greater percentage of stress relaxation at longer times after construction, eventually resulting in the cessation of creep in the geosynthetic wall.

In some cases, reinforcement load increased after the end of wall construction, which may have been due to the following:

1. time dependent load transfer from the props to the reinforcement in the case of Wall GW18 during the first 1,000 hours
2. post peak soil shear strength behavior, resulting in a decrease in the soil stiffness and an increase in the load carried by the soil reinforcement as failure of the soil-geosynthetic system progresses, in the case of walls GW14 and GW15
3. an unknown source, but potentially soil creep near the wall face, in the case of Wall GW7.

In these cases, the measured creep strain rates were greater than the in-isolation laboratory creep strain rates estimated at the load levels provided in Table 6.5, at least initially. These load increases appear to be less than 10 to 20 percent of the load measured at the end of wall construction. Note that load increase due to post peak soil shear strength behavior should be avoided through proper design, as for all practical purposes, the wall has failed when this condition occurs.

Post-construction, long-term wall face deformation data show that geosynthetic wall face deformations, if the wall is properly designed, will generally be less than 25 to 30 mm during the first year of service and less than 35 mm during the design lifetime for walls shorter than 13 m. This long-term face deformation is generally greatest at the wall top, decreasing linearly to zero at the base of the wall, and it appears to be independent of wall height or facing type for the range of conditions available in the database. This long-term deformation can easily be taken into account through selection of a wall face pre-batter and by designing the facing system to be tolerant of this movement.

A substantial body of long-term evidence demonstrates that geosynthetic walls can be used reliably for permanent applications. Current procedures provided in design codes for

geosynthetic walls are conservative, and new design methodologies that can reduce the level of conservatism in geosynthetic wall designs could provide significant economic benefits without compromising long-term reliability.

7.0 A NEW WORKING STRESS METHOD FOR PREDICTING REINFORCEMENT LOADS IN GEOSYNTHETIC WALLS

7.1 Introduction

Accurate prediction of loads and their distribution in reinforcement layers is necessary to produce cost effective, internally stable reinforced soil wall designs. The predicted reinforcement loads affect the strength and spacing required for the reinforcement, as well as the reinforcement length required to resist pullout.

The three primary methods identified in the most recent design specifications in North America for estimating loads in geosynthetic reinforced soil walls include the Coherent Gravity Method (AASHTO 1996), the FHWA Structure Stiffness Method (Christopher et al. 1990), and the Simplified Method (AASHTO 2002, Elias et al. 2001) or variants (Simac et al. 1993, Bathurst et al. 1993a). Chapter 5.0 provides an assessment of the predictive accuracy of these methods for geosynthetic walls, and Allen et al. (2001) evaluated the predictive accuracy of these methods for steel reinforced structures. These approaches have worked reasonably well for typical steel reinforced soil walls (Allen et al. 2001), but they have worked poorly for predicting loads in geosynthetic reinforced structures (Bell et al. 1983, Rowe and Ho 1993; see also Chapter 5.0).

All of these methods are semi-empirical in nature, using limit equilibrium concepts to develop the design model, but incorporating working stress observations to adjust the models to fit what has been observed in full-scale structures. The development of these methods assumed that reinforcement loads can be equated directly to the soil state of stress and that limit equilibrium concepts are applicable. The developers of these design methods have not hesitated to adjust the load predictions to match the empirical data for steel reinforced soil walls because the reinforcement loads in steel reinforced structures have been measured to be equal to or greater than the loads calculated by integration of active or at-rest lateral earth pressures over the tributary area of the reinforcement.

However, for geosynthetic reinforced walls, the measured strains converted to loads with reinforcement stiffness values have shown that reinforcement loads are less than those predicted by integrating the active earth pressure over the tributary area. To maintain the assumption that the reinforcement loads should directly reflect the soil state of stress, the data that appeared to

support lower reinforcement load levels have in effect been ignored, and the design reinforcement load has been maintained at active earth pressure levels for these methods.

Uncertainties about the effects of time (creep or stress relaxation), temperature and soil confinement on the determination of the geosynthetic stiffness has hindered acceptance of the lower reinforcement loads inferred from strain measurements. Fannin and Hermann (1991), Bathurst (1990) and Bathurst and Benjamin (1990) suggested that the in-isolation isochronous creep stiffness be used to convert measured geosynthetic strains to load for geogrid reinforcement products rather than the stiffness from an index tensile test such as ASTM D4595. Chapter 4.0 investigates this issue in detail, and confirms that for geogrids and woven geotextiles, the in-isolation isochronous creep stiffness, with consideration of the time necessary to construct the wall and apply any surcharges, provides a reasonably accurate stiffness for converting measured reinforcement strains to load. It also confirms that the short-term, wide-width tensile stiffness is much too high for this purpose.

The proper estimation of the geosynthetic stiffness value needed to convert measured strain to load is a source of uncertainty in determining actual load levels in geosynthetic reinforcement layers. This uncertainty is compounded by the need to correctly interpret measured strains. However, through proper strain gauge calibration and redundancy in monitoring points and strain measurement type, reasonable estimates of in-soil reinforcement strain are possible. Chapters 3.0, 4.0, and 5.0 address and quantify these sources of uncertainty and their effect on the "measured" reinforcement loads in instrumented, full-scale structures. Notwithstanding these uncertainties, Chapter 5.0 shows that current design approaches greatly over-estimate geosynthetic reinforcement loads, even when less conservative (for design) plane strain soil strength parameters are used.

The past performance of geosynthetic reinforced soil walls has also provided strong evidence that current design methodologies for internal stability, in particular the prediction of reinforcement loads, are very conservative. Chapter 2.0 shows that a number of well-documented geosynthetic walls that have demonstrated good long-term performance for up to 25 years were designed with significantly lower global resistance to demand ratios than would be required by current practice. Furthermore, Chapter 6.0 demonstrates that the measured long-term creep rates in full-scale geosynthetic structures corroborate reinforcement load levels that are much lower than previously thought.

In this chapter a new working stress methodology, termed the K-Stiffness Method, is proposed. The method has been calibrated against measurements of strain and load in the monitored, full-scale walls reported in the previous chapters. The proposed design methodology, in addition to being relatively easy to apply, provides a seamless transition between geosynthetic and steel reinforced soil walls.

The scope of this chapter and the proposed design methodology are limited to walls with granular (non-cohesive) backfills.

7.2 Summary of Case Histories Evaluated

The key properties and parameters for each of the case histories referenced in this report are summarized in Table 7.1. Additional details for each of these case histories, including wall type, reinforcement geometry, reinforcement type, soil properties, and construction history, are provided in chapters 2.0, 3.0, and 5.0.

A total of 11 geosynthetic wall cases from Table 7.1 were analyzed (the same wall with and without a surcharge was considered to be one case). These wall cases included a variety of wall geometries and materials, surcharge conditions, and granular backfill. Wall reinforcement products included geotextiles and geogrids, different polymers—polypropylene (PP), high density polyethylene (HDPE) and polyester (PET), strip and continuous reinforcements, a range of tensile strengths from 12 to 200 kN/m (See Chapter 2.0), and a range of reinforcement stiffnesses from 90 to 7,400 kN/m. Reinforcement vertical spacing varied from 0.3 to 1.6 m. Wall facing batter angles varied from 0^o (vertical) to 27^o, although most of the walls had facing batter angles of 5^o or less. Wall heights varied from 3.0 m to 12.6 m, with surcharge heights of up to 5.3 m of soil. Facing types included geosynthetic wrapped-face, welded wire, pre-cast concrete panels, and modular concrete blocks (segmental retaining wall units). Estimated plane strain peak soil friction angles varied from 42^o to 57^o. See Chapter 2.0 for the specific procedures used to estimate plane strain friction angles from measured triaxial or direct shear values.

Although it is generally not possible to isolate the effect of a specific variable, many of the conditions that are likely to be encountered in the field were included within the database of case histories described above.

Table 7.1. Summary of geosynthetic wall case histories.

Wall Case History	Date Wall Built	Wall Height (m)	Facing Type	Surcharge Conditions	Face Batter Angle from Vertical ω (^{o})	Backfill Friction Angle ϕ_{tx} or ϕ_{ds} (^{o})	Backfill Friction Angle ϕ_{ps} (^{o})	Geosynthetic	$J_{2\%}$, for Layer (at end of wall construction, considering creep, kN/m)*	Global Wall Stiffness at End of Wall Construction (kN/m^2)
Tanque Verde Wall (GW5)	1984	4.9	Full-height propped concrete panel	None	0	53	53	Tensar SR-2 (HDPE geogrid)	340	720
Oslo, Norway Wall, Sections J and N (GW7)	1987	4.8	Welded wire	3 m steeply sloping soil surcharge	27	41	46	Tensar SR-55 (HDPE geogrid)	350 at surcharge completion	430 for Section J, 590 for Section N
Algonquin Wall (GW8)	1988	6.1	Incremental concrete panel	2.1 m sloping surcharge	0	40	43	Tensar SR-2 (HDPE geogrid)	500	660
Algonquin Wall (GW9)	1988	6.1	Modular masonry block	2.1 m sloping surcharge	2.9	40	43	Miragrid 5T (PET geogrid)	200	260
Algonquin Wall (GW10)	1988	6.1	Wrapped face	None	0	40	43	Quline 160 (PET nonwoven geotextile)	Approximately 180	210
Rainier Ave. Wall (GW16)	1989	12.6	Wrapped face	5.3 m sloping surcharge	3	45	54	GTF 200 (PP woven geotextile)	100	1000
								GTF 375(PP woven geotextile)	190	
								GTF 500(PP woven geotextile)	340	
								GTF 1225T (PET woven geotextile)	1000	
Fredericton, New Brunswick Wall (GW18)	1990	6.1	Full-height propped concrete panel	None	0	42	45	Tensar SR-2 (HDPE geogrid)	500	740
St Remy Wall (GW19)	1993	6.4	Incremental concrete panel	None	0	39	42	Parweb 2S Strap (PET)	7400	9200
Vicenza, Italy Wall (GW20)	1998	4.0	Welded wire	3.5 m steeply sloping soil surcharge	5	49	57	Tenax TT201 SAMP (HDPE geogrid)	300	220
Vicenza, Italy Wall (GW20)	1998	4.0	Welded wire	3.5 m steeply sloping soil surcharge	5	49	57	Tenax LBO220 SAMP (PP geogrid)	90 to 100	75

Notes: HDPE = high density polyethylene; PET = polyester; PP = polypropylene; * see Walters et al. (2002) for procedure to estimate $J_{2\%}$ stiffness values from laboratory in-isolation creep data; References: GW5 (Bright et al. 1994; Desert Engineering 1989; Berg et al. 1986); GW7 (Fannin and Hermann 1990, 1991; Fannin 1988, 1994, 2001); GW8 (Christopher 1993, 1998); GW9 (Bathurst et al. 1993b); GW10 (Christopher 1993, 1998); GW16 (Allen et al. 1992); GW18 (Knight and Valsangkar 1993); GW19 (Schlosser et al. 1993); GW20 (Carrubba et al. 1999; Montanelli 2000)

Note that the peak plane strain friction angle and the measured peak triaxial or direct shear friction angle are included in Table 7.1 for each case history. Plane strain conditions typically exist in reinforced soil walls. Peak plane strain friction angles for granular soils are larger than values from triaxial compression or direct shear testing and hence are less conservative for design. Furthermore, recent work indicates that the peak plane strain soil friction angle in calculations gives a better estimate of reinforcement loads, at least for geosynthetic walls (Rowe and Ho 1993, Zornberg et al. 1998a,b, Lee et al. 1999, Allen and Bathurst 2002a).

The isochronous reinforcement stiffness at 2 percent strain ($J_{2\%}$) was estimated from project-specific, in-isolation creep testing results where available. If these data were not available, in-isolation creep testing for the same product reported in the literature or supplied by the manufacturer were used. The stiffness values were corrected for temperature as required. A detailed description of the determination of isochronous stiffness values for each case study in Table 7.1 can be found in Chapter 5.0.

7.3 Analysis of Reinforcement Loads

In Chapter 5.0, current North American methods for predicting reinforcement loads were investigated. The conclusion was that the AASHTO Simplified Method produces results similar to those of the other methods, yet it has the advantage of being simpler to use and more broadly applicable. Therefore, the Simplified Method will be used herein as the baseline of comparison for reinforcement loads predicted with the new working stress method.

Figure 7.1 summarizes how well the Simplified Method predicts reinforcement loads in geosynthetic walls built in the field (see Chapter 5.0 for additional details). Triaxial or direct shear friction angles were used in the original development of the Simplified Method. However, this method was only adjusted to fit the empirical data for steel reinforced walls. To provide a common basis of comparison with the proposed K-Stiffness Method that uses plane strain soil friction angles, and to eliminate any conservatism in the prediction of loads resulting from conservative soil parameter selection, peak plane strain soil friction angles estimated from triaxial or direct shear strength tests and project-specific measured unit soil weights were used to estimate loads with the Simplified Method.

Loads predicted for geosynthetic walls using the Simplified Method were generally very conservative relative to the “measured” loads (Figure 7.1). The only exceptions were walls GW7

(Section N) and GW19. The reinforcement loads in Wall GW7 (Section N) and GW19 were under-predicted by the Simplified Method. However, these walls had unusual features that may have contributed to their different behavior with respect to reinforcement loads. For example, the face of Wall GW7 was heavily battered and could be classified as a reinforced slope. Wall GW19 was the only wall reinforced with PET straps rather than continuous sheets. The global wall stiffness for this wall was also very high, indicating that reinforcement stiffness may have significantly affected the amount of load carried by the reinforcement. In practice, the Simplified Method as described in AASHTO (2002) would not be used to design heavily battered or polymer strap walls. However, for the sake of direct comparison of the Simplified Method to the proposed K-Stiffness Method, the data for walls GW7 and GW19 have been included in Figure 7.1. Even when data for walls GW7 and GW19 are omitted from Figure 7.1, there is a large amount of scatter in the predicted loads, and the correlation of predicted to measured values with the current design methodology remains poor.

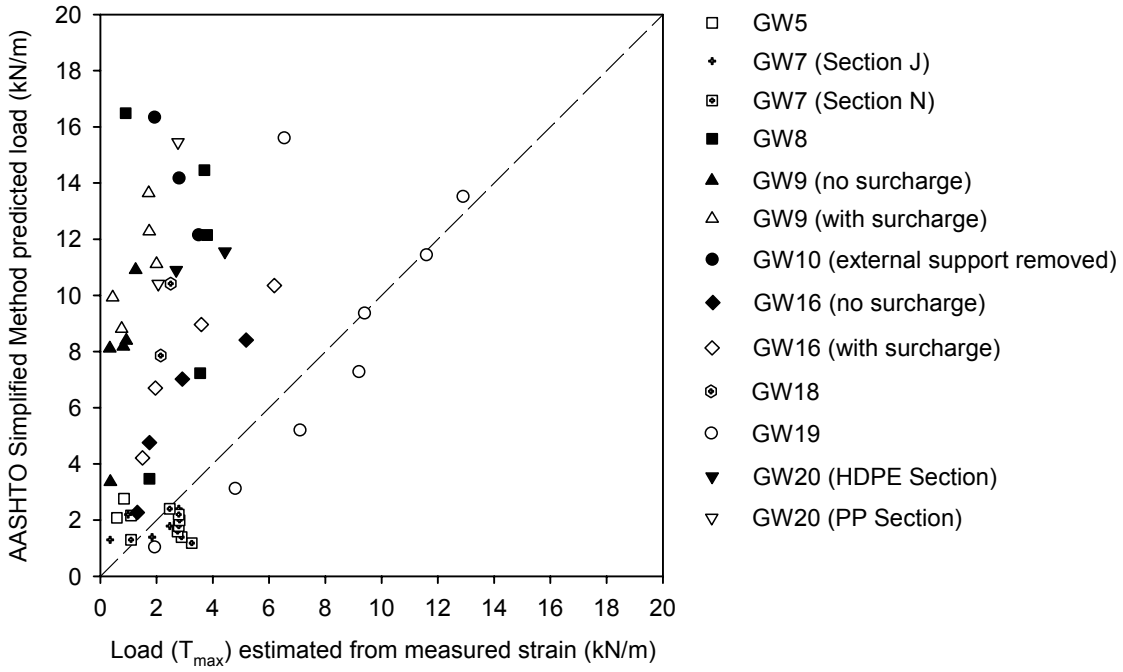

Figure 7.1. Predicted versus measured values of T_{max} in reinforcement layers for geosynthetic walls, using the AASHTO Simplified Method and peak plane strain soil friction angles.

7.4 Development of a New Approach to Predict Maximum Reinforcement Loads

7.4.1 General

The following key factors influence the magnitude of maximum reinforcement load, T_{max}:

- height of the wall and any surcharge loads
- global and local stiffness of the soil reinforcement
- resistance to lateral movement caused by the stiffness of the facing and restraint at the wall toe
- face batter
- shear strength and modulus of the soil
- unit weight of the soil
- vertical spacing of the reinforcement.

These factors are introduced analytically in the following general expression for the maximum load per running unit length of wall in reinforcement layer i:

$$T^{i}_{max} = S^{i}_{v}\ \sigma_h\ D_{tmax}\ \Phi \tag{7.1}$$

where S^{i}_{v} = tributary area (equivalent to the average vertical spacing of the reinforcement near each layer when analyses are carried out per unit length of wall); σ_h = lateral earth pressure acting over the tributary area; D_{tmax} = load distribution factor based on layer location that modifies the reinforcement load ; and Φ = influence factor that is the product of factors that account for the influence of local and global reinforcement stiffness, facing stiffness, and face batter.

The lateral earth pressure is calculated as the average value acting over the height of the wall, H, according to conventional earth pressure theory, hence:

$$\sigma_h = \frac{1}{2} K \gamma (H + S) \tag{7.2}$$

Here K = lateral earth pressure coefficient, γ = unit weight of the soil, H = height of the wall, and S = equivalent height of uniform surcharge pressure q (i.e., S = q/γ). The coefficient of lateral earth pressure, K, is calculated with the Jaky equation (Holtz and Kovacs 1981):

$$K = K_o = 1 - \sin \phi_{ps} \tag{7.3}$$

where ϕ_{ps} is the peak plane strain friction angle. The use of $K = K_o$ in this proposed method does not imply that at-rest conditions exist within the reinforced backfill. K_o is simply used as a familiar index parameter to characterize soil behavior. This point is discussed in more detail later in this chapter.

Substitution of equations 7.2 and 7.3 into Equation 7.1 leads to:

$$T_{max}^{i} = \frac{1}{2} K \gamma (H + S)\, S_v^i\, D_{tmax}\, \Phi \tag{7.4}$$

Equation 7.4 contains an expression for reinforcement loads that is similar to the conventional expression used in current limit equilibrium methods of analysis but represents the average load applied to the reinforcement layers rather than a load that increases linearly as a function of the vertical overburden stress. The empirical reinforcement load distribution parameter D_{tmax} is used to distribute the load as a function of depth, accounting for the reinforcement properties, load redistribution among layers, and foundation conditions. It is expressed here as a function of normalized depth below the top of the wall (z+S)/(H+S), including the effect of the soil surcharge, S, and varies over the range $0 \leq D_{tmax} \leq 1$. The modifier Φ is an empirically determined parameter or function that captures the effect the major wall components have on reinforcement load development. On the basis of an examination of a large number of case studies, these parameters are used to improve the correlation between predicted and measured reinforcement loads at working stress conditions based. For brevity, the influence factor Φ in Equation 7.4 is used to represent the product of four factors as follows:

$$\Phi = \Phi_g \times \Phi_{local} \times \Phi_{fs} \times \Phi_{fb} \tag{7.5}$$

Parameter Φ_g is a global stiffness factor that accounts for the influence of the stiffness and spacing of the reinforcement layers over the entire wall height. It has the following general form:

$$\Phi_g = \alpha \left(\frac{S_{global}}{p_a} \right)^{\beta} \tag{7.6}$$

Here, S_{global} is the global reinforcement stiffness and α and β are constant coefficients. The non-dimensionality of the expression is preserved by dividing the global reinforcement stiffness by p_a = 101 kPa (atmospheric pressure). The global reinforcement stiffness value for a wall is calculated as follows (Christopher et al. 1990):

$$S_{global} = \frac{J_{ave}}{(H/n)} = \frac{\sum_{i=1}^{n} J_i}{H} \tag{7.7}$$

Here, J_{ave} is the average tensile stiffness of all "n" reinforcement layers over the wall height, and J_i is the tensile stiffness of an individual reinforcement layer expressed in units of force per unit length of wall.

Parameter Φ_{local} is a local stiffness factor that accounts for relative stiffness of the reinforcement layer with respect to the average stiffness of all reinforcement layers. It is expressed as follows:

$$\Phi_{local} = \left(\frac{S_{local}}{S_{global}} \right)^{a} \tag{7.8}$$

The coefficient term "a" is taken as a = 0 for steel reinforcement and a =1 for geosynthetic reinforced soil walls. S_{local} is the local reinforcement stiffness for reinforcement layer i, calculated as:

$$S_{local} = \left(\frac{J}{S_v} \right)_i \tag{7.9}$$

It is used to quantify the local combined influence of the individual layer stiffness and spacing on reinforcement load.

Parameters Φ_{fs} (facing stiffness factor) and Φ_{fb} (facing batter factor) in Equation 7.5 are factors that account for the influence of the facing stiffness (Section 7.4.5) and facing batter (Section 7.4.6), respectively, and are constant values for a given wall.

Equations 7.1 and 7.5 show that the maximum load in a reinforcement layer is the product of seven terms that have some uncertainty associated with their value and/or require back-analyses to determine the magnitude of coefficient terms. In addition, some terms are highly non-linear. It is assumed *a priori* that parameters K, γ and factors D_{tmax} , Φ_g , Φ_{local} , Φ_{fs} and Φ_{fb} are, for practical purposes, uncorrelated. This assumption allows the influence of each factor on predicted reinforcement loads to be examined separately while keeping other parameters at baseline values. The baseline values for coefficient terms in expressions for Φ_g , Φ_{local} , Φ_{fs} and

Φ_{fb} are identified in the following sections. For example, the constant in Equation 7.8 is taken as a = 1, corresponding to the case of geosynthetic reinforced soil walls unless noted otherwise.

The accuracy of the K-stiffness method when different expressions for the influence factors and associated constant coefficient values identified above are used is evaluated in the following sections in two ways:

1. direct comparison of predicted and measured reinforcement load values for the walls summarized in Table 7.1 and,
2. comparison of the mean and coefficient of variation (COV) of the bias, defined as the ratio of the reinforcement loads estimated from strain measurements to the predicted reinforcement loads for all case studies (Table 7.2).

Values of the mean of the bias of reinforcement loads close to but slightly less than unity are desirable while a minimum value for the coefficient of variation (COV) is maintained.

7.4.2 Load Distribution Factor, D_{tmax}

Current design methodologies assume a triangular distribution of T_{max} with depth below the wall top for geosynthetic walls (Figure 7.2a), and a modified triangular distribution with depth for steel reinforced soil walls (Figure 7.2b), where K varies as a function of depth. Other types of reinforced soil structure design, such as anchored walls, have used trapezoidal distributions for T_{max} versus depth (Figure 7.2d). Two other distributions that have been proposed for geosynthetic reinforced soil walls are also illustrated (figures 7.2c, 7.2e).

Table 7.2. Summary of the ratio of predicted to measured reinforcement load for geosynthetic walls.

Parameter	Number of Data Points	Ratio of Measured/Predicted T_{max} or T_{mxmx} (Bias)												
		AASHTO Simplified Method			K-Stiffness Method (Equation 7.4)									
						Influence of Selected Values on Bias								
						Coefficient of Earth Pressure		Soil	Local Stiffness Factor Φ_{local} (Eq. 10)		Facing Stiffness Factor	Facing Batter Factor		S_v
		plane strain ϕ	triaxial/direct shear ϕ	w/o GW7 and GW19 (triaxial/direct shear ϕ)	Proposed Approach: $K = K_o$ (a=1 in Eq. 10, d=0.25 in Eq. 18)	$K = K_{ah}$	K = 0.3 for all soils	γ = 19.5 kN/m^3 for all walls	a = 0 (Φ_{local} =1)	a = 0.5	Φ_{fs} =1 for all walls	Φ_{fb} = 1 (d = 0 in Eq. 18)	Φ_{fb} < 1 (d = 1 in Eq. 18)	0.6 m for all walls
Mean T_{max}	56	0.65	0.45	0.20	0.99	1.16	0.9	0.96	1.10	1.02	0.79	0.90	1.62	1.15
COV T_{max} (%)	56	95	91	59	36	64	39	35	61	44	52	34	86	58
Mean T_{mxmx}	12	0.58	0.39	0.23	0.99	1.07	0.83	0.98	1.05	1.01	0.74	0.91	1.42	1.34
COV T_{mxmx} (%)	12	99	86	53	17	40	30	18	35	24	37	22	60	83

Note: T_{max} = maximum load in reinforcement layer; T_{mxmx} = maximum reinforcement load in the wall; COV = coefficient of variation = (standard deviation of bias values/mean of bias values) x 100%; K_{ah} using Coulomb analysis with full wall-soil friction ($\delta = \phi$) and wall batter ω.

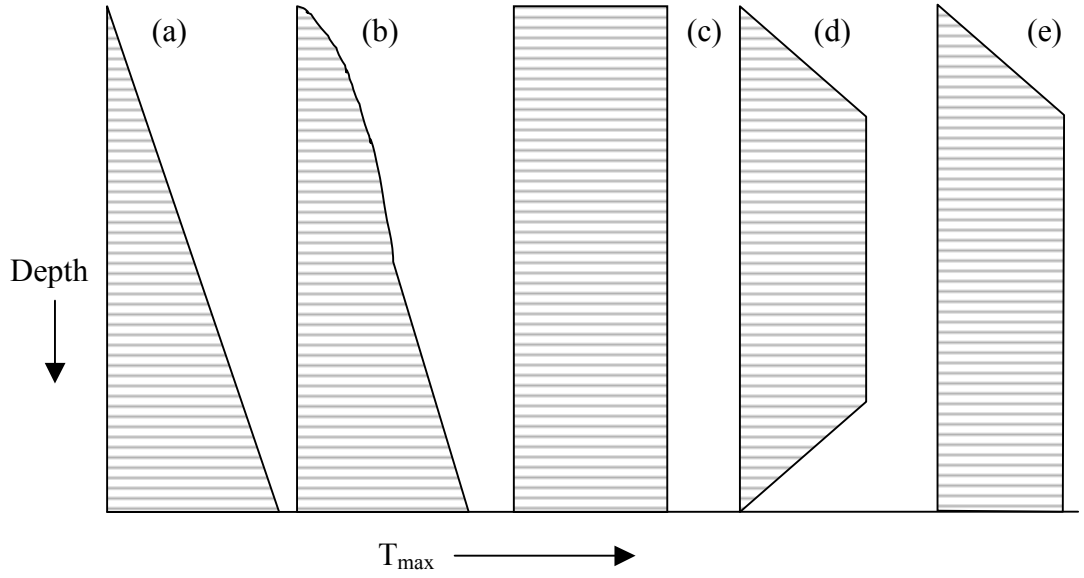

Figure 7.2. Typical distributions of T_{max} with depth below the wall top for reinforced soil walls: (a) triangular distribution used in Tieback Wedge Method (Bell et al. 1975), (b) modified triangular distribution used in Coherent Gravity (AASHTO 1996) and Simplified methods (AASHTO 2002), (c) rectangular distribution for geosynthetic walls (Broms 1978), (d) trapezoidal distribution for anchored walls (Sabatini et al. 1999), and (e) distribution for geogrid reinforced soil walls (Collin 1986).

Lee (2000) carried out a numerical investigation of geosynthetic reinforced soil wall performance. The numerical model was calibrated against some of the case studies referenced in this paper, and the numerical study extended to a wider range of wall geometry, reinforcement stiffness, and soil properties. He found that a trapezoidal distribution of maximum reinforcement layer loads, similar to that shown in Figure 7.2d, was applicable to all of the cases evaluated. Allen and Bathurst (2002a) adopted a similar approach and proposed the trapezoidal envelope in Figure 7.3a for the geosynthetic wall case studies in Table 7.1. In this figure the ratio of maximum reinforcement load in a layer, T_{max}, to the maximum reinforcement load for all layers, T_{mxmx}, is plotted against the depth of the layer plus surcharge height normalized by the total wall height plus average surcharge height (z+S)/(H+S). Over the normalized depth range 0.4 to 0.8, the reinforcement loads match the maximum reinforcement load value (T_{mxmx}) taken from all reinforcement layers, while the predicted reinforcement loads tend to zero at the wall top and to a small but finite value representing 20 percent of the maximum reinforcement load at the wall

base. The coordinates for this distribution are approximate only and have been selected to capture the majority of the data while simplifying the envelope geometry.

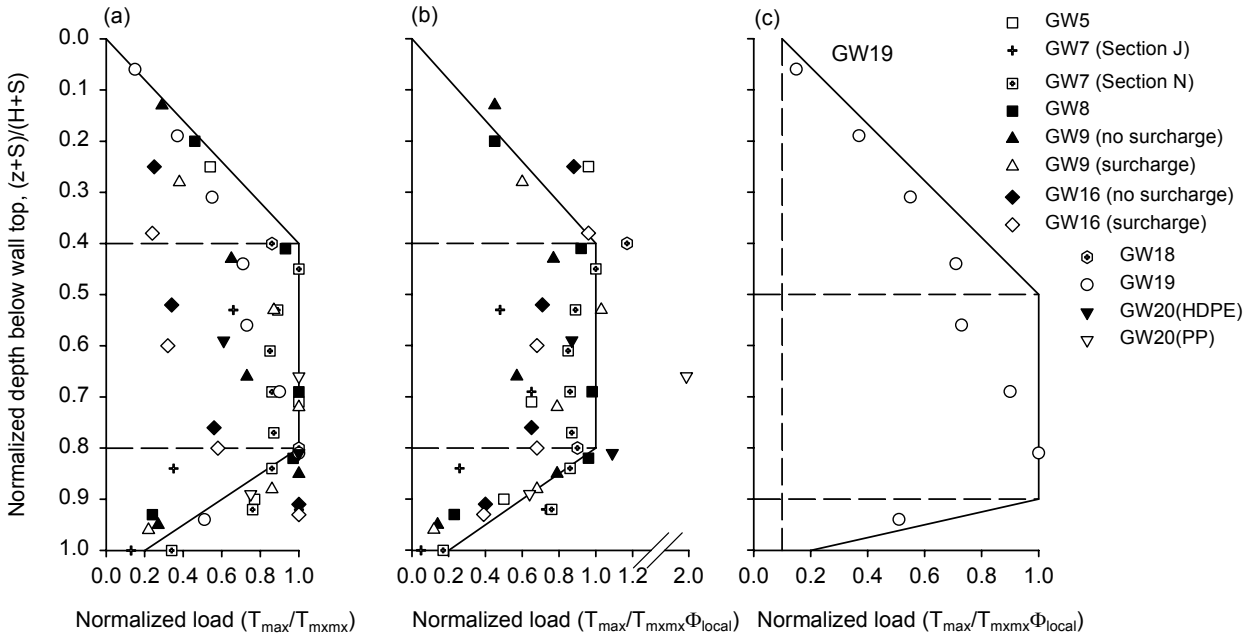

Figure 7.3. Distribution D_{tmax} as a function of normalized depth plus average surcharge height versus (a) T_{max} normalized by T_{mxmx}, (b) T_{max} normalized by $T_{mxmx} \times \Phi_{local}$, and (c) T_{max} normalized by $T_{mxmx} \times \Phi_{local}$ for Wall GW19 and showing the distribution proposed in Chapter 8.0 for polymer strap walls.

Numerical simulation results of geosynthetic reinforced soil walls reported by Lee (2000) and Rowe and Ho (1993) also predicted that load in the reinforcement layers near the bottom of the wall will be less than the reinforcement loads within the middle third of the wall height. Rowe and Ho provided a summary of physical data from reduced-scale and full-scale walls that confirms this observation for walls with a pinned toe. Bathurst and Hatami (1998) demonstrated the same effect through numerical parametric analyses of an idealized, full-height, panel reinforced soil wall with a toe that was free to rotate. However, they also showed that attenuation of reinforcement loads at the base of the wall did not occur if the toe was free to slide. Given the observations made here, it is clear that the stiffness of the foundation and the degree of fixity of the wall facing toe influence the distribution of reinforcement loads at the base of a geosynthetic reinforced soil wall. However, most walls have a fixed toe condition due to wall embedment, and

hence the attenuation of reinforcement load in proximity to the foundation predicted by a trapezoidal distribution is reasonable for walls constructed on stiff competent foundations.

It is shown later in this chapter that local reinforcement stiffness, Φ_{local} , can have a significant effect on the magnitude and distribution of T_{max}. Figure 7.3b illustrates this effect. With one notable exception (Wall GW20 (PP) with an unusually large vertical reinforcement spacing), the distribution of normalized T_{max} values was improved when the data were normalized by the local stiffness factor in addition to T_{mxmx}. This figure indicates that truncating the trapezoidal distribution at a normalized depth of 0.8 appears to be appropriate, and it also lends support to the argument that increasing foundation stiffness and wall toe fixity tend to reduce reinforcement loads near the bottom of the wall.

Overall, the global stiffness of the reinforcement does appear to influence the D_{tmax} distribution, causing the distribution to tend toward a more triangular shape as the global stiffness value increases (see Chapter 8.0). Because of the significantly greater stiffness of Wall GW19 (PET strap reinforcement), the D_{tmax} distribution is modified for polymer strap walls as illustrated in Figure 7.3c.

7.4.3 Global Reinforcement Stiffness Factor, Φ_g

As discussed in Chapter 5.0, the stiffness of the various internal components of the wall directly affects the distribution of loads to each of the wall components at working stress conditions. This is true of any composite material in which the components of the system have different stiffness values and in which the components are perfectly bonded together (e.g., steel or fiber reinforced concrete). To account for the effect of stiffness, the relationship between reinforcement load and reinforcement stiffness must be quantified. The influence of reinforcement stiffness on reinforcement loads can be assessed from both a global perspective (i.e., the influence of all reinforcement layers in the wall section - Equation 7.7) and a local perspective (i.e., individual reinforcement layer – Equation 7.9). Christopher (1993) showed that maximum reinforcement loads increase with increasing magnitude of global reinforcement stiffness value, S_{global}. In other words, as the average stiffness of the reinforcement layers increases, the reinforcement loads increase. Equation 7.1 is rewritten below to enable back-calculation of global stiffness factor values, Φ_g (measured), from measured maximum reinforcement load (T_{mxmx}) values:

$$\Phi_g \text{ (measured)} = \frac{T_{mxmx}}{S_v^i \, \sigma_h \, D_{tmax} \, \Phi_{local} \, \Phi_{fs} \, \Phi_{fb}} \tag{7.10}$$

Data for Φ_g (measured) versus (S_{global}/p_a) are plotted in Figure 7.4 for all of the geosynthetic wall case histories in Table 7.1 plus the steel wall case histories identified in Chapter 8.0.

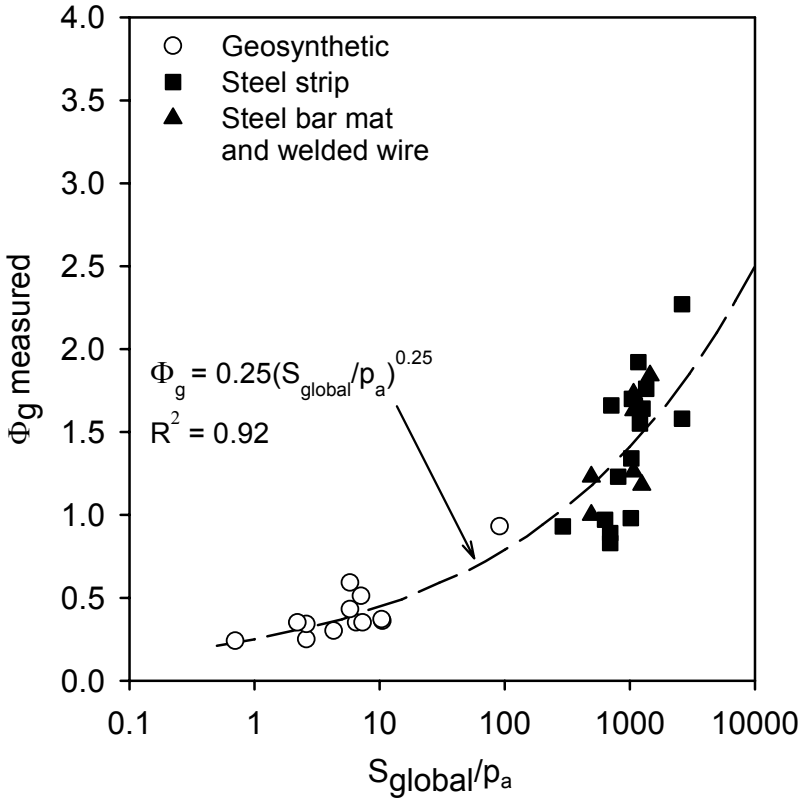

Figure 7.4. Measured Φ_g (Equation 7.10) versus normalized global reinforcement stiffness value (S_{global}/p_a).

Data for Φ_g (measured) versus (S_{global}/p_a) are plotted in Figure 7.4 for all of the geosynthetic wall case histories in Table 7.1. The data in Figure 7.3 indicate that the maximum reinforcement load in the wall corresponds to the case with $D_{tmax} = 1$. Hence, D_{tmax} was set equal to 1 in Equation 7.10. The constant for the local stiffness factor, Φ_{local}, in these calculations (Equation 7.8) was taken as a = 1 for geosynthetic reinforced soil walls and a = 0 for steel reinforced soil walls, as noted earlier in this chapter. Values for Φ_{fs} (facing stiffness factor) and Φ_{fb} (facing batter factor) are presented later in this report. Superimposed on Figure 7.4 is a regressed

approximation to the trend in data for the geosynthetic case histories in Table 7.1 and for steel reinforced wall case studies reported by Allen et al. (2001) and in Chapter 8.0 using a power function. The data for steel reinforced soil walls were used in the regression analysis to extend the predicted relationship to reinforcement stiffness values beyond those available for the geosynthetic reinforced soil walls in Table 7.1. Hence, the regression equation is applicable to both the geosynthetic and steel data sets. The power curve fit to the physical data is reasonably accurate, although there is some scatter for the steel data, which may be due to factors unique to steel reinforced soil walls (see Chapter 8.0). In the parametric analyses to follow, coefficient terms $\alpha = 0.25$ and $\beta = 0.25$ are used in the power function plotted in Figure 7.4.

7.4.4 Local Stiffness Factor, Φ_{local}

Local deviations from overall trends in reinforcement loads can be expected when the reinforcement stiffness and/or spacing of the reinforcement change from average values over the height of the wall (i.e., $S_{local}/S_{global} \neq 1$). This effect is captured by a local stiffness factor, Φ_{local}, expressed by Equation 7.8. Figure 7.5 shows the best predictions for maximum load in the geosynthetic reinforcement layers for three different case studies. The predictions were calculated with the working stress method and correspond to local stiffness factor calculations with a = 1. A value of a = 1 was selected as a preliminary estimate in the working stress method for structures built with geosynthetic reinforcement layers.

A parametric investigation, similar to what was done in Section 7.4.3 for the global reinforcement stiffness factor, was conducted for the local stiffness factor. Equation 7.1 is rewritten below to back-calculate values of local stiffness factor, Φ_{local} (measured), from measured maximum reinforcement load (T_{mxmx}) values:

$$\Phi_{local} \text{ (measured)} = \frac{T_{mxmx}}{S_v^i \, \sigma_h \, D_{tmax} \, \Phi_g \, \Phi_{fs} \, \Phi_{fb}} \tag{7.11}$$

The values of these variables are as described in Section 7.4.3. Values of Φ_{local} (measured) versus (S_{local}/S_{global}) are plotted in Figure 7.6 for the geosynthetic wall case histories in Table 7.1. As shown in the figure, an exponent "a" that is approximately equal to 1.0 provides the best fit for geosynthetic walls.

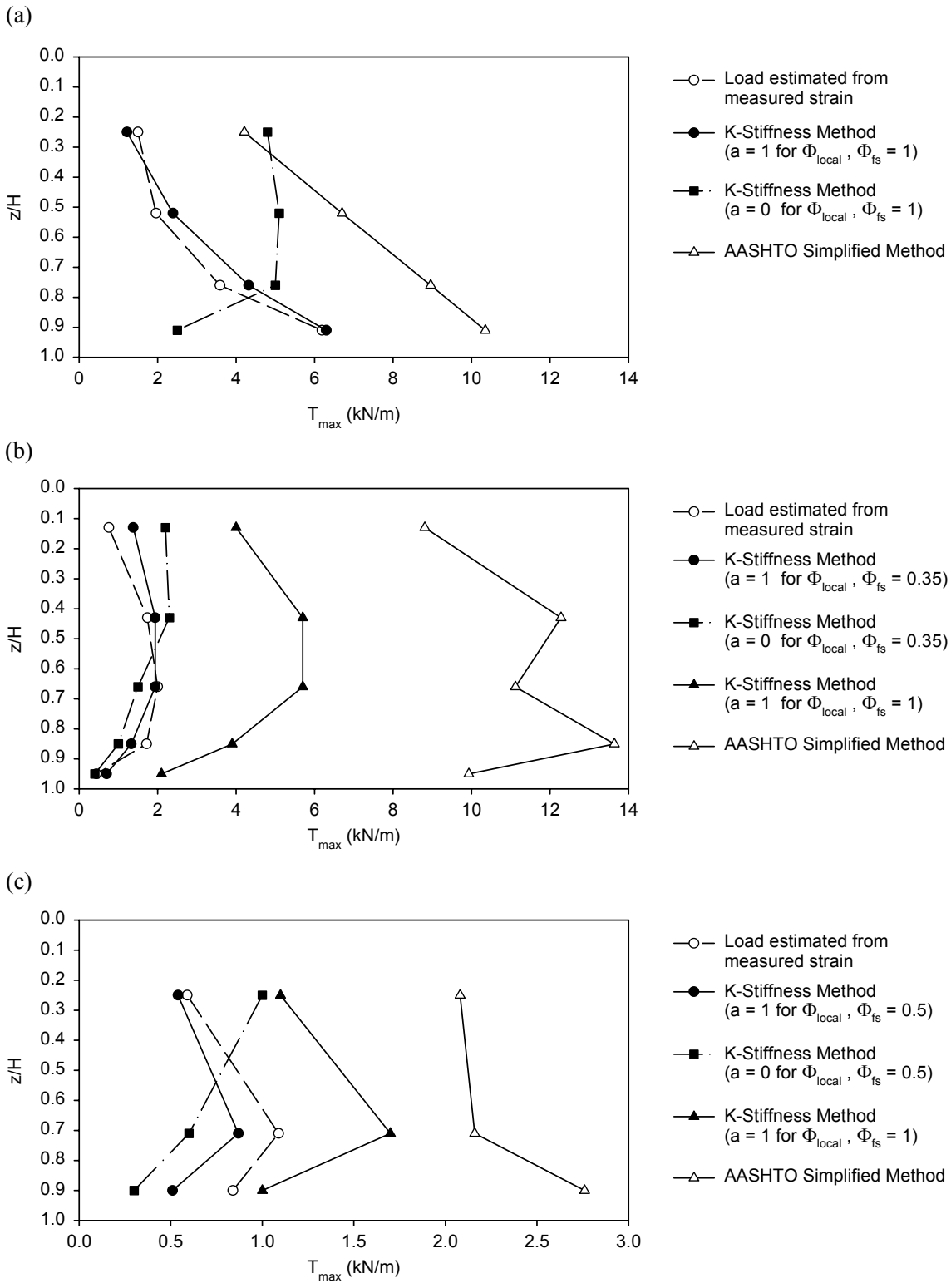

Figure 7.5. Influence of magnitude of facing stiffness factor and local stiffness factor on magnitude and distribution of reinforcement load T_{max} (a) GW16 (wrapped-face wall) with soil surcharge, (b) GW9 (modular block wall) with soil surcharge, and (c) GW5 (incremental precast panel wall).

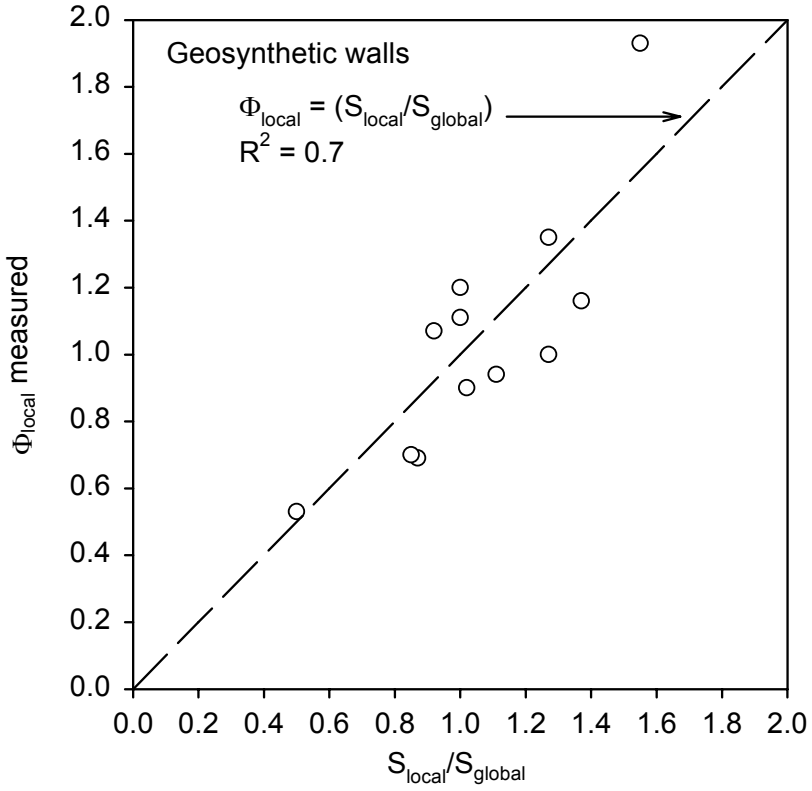

Figure 7.6. Measured Φ_{local} (Equation 7.11) versus S_{local}/S_{global}.

A similar parametric investigation discussed in Chapter 8.0 showed that for steel reinforced soil walls, a value of a = 0 for the constant coefficient in the local stiffness factor equation is more accurate. An explanation for the difference in values is that steel reinforcement is much stiffer than the soil, and hence local variations in reinforcement stiffness may have little effect on redistribution of reinforcement loads. Table 7.2 shows the influence of assigning values of a = 0 ($\Phi_{local} = 1$, i.e., ignoring any possible local reinforcement stiffness effect) and a = 0.5 in stiffness method calculations on predicted reinforcement loads in geosynthetic walls. (See also figures 7.5a, 7.5b, and 7.5c, in particular comparing curves for a = 0 and a = 1 with the same facing stiffness factor Φ_{fs}). The COV values in Table 7.2 are nearly twice as large if the local stiffness effect is not considered (a = 0), indicating a strong relationship between T_{max} and the corresponding local stiffness value.

7.4.5 Facing Stiffness Factor, Φ_{fs}

Previous research has indicated that the stiffness of the facing and the lateral restraint of the wall facing at the wall toe can have a significant influence on the loads carried by the soil reinforcement, at least for geosynthetic walls. Tatsuoka (1993) provided an overview of facing stiffness effects on soil wall reinforcement loads. He categorized facings on the basis of their stiffness characteristics as follows: Types A and B - very flexible wrapped geosynthetic, gabion, or steel skin facings; Type C - articulated (incremental) concrete panels; Type D - full-height, precast concrete panels; and Type E - concrete gravity structures. Facing rigidity was defined in terms of local, axial, shear, and bending rigidity, and overall mass as a gravity structure. Tatsuoka concluded that soil reinforcement strains tend to decrease as facing rigidity increases because of the increase in soil confinement caused by a very stiff facing, thereby reducing reinforcement loads. Loads carried axially by the facing to the toe may also contribute to the increased stability that occurs in stiffer facings. If the wall facing is massive enough to behave as a gravity structure, the loads in the reinforcement may be reduced to very low values.

Rowe and Ho (1993) concluded that both the facing and foundation stiffness affect the overall stiffness of the system as well as influence the portion of horizontal load carried by the reinforcement and the footing. In fact, for stiff facings (e.g., full-height concrete panel walls), force equilibrium cannot be satisfied without considering the toe forces transferred to the bottom of a facing with a restrained toe (Rowe and Ho 1993, Bathurst et al. 1989). Bathurst (1993) investigated the issue of facing stiffness/toe restraint for two full-scale laboratory test walls with full-height propped and incremental aluminium panel facings. For these two walls, he found that 25 percent of the total lateral load at collapse caused by surcharging was carried by the wall toe. In more recent work, using 3.6-m-high modular block-faced systems, Bathurst et al. (2000) found that the wall toe carried approximately 40 percent of the lateral load when the wall was loaded to near collapse. This more recent work appears to indicate, however, that as wall lateral deformations develop, the reinforcement layers carry a greater proportion of the total lateral load while the facing approaches a limiting capacity beyond which additional surcharge load increments are carried by the reinforcement layers. Information provided in Chapter 5.0 also indicates that propping a full-height panel wall during backfilling caused the wall facing to behave as a very stiff column, even after final equilibrium was reached following prop release. However, after surcharge loading of the wall, reinforcement loads approached values recorded

for an otherwise identical wall with a more flexible incremental panel facing that was not externally supported during wall construction.

The numerical parametric studies by Lee (2000) mentioned previously were also used to investigate the effect of facing stiffness on reinforcement loads. Two categories of facings were used: 1) flexible face (e.g., wrapped-face walls) and 2) stiff-faced walls (e.g., propped precast concrete panel walls and modular block-faced walls). Lee found that the reinforcement loads in the stiff-faced walls were approximately 50 percent of the reinforcement loads in the flexible-faced walls.

The empirical data available from the full-scale wall case histories with stiff facings and those with flexible facings were compared to determine the effect of facing stiffness on reinforcement loads. A parametric investigation similar to that described in the previous sections was carried out for the facing stiffness factor Φ_{fs}. Equation 7.1 was rewritten, below, to back-calculate values of the local stiffness factor, Φ_{fs} (measured), from maximum reinforcement load (T_{mxmx}) values estimated from strain measurements:

$$\Phi_{fs}\ (\text{measured}) = \frac{T_{mxmx}\ (\text{measured})}{S_v^i\ \sigma_h\ D_{t\,max}\ \Phi_g\ \Phi_{local}\ \Phi_{fb}} \tag{7.12}$$

The facing for each of the field walls can be treated as a conventional, uniformly loaded cantilevered beam. The stiffness of this "equivalent beam" is a function of its elastic modulus, E, and moment of inertia, I. The maximum elastic beam deflection can be expressed as follows (Popov 1978):

$$y_{max} = \frac{1.5wH^4}{ELb^3} \tag{7.13}$$

Here, b is the thickness of the facing column, L is the unit length of the facing (e.g., L = 1 m), H is the height of the facing column, and w is the distributed load. The elastic beam model is admittedly crude, given that the wall toe may not be completely fixed, the facing column often contains joints (i.e., the beam is not continuous), and the facing column is attached to the reinforcement at intervals. However, the objective here is not to predict wall deflections but rather to introduce a normalized facing column stiffness parameter, F_f, that captures the trend in

relative facing column stiffness for a range of facing types and geometry. F_f is defined here as follows:

$$F_f = \frac{1.5H^4}{ELb^3(h_{eff}/H)} p_a \quad (7.14)$$

The term h_{eff} is the equivalent height of an un-jointed facing column that is 100 percent efficient in transmitting moment through the height of the facing column. The ratio h_{eff}/H is used to estimate the efficiency of a jointed facing system to transmit moment throughout the facing column. The non-dimensionality of the expression is preserved by the use of p_a = 101 kPa.

For modular block wall systems, h_{eff} = H because these systems have greater width (typically ≥ 300 mm) than other concrete facing systems. In addition, the blocks are in compression, partially because of self weight and partially because downdrag forces on the back of the facing, and can transmit moment through the height of the column (Bathurst et al. 2000, 2001). Incremental concrete panel systems are generally thinner (approximately 100 to 140 mm) and tend to behave as beams that are pinned at the panel joints. Therefore, h_{eff} is assumed to be equal to the panel height for this type of facing. The influence of facing type on stiffness of flexible wall facings is more challenging. The approach taken here is to consider the column of soil confined by the flexible facing system to be the facing column. For welded wire walls, the length of the horizontal leg of the welded wire facing panel is taken as the width of the facing, b. For wrapped-face geosynthetic walls, b is taken as the approximate width of the facing wrap. The elastic modulus of the column in both cases is taken as 35,000 kPa, which corresponds to the soil modulus value used by Lee (2000) in numerical modelling work that included some of the case studies in this report.

The value of F_f for the walls in this study varies over three orders of magnitude and thus allows the structures to be differentiated on the basis of relative facing stiffness. Values of Φ_{fs} (measured) versus F_f are plotted in Figure 7.7 for the geosynthetic wall case histories in Table 7.1. This figure shows that the measured data can be correlated to the facing stiffness parameter (Equation 7.14) by using a power function expressed here as:

$$\Phi_{fs} = \eta (F_f)^{\kappa} \quad (7.15)$$

From regression analysis, η and κ are 0.5 and 0.14, respectively. This equation results in Φ_{fs} being equal to approximately 1.0 for flexible faced walls, and to as low as 0.35 for the relatively stiff modular block systems. Incremental concrete panel-faced systems fall between these two values.

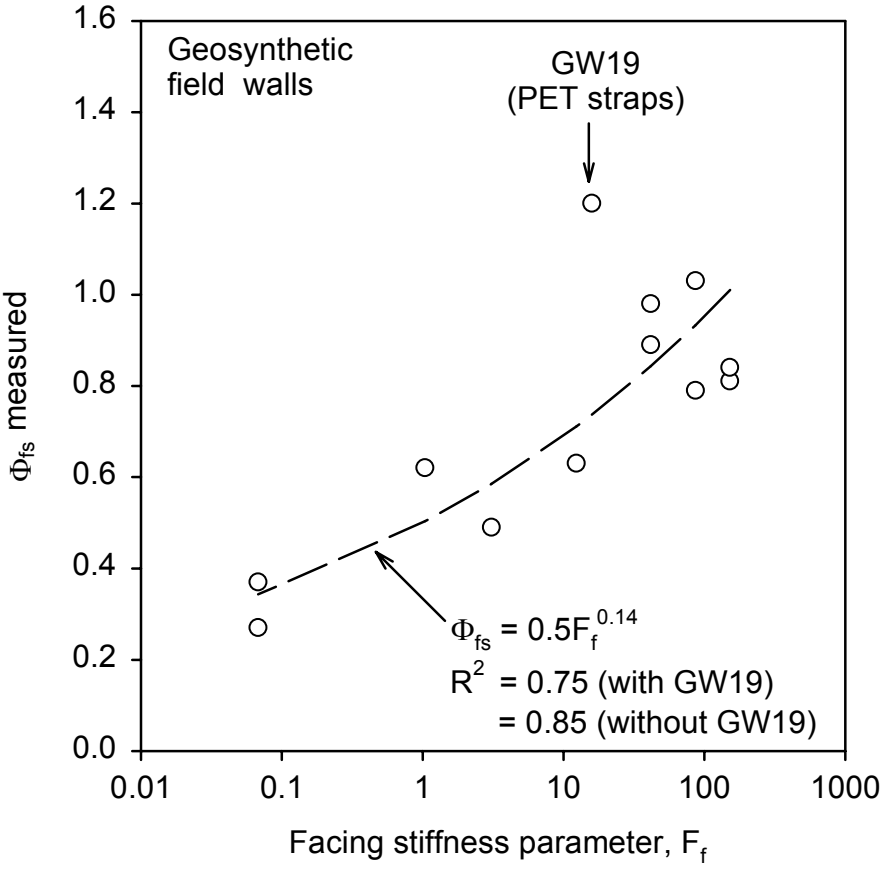

Figure 7.7. Measured Φ_{fs} (Equation 7.12) versus facing stiffness parameter F_f for geosynthetic reinforced soil walls.

Note that the regression analysis in Figure 7.7 to calculate the constant coefficient values η and κ does not include the data point for Wall GW19, which fell well above the rest of the data. Recall that Wall GW19 was constructed with a very stiff reinforcement and had the highest global stiffness value of all the walls in the database (i.e., one to two orders of magnitude higher). An explanation for this result is that the influence of the facing stiffness on reinforcement loads is low for very high global stiffness values. In other words, regardless of the facing type, for very high reinforcement global stiffness values, the reinforcement carries most of

the load acting at the back of the facing, and the stiffness of the facing type plays a lesser role to resist earth pressures.

Figures 7.5b and 7.5c demonstrate the improvement in predicted maximum reinforcement loads for modular block and incremental concrete panel walls by using $\Phi_{fs} = 0.35$ to 0.5, respectively, rather than a value of $\Phi_{fs} = 1.0$ to represent flexible-faced structures. Table 7.2 also shows the result of assuming $\Phi_{fs} = 1.0$ for all case studies, in effect treating all wall facings as flexible. Doing so causes COV values for the ratio of measured to predicted loads to increase substantially, demonstrating the importance of considering the facing stiffness when T_{max} is estimated for typical geosynthetic walls.

For preliminary design purposes, Equation 7.15 results in the following facing stiffness factor values for typical geosynthetic walls:

1. $\Phi_{fs} = 0.35$ for modular block and propped concrete panel-faced walls (stiff facings)
2. $\Phi_{fs} = 0.5$ for incremental precast concrete facings
3. $\Phi_{fs} = 1.0$ for all other types of wall facings (flexible facings - e.g., wrapped-face, welded wire or gabion faced).

More data are required to quantify the relationship between facing stiffness and reinforcement global stiffness and their combined influence on the magnitude of reinforcement loads in geosynthetic reinforced walls that are constructed with very stiff reinforcement products and for walls with greater facing flexibility than those available at the time of this investigation.

7.4.6 Facing Batter Factor, Φ_{fb}

In current practice, wall face batter (i.e., inclination from the vertical) is taken into account explicitly with Coulomb earth pressure theory. While calculations with the new working stress method described up to this point in this chapter improved reinforcement load predictions, significant discrepancies remained for the battered walls in Case Study GW 7 (see Figure 7.9 later in this section). Limit equilibrium methodologies attempt to capture this effect through the Coulomb earth pressure coefficient. However, as demonstrated in Chapter 5.0 and as will be shown later, the Coulomb earth pressure coefficient tends to reduce reinforcement loads

excessively for heavily battered walls. The influence of reduced confining pressure near the wall face cannot be captured explicitly by limit equilibrium methods.

The influence of wall facing batter on maximum reinforcement loads is adjusted in the proposed working stress method by using an empirical facing batter factor expressed as:

$$\Phi_{fb} = \left(\frac{K_{abh}}{K_{avh}} \right)^{d} \tag{7.16}$$

where K_{abh} is the horizontal component of the active earth pressure coefficient accounting for wall face batter, and K_{avh} is the horizontal component of active earth pressure coefficient, assuming the wall is vertical and d is a constant coefficient. The form of the equation shows that as the wall face batter angle $\omega \rightarrow 0$ (i.e., the wall facing batter approaches the vertical), the facing batter factor $\Phi_{fb} \rightarrow 1$. With the exception of case study GW7, the structures in Table 7.1 correspond to values of Φ_{fb} that are greater than 0.85. Different values of the constant coefficient "d" in Equation 7.16 were examined to improve the fit between measured and predicted values of reinforcement loads for the case studies with wall batter, especially case study GW7 (facing batter angle $\omega = 27$ degrees from vertical).

A parametric investigation, similar to what was done in Section 7.4.3 for the global reinforcement stiffness factor, was attempted for the facing batter factor. Equation 7.1 is rewritten below to back-calculate values of facing batter factor, Φ_{fb} (measured), from measured maximum reinforcement load (T_{mxmx}) values:

$$\Phi_{fb} \text{ (measured)} = \frac{T_{mxmx} \text{ (measured)}}{S_v^i \, \sigma_h \, D_{tmax} \, \Phi_g \, \Phi_{local} \, \Phi_{fs}} \tag{7.17}$$

The values of these variables are as described in Section 7.4.3. Values of Φ_{fb} (measured) versus (K_{abh}/K_{avh}) are plotted in Figure 7.8 for the geosynthetic wall case histories in Table 7.1. The regression analysis for the data in the figure yielded an exponent "d' of approximately 0.25. Note that the data are limited at lower ratios of (K_{abh}/K_{avh}), and the R^2 value is quite low. Because the reliability of this regression as marginal, additional analyses were conducted to assess the best value of "d" to use until more data on face batter effects can be gathered.

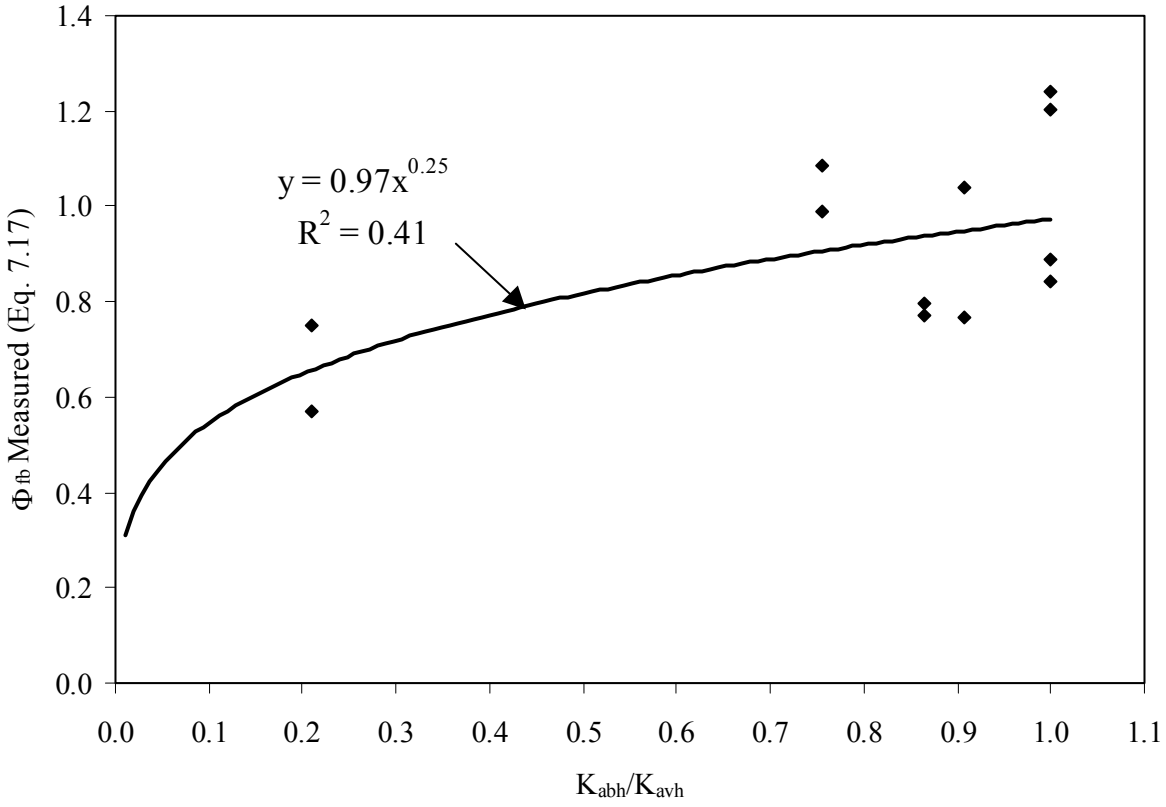

Figure 7.8. Measured Φ_{fb} (Equation 7.17) versus K_{abh}/K_{avh}.

Figure 7.9 shows plots of predicted reinforcement loads using equations 7.1 and 7.16 with d = 0 (curve 3), 1 (curve 4) and 0.25 (curve 2). Predictions calculated with the Simplified Method (AASHTO 2002) are also provided for comparison. For Sections J and N of case GW7 in Figure 7.9, the loads predicted with Equation 7.1 and Equation 7.16 with d = 0.25 (curve 2) are reasonably close to the measured values (curve 1). However, fully accounting for the face batter in the Coulomb equation (i.e., d = 1) clearly results in the under-prediction of the loads using the K-Stiffness Method and tends to result in an under-prediction of loads using the AASHTO Simplified Method, especially for Wall Section N. Conversely, this figure shows that ignoring the effect of facing batter on the reinforcement loads (i.e., d = 0), consistently results in a conservative prediction of reinforcement load.

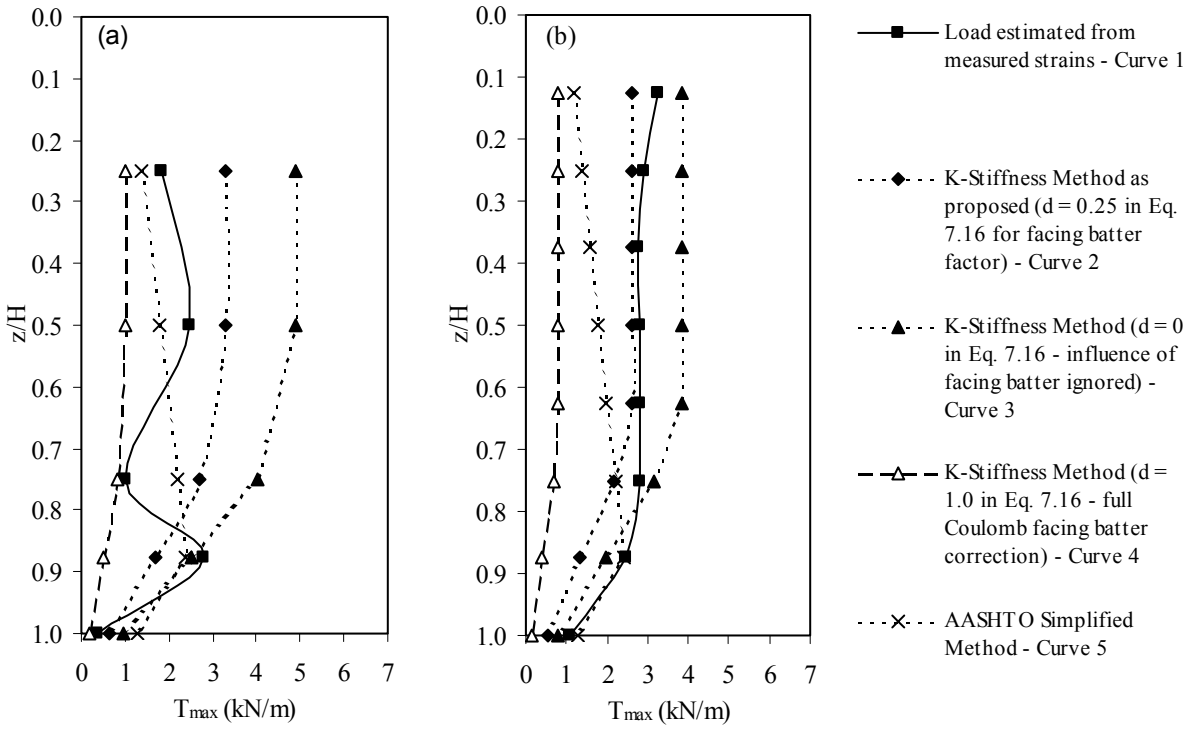

Figure 7.9. T_{max} distribution versus normalized depth for GW7 (a) Section J, and (b) Section N, showing effect of secondary reinforcement and facing batter on T_{max} prediction.

Table 7.2 provides a comparison of the spread (represented by the coefficient of variation - COV) in the ratios of measured to predicted reinforcement loads for the proposed method by ignoring the facing batter effect (d = 0), using d = 0.25, or assigning a constant coefficient of d = 1 (which corresponds to the full effect of facing batter in the Coulomb equation) in Equation 7.16 for all cases. Note that if the full facing batter effect is allowed (i.e., d = 1), the COV value for T_{max} is more than twice the value obtained by using d = 0.25.

On the basis of this "trial and error" selection of the exponent "d", a value of d = 0.25 gives the best fit with the available T_{max} data and is recommended as the default value in the proposed K-Stiffness Method. The scatter in the data indicates that improvement in the formulation of the batter factor proposed herein may be needed, though the writers believe that the proposed facing batter factor is an improvement over the Coulomb earth pressure coefficient to account for facing batter effects, especially in the context of the K-Stiffness approach.

7.4.7 Influence of Soil Strength on Reinforcement Loads

For working stress conditions in MSE walls, the soil property that most likely affects the distribution of load to the reinforcement layers in the wall is the soil modulus. This is due to the relatively low strain levels and the fact that limit equilibrium conditions have not been reached. However, the soil modulus is difficult to determine and is dependent on strain and stress levels. The peak soil friction angle is routinely available, familiar to designers, and is relatively easy to measure or estimate. In general, as peak friction angle for a granular soil increases, the soil modulus also increases (Duncan et al. 1980). Hence, peak friction angle can be interpreted as an indicator of relative soil modulus value between soil types.

In the development of the proposed stiffness method, values of $K = K_o$ (Equation 7.3) and $K = K_{ah}$ were examined to investigate the relative accuracy of predicted values of T_{max} and T_{mxmx}. K_o was used because it is simple to calculate, and its value is independent of wall face batter. K_{ah} (the horizontal component of active earth pressure) was determined by using the Coulomb method, assuming full interface friction for all walls (i.e., $\delta = \phi$) and continuous or nearly continuous reinforcement layers. For these structures the reinforcement-facing connections restricts downward movement of the backfill soil against the face, effectively resulting in an interface friction angle at the back of the wall face equal to the backfill soil friction angle. In wall GW19, the reinforcement comprised discrete straps, and hence full mobilization of soil shear strength behind the wall facing panels was not expected. For this wall, an interface friction angle of two-thirds the soil backfill friction angle was used to calculate the Coulomb K_{ah} value, which is typical practice for concrete-soil interface friction angles. The data in Table 7.2 show that there was less spread in the ratios of measured to predicted reinforcement loads when $K = K_o$ rather than K_{ah} was used. Some of the spread caused by use of K_{ah} was likely due to an inaccurate accounting of the wall face batter effect on the calculation of T_{max}. Interestingly, setting K equal to a constant value of 0.3 for all soil friction angles yielded only a modest increase in the COV value for the bias in all T_{max} values in comparison to the COV value resulting form use of $K = K_o$ calculated from the measured peak friction angle. The improvement in prediction accuracy of the proposed method using Equation 7.3 was more pronounced when the COV values were compared for the bias in T_{mxmx} values.

A parametric investigation, similar to that reported in Section 7.4.3 for the global reinforcement stiffness factor, was conducted to back-calculate K in the K-Stiffness Method from measured maximum reinforcement load (T_{mxmx}) values normalized as shown below:

$$K \text{ (measured)} = \frac{T_{mxmx}}{S_v^i \left(0.5\gamma(H+S)\right) D_{tmax} \Phi_g \Phi_{local} \Phi_{fb} \Phi_{fs}} \tag{7.18}$$

The values of factors in the denominator are calculated by using baseline values described earlier in the report. The back-calculated values of K determined from the measured values of T_{mxmx} versus K from Equation 7.3 are plotted in Figure 7.10 for the geosynthetic wall case histories in Table 7.1. This figure indicates that the load in the reinforcement is influenced by the soil response to load, if K_o is used as the soil index parameter. However, there is scatter in the data, which is consistent with the fact that the use of $K = K_o$ can only approximate the real parameter of interest, the soil modulus. In addition, this scatter may indicate that other factors related to soil properties and construction may be in play (e.g., compaction effort). Until these other factors are identified, the use of $K = K_o$ is considered to be a reasonable approach to approximate the role of soil strength and modulus in the development of reinforcement load.

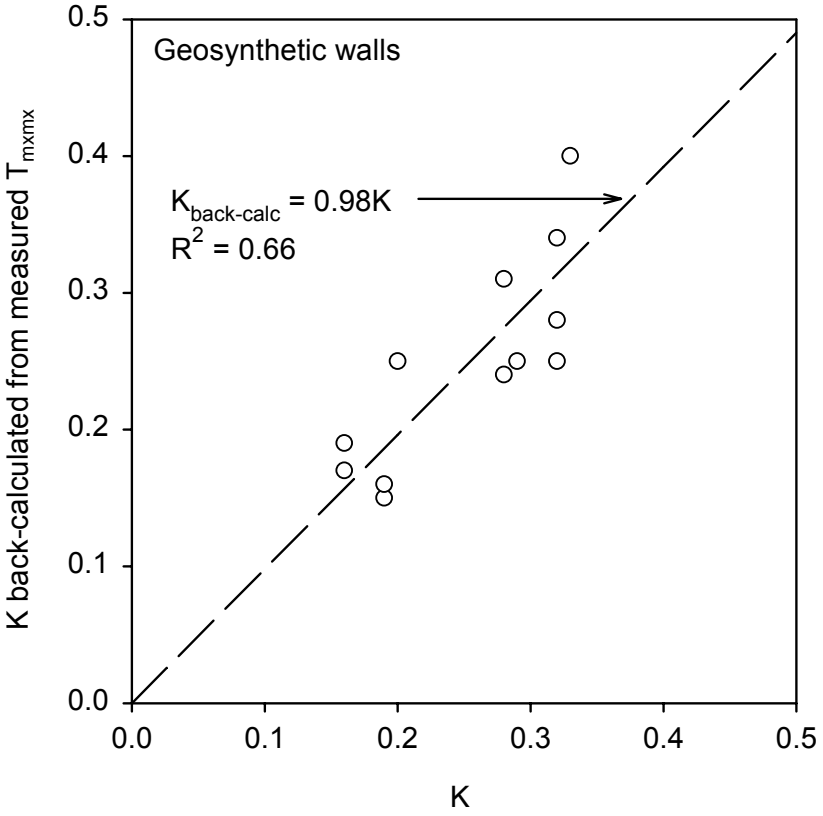

Figure 7.10. Back-calculated K (Equation 7.18) versus K calculated from Equation 7.3.

7.4.8 Effect of Soil Unit Weight on Soil Reinforcement Loads

The soil unit weight recorded for each case study was within 16 percent of the mean value for all of the walls (γ_{mean} = 19.5 kN/m^3) and ranged from 16.4 to 21.1 kN/m^3 (see Chapter 2.0). This variation was considered to be small in comparison to the uncertainty associated with other parameter values in this investigation, including estimated reinforcement loads. However, the fundamental expression for reinforcement loads (Equation 7.4) with the Stiffness Method shows that loads (and hence strains) should vary linearly with soil unit weight. To investigate the influence of soil unit weight on predicted reinforcement loads, calculations for T_{max} and T_{mxmx} were carried out with a constant value of γ = 19.5 kN/m^3. Table 7.2 shows that the difference in the accuracy of predicted reinforcement loads using a default constant unit weight of 19.5 kN/m^3 in the calculations rather than project-specific values was only minor. This minor difference is consistent with the small variation in the magnitude of measured soil unit weight values. A practical implication of this result is that the selection of soil unit weight is not a critical factor for design accuracy with the K-Stiffness Method.

7.4.9 Effect of Reinforcement Layer Spacing on Soil Reinforcement Loads

The vertical distance between reinforcement layers in the case studies for this investigation varied from 0.3 to 1.6 m. Note that this is not necessarily the same as the vertical zone in the wall that contributes to load in a given reinforcement layer (i.e., the tributary area). S_v is representative of the tributary area when loads are calculated on the basis of load per unit of wall length and the spacing between layers is uniform. When the spacing is not uniform, this parameter is representative of the average distance between the layers that are adjacent to the layer in question. At the top of a wall, S_v includes the full distance between the top layer and the top of the wall, plus the distance to the mid-point between the top layer and the next layer below.

The magnitude of reinforcement loads (and strains) can be expected to vary linearly with S_v, as assumed in the Stiffness Method and conventional design methods. Calculations were redone with a default value of S_v = 0.6 m, which is a typical reinforcement spacing value for all of the walls. Table 7.2 shows that S_v has a significant effect on the accuracy of the predicted reinforcement loads for all of the case histories.

A parametric investigation, similar to what was done in Section 7.4.3 for the global reinforcement stiffness factor, was carried out to evaluate the accuracy of the assumption that

maximum reinforcement loads in a wall vary linearly with S_v. Equation 7.1 is rewritten below to back-calculate values of S_v from measured maximum reinforcement load (T_{mxmx}) values:

$$S_v \text{ (back-calculated)} = \frac{T_{mxmx}}{\sigma_h D_{tmax} \Phi_g \Phi_{local} \Phi_{fs} \Phi_{fb}} \tag{7.19}$$

The values of the variables are as described in Section 7.4.3. Values of S_v, back-calculated from the measured values of T_{mxmx}, versus S_v, as determined directly from the spacing of the reinforcement in the wall, are plotted in Figure 7.11 for the geosynthetic wall case histories in Table 7.1. The regressed data demonstrate a linear relationship between reinforcement load and S_v, as predicted by both the proposed method and current design methods. This correlation appears to hold reasonably well even to large values of S_v. From a practical point of view, the multiplier on S_v that results from the linear regression in Figure 7.11 can be ignored without influencing design accuracy.

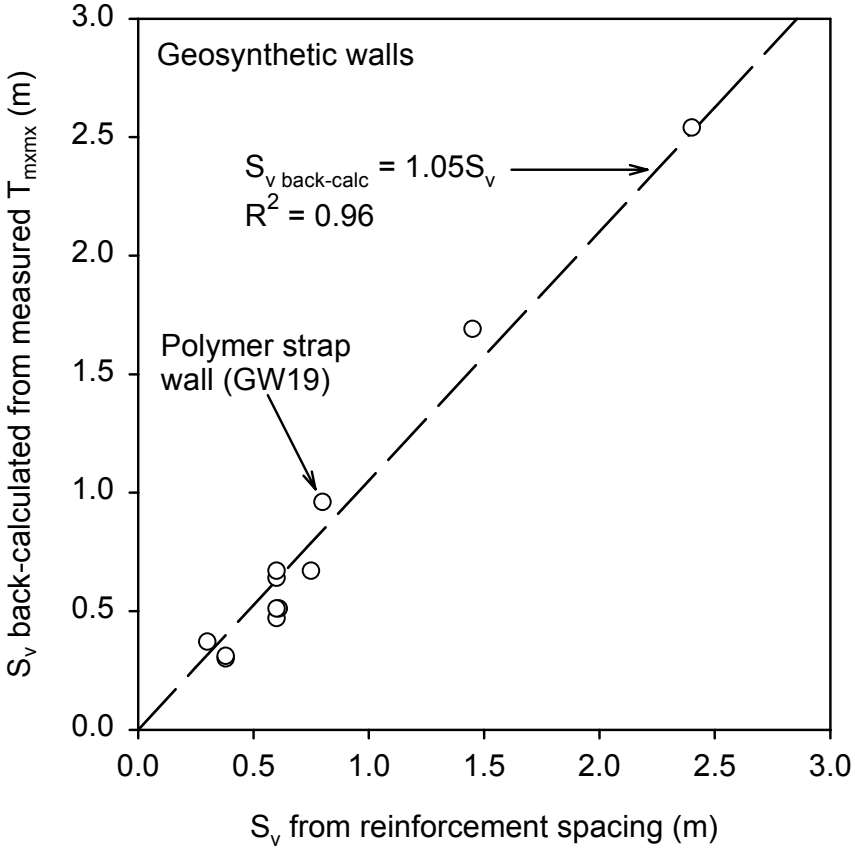

Figure 7.11. Back-calculated S_v from measured T_{mxmx} (Equation 7.19) versus S_v determined directly from the spacing of reinforcement in the wall.

7.5 Overall Performance of the K-Stiffness Method

The accuracy of the proposed K-Stiffness Method (Equation 7.4) for geosynthetic walls is illustrated in Figure 7.12 for all of the full-scale field wall case histories in Table 7.1. The improvement in predicted loads versus loads estimated from measured strains with the proposed Stiffness Method in comparison to the AASHTO Simplified Method is apparent when Figure 7.12 is compared to Figure 7.1. The same conclusion is reached by examination of values for the mean and spread (COV) of the bias values for the two methods in Table 7.2.

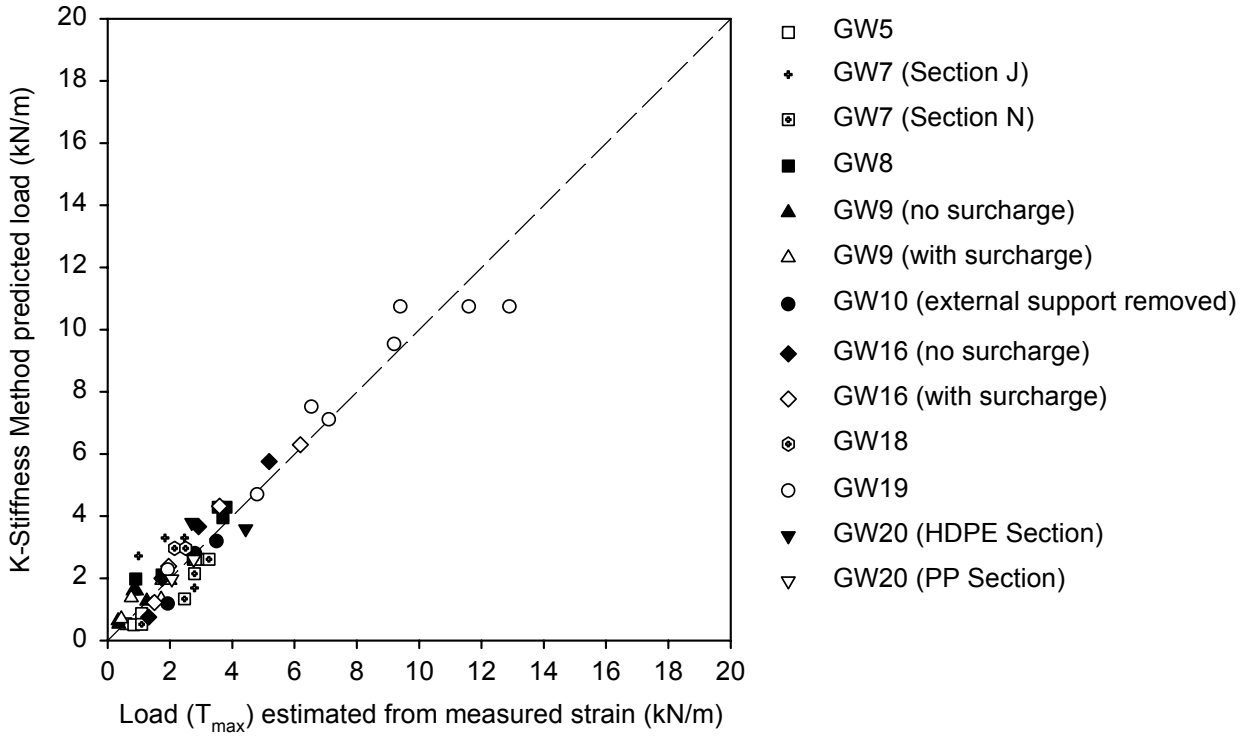

Figure 7.12. Predicted versus measured values of T_{max} in reinforcement layers for geosynthetic walls, using the K-Stiffness Method.

The data in Table 7.2 indicate that there is twice as much variation in the prediction of reinforcement load T_{max}, given all reinforcement layers, than in the prediction of the maximum reinforcement load, T_{mxmx} (compare the COV for T_{max} with the COV for T_{mxmx}). Therefore, better prediction of the distribution of T_{max} versus depth could greatly improve the prediction accuracy of the K-Stiffness Method.

The strain level in the reinforcement also appears to have a significant effect on the prediction accuracy of the K-Stiffness Method. Figure 7.13 shows maximum reinforcement strains predicted with the K-Stiffness Method and T_{mxmx}, plotted against the maximum measured

reinforcement strain in the backfill in each geosynthetic wall at the end of wall construction (i.e., the data do not include any locally high connection strains). The predicted strains were calculated by dividing T_{mxmx} at the end of construction (EOC) by the reinforcement layer stiffness value, J (determined at the applicable strain level and time – EOC). It appears that once reinforcement strains exceed approximately 3 to 4 percent for the available case histories, the K-Stiffness Method consistently under-predicts the measured strain. Note that all of the strains greater than about 3 percent were measured in full-scale laboratory test walls that were surcharged to loads well in excess of working stress conditions (see Bathurst 1993, Bathurst et al. 1993b, 2000, 2001 for details regarding these full-scale laboratory test walls).

Bathurst and co-workers noted that in their full-scale laboratory tests, soil failure occurred before reinforcement rupture. Evidence of soil failure included a sudden and large outward movement of the wall face, soil settlement directly behind the wall face, and a concurrent increase in reinforcement strains. None of the full-scale field walls recorded reinforcement strains that were consistent with soil failure, with the exception of Wall GW10. It exhibited signs of soil failure, but only after the strain gauges mounted directly on the reinforcement ceased to function (at about 3 percent strain). Wall GW20 appeared to be stable at the end of surcharge completion at a reinforcement strain of just over 3 percent. However, after several months of reinforcement creep, the reinforcement strains exceeded 4 percent. On the basis of observations made by Carrubba et al. (1999) and the pattern observed in the creep data (see Chapter 6.0), it can be concluded that the wall was approaching soil failure.

Given the correlation between the physical observations of soil failure within the reinforced wall backfill made by Bathurst and co-workers and the measured maximum strain in the wall backfill reinforcement, it appears that backfill soil failure matches strain values in Figure 7.13 where the K-Stiffness Method begins to consistently under-predict the reinforcement strain. However, soil failure does not appear to be the only cause of this under-prediction. The crudeness of the facing stiffness factor in capturing the effect of facing stiffness on reinforcement strain and load development appears to also contribute to this under-prediction. Note that in Figure 7.13, at high reinforcement strains, the data points for walls with stiff facings are consistently below those for walls with flexible facings. In fact, while the K-Stiffness Method tends to begin to under-predict loads at just over 3percent strain for the flexible-faced walls, this under-prediction begins at approximately 1.5 to 2percent strain for the stiff-faced walls. This

may be an indicator that the facing stiffness correction factor used in the K-Stiffness method is not a constant as proposed but, instead, increases toward 1.0 (i.e., less effect of facing stiffness) as strain increases. At higher strains, the facing appears to have reduced reserve capacity to carry additional load, consistent with the observations made by Bathurst et al. (2000). While the facing has not failed at reinforcement strains greater than 1.5 to 2 percent, the reinforcement takes on additional load to maintain facing column equilibrium. Once the reinforcement strain exceeds 3 to 4 percent, the soil begins to fail for both flexible and stiff-faced walls.

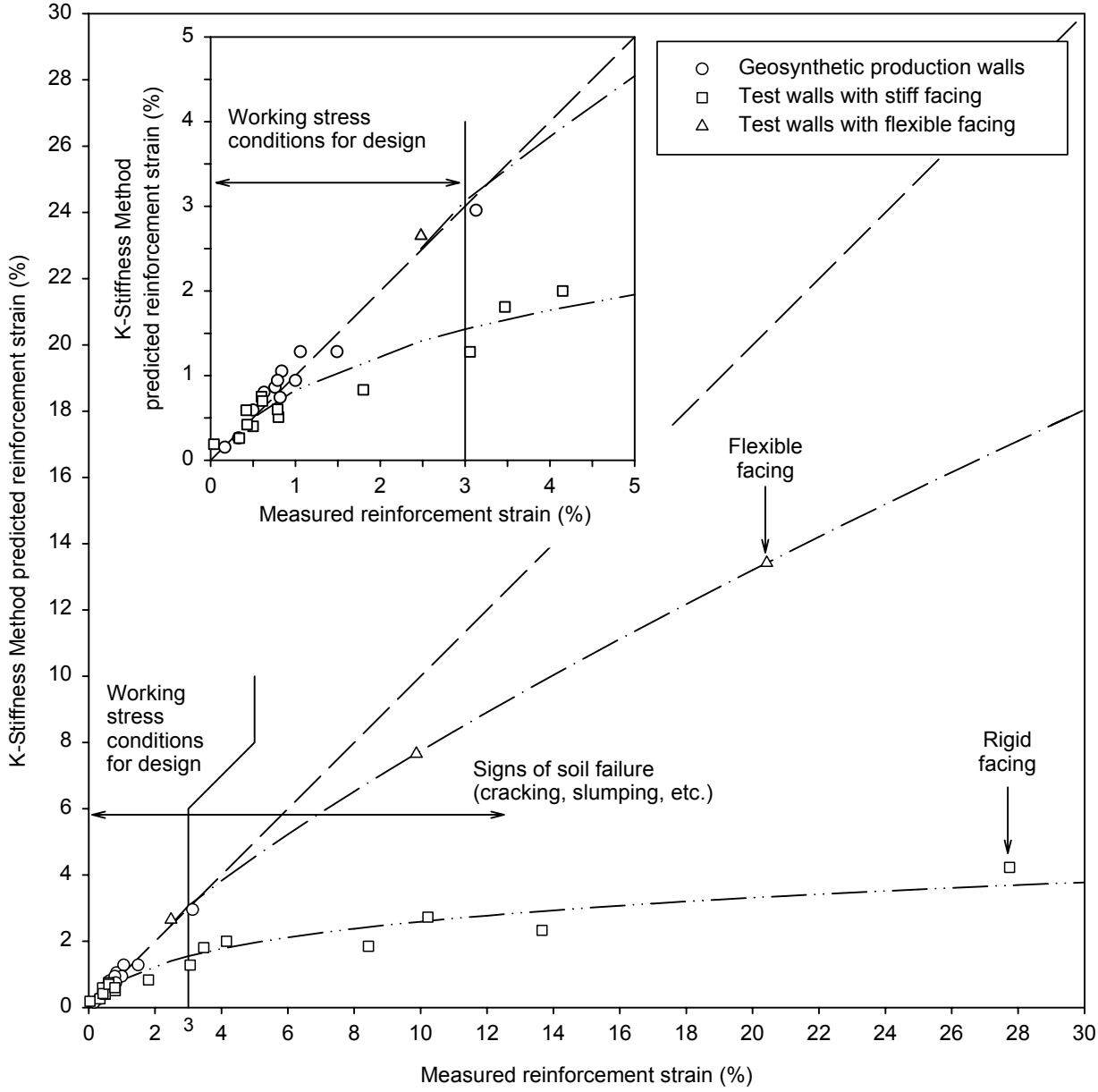

Figure 7.13. Predicted versus measured reinforcement strain (based on T_{mxmx}) using the K-Stiffness Method for full-scale production (field) and full-scale laboratory geosynthetic walls. Note: Inset figure corresponds to a reinforcement strain range from 0 to 5 percent.

Plane strain shear strength data for the same backfill used in Wall GW16 indicated that peak soil strength occurred at strains of about 2 to 3 percent (Boyle 1995). Since the backfill used for this wall was at the upper end of the range of soil shear strength for the case histories considered herein, these plane strain peak strains are likely at the lower end of the typical range for granular soils. Plane strain shear strength data reported by Lee (2000) for RMC soil specimens at confining pressures comparable to surcharge pressures required to initiate large wall deformations indicated that peak soil strains were also about 2 to 3 percent. In both cases (Boyle 1995, Lee 2000), the plane strain test results indicated that the peak soil strain increases with increasing confining stress.

As indicated by data from the RMC full-scale walls, geosynthetic reinforcement tensile strains large enough to cause signs of soil failure are typically numerically greater than the 2 to 3 percent peak strain values required to cause the soil to begin to fail in a plane strain shear test. That is, reinforcement strain levels of approximately 3 to 4 percent or more appear to correspond to soil peak shear strains of 2 to 3 percent, as indicated by laboratory plane strain testing of RMC granular soils.

Prevention of reinforcement strains that are great enough to allow failure of the soil should be an objective of any working stress design method. Soil failure is defined as contiguous or near-contiguous zones of soil with shear strains in excess of the strain at peak strength. Contiguous shear zones have been observed in test walls taken to collapse under uniform surcharge loading (Bathurst 1990, Bathurst et al. 1993b; see also Chapter 6.0). As indicated by analysis of long-term creep strains measured in walls taken from working stress conditions to near collapse, once a wall goes beyond working stress conditions, the load levels in the reinforcement begin to increase as internal soil shear surfaces continue to develop and the soil approaches a residual strength (see Chapter 6.0). This in turn leads to higher creep rates and an acceleration of strain development in the wall. Nevertheless, this condition does not necessarily result in reinforcement rupture and wall collapse if the reinforcement has sufficient strength. However, it does mean that wall deformations may become excessive. Once the soil has failed, for all practical purposes the wall has failed, and an internal strength limit state for the soil has been achieved.

The key to preventing the soil from reaching a failure limit state is to estimate how much strain can be allowed in the reinforced wall system (i.e., the soil reinforcement) without causing

the soil to reach a soil failure condition. It appears that preventing the reinforcement strain from exceeding a 3 to 3.5 percent design value will be adequate for the high shear strength granular backfill soils in this study and likely conservative for weaker backfill soils. Since the maximum reinforcement strain to prevent soil failure was derived from high shear strength soils, the 3 to 3.5 percent strain value represents what is effectively a lower bound value and is therefore recommended for design, given available data. However, the relationship between reinforcement strain and the soil shear strain at peak strength needs to be investigated for a wider range of soils.

7.6 Summary and Conclusions

A new approach, termed the K-Stiffness Method, is proposed to predict reinforcement loads and strains for designing the internal stability of reinforced soil walls. The working stress methodology has been developed and calibrated by using a database of reinforced soil wall reinforcement strain and load data. This new methodology considers the stiffness of the various wall components and their influence on reinforcement loads. An objective of the method is to design the wall reinforcement so that the soil within the wall backfill is prevented from reaching a state of failure consistent with the notion of working stress conditions. This soil failure limit state is not considered in the reinforced soil wall internal stability design methods currently available, yet, as indicated by the research results presented herein, is likely to be a controlling limit state for geosynthetic structures. This new approach is largely empirically based, using back-analysis and curve fitting of measured data from full-scale reinforced soil walls. The database used captures the typical range of wall types and geosynthetic reinforcement materials. This gives confidence that the new method is applicable to most typical geosynthetic reinforced soil walls constructed with granular backfill soils.

8.0 DEVELOPMENT OF THE K-STIFFNESS METHOD FOR STEEL REINFORCED SOIL WALLS

8.1 Introduction

In Chapter 7.0, a new working stress method, called the K-Stiffness Method, is developed for geosynthetic walls. A desirable feature of any new methodology for designing reinforced soil wall internal stability is a seamless transition between geosynthetic and steel reinforced soil walls. Such a feature will keep the design approach for reinforced soil walls simpler, allow different reinforcement options to be evaluated within a common framework, and provide the designer confidence that the approach can be applied to a wide range of geosynthetic and metallic soil reinforcement products.

This chapter demonstrates how the K-Stiffness Method proposed by the writers for geosynthetic reinforced soil walls can be extended to steel reinforced walls. As is true in Chapter 7.0, the scope of this chapter is limited to reinforced soil walls with granular (non-cohesive) backfill.

8.2 Summary of Case Histories Evaluated

The key properties and parameters for each of the case histories referred to in this chapter are summarized in Table 8.1 for steel reinforcedsoil walls. Additional details for each of these case histories, including wall and reinforcement geometry, reinforcement type, soil properties, and construction history, are provided by Allen et al. (2001).

The database of steel reinforced soil wall case histories includes 20 instrumented wall sections that were built to full scale in the field. These case histories include walls with steel strip, bar mat, and welded wire reinforcement (reinforcement stiffness values varied from 18,000 to 166,000 kN/m). All of the walls have precast concrete panel or welded wire facings. Included in the database are walls with and without significant soil surcharges, narrow base- and wide base-width walls, walls with trapezoidal cross-sections, very tall walls up to 18 m high, walls with a wide range of reinforcement coverage ratios varying from R_c = 0.053 to 1.0, and walls with a range of plane strain peak friction angles (ϕ_{ps} = 35^o to 56^o).

Table 8.1. Summary of steel strip, bar mat, and welded wire reinforced soil wall case histories.

Wall Case History	Project Date	Wall Height (m)	Surcharge Condition	Measured Backfill Triaxial or Direct Shear Friction Angle ϕ_{tx} or ϕ_{ds} (^{o})	Estimated Backfill Plane Strain Friction Angle ϕ_{ps} (^{o})	Reinforcement Stiffness J (MN/m)	Global Wall Stiffness S_{global} (MN/m^2)	Reference
Lille, France Wall (SS1)	1972	6.0	None	44	49	48	64	Bastick 1984
UCLA Test Wall (SS2)	1974	6.1	None	38	40	63	104	Richardson et al. 1977
WES Test Wall (SS3)	1976	3.66	Uniform (90 kPa)	36	40	18	30	Al-Hussaini and Perry 1978
Fremersdorf Wall (SS4)	1980	7.3	None	37	40	79	103	Thamm 1981
Waltham Cross Wall (SS5)	1981	8.2	None	56	56	53 to 105	105	Murray and Farrar 1990
Guildford Bypass Walls (SS6)	1981	6.0	None	48	53	83	264	Hollinghurst and Murray 1986
Asahigaoka, Japan Wall (SS7)	1982	12.0	Sloping $\leq$ 1 m high	36	40	80 to 121	128	Bastick 1984
Ngauranga Wall (SS10)	1985	12.6	5^o negative slope	50*	50*	79 to 118	122	Boyd 1993
Algonquin Wall (SS11)	1988	6.1	None	40	43	55	72	Christopher 1993
Gjovik (Norway) Wall (SS12)	1990	12.0	1.5:1 slope $\leq$ 3 m high	38	41	53	70	Vaslestad 1993
Bourron Marlotte (rectangular section) Test Wall (SS13)	1993	10.5	None	37	40	79 to 118	137	Bastick et al. 1993
Bourron Marlotte (trapezoidal section) Test Wall (SS14)	1993	10.5	None	37	40	79 to 118	118	Bastick et al. 1993
INDOT Minnow Creek Wall (SS15)	2001	16.9	None	38	40	38 to 105	81	Runser et al. 2001
Hayward Wall, Section 1 (BM1)	1981	6.1	2:1 slope	41	44	66	109	Neely 1993
Hayward Wall, Section 2 (BM2)	1981	4.3	2:1 slope	41	44	66	108	Neely 1993
Algonquin Wall (sand) (BM3)	1988	6.1	None	40	43	38	48	Christopher 1993
Algonquin Wall (silt) (BM4)	1988	6.1	None	35	35	39	48	Christopher 1993
Cloverdale Wall (BM5)	1988	18.2	None	40	43	57 to 166	126	Jackura 1988
Rainier Ave. Wall (WW1)	1985	16.8	0.3 m soil surcharge	43$^+$	48	39 to 103	147	Anderson et al. 1987

*Estimated from in-soil pullout tests. $^+$Estimated from triaxial shear strength tests on soil obtained from the same source used at an adjacent project.

Note: SS = steel strip reinforced soil wall; BM = steel bar mat reinforced soil wall; WW = welded wire reinforced soil wall. The stiffness J was determined assuming a steel modulus of 200 GPa, with the exception of SS3 which used the value reported in reference. The stiffness was computed as force per unit width of wall, based on geometry and horizontal spacing of the reinforcement.

Vertical spacing of reinforcement layers varied from 0.3 to 0.75 m. The facing batter for all of the steel reinforced walls was near vertical.

Although it is generally not possible to isolate the effect of a specific variable, most of the conditions that are likely to be encountered in the field are included within the database of case histories described above.

Plane strain friction angles were used to characterize soil shear strength in the case histories. Plane strain conditions typically exist in soil walls, and recent work (see Chapter 7.0) indicates that the plane strain soil friction angle provides a better correlation to reinforcement loads, at least for geosynthetic walls (see also Rowe and Ho 1993, Zornberg et al. 1998a,b, Lee et al. 1999). Measured plane strain friction angles were not available for these case histories, but were estimated from measured triaxial or direct shear friction angles (Table 8.1). Peak friction angles reported in the source references from triaxial compression tests, ϕ_{tx} , were adjusted to peak plane strain friction angles by using the methods provided in Chapter 2.0.

8.3 Analysis of Reinforcement Loads

Allen et al. (2001) investigated North American methods for predicting reinforcement loads and concluded that the AASHTO (2002) Simplified Method produces results similar to those of the other methods in use today, yet has the advantage of being simpler to use and more broadly applicable. Therefore, the Simplified Method will be used herein as the baseline of comparison for reinforcement loads predicted with the new working stress method.

Figure 8.1 indicates how well the Simplified Method predicts reinforcement loads in steel and geosynthetic reinforced soil walls built in the field. A log-log scale has been used to better display the wide range of load levels in the walls. The reinforcement load T_{max} in the figure is the maximum load in the reinforcement layer. Triaxial or direct shear friction angles were originally used to develop the Simplified Method, and the method was adjusted only to fit the empirical data for the steel reinforced soil walls. For geosynthetic reinforced soil walls, the active lateral earth pressure coefficient was used directly to calculate reinforcement loads. Measured triaxial or direct shear strength friction angles and measured unit weights were used to estimate loads with the Simplified Method to maintain consistency with the empirical calibration of the Simplified Method, and to be consistent with the type of friction angle used to develop Figure 8.1. The use of measured soil parameters eliminates the conservatism in the estimate due to soil

parameter selection, making it possible to evaluate the accuracy of the method itself. However, current AASHTO (2002) design specifications require a maximum friction angle of 40^o even if the measured friction angle is higher, so that specifications are consistent with the empiricism in the Simplified Method for steel reinforced walls (Allen et al. 2001). Therefore, to maintain consistency between the Simplified Method and the K-Stiffness Method (which effectively caps the plane strain soil friction angle at 44^o and is discussed later in this chapter), the triaxial or direct shear friction angle was capped at a maximum value of 40^o for steel reinforced walls. For the geosynthetic reinforced walls because the empirical evidence does not dictate the need to cap friction angle values, and to be consistent with the K-Stiffness Method which does not have a maximum friction angle criterion for geosynthetic walls (see Chapter 7.0), the friction angles used for load prediction were not capped for geosynthetic walls in Figure 8.1. \

The data in Figure 8.1 show that the Simplified Method tends to overestimate reinforcement loads in geosynthetic reinforced soil walls. Chapter 5.0 demonstrates that predicted loads for geosynthetic reinforced soil walls, if triaxial or direct shear friction angles are used, are approximately 5 to 8 times greater than observed values for full-scale field walls. For steel reinforced walls, the Simplified Method predictions are more accurate, with maximum reinforcement loads (on average) approximately equal to the measured values. This better agreement should not be surprising, since the Simplified Method was largely developed and calibrated against the results of instrumented steel reinforced structures (Allen et al. 2001a).

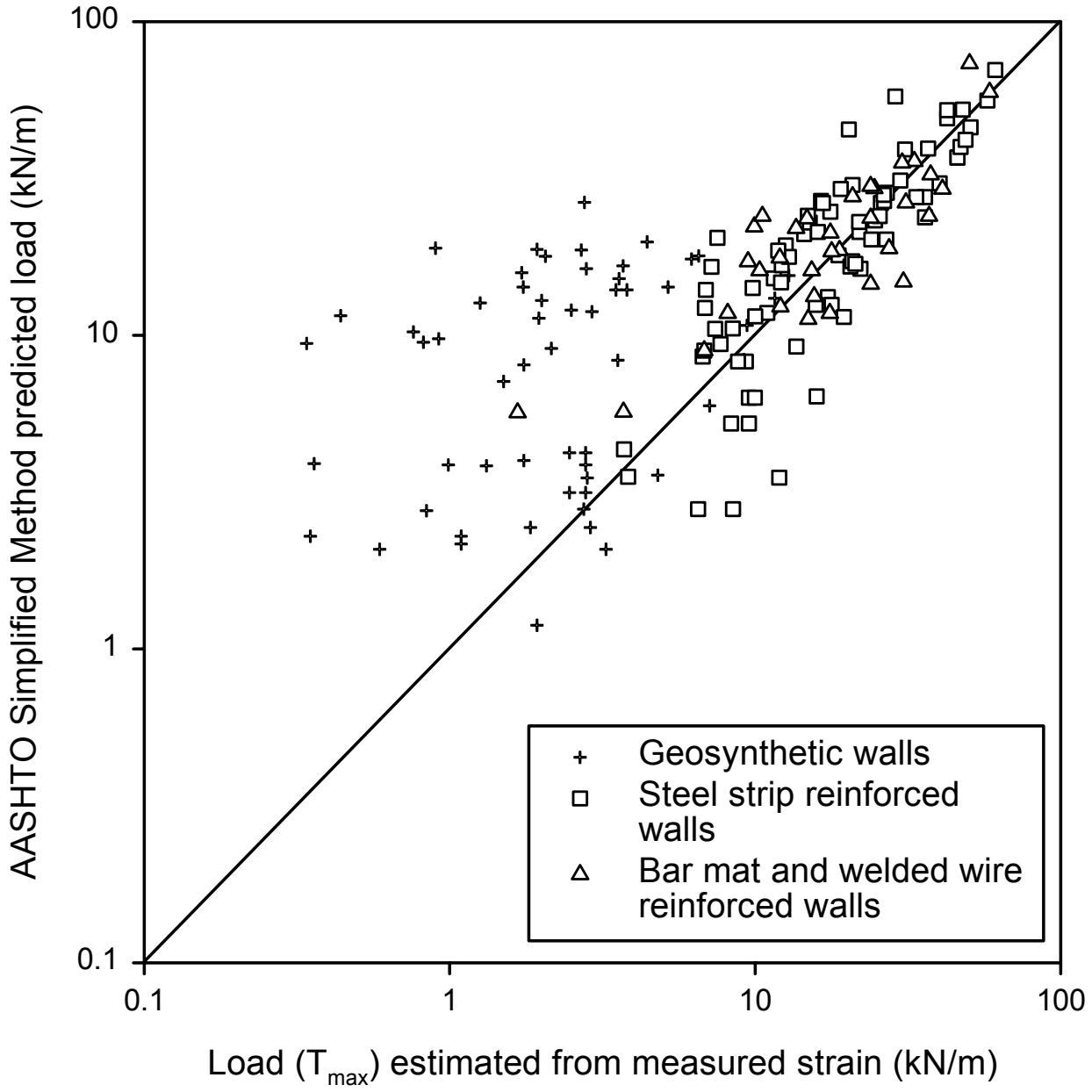

Figure 8.1. Predicted T_{max} versus T_{max} estimated from measured strains using the AASHTO Simplified Method. Note : Based on peak triaxial or direct shear friction angles (capped at 40^o max. for steel walls).

8.4 Development of The K-Stiffness Method to Predict T_{max} for Steel Reinforced Systems

8.4.1 General

As discussed in Chapter 7.0, the following key factors influence the magnitude of maximum reinforcement load, $T_{max,}$ in reinforced soil walls:

- height of the wall and any surcharge loads

- global and local stiffness of the soil reinforcement
- resistance to lateral movement caused by the stiffness of the facing and restraint at the wall toe
- face batter
- shear strength and modulus of the soil
- unit weight of the soil
- vertical spacing of the reinforcement
- degree of backfill compaction, including local effects such as compaction in proximity to the wall face.

Chapter 7.0 addresses each of these factors in the development of the K-Stiffness Method for geosynthetic walls. Each of these factors must also be addressed to develop the K-Stiffness Method for steel reinforced systems. Details of the derivation of the K-Stiffness Method are provided in Chapter 7.0. For convenience, the method is summarized below.

T_{max} is calculated with the following general expression, per running unit length of wall in reinforcement layer i:

$$T_{max}^{i} = \frac{1}{2} K \gamma (H + S) S_v^i D_{tmax} \Phi_g \Phi_{local} \Phi_{fs} \Phi_{fb} \quad (8.1)$$

where S_v^i = tributary area (equivalent to the vertical spacing of the reinforcement near each layer location when analyses are carried out per unit length of wall); D_{tmax} = load distribution factor that modifies the reinforcement load on the basis of layer location; K = lateral earth pressure coefficient; γ = unit weight of the soil; H = height of the wall; S = equivalent height of uniform surcharge pressure q (i.e., $S = q/\gamma$); and Φ_g, Φ_{local}, Φ_{fs} and Φ_{fb} are influence factors that individually account for the influence of local and global reinforcement stiffness, facing stiffness, and face batter. For reinforced soil structures, conventional practice is to assume that the lateral earth pressure acting at any level in the wall is directly proportional to the overburden stress. Equation 8.1 makes no such *a priori* assumption, making it possible to more fully evaluate the mechanisms that affect the distribution of loads in the reinforcement layers.

The coefficient of lateral earth pressure, K, is calculated by using the Jaky equation for "at rest" earth pressure (Holtz and Kovacs 1981):

$$K = K_0 = \left(1 - \sin \phi_{ps}\right) \text{ and } K_0 \geq 0.3 \tag{8.2}$$

where ϕ_{ps} is the peak plane strain friction angle. The use of K_0 in this proposed method does not imply that at-rest conditions exist within the reinforced backfill. K_0 is simply used as an index parameter to characterize the soil behavior. This issue, as well as the limitation on the minimum value of K_o, are explained in Section 8.4.7.

Equation 8.1 contains an expression for reinforcement loads that is similar to the conventional expression used in current limit equilibrium methods of analysis, but it represents the average load applied to the reinforcement layers rather than a load that increases linearly as a function of the vertical overburden stress. The empirical reinforcement load distribution parameter, D_{tmax}, is used to distribute the load as a function of depth, accounting for the reinforcement characteristics, load redistribution among layers, and foundation conditions. The modifiers Φ_g, Φ_{local}, Φ_{fs}, and Φ_{fb} are empirically determined parameters or functions that capture the effect the major components have on reinforcement load development. These parameters are used to improve the correlation between measured and predicted reinforcement loads at working stress conditions on the basis of an examination of a large number of case studies. Parameter D_{tmax} is a function of normalized depth below the top of the wall (z+S)/(H+S), including the effect of the soil surcharge S, and varies over the range $0 \leq D_{tmax} \leq 1$.

Parameter Φ_g is a global stiffness factor that accounts for the influence of the stiffness and spacing of the reinforcement layers over the entire wall height. It has the following general form:

$$\Phi_g = \alpha \left(\frac{S_{global}}{p_a} \right)^{\beta} \tag{8.3}$$

Here, S_{global} is the global reinforcement stiffness, and α and β are constant coefficients. The non-dimensionality of the expression is preserved by dividing the global reinforcement stiffness by p_a = 101 kPa (atmospheric pressure). The global reinforcement stiffness value for a wall is calculated as shown in Chapter 7.0.

Parameter Φ_{local} is a local stiffness factor that accounts for relative stiffness of the reinforcement layer with respect to the average stiffness of all reinforcement layers. It is expressed as follows:

$$\Phi_{local} = \left(\frac{S_{local}}{S_{global}} \right)^{a} \tag{8.4}$$

Here, parameter S_{local} is the local reinforcement stiffness for reinforcement layer i, calculated as shown in Chapter 7.0. It is used to quantify the local combined influence of the individual layer stiffness and spacing on reinforcement load. The coefficient term "a" in Equation 8.4 is taken as a = 0 for steel reinforcement, resulting in Φ_{local} = 1 and a =1 for geosynthetic reinforced soil walls.

Parameters Φ_{fs} (facing stiffness factor) and Φ_{fb} (facing batter factor) in Equation 8.1 account for the influence of the facing stiffness (Section 8.4.5) and facing batter (Section 8.4.6), respectively, and are constant values for a given wall.

Examination of Equation 8.1 shows that the maximum load in a reinforcement layer is the product of seven terms that have some uncertainty associated with their value (i.e., are not deterministic) and/or require back-analyses to determine the magnitude of coefficient terms. In addition, some terms are highly non-linear. It is assumed *a priori* that parameters K and γ, and factors D_{tmax} , Φ_g , Φ_{local} , Φ_{fs} and Φ_{fb} are for practical purposes statistically independent. This assumption allows the influence of each term on predicted reinforcement loads to be examined separately while keeping other parameters at baseline values. Baseline values for coefficient terms in expressions for Φ_g , Φ_{local}, Φ_{fs} and Φ_{fb} are discussed in the following sections.

The accuracy of the K-Stiffness Method when different expressions for the influence factors and associated constant coefficient values identified above are used is evaluated in the following sections in two ways:

1. direct comparison of predicted and measured reinforcement values for the walls summarized in Table 8.1 and by Allen et al. (2001a) and
2. comparison of the mean and coefficient of variation (COV) of the bias, defined as the ratio of the reinforcement loads estimated from strain measurements to the predicted reinforcement loads for all case studies (Table 8.2).

Values of the mean of the ratio of reinforcement loads close to but slightly less than unity are desirable while maintaining a minimum coefficient of variation (COV). Analyses of the major factors contained in Equation 8.1 are described in the following sections.

8.4.2 Load Distribution Factor, D_{tmax}

Rowe and Ho (1993) and Lee (2000), as well as Chapters 5.0 and 7.0 herein, demonstrate that the distribution of T_{max} from measured geosynthetic reinforcement loads versus normalized depth below the top of the wall is trapezoidal in shape. An empirical approach similar to that used in Chapter 7.0 was applied here to generate the normalized reinforcement load distribution envelope shown in Figure 8.2 for the steel reinforced soil wall case histories in Table 8.1. Data points for both geosynthetic (Chapter 7.0) and steel reinforced soil walls are plotted in Figure 8.2. The normalized reinforcement load for the steel reinforced walls is calculated as the ratio of the maximum load in a reinforcement layer (T_{max}) divided by the maximum reinforcement load in the wall (T_{mxmx}). For the geosynthetic walls, this ratio is also divided by the local stiffness factor to account for the effects of local stiffness. Local stiffness effects are not significant for steel reinforced walls, as discussed later in this chapter.

The load distribution factor, D_{tmax}, is assumed to be coincident with the envelope traced on the figures. The coordinates for this distribution are approximate only and have been selected to capture the majority of the data while simplifying the envelope geometry for all classes of steel reinforced wall structures. The more triangular envelope used for the steel reinforced soil wall data (figures 8.2c and 8.2d) appears to be a better predictor of the measured data than the trapezoidal distribution recommended for geosynthetic reinforced soil walls (figure 8.2a and 8.2b). The difference is likely due to differences in the ability of the two types of reinforcement to deform and redistribute load. Steel reinforcement is stiffer, and the reinforcement load distribution tends to more closely follow the increase in earth pressure with depth than is the case for geosynthetic walls. However, the distribution for steel walls is not fully triangular, possibly because of the effects of compaction stresses, as discussed later in the paper. As indicated by Figure 8.2, improved prediction accuracy could likely be obtained through further investigation of the effect of reinforcement stiffness on D_{tmax}.

Numerical simulation of propped panel walls with a range of soil reinforcement stiffness values corresponding to both typical geosynthetic and steel reinforced walls have been reported by Bathurst and Hatami (1998). They showed that the distribution of reinforcement loads is triangular for stiffness values associated with steel reinforcement products. For geosynthetic reinforced walls, the loads in the reinforcement layers near the bottom of the wall tend to be less than the loads observed in the layers within the middle third of the wall height. Rowe and Ho

(1993) also provide a summary of data from reduced-scale model and full-scale walls that is consistent with the trends in Figure 8.2.

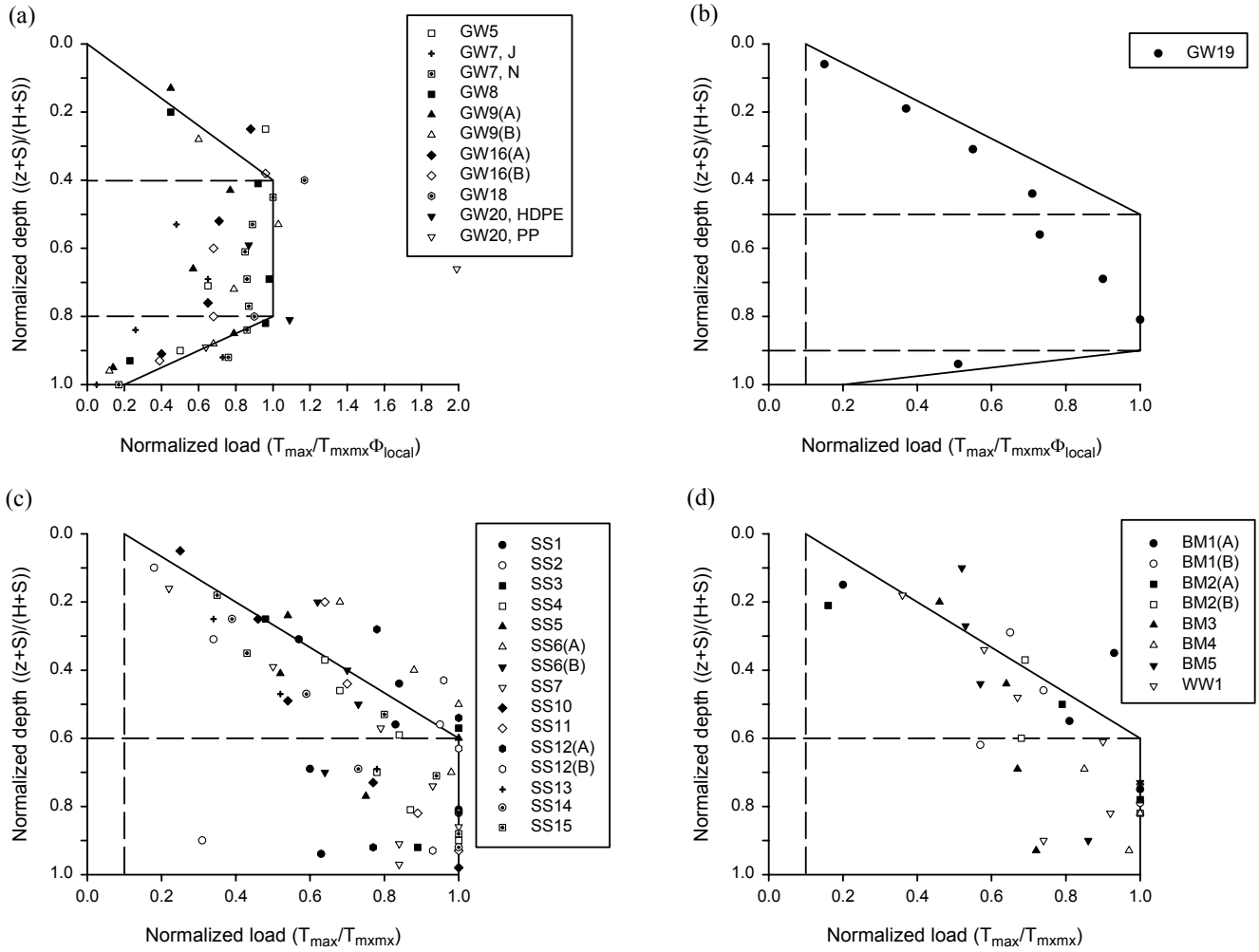

Figure 8.2. Normalized distribution of values of T_{max} estimated from measured strains: (a) geogrid and geotextile reinforced soil walls, (b) polyester strap reinforced soil walls, (c) steel strip reinforced soil walls, and (d) steel bar mat and welded wire reinforced soil walls. Note: T_{max} = maximum load in reinforcement layer; T_{mxmx} = maximum reinforcement load in the wall..

8.4.3 Global Reinforcement Stiffness Factor, Φ_g

As discussed in chapters 5.0 and 7.0, the stiffness of the various internal components of the wall directly affects the distribution of loads to each of the wall components at working stress conditions. In other words, as the average stiffness of the reinforcement layers increases, the reinforcement loads increase. Chapter 7.0 develops and applies this concept to reinforced soil

walls by rewriting Equation 8.1 to back-calculate values of global stiffness factor, Φ_g (measured) from maximum reinforcement load (T_{mxmx}) values estimated from measured strains:

$$\Phi_g \text{ (measured)} = \frac{T_{mxmx}}{S_v^i \, \sigma_h \, D_{Tmax} \, \Phi_{local} \, \Phi_{fs} \, \Phi_{fb}} \tag{8.5}$$

Data for Φ_g (measured) versus (S_{global}/p_a) are plotted in Figure 7.3 (Chapter 7.0) for all of the steel reinforced wall case histories in Table 8.1 and the geosynthetic wall case histories summarized in Chapter 7.0. Since the regression between the measured Φ_g and the normalized global stiffness included both the geosynthetic and steel reinforced soil wall case histories, no additional adaptation is needed to determine Φ_g for steel reinforced systems. As noted in Chapter 7.0, the regression of these data results in values of $\alpha = 0.25$ and $\beta = 0.25$ for the global stiffness power function constants. The power curve fit to the physical data is reasonably accurate, although there is some scatter for the steel reinforced soil walls data. This may be due to factors unique to steel soil walls (see below). In the parametric analyses to follow, coefficient terms $\alpha = 0.25$ and $\beta = 0.25$ are used.

8.4.4 Local Stiffness Factor, Φ_{local}

Local deviations from overall trends in reinforcement loads can be expected when the reinforcement stiffness and/or spacing of the reinforcement change from average values over the height of the wall (i.e., $S_{local}/S_{global} \neq 1$). This effect has been shown to be captured for geosynthetic reinforced soil walls by introducing a local stiffness factor, Φ_{local}, expressed by Equation 8.4 and by setting the coefficient term to a = 1. A range of parameter values corresponding to a = 1, 0.5, and 0 were assumed in Equation 8.1, together with baseline values for the other factors described in the previous and following sections. The results are summarized in Table 8.2, which shows that ignoring the local stiffness factor previously introduced for geosynthetic reinforced soil walls in Chapter 7.0 provides the best prediction of reinforcement loads. It appears that for steel reinforcement, local variations in reinforcement stiffness have little effect on the redistribution of the reinforcement loads.

Table 8.2. Summary of the mean and COV of the ratio of measured to predicted reinforcement loads (bias) for steel reinforced soil walls.

Parameter	No of Data Points	Ratio of Measured/Predicted (bias) T_{max} or T_{mxmx}											
		AASHTO Simplified Method				K-Stiffness Method (Equation 8.1)							
						Coefficient of Earth Pressure				Influence of Selected Values on Ratio of Measured/Predicted Loads			
		Triaxial or Direct Shear ϕ	Triaxial or Direct Shear ϕ Capped at 40°	Plane Strain ϕ	Plane Strain ϕ Capped at 44°	Proposed Method: K, Capped to Minimum Value of 0.3 (a=0 in Eq. 8.4, d=0.25 in Eq. 8.6)	K_{ah}	K = 0.3 for all Soils	$K = K_0$	$\gamma = 20$ kN/m^3 for all Walls	Local Stiffness Factor Φ_{local} (Eq. 8.4)		$S_v = 0.6$ m for all Walls
											a = 0.5	a = 1	
Mean T_{max}	102	1.28	1.12	1.49	1.25	0.95	0.95	1.03	1.07	0.95	0.95	0.97	1.03
COV T_{max} (%)	102	67.0	45.3	66.4	48.2	32.0	43.8	30.6	41.9	35.5	34.5	40.3	35.5
Mean T_{mxmx}	22	1.21	1.07	1.39	1.17	1.01	0.92	0.94	1.13	1.01	0.97	0.94	1.12
COV T_{mxmx} (%)	22	55.3	27.7	55.5	30.3	20.6	35.3	23.1	32.1	22.3	21.0	23.3	27.5

Notes: T_{max} = maximum load in reinforcement layer; T_{mxmx} = maximum reinforcement load in the wall; COV = coefficient of variation = (standard deviation of ratio of reinforcement load values/mean of ratio of reinforcement load values) x 100%; K_{ah} is based on Coulomb analysis, assuming wall batter $\omega = 0$.

It is possible that a steel reinforced soil wall with a very low global stiffness value (for example, gabion hexagonal wire mesh) could require an exponent value of "a" between 0 and 1. As additional case studies become available, and/or calibrated numerical models are developed, the magnitude of this coefficient term may need to be adjusted to reflect a wider range of metallic reinforcement products and spacing.

8.4.5 Facing Stiffness Factor, Φ_{fs}

Chapters 5.0 and 7.0 examine the influence of wall facing stiffness and toe restraint on the load levels observed in geosynthetic reinforced walls. Analysis found that very stiff facings could reduce the reinforcement loads by a factor of 2 to 4 relative to the loads in geosynthetic reinforced walls with a more flexible facing. This effect could not be evaluated for steel reinforced walls because not enough different wall facing types are in the database. In fact, all but one of the walls in Table 8.1 were built with incremental precast concrete facing panels. However, it may be reasonable to assume that the high global stiffness of steel reinforced walls in relation to that of geosynthetic reinforced walls minimizes the influence of the stiffness of the facing and wall toe on reinforcement loads. In the absence of available data to the contrary, the facing stiffness factor for all steel reinforced soil walls is recommended to be $\Phi_{fs} = 1.0$.

8.4.6 Facing Batter Factor, Φ_{fb}

In current practice, wall face batter (i.e., ω = inclination from the vertical) is taken into account explicitly by using Coulomb earth pressure theory. Limit equilibrium methods include the facing batter in the calculation of the Coulomb earth pressure coefficient. However, as demonstrated in Chapter 7.0, the Coulomb earth pressure coefficient tends to reduce reinforcement loads excessively for heavily battered walls. The influence of reduced confining pressure near the wall face cannot be captured explicitly by limit equilibrium methods. The influence of wall facing batter on maximum reinforcement loads is adjusted in the proposed working stress method for geosynthetics by using an empirical facing batter factor expressed as follows:

$$\Phi_{fb} = \left(\frac{K_{abh}}{K_{avh}} \right)^{d} \tag{8.6}$$

where K_{abh} is the horizontal component of active earth pressure coefficient accounting for wall face batter, and K_{avh} is the horizontal component of active earth pressure coefficient, assuming that the wall is vertical and d is a constant coefficient. A value of d = 0.25 was demonstrated in Chapter 7.0 to be a convenient numerical value to match measured reinforcement loads for geosynthetic reinforced soil walls with a range of facing batters and to provide a crude match to the available data. There are no data available in the literature for instrumented battered steel reinforced soil walls (i.e., for $\omega > 0$). However, a value of d = 0.25 may be reasonable for steel reinforced soil walls as well as for geosynthetic reinforced soil walls, is more conservative than the current practice, and is recommended until more data are available.

8.4.7 Soil Strength Effects on Soil Reinforcement Loads

For working stress conditions in soil walls, the soil property that most likely affects the distribution of load to the reinforcement layers in the wall is the soil modulus. This is because of the relatively low strain levels observed in these systems and the fact that limit equilibrium conditions have not been reached. However, the soil modulus is difficult to determine, is strain and stress level dependent, and for the case histories reported herein, measured soil modulus data were not available. The peak soil friction angle is routinely available, familiar to designers, and is relatively easy to measure or estimate. In general, as peak friction angle for a granular soil increases, the soil modulus also increases (Duncan et al. 1980). Hence the peak friction angle can be interpreted as an indicator of relative soil modulus value between soil types.

In the development of the stiffness method proposed herein, values of $K = K_o$ (Equation 8.2) and $K = K_{ah}$ were examined to investigate the relative accuracy of predicted values of T_{max} and T_{mxmx}. K_0 was considered because it is simple to calculate and is calculated independent of wall face batter (face batter is being handled by a separate factor—see Section 8.4.6). K_{ah} was determined with the Coulomb method and the assumption that the wall interface friction angle is equal to the soil backfill friction angle (i.e., $\delta = \phi_{ps}$) for coverage ratios $R_c \geq 0.7$ and decreases linearly with coverage ratios between 0.7 and 0.0 to a minimum value of $\delta = 0.65\phi$ for concrete faced walls. Full interface friction was assumed for coverage ratios greater than 0.7 because the continuous or nearly continuous reinforcement layers will restrict downward movement of the backfill soil immediately against the face and effectively generate an interface friction angle at

the back of the wall face that is equal to the backfill soil friction angle. The data in Table 8.2 show that reinforcement load ratios were closer to unity with K_0 (see the columns in the table for K_{ah} and K_0) than with K_{ah} in Equation 8.1, and the spread in ratio values was slightly less.

Allen et al. (2001) observed that current methods in use (e.g. the Simplified and Coherent Gravity methods) tend to under-predict reinforcement loads in steel reinforced MSE walls when triaxial or direct shear peak soil friction angles (ϕ) greater than 40^o are used. (The peak friction angle from these test methods can be used to estimate a peak plane strain friction angle value of approximately $\phi_{ps} = 44^o$.)

The influence of friction angle and the choice of $K = K_0$ was explored further by either capping the soil friction angle at $\phi_{ps} = 44^o$, placing no restriction on the soil friction angle, or using a constant soil friction angle of 44^o for the data set (see Table 8.2). Providing no restriction on the soil friction angle value clearly increases the COV value and makes the prediction less conservative for the K-Stiffness method. The same is true for the AASHTO Simplified Method. However, using a constant value of plane strain friction angle of 44^o ($K = 0.3$) for all the walls resulted in a prediction accuracy similar to simply capping the soil plane strain friction angle at 44^o ($K = 0.3$), given the data available. However, there were few case studies with plane strain friction angles of less than 44^o, and hence, it is not surprising that there was not much difference between the two sets of results.

Taken together, the results of this investigation lead to the recommendation that the value of K_o should be calculated according to Equation 8.2 but should not be less than 0.3. This approach preserves the current practice of accounting for the soil response on the basis of the peak soil friction angle; at the same time, it reduces the spread in the predicted load by accounting for the lack of correlation between soil friction angle and peak reinforcement load at higher soil friction angles, by adopting a constant value of $K = K_0$.

For geosynthetic reinforced systems, the correlation between T_{max} and the peak soil friction angle throughout the range of values was stronger than it was for steel reinforced systems (see Chapter 7.0). The influence of soil strength and stiffness on T_{max} appears, on the basis of this observation, to be affected by the global wall stiffness value. That is, the higher the global wall stiffness value, the less that changes in soil strength affect the magnitude of T_{max}, especially for very high shear strength soils. This reinforcement stiffness effect provides support to cap K at 0.3 for steel reinforced systems.

It is recognized that the use of $K = K_0$ can only be an indicator of the magnitude and influence of the real parameter of interest, which is the soil modulus or stiffness. However, K_0 is considered to be a readily available parameter and at this stage in the development of the general stiffness approach is a reasonable index for approximating the influence of soil strength and stiffness on the development of reinforcement loads.

8.4.8 Effect of Soil Unit Weight on Soil Reinforcement Loads

The soil unit weight recorded for each case study was within 16 percent of the mean value for all of the walls (γ_{mean} = 20 kN/m^3) and ranged from 16.8 to 22.6 kN/m^3. This variation was considered to be small in comparison to the uncertainty associated with other parameter values in this investigation, including estimated reinforcement loads. However, the fundamental expression for reinforcement loads (Equation 8.1) calculated with the Stiffness Method shows that loads (and hence strains) should vary linearly with soil unit weight. To investigate the influence of soil unit weight on predicted reinforcement loads, calculations for T_{max} and T_{mxmx} were carried out with a constant value for γ of 20 kN/m^3. Table 8.2 shows that there was only a minor difference in the accuracy of predicted reinforcement loads when a default constant unit weight of 20 kN/m^3 was used in the calculations rather than project-specific values. This minor difference was consistent with the variation in the measured value of this parameter. A practical implication of this result is that the selection of soil unit weight is not a critical factor for design accuracy with the K-Stiffness Method.

8.4.9 Effect of Reinforcement Layer Spacing on Soil Reinforcement Loads

The vertical distance between reinforcement layers in the case studies investigated varied from 0.3 to 0.75 m. Note that this is not necessarily the same as the vertical zone in the wall that contributes to load in a given reinforcement layer (i.e., the tributary area). S_v is representative of the tributary area when loads are calculated on the basis of load per unit of wall length and the spacing between layers is uniform. When the spacing is not uniform, this parameter is representative of the average distance between layers that are adjacent to the layer in question. At the top of a wall, S_v includes the full distance between the top layer and the top of the wall, plus the distance to the mid-point between the top layer and the next layer below.

The magnitude of reinforcement loads (and strains) can be expected to vary linearly with S_v, as assumed in the Stiffness Method proposed here and conventional design methods. Calculations were redone with a default value of S_v = 0.6 m, which was an average value from the steel reinforced wall case studies in Table 8.1. Table 8.2 shows that reinforcement spacing does influence calculated results, particularly the spread in the ratios of predicted to measured reinforcement loads in comparison to values calculated with the full procedure.

A parametric investigation, similar to what was done in Section 8.4.3 for the global reinforcement stiffness factor, was conducted to evaluate S_v. Equation 8.1 is rewritten below to back-calculate values of S_v from measured maximum reinforcement load (T_{mxmx}) values:

$$S_v \text{ (back-calculated)} = \frac{T_{mxmx}}{\sigma_h D_{tmax} \Phi_g \Phi_{local} \Phi_{fs} \Phi_{fb}} \quad (8.7)$$

The values of the variables are as described in Section 8.4.1. Data for S_v, back-calculated from the measured values of T_{mxmx}, versus S_v as determined directly from the spacing of the reinforcement in the wall are plotted in Figure 8.3 for both steel and geosynthetic reinforced wall systems (the case histories used are provided in Table 8.1, in Allen et al., 2001, and in Chapter 7.0). The regressed data demonstrate a linear relationship between reinforcement load and S_v, as predicted by both the proposed method and current design methods. This correlation appears to hold reasonably well even for large values of S_v.

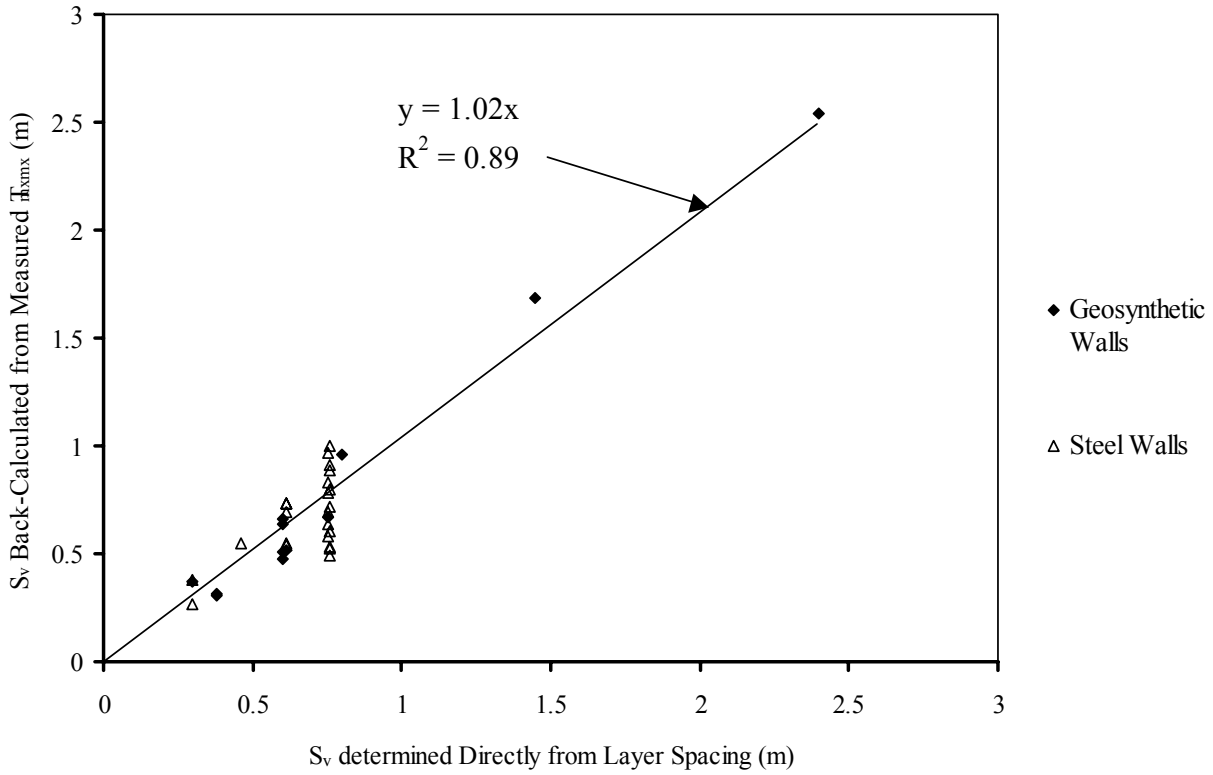

Figure 8.3. Back-calculated S_v from measured T_{mxmx} (Equation 8.7) versus S_v determined directly from spacing of reinforcement in wall.

8.4.10 Overall Performance of the K-Stiffness Method Applied to Steel Reinforced Soil Walls

Examples of measured values of T_{max} as a function of depth for several wall case histories are presented in Figure 8.4. The following observations can be made:

1. Both the AASHTO Simplified Method and the proposed K-Stiffness Method capture the general trend in reinforcement loads, which can be seen to increase with depth below the top of the wall.
2. Even with the friction angle capped at 40^o (triaxial/direct shear), or 44^o (plane strain), the Simplified Method does not appear to predict the loads estimated from measured strains as well as the K-Stiffness Method.

Furthermore, the proposed K-Stiffness Method matches the measured data more consistently than does the AASHTO Simplified Method, as shown by the COV values in Table 8.2, although both methods produce an average ratio of measured to predicted T_{max} that is near 1.0, provided that triaxial or direct shear soil friction angles are used with the Simplified Method.

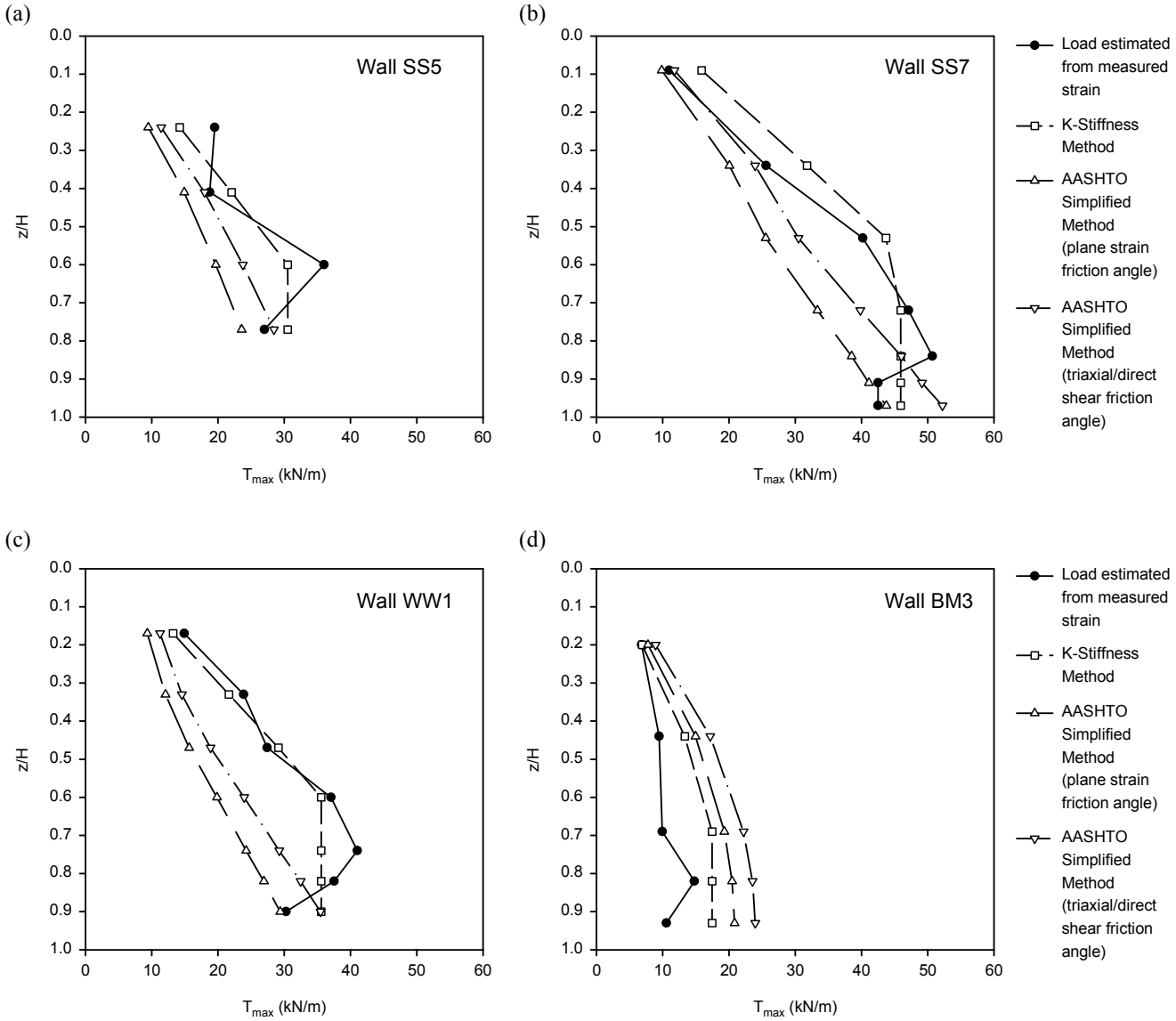

Figure 8.4. T_{max} distribution versus normalized depth for (a) steel strip reinforced soil wall (SS5), (b) steel strip reinforced soil wall (SS7), (c) welded wire reinforced soil wall (WW1), and (d) bar mat reinforced soil wall (BM3).

The K-Stiffness Method has been developed to work for both geosynthetic and steel reinforced soil walls. Data reported in Chapter 7.0 for 11 different geosynthetic reinforced soil wall sections are plotted with the steel reinforced wall data points in Figure 8.5. Comparison with Figure 8.1 presented earlier shows that the K-Stiffness Method provides a large improvement in prediction accuracy for geosynthetic walls. The improved prediction accuracy illustrated in this figure for steel reinforced soil walls relative to the Simplified Method is smaller

but is nevertheless visually apparent in the figures. Quantitative support for the improvement in predicted reinforcement loads using the proposed method can be found in Table 8.2, specifically, the COV of the ratio of measured to predicted T_{max} was 67 percent for the AASHTO Simplified Method (45 percent if ϕ_{tx} or ϕ_{ds} is capped at 40^o according to AASHTO (2002)), and 32 percent for the K-Stiffness Method, which is a significant improvement.

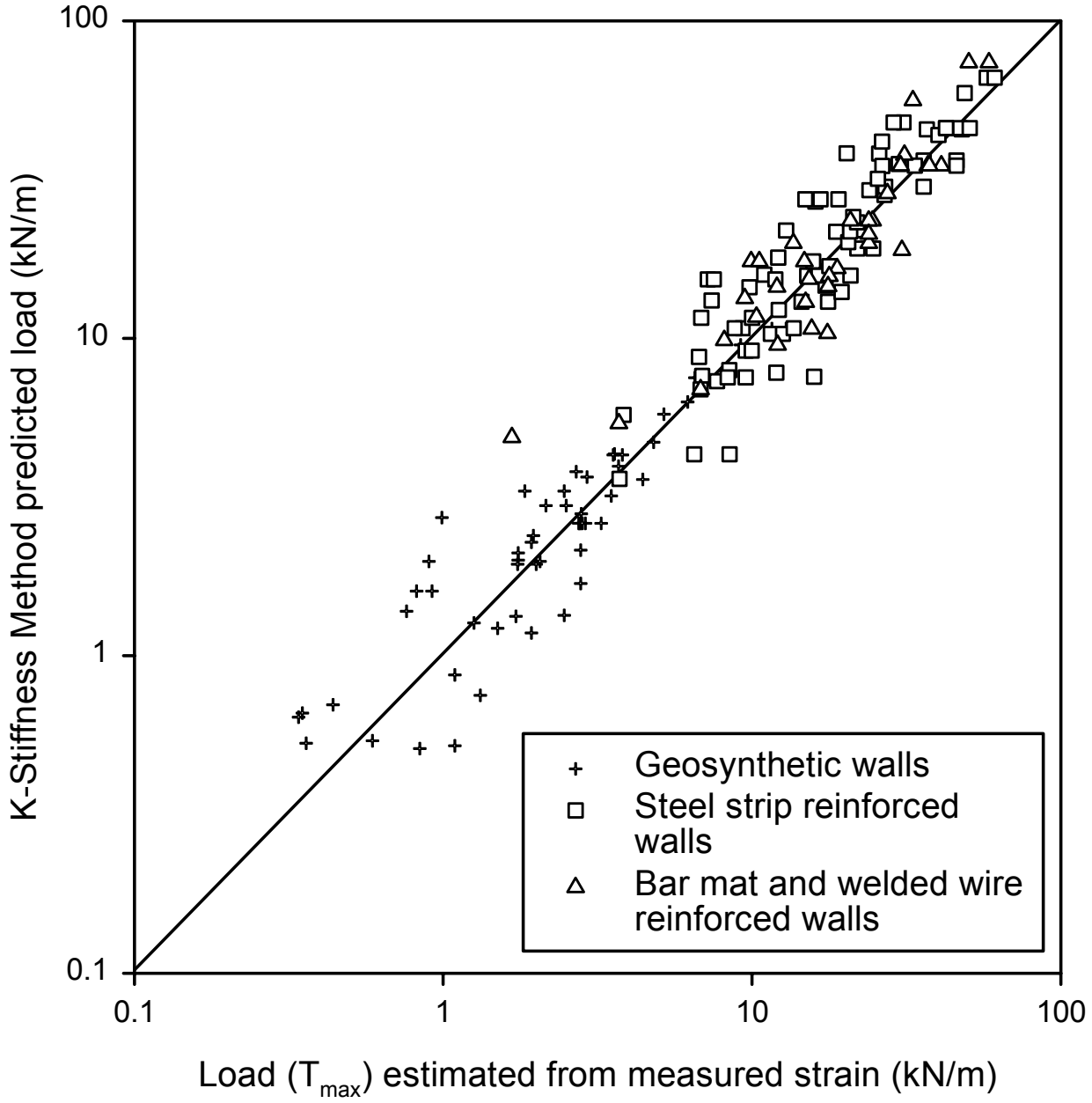

Figure 8.5. Predicted T_{max} versus T_{max} estimated from measured strains using the K-Stiffness Method (plane strain ϕ).

For both steel and geosynthetic reinforced systems, as shown by Table 8.2 and similar data reported in Chapter 7.0, it appears that approximately 50 percent of the coefficient of variation for the data set is due to variations in the distribution of T_{max} with depth (compare the COV for T_{max} with the COV for T_{mxmx}). Therefore, additional data and refinement of the proposed method to better predict the distribution of T_{max} versus depth should be a topic of further investigation.

Another potential contributing factor to the spread in the ratios of predicted to measured steel reinforcement loads for both the K-Stiffness Method and the Simplified Method are compaction stresses, which have not specifically been taken into account by these methods. Allen et al. (2001) found that, at least for the Simplified Method, the degree of compaction did not appear to have a significant effect on the reinforcement load levels in the completed walls. On the basis of their stress path analysis, Ehrlich and Mitchell (1994) indicated that the degree of compaction may increase reinforcement loads near the top of the wall, while in the lower portions of the wall, the stress history imparted to the soil by the compaction process is overcome by the increased vertical stress from the weight of soil above. The magnitude of increased reinforcement load is likely dependent on the location of the reinforcement relative to the wall top, the rigidity of the wall facing, the compaction effort used, the reinforcement stiffness, and the ability of the soil and reinforcement to lock in compaction stresses.

To further investigate the influence of compaction effects on steel reinforcement loads, case histories with light compaction (typical of test walls) were compared to case histories with typical field compaction. Typical field compaction is defined here as the use of full-size compaction equipment, with sufficient compaction effort applied to meet contract specification requirements. To minimize the influence of friction angle on the interpretation of compaction effects, case histories for this comparison were selected that had plane strain soil friction angles ranging from 40 to 43^{o}. The mean of the ratio of measured to predicted T_{max} was 0.94 for the light compaction group and 0.89 for the typical field compaction group, while the corresponding COV values were 22 percent and 34 percent, respectively. These data indicate that, on average, there is little effect on predicted reinforcement loads if compaction effects are considered. This was expected, since the K-Stiffness Method is empirically derived and based on the average value of input parameters.

Figure 8.6 provides plots of the ratio T_{max}/T_{mxmx} from measured data for walls known to have been compacted with typical field compaction and for structures known to have been lightly compacted. Superimposed on the figure is the distribution for the load distribution factor D_{tmax} introduced in Section 8.4.2. The data in this figure show that if compaction is light, the T_{max} distribution tends to be linear (triangular shaped), whereas if a more typical level of compaction is used, the distribution tends to become more trapezoidal. The trapezoidal shape of the T_{max} distribution appears to be the result of elevated reinforcement stresses remaining from the compaction process rather than mechanisms associated with geosynthetic reinforced soil walls, which also have a trapezoidal distribution for D_{tmax}. Because the recommended envelope shown in Figure 8.2 captures the distribution of T_{max} for the walls with typical compaction, the K-Stiffness Method can be argued to take into account the influence of compaction stresses on reinforcement loads. However, this recommended envelope only accounts for an average degree of "typical" compaction, and reinforcement load increases due to compaction could be greater if backfill soils are heavily compacted and are able to lock in compaction stresses. This observed apparent compaction stress effect may explain a number of other data points in figures 8.2 and 8.4 that fall well above the proposed envelope at the top of the walls.

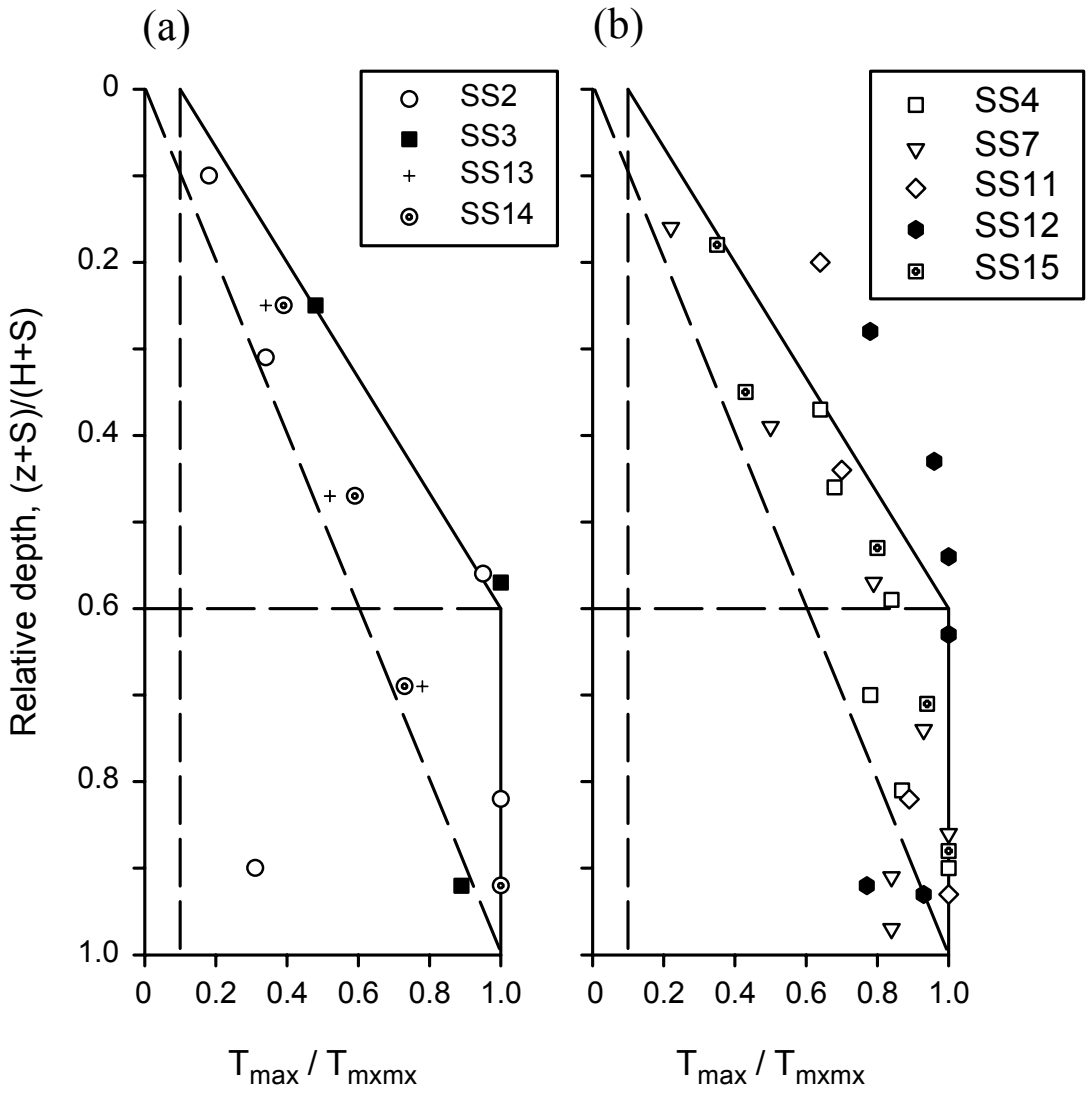

Figure 8.6. Normalized T_{max} as a function of relative depth below the wall top for steel strip reinforced soil walls with $\phi_{ps} \leq 44^{o}$: (a) light compaction (typical for test walls), and (b) typical field compaction. Note: The triangular distribution in the figures corresponds to the distribution of normalized load assumed in the AASHTO Simplified Method.

8.5. Concluding Remarks

A new approach, termed the "K-Stiffness Method," is proposed to predict reinforcement loads and strains for internal stability design of reinforced soil walls. Note that the value of K = K_o in the calculation of reinforcement loads was not chosen to imply that the state of stress in the soil backfill corresponds to an at-rest condition. Rather, parameter K was chosen by using the well-known Jaky equation for K_o as a characteristic index parameter of the new method and to

distinguish the new "K-Stiffness Method" from "stiffness methods" that appear in older versions of AASHTO/FHWA design guidance documents and some of the references cited in this report.

The K-Stiffness Method has been shown to improve the accuracy of predicted reinforcement loads in comparison to the Simplified Method and provides a way to estimate reinforcement loads on the basis of measured parameters. While the improvement in the accuracy of the method is not as great as for geosynthetic reinforced systems (see Chapter 7.0), the improvement for steel reinforced systems is still significant. However, an additional benefit of the method is that it provides a seamless transition between walls constructed with steel reinforcement and similar walls constructed with geosynthetic reinforcement.

For geosynthetic walls, the focus of the method is to design the wall reinforcement so that the soil within the wall backfill is prevented from reaching a state of failure, preserving working stress conditions (see Chapter 7.0). This soil failure limit state is not considered in the reinforced soil wall internal stability design methods currently available, yet given the research results presented herein, is likely to be a controlling limit state for geosynthetic structures. For steel reinforced walls, soil failure is only an issue if the reinforcement is allowed to yield. Since the proposed method should prevent the steel reinforcement from reaching its yield strength, the prevention of soil failure will generally not be a controlling limit state for steel reinforced walls.

9.0 CONCLUDING REMARKS AND RECOMMENDATIONS FOR FUTURE RESEARCH

A large database of case histories has been used to calibrate the empirically based model proposed herein. The proposed K-Stiffness Method represents a first step in the development of an empirically based working stress design method. This proposed method significantly improves the accuracy of reinforcement load prediction in relation to current design protocols, especially for geosynthetic walls, and provides a consistent approach for both geosynthetic and steel reinforced soil wall systems. However, refinement of the methodology, including formulations for influence factor expressions and associated constant coefficient values that are a primary feature of the method, is warranted. Specific areas of research needed to accomplish this refinement are summarized below for each variable or influence factor.

9.1 Reinforcement Spacing

Conventional design practice and back-analyses of the full-scale field wall data indicate that the value of T_{max} is directly proportional to the vertical spacing of the reinforcement, S_v. However, very small vertical spacing or very large vertical spacing could result in a deviation from this linear relationship. For example, at small spacing, it may be possible to derive additional benefit (i.e., reduced reinforcement loads) as a result of improved confinement of the soil. At some larger spacing, it is reasonable to assume that the reinforced backfill will cease to function as a coherent mass and will thus require refinement of the methodology presented in this report. Analysis of full-scale structures and analytical models calibrated against full-scale data in which S_v is the primary variable are needed to more clearly establish this relationship.

The horizontal distribution of the reinforcement, as represented by the coverage ratio, R_c, is currently considered in the methodology as a modifier to the available reinforcement tensile strength expressed as a force per unit width of wall. However, the use of R_c in this manner may not account for the possible effect of the reinforcement to confine the soil. The proposed methodology is based on continuous reinforcement layers for geosynthetic-reinforced systems but on discontinuous strip reinforced systems for steel reinforced walls because of the available database of case histories. What effect, if any, does R_c have on reinforcement stresses other than what has already been assumed? Furthermore, what effect does reinforcement continuity have

on downdrag forces that develop on the back of the wall facing, and what effect does downdrag have on reinforcement stresses, both in the backfill and at the connection?

9.2 Lateral Earth Pressure Coefficient, K

The correlation between lateral earth pressure/peak soil friction angle and the value of T_{max} is not as obvious as it is for other variables such as S_v, at least from the standpoint of load prediction accuracy. For geosynthetic-reinforced systems, the correlation between the earth pressure coefficient based on peak soil strength parameters (K_0 as proposed herein) and the reinforcement load is fairly strong. However, for steel reinforced systems, this correlation appears to be very poor, especially for high shear strength soils. The difference in this correlation for steel and geosynthetic-reinforced systems may be related to the relative stiffness between the soil and the reinforcement. As the reinforcement becomes much stiffer than the soil (e.g., steel), the influence of the soil stiffness on the reinforcement load may decrease, possibly to the point of having no influence at all. Additional research is needed to determine how to best incorporate the soil properties into the design method, with particular emphasis on the relative stiffness of the soil and the reinforcement. Furthermore, very few data are available for walls that use lower quality (i.e., very silty) backfills. The availability of high quality backfill is the exception rather than the rule in much of North America. Significant cost reductions can be obtained by using poorer quality backfills.

9.3 Soil Unit Weight, γ

Only minor variations in the magnitude of reinforcement load with soil unit weight were observed. This variation was considered to be small in comparison to the uncertainty associated with other parameter values in the current investigation, including estimated reinforcement loads. However, the fundamental expression for reinforcement loads with the Stiffness Method shows that loads should vary linearly with soil unit weight. This linearity is preserved in the back-analyses resulting from the available database of case histories. Therefore, specific research regarding the influence of soil weight on reinforcement loads is not warranted at this time.

9.4 Wall Height Plus Surcharge (H + S)

This variable is used to characterize the overall wall geometry by an equivalent height. The fundamental expression for the stiffness method shows that reinforcement loads vary linearly with this quantity. The surcharge (S) is currently defined as the average equivalent height of soil over the reinforced backfill zone. Investigation is warranted to better understand the depth of influence of surcharge loads below the top of the wall for different wall heights (H) and the overall effect of the surcharge on the distribution of reinforcement loads within the wall. Full-scale wall reinforcement data for very tall walls are also needed to extrapolate the K-Stiffness Method to large values of H.

9.5 Load Distribution Factor, D_{tmax}

The load distribution with depth shown in chapters 5.0, 7.0, and 8.0 is likely to be influenced by foundation conditions (soft versus hard, for example). Better quantification of the load distribution with depth is needed to determine the effect of various foundation soil conditions and various facing types on the distribution. The shape of the load distribution envelope is trapezoidal for extensible reinforcement (geosynthetics) but becomes more triangular for stiff reinforcement (steel). This indicates the possible influence of reinforcement stiffness on the distribution of reinforcement loads. Variation in the load distribution with depth appears to account for approximately 50 percent of the total variation in the loads predicted by the K-Stiffness Method relative to the measured reinforcement loads. Additional research to refine the load distribution factor is considered to be a major requirement to improve reinforcement load prediction accuracy within the framework of the new design methodology.

9.6 Local Stiffness Factor, Φ_{local}

This factor is related to the distribution factor, in that the local stiffness affects how load is distributed among reinforcement layers with different stiffness and spacing values. The effect of local stiffness appears to be significant for geosynthetic reinforcement, but the available data suggest that it has little effect on steel reinforced wall systems. On the basis of this observation, the exponent "a" has been set to 1.0 for geosynthetics and 0.0 for steel reinforcements. Additional study is needed to determine why there is a difference in the effect of this local

stiffness factor for geosynthetic and steel reinforcements and whether the preliminary values of "a" assigned for this factor are accurate.

9.7 Wall Face Batter Factor, Φ_{fb}

The proposed batter factor is an approximation based on limited empirical evidence. To date, only two wall sections within the database of geosynthetic structures with facing batters are large enough to fully investigate this issue, and no steel reinforced MSE walls are available with significant facing batters. Batter affects the loads in the reinforcement in the backfill, connection loads, and for frictional modular block systems, the connection strength. The analysis provided herein indicates that use of the Coulomb method to account for facing batter excessively reduces reinforcement loads. For frictional modular block faced systems, the hinge height concept also appears to cause too severe a reduction in the connection strength available for the typical range of facing batters used today. The influence of the magnitude of facing batter on reinforcement loads, connection loads, and connection strength in reinforced soil walls is an important area of further research.

9.8 Facing Stiffness Factor, Φ_{fs}

The empirical evidence suggests that facing stiffness has a strong influence on reinforcement loads for walls with modular block facings and full-height propped panel facings (see Chapter 7.0). The methodology proposed in this report to account for facing stiffness effects is admittedly crude and requires further development. It may be especially important to

- develop better approaches to characterize the stiffness of the facing with consideration to its segmental nature (i.e., its efficiency in transferring moment throughout the facing column)
- formulate an improved approach to characterize and quantify the stiffness of flexible faced walls
- obtain data to validate the use of the proposed facing stiffness methodology for very tall walls.

Furthermore, no empirical evidence is currently available to validate the effect of facing stiffness on steel reinforced walls. Because steel is much stiffer than geosynthetic reinforcement, the effect of facing stiffness observed for geosynthetic-reinforced walls may not be as strong for

steel reinforced wall systems. Improved quantification of how facing stiffness and wall toe restraint affect reinforcement loads, especially for steel reinforced walls, is needed.

9.9 Global Reinforcement Stiffness, S_{global}

All of the variables discussed previously affect the correlation between global stiffness and maximum reinforcement loads, as shown by the regression analyses performed to obtain the power function relationship between global stiffness and maximum reinforcement stress within the K-Stiffness method. Hence, the form and magnitude of coefficients that relate the global stiffness parameter to reinforcement loads will need to be reevaluated if other fundamental variable values are refined.

9.10 Application of the K-Stiffness Method to Reinforced Soil Wall Internal Stability Design

Because the new method for estimating reinforcement loads must be in Load and Resistance Factor Design (LRFD) format (i.e., a limit states approach) to be implemented in current public sector design specifications (e.g., AASHTO), multiple full-scale laboratory test walls and field walls are needed to assess the variability in key parameters so that both load and resistance factors can be determined at each of the appropriate limit states. The accuracy of load and resistance factor values can be expected to increase as the database of monitored and instrumented wall structures grows.

Though the proposed design method can accurately predict reinforcement strains, these values need to be better linked to global wall deformations so that serviceability limit state deformations can be accurately predicted and reasonable design criteria can be developed. Some relevant data have been gleaned from full-scale field walls, but at the time of this writing, a strategy for predicting both short-term and long-term deformations is needed.

The development of the K-Stiffness Method has primarily focused on predicting peak reinforcement loads within the wall backfill. Prediction of loads at the connection between the facing and soil reinforcement is also a necessary part of a complete reinforced soil wall design procedure. Internal reinforcement failures that have occurred in full-scale field walls to date may have been, at least in part, the result of poor connections with the facing. How many of these failures can be assigned to fundamental flaws in design and how many to other factors such as

poor construction is a topic of debate in the industry. The influence of connection design on wall performance requires further study if the risk of failure is to be properly quantified. Load factors for connection design must also be determined.

One of the limit states that must be evaluated to implement the new method is the strength limit state to prevent soil failure within the reinforced backfill. To accomplish this, data are needed to assess how much strain can be allowed in the reinforcement without causing the soil to reach a state of failure. This limit reinforcement strain is likely related to the plane strain peak soil shear strain for the backfill. Very few field walls have been taken to a high enough load level to assess this limit state. Necessarily, only an approximate lower bound quantification of the limit reinforcement strain has been provided herein. More research is needed to better quantify this limit strain for a range of backfill soils.

Furthermore, for steel reinforced systems, it has been assumed that the stiffness and deformability of the steel reinforcement are strictly a function of the modulus of the steel and its cross-sectional area per unit of tributary area in the wall. For grid or welded wire reinforcements, the true stiffness may be affected by the deformability of the transverse members of the grid and the spacing between longitudinal members of the grid. This could affect the potential for the reinforcement to allow enough strain in the system to approach a soil failure limit state as well as the stress levels in the reinforcement resulting from the wall's global stiffness. This could possibly affect geogrid reinforced walls as well, if longitudinal grid members are spaced too widely.

A systematic program of monitoring full-scale walls should be carried out in which one key parameter is varied in each test (e.g., reinforcement spacing, facing stiffness/toe restraint, soil modulus and shear strength, soil compaction, foundation stiffness, and reinforcement stiffness). Finally, additional analytical modeling, properly calibrated to match the existing case history data, must be conducted to provide some theoretical verification of the trends observed herein, and to extrapolate the available case history data to a wider range of wall geometry, reinforcement type, and soil materials.

ACKNOWLEDGMENTS

The writers would like to acknowledge the financial support of the Washington State Department of Transportation and the following organizations:

- Alaska Department of Transportation
- Arizona Department of Transportation
- California Department of Transportation
- Colorado Department of Transportation
- Idaho Transportation Department
- Minnesota Department of Transportation
- New York Department of Transportation
- North Dakota Department of Transportation
- Oregon Department of Transportation
- Wyoming Department of Transportation

The writers would also like to acknowledge the financial support of the National Concrete Masonry Association, the Reinforced Earth Company, Natural Sciences and Engineering Research Council of Canada, Academic Research Program of the Department of National Defense (Canada) and grants from the Department of Infrastructure and Environment (DND Canada). In addition the writers would like to acknowledge the contribution of Dave Walters, who assisted with the development of Chapter 4.0 of this report and who performed some of creep and stress relaxation testing and modelling referenced in that chapter. Finally, the writers would like to acknowledge the contributions of Dr. Robert Holtz, Dr. Barry Christopher, Dr. Wei Lee, Dr. Stan Boyle, and Mr. Ryan Berg for reviewing various portions of this document, assistance in gathering data, and for many interesting technical discussions that helped to improve the thinking of the writers during the development of this document.

REFERENCES

AASHTO, 1996, *Standard Specifications for Highway Bridges,* American Association of State Highway and Transportation Officials, Sixteenth Edition, Washington, D.C., USA, 686 p.

AASHTO, 1998, LRFD Bridge Design Specifications, with 2003 Interims, American Association of State Highway and Transportation Officials, Second Edition, Washington, D.C., USA, 686 p.

AASHTO, 2002, *Standard Specifications for Highway Bridges,* American Association of State Highway and Transportation Officials, Seventeenth Edition, Washington, D.C., USA, 686 p.

Adib, M. E., 1988, *Internal Lateral Earth Pressure in Earth Walls*, Doctoral Thesis Submitted to the University of California, Berkeley, California, 376 pp.

Alberto, L. V., 1998, *Studio Teorico E Sperimentale Del Comportamento Statico Di Un Rilevato in Terra Rinforzata*, Dissertation, Universita' Degli Studi di Padova, 285 pp.

Allen, T. M., 1983, *Properties of Geotextiles in Cold Regions Applications*, Transportation Research Report 83-6, Oregon State University.

Allen, T. M., 1991, "Determination of Long-Term Strength of Geosynthetics: a State-of-the-Art Review", *Proceedings of Geosynthetics '91*, Atlanta, GA, USA, Vol. 1, pp. 351-379.

Allen, T. M., 1997, "Viscoelastic Behavior of Geosynthetics in MSB Systems," *Mechanically Stabilized Backfill,* J. T. H. Wu, ed., Balkema, Rotterdam, pp. 401-406.

Allen, T. M., and Bathurst, R. J., 1994, "Characterization of Geosynthetic Load-Strain Behavior After Installation Damage," *Geosynthetics International*, Vol. 1, No. 2, pp. 181-199.

Allen, T. M., and Bathurst, R. J., 1996, "Combined Allowable Strength Reduction Factor for Geosynthetic Creep and Installation Damage," *Geosynthetics International,* Vol. 3, No. 3, pp. 407-439.

Allen, T. M., and Elias, V., 1996, *Durability of Geosynthetics for Highway Applications - Interim Report,* FHWA-RD-95-016, Washington, D.C.

Allen, T. M., and Holtz, R. D., 1991, "Design of Retaining Walls Reinforced with Geosynthetics," *ASCE Geotechnical Engineering Congress*, Vol. II, Geotechnical Special Publication No. 27, Boulder, CO, pp. 970-987.

Allen, T. M., Christopher, B. R., Elias, V., and DiMaggio, J. D., 2001, *Development of the Simplified Method for Internal Stability Design of Mechanically Stabilized Earth (MSE) Walls*, WSDOT Research Report WA-RD 513.1, 108 pp.

Allen, T. M., Christopher, B.R., and Holtz, R.D., 1992, "Performance of a 12.6 m High Geotextile Wall in Seattle, Washington", *Geosynthetic Reinforced Soil Retaining Walls*, J. T. H. Wu (editor), Balkema, Rotterdam, pp. 81-100.

Ang, A. H-S., and Tang, W.H., 1975, *Probability Concepts in Engineering Planning and Design: Volume 1 – Basic Principles*, John Wiley and Sons, New York, NY, USA, 409 pp.

ASTM D4595. *Standard Test Method for Tensile Properties of Geotextiles by the Wide-Width Strip Method. American Society for Testing and Materials*, West Conshohocken, PA, USA.

ASTM D5262. *Standard Test Method for Evaluating the Unconfined Tension Creep Behavior of Geosynthetics*. American Society for Testing and Materials, West Conshohocken, PA, USA.

ASTM D6637. *Standard Test Method for Determining Tensile Properties of Geogrids by the Single or Multi-Rib Tensile Method. American Society for Testing and Materials*, West Conshohocken, PA, USA.

ASTM E328-86. *Standard Test Method for Stress Relaxation for Materials and Structures. American Society for Testing and Materials*, West Conshohocken, PA, USA.

Bathurst, R. J., 1990, "Intrumentation of Geogrid-Reinforced Soil Walls," Transportation Research Record 1277, Washington, DC, pp. 102-111.

Bathurst, R. J., 1992, "Case Study of a Monitored Propped Panel Wall," Proceedings of the International Symposium on Geosynthetic-Reinforced Soil Retaining Walls, Denver, Colorado, pp. 159-166.

Bathurst, R. J., 1993, "Investigation of Footing Restraint on Stability of Large-Scale Reinforced Soil Wall Tests," 46'th Annual Canadian Geotechnical Conference, Saskatoon, Saskatuan, pp. 389-398.

Bathurst, R. J., and Benjamin, D. J., 1990, "Failure of a Geogrid-Reinforced Soil Wall," Transportation Research Record 1288, Washington, D.C., pp. 109-116.

Bathurst, R.J. and Hatami, K., 1998, "Seismic Response Analysis of a Geosynthetic Reinforced Soil Retaining Wall," *Geosynthetics International*, Vol. 5, Nos. 1&2, pp. 127-166.

Bathurst, R. J., Jarrett, P.M., and Lescoutre, S. R., 1988, "An Instrumented Wrap-Around Geogrid Reinforced Soil Wall," Third Canadian Symposium on Geosynthetics, Kitchener, Ontario, pp. 71-78.

Bathurst, R. J., Benjamin, D. J., and Jarrett, P.M., 1989, "An Instrumented Geogrid Reinforced Soil Wall," Proceedings of the 12th International Conference on Soil Mechanics and Foundation Engineering, Rio de Janerio, Brazil, pp. 1223-1226.

Bathurst, R. J., Jarrett, P.M., and Benjamin, D. J., 1993a, "A Database of Results from an Incrementally Constructed Geogrid-Reinforced Soil Wall Test," Reinforcement Des Sols: Experimentations en Vraie Grandeur des Annees 80, Paris, pp. 401-430.

Bathurst, R. J., Simac, M. R., Christopher, B. R., and Bonczkiewicz, C., 1993b, "A Database of Results from a Geosynthetic Reinforced Modular Block Soil Retaining Wall," Renforcement Des Sols: Experimentations en Vraie Grandeur des Annees 80, Paris, pp. 341-365.

Bathurst, R. J., Wawrychuk, W. F., and Jarrett, P. M., 1987, "Laboratory Investigation of Two Large-Scale geogrid Reinforced Soil Walls," *The Application of Polymeric Reinforcement in Soil Retaining Structures*, NATO Advanced Study Institutes Series, Kluwer Academic Publishers, pp. 75-125.

Bathurst, R.J., and Jones, C.J.F.P., 2001, "Chapter 17: Earth Retaining Structures and Reinforced Slopes," *Geotechnical and Geoenvironmental Engineering Handbook*, Kluwer Academic Publishing, Norwell, MA, U.S.A. (R.K. Rowe, Editor) 1088p.

Bathurst, R.J., Simac, M.R., and Sandri, D., 1995, "Lessons Learned from the Construction Performance of a 14m High Segmental Retaining Wall," *Proceedings of Geosynthetics: Lessons Learned from Failures*, Nashville, Tennessee, pp. 15.

Bathurst, R.J., Walters, D., Vlachopoulos, N., Burgess, P., and Allen, T.M., 2000, "Full Scale Testing of Geosynthetic Reinforced Walls", Keynote paper, *ASCE Special Publication No. 103, Advances in Transportation and Geoenvironmental Systems using Geosynthetics, Proceedings of GeoDenver 2000*, Denver, Colorado, pp. 201-217.

Bathurst, R.J., Walters, D.L., Hatami. K., and Allen. T.M., 2001, "Full-scale performance testing and numerical modeling of reinforced soil retaining walls", Special plenary lecture: *International Symposium on Earth Reinforcement*, IS Kyushu 2001, Fukuoka, Japan, 26 p.

Bathurst, R.J., Blatz, J., and Burger, M.H., 2003, "Performance of Full-Scale Reinforced Embankments Loaded to Failure," submitted to *Canadian Geotechnical Journal*.

Bell, J. R., 1998, personal communication.

Bell, J. R., and Barrett, R. K., 1995, "Survivability and Durability of Geotextiles Buried in Glenwood Canyon Wall," *Transportation Research Record 1474*, Washington, DC, pp. 55-63.

Bell, J. R., and Steward, J. E., 1977, "Construction and Observations of Fabric Soil Walls," Proceedings International Conference on Use of Fabrics in Geotechniques, Paris, Vol. 1, pp. 123-128.

Bell, J. R., Barrett, R. K., and Ruckman, A. C., 1983, "Geotextile Earth-Reinforced Retaining Wall Tests: Glenwood Canyon, Colorado," Transportation Research Record 916, Washington, DC, pp. 59-69.

Bell, J. R., Stilley, A. N., and Vandre, B., 1975, "Fabric Retained Earth Walls," Proceedings of the Thirteenth Annual Engineering Geology and Soils Engineering Symposium, University of Idaho, Moscow, Idaho, pp. 271-287.

Bell, J.R., Szymoniak, T. and Thommen, G.R., 1985, "Construction of a Steep Sided Geogrid Retaining Wall for an Oregon Coastal Highway," *Proceedings of the Polymer Grid Reinforcement Conference,* London England, March 22-23, 1984, Thomas Telford, London, pp 198-202.

Benjamin, J. R. S., 1989, *Performance of Full Scale Geogrid Reinforced Soil Retaining Walls*, MEng Thesis, Royal Military College, Kingston, Ontario, 256 pp.

Berg, R. R., 2002, Personal Communication.

Berg, R. R., Allen, T. M., and Bell, J. R., 1998, "Design Procedures for Reinforced Soil Walls - A Historical Perspective," *Proceedings of the Sixth International Conference on Geosynthetics,* Atlanta, GA, Vol. 2, pp. 491-496.

Berg, R.R., Bonaparte, R., Anderson, R. P., and Chouery, V.E., 1986, "Design, Construction, and Performance of Two Geogrid Reinforced Soil Retaining Walls," *Proceedings of the Third International Conference on Geotextiles*, Vienna, pp. 401-406.

Bernardi, M., and Paulson, J., 1997, "Is Creep a Degradation Phenomenon?," Mechanically Stabilized Backfill, J. T. H. Wu, ed., Balkema, Rotterdam, pp. 289-294.

Bolton, M.D. 1986, "The Strength and Dilatancy of Sands," Geotechnique, Vol. 36, No. 1, pp. 65-78.

Boyce, M.C., Socrate, S., and Llana, P.G., 2000, "Constitutive Model for the Finite Deformation Stress-Strain Behaviour of Poly(ethylene Terephthalate) above the Glass Transition", *Polymer*, Vol. 41, No. 6, pp. 2183-2201.

Boyle, S. R., 1995*, Deformation Prediction of Geosynthetic Reinforced Soil Retaining Walls*, Ph.D. Dissertation, University of Washington, 391 pp.

Boyle, S. R., and Holtz, R. D. 1996, "Discussion of 'A Performance Test for Assessment of Long-Term Creep Behavior of Soil-Geosynthetic Composites' by Wu, J. T. H., and Helwany, S. M. B.", *Geosynthetics International*, Vol. 3, No. 4, pp. 551-557.

Boyle, S. R., Gallager, M. and Holtz, R. D., 1996, "Influence of Strain Rate, Specimen, Length and Confinement on Measured Geotextile Properties*," Geosynthetics International*, Vol. 3, No. 2, pp. 205-225.

Boyle, S.R, and Holtz, R.D. 1998, "Measuring Geotextile Strains with Strain Gauges", *Proceedings of the Sixth International Conference on Geosynthetics*, Atlanta, Georgia, Vol 1. pp.517-522.

Bright, D. G., Collin, J. G., and Berg, R. R., 1994, "Durability of Geosynthetic Soil Reinforcement Elements in Tanque Verde Retaining Wall Structures," Transportation Research Record 1439, Washington, DC, pp. 46-54.

Broms, B. B., 1978, "Design of Fabric Reinforced Retaining Structures," Proceedings ASCE Symposium on Earth Reinforcement, Pittsburgh, pp. 282-303.

Burgess, G. P., 1999, *Performance of Two Full-Scale Model Geosynthetic-Reinforced Segmental Walls*, M. S. Thesis, Royal Military College of Canada, Kingston, Ontario, 206 pp.

Bush, D.I. and Swan, D.B.G., 1987, "An Assessment of the Resistance of Tensar SR-2 to Physical Damage during Construction and Testing of a Reinforced Soil Wall," *The Application of Polymeric Reinforcement in Soil Retaining Structures*, NATO Advanced Study Institutes Series, Kluwer Academic Publishers, pp. 173-180.

Bush, D.I., 1990, "Variation of Long-Term Design Strength of Geosynthetics in Temperatures up to 40^{O}C," *Proceedings of the Fourth International. Conference on Geotextiles, Geomembranes, and Related Products*, The Hague, Netherlands, pp. 673-676.

Carrubba, P., Moraci, N., and Montanelli, F., 1999, "Instrumented Soil Reinforced Retaining Wall: Analysis of Measurements," *Geosynthetics '99 Conference Proceedings*, Boston, MA, pp. 921-934.

Cazzuffi, D., and Sacchetti, M., 1999, "Temperature Effects on Tensile-Creep Behaviour of High Strength Geosynthetics," *Geosynthetics '99*, Boston, Vol. 2, pp. 723-734.

Christopher, B. R., 1993, *Deformation Response and Wall Stiffness in Relation to Reinforced Soil Wall Design,* Ph.D. Dissertation, Purdue University, 352 pp.

Christopher, B. R., 1998, Personal Communication.

Christopher, B. R., Holtz, R. D., and Bell, W. D., 1986, "New Test for Determining the In-Soil-Stress-Strain Properties of Geotextiles," *Proceedings of the Third International Conference on Geotextiles*, Vol. 2, Vienna, Austria, pp. 683-686.

Christopher, B. R., Gill, S. A., Giroud, J.-P., Juran, I., Mitchell, J. K., Schlosser, F., and Dunnicliff, J., 1990, *Reinforced Soil Structures, Vol. 1 Design and Construction Guidelines*, FHWA Report FHWA-RD-89-043, 285 pp.

Davis, G.W. and Talbot, J.R., 1985, "Polyester, Fibers", *Encyclopedia Of Polymer Science And Engineering*, Vol 12., Mark, H.F., Bikales, N.M., Overberger, C.G. and Menges, G., Editors, John Wiley & Sons, New York, 858 p.

Delmas, Ph., Blivet, J.C. and Matichard, Y., 1987, "Geotextile-Reinforced Retaining Structures: A few Instrumented Examples," *The Application of Polymeric Reinforcement in Soil Retaining Structures*, NATO Advanced Study Institutes Series, Kluwer Academic Publishers, pp. 285-311.

Desert Earth Engineering, 1989, Experimental Project 1: Ground Modification Techniques - Tensar Geogrid Reinforced Soil Wall, Final Report, FHWA-EP-90-001-005, Federal Highway Administration, Washington, DC, 133 p.

Duncan J.M., Byrne, P., Wong, K.S. and Mabry, P., 1980, "Strength, Stress-Strain and Bulk Modulus Parameters for Finite Element Analyses of Stresses and Movements in Soil Masses", Geotechnical Engineering Report No. UCB/GT/80-01, University if California, Berkeley, 70p.

Ehrlich, M., and Mitchell, J. K., 1994, "Working Stress Design Method for Reinforced Earth Soil Walls," *ASCE Journal of Geotechnical Engineering*, Vol. 120, No. 4, pp. 625-645.

Elias, V., 2001a, *Corrosion/Degradation of Soil Reinforcements for Mechanically Stabilized Earth Walls and Reinforced Soil Slopes*, FHWA-NHI-00-044, Federal Highway Administration, Washington, D.C.

Elias, V., 2001b, *Long-Term Durability of Geosynthetics Based on Exhumed Samples from Construction Projects*, FHWA Report FHWA RD-00-157, 53 pp.

Elias, V., and Christopher, B.R., and Berg, R. R., 2001, *Mechanically Stabilized Earth Walls and Reinforced Soil Slopes - Design and Construction Guidelines*, No. FHWA-NHI-00-043, Federal Highway Administration.

Elias, V., Salman, A., and Goulias, D., 1998, "The Effect of pH, Resin Properties, and Manufacturing Process on Laboratory Degradation of Polyester Geosynthetics," *Geosynthetics International*, Vol. 5, No. 5, pp. 459-490.

Elias, V., Yuan, Z., Swan, R. H., and Bachus, R. C., 1998b, *Development of Protocols for Confined Extension/Creep Testing of Geosynthetics in Highway Applications*, Federal Highway Administration, No. FHWA-SA-97-143.

Fannin, R. J., 1988, *Soil Reinforcement for Norwegian Conditions - An Instrumented Field Study of the Analysis and Design of Geogrid Reinforced Slopes,* Report to the Norwegian Geotechnical Institute.

Fannin, R. J., 1994, "Field Observations on the Load-Strain-Time Behavior of Geogrid Reinforcement," *Canadian Geotechnical Journal*, No. 31, pp. 564-569.

Fannin, R. J., 2001, "Long-Term Variations of Force and Strain in a Steep Geogrid-Reinforced Soil Slope," *Geosynthetics International*, Vol. 8, No. 1, pp. 81-96.

Fannin, R. J., and Hermann, S., 1990, "Performance Data for a Sloped Reinforced Soil Wall," *Canadian Geotechnical Journal*, No. 27, pp. 676-686.

Fannin, R. J., and Hermann, S., 1991, "Creep Measurements on Polymeric Reinforcement," *Geosynthetics '91 Conference*, Atlanta, pp. 561-573.

Gallagher, M. D., 1995, *In-Isolation Wide Width Tests on Geotextiles*, MS Thesis, University of Washington, Seattle, 132 pp.

Gnanendran, C.T., and Selvadurai, A.P.S., 2001. "Strain Measurement and Interpretation of Stabilizing Force in Geogrid Reinforcement", Geotextiles and Geomembranes 19: pp. 177-194.

Gourc, J.-P., and Matichard, Y., 1992, "Development of Geotextile Reinforcement Techniques in France," *Geosynthetic Reinforced Soil Retaining Walls*, J. T. H. Wu (editor), Balkema, Rotterdam, pp. 131-152.

Greenway, D., Bell, J. R., and Vandre, B.,1999, "Snailback Wall - First Fabric Wall Revisited at 25 Year Milestone," *Geosynthetics '99 Conference Proceedings*, Boston, MA, pp. 905-919.

Greenwood, J. H., 1990, "The Creep of Geotextiles," *Proceedings of the Fourth International. Conference on Geotextiles, Geomembranes, and Related Products*, The Hague, Netherlands, pp. 645-650.

Greenwood, J. H., 1997, "Designing to Residual Strength of Geosynthetics Instead of Stress-Rupture," *Geosynthetic International,* Vol. 4, No. 1, pp. 1-10.

Helwany, S. M. B., and Shih, S., 1998, "Creep and Stress Relaxation of Geotextile Reinforced Soils," *Geosynthetics International*, Vol. 5, No. 4, pp. 425-434.

Holtz, R. D., and Kovacs, W. D., 1981, *An Introduction to Geotechnical Engineering*, Printice-Hall, Inc., New Jersey, 733 pp.

Jewell, R. A., and Wroth, C. P., 1987, "Direct Shear Tests on Reinforced Sand," Geotechnique, Vol. 37, No. 1, pp. 53-68.

Jewell, R.A. and Greenwood, J.H., 1988, "Long-Term Strength and Safety in Steep Soil Slopes Reinforced by Polymer Materials", *Geotextiles and Geomembranes*, Vol. 7, Nos. 1 and 2, pp. 81-118.

Kaliakin, V. N., Dechasakulsom, M., and Leshchinsky, D, 2000, "Investigation of the Isochrone Concept for Predicting Relaxation of Geogrids," *Geosynthetics International*, Vol. 7, No. 2, pp. 79-99.

Knight, M. A., Valsangkar, A. J., 1993, "Intrumentation and Performance of Tilt-Up Panel Wall," *Proceedings of the Geosynthetics '93 Conference*, Vancouver, BC, pp. 123-136.

Koutsourais, M., 1995, "Correlating the Creep Strain Component of the Total Strain as a Function of Load-Level for High-Tenacity Polyester Yarns, Geogrids, and Geotextiles," *Proceedings of the Geosynthetics '95 Conference*, Nashville, TN, Vol. 3, pp. 989-1002.

Kuhn, M. R. and Mitchell, J. K., 1993, "New Perspectives on Soil Creep," *Journal of Geotechnical Engineering*, ASCE, Vol. 119, No. 3, pp. 507-524.

Lade and Lee, 1976, "Engineering Properties of Soils," *Report UCLA-ENG-7652*, 145 pp. [As cited by Holtz and Kovacs (1981)].

Leclercq, B., Schaeffner, M., Delmas, Ph., Blivet, J. C., and Matichard, Y., 1990, "Durability of Geotextiles: Pragmatic Approach Used in France," *Proceedings of the Fourth International Conference on Geotextiles, Geomembranes, and Related Products*, The Hague, pp. 679-684.

Lee, K. L., Adams, B. D., and Vagneron, J. J., 1973, "Reinforced Earth Retaining Walls," *Journal, Soil Mechanics Division*, ASCE, Vol. 99, No. SM10, pp. 745-764.

Lee, W. F., 2000, *Internal Stability Analysis of Geosynthetic Reinforced Retaining Walls*, Ph.D. Dissertation, University of Washington, 355 pp.

Leflaive, E., 1988, "Durability of Geotextiles: The French Experience," *Geotextiles and Geomembranes*, No. 7, pp. 23-31.

McCrum, N.G., Buckley, C.P. and Bucknall, C.B., 1988, *Principles of Polymer Engineering*, Oxford University Press, Oxford, 391 pages.

McGown, A., Paine, N., and DuBois, D. D., 1984, "Use of Geogrid Properties in limit Equilibrium Analysis," *Proceedings Symposium on Polymer Grid Reinforcement in Civil Engineering*, Paper No. 1.4, pp. 1-5.

McMahon and Mann Consulting Engineers, 1996, *Addendum #6 Report Tensar Wall Instrument Readings, Tucson, Arizona*, Unpublished Report.

Montanelli, F., 2000 (personal communication).

Murray and Farrar, 1990, "Reinforced Earth Wall on the M25 Motorway at Waltham Cross," *Proceedings of the Institution of Civil Engineers*, Part 1, No. 88, 261-282.

Orsat, P., Khay, M., and McCreath, M., 1998, "Study on Creep-Rupture of Polyester Ttendons: Full Scale Tests," *Proceedings of the Sixth International Conference on Geosynthetics,* Atlanta, GA, Vol. 2, pp. 675-678.

Perkins, S.W., and Lapeyre, J.A., 1997, "In-Isolation Strain Measurement of Geosynthetics in Wide-Width Strip Tension Test," *Geosynthetics International*, Vol. 4, No. 1, pp. 11-32.

Powell, B., and Mohney, J., 1994, "Durability of Geotextiles Used in Reinforcement of Walls and Road Subgrade," Transportation Research Record 1439, Washington, DC, pp. 20-24.

Puig , J., Blivet, J. C., and Pasquet, P., 1977, "Earth Reinforced Fill with Synthetic Fabric," *Proceedings international Conference on the Use of Fabrics in Geotechniques*, Paris, Vol. 1, pp. 85-90.

Rimoldi, P., and Montanelli, F., 1993, "Creep and Accelerated Creep Testing for Geogrids," *Proceedings of the Geosynthetics '93 Conference*, Vancouver, BC, pp. 773-785.

Rowe, R. K., and Ho, S. K., 1993, "Keynote Lecture: A Review of the Behavior of Reinforced Soil Walls," *Earth Reinforcement Practice*, Ochiai, Hayashi, and Otani, ed's, Balkema, Rotterdam, pp. 801-830.

Sabatini, P. J., Pass, D. G., and Bachus, R. C., 1999, *Ground Anchors and Anchored Systems*, Geotechnical Engineering Circular No. 4, FHWA SA-99-015, Washington, DC, 281 pp.

Salman, A., Elias, V., and DiMillio, A., 1998, "The Effect of Oxygen Pressure, Temperature, and manufacturing Processes on Laboratory Degradation of Polyolefin Based Geosynthetics," *Sixth International Conference on Geotextiles, Geomembranes, and Related Products,* Atlanta, GA, Vol. 2, pp. 683-690.

Salman, A., Elias, V., Juran, I., Lu, S., and Pearce, E., 1997, "Durability of Geosynthetics Based on Accelerated Laboratory Testing," Geosynthetics '97, IFAI, San Diego, CA, pp. 217-234.

Saunders, D. 2001. The Performance of Two Full-Scale Reinforced Segmental Soil Retaining Walls, Master of Engineering Thesis, Civil Engineering Department, Royal Military College of Canada, May 2001, 304p.

Sawicki, A., 1999, "Rheological Model of Geosynthetic-Reinforced Soil", *Geotextiles and Geomembranes*, Vol. 17, pp 33-49.

Schlosser, F., Hoteit, N., and Price, D., 1993, "Instrumented Full Scale Freyssisol-Websol Reinforced Wall," Reinforcement Des Sols: Experimentations en Vraie Grandeur des Annees 80, Paris, pp. 299-320.

Simac, M.R., Bathurst, R.J., Berg, R.R., and Lothspeich, S.E., 1993, *National Concrete Masonry Association Segmental Retaining Wall Design Manual*, National Concrete masonry Association, Herdon, Virginia, USA, 250 p.

Soong, T.-Y. and Koerner, R.M., 1998, "Modelling and Extrapolation of Creep Behaviour of Geosynthetics", *Proceedings of the 6th International Conference on Geosynthetics*, Vol. 2, Atlanta, Georgia, USA, March 1998, pp. 707-710.

Soong, T.-Y. and Lord, A.E., Jr., 1998, "Slow Strain Rate Modulus Assessment Via Stress Relaxation Experiments", *Proceedings of the 6th International Conference on Geosynthetics*, Vol. 2, Atlanta, Georgia, USA, March 1998, pp. 711-714.

Steward, J., Williamson, R., and Mohney, J., 1977, *Guidelines for the Use of Fabrics in Construction and Maintenance of Low-Volume Roads*, Report No. FHWA-TS-78-205.

Tatsuoka, F. 1993, "Keynote Lecture: Roles of Facing Rigidity in Soil Reinforcing," *Earth Reinforcement Practice*, Ochiai, Hayashi, and Otani, ed's, Balkema, Rotterdam, pp. 831-870.

Thornton, J. S., Allen, S. R., and Thomas, R. W., 1997, "Approaches for the Prediction of Long Term Viscoelastic Properties of Geosynthetics from Short Term Tests," *Geosynthetics '97*, IFAI, Long Beach, CA, Vol. 1, pp. 277-291.

Thornton, J.S., 2001, "Characterization of Short and Long Term Creep and relaxation properties of a Polypropylene Geogrid", *Geosynthetics 2001*, IFAI, Portland, Oregon, pp. 835-845.

Vlachopoulos, N., 2000, *The Performance of Two Full-Scale Model Geosynthetic-Reinforced Walls: Segmental and Wrapped-Face*, M. S. Thesis, Royal Military College of Canada, Kingston, Ontario, 242 pp.

Voskamp, W. and van Vliet F., 2001, "Variation in Creep Rate at Constant Loading of PET Geogrid Strapping", *Landmarks in Earth Reinforcement*, Vol. 1, Ochiai, H., Otani, J, Yasufuku, N. and Omine, K., Editors, A.A. Balkema, Lisse, 159-164 p.

Walters, D. (2001) personal communication.

Washington State Department of Transportation, 1998, "Determination of Long-Term Strength of Geosynthetics," *WSDOT Test Method 925*, FOSSC Materials Laboratory, Tumwater, WA.

Wilding, M.A. and Ward, I.M., 1981, "Creep and Recovery of Ultra High Modulus Polyethylene", *Polymer*, Vol. 22, pp. 870-876.

Williams, J.G., 1980, *Stress Analysis of Polymers,* 2nd Edition, Ellis Horwood Limited, Chichester, John Wiley & Sons, New York, 360 pp.

Wilson-Fahmy, R. F., Koerner, R. M., and Fleck, J. A., 1993, "Unconfined and Confined Width Width Tension Testing of Geosynthetics," *Geosynthetic Soil Reinforcement Testing Procedures*, ASTM STP 1190, pp.

Yako, M. A., and Christopher, B. R., 1987, "The Application of Polymeric Reinforcement in Soil Retaining Structures," *NATO Advanced Study Institutes Series*, Kluwer Academic Publishers.

Yeo, K. C., 1985, *The Behavior of Polymeric Grids Used for Soil Reinforcement*, Ph.D. Dissertation, University of Strathclyde, pp.185 + Appendices.

Yuan, Z., Swan, R. H., Jr., and Bachus, R. C. 1998, "Soil Confinement Effect on Stress-Strain Properties of Geosynthetics," *Proceedings of the Sixth International Conference on Geosynthetics*, Atlanta, GA, pp. 523-528.

Zhang, C. and Moore, I.D., 1997, "Nonlinear Mechanical Response of High Density Polyethylene, Part II: Uniaxial constitutive modeling", *Polymer Engineering and Science*, Vol. 37, No. 2, pp. 414-420.

Zornberg, J. G., Sitar, N., and Mitchell, J. K., 1998(a), "Performance of Geosynthetic Reinforced Slopes at Failure," Journal of Geotechnical and Geoenvironmental Engineering, ASCE, Vol. 124, No. 8, pp. 670-683.

Zornberg, J. G., Sitar, N., and Mitchell, J. K., 1998(b), "Limit Equilibrium as basis for Design of Geosynthetic Reinforced Slopes," Journal of Geotechnical and Geoenvironmental Engineering, ASCE, Vol. 124, No. 8, pp. 684-698.

ADDITIONAL RESOURCES

Elias, V., DiMaggio, J., and DiMillio, A., 1997, "FHWA Technical Note on the Degradation-Reduction Factors for Geosynthetics," *Geotechnical Fabrics Report*, Vol. 15, No. 6, pp. 24-26.

Federal Highway Administration (FHWA), 1997, "Degradation Reduction Factors for Geosynthetics," *Federal Highway Administration Geotechnology Technical Note*.

Lescoutre, S. R., 1986, *The Development of a Large Scale Facility for Reinforced Soil Retaining Walls*, M.S. Thesis, Royal Military College of Canada, Kingston, Ontario, 294 pp.

Leshchinsky, D., Dechasakulsom, M., Kaliakin, V. N., and Ling, H. I., 1997, "Creep and Stress Relaxation of Geogrids," *Geosynthetics International*, Vol. 4, No. 5, pp. 463-479.

APPENDIX A: T_{MAX} DISTRIBUTIONS AS A FUNCTION OF DEPTH BELOW THE WALL TOP

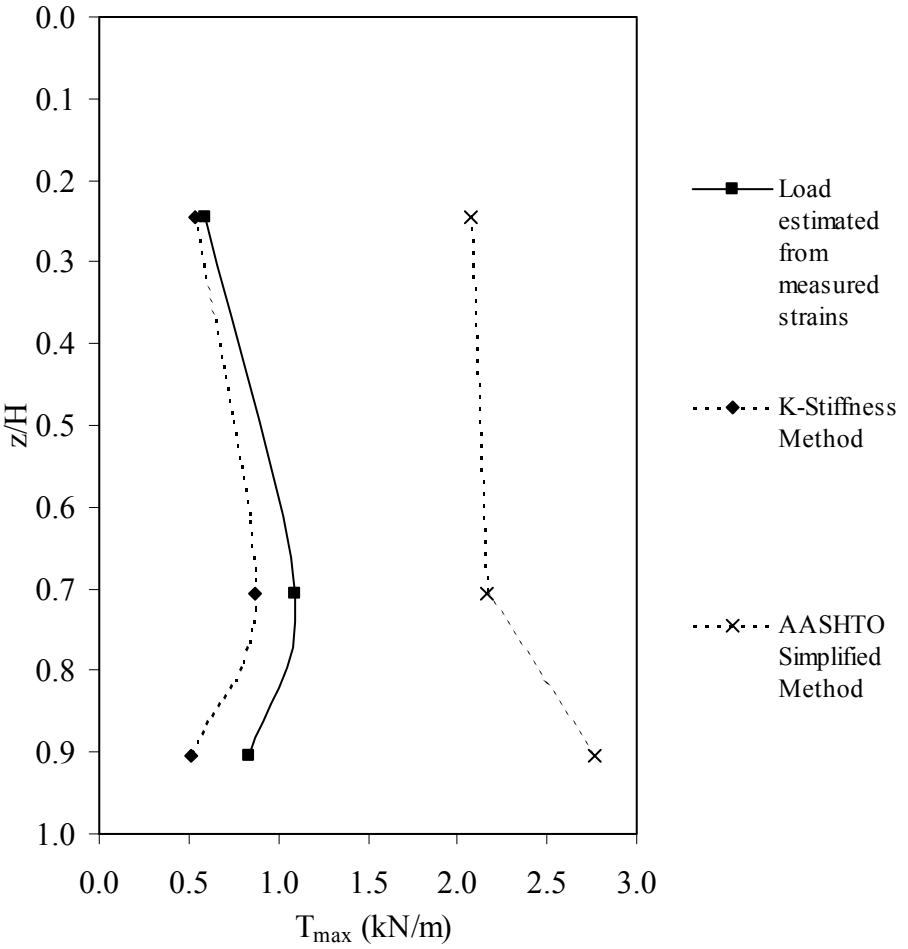

Figure A.1. T_{max} as a function of depth below wall top for Wall GW5 (plane strain ϕ_{ps}).

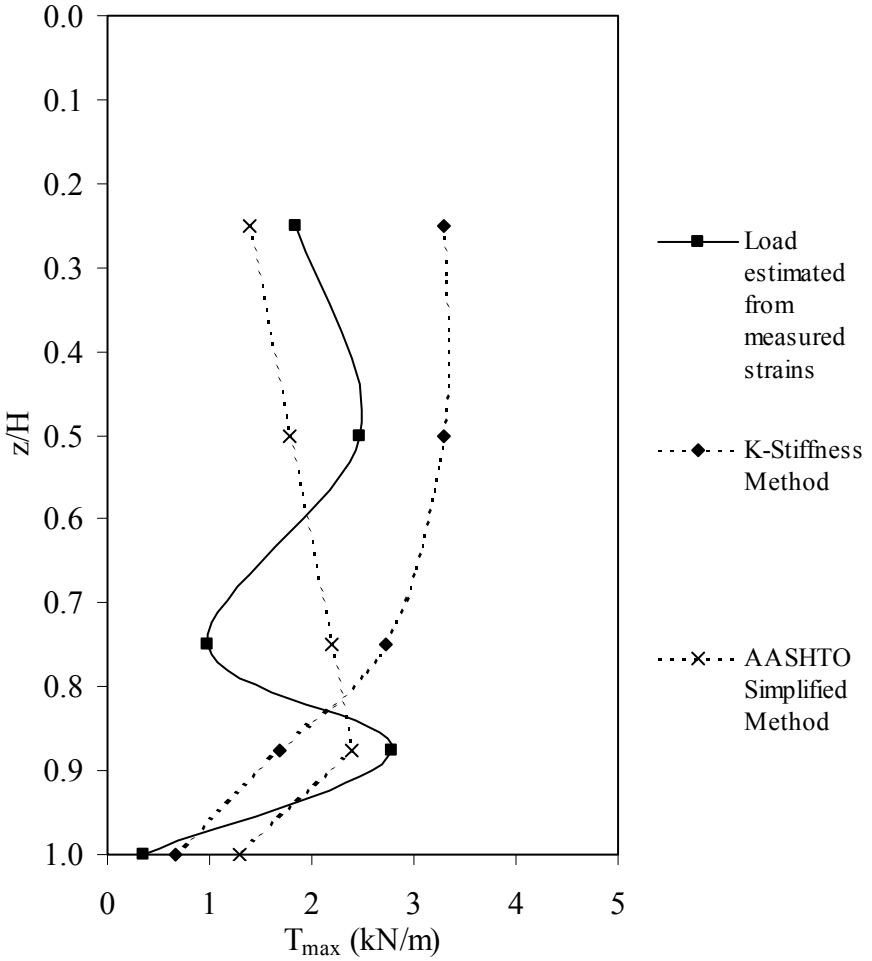

Figure A.2. T_{max} as a function of depth below wall top for Wall GW7 (Section J - plane strain ϕ_{ps}).

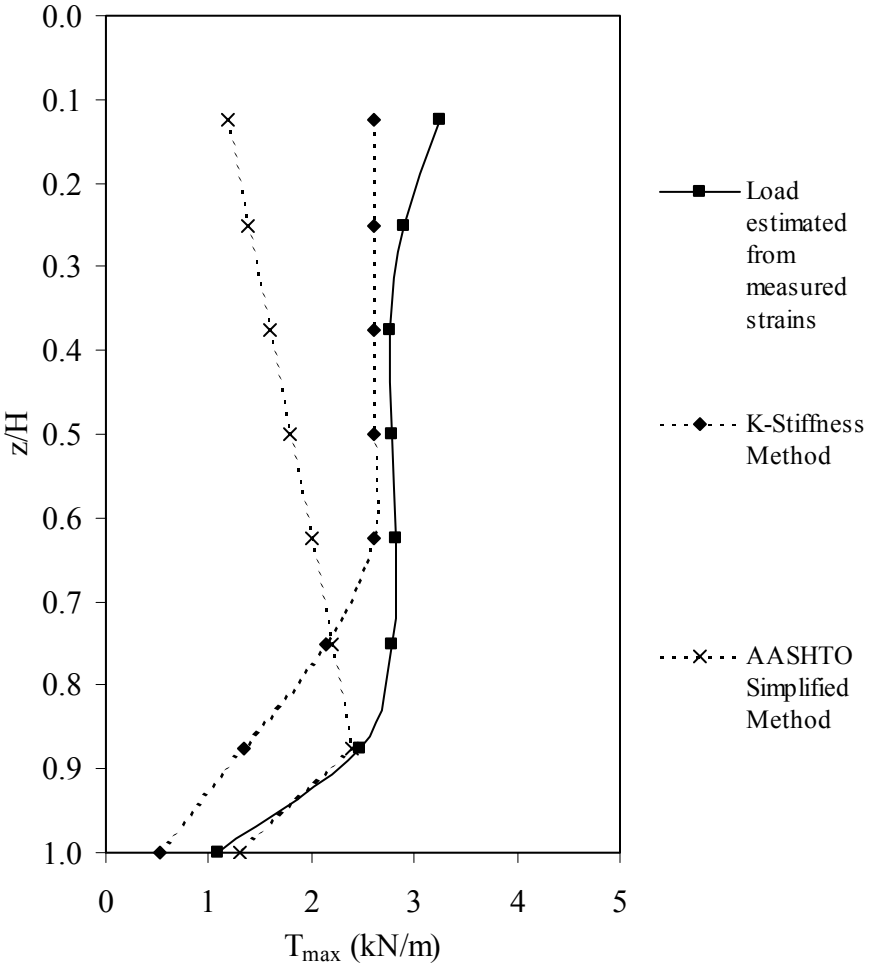

Figure A.3. T_{max} as a function of depth below wall top for Wall GW7 (Section N - plane strain ϕ_{ps}).

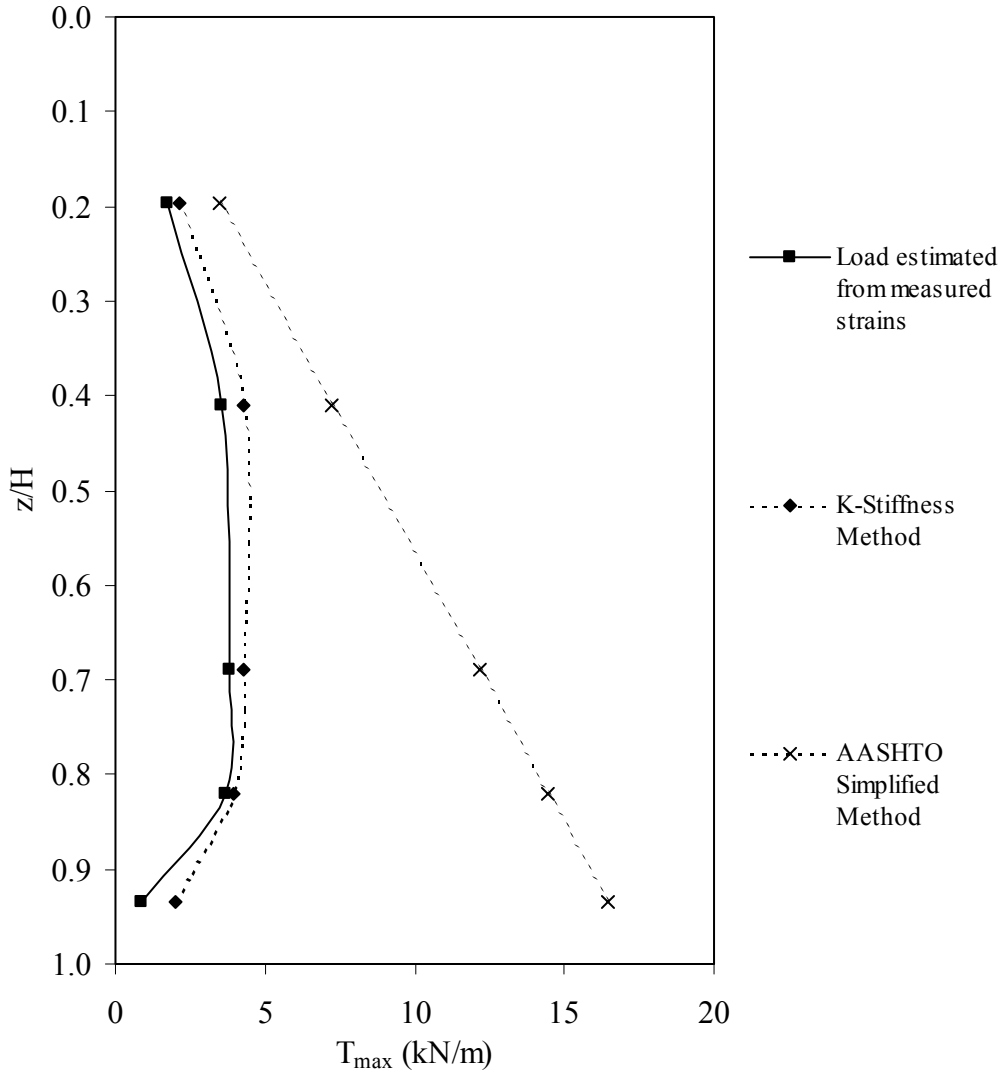

Figure A.4. T_{max} as a function of depth below wall top for Wall GW8 (plane strain ϕ_{ps}).

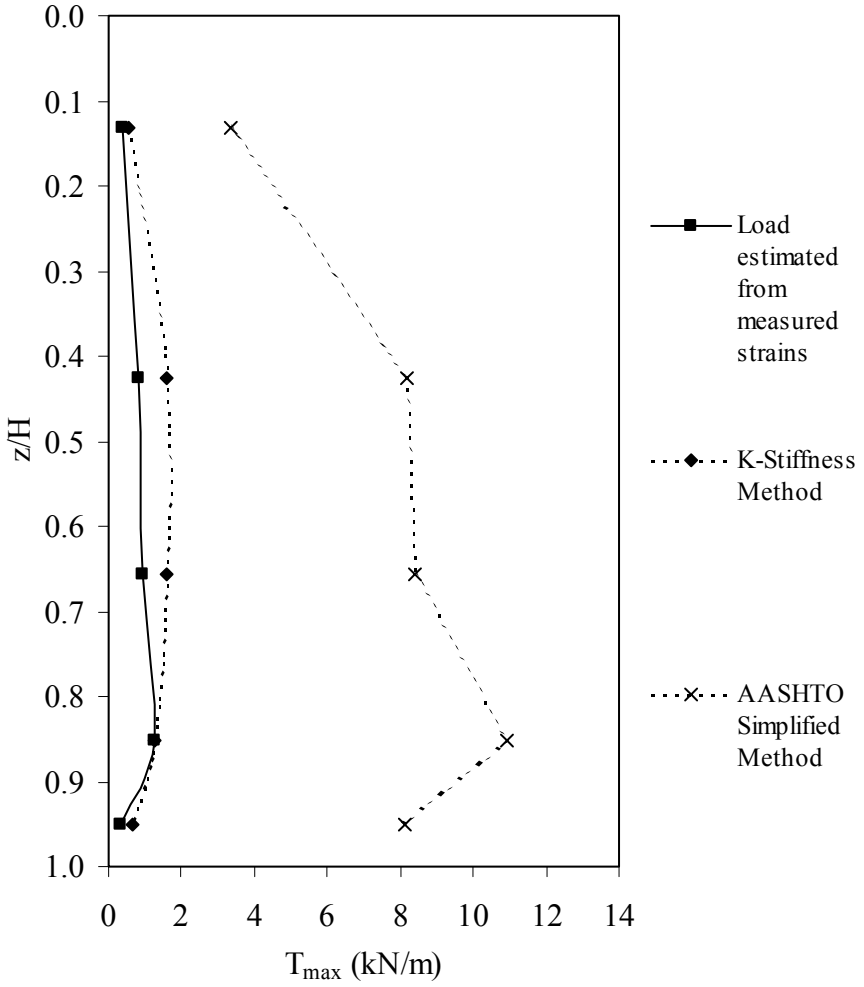

Figure A.5. T_{max} as a function of depth below wall top for Wall GW9 (no surcharge - plane strain ϕ_{ps}).

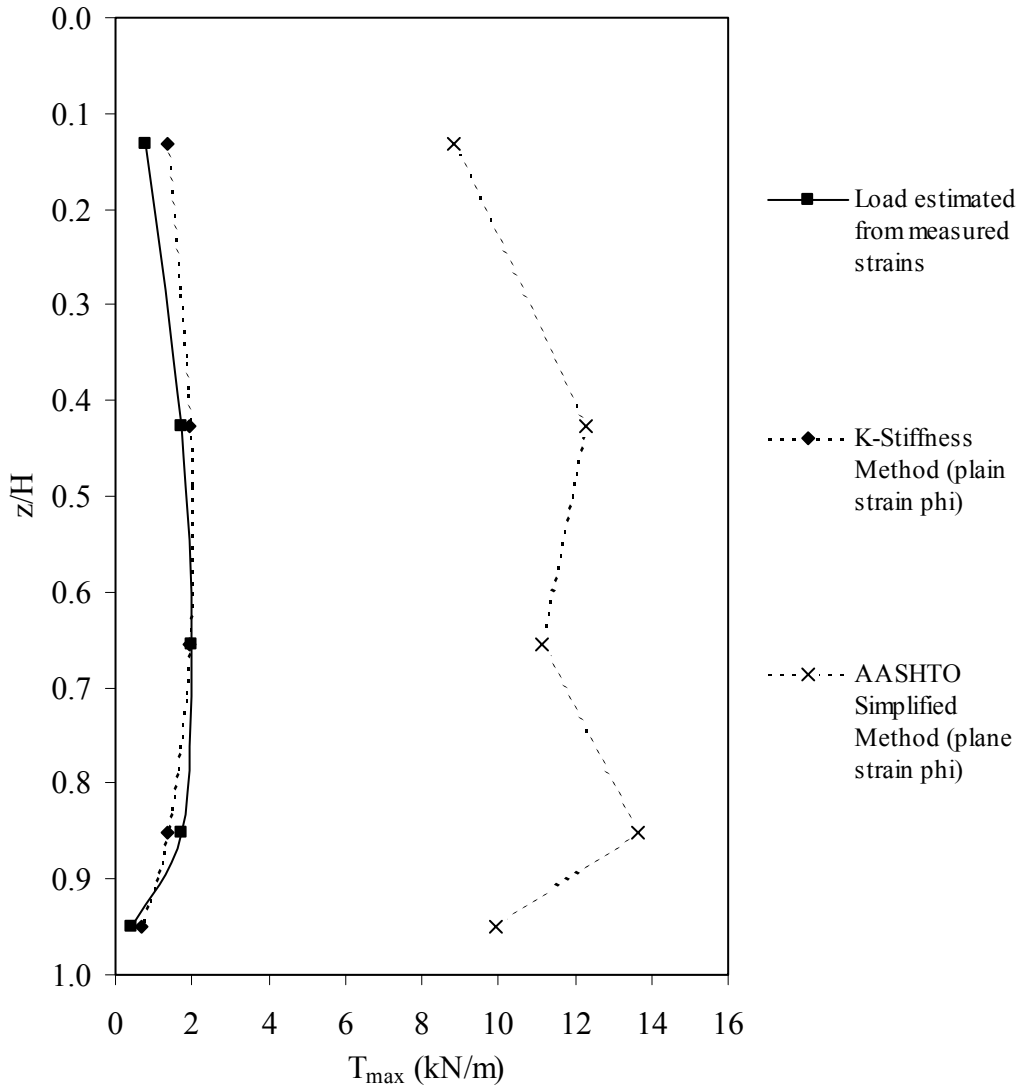

Figure A.6. T_{max} as a function of depth below wall top for Wall GW9 (with surcharge - plane strain ϕ_{ps}).

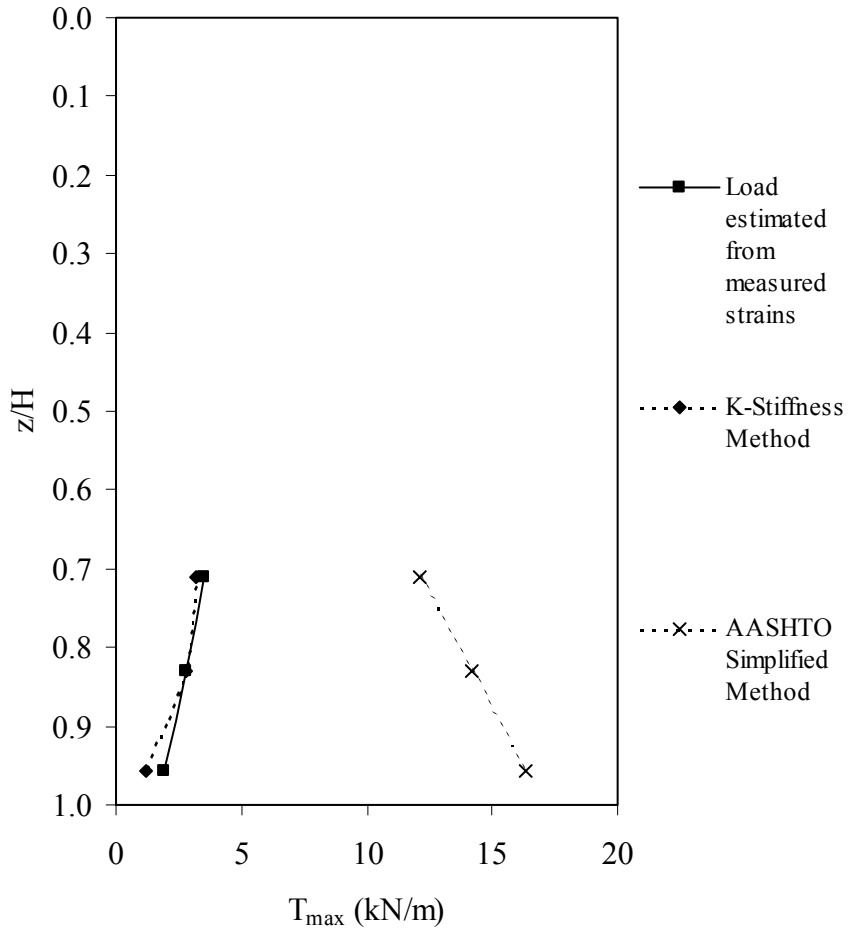

Figure A.7. T_{max} as a function of depth below wall top for Wall GW10 (after water restraint removed - plane strain ϕ_{ps}).

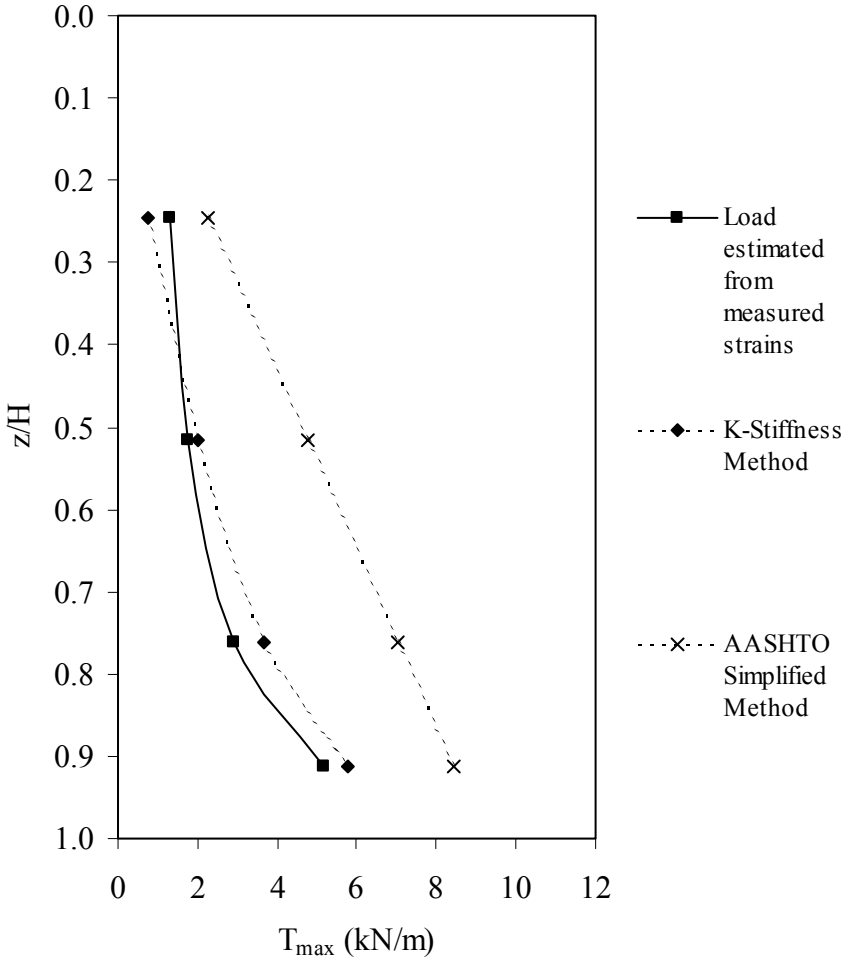

Figure A.8. T_{max} as a function of depth below wall top for Wall GW16 (no surcharge - plane strain ϕ_{ps}).

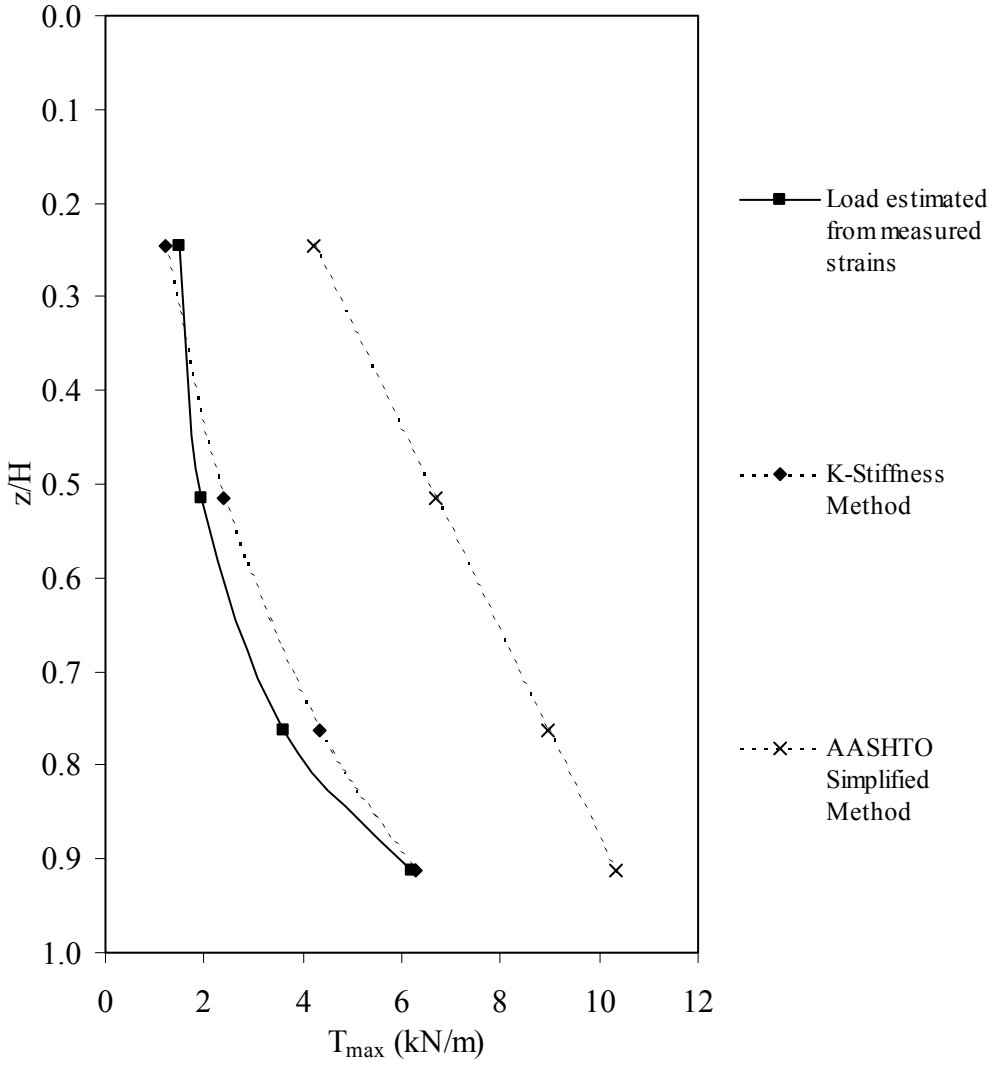

Figure A9. T_{max} as a function of depth below wall top for Wall GW16 (with surcharge - plane strain ϕ_{ps}).

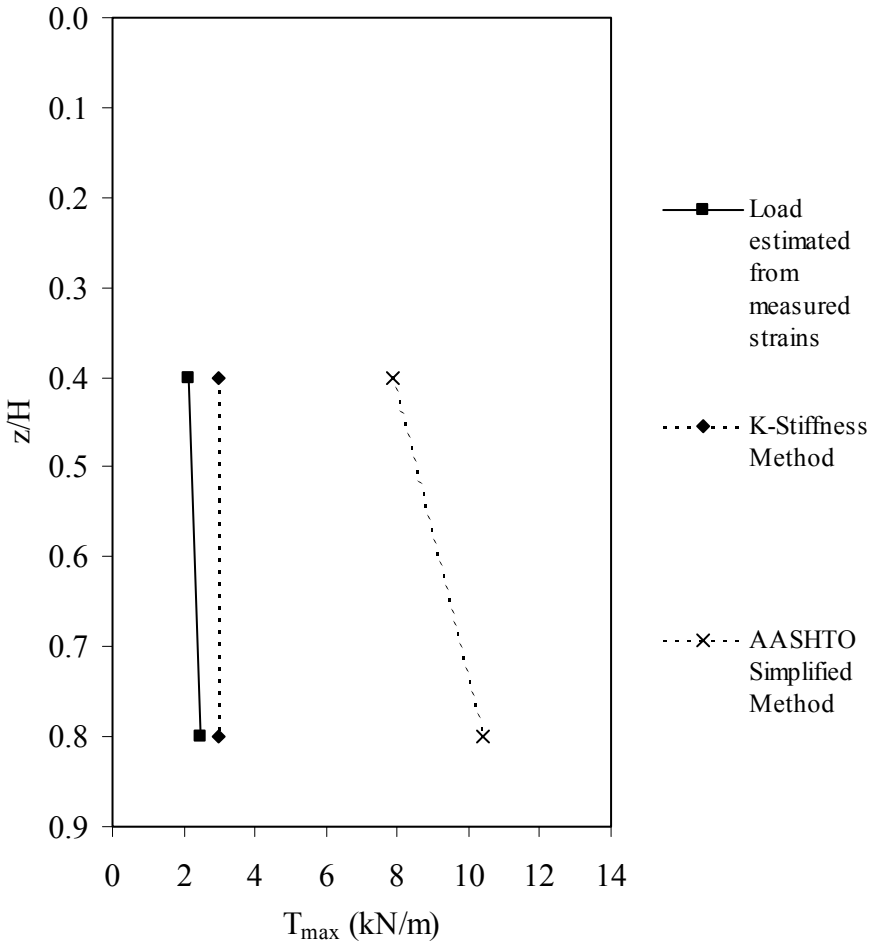

Figure A10. T_{max} as a function of depth below wall top for Wall GW18 (plane strain ϕ_{ps}).

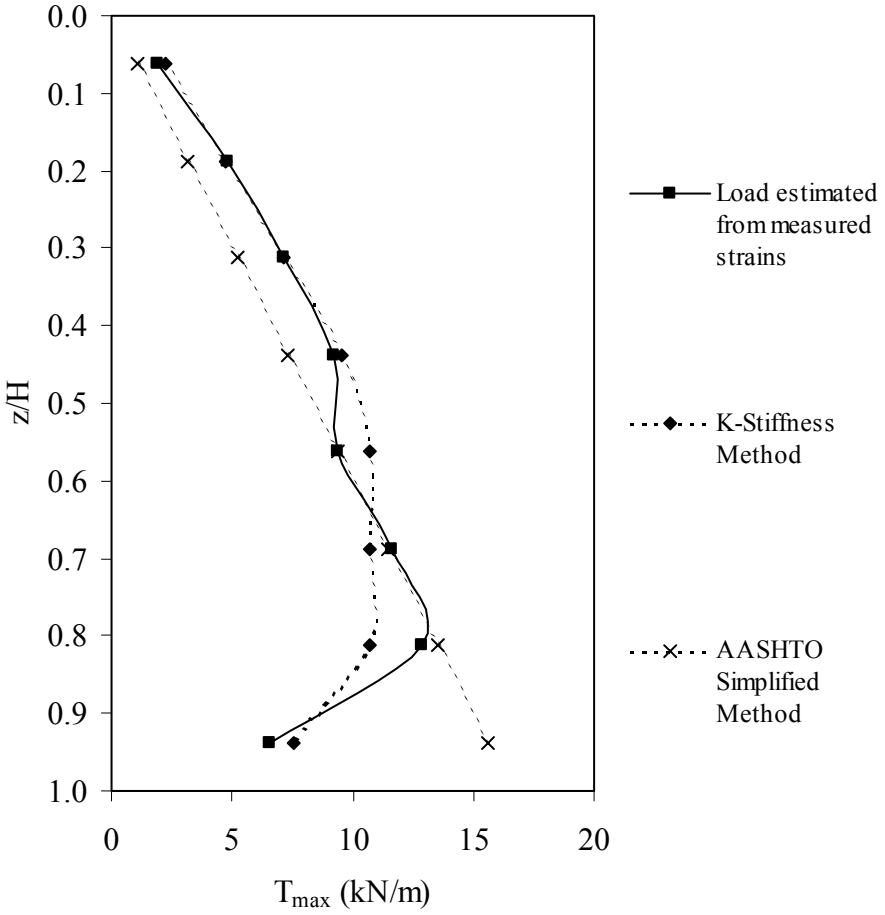

Figure A11. T_{max} as a function of depth below wall top for Wall GW19 (plane strain ϕ_{ps}).

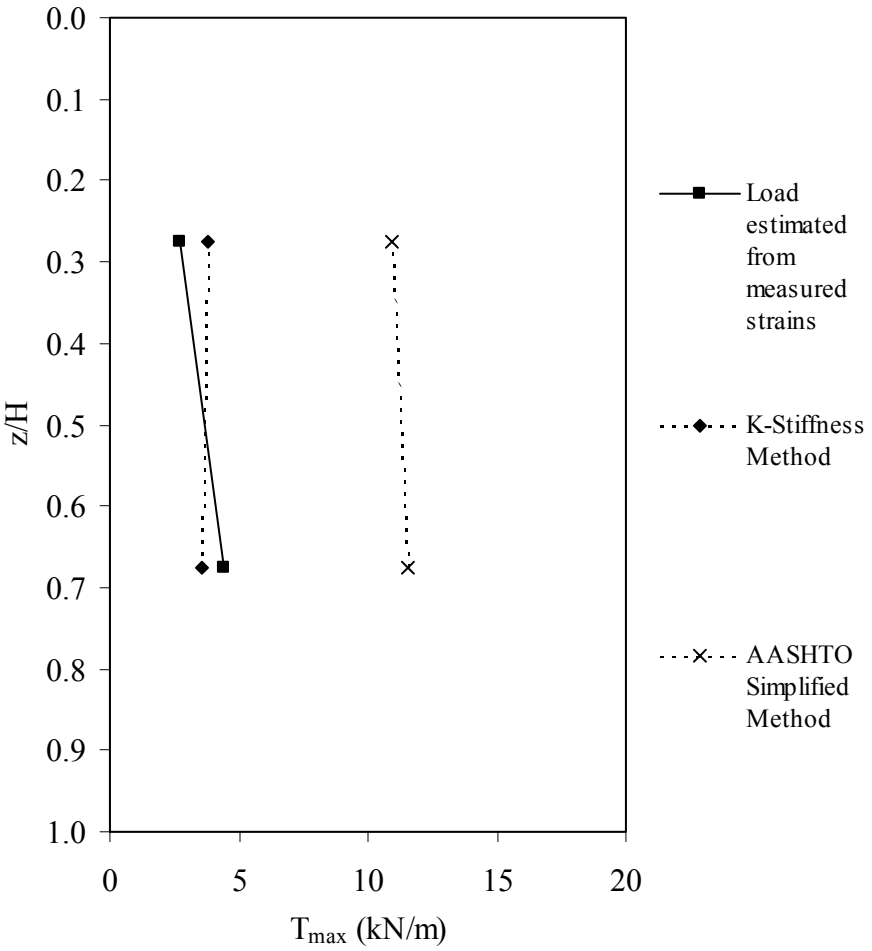

Figure A12. T_{max} as a function of depth below wall top for Wall GW20, HDPE Section (with surcharge - plane strain ϕ_{ps}).

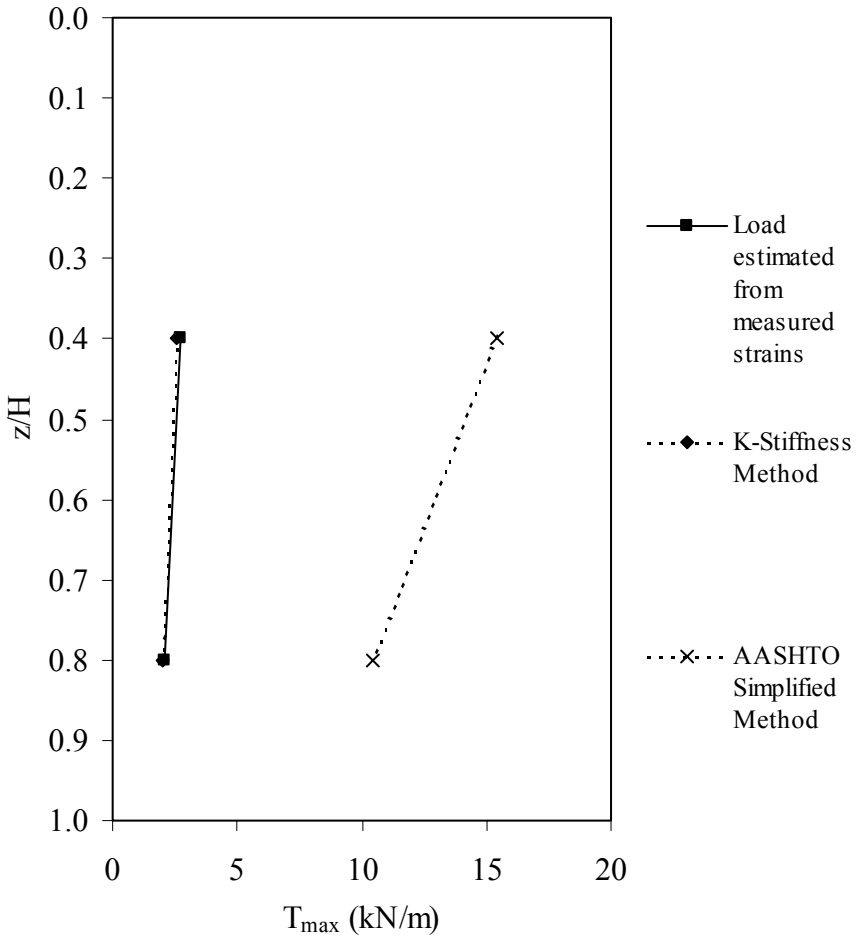

Figure A13. T_{max} as a function of depth below wall top for Wall GW20, PP Section (with surcharge - plane strain ϕ_{ps}).

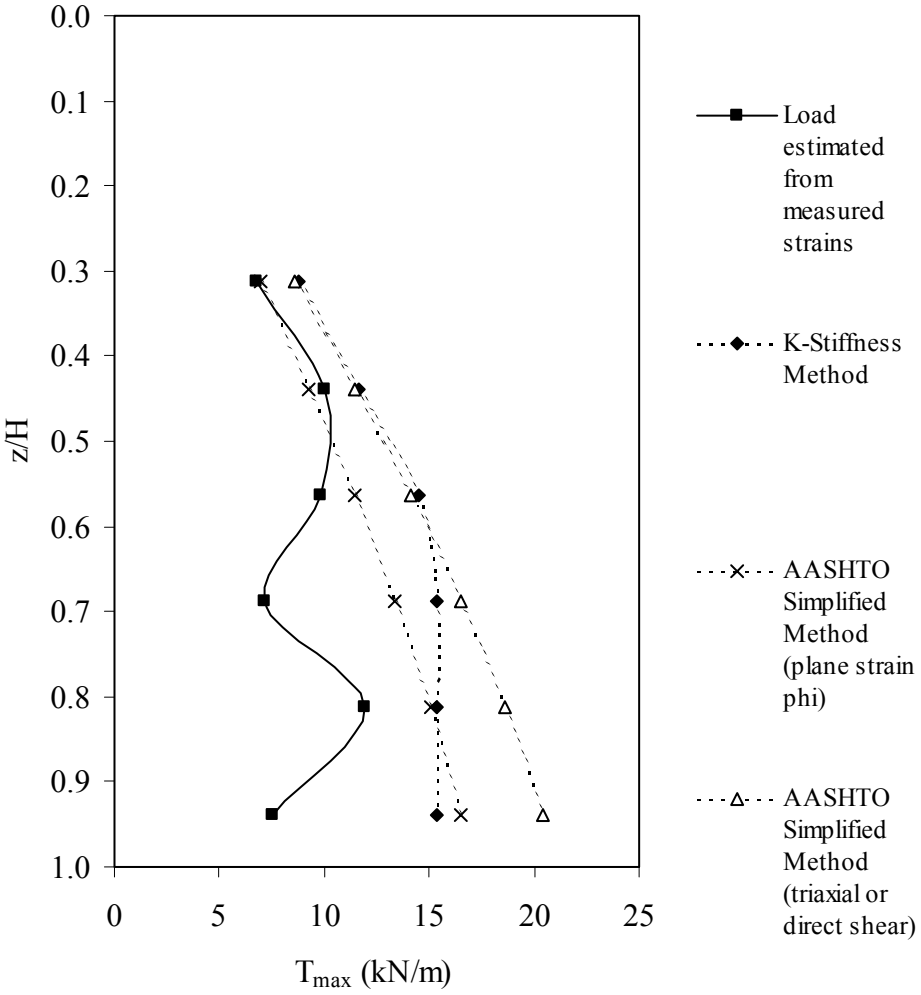

Figure A14. Measured and predicted T_{max} as a function of depth below wall top for Wall SS1.

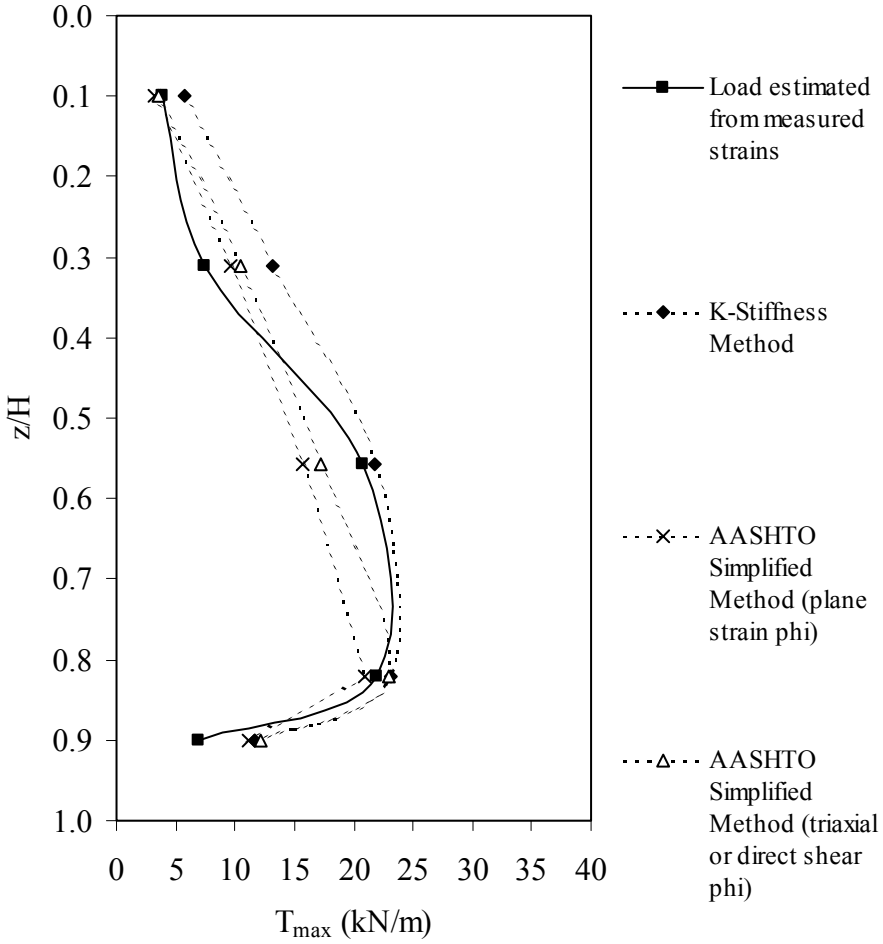

Figure A15. T_{max} as a function of depth below wall top for Wall SS2.

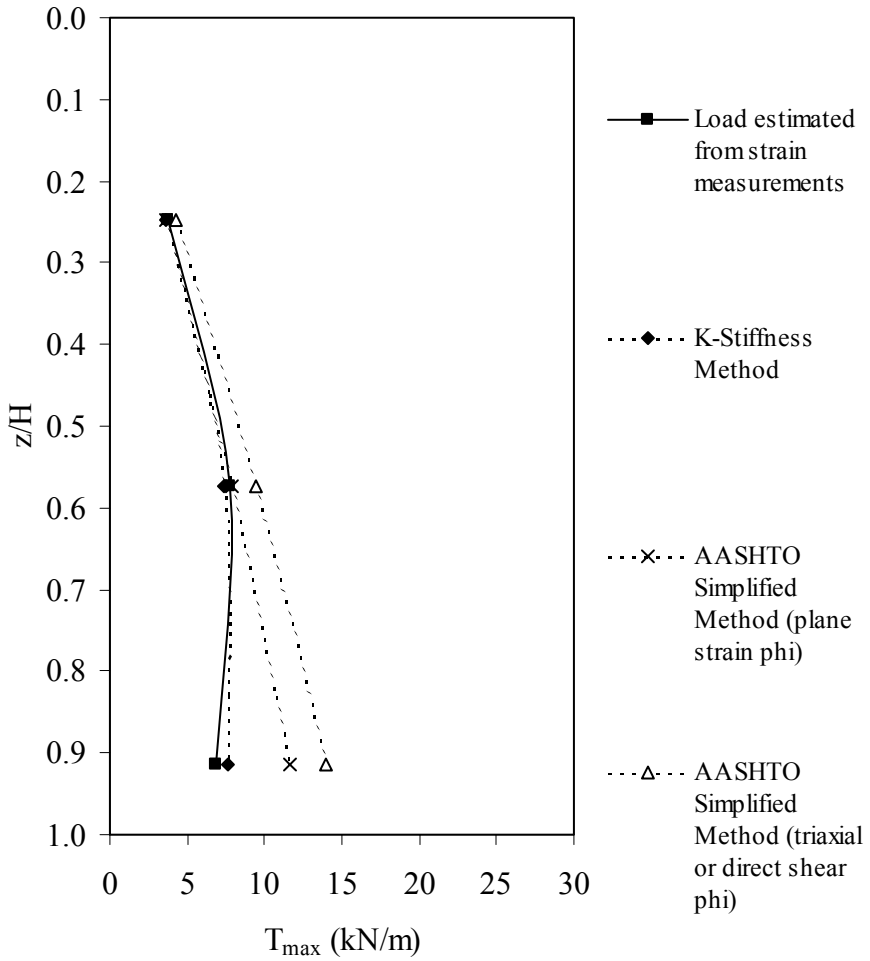

Figure A16. T_{max} as a function of depth below wall top for Wall SS3 (no surcharge).

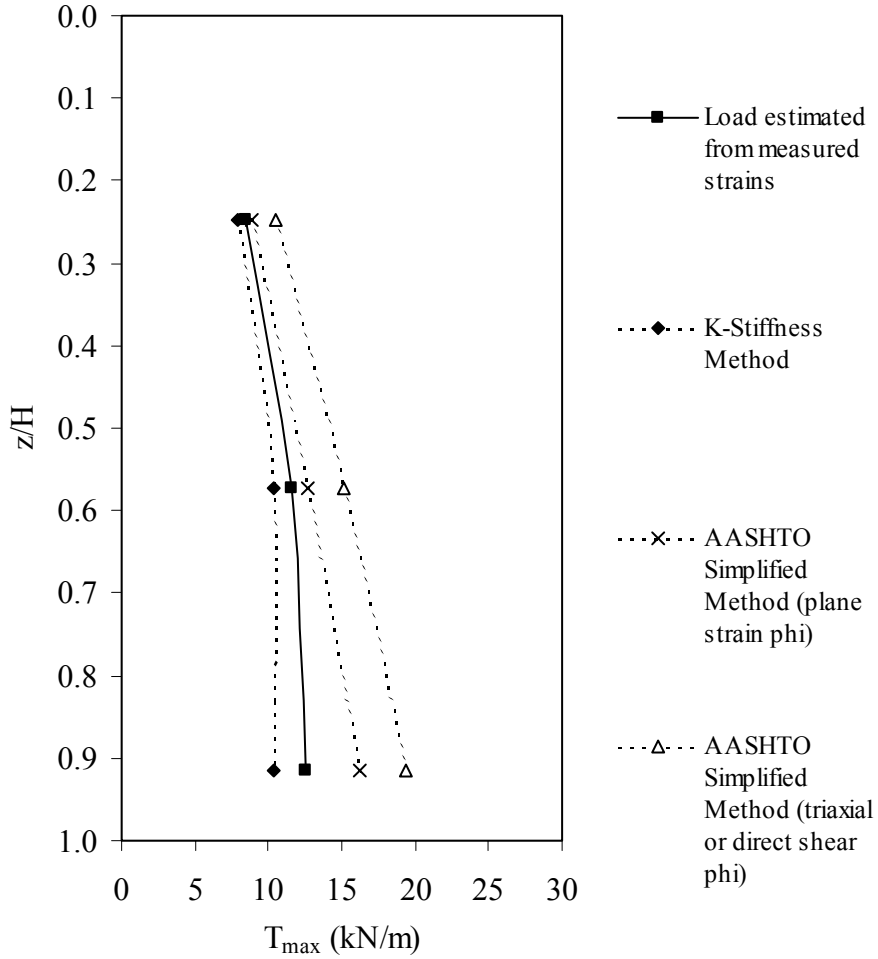

Figure A17. T_{max} as a function of depth below wall top for Wall SS3 (24 kPa surcharge).

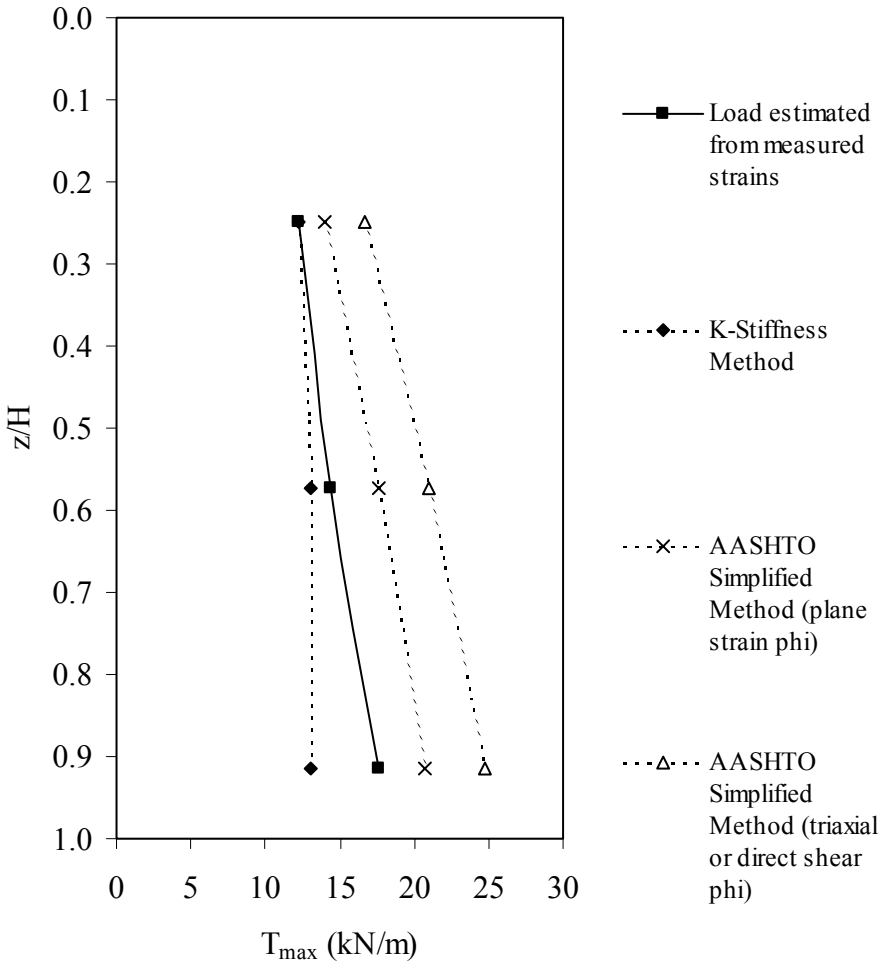

Figure A18. T_{max} as a function of depth below wall top for Wall SS3 (48 kPa surcharge).

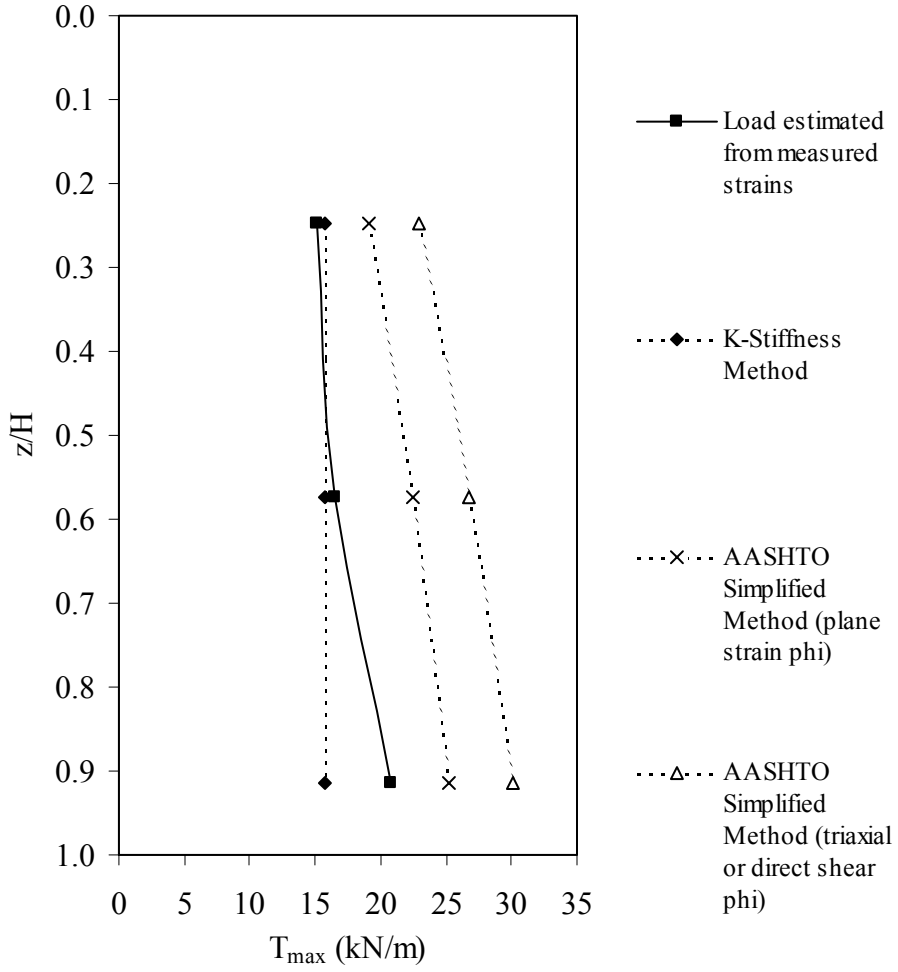

Figure A19. Measured and predicted T_{max} as a function of depth below wall top for Wall SS3 (72 kPa surcharge).

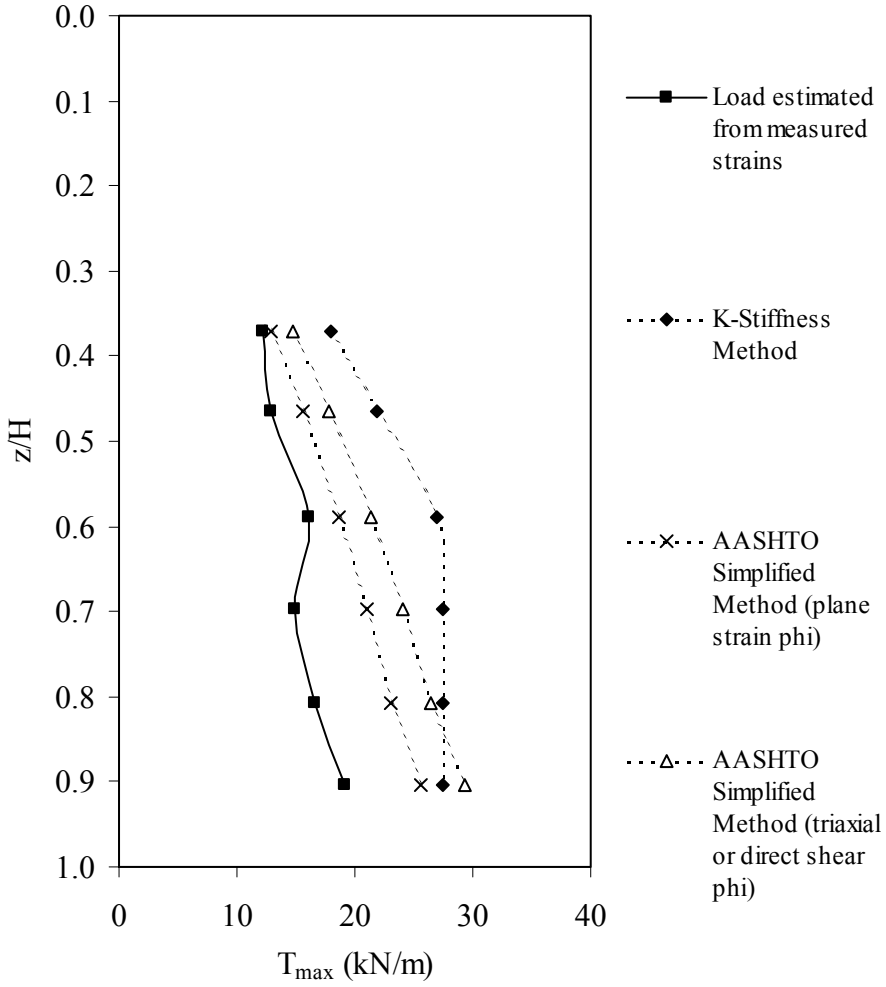

Figure A20. T_{max} as a function of depth below wall top for Wall SS4.

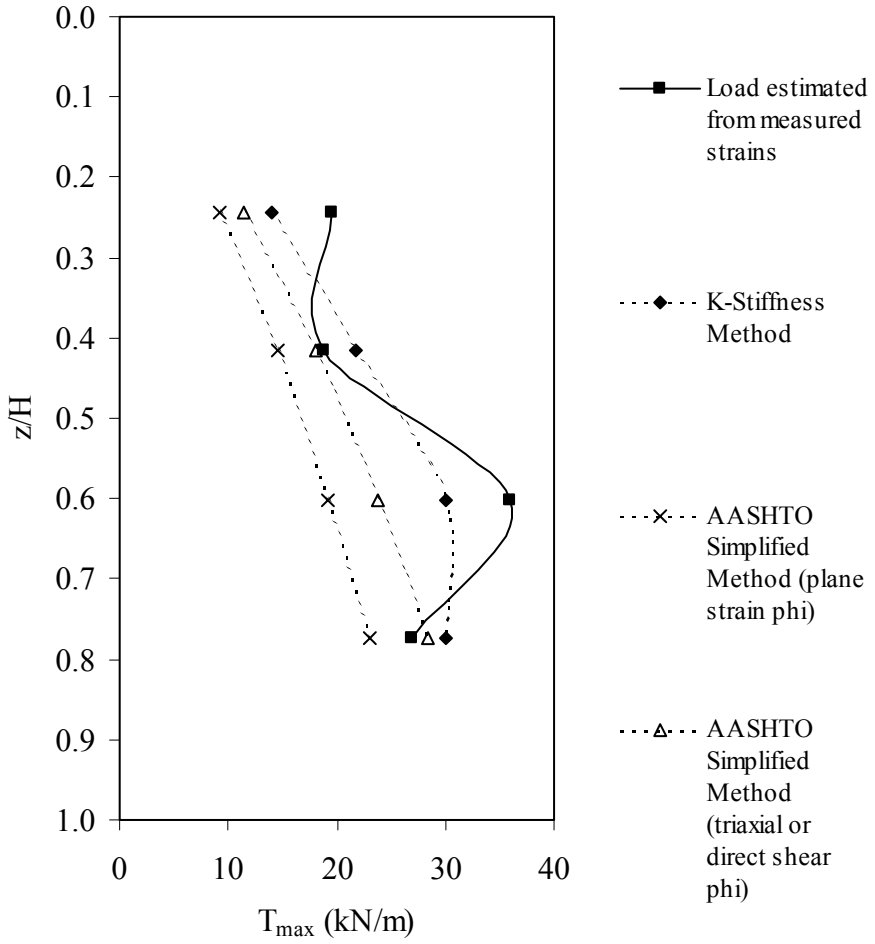

Figure A21. T_{max} as a function of depth below wall top for Wall SS5.

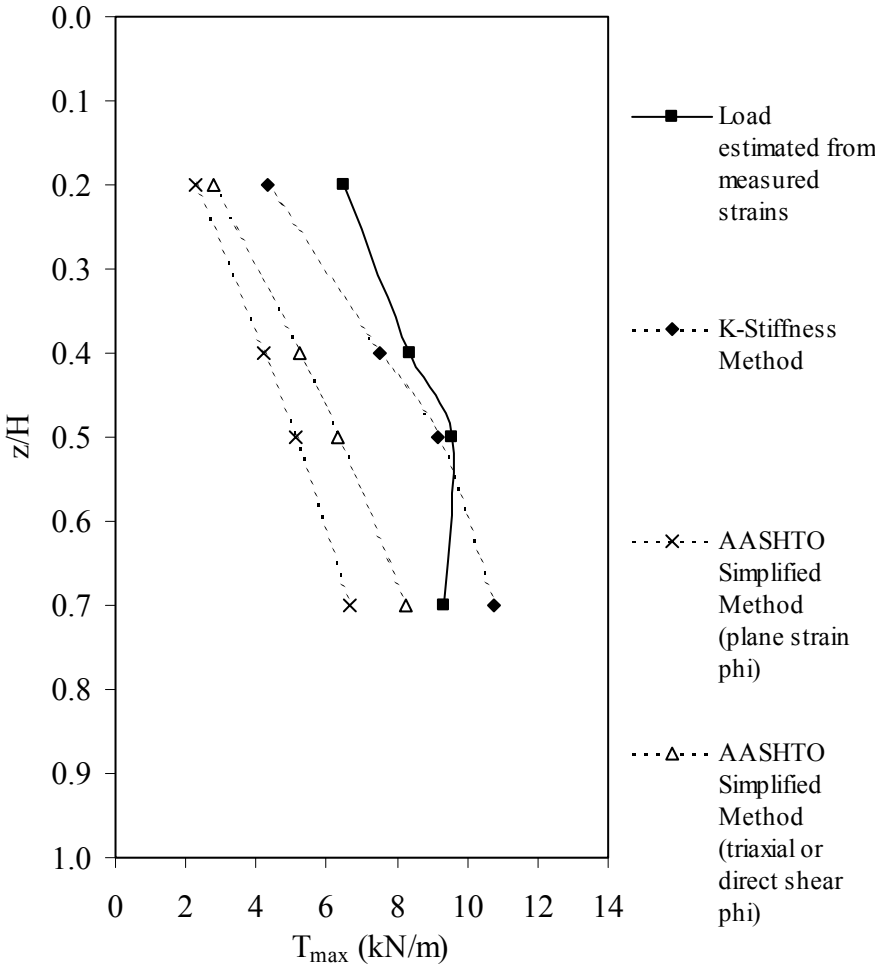

Figure A22. T_{max} as a function of depth below wall top for Wall SS6 (Section A).

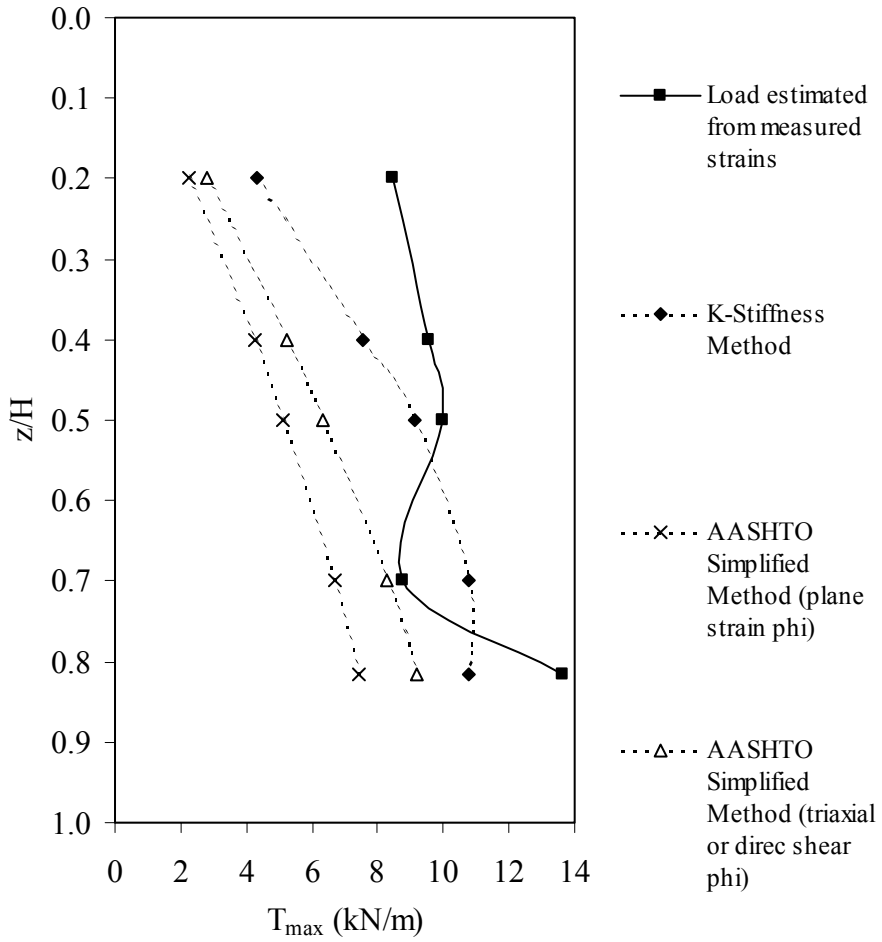

Figure A22. T_{max} as a function of depth below wall top for Wall SS6 (Section B).

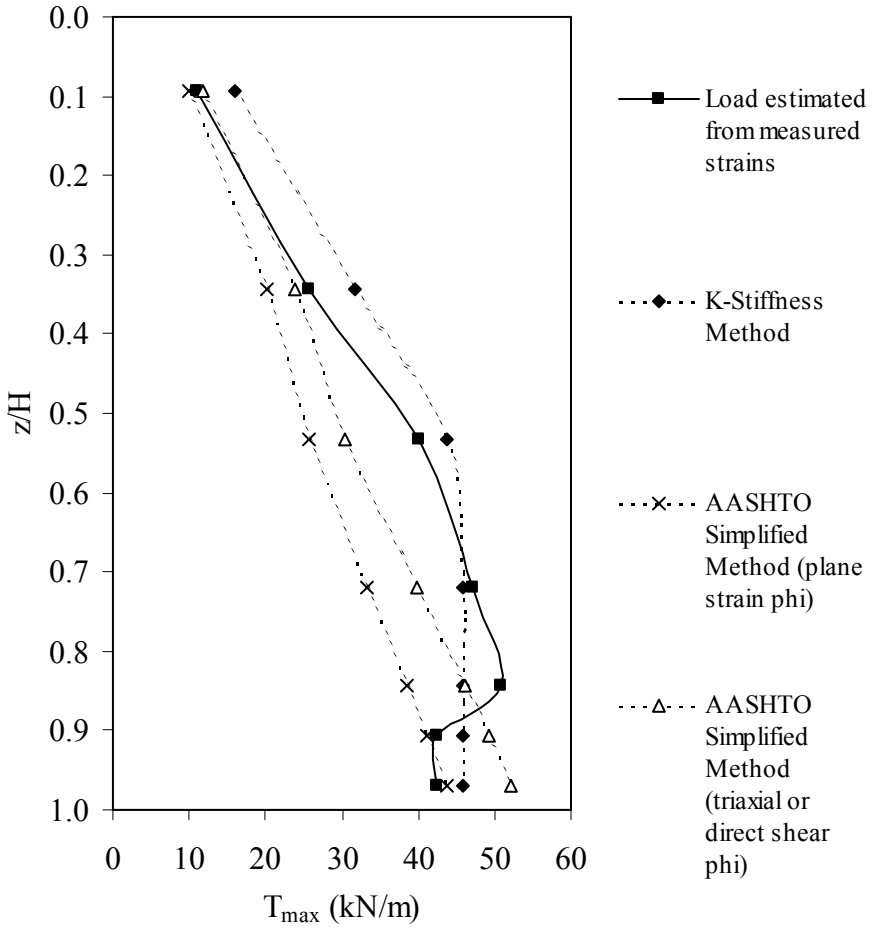

Figure A23. T_{max} as a function of depth below wall top for Wall SS7.

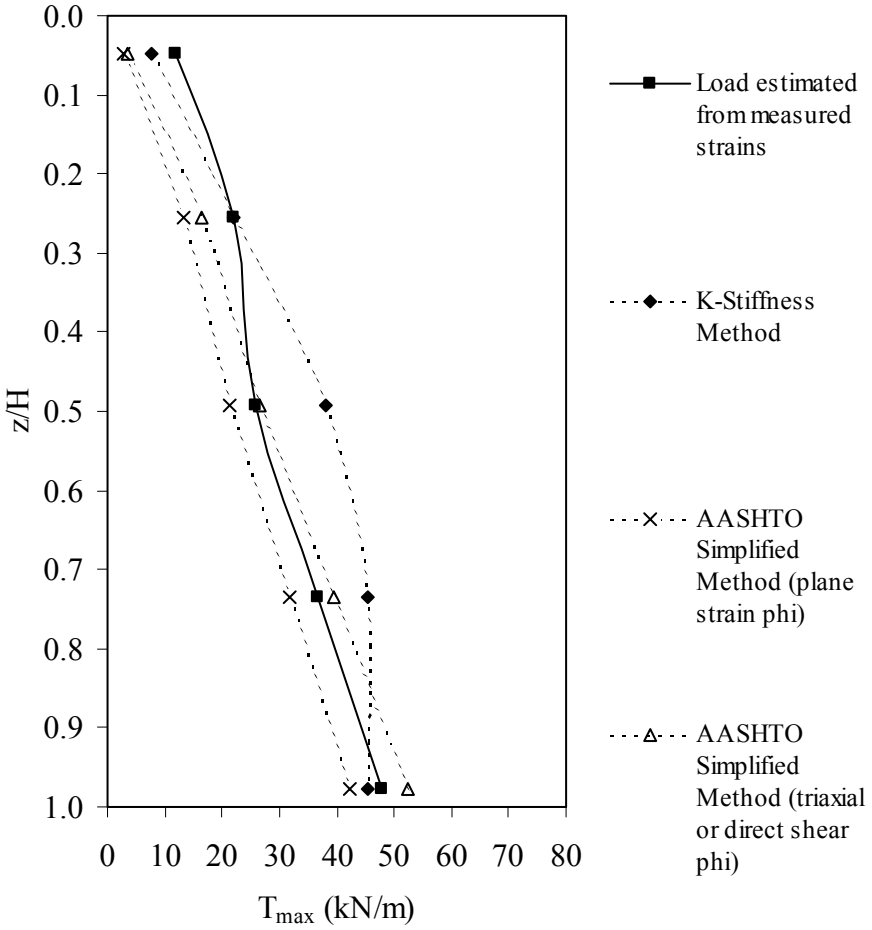

Figure A24. T_{max} as a function of depth below wall top for Wall SS10.

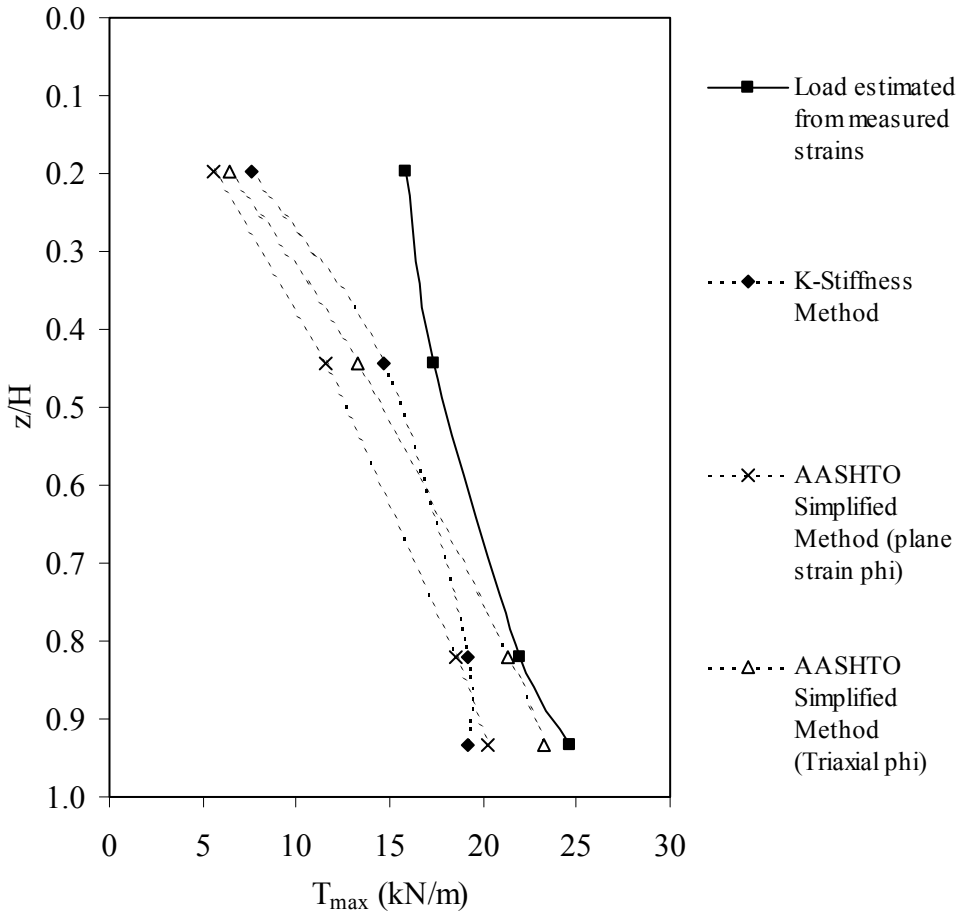

Figure A25. T_{max} as a function of depth below wall top for Wall SS11.

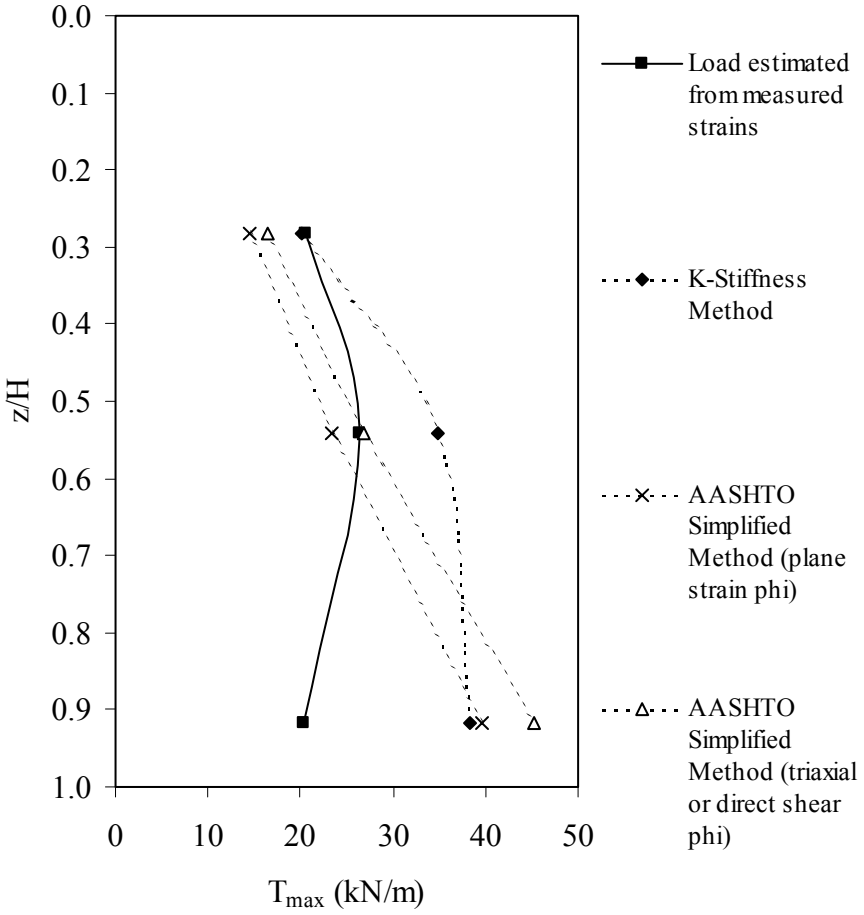

Figure A26. T_{max} as a function of depth below wall top for Wall SS12 (no surcharge).

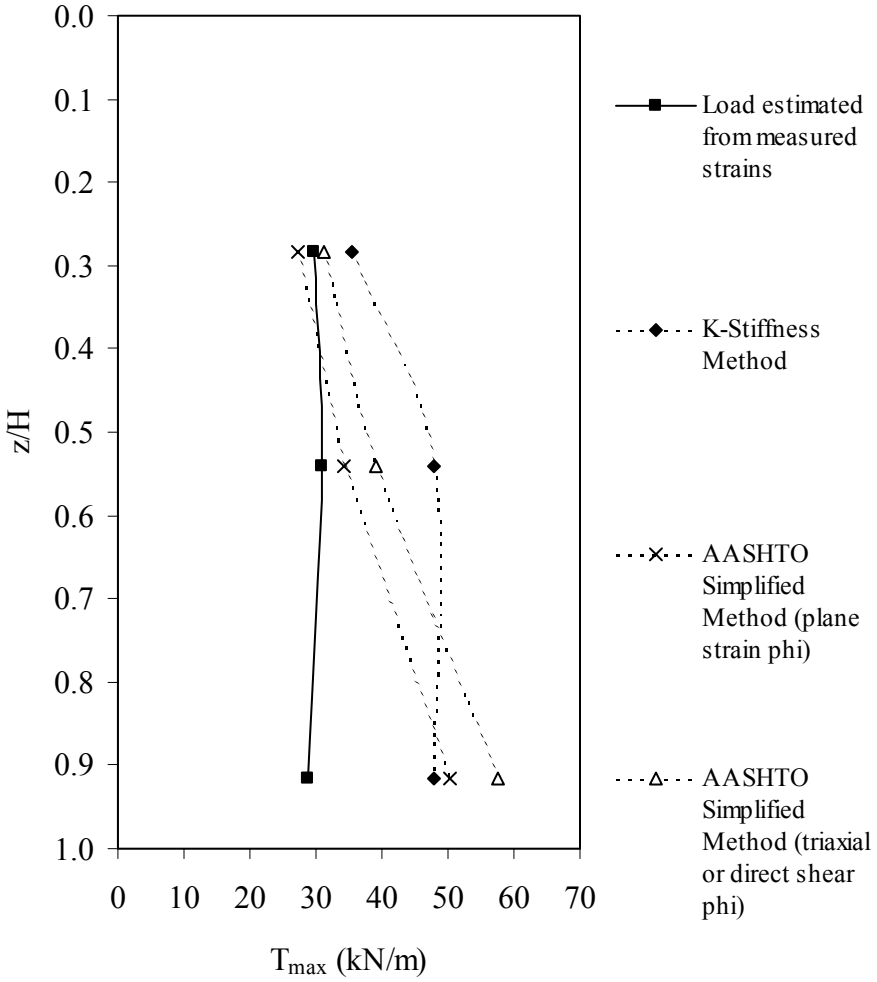

Figure A27. T_{max} as a function of depth below wall top for Wall SS12 (with surcharge).

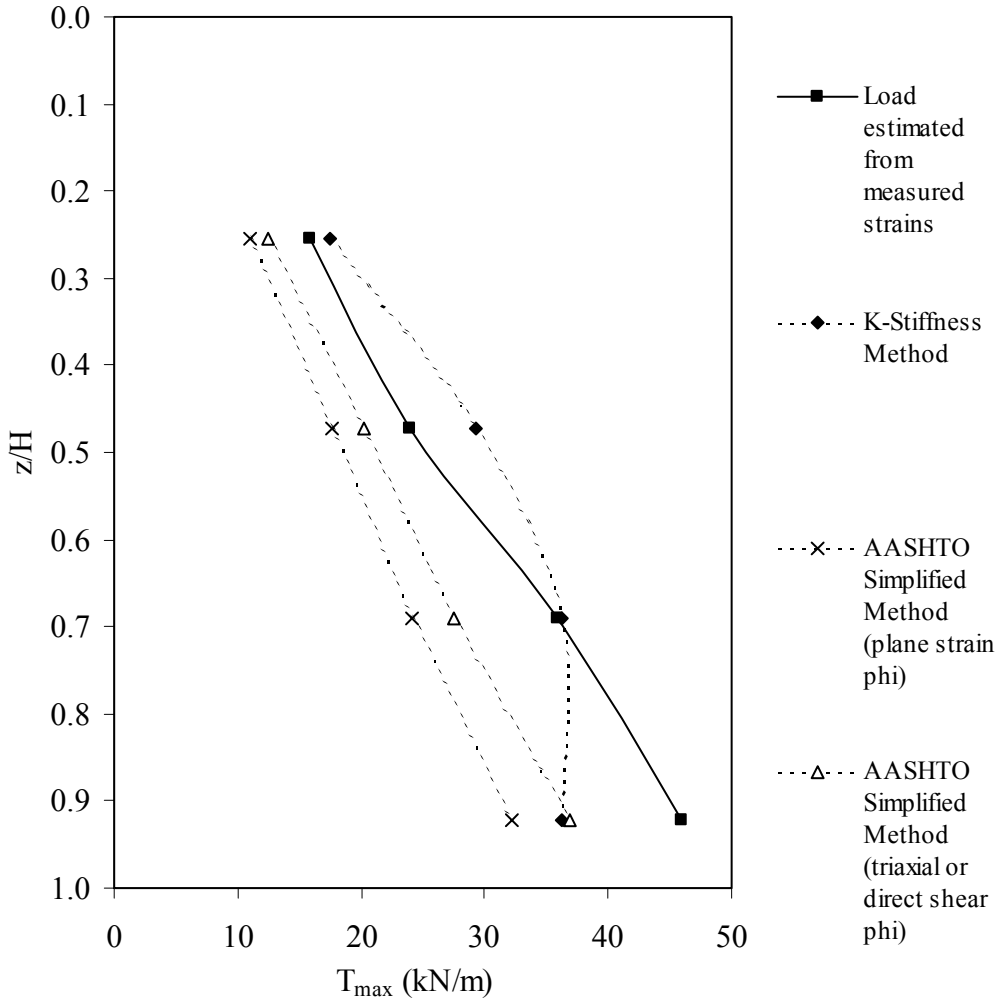

Figure A28. T_{max} as a function of depth below wall top for Wall SS13 (rectangular section).

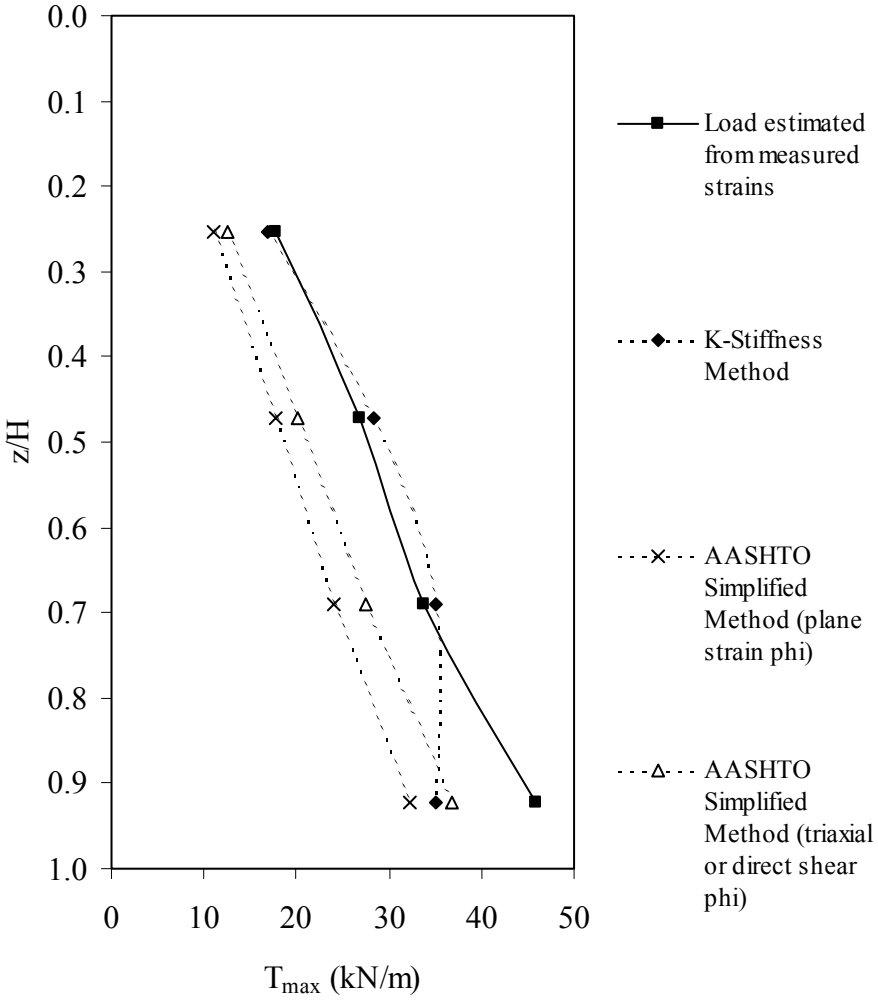

Figure A29. T_{max} as a function of depth below wall top for Wall SS14 (trapezoidal section).

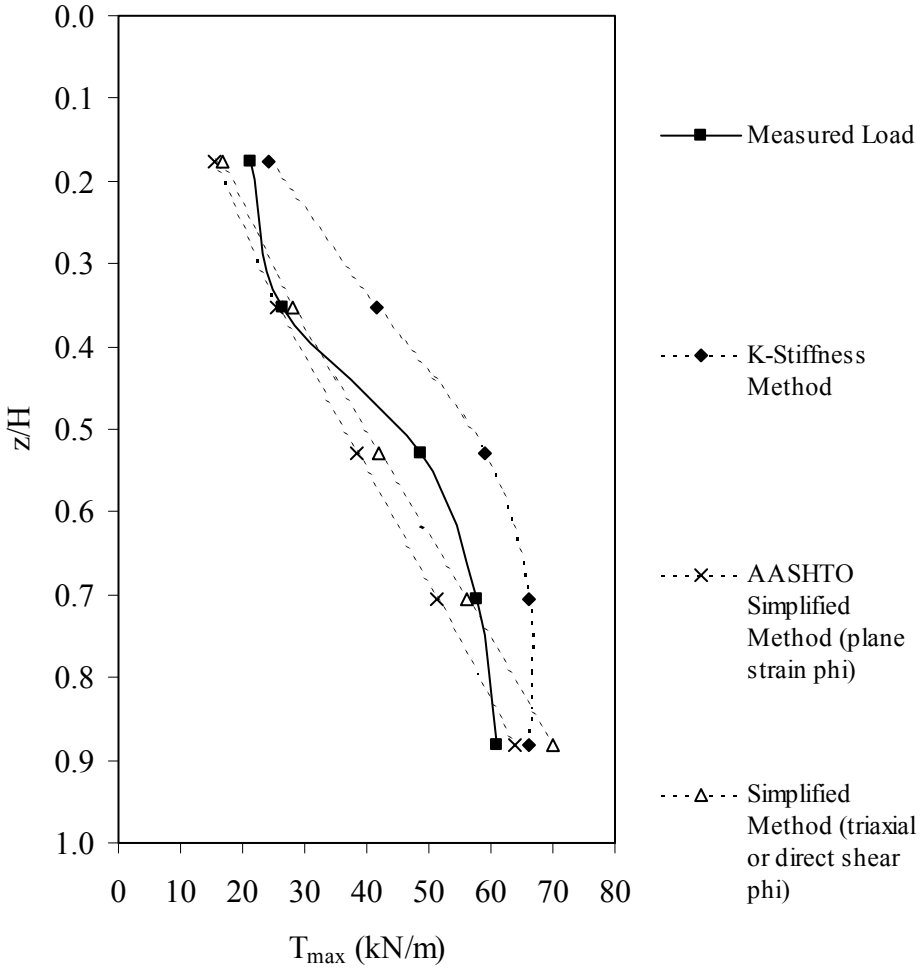

Figure A30. T_{max} as a function of depth below wall top for Wall SS15.

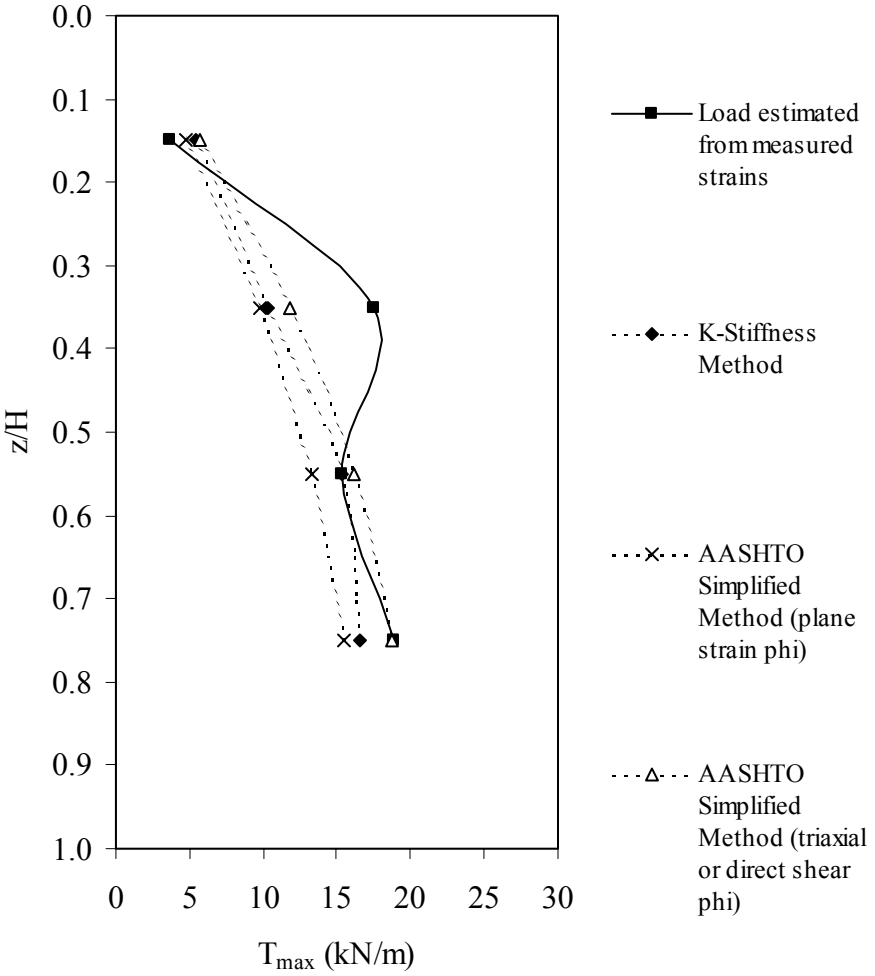

Figure A31. T_{max} as a function of depth below wall top for Wall BM1 (no surcharge).

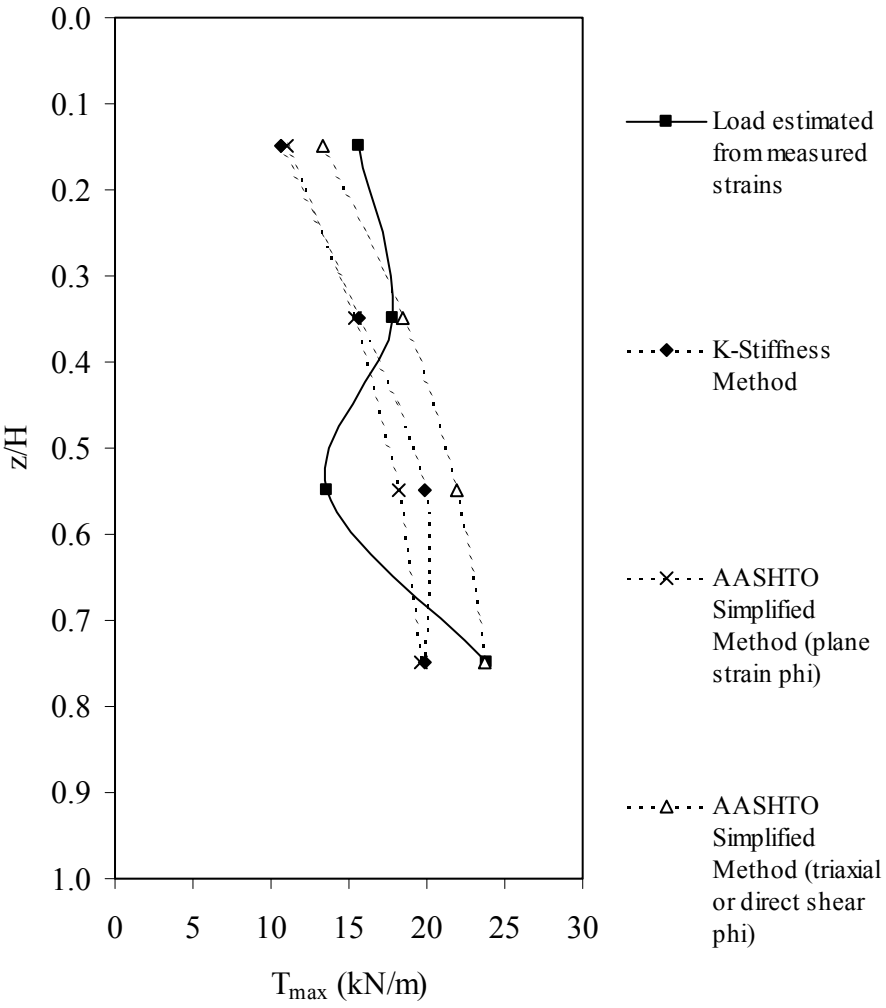

Figure A32. T_{max} as a function of depth below wall top for Wall BM1 (with surcharge).

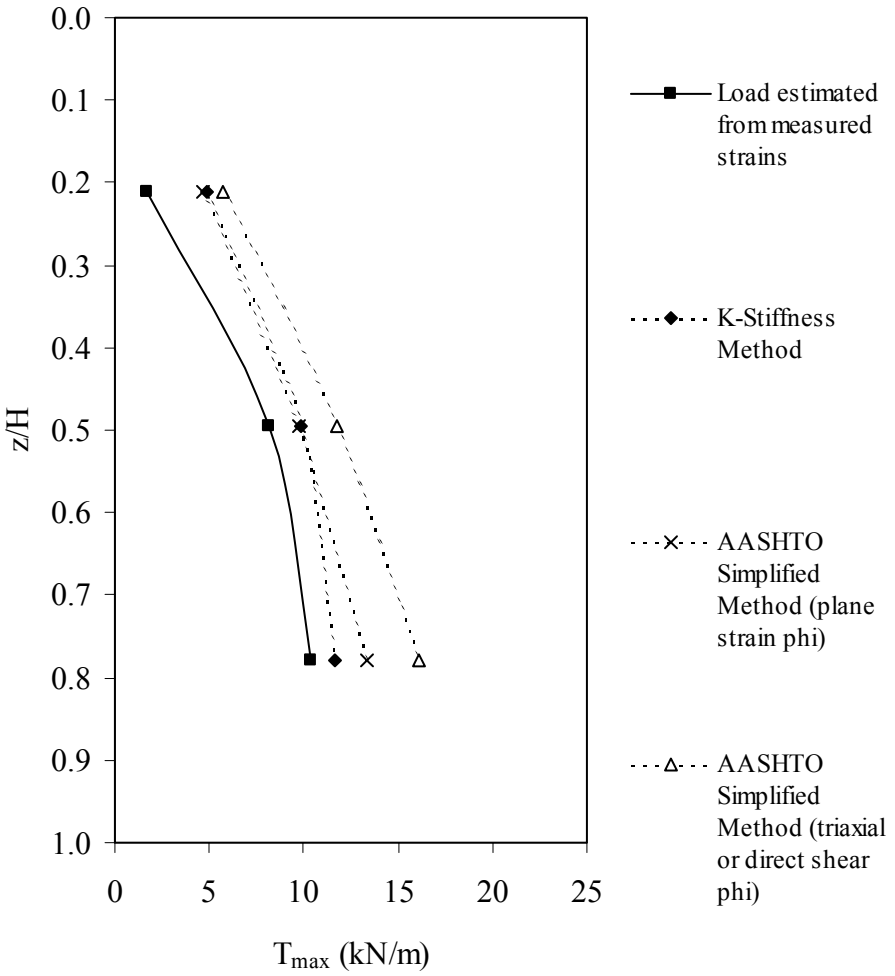

Figure A33. T_{max} as a function of depth below wall top for Wall BM2 (no surcharge).

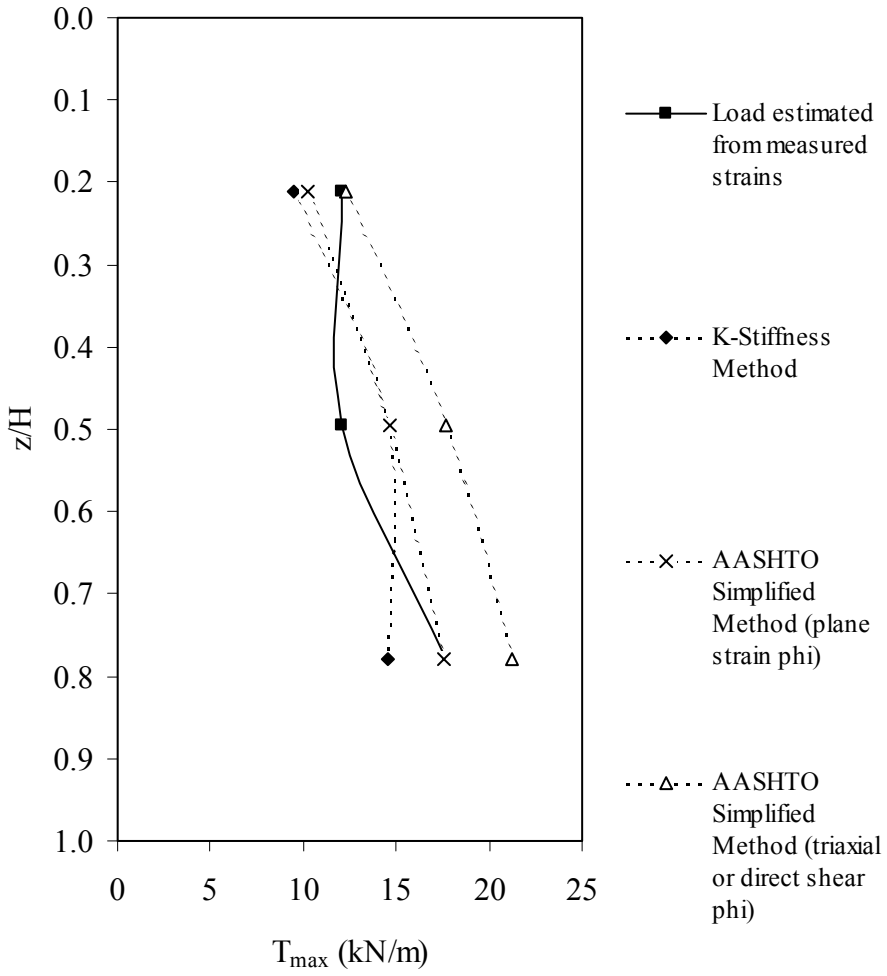

Figure A34. T_{max} as a function of depth below wall top for Wall BM2 (with surcharge).

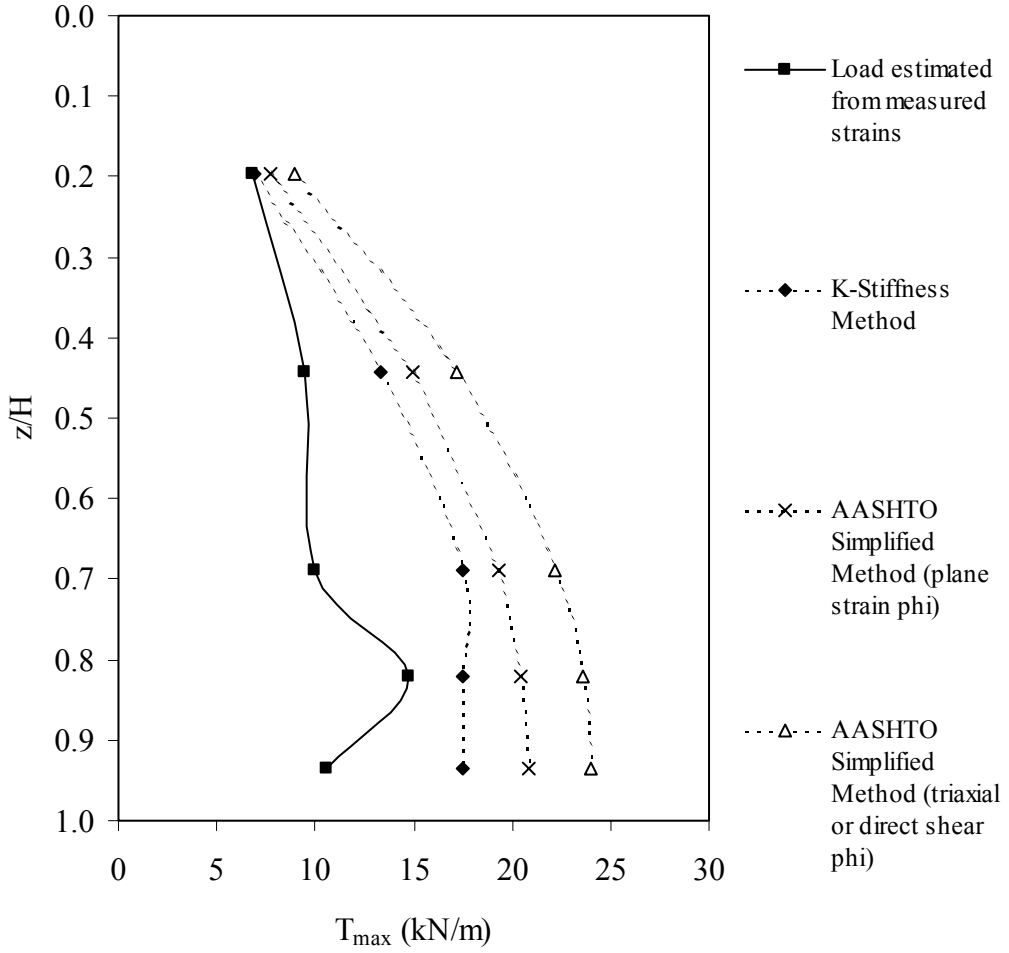

Figure A35. T_{max} as a function of depth below wall top for Wall BM3.

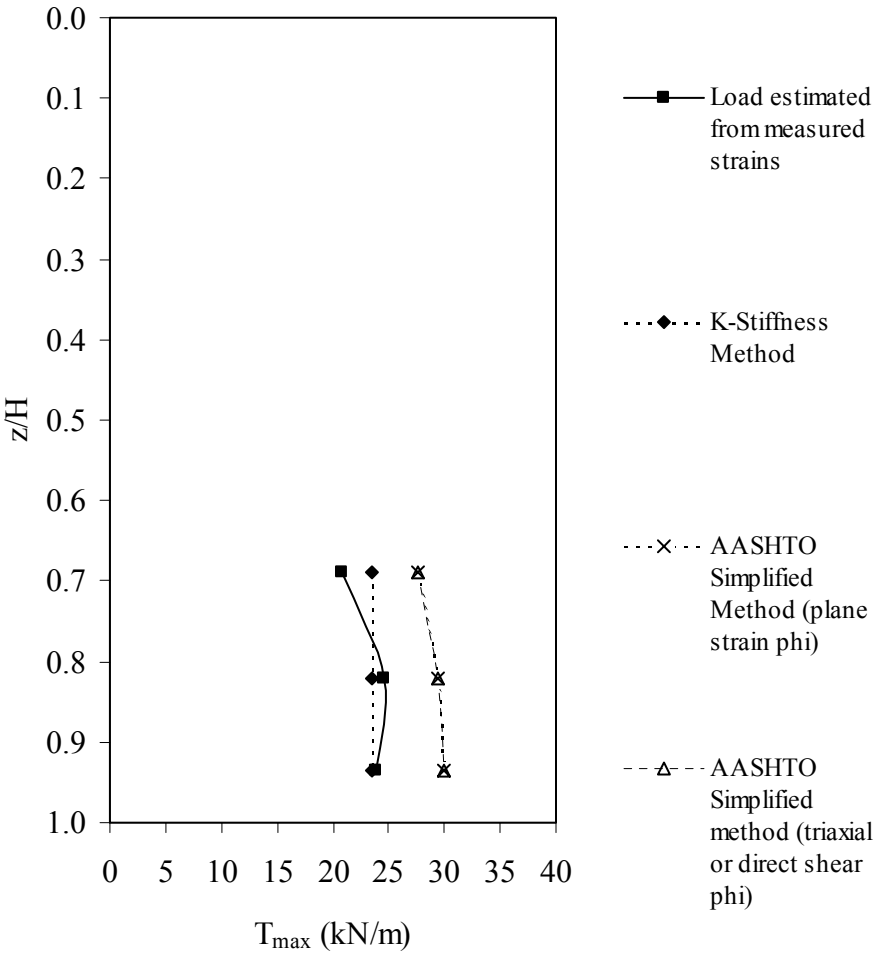

Figure A36. T_{max} as a function of depth below wall top for Wall BM4.

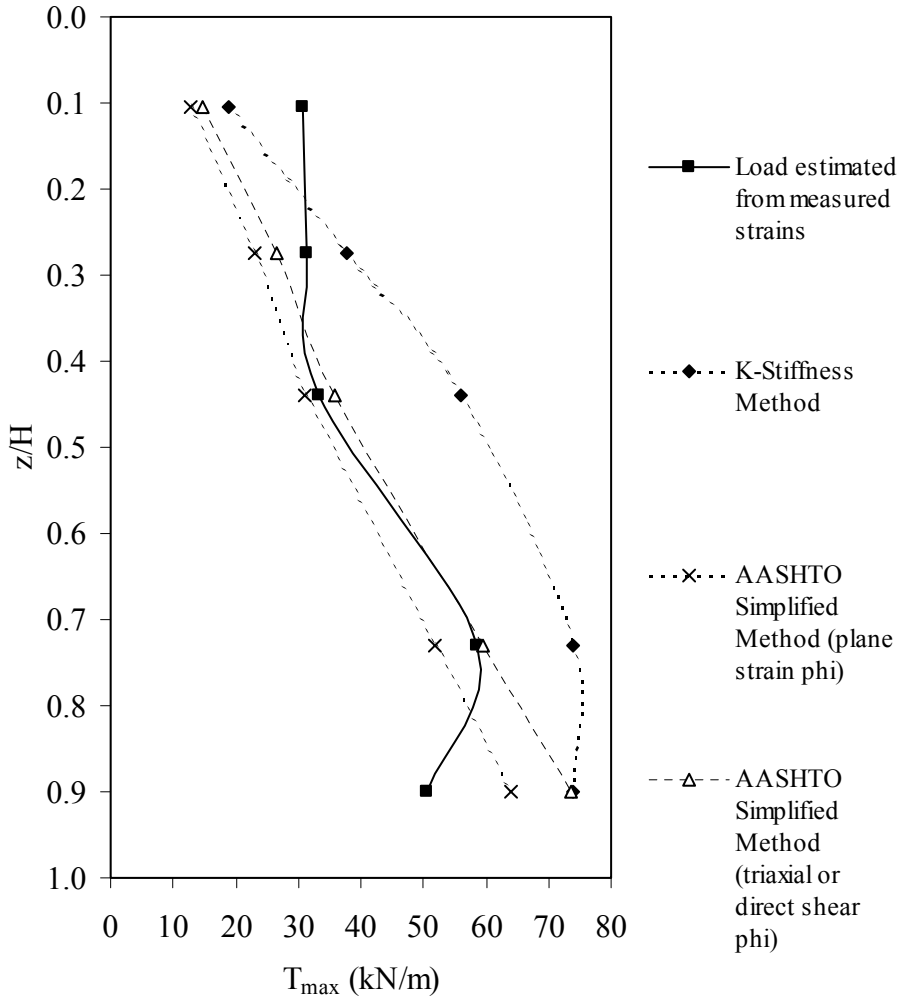

Figure A37. T_{max} as a function of depth below wall top for Wall BM5.

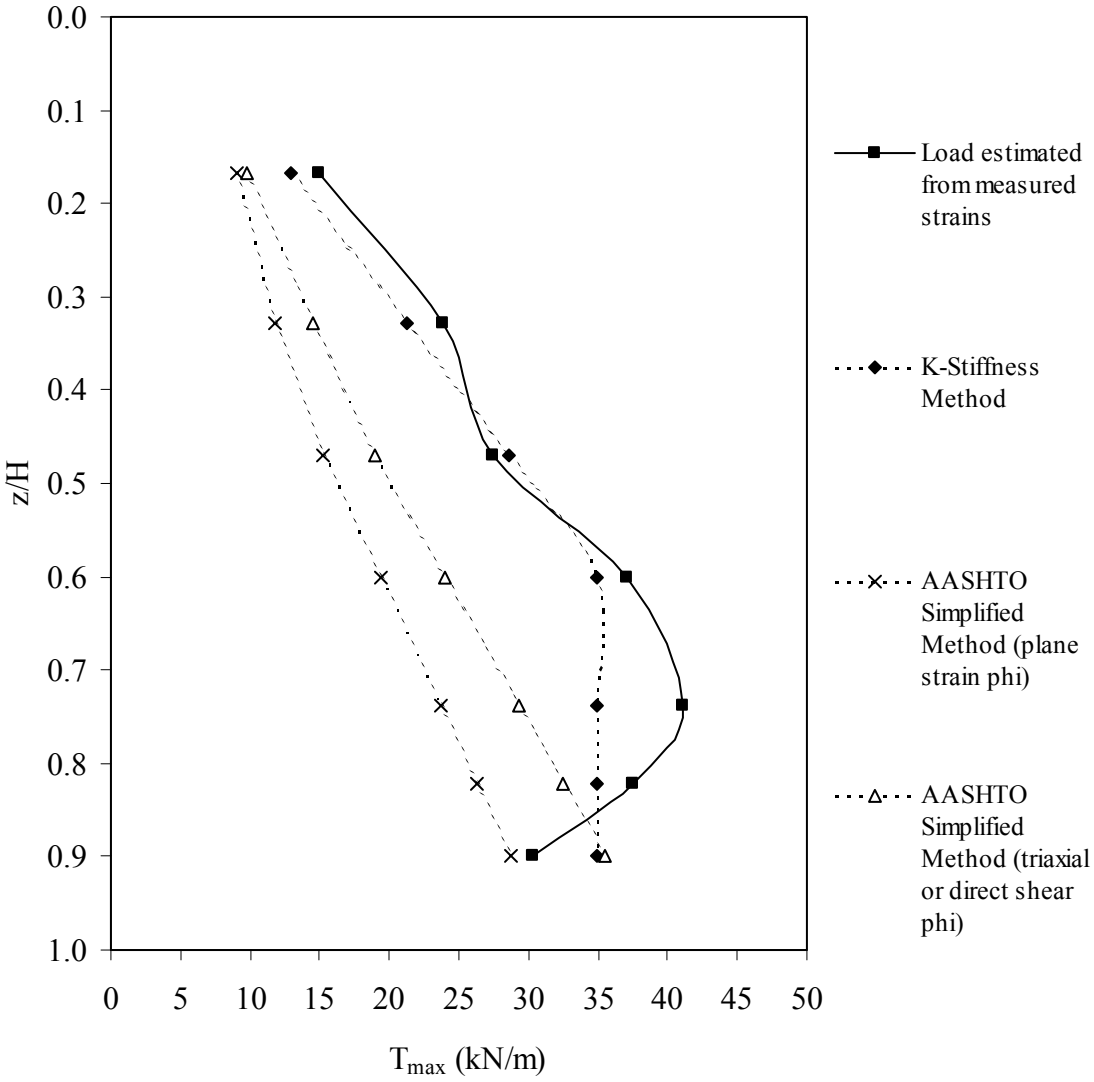

Figure A38. T_{max} as a function of depth below wall top for Wall WW1.

APPENDIX B: NOMENCLATURE

a = constant coefficient
b = thickness of facing column (m)
c = soil cohesion (kPa)
COV_1, COV_2, COV_{total} = coefficient of variation (%)
d = constant coefficient
D = demand (the total horizontal earth force to be carried by the reinforcement layers) (kN/m)
D_{actual} = demand based on the measured shear strength of the soil using plane strain peak friction angles (kN/m)
D_{design} = demand on the reinforcement layers based on the design value of soil shear strength (kN/m)
D_{tmax} = reinforcement load distribution factor (dimensionless)
E = elastic modulus (N/m^2)
F_f = facing column stiffness parameter (dimensionless)
FS = factor of safety
FS_{design} = design global factor of safety
h_{eff} = equivalent height of facing column (m)
H = height of the wall (m)
i = counter (1,2,3 …n)
I = moment of inertia (m^4)
J = tensile stiffness of the reinforcement (kN/m)
$J_{1\%}$ = secant stiffness of the reinforcement at 1% strain (kN/m)
$J_{2\%}$ = secant stiffness of the reinforcement at 2% strain (kN/m)
J_{ave} = average tensile stiffness for all the reinforcement layers (kN/m)
J_c = creep stiffness (kN/m)
J_{crs} = constant rate of strain stiffness (kN/m)
J_i = tensile stiffness of an individual reinforcement layer (kN/m)
J_r = relaxation stiffness (kN/m)
K = coefficient of lateral earth pressure (dimensionless)
K_a = active lateral earth pressure coefficient (dimensionless)
K_{abh} = horizontal component of active earth pressure coefficient accounting for wall face batter (dimensionless)
K_{ah} = horizontal component of active earth pressure coefficient (dimensionless)
K_{avh} = horizontal component of active earth pressure coefficient for vertical wall (dimensionless)
K_o = coefficient of lateral earth pressure at-rest (dimensionless)
K_r = lateral earth pressure coefficient (dimensionless)
L = unit length of wall facing (m)
n = total number of reinforcement layers in wall section
p_a = 101 kPa (atmospheric pressure)
P_{ah} = horizontal component of earth force (kN/m)
q = uniformly distributed surcharge pressure, or specifically the vertical stress due to traffic surcharge (kPa)
R = resistance (the total tensile capacity of the reinforcement layers in the structure) (kN/m)
R_{actual} = actual long-term resistance value (total for wall) (kN/m)

R_c = reinforcement coverage ratio (dimensionless)
$RD_{aldesign}$ = allowable long-term resistance-demand ratio (dimensionless)
R_{design}= long-term resistance value (total for wall) based on the design value of soil shear strength (kN/m)
$RD_{long\text{-}term}$ = estimated long-term resistance-demand ratio (dimensionless)
RD_{index} = index resistance-demand ratio (dimensionless)
$RD_{ultdesign}$ = ultimate design resistance-demand ratio (dimensionless)
RF = combined reduction factor to account for geosynthetic strength loss
RF_{actual} = actual strength reduction factor
RF_{CR} = reduction factor to account for strength loss due to creep
RF_D = reduction factor to account for chemical and biological degradation
RF_{design} = design reduction factor
RF_{ID} = reduction factor to account for installation damage
R_{index} = short-term reinforcement resistance values (total for wall) (kN/m/m width of wall)
$R_{ultdesign}$ = short-term reinforcement resistance value (total for wall) based on the design value of soil shear strength (kN/m)
S = average soil surcharge depth above the wall top, or equivalent height of uniform surcharge pressure (m)
S_{global} = global reinforcement stiffness value for wall (kN/m^2)
S_{local} = local reinforcement stiffness value (kN/m^2)
S_r = global reinforcement stiffness for the wall (kN/m^2)
S_v, S_i, S_v^i = tributary area for reinforcement layer (assumed equivalent to the vertical spacing of the reinforcement per unit length of wall) (m)
T, T(t), T_i = reinforcement load at any time (kN/m)
T_{al}, T_{al}^i, $T_{aldesign}^i$ = long-term strength for reinforcement layer (kN/m)
T_i = tensile capacity for reinforcement layer i (kN/m)
T_{max}^i, T_{max} = maximum measured or design reinforcement load for a layer (kN/m)
T_{mxmx} = maximum reinforcement load from all layers in the wall (kN/m)
T_{ult} = short-term (index or ultimate) strength of the reinforcement (kN/m)
T_{ult}^i = short-term (index or ultimate) strength of the reinforcement for layer i (kN/m)
$T_{ultdesign}$, $T_{ultdesign}^i$ = ultimate design (index or ultimate) tensile strength for reinforcement layer i (kN/m)
W = uniformly distributed load (N/m)
y_{max} = maximum deflection of uniformly loaded cantilever beam (m)
z = depth to the reinforcement level relative to the wall top at the wall face (m)
z_i = depth below top of wall to reinforcement layer i (m)
α = constant coefficient
β = constant coefficient
δ = interface shear angle between wall facing and backfill soil (degrees)
$\varepsilon(t)$, ε_i = reinforcement strain at any time (dimensionless)
$\dot{\varepsilon}$ = reinforcement strain rate
Φ = influence factor = $\Phi_g \times \Phi_l \times \Phi_{fs} \times \Phi_{fb}$ (dimensionless)
Φ_{fb} = facing batter factor (dimensionless)

Φ_{fs} = facing stiffness factor (dimensionless)
Φ_g = global stiffness factor (dimensionless)
Φ_{local} = local stiffness factor (dimensionless)
ϕ = friction angle of the soil (degrees)
ϕ_{des} = design friction angle for the soil (degrees)
ϕ_{ds} = peak direct shear friction angle of the soil (degrees)
ϕ_{tx} = peak triaxial friction angle (degrees)
γ = unit weight of the soil (kN/m^3)
η = constant coefficient (dimensionless)
κ = constant coefficient (dimensionless)
σ_1 = axial principal stress (kPa)
σ_3 = confining principal stress (kPa)
σ_h = lateral earth pressure acting over the tributary area (kPa)
ω = wall face batter from vertical (degrees)
$\Omega_{1,2}$ = constant coefficient (dimensionless)